SSME BEARING AND SEAL TESTER DATA COMPILATION, ANALYSIS AND REPORTING; AND REFINEMENT OF THE CRYOGENIC BEARING ANALYSIS MATHEMATICAL MODEL

Final Report

for

Contract No.: NAS8-39379

Prepared for

Mr. Howard G. Gibson
Materials and Processes Laboratory
Engineering Physics Division
George C. Marshall Space Flight Center
Marshall Space Flight Center

SRS TECHNOLOGIES

NASA

FOREWORD

This final report was prepared by SRS Technologies under Contract No. NAS8-39379 for the George C. Marshall Space Flight Center of the National Aeronautics and Space Administration. This work was administered under the technical direction of the Contract Officer's Technical Representative, Mr. Howard G. Gibson of the Materials and Processes Laboratory, Engineering Physics Division.

This final report describes the work performed by SRS Technologies during the period of January 1992 through January 2000. Mr. James D. Moore served as the SRS Technologies Principal Investigator. Mr. Joe C. Cody serves as an SRS Consultant on this contract.

CONTENTS

LIST OF EXHIBITS

LIST OF EXHIBITS (Continued)

LIST OF EXHIBITS (Continued)

LIST OF EXHIBITS (Continued)

LIST OF EXHIBITS (Continued)

LIST OF EXHIBITS (Continued)

LIST OF EXHIBITS (Continued)

LIST OF EXHIBITS (Continued)

LIST OF EXHIBITS (Continued)

LIST OF EXHIBITS (Concluded)

LIST OF TABLES

Introduction

The material presented in this report presents an attempt to document eight years of engineering support to Marshall Space Flight Center's cyrogenic bearing testing, design, and analysis efforts. The diverse nature of the many task performed in this support role and the extended period of performance for this effort make it very difficult to generate a single document that captures all of the effort. In fact many test reports, technical papers, and other standalone documents have been produced in the past and these publications provide more detailed documentation of certain topics. However, this document does attempt to at lest identify and summarize the majority of the tasks performed under this effort.

SRS Technologies support functions can be loosely categorized into three functional areas; thermomechanical bearing analysis software development, bearing analysis in support of hardware anomalies and new hardware design, and on-site test support. It is along these functional lines that the material in this report is organized. The material has been divided into six chapters, each falling under one of the functional areas described above.

The first chapter captures the majority of the software development that was accomplished under this contract. The core of the thermomechanical bearing model SINSHA had largely been developed at the beginning of this effort. However, significant modifications and improvements to the software were accomplished under this effort. The most significant involved integration of the Hydroseal[1] fluid bearing model into the SINSHA simulation. The improved system simulation now has the capability of incorporating a high fidelity simulation of the hydrostatic and or journal bearing in the coupled thermomechanical shaft bearing system model. The improved code was tested by incorporating the fluid damper seal into the Rocketdyne high pressure oxidizer turbopump shaft bearing simulation. The addition of the high fidelity damper seal model significantly improved the correlation of simulation results and observed hardware operating characteristics. The bearing diametrical fit/clearance analysis was also completely overhauled during this effort. The new model accommodates the use of fit modifying sleeves and provides improved analysis of temperature effects on diametrical clearance. The axial preload spring model was also overhauled and made more generic under this effort. Finally, in addition to these major changes, there were many minor improvements and refinements that were implemented.

The next three chapter of this report focus on applications of the analytical tools to support NASA in design and analysis of various cyrogenically cooled bearings. Chapter 2 addresses a diverse set of bearing design tasks that were performed using the arsenal of analysis tools supported by SRS. Many of the studies are related to designing bearings to maximize the benefits of improved wear and durability characteristics of silicon nitride rolling elements. Advanced cage designs were also performed in an effort to provide better lubrication to the rolling elements. This chapter also documents some of the design evaluation performed in support of the Advanced Techology Turbopump Program. The third chapter specifically documents the design analysis SRS performed in support of the Simplex pump development program. The fourth chapter documents analysis that was performed in support of various specific hardware anomalies that occurred during the period of performance of this effort.

Chapter five and six of this report document the two separate test support efforts performed by SRS during this effort. Chapter 5 covers the high payoff bearing seals and materials test program (BSMT). This program was a continuation of the testing completed and covered under earlier contracts. Support under this contract covered three BSMT builds; Unit 3, Build 6; Unit 2, Build 14; and Unit 3, Build 7. These three builds were the last test conducted under this very important test program that can be justifiably credited with enabling realization of long life cryogenic turbopumps. This rig program identified and demonstrated the benefits and feasibility of using ceramic rolling elements in the harsh turbopump environment. Chapter 6 covers the LH2 Bearing Test Rig, Build 0 through 5. This program provided a means of accelerated testing of bearings up to and through the 30,000 second design life criterion. Most importantly the program demonstrated that bearings displaying the surface distress anomaly, which has been called "river marking", can be depended on for continued safe and reliable operation for a complete 30,000 second life application.

As previously stated, these six chapters cover an eight year compilation of a large number of diverse efforts. Thus, this reports is necessarily a summary of these efforts. A list of topics by month is provided as a cross reference to monthly reports that can be referenced for more detailed coverage of selected topics.

SYNOPSIS OF REPORTS

September 1999

- Stress Analysis for FEP Coated Cage Debond Investigation

August 1999

- ADORE Analysis Supporting FEP Coated Cage Debond Investigation

July 1999

- Final Report Preparation
- SINDA/SHABERTH Code Modifications

June 1999

- Fluid Film Bearing Off-Design Analysis

May 1999

- NAS8-39379 Final Report Compilation
- Hydrostatic Bearing Test Review

April 1999

- Status of Build 5 Testing

March 1999

- Status of Build 5 Testing
- Final Report Preparation

February 1999

- Build 5 Rotational Testing (Tests 02096013.500 - P2096017.500)
- Mid Term Inspection Results

January 1999

- Build 5 Rotational Testing (Tests 007 - 012)

December 1998

- Build 5 Rotational Testing (Test 006)

November 1998

- Build 5 Rotational Resting (Tests 000 - 005)

October 1998

- Status of LH_2 Rig Support
- SHABERTH model update

September 1998

- Status of LH_2 Rig Support

August 1998

- Status of LH_2 Rig Support

July 1998

- Status of LH_2 Rig Support

June 1998

- Improvements to SHABERTH Bearing Code to Support Future LH_2 Rig Testing

May 1998

- Improvements to SHABERTH Bearing Code to Support Future LH_2 Rig Testing

April 1998

- Status of LH_2 Rig Build 5

March 1998

- Ball Bearing Analysis for LH_2 Rig Roller Bearing Test
- Modification of SHABERTH Only Code

February 1998

- Build 4A Rotational Testing (Test 125 - 126)
- Radial Load Capability Analysis of the LH_2 Rig Hydrostatic Bearing
- Contact Geometry Characteristics for the Fuel Pump Ball Bearing

January 1998

- Build 4A Rotational Testing (Test 119 - 124)

December 1997

- Build 4A Rotational Testing (Test 115 - 118)

November 1997

- Build 4A Rotational Testing (Test 109 - 114)
- Hydroject Analysis of LH_2 Rig Hydrostatic Bearing

October 1997

- Build 4A Rotational Testing (Test 108)
- Modification of SHABERTH Software
- Hardware Inspection of Ball Bearings From Flight Fuel Pump 6-5

September 1997

- LH_2 Bearing Build 4A Testing Initiated

August 1997

- Status of the LH_2 Bearing Tester Build 4

July 1997

- Status of the LH_2 Bearing Tester Build 4 (Tests 92 to 103)

June 1997

- Status of the LH_2 Bearing Tester Build 4 (Tests 81 to 91)

May 1997

- Liquid Hydrogen Bearing Tester Support

April 1997

- Preparation for Build 4

March 1997

- Status of MSFC LH_2 Bearing Tester Build 3A
- SINDA/SHABERTH Computer Modeling of LH_2 Bearing Tester

February 1997

- Status of MSFC LH_2 Bearing Tester Build 3A
- SINDA/SHABERTH Modeling of MSFC LH_2 Bearing Tester

January 1997

- Status of LH_2 Bearing Rig Build 3A

December 1996

- LH_2 Bearing Rig Build 3 Test Summary

November 1996

- ADORE Analysis of HPFTP/AT and HPOTP/AT Contact Traction Forces
- Status of Build 3 Testing

October 1996

- Build 2 Hardware Tear Down and Inspection
- Status of Build 3 Testing

September 1996

- LH_2 Bearing Rig Build 2 Test Summaries and Results
- Estimated Overspeed for Test 0202606 and Test 02026028
- Analysis of Speed and Thermal Effect on LH_2 Rig Operating Loads

August 1996

- Hydrogen Bearing Tester Liquid Nitrogen Shakedown Test P2026022

July 1996

- Hydrogen Bearing Tester Liquid Nitrogen Shakedown Test P2026021

June 1996

- Pretest Support for Ball and Roller Bearing Test Series

May 1996

- Incorporation of Roller Bearing Into LH_2 Bearing Tester Model

April 1996

- MSFC LH_2 Bearing Tester Post Test Hardware Review

March 1996

- MSFC Liquid Hydrogen Bearing Tester Status

February 1996

- Summary of LH_2 Test Series Status

January 1996

- Planning for Hydrogen Bearing Testing

December 1995

- Preparation for Hydrogen Test Series

November 1995

- Modification of SHABERTH Code to Output Additional Contact Data

October 1995

- Preparation for Hydrogen Testing of HPFTP/AT Ball Bearing
- Bearing Fluid Flow Model Demonstration Attended

September 1995

- Completion of SINDA/SHABERTH Preload Model
- LH_2 Bearing Tester Computer Simulation with Liquid Nitrogen
- Test Support for the MSFC Bearing Tester

August 1995

- Rolling Element Bearing Tester Test Readiness Review
- Modification of SINDA/SHABERTH Model Preload Routine

July 1995

- Modification of SINDA/SHABERTH Model Preload Routine

June 1995

- Fluid Film Bearing Tester SSH Model Updates and Pretest Predictions
- SIMPLEX Bearing Stick-out Prediction

May 1995

- Completion and Delivery of Updated SHABERTH Bearing Code
- Development of SINDA/SHABERTH/HYDROSEAL Model of MSFC Fluid Film Bearing Tester

March/April 1995

- Three Ring Fit Analysis Added to SINDA/SHABERTH Bearing Model
- Development of SINDA/SHAVERTHE/HYDRODEAL Model of MSFC Fluid Film Bearing Tester
- Fluid Film Bearing tester Redline Review

February 1995

- MathCAD Program for Three Ring Fit Analysis

January 1995

- ALGOR Thermal Analysis of MSFC Hybrid Bearing Test Rig

November/December 1994

- Analysis of Instrumentation Redline Limits for SIMPLEX Liquid Oxygen Pump
- User Group Meeting for General Fluid System Simulation Program (GFSSP)
- SHABERTH Fit Routine Modified to Correct Fit Pressure Calculations

October 1994

- SSH Hybrid Bearing Thermal Code Beta Version Completed

September 1994

- SSH Hybrid Bearing Code Development

August 1994

- Hybrid Bearing Code Development
- Space Shuttle APU Bearing Torque Investigation

July 1994

- Improvements to Hybrid Rolling Elements/Fluid Bearing Model
- Power Requirements for Ball Bearing Modification of Fluid Film Bearing Tester

June 1994

- SHABERTH/HYDROSEAL Fluid Film Bearing Code Development

May 1994

- Development of SHABERTH Fluid Film Bearing Code
- Documentation of EHD Film Models
- SINDA/SHABERTH Code Installed on Pentium Personal Computer
- Documentation of Friction Models Used in SHABERTH

April 1994

- Development of Hybrid Fluid Film/Rolling Element Bearing Shaft Support Analysis

March 1994

- Development of Finite Element Shaft Model for Shaft/Bearing System Modeling
- Hybrid Bearing Load Support System Model Development

February 1994

- Hybrid Fluid Film Bearing System Model Development
- Analysis of 85mm LPOTP Bearing Ball Excursion

January 1994

- Simplex LO_2 Pump Bearing Spacer Length Determination
- Hydroseal Fluid Film Bearing Program Evaluation

December 1993

- Unit 3 Build 7 Post Test Bearing Summary

November 1993

- Analysis of Rocketdyne HPOTP 2315R3 Pump End Bearing
- Development of Hybrid Fluid-Film/Rolling Element Bearing System Model

October 1993

- Simplex LO_2 Pump Preload and Radial Stiffness
- Investigation of Bearing Ring Flexing Modeling

September 1993

- Development of Hybrid Fluid Film Bearing/Rolling Element Bearing Shaft Support Analyses
- Analysis of Simplex LO_2 Pump Bearing

August 1993

- Testing of BSMT Unit 3 Build 7
- Analysis of SIMPLEX LO_2 Pump Bearings

July 1993

- Analysis of Support Preliminary Design of Simplex Pump Bearings
- ADORE Version 3.2 Installed on EADSII Computer System
- Testing of BSMT Unit 3 Build 7

June 1993

- Testing of BSMT Unit 3 Build 7
- Evaluation of Bearing Stiffness Loss as a Function of Ball Wear for Rocketdyne SSME Fuel Pump Bearings
- Static Load Capacity of High Pressure Fuel Pump Ball Bearings

May 1993

- Testing of BSMT Unit 3 Build 7
- Investigation of Ball Size Variation Effects in ATD LO_2 Pumps

April 1993

- Simplex Turbopump Bearing Thermo-Mechanical Model Development
- Comparison of Cage Loads from BSMT Testing of Battelle Cages to Expected Cage Loads for 45mm Bearings with Battelle Cages in Turbopump

February/March 1993

- Support to ATD Pump End Bearing Problem Assessment
- Tests of Si_3N_4 Ball Bearings with Axial and Radial Loads in BSMT
- Analysis of Battelle Cage with Oval Ball Pockets

December 1992 - January 1993

- Support to ATD Pump End Bearing Problem Assessment
- Tests of Si_3N_4 Ball Bearings with Axial and Radial Loads in BSMT

November 1992

- Support to ATD Pump End Bearing Problem Assessment
- Bearing Preload Spring Tilting Moment Tests

October 1992

- Support to ATD Pump End Bearing Problem Assessment
- Radial Load Analysis for Si_3N_4 Ball Bearings in the BSMT

September 1992

- ATD LOX Pump PEBB Radial Stiffness with Straight and Diverged Deadband

August 1992

- BSMT Radial Loading
- Version 1.2 of P.C. SHABERTH Completed

July 1992

- PEBB Beam Preload Spring Tilting Moment Test
- P&W PEBB Operation with High Axial Preloads

June 1992

- Investigation of Ball Pocket Clearances for 45mm Bearing with Battelle Cages
- Summary of Unit 3 Build 6 Test Series
- Radial Load of BSMT Bearings

May 1992

- Assessment of Outer Race Tilt Effects on the 45 mm HPOTP Bearing Operating Characteristics
- Summary of BSMT Unit 3 Build 6 Test Series

April 1992

- Determination of Outer Race Curvature Effects on HPOTP Pump End Bearing Operating Parameters
- Investigation of Hybrid Pump End Bearing Pair

March 1992

- Investigation of Operating Stresses in the Fluoroly-C Cage Design
- HPOTP Pump End Bearing Optimization Using Silicon Nitride Rolling Elements

February 1992

- Conversion and Verification of the 45mm HPOTP Pump End Bearing Thermo-Mechanical Model for Use on the PC SHABERTH/SINDA Code
- Investigation of Replacement of the 440-C Rolling Elements in the 45mm HPOTP Pump End Bearing with Silicon Nitride Balls
- Investigation of Spiral Scarring Found on ATD LOX Pump PEBB Using the ADORE Software

1.0 Bearing Analysis Software Improvements

SRS and NASA/MSFC have developed software with unique capabilities to couple bearing kinematic modeling with high fidelity thermal modeling. The core thermomechanical modeling software was developed by SRS and others in the late 1980's and early 1990's under various different contractual efforts. SRS originally developed software that enabled SHABERTH (Shaft Bearing Thermal Model) and SINDA (Systems Improved Numerical Differencing Analyzer) to exchange data and autonomously allowing bearing component temperature effects to propagate into the steady state bearing mechanical model. A separate contract was issued in 1990 to create a personal computer version of the software. At that time SRS performed major improvements to the code. Both SHABERTH and SINDA were independently ported to the PC and compiled. SRS them integrated the two programs into a single program that was named SINSHA. This was a major code improvement.

By combining the software into a simple FORTRAN code, we eliminated the dependency of the software on a particular operating system. Prior to this modification, even small operating system version changes or upgrades often created problems. In a latter modification, transient analysis capability was added to the software. This unified steady-state and transient, personal computer based program, SINSHA, was the baseline analysis tool that was used for various test support modeling, hardware anomaly investigations and bearing design tasks that were completed under this contract.

At the beginning of this effort the core SINSHA program existed. However, in the course of this contract two major software modifications and numerous minor changes to the program were implemented. The largest major changed accomplished involved the addition of fluid film bearing modeling capabilities to the SINSHA program. This was accomplished by integrating portions of the hydroseal code, developed by Dr. L. San Andres of the University of Texas A&M, directly into the SINSHA code. The hydroseal model provided fluid bearing stiffness as a function of shaft displacement. Hence, we were able to use this code in the same manner as the ball bearing, roller bearing, and tapered roller bearing modules are used in SINSHA. The standard SINSHA input file was modified for the fluid film bearing mode. It is now possible to include up to five fluid film bearings in the SINSHA bearing system model. To the best of our knowledge, SINSHA is the only shaft/load support system model that can incorporate detailed analysis of hydrostatic bearings in the system level analysis. This feature proved valuable for evaluating the SSME turbopump bearing support system and including the load support from the damper seal. In fact, model results were found to agree much better with observed operating characteristics once this modification was implemented and the damper seal was modeled in detail.

The second major revision to the code involved an improvement to the diametrical clearance change analysis in the bearing model. The motivation for this modification was to enable better modeling of bearings that use a sleeve between the inner ring and shaft or between the outer ring and the housing. In many designs a sleeve is used to provide an additional parameter to control the internal radial clearance (IRC) and other critical fits in the bearing stack-up. To provide detail analysis of these types of bearings, a three ring analysis was developed. This new code completely replaced the previous "fit" rou-

tine in SINSHA. The input data deck was changed to accommodate the additional data required to define any sleeves that may exist on a bearing design.

Other modeling efforts accomplished under this effort include: improvements to the preload spring model, development of a standalone SHABERTH only version of the software that includes the modeling improvements described above, and the development of some independent codes to look at special issues. All of these accomplishments are described in this section of the report.

1.1 45 MM Bearing Model Conversion to PC SINDA/SHABERTH

One of the first tasks accomplished under this contract involved converting one of the Rocketdyne turbopump bearing models from the older format into the PC SINSHA format. The thermomechanical model of the Rocketdyne HPOTP pump end 45 mm bearing, which was initially developed and operated on the MSFC EADS, was converted for operation on the personal computer version of SINDA/SHABERTH developed by SRS. The conversion involved changing the SINDA portion of the model from SINDA '87 which is supported by DR. J D. Gaski to SINDA '85/FLUINT which was written by Martin Marietta Corporation and is distributed through Cosmic. These SINDA formats are basically the same with only HEADER BLOCK format differences, thus, SINDA model conversion was relatively simple. However, the interaction between SINDA and SHABERTH had been radically changed for the personal computer version. The EADS version used Job Control Language (JCL) to perform the iterations between SINDA and SHABERTH, whereas, in the PC version, SHABERTH is accessed from within SINDA through a subroutine call statement. A solution can be obtained much faster with the PC version simply because the SINDA preprocessor is only executed once and not at every SINDA/ SHABERTH iteration as with the EADS version.

1.2 Version 1.2 of PC SHABERTH Completed

Early in this program, improvements were made to PC SHABERTH software. PC SHABERTH is a standalone version of SHABERTH that can be used when the advanced thermal modeling capability of SINSHA is not required. Version 1.1 of this software was previously distributed by COSMIC. Version 1.2 incorporated improvements suggested by users around the country. Two modifications were incorporated that improve the features of Version 1.2 over previous versions. The first modification involves input and modification of shaft loading data. In previous versions of P.C. SHABERTH, separate data input screens were called for each radial load in X-Y plane and each radial load in the X-Z plane. It could be confusing determining which loads were being requested for input. Additionally, previous version required that the user reenter the entire load set each time any of the shaft loads were changed for additional analysis. This made it difficult to perform parametric type studies. For Version 1.2 new input screens were developed for inputting and modifying shaft loading data. Any of the shaft loads can now be modified from a single input screen. This feature supports parametric analysis requiring multiple runs.

The second modification incorporated in Version 1.2 was the addition of new source code to calculate and output additional design parameters. Selected pages of Version 1.2 output are shown in **Exhibit 1** through **5**. The second

*** S H A B E R T H / P C ********** S H A B E R T H / P C ********** S H A B E R T H / P C ****

SAM2

R O L L I N G E L E M E N T O U T P U T FOR BEARING NUMBER 2

AZIMUTH	ANGULAR SPEEDS (RADIANS/SECOND)					SPEED VECTOR ANGLES (DEGREES)		SPIN TO ROLL RATIO	
ANGLE (DEG.)	WX	WY	WZ	TOTAL	ORBITAL	TAN-1(WY/WX)	TAN-1(WZ/WX)	OUTER	INNER
0.00	-7259.450	1741.077	-25.955	7465.363	1490.772	166.51	-179.80	0.0000	0.3327
32.73	-7092.426	1973.759	-29.082	7362.002	1473.425	164.45	-179.77	0.0000	0.2666
65.45	-7052.890	2095.106	-30.888	7357.559	1474.285	163.46	-179.75	0.0000	0.2423
98.18	-7106.725	2123.985	-31.572	7417.402	1486.451	163.36	-179.75	0.0000	0.3013
130.91	-7345.679	1978.779	-30.112	7607.593	1521.751	164.92	-179.77	0.0000	0.4064
163.64	-7785.451	1682.350	-26.726	7965.191	1588.609	167.81	-179.80	0.0000	0.5639
196.36	-8212.207	1376.173	-22.805	8326.747	1657.103	170.49	-179.84	0.0000	0.7015
229.09	-8442.695	1135.752	-19.232	8518.768	1693.295	172.34	-179.87	0.0000	0.7705
261.82	-8389.945	1028.718	-17.278	8452.795	1679.561	173.01	-179.88	0.0000	0.7470
294.55	-8081.725	1109.732	-17.996	8157.589	1621.649	172.18	-179.87	0.0000	0.6390
327.27	-7640.225	1383.233	-21.386	7764.459	1546.061	169.74	-179.84	0.0000	0.4809

SRS TECHNOLOGIES

Exhibit 1 Version 1.2 Rolling Element Output Including Spin to Roll Ratios

*** S H A B E R T H / P C ********** S H A B E R T H / P C ********** S H A B E R T H / P C *****

SAM2

F R I C T I O N A L H E A T G E N E R A T I O N I N C O N T A C T E L L I P S E
R O L L I N G E L E M E N T N U M B E R 1
------ BRG NO. 2 ------

I N N E R R A C E

# LAMINA	CONTACT AREA (MM**2)	SEMI-MAJOR AXIS (MM)	SEMI-MINOR AXIS (MM)
20	0.2447	0.9170	0.8479E-01

WIDTH OF LAMINUM (MM)	HEAT GEN. PER LAM. (WATTS)
0.0902578200	0.275
0.0902578200	0.711
0.0902578200	0.766
0.0902578200	0.712
0.0902578200	0.602
0.0902578200	0.462
0.0902578200	0.315
0.0902578200	0.180
0.0902578200	0.075
0.0902578200	0.015
0.0931477600	0.016
0.0931477600	0.096
0.0931477600	0.263
0.0931477600	0.519
0.0931477600	0.858
0.0931477600	1.214
0.0931477600	1.469
0.0931477600	1.509
0.0931477600	1.413
0.0931477600	0.544

O U T E R R A C E

# LAMINA	CONTACT AREA (MM**2)	SEMI-MAJOR AXIS (MM)	SEMI-MINOR AXIS (MM)
20	0.4126	1.003	0.1309

WIDTH OF LAMINUM (MM)	HEAT GEN. PER LAM. (WATTS)
0.1003173000	0.077
0.1003173000	0.097
0.1003173000	0.079
0.1003173000	0.057
0.1003173000	0.039
0.1003173000	0.026
0.1003173000	0.018
0.1003173000	0.014
0.1003173000	0.012
0.1003173000	0.012
0.1003173000	0.012
0.1003173000	0.012
0.1003173000	0.014
0.1003173000	0.018
0.1003173000	0.026
0.1003173000	0.039
0.1003173000	0.057
0.1003173000	0.079
0.1003173000	0.097
0.1003173000	0.077

SRS TECHNOLOGIES

Exhibit 2 Version 1.2 Heat Geneation Distribution to Contact Ellipse

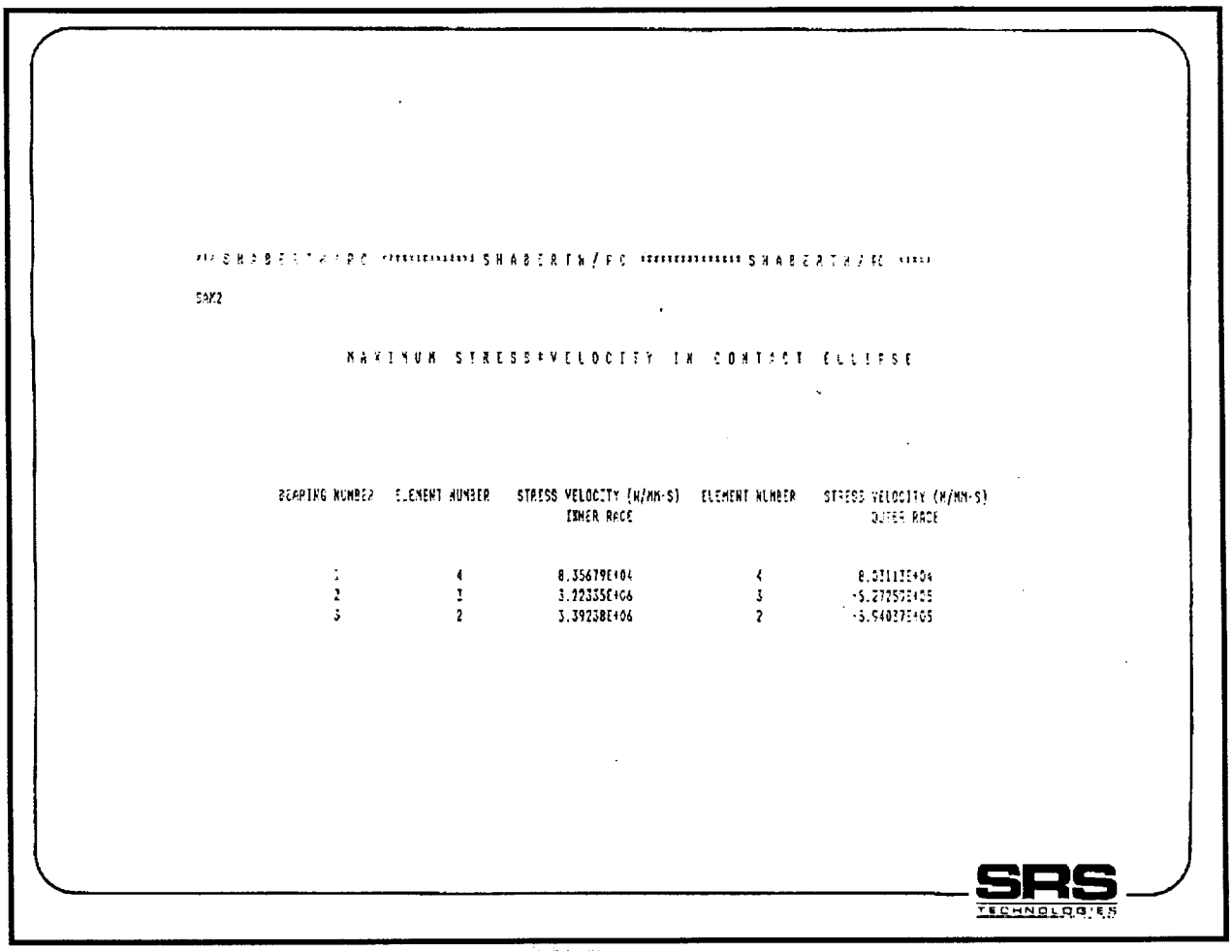

Exhibit 3 Maximum Stress Velocity Output for Version 1.2

*** SHABERTH/PC ********** SHABERTH/PC ********** SHABERTH/PC *****

SAM2

STRESS VELOCITY PROFILE IN CONTACT ELLIPSE

ROLLING ELEMENT NUMBER 1

------ BRG NO. 2 ------

LAMINA POSITION FROM LOWER CONTACT ANGLE EDGE OF CONTACT ELLIPSE

INNER RACE		OUTER RACE	
LAMINA POSITION (MM)	STRESS VELOCITY (N/MM-S)	LAMINA POSITION (MM)	STRESS VELOCITY IN/MM-S)
5.77027E-02	-7.46742E+05	5.92426E-02	-2.97511E+05
1.73108E-01	-1.22523E+06	1.77728E-01	-5.07257E+05
2.88514E-01	-1.46540E+06	2.96213E-01	-5.21604E+05
4.03919E-01	-1.56614E+06	4.14698E-01	-4.38752E+05
5.19325E-01	-1.55554E+06	5.33183E-01	-3.72316E+05
6.34730E-01	-1.44747E+06	6.51668E-01	-2.81015E+05
7.50136E-01	-1.25153E+06	7.70154E-01	-1.96787E+05
8.65541E-01	-9.76177E+05	8.88639E-01	-1.27553E+05
9.80947E-01	-6.30137E+05	1.00712E+00	-7.57601E+04
1.09635E+00	-2.23037E+05	1.12561E+00	-5.35594E+04
1.21378E+00	2.42384E+05	1.24409E+00	-5.35594E+04
1.33324E+00	7.54570E+05	1.36258E+00	-7.87601E+04
1.45270E+00	1.28823E+06	1.48106E+00	-1.27559E+05
1.57216E+00	1.82155E+06	1.59955E+00	-1.96787E+05
1.69162E+00	2.32682E+06	1.71804E+00	-2.81015E+05
1.81108E+00	2.76751E+06	1.83652E+00	-3.72212E+05
1.93054E+00	3.09253E+06	1.95501E+00	-4.38703E+05
2.04999E+00	3.22335E+06	2.07349E+00	-5.21604E+05
2.16945E+00	3.01618E+06	2.19198E+00	-5.07259E+05
2.28891E+00	2.06939E+06	2.31046E+00	-3.97813E+05

SRS TECHNOLOGIES

Exhibit 4 Stress Velocity Profile Output for Version 1.2

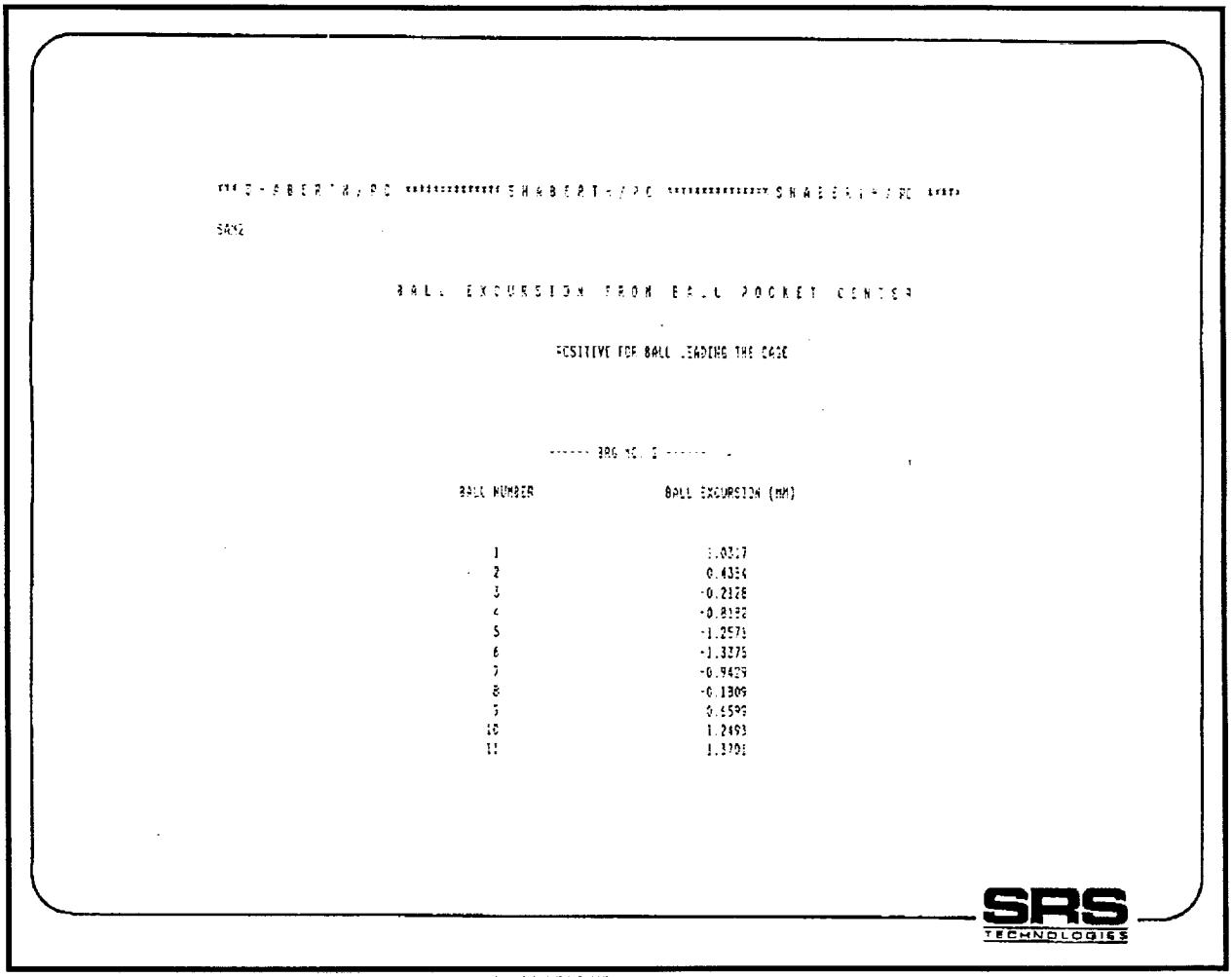

Exhibit 5 Ball Bearing Ball Excursion Output

rolling element output page was modified to display the inner race and outer race spin to roll ratio, this page is shown in Exhibit 1. The spin to roll output columns are included in the output for all bearing types. However, both columns should be zero unless the bearing output data is for a ball bearing. The rolling element contact frictional heat generation output was also improved in Version 1.2. This page illustrated in Exhibit 2, shows how the heat generation rate varies across the contact ellipse. In previous version of P.C. SHABERTH this page was printed out for ball bearings only. For Version 1.2, the heat generation distribution for cylindrical roller bearings is also output. Several completely new output pages were developed for Version 1.2. Two pages are used to output bearing SV. This parameter is the product of Hertzian contact stress and slip velocity in the contact ellipse. The page shown in Exhibit 3 outputs the maximum SV for each bearing on both the inner and outer race. The output also indicates which rolling element experiences this maximum SV. The second SV output page is shown in Exhibit 4. This page shows the distribution of SV across inner and outer contact ellipses for the rolling element with maximum SV. The sign of the SV value indicates the direction of relative slip across the lamina. Finally, an output page (Exhibit 5) was developed to show the magnitude of ball excursions from the cage pocket center. This page is output for ball bearings only.

The PC SHABERTH users manual was updated to reflect the changes in Version 1.2. This code is still available for public distribution through the distribution system that replaced the COSMIC software center.

1.3 ADORE Version 3.2 Installed on EADSII Computer System

In addition to the SINSHA code development effort, SRS provided support and maintenance of the ADORE dynamics model that MSFC licenses from PKG, Inc. ADORE V3.2 was installed on the EADSII Computer System. This version of ADORE has improvements to the shaft equilibrium equations which simplify the task of modeling certain bearing operating condition such as those resulting from ball size variations in ball bearings. The source code for version 3.2 was installed on the EADS II common file system (CFS1). All of the bearing models that were developed on the EADS I system were transferred to EADSII. However, the input format for version 3.2 was slightly different from the format for previous versions. Therefore, the existing bearing models was updated prior to execution with version 3.2 on EADS II. A new version of the ADORE plotting package ADRP was also installed. This program requires linking with the DISSPLA software and therefore must be run on the Silicon Graphics (VMCS) System.

1.4 Development of Hybrid Fluid Film Bearing/Rolling Element Bearing Shaft Support Analysis

Rocketdyne SSME turbopumps and the Advanced Technology Development (ATD) turbopumps for the SSME use rolling element bearings to support the turbine/pump shaft. These bearings are subject to wear and thermal conditions which can limit pump life. Recent research efforts have investigated the application of fluid film bearings as an alternative technology with potential to improve cryogenic turbopump life, reliability, and possibly performance. Analysis capabilities have been developed to support design and optimization of fluid film bearings for cryogenic applications. These codes typically provide a detailed analysis of a single bearing subjected to a set of specified boundary conditions (applied loads, misalignment, inlet flow properties, etc.). However, it can be difficult to determine the appropriate boundary conditions for modeling a single bearing when the bearing is used in a complex multi-bearing load support system such as a turbopump. For rolling element bearings this problem is addressed through shaft-bearing system modeling using computer codes such as SHABERTH. The system model accounts for the effects of load sharing between bearings and for the influences of shaft flexing and rotational stiffness of the bearings in response to loads applied at arbitrary points along the shaft. The intent of this modeling effort was to integrate fluid film bearing models into SHABERTH so that system modeling of turbopumps or other turbo-machinery can include fluid film bearings and/or damping seals. This capability significantly improved the simulation results for turbopumps that use damping seals and provided for design simulation of future turbopumps that use fluid-film bearings or hybrid systems using both fluid-film and rolling element bearings.

The fluid film bearing code Hydroseal, developed under NASA Grant NAG3-1434 by Dr. Luis San Andres at Texas A&M University, can numerically solve for the pressure, flow, film forces, and dynamic force coefficients of hydrostatic bearings, annular seals, and fixed arc bearings. One of the capabilities of Hydroseal is the

calculation of the 16 stiffness coefficients that define the fluid forces (Fx, Fy) and restoring moments (Mx, My) in terms of shaft displacements and misalignment angles. These stiffness coefficients provide the input needed to simulate the effects of a fluid film bearing on a shaft/bearing load support system using a system model like SHABERTH. A major software development effort was accomplished under this contract that resulted in the integration of the hydroseal model capabilities in the SINSHA software.

Evaluation of the Hydroseal program was initially performed on a silicon graphics workstation to facilitate its incorporation into the SINDA/SHABERTH rolling element/shaft program. The evaluation of the fluid film bearing code included a familiarization with the workings of the program itself. The program was used to simulate the damper seal of the Rocketdyne SSME high pressure oxygen pump to gain experience with the program's execution and to give a comparison case for later personal computer versions. The input to the program is accomplished through the use of menu driven prompts or, alternatively, the user can call a previously constructed and saved input file. After the type of fluid film bearing (hydrostatic, seal, or journal) has been chosen and the dimensions and specifics of the bearing design (number and location of pads, recesses, surface finish, fluid conditions, speed, etc.) have been input, the program can calculate operating parameters such as fluid flow, eccentricity, force, stiffness, damping, and inertia coefficients.

Graphical output can also be generated by the program through the use of the Plot 2 graphics package (operational on Silicon Graphics) which was provided with the code. Plots showing the x-axis representing the width of the bearing parallel to the shaft, the y-axis depicting the magnitude of the fluid pressure, and the z-axis representing the circumferential direction of the bearing clearance can be generated.

After the initial check out on a Unix system, a personal computer version of the code, was developed. In order to integrate the code into the SRS shaft, bearing, thermal model it was necessary to have the code running on a personal computer. The source code was loaded onto the Northgate Elegance 486 PC and compiled using Lahey FORTRAN version 5.0. Minor modifications to the source code were required to get the program to execute on the PC. The majority of the modifications were simply due to the differences in file naming conventions between DOS and UNIX. It was also necessary to modify some of the calls to intrinsic FORTRAN functions. Several of the functions called are not supported in Lahey FORTRAN. This problem was corrected by using alternative functions that are supported by the PC compiler. After correcting the syntax problems a PC version of Hydroseal was successfully compiled.

The Hydroseal Users Manual contains examples of input and output for the various types of fluid film bearings modeled by Hydroseal. These example cases were run on the PC to verify the PC version. Initially, it was found that the code would run successfully for cases where fluid properties were implicitly input. However the code would not run correctly for cases where the user requested that fluid properties be calculated by the MIPROPS subroutine of Hydroseal. The problem was investigated and it was found that an error was caused when the program attempted to read fluid property coefficients from files stored on the disk. The cause of the disk file read error could not be readily determined. However, a work around solution to the problem was implemented which worked for the case of a

bearing operating in oxygen. Later fixes resolved the problem and now bearings operating in methane, nitrogen, and parahydrogen can be modele.d

Comparison of the outputs from the PC version of the code to the examples showed that the PC version obtained answers that were very close (within 5%) of the results included in the manual. We were concerned that the answers did not agree exactly with the results from the manual. To investigate further we ran the same cases with the original version of the code on an in house Silicon Graphics computer. The results obtained agreed exactly with the PC version. Therefore, we have concluded that the code must have been modified slightly since the manual was published.

A finite element model was developed to solve for reaction loads and deflections of a shaft supported by bearings that provide linear and torsional stiffness. The model was developed to support integration of fluid film bearings into the SINDA/SHABERTH load support system simulation. A shaft/bearing system consists of a rotating shaft supported by one or more bearings. Each bearing typically provides both radial and rotational stiffness. If the system includes more than one bearing, the problem is statically indeterminate and the equations of static equilibrium are insufficient to solve for the forces and moments reacted by the bearings. The finite element approach provides the additional equations needed to solve for the reactions by the use of strain energy equations.

The system modeled for this application is shown in **Exhibit 6**. The shaft is modeled with beam elements, each defined by the location of two nodes. The model assumes that each element has a constant modulus of elasticity and moment of inertia along its length (EI). Loads and moments can be applied only at nodal locations. When defining the shaft, nodes must be located at all positions were bearings are fitted to the shaft, at all locations were external loads are applied to the shaft, and at locations were the shaft geometry (EI) changes. Two sets of data are required to solve for shaft reactions in either the x-y plane or the x-z plane. First a node data set is input. Node data includes the nodal coordinates in the global reference plane, boundary condition flags for each degree of freedom at the node, and boundary conditions at the node. The flags are set to one if the boundary condition is an enforced displacement and to zero if the boundary condition is a prescribed force. As shown in Exhibit 6, each node has three degrees of freedom two displacements and one rotation. The shaft must be adequately constrained to prevent any rigid body motion. The second set of input data is the element data. The element data includes the two node numbers for the nodes that define the element, the modulus of elasticity for the element, and the bending moment of inertia for the element. To model a shaft with general loading (a case were the applied loads do not all lie in one plane) the loads must be resolved into two planes

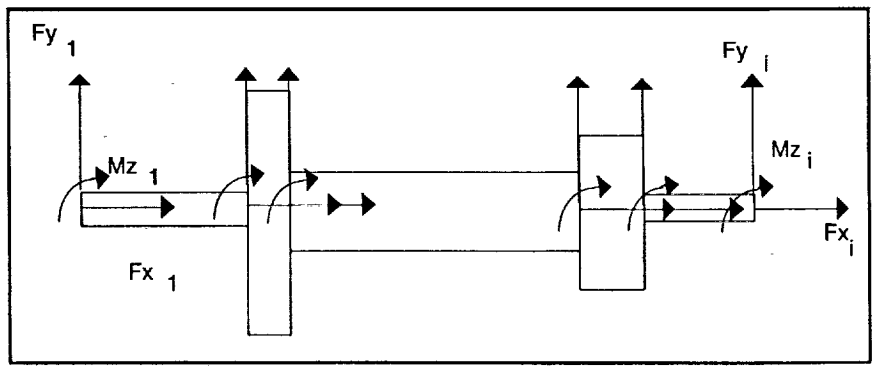

Exhibit 6 Shaft System Modeled with Beam Elements

and the model can be run twice to obtain reaction forces in each of the planes.

The finite element code solves the equation |K| x |D| = |F|. The K matrix is the global stiffness matrix. The D matrix contains nodal deflections and rotations and the F matrix is the vector of applied loads. The global stiffness matrix is assembled from the element stiffness matrix's shown in **Exhibit 7**.

A is the elements cross-sectional area, E is the element modulus of elasticity, I is the moment of inertia, and L is the section length. To obtain the displacement solution global stiffness and load matrix's are constructed from the input data. These matrix's are the modified to remove unnecessary degrees of freedom that result when enforced displacements are input as boundary conditions. The global stiffness matrix is then inverted and multiplied by the load matrix to solve for displacements. This procedure was implemented by developing a FORTRAN program to model the shaft using the finite element approach. This code was initially used to couple in coupling the hydroseal and SINSHA models.

The SHABERTH system model solves for bearing loads and reactions by modeling the shaft as a beam with external loads reacted by the bearings. This is a nonlinear problem because the stiffness of each bearing is dependent on the magnitude of load and moment applied to the bearing. SHABERTH uses an iterative solution technique to solve the problem. SHABERTH iterates bearing displacements and shaft displacements until compatible reaction loads are obtained. To develop a fluid bearing interface to SHABERTH it was necessary to introduce the stiffness of the fluid film bearing into the SHABERTH shaft/bearing equilibrium algorithm. The stiffness of the fluid film bearing is also nonlinear with respect to displacement. Therefore, the most direct approach to modeling a hybrid system was to integrate the fluid film bearing model (Hydroseal) directly into the SHABERTH code. Hydroseal could then be called to calculate fluid film bearing loads each time the shaft bearing equilibrium model calls for bearing deflections. Towards this end, the shaft modeling equations in the SHABERTH code were reviewed in detail. It was found that the shaft model in SHABERTH is general enough to calculate deflections at any point on the shaft. However, the arrays used to contain the data needed to solve for deflections were sized such that SHABERTH can calculate deflections only for locations were bearings are located. The maximum number of bearings is limited to five. The data structure of the program is quite complicated and involves numerous data overlays. It was determined that modifying the code to accept additional fluid film bearings would be very complicated. To avoid the necessity of a major SHABERTH code modification an alternative approach was developed. An independent shaft model was developed to solve for fluid film bearing to shaft reactions (the finite element model previously described). This approach adds another layer of iteration to the solution, however, implementation is straight forward. First , SHABERTH runs and solves for the reaction loads and displacements for any and all rolling element bearings on the shaft. The calcu-

$$\begin{bmatrix} S & 0 & 0 & -S & 0 & 0 \\ 0 & D & C & 0 & -D & C \\ 0 & C & A & 0 & -C & B \\ -S & 0 & 0 & S & 0 & 0 \\ 0 & -D & -C & 0 & D & -C \\ 0 & C & B & 0 & -C & A \end{bmatrix}$$

S=AE/L
A=4EI/L
B=2EI/L
C=6EI/(L**2)
D=12EI/(L**3)

Exhibit 7 Element Stiffness Matrix

lated displacements are output to a file. Hydroseal is then run with displacement boundary conditions and solves for reaction loads for each of the fluid bearings on the shaft. For the initial case, the input displacements used are simply guesses that are input to start the iteration process. The loads calculated by Hydroseal are output to a file. Next the finite element shaft code reads the rolling element bearing deflections and the fluid film bearing loads and applies them to the finite element shaft model as boundary conditions. The finite element model then solves for displacements on the shaft at the locations of the fluid film bearings. These displacements are compared to the displacements that were used to predict the fluid film bearing loads. If the displacements are not the same (within a user specified tolerance) the fluid bearing displacements are updated and new loads are predicted. These loads are input back into SHABERTH and the rolling element bearing deflections are recalculated. This process is repeated until the displacements used for the fluid film bearing analysis are compatible with the rolling element bearing solution. Typically, results converge after four or five iterations.

The iteration procedure outlined above was shown to converge relatively quickly for the cases evaluated. However, the process was not fully automated and user intervention was required to manually converge the solution. Therefore, the option of more fully integrating the fluid model into SHABERTH was investigated. If the total number of bearings (fluid + rolling element) is limited to five, it was found it was possible to incorporate the fluid film bearing model more directly to the SHABERTH code. This approach eliminated one layer of iteration from the earlier solution method. It also eliminated the requirement for the external finite element model.

A study of the capabilities of the hybrid system model was conducted in April of 1994. The shaft/bearing system used for this investigation was the Rocketdyne High Pressure Oxygen Turbopump which uses four ball bearings and one fluid film bearing (damper seal) to support the shaft. The results of this preliminary investigation are discussed in the following sections which are excerpts form the SRS paper prepared for the 1994 Earth-to-Orbit Propulsion Conference.

Introduction. Cryogenic liquid propulsion systems for spacecraft use high performance turbopumps to deliver fuel and oxidizer to the combustion chamber at high pressure and flow rate. The pump system consists of a structural casing/valve, pump impeller(s), turbine disk, shaft, and bearings. The impellers and turbine are mounted to the shaft which is supported by bearings. Most contemporary pump designs use conventional rolling element bearings as the primary load support mechanism. Design for minimum weight requires high speed operation creating a severe environment for bearings in terms of thermal effects and loads. Consequently, cryogenically cooled rolling element bearings have proven to be one of the most critical life limiting components of pump systems.

More robust bearings systems are needed for applications in long life reusable liquid propulsion systems. Various different bearing technologies, including magnetic bearings, foil bearings, and fluid film bearings, have been proposed as candidates for application in long life turbopumps. Of these technologies, fluid film bearings are probably the most near term candidate in terms of technology readiness. A data base of cryogenic fluid film bearing performance characteristics has been developed from various applications. The current Space Shuttle Main Engine (SSME) turbopumps utilize annular axial flow damper seals which also function in a bearing capacity and carry a fraction of the radial loading on the shaft. A test configuration of the SSME High Pressure Oxidizer Turbopump

(HPOTP) that used a fluid film bearing, in place of the pump end ball bearings, was successfully tested on the Technology Testbed Development engine at Marshall Space Flight Center. The data generated from these applications has demonstrated that cryogenic fluid film bearings are capable of producing high stiffnesses and are viable candidates for serving as primary load support bearings in cryogenic turbopumps. Therefore, design of future pumps or improved version of current pumps will certainly involve consideration of fluid film bearings as primary load support devices.

Several issues must be addressed for design of pumps using fluid film bearings. These include axial load imbalances and radial load support during start up and shut down of the pump. Annular seal bearings do not provide axial stiffness. During steady state pump operation this is not a problem because most pumps use an axial load balancing device to position the shaft. However, during start up and shut down transients, bearing axial stiffness may be required to position the shaft. Additionally, rubbing of the journal lands during start up and shut down is a concern. One approach for addressing these issues is to develop hybrid systems that use both fluid film and rolling element bearings. The rolling element bearings would be highly loaded only under transient conditions, during steady state operation the fluid film bearings would serve as the primary load supports. The design of such systems requires accurate system modeling to evaluate the load sharing characteristics between the bearings and to design the bearings to accommodate those loads. The software development effort described in this paper is intended to provide that analysis capability required to design future pump bearing systems and to improve the capability to analyze current SSME, hardware by more thoroughly modeling damper seal effects on the rolling element bearings.

Objectives. The objective of this effort is to improve current cryogenic turbopump shaft-bearing-thermal analysis capabilities by incorporating detailed modeling of fluid film bearings into the SINDA/SHABERTH bearing code [2, 3]. This code is used extensively for simulation of cryogenic turbopump systems. The SINDA/SHABERTH code provides for coupled thermomechanical analysis of a shaft bearing system. The system model includes the elastic shaft and the supporting bearings as illustrated in **Exhibit 8**. The system model allows the analyst to specify the shaft geometry, the types and specifications of the supporting bearings, the locations of the bearings on the shaft, and the applied loads on the shaft. The code then predicts bearing reaction loads, shaft displacements, and solves for bearing performance characteristics (contact stresses, stress velocity, operating temperatures, fatigue life, etc.). The version of SHABERTH used in the original SINDA/SHABERTH model incorporates bearing models for ball bearings, roller bearings, and tapered roller bearings. To meet the objective of this effort, a fluid film bearing model was integrated into the code.

Code Development. Predicting bearing reaction loads requires modeling the complete shaft/bearing system. The reaction load on each of the bearings is a function of the shaft stiffness distribution, the bearing's stiffness, and the stiffness of each of the other bearings in the system. Bearing stiffness is a non-linear function of reaction loads, operating temperatures, and geometry. This coupling results in a set of constitutive equations that must be solved using an iterative solution algorithm. The algorithm searches for the reaction loads that satisfy the constraints of both shaft equilibrium and bearing equilibrium.

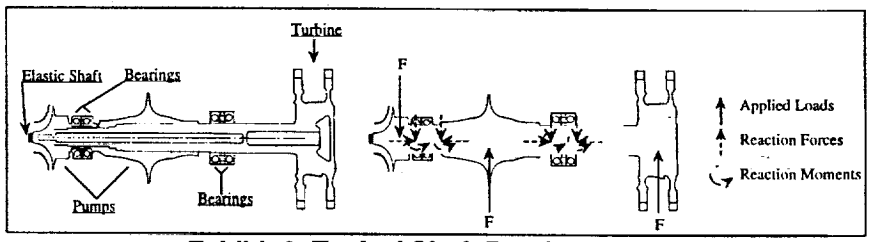

Exhibit 8 Typical Shaft Bearing System with Applied Loading and Bearing Reactions

The SHABERTH solution algorithm obtains the inner ring equilibrium solution by solving the system [4]:

$(F_b)_i - (F_s)_i = 0$ for all bearings, i

$(F_b)_i$ = vector of bearing loads and moments resulting from rolling element to inner race interactions

$(F_s)_i$ = vector of shaft loads exerted on the shaft by the inner rings

$$(F_b)_i = \begin{bmatrix} F_{bxi} \\ F_{byi} \\ F_{bzi} \\ M_{byi} \\ M_{bzi} \end{bmatrix} \qquad (Fs)_i = \begin{bmatrix} F_{sxi} \\ F_{syi} \\ F_{szi} \\ M_{syi} \\ M_{szi} \end{bmatrix}$$

The variables in the system are (Δ_{bi}) and (Δ_{si}) where (Δ_{bi}) is the vector of bearing deflections and (Δ_{si}) is the vector of shaft deflections. The deflection degrees of freedom are the x, y, z deflections, and the rotations about the y and z axis. Compatibility requires that (Δ_{bi})equal (Δ_{si}).

Solution of the system described above requires constitutive models which relate deflections to forces. The shaft is modeled as an elastic beam governed by the differential equation **[4]**.

$$\frac{d^2y}{dx^2} = -\frac{M_{(x)}}{EI_{(x)}}$$

Applied shaft loads, and bearing reaction loads, forces and moments, define $M_{(x)}$. Shaft deflections are calculated by solving the beam equation once for the x-y plane and once for the x-z plane. Rolling element bearings are modeled by solving kinetic equations which relate applied bearing loads to inner ring deflections (Δ_{bi}). Each of the bearing types, ball, roller, and tapered is represented by a separate constitutive model. These models are documented in **Reference 4**.

To achieve the objective of incorporating fluid film bearings into the simulation a constitutive fluid film bearing model is required. A model with the required capabilities has been developed and implemented in the computer code Hydroseal **[1]**. The Hydroseal program was developed by Dr. Luis San Andres, Texas A&M University, Turbomachinery Laboratory. The program is capable of modeling hydrostatic journal bearings, annular pressure (damper) seals and hydrodynamic pad journal bearings **[5]**. **Reference 5**, "An Introduction to the Analysis of Barotropic Fluid, Turbulent Flow, Fluid Film Bearings", provides detailed documentation of the governing fluid flow equations and bearing geometries modeled.

The flow diagram shown in **Exhibit 9** illustrates the functional flow of the shaft bearing simulation and shows the interface that was developed to integrate fluid film bearing modeling into the algorithm. The simulation begins with data input defining the bearings, the shaft, initial temperatures, loads, and operating speed. The program then initializes the solution algorithm by calculating various system constants and making initial guesses for the dependent variables (load vector) and for the independent variables (displacement vector). The initial displacements are passed to the bearing models. The bearing models determine the reaction loads based on the current displacement vector. The displacement vector contains the x, y, and z deflections and the y and z rotations for each of the bearings in the system. The program checks the input data to determine the appropriate bearing type for each of the displacement vectors $(\Delta_b)_i$. If the bearing is a rolling element bearing the appropriate SHABERTH bearing model is called to solve for reaction forces **[4]**. If the bearing is a fluid film bearing the Hydroseal program is used to calculate reaction forces. The reaction forces and moments calculated by the bearing models are then passed to the shaft model. The predicted bearing loads are applied to the shaft and used as boundary conditions to predict a new set of displacement vectors. A convergence test is then

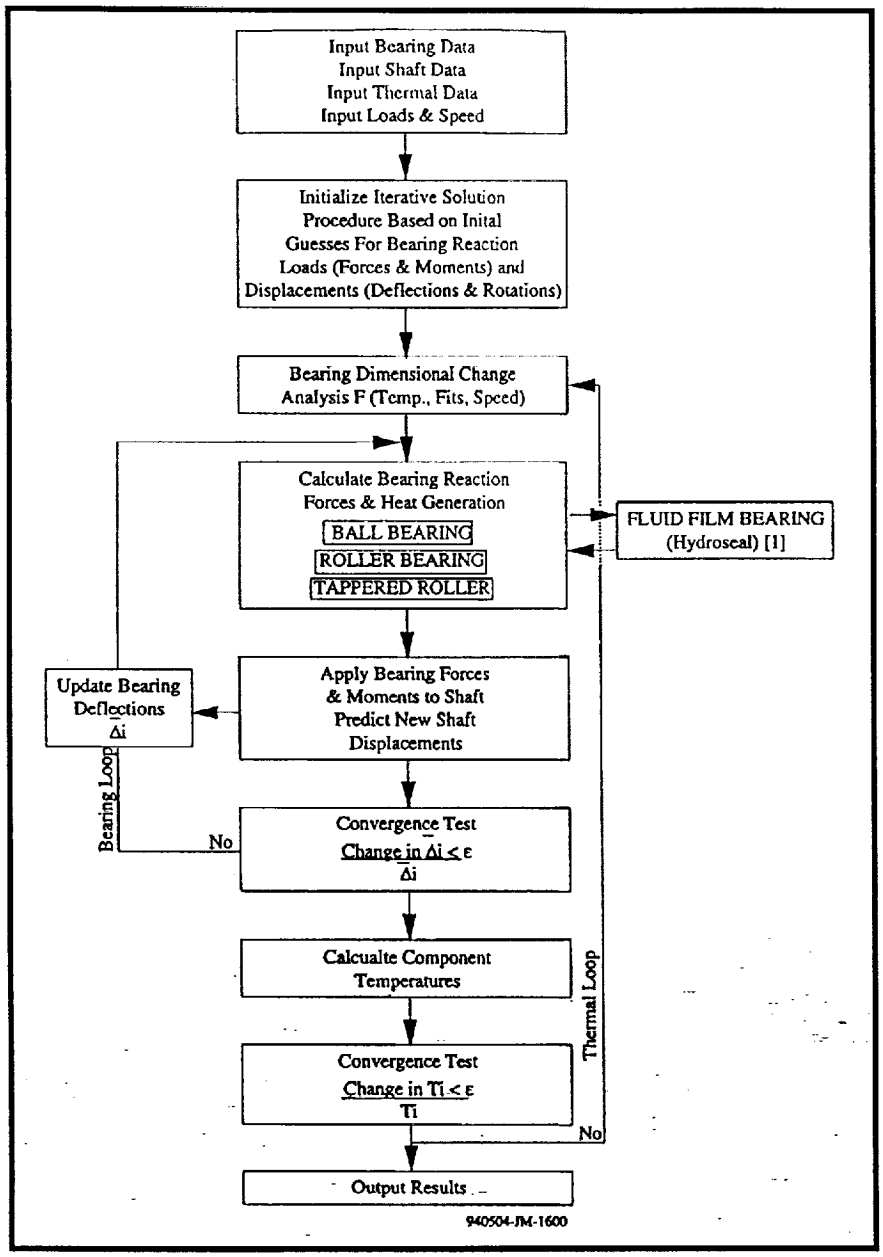

Exhibit 9 Bearing Thermomechanical Model Flow Diagram Showing Interface to Hydroseal

performed to see if the bearing deflections used agree with the predicted shaft deflections. If not, a Newton-Raphson Algorithm is used to update the deflections and another iteration is performed. Once a converged bearing solution is obtained, the predicted bearing heat generation rates are passed to the SINDA thermal model to predict new operating temperatures. The updated fluid and bearing component temperatures are then passed back to the dimensional change analysis routine in SHABERTH. This iteration continues until a thermally converged solution is obtained.

The basic solution algorithm described in Exhibit 9 was developed and coded in the original SHABERTH program [4]. The thermal modeling loop has since been updated, for improved modeling of cryogenic cooling, by SRS Technologies [2, 3, 6]. Therefore, the main code development effort required to include fluid film bearing modeling in the simulation is the development of the interface to Hydroseal. The minimum requirements for the interface includes two functions. First, it must pass bearing displacements to Hydroseal. Then it must pass predicted bearing reaction loads back to SHABERTH/ SINDA. An interface meeting these minimum requirements has been developed and used to simulate the SSME lox pump including modeling of the damper seal. The results of this simulation are presented in Section IV.

The interface developed consists of a FORTRAN subroutine added to SHABERTH that writes deflections to a file, reads forces output by Hydroseal and incorporates them into the solution algorithm. A DOS batch file was also developed to execute Hydroseal at the appropriate point in the simulation. As currently implemented, the interface does not pass any bearing geometry data or fluid property data between the codes. Therefore, the analyst must first run through

Hydroseal manually and enter the data required to define the fluid film bearing and fluid. The model data is stored in a default data file generated by Hydroseal. A simulation can be performed after the Hydroseal model is created. Running SHABERTH with the interface active, results in a call to Hydroseal at each shaft/bearing equilibrium iteration. During each iteration, the interface outputs predicted displacements to a file, executes Hydroseal using option 33 [1], and imports predicted shaft forces and moments into the SHABERTH code. Hydroseal option 33 solves for bearing flow rate, bearing reaction forces, moments, and torque, for specified values of pressure drop and journal displacement and tilt.

The current version of the interface links Hydroseal to the shaft/bearing equilibrium loop of the simulation only. The thermal loop of the SINDA/SHABERTH simulation still functions; however, fluid film bearing component temperatures are not updated. Planned improvements include integrating Hydroseal results into the thermal loop and integration of fluid film bearing data directly into the SHABERTH model input file.

Initial Results. The SSME HPOTP shaft and bearing system model was used as a test case to evaluate the function of the Hydroseal interface. The baseline SINDA/SHABERTH model has been used in the past to evaluate rolling element bearing performance for many different pump operating conditions. The shaft and bearing geometry modeled is shown in **Exhibit 10**. The applied loads and reaction loads are also illustrated in Exhibit 10. The largest applied load is the static side load on the main impeller. Static radial loads are also applied to the preburner impeller, turbine disk, and damper seal. The radial loads and reactions have been normalized with respect to the main impeller load. The bearing reaction moments are normalized with respect to the inboard 57mm ball bearing (bearing 3) reaction moment.

The influence of the damper was simulated in the original SINDA/SHABERTH model by inputting an applied radial load on the shaft at the location of the damper seal. The magnitude of the damper reaction load was estimated by reviewing test data from instrumented engine tests. Several pumps have been run with an instrumented bearing carrier capable of resolving the radial load reacted by the pump-end bearing pair (bearings 1 and 2). The magnitude of the damper seal reaction load was estimated by incrementally increasing the damper seal load in the simulation until the predicted bearing loads agreed with test results. It was estimated that the damper seal carried approximately 28% of the main impeller load.

The results from the baseline case described above were compared to results obtained using the hybrid system model. The simulated damper seal load was removed from the shaft and a Hydroseal model of the damper seal was developed. A simulation of the pump was performed with the Hydroseal interface option on. The results of this simulation are illustrated in **Exhibit 11**. The predicted reaction loads compare favorably with the baseline simulation. The damper seal was predicted to carry 33% of main impeller load as compared to the 28% load used in the baseline model. The hybrid model predicts 1% and 10% of

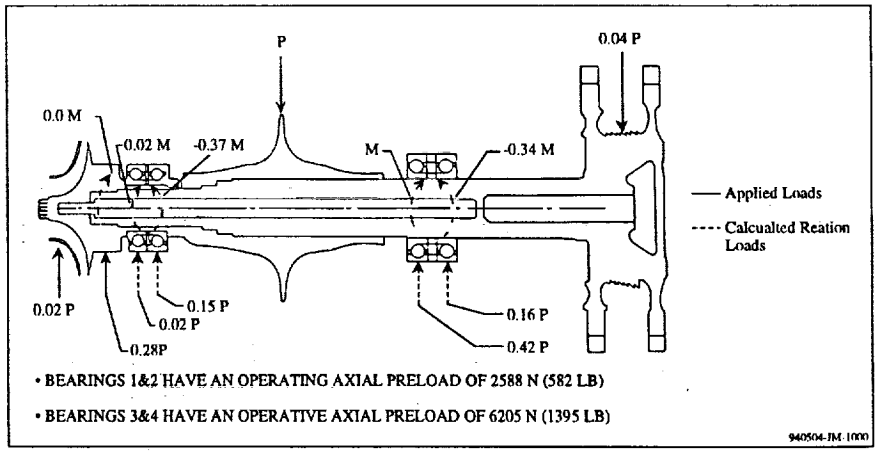

Exhibit 10 SSME LOX Turbopump Bearing/Shaft Reaction Load Predictions for Prescribed Damper Seal Load

the main impeller load carried by bearings 1 and 2, respectively. This compares to 2% and 15% predicted by the baseline model. Hydroseal also predicts the magnitude of the moment reacted by the damper seal. This moment was assumed to be zero for the baseline case. With the exception of bearing 4, the hybrid code predicts that the magnitudes of the bearing reaction moments are slightly lower than the moments predicted by the baseline model. The predicted bearing operating misalignments also agreed well. In both cases, bearing 1 and 2 outer races are predicted to tilt in a clockwise direction with respect to the bearing carrier. For the baseline case the predicted magnitude of the bearing 1 tilt is very small, almost zero. The hybrid simulation predicted a larger bearing 1 tilt in the same direction. Post run hardware observations of bearing 1 show that the bearing does tend to tilt in the direction predicted. In this respect the hybrid code results seem to yield a more realistic prediction.

The results from the test cases demonstrated an additional capability of the hybrid simulation. The hybrid simulation was able to introduce the effects of damper seal cross-coupled stiffness into the simulation. For this case, the magnitudes of the predicted transverse radial loads were small; $5.2 \times 10^{-3}P$, $-1.2 \times 10^{-3}P$, $-3.0 \times 10^{-3}P$, $-7.8 \times 10^{-3}P$, and $6.9 \times 10^{-3}P$ for the damper seal and bearings 1 through 4, respectively. For the baseline simulation the effect of these transverse loads was not considered. It should be noted that for this case the transverse loads are small; however, the predicted transverse shaft displacement is significant. The low loads are a result of the radial clearance between the bearing outer races and the bearing carrier. These loads could become quite significant for systems where the outer race is tightly fitted in the carrier.

In summary, the results from the hybrid simulation agreed quite well with the results from the baseline model. The comparison demonstrated the functionality of the SINDA/SHABERTH to Hydroseal interface. Additionally, simulating the fluid-film bearing provided additional analysis capabilities that will be useful for design and analysis for future pump systems.

1.5 Later Revision and Improvements to the Hybrid Fluid Film/Rolling Element Bearing System Model

The initial successful version of the hybrid code was somewhat difficult to use because separate hydroseal and SHABERTH models had to be maintained. The model was improved in terms of input data structure and execution time. The original version of the code was developed by using DOS commands in batch files to transfer data between the SINDA/SHABERTH code , which models the shaft and rolling element bearings, and the Hydroseal code, which models fluid film bearings. This approach was used because it was the easiest way to couple the two portions of the simulation and verify the feasibility of incorporating a fluid film bearing model in SHABERTH analysis. On the other hand, this approach is not very computational efficient and results in awkwardly structured input files. Using this technique the two

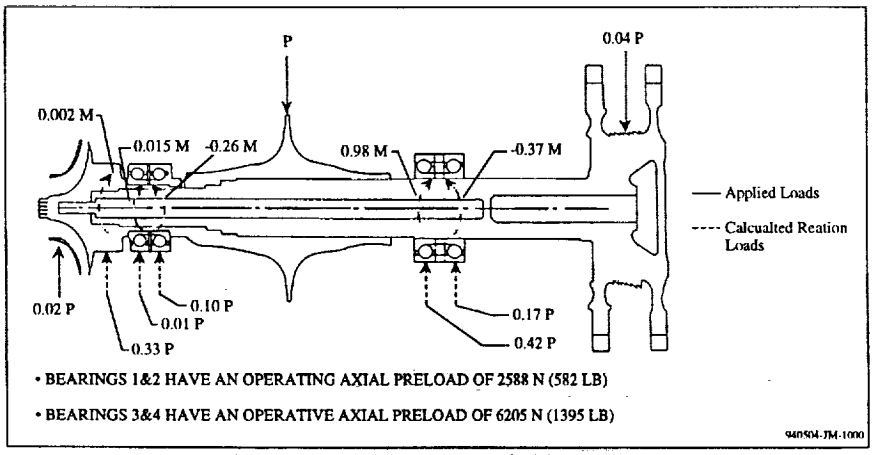

Exhibit 11 SSME LOX Turbopump Bearing/Shaft Reaction Load Predictions for Simulated Damper Seal

codes, SINDA/SHABERTH and Hydroseal, are completely separate, independently compiled programs. During a coupled simulation , SINDA/ SHABERTH needs to calculate bearing reaction forces many times. Each time fluid film bearing reaction forces were required, SHABERTH had to stop, write data to a disk, and call Hydroseal. Hydroseal then had to load, read data from the separate Hydroseal input data file , perform a fluid film bearing analysis, output reaction forces to the disk, and then call SHABERTH to continue the analysis. This sequence of events was repeated many times during a SHABERTH analysis. As a result of this overhead, a typical analysis required about two hours on a 33MHz 486 computer. The integration changes made later reduced the typical run time to about twenty minutes on the same computer.

The coupled simulation runtime improvements were obtained by integrating the source codes for the two programs and incorporating the bearing definition data into a single input file. Hydroseal was converted into a subroutine called by SHABERTH. This improvement eliminates the need to access the disk and load source code each time fluid film bearing reactions are required. Additionally, the two codes can now pass data in RAM memory through the use of common blocks and argument lists. The ability to pass and store data through multiple iterations eliminates the requirement for Hydroseal to read an input file at each iteration. Thus, the SHABERTH code was modified to read the fluid film bearing data along with the rolling element bearing data. Once input in SHABERTH, the input data is available to Hydroseal at each iteration. The elimination of multiple disk reads for fluid film bearing data is responsible for much of the speed increase obtained. Data input for fluid film bearings was structured to mimic the format of SHABERTH rolling element bearing data input. The user includes a fluid film bearing in a SHABERTH analysis by specifying a bearing data block for the fluid film bearing in the SHABERTH input file. An example of the new input format is found in **Attachment A** . The example is for simulation of a proposed configuration of the EH-14 fluid film bearing tester. The SHABERTH model simulates a modified tester configuration that could be used for testing both fluid film bearings and rolling element bearings. The input file shows that bearings one and two are ball bearings. These bearings are defined with "bearing data" blocks that are identical to bearing data blocks in the original SHABERTH code. The third bearing (turbine end) is defined by a fluid film bearing data block. The letter "F" in the first line of the data block signifies that this bearing is a fluid film bearing. The data required to define the bearing geometry and operating characteristics constitutes the rest of the data block. The remainder of the data file; thermal data, shaft data, and load data, is identical to the data for the original SHABERTH code. This model was used to determine power requirements for the liquid hydrogen bearing tester.

The evolution of the hybrid fluid film/rolling element bearing code continued by combining the hybrid simulation with the thermal modeling capabilities of SINDA. The detailed thermal analysis of the rolling element bearings provided by SINDA has in the past proven very valuable in cryogenic bearing anomaly investigations. It is believed that thermal effects will also have a strong influence on the performance of fluid film bearings as well. Thus, the Shaberth/Hydroseal hybrid bearing code was integrated with SINDA. The basic work of combining the code with SINDA was previously performed when SHABERTH was made a subroutine of SINDA

in 1991 under another contract. The format will be very similar to that used previously since Hydroseal was made a subroutine of SHABERTH.

The execution of the SSH hybrid bearing code is performed with the same procedure used to execute any SINDA model. As part of the SINDA model, a call statement to the SHABERTH program is placed in the Output Calls section of the SINDA input file. SHABERTH will then read the bearing geometry and shaft loading data from an external file. The SHABERTH program includes the capability to read fluid film bearing data. This was accomplished by integrating into the SHABERTH subroutine SKF the Hydroseal subroutine that is used to read the fluid film bearing data from the DEFAULT.DAT file. DEFAULT.DAT is a file created by Hydroseal to store the bearing data which was entered during an interactive Hydroseal session. Thus, a DEFAULT.DAT file can be directly added to a SHABERTH input file to simulate a fluid film bearing. The fluid film bearing capability is activated if Shaberth reads a bearing designation character "F" at the beginning of the bearing data section signifying a fluid film bearing.

Currently, the SSH hybrid bearing code has the capability to read and model any fluid film bearing that is within the capability of Hydroseal. Additionally, the SSH bearing code can simulate up to four fluid film bearings or five rolling element bearings on a common shaft. However, early versions of the SSH program model had to have at least one ball bearing with the fluid film bearings to act as a stop for the axial motion of the shaft since radial fluid bearings have no axial load capacity.

The execution of a SSH simulation is quite computer time intensive if a fluid bearing is chosen. SHABERTH uses radial tangent stiffnesses in the Y and Z directions as well as rotational tangent stiffnesses about the Y and Z for each bearing on the shaft to determine a shaft/bearing load equilibrium. These stiffness calculations are performed about seven times per bearing for a simple shaft loading configuration. Thus, for a fluid film bearing, Hydroseal must be executed a total of five times to determine the four tangent stiffnesses which add up to about 35 times per average SHABERTH run. SINDA then executes SHABERTH, usually four times for a nominally loaded bearing, giving a grand total of about 140 Hydroseal runs. This results in a total execution time for a converged SSH simulation with one fluid film bearing of approximately 100 minutes on a 486/33mHz machine, whereas without the fluid bearing the execution time would be approximately 15 minutes. In addition, the execution time is almost a direct multiple of the number of fluid film bearings leading to long but manageable execution times.

The final code developments, accomplished in the evolution of the hybrid model, involved changes to allow for modeling multiple fluid film bearing types supporting the shaft. Earlier versions of the SSH code could model only one type of fluid film bearing per shaft. The reason for this limitation was that the portions of HYDROSEAL used to read bearing geometry and configuration data were originally scalar values since hydroseal is a single bearing model. To provide for multiple bearing types, the fluid film bearing input data is now read from new arrays set up in SHABERTH. The solution routine keeps track of which bearing is being analyzed in the equilib-

rium analysis and extracts the appropriate data to send to the HYDROSEAL model. With this new capability each of the fluid film bearings on the shaft can be unique. Modifications to the code were also developed to prevent a numerical instability that occurred when modeling systems supported solely by fluid film bearings. The solution scheme used in SHABERTH provides a degree-of-freedom in the shaft axial direction. Therefore some boundary condition must be provided to react any axial load on the shaft. Damper seals provide no axial load support, therefor, the model could not converge for cases where all the bearings in the system are fluid film bearings. A numerical problem developed even for cases which involved no applied axial loading. To correct this problem, SHABERTH was modified to introduce a very small axial stiffness for cases in which all the bearings are fluid film types. The small stiffness does not effect the accuracy of the simulation and prevents numerical instability.

With the incorporation of the above modifications, SSH is now fully functional. The first version was considered the Beta version. This version was used to model the new bearing tester that came on-line in 1995. The code was used to support development of pretest red-lines and evaluate bearing configurations for test. Test results were compared to code predictions for verification and validation (V&V) of the software. Improvements and modifications to the software were incorporated as dictated by the V&V efforts. In general, the code has been found to be functional and accurate. To the best of our knowledge, SSH is the only tool currently available to perform system level thermomechanical analysis of hybrid bearing systems.

1.6 Analysis of ATD Beam Springs

An analysis was performed on a preload spring of similar design to that used in the Pratt and Whitney ATD LOX pump ball bearing to determine the amount of tilt produced for a known tilting moment. The analysis was performed with both lab experimentation and computer modeling. The results showed that the spring would allow more tilt for a given moment than was previously expected based on hand calculations. These results were used to modify our predictions of tilting for the preload spring of the Pump End Ball Bearing (PEBB) in the Pratt pump.

Analysis of high vibration anomalies experienced by the Pratt and Whitney ATD LOX pump had indicated that a possible cause could be reduced radial stiffness of the Pump End Ball Bearing (PEBB) due to outer race tilting. Computer analysis of the ATD LOX pump shaft/bearing system has shown that the inner race will tilt with respect to the housing due to shaft deflection caused by the radial load and that the outer race will follow the inner race to reduce the moment in the bearing. The preload spring will, however, support the outer race and resist its tilting in the housing. The amount of moment the beam preload spring would exert on the outer race for a given tilt angle and the effect of three contact pads per side of the spring would have on tilt were not certain. To address these issues the PEBB preload spring was modeled with the ANSYS computer code, deflection calculations were made, and hardware component testing was performed.

The hardware testing was performed utilizing a spring of similar design and dimensions as the PEBB preload spring except the spring constant

(K) was higher for the test spring. A schematic of the apparatus used to perform the spring tilting moment test is shown in **Exhibit 12**. The apparatus consisted of an Instron machine to apply and measure the axial compression force on the spring, a ball and cup joint to allow application of the tilting moment while the spring is under the compression load, and two load plates for the spring to react against. **Exhibit 13** shows an axial view of the spring indicating the location of the contact pads, the twelve positions where the tilting force was applied, and where the three tilt displacement measurements were taken. The hardware testing was performed by Howard Gibson and Lewis Moore of NASA Marshall.

The first experiment was to verify the overall spring rate of this spring. This was done by applying a know load to the spring while measuring the axial movement of both the top and bottom plates. The displacement of the top plate was subtracted from the displacement of the bottom plate to determine the compression of the spring. The value of the applied load was then divided by the corresponding spring compression value to calculate the spring constant. **Exhibit 14** shows the resulting spring rate as a function of applied load. The data below approximately 1,000 N (225 lbs) is questionable due to the very low deflections and the limited precision of the displacement measurements (+/-0.0127 mm, or 0.0005 in.). The data for higher loads looked very good and the resulting spring rate was reasonably constant at an average value of 4100 N/mm (23,400 lb/in).

The tilting deflections were then determined for known tilting moments applied to the spring while preloaded to 4,448 N (1,000 lbs). The tilting moments were produced by applying measured forces on the top load plate at a known radius from the center of the spring. Forces of 89, 178, 267, and 356 N (20, 40, 60, and 80 lbs) were applied at a radius of 81.3 mm (3.2 in) for twelve positions evenly spaced around the circumference of the spring (see Exhibit 13) to produce the tilting moments at different locations relative to the spring contact pads. The tilt angle of the spring was then calculated from the three displacement measurements which were spaced 120 degrees apart at a radius of 61 mm (2.4 in).

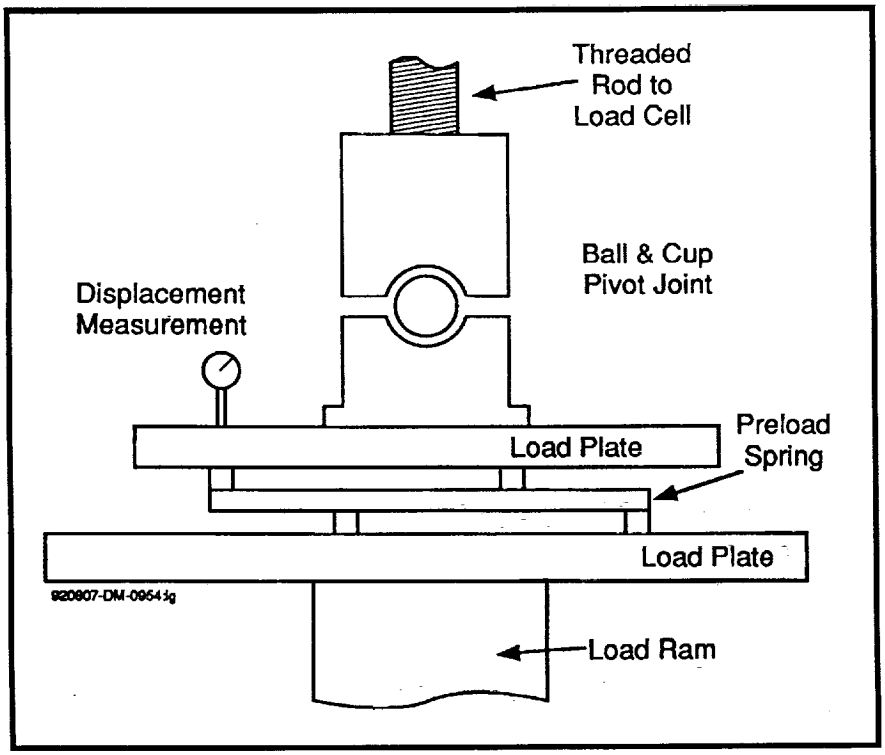

Exhibit 12 Schematic of Test Apparatus for Pratt & Whitney Preload Spring Moment Test

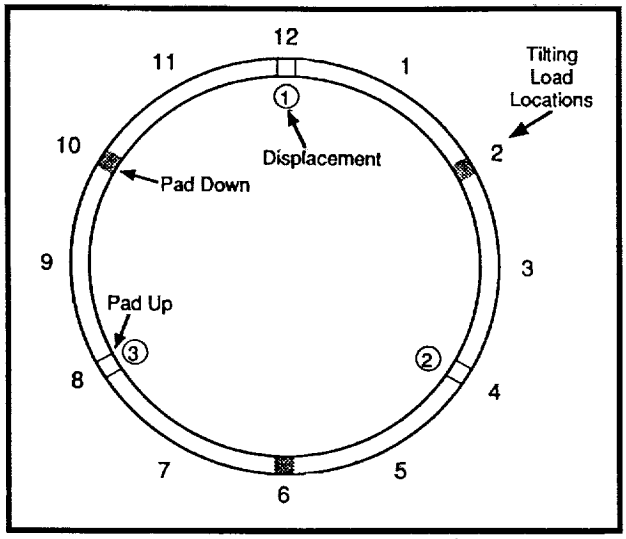

Exhibit 13 Schematic of Preload Spring Depicting Location of Tilting Load Application Points, Displacements, and Spring Pads

The resulting experimental average tilt angle is plotted in **Exhibit 15** as a function of the applied tilting moment. This angle is an average of all twelve positions around the circumferential of the spring. The location of the tilting moment relative to the spring pads did not have a significant affect on the value of the resulting tilt as best could be determined with the experiment. Thus, the use of only three contact pads per side does not cause a lower restoring moment to the outer race to be produced when the resulting tilt occurs between two pads on the same side or on opposite sides of the spring.

The hand calculations predicted a lower amount of tilt for the same applied moment, as shown in **Exhibit 15**, than measured in the experiment at the higher moments. The equation used in the calculations is based on two assumptions about the spring. The first assumption was that each of the three pads on one side of the spring would possess a third (1/3) of the total spring constant. The other assumption was that the spring constant would remain the same no matter how the spring was compressed or relaxed. Thus, when one pad is at the 12 o'clock position and the other two are at 4 and 8 o'clock and the spring is deformed so that it tilts about an axis that runs through 3 and 9 o'clock, the resulting tilting moment equation would be:

$$\text{SPRING MOMENT} = K/2 \cdot r^2 \text{ THETA}$$

K = Total spring rate
r = Radius out to center of pad
THETA = Tilt angle

The above equation assumes that each of the three load pads on one side of the spring behaves as a linear spring with a stiffness equal to 1/3 of the total stiffness of the spring. The validity of this assumption is questionable when each of the pads is displaced by a different amount of deflection as occur during bearing outer race tilting. Therefore, an ANSYS finite element model of

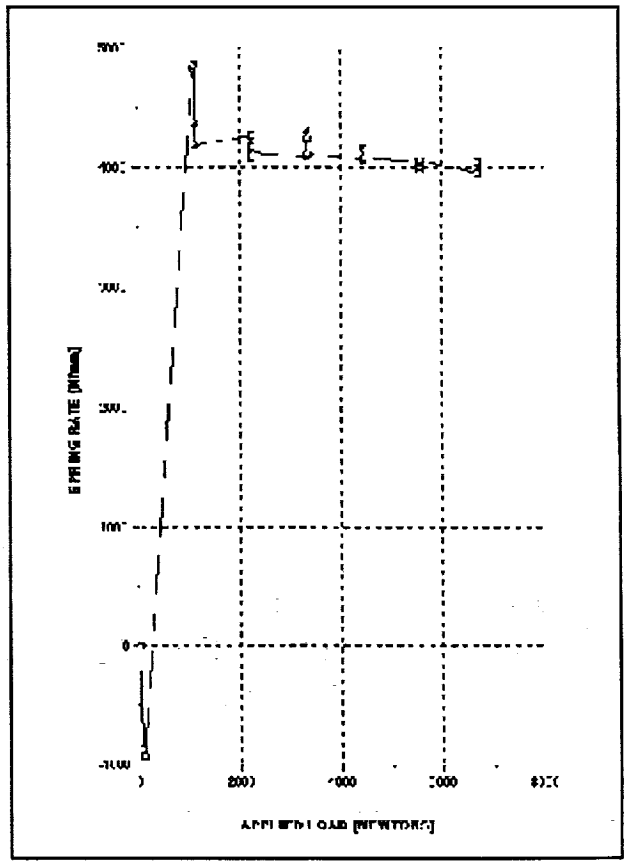

Exhibit 14 P&W Preload Spring Rate Test Results

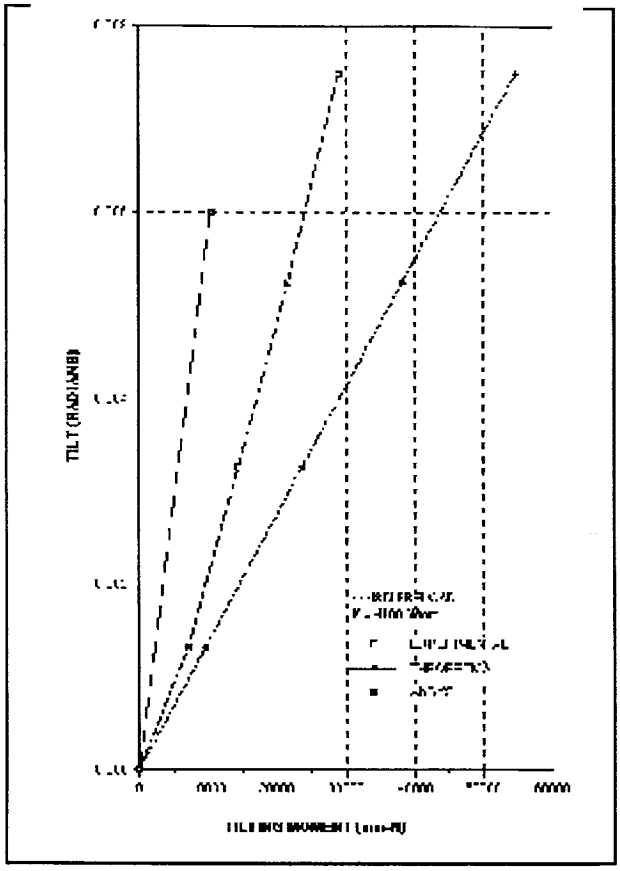

Exhibit 15 P&W Preload Spring Rate Test Results

the spring was developed to investigate the moment stiffness of the spring. The model was constructed of six sided quadratic brick elements. The nodes on the faces of the pads on one side of the spring were constrained to zero displacement in the out of plane direction. This side corresponds to the side of the spring contacting the bearing corner. For validation of the model an axial deflection test of the spring was modeled. For this test, each of the pads on the non-constrained side of spring were deflected by 1.105 mm (0.0435 in) and the reaction forces were calculated. The spring constant calculated by the model was 4,027 N/mm (23,000 lb/in) which agrees with the test data. After validation, the model was used to calculate a rotational stiffness of the spring. For this analysis, the pads on the non-constrained side of the bearing were deflected individually by a prescribed amount. The enforced deflections were calculated as shown in **Exhibit 16**.

The reaction forces were calculated by ANSYS for this case and used to calculate the resultant moment. This single point curve is plotted in Exhibit 15. The ANSYS model calculated a lower rotational stiffness than test data or the initial calculation. The test data is expected to be slightly high because of friction in the test rig. The spring rotational stiffness used to calculate outer race operating tilt should lie between the value calculated by ANSYS and the test data. The simple linear spring equation seems to significantly over predict the rotational stiffness. On-the-other-hand, the ANSYS model seems to underpredict the rotational stiffness. This is probably because the feet on the carrier side of the spring were constrained at only a single point. These constraints allow for more twisting of the spring than occurs in the actual hardware. **Exhibit 17** shows two views of the deflections calculated by ANSYS for the case with no tilt and 1,000 lbs preload and for the case with 0.006 rad tilt and 1,000 lbs preload.

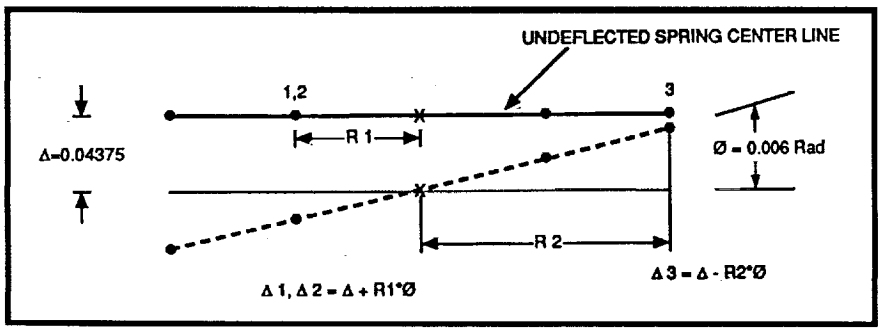

Exhibit 16 Enforced Displacement for Tilt Analysis

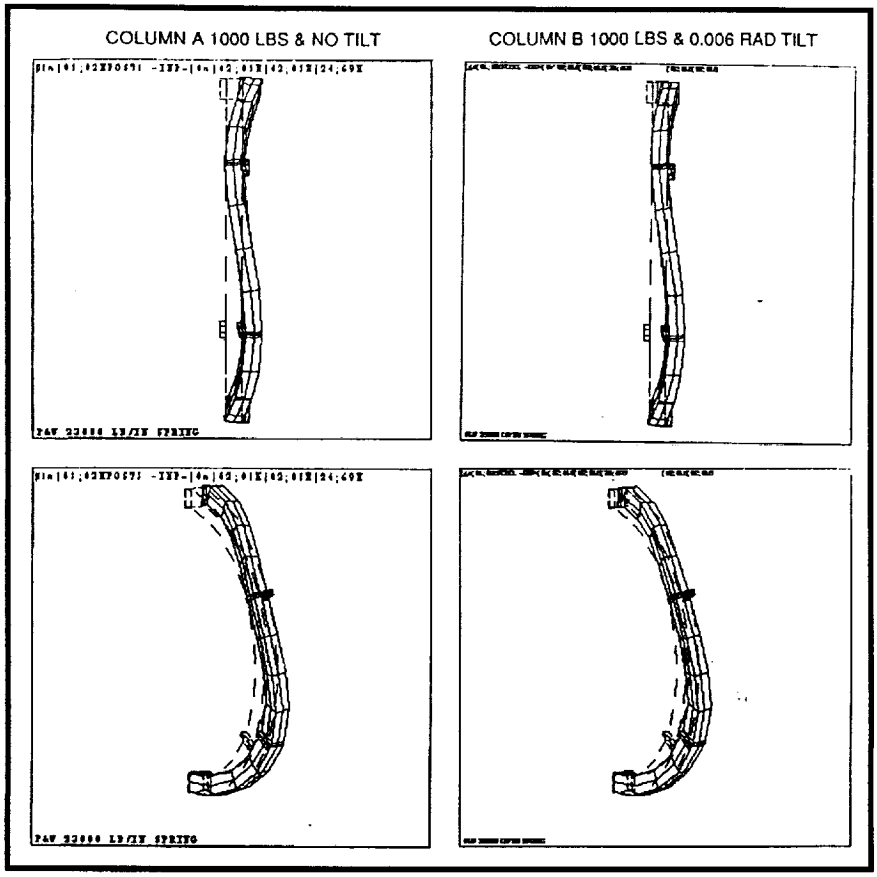

Exhibit 17 Deformed Structure Plots for Spring

1.7 MathCAD Program for Three Ring Fit Analysis

Internal clearance of ball and roller bearings affects the stiffness, contact stresses, and other performance characteristics of the bearings. The affects of press fits, temperature, and centrifugal body forces cause the operating internal clearance of the bearing to change significantly from the as-built free internal clearance. Therefore, accurate analysis of bearing performance must account for the effects of clearance change due to the operating environment. Fit analysis is usually performed using classical engineering mechanics relations for thick walled cylinders and spinning disks. This approach is used in both the SHABERTH and ADORE codes that are frequently used for bearing design. However, both codes were at one time limited to analysis of two ring fit problems (cases were the inner race is fit directly on the shaft and/or the outer race is fit directly in the housing). Bearings such as those used in the Pratt & Whitney AT turbopumps make use of an intermediate ring between the race and shaft or housing. Fit analysis of these bearings requires a three ring analysis. A MathCAD program was developed for manual analysis of three-ring problems. The calculated three ring fits can then be used as input for SHABERTH or ADORE for accurate analysis of bearing performance.

The MathCAD spread sheet is included in . To use the program the user opens the spread sheet with MathCAD for Windows version 5+. Ring geometries, material properties, fits, temperatures, and spinning velocity, are entered directly on the spread sheet. The spread sheet can be used for shaft/sleeve/inner race or for outer race/sleeve/housing fits analysis. The interference fits input are based on drawing specifications. The spread sheet then calculates the interference fit changes resulting from temperature and spinning effects. The fit pressures resulting from the modified interference fits can then be determined by equating the sum of the radial deflections, at a ring to ring interface, to the modified interference fit at the interface. The three ring case has two ring interfaces resulting in two equations in terms of the two unknown fit pressures. MathCAD's numerical SOLVE routine is used to solve for the fit pressures. It should

be noted that the routine will return a negative value for fit pressure for the case of loose fits. If a negative pressure is predicted the MathCAD results are invalid and a standard two ring fit analysis can be used for the two rings with positive interference. Once the fit pressures are determined calculation of the radial dimensional changes is preformed for the inner most radius and for the outer most radius. If the three ring set analyzed is an outer race/sleeve/housing combination then the change in inner ring, inner diameter indicates the net affect of the fits on bearing diametrical clearance. If the three ring set analyzed is shaft/sleeve/inner race combination then the change in outer ring, outer diameter indicates the net affect of fits on bearing diametrical clearance. For a complete analysis both the inner ring set and outer ring set must be analyzed. The total bearing diametrical clearance change is determined by summing the effects of outer race inner diametrical change, the inner race outer diametrical change, and two times the diametrical change of the rolling elements. Typically, the rolling element diametrical change is dominated by thermal affects thus only delta temperature of the rolling element is needed to calculate the dimensional change of the rolling element.

1.8 Three Ring Fit Analysis Added to SINDA/SHABERTH Bearing Model

The February 1995 progress report documented the development of a three ring fit analysis program developed to perform fit analysis of bearings mounted on a shaft or in a housing that employs an intermediate spacing ring in the stack. Spacing rings have been used in the AT turbopumps developed by Pratt & Whitney and in the turbine powered bearing tester developed by MSFC. Spacing rings provide a simple means for controlling the race hoop stresses and bearing operating clearances. The objective of developing the three ring model is to improve the current bearing analysis capability for the bearings used in these systems. The primary code used to evaluate the performance of cryogenic bearings is the SINDA/SHABERTH thermomechanical model. The original fit analysis incorporated in the SHABERTH portion of the code was limited to two ring analysis thus precluding completely accurate modeling of bearings that are mounted on spacing rings. In the past the effects of the spacing ring have been approximately accounted for by manually calculating the diametrical change effects of the spacer and manually forcing those changes in the model. The MathCAD program (previously discussed) was used to evaluate the magnitude of error associated with use of the two ring model on three ring systems. It was determined that the procedure resulted relatively small errors; however, a considerable amount of manual calculation is required to determine the fit modifications needed to account for the intermediate ring. It was apparent that the preferred approach is to accurately model the three ring system directly within SHABERTH.

Several approaches were evaluated for developing a three ring SHABERTH analysis. The first approach was to modify the existing SHABERTH fit subroutine to include a spacer. By reviewing the code and documentation it was determined that this approach would involve considerable reverse engineering, a lengthy process. It was decided that it would be more efficient to scrap the existing SHABERTH fit routine and develop a new routine for integration with SHABERTH. While developing the new routine, it was discovered that several generic FORTRAN routines for evaluating three ring fits were available in the literature. Therefore, an existing three ring model was selected and inte-

grated into the SHABERTH code. The results have been verified using the MathCAD routine documented in the February report.

The integration involved carefully identifying the parameters required by SHABERTH from the existing fit routine and vice versa. A careful one-to-one mapping of the parameters was conducted and used to design the SHABERTH fit interface. It was necessary to modify the inputs that are used to define the SHABERTH model to accommodate the additional data needed to define any spacer rings existing in the system. The model input changes required are documented below in terms of bearing data cards. The bearing data cards described are consistent with the BD cards documented in the original SHABERTH model.

- Card BD 9 was split into two cards, BD 9a and BD 9b. The entries on card BD 9a are inner shaft to shaft fit, shaft fit, housing fit, and housing to casing fit. The entries on card BD 9b are inner shaft effective length, shaft effective length, inner ring width, outer ring width, and casing effective width. A zero value for inner shaft effective width or casing effective width flags the code to perform a two ring analysis for the inner race or outer race respectively.
- Card BD 10 is modified by adding an entry in columns 1 through 10 for the inner shaft ID. The remaining data items are shifted 10 columns to the right. Casing OD is entered in columns 71 through 80.
- Cards BD 11 through BD 14, which define component material properties, are modified by adding the inner shaft property to columns 1 through 10. The remaining data items are shifted 10 places to the right. Casing properties are added in columns 61 through 70. Zero values are entered for inner shaft and casing properties if not applicable to the geometry analyzed.
- Card T2 is modified by inserting the inner shaft temperature in columns 41 through 45. The remaining data is shifted five places to the right. Casing temperature is entered in columns 71 through 75. Zero values are entered for inner shaft and casing properties if not applicable to the geometry analyzed

With the exceptions noted above the SINDA/SHABERTH model input is identical to previous versions of the code.

The three ring version of SINDA/SHABERTH is now operational. The code has been successfully used to model the three ring bearing designs that were tested in the turbine powered bearing tester and to model the Pratt & Whitney AT high pressure fuel turbopump (AT HPOTP) bearings. Selected pages from the AT HPOTP bearing model output are included in **Exhibits 18** and **19**. Exhibit 18 shows the changes to the portion of the output that echo the input. The inner shaft and casing initial fits, material properties, and temperatures are now included. **Exhibit20** shows the outputs of the new fit routine which now includes shaft to inner shaft and housing to casing interference fits and fit pressures.

The new version of SHABERTH was also used to update the SINDA/SHABERTH/HYDROSEAL thermal/mechanical bearing code to include the three ring fit analysis.

Verification of the updated SHABERTH code for a three ring system was performed by simulating a roller bearing with both inner and outer race sleeves. The SHABERTH results were then compared to the results from a CYLFLEX model of the same bearing under the same operating conditions. The results for the press fits differed by approximately 4% while the roller loads dif-

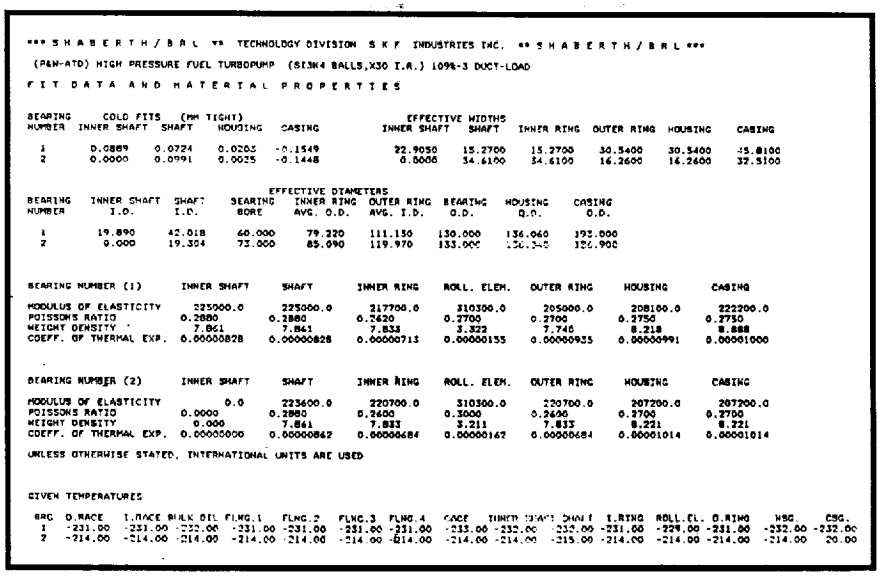

*** S H A B E R T H / B R L ** TECHNOLOGY DIVISION S K F INDUSTRIES INC. ** S H A B E R T H / B R L ***

(P&W-ATD) HIGH PRESSURE FUEL TURBOPUMP (SI3N4 BALLS,X30 I.R.) 109%-3 DUCT-LOAD

F I T D A T A A N D M A T E R I A L P R O P E R T I E S

BEARING NUMBER	COLD FITS (MM TIGHT) INNER SHAFT	SHAFT	HOUSING	CASING	EFFECTIVE WIDTHS INNER SHAFT	SHAFT	INNER RING	OUTER RING	HOUSING	CASING
1	0.0889	0.0724	0.0203	-0.1549	22.9050	15.2700	15.2700	30.5400	30.5400	45.8100
2	0.0000	0.0991	0.0025	-0.1448	0.5008	34.6100	34.6100	16.2600	16.2600	32.5100

BEARING NUMBER	EFFECTIVE DIAMETERS INNER SHAFT I.D.	SHAFT I.D.	BEARING BORE	INNER RING AVG. O.D.	OUTER RING AVG. I.D.	BEARING O.D.	HOUSING O.D.	CASING O.D.
1	19.890	42.018	60.000	79.220	111.130	130.000	136.060	195.000
2	0.000	19.304	73.000	85.090	119.970	153.000	156.340	156.900

BEARING NUMBER (1)	INNER SHAFT	SHAFT	INNER RING	ROLL. ELEM.	OUTER RING	HOUSING	CASING
MODULUS OF ELASTICITY	225000.0	225000.0	217700.0	310300.0	205000.0	208100.0	222200.0
POISSONS RATIO	0.2880	0.2880	0.2620	0.2700	0.2700	0.2750	0.2750
WEIGHT DENSITY	7.861	7.861	7.833	3.322	7.746	8.218	8.888
COEFF. OF THERMAL EXP.	0.00000828	0.00000828	0.00000713	0.00000155	0.00000935	0.00000991	0.00001000

BEARING NUMBER (2)	INNER SHAFT	SHAFT	INNER RING	ROLL. ELEM.	OUTER RING	HOUSING	CASING
MODULUS OF ELASTICITY	0.0	223600.0	220700.0	310300.0	220700.0	207200.0	207200.0
POISSONS RATIO	0.0000	0.2980	0.2600	0.3000	0.2600	0.2700	0.2700
WEIGHT DENSITY	0.000	7.861	7.833	3.211	7.833	8.221	8.221
COEFF. OF THERMAL EXP.	0.00000000	0.00000862	0.00000684	0.00000162	0.00000684	0.00001014	0.00001014

UNLESS OTHERWISE STATED, INTERNATIONAL UNITS ARE USED

GIVEN TEMPERATURES

BRG	O.RACE	I.RACE	BULK OIL	FLNG.1	FLNG.2	FLNG.3	FLNG.4	CAGE	INNER SHAFT	SHAFT	I.RING	ROLL.EL.	O.RING	HSG.	CSG.
1	-231.00	-231.00	-232.00	-231.00	-231.00	-231.00	-231.00	-233.00	-232.00	-232.00	-231.00	-229.00	-231.00	-232.00	-232.00
2	-214.00	-214.00	-214.00	-214.00	-214.00	-214.00	-214.00	-214.00	-214.00	-214.00	-215.00	-214.00	-214.00	-214.00	20.00

Exhibit 18 Changes to SHABERTH Input Resulting from Three Ring Fit Analysis Modification

fered by the same percentage. The reason for the small differences may be due to the fact that the two programs converged on slightly different roller loads due to the flexible outer race capability of CYLFLEX resulting in different fits or that the slightly different fits caused the different roller loads. By adjusting the input parameters, the roller loads probably could be made to match and then the fits compared. However, the observed differences were so small that further comparison was judged unnecessary.

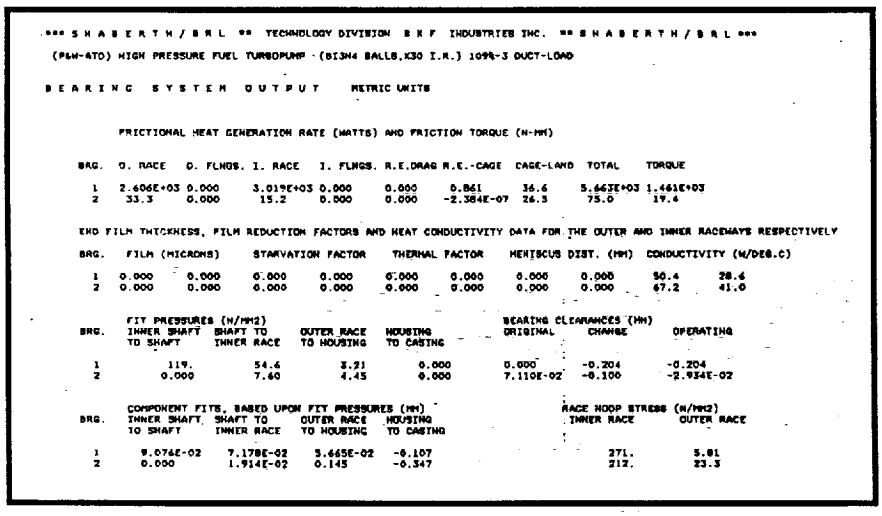

*** S H A B E R T H / B R L ** TECHNOLOGY DIVISION S K F INDUSTRIES INC. ** S H A B E R T H / B R L ***

(P&W-ATD) HIGH PRESSURE FUEL TURBOPUMP (SI3N4 BALLS,X30 I.R.) 109%-3 DUCT-LOAD

B E A R I N G S Y S T E M O U T P U T METRIC UNITS

FRICTIONAL HEAT GENERATION RATE (WATTS) AND FRICTION TORQUE (N-MM)

BRG.	O. RACE	O. FLNGS.	I. RACE	I. FLNGS.	R.E.DRAG	R.E.-CAGE	CAGE-LAND	TOTAL	TORQUE
1	2.606E+03	0.000	3.019E+03	0.000	0.000	0.861	36.6	5.663E+03	1.461E+03
2	33.3	0.000	15.2	0.000	0.000	-2.384E-07	26.5	75.0	19.4

END FILM THICKNESS, FILM REDUCTION FACTORS AND HEAT CONDUCTIVITY DATA FOR THE OUTER AND INNER RACEWAYS RESPECTIVELY

BRG.	FILM (MICRONS)		STARVATION FACTOR		THERMAL FACTOR		MENISCUS DIST. (MM)		CONDUCTIVITY (W/DEG.C)	
1	0.000	0.000	0.000	0.000	0.000	0.000	0.000	0.000	50.4	28.4
2	0.000	0.000	0.000	0.000	0.000	0.000	0.000	0.000	67.2	41.0

BRG.	FIT PRESSURES (N/MM2) INNER SHAFT TO SHAFT	SHAFT TO INNER RACE	OUTER RACE TO HOUSING	HOUSING TO CASING	BEARING CLEARANCES (MM) ORIGINAL	CHANGE	OPERATING
1	119.	54.6	3.21	0.000	0.000	-0.204	-0.204
2	0.000	7.60	4.45	0.000	7.110E-02	-0.100	-2.934E-02

BRG.	COMPONENT FITS, BASED UPON FIT PRESSURES (MM) INNER SHAFT TO SHAFT	SHAFT TO INNER RACE	OUTER RACE TO HOUSING	HOUSING TO CASING	RACE HOOP STRESS (N/MM2) INNER RACE	OUTER RACE
1	9.076E-02	7.178E-02	5.665E-02	-0.107	271.	5.81
2	0.000	1.914E-02	0.145	-0.347	212.	23.3

Exhibit 19 Changes to SHABERTH Output Resulting from Three Ring Fit Analysis Modification

The new versions of both the "stand alone" SHABERTH and the SINDA/SHABERTH/HYDROSEAL computer programs were delivered to MSFC and installed on a personal computer. A short tutorial session was performed for Tim Jett to acquaint him with the modifications to the SHABERTH inputs and the techniques of building thermal/mechanical bearing models with the SINDA/SHABERTH/HYDROSEAL program. Mr. Jett, with minimal assistance, was able to use the programs to begin an analysis of the turbine end bearings of the Rocketdyne fuel turbopump.

1.9 Modification of SINDA/SHABERTH Model Preload Routine

The SRS SINDA/SHABERTH shaft bearing system model includes a subroutine that allows the effects of a preload spring to be incorporated in the simulation. The SRS spring routine simulates the axial travel of bearing outer races which occurs due to bearing internal clearance changes resulting from thermal and speed effects. The original version of SHABERTH assumed that the axial position of the outer races remained as initially specified regardless of the bearing temperatures. As a result, the predicted axial

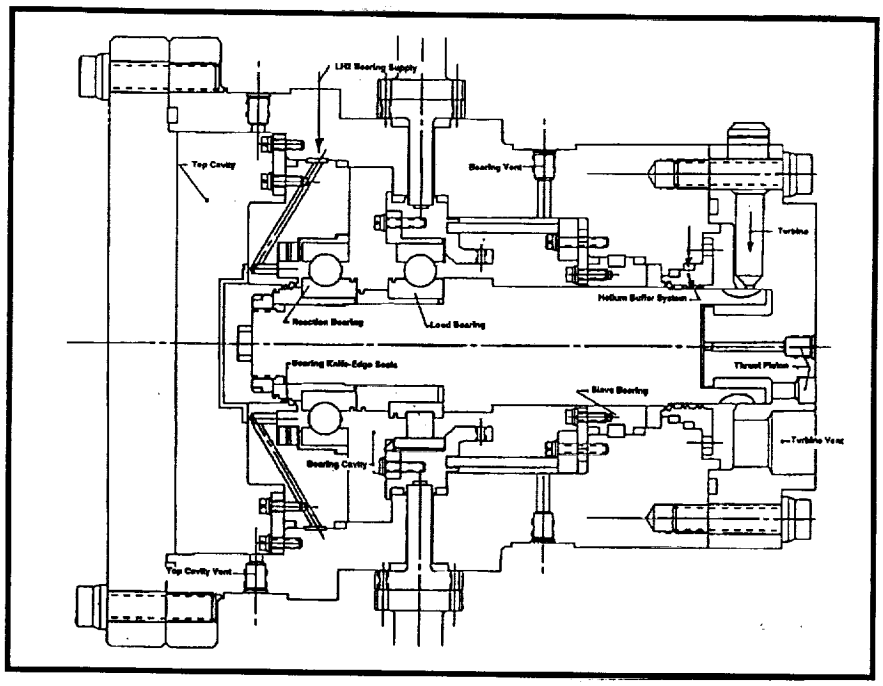

Exhibit 20 Fluid Film Bearing Tester
Showing Optional Ball and Roller Bearing Installation

load of the bearing would increase dramatically with a small increase in rolling element temperature. The preload spring allows the outer race positions to change, thus reducing axial load for a given rolling element temperature. Therefore, proper modeling of the spring is imperative for accurate prediction of bearing operating loads, temperatures, and thermal margin.

The original preload spring model incorporated in SHABERTH was developed specifically for the Rocketdyne SSME LOX turbopump ball bearings. The routine has since been modified for other spring and bearing designs. However, the basic routine was valid only for two identical bearings preloaded against one another. The reason for this limitation is that only one set of bearing deflections were used to define the initial axial offsets of the duplex bearing pair outer races. There was no means of initializing the model if the bearings preloading each other have different axial deflections for a give magnitude of axial preload. This limitation had to be eliminated in order for the preload spring routine to be capable of modeling the proposed test configurations for the turbine-powered hybrid bearing tester. One test configuration uses a steel rolling element bearing preloading a silicon nitride rolling element bearing.

A method for initializing the spring model based on the stiffness of only one of the bearings in the duplex bearing set was formulated. This approach is much more general than the current technique and allowed the spring model to be valid for a much larger number of bearing preloading configurations. The basic relationships needed to implement this technique were developed. The FORTRAN code needed to integrate the new spring model in SHABERTH was developed.

The improved spring routine is generic and was developed to allow modeling of preload spring configurations similar to the setup used in the dual ball bearing configuration of the MSFC hydrogen bearing test rig. **Exhibit 21** illustrates the tester preloading configuration modeled.

The preload spring model functions by adjusting the SHABERTH input parameters Sd (input diametrical play) and a (input contact angle), for one of the bearings in the complement. The effect of varying these parameters, via appropriate relationships, is to slightly change the distance between the preloaded bearings outer races. The relative race motion either increases or decreases the axial loading of the bearings against

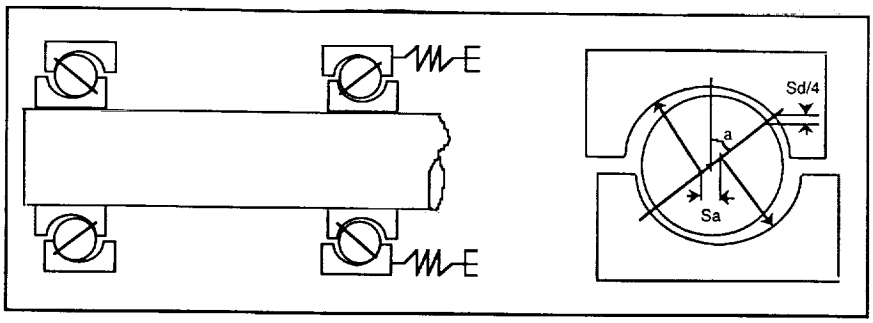

Exhibit 21 Preload Spring Configuration Model Incorporated In SINDA/SHABERTH

one another. Once the race spacing is established using the parameters from the input file, SHABERTH does not allow any motion of the outer races. As a result of this limitation, increases in rolling element temperatures cause a significant axial load to develop between the bearings due to loss of internal clearance. In the actual hardware, the slope of the load rise is significantly reduced by the use of a preload spring which allows the outer races to separate by compressing the preload spring. For given temperatures, loads and speed the bearing axial load condition is specified using the following relationships:

ro = outer race radius of curvature
ri = inner race radius of curvature
D = ball diameter
A = ro+ri-D
Pd = free diametrical clearance
Sd= disine(2A-Pd+Sd/2A)*

To use the model, Sd and a are varied parametrically during the set up of the bearing model until the model predicts that the bearing axial reaction loads equal the design preload. This procedure involves selecting an arbitrary value of Sd and then calculating the corresponding value of a. The procedure continues until the calculated load equals the design load under the specified conditions. Using the new preload model setup, only the inputs for bearing 2 are changed to vary the load. Bearing 1 clearance and contact angle can be set to any values that satisfy the relationships above for that bearing. Experience has shown that choosing bearing 1 parameters such that the axial offset of the bearing 1 is maximized works best for most load conditions. Axial offset can be calculated using the following relationship:

$$Sa = \tan(a) \times (A - Pd/2)$$

After preloading the model using the procedure described above, the preload values of Sa and the preload spring constant K are input into the model for use by the automated spring subroutine.

The spring routine developed for this model works by iteratively adjusting the parameters Sa and a during combined SINDA/SHABERTH thermomechanical analysis. During the analysis, SINDA executes to calculate bearing component temperatures. Typically a rise in ball temperature results in a loss of clearance in the bearing causing SHABERTH to predict larger axial reaction loads. During the Shaberth run the spring model initially adjusts the bearing 2 clearance and contact angle to the values which result in minimum race offset. This initial guess for the parameters results in very large axial load predictions. A value for axial offset (Sa) is calculated for this condition. The change in Sa from the preload condition is multiplied by the spring constant (k) to calculate a spring compression force (F). The spring subroutine then opens the clearance a small amount and reruns the SHABERTH simulation. This automated itera-

tion procedure is performed until the predicted axial reaction force equals the calculated preload spring force. When the forces converge SHABERTH iteration terminates and the calculated heat generation rates are exported to SINDA for another thermal iteration.

The new spring routine was implemented and is now functional in the SINDA/SHABERTH code. The robust bisection root finding algorithm used in the previous spring model was retained in this model. Other features in the model include: maximum spring travel checks to simulate bottoming of the preload spring, no geometric similarity requirements for preloaded bearings, and the ability to function correctly even under conditions of applied axial loading on the shaft. These features enhance the capabilities of the code significantly. The improved spring modeling was utilized for analysis of the MSFC bearing tester shake down tests.

1.10 Invesigation of Bearing Ring Flexing Model

Many analytical models of rolling element bearings have been developed without including the effects of race flexing. These simulations typically model the races as rigid rings considering only the local contact deformations as calculated using Hertzian contact theory. For many bearings this model provides a very good approximation of the actual geometry of the bearing. However, for some applications bearing races are designed with a relatively thin cross-section and lower bending stiffness. Accurate modeling of these bearings requires incorporating the race bending deflections into the model. There are many possible approaches that could be used to model ring flexing. One model that has been used for flexible ring analysis is based on the work of J. Y. Lui and Y. P. Chiu. This analysis is presented in the paper "Analysis of a Thin Elastic Ring Under Arbitrary Loading"; published in Transactions of the ASME, August, 1974.

Recently, analysis results from two different flexible race bearing simulations were reviewed and compared. Both simulations modeled the race using the analysis developed by Lui and Chiu. Different deflected ring shapes were predicted for two cases with similar rolling element loading. The source of the differences between the two cases was investigated. It was found that the source of the differences in the two solutions was due to the way in which the radial load on the ring was reacted. Both models use the solution developed for a ring subjected to a radial load that is reacted by a sinusoidal distributed shear force. This loading condition is illustrated in **Exhibit 22**. The solution of Lui and Chiu states that the radial displacement at any location (Q') is given by the following relationship:

$$\delta_r = \frac{PR^3}{4\pi EI}\left[(\Theta - \pi)\sin\Theta + \left(\pi\Theta - \frac{\Theta^2}{2} + \frac{3}{4} - \frac{\pi^2}{3}\right)\times\cos\Theta + 2\right]_{\Theta=\Theta'} \qquad \Theta \le \Theta' \le 2\pi$$

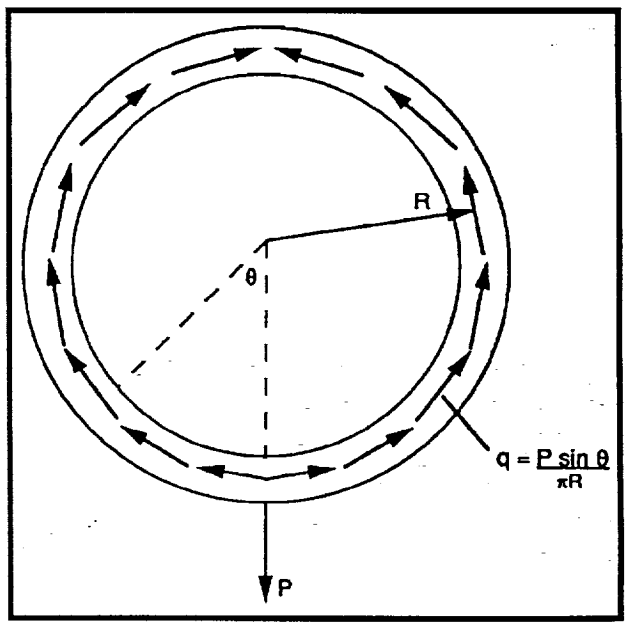

Exhibit 22 Ring Under a Radial Load and Distribution Shear Forces

For a bearing the radial deflection at each rolling element position must be determined. Therefore, the complete deflected ring shape is determined by individually applying each radial load and calculating the deflection at every roller location resulting from the applied load. The deflections at each roller location, for each load, are summed to obtain the deflected ring shape.

The difference in the results from the models is due to the inclusion of an applied reaction load in one case, whereas in the other case the resultant radial load was reacted through residual distributed shear forces. The two cases are shown in **Exhibit 23** and **Exhibit 24**. In the first case, it is assumed that the ring is sitting on a surface and the entire radial load is reacted through a single point. This case is not entirely realistic because in reality a bearing is usually supported in a curved deadband and the reaction forces assume a distributed Hertzian type variation. For the second case it is assumed that the reaction load is supported by distributed shear forces which are maximum at a location 90 degrees away from the location of the resultant radial load. It is difficult to imagine how this type of reaction force could actually be applied to the bearing. Therefore, both models use relatively rough approximations to describe the constraints on the ring. However, it could be expected that for cases with relatively small resultant radial loads either model should provide fairly accurate results. For the two cases studied the radial load was 11120 N (2500 lbs) which is a fairly large radial load in relation to the size of the bearing. The deflected shapes predicted from the two methods described are shown in **Exhibit 25**. It can be seen that the magnitude of the deflections vary by an order of magnitude and the general shape of the deflected ring is also changed. Exhibit 25 was generated by scaling the deflections and plotting them on a circular ring with a two inch radius.

The results of this comparison show that for larger radial loads the solution of the ring flexing equations is extremely sensitive to the manner in which the radial load is reacted. Based on this observation it appears that a more detailed analysis is required to accurately model ring flexing

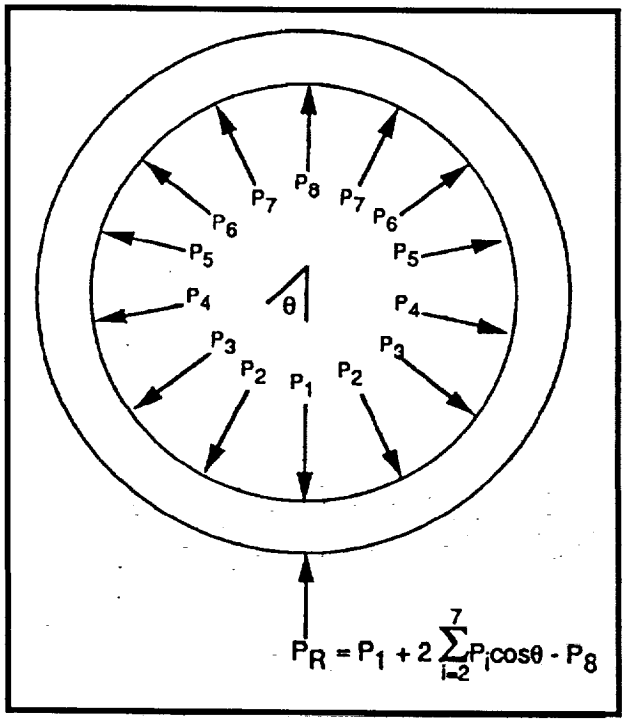

Exhibit 23 Ring Loading for Case of Applied Reaction Load

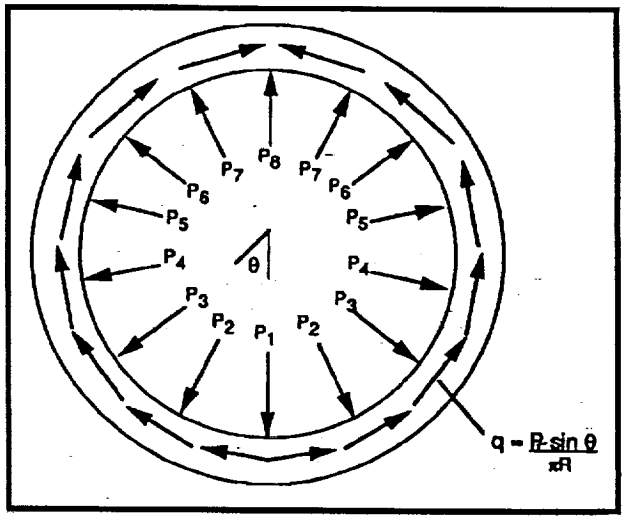

Exhibit 24 Ring Loading for Case of Distributed Reaction Load

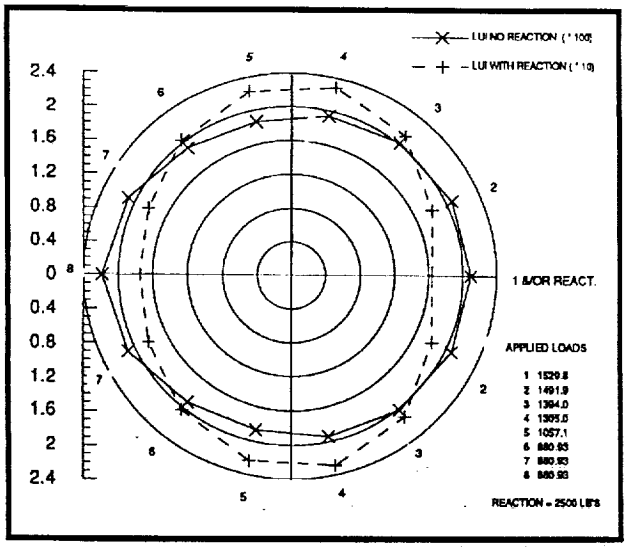

Exhibit 25 Deflected Ring Shapes for Two

when the radial loads are large. The general form of the solution developed by Lui and Chiu provides for arbitrary loading of a thin ring. Therefore, one approach to improving the bearing model results would be to solve for the actual reaction force distribution, using Hertzian contact theory, and then solve for the ring deflections using the general form of the thin ring solution subject to the actual distributed reaction force.

1.11 Modification of SHABERTH Code to Output Additional Contact Data

The SHABERTH code was modified to provide additional output describing the tribological conditions in the rolling element contacts for ball bearings. Previous modifications to the code were developed to provide the wear parameter stress times velocity (SV). Using the earlier version of the code the maximum and minimum values of stress velocity were output for each bearing. The stress velocity profile across the rolling element contact was output for the contact with the maximum stress velocity. With this modification, the code now includes outputs for contact stress and slip velocity, for each contact lamina in the contact with the largest SV parameter. This modification provides data in a format more useful for planing traction testing to simulate the rolling friction characteristics.

1.12 SHABERTH Shoulder Run-Out Model Update

A minor modification was made to the SINDA/ SHABERTH bearing design software for improved data output. The original SHABERTH code has been modified many times in order to calculate and output additional bearing performance metrics. One of these additional metrics is shoulder run-out. The code now calculates how far up the inner and outer race shoulder the edge of the Hertzian contact ellipse rides. Prior to the subject modifications, this data was calculated in SHABERTH and then transferred to SINDA for output. Therefore, the data was not available for studies performed using known bearing temperatures and not requiring SINDA analysis. The subject modification provides a print out of calculated shoulder run out directly from SHABERTH. The modifications were performed at SRS and then the modified code was installed on Mr. Tim Jetts computer at MSFC.

1.13 Improvements to SHABERTH Bearing Code to Support Future LH_2 Rig Testing

A modification was performed to the SHABERTH bearing software to facilitate data processing of bearing rig test results. SRS maintains two software packages that are used to support bearing rig testing and flight pump bearing issues. One package is integrated with a thermal model and is able to solve for component temperatures and the effects that temperatures have on bearing components. The other model, which is much simpler to set up, uses temperatures input as know quantities. This second

version of the code is very useful for performing quick turn-around analysis and parametric studies that are often used to evaluate and analyze rig test data. Over a period of time these two packages diverged, often new features were added to the full-up thermomechanical model and not incorporated into the simple bearing only version. The two separate versions of the code required different input files to run the same bearing. The recent modifications performed have brought the standalone bearing only code up to the same level as the thermomechanical code. The two versions can now be run from the same SHABERTH bearing input file. This consolidation eliminates the need to maintain multiple models of the same bearing/rig configuration. The new version of the SHABERTH only code was compiled on a Pentium based PC using 32-bit Digital FORTRAN. This new compiler eliminated the compatibility problems sometimes encountered when using the old software on modern PCs. The new software was delivered, via e-mail, to Mr. Tim Jett for in-house use.

2.0 — Bearing Design Studies

SRS performed various bearing design functions over the course of this effort. The studies presented in this chapter cover three major areas. First, SRS performed design studies to determine the best approach for integrating silicon nitride rolling elements into the Rocketdyne SSME high pressure oxidizer turbopump bearings. In particular, it was desired to substitute silicon nitride balls for 440C stainless steel balls in the 45mm bearing. SRS performed many design trades to evaluate the feasibility and best approach for accomplishing this objective. It was shown that a direct substitution of rolling elements was possible provided they were sized correctly. It was shown that the Phase II races would work with ceramic balls.

SRS also provided design analysis to support evaluation of advanced ball separator designs. This analysis looked primarily at the Bronze/ Salox cage design by Battelle Laboratories. SRS supported investigations of problems that developed during testing. The analysis resulted in identifying a simple resolution of the problem. Simulations were also performed to support scaling of 57 mm bearing test results to future application.

Additionally, SRS developed simulations of the Pratt and Whitney Advanced Technologies turbopump bearings to support these bearing design efforts. A significant effort was devoted to characterizing the performance of these bearings in off design operating conditions.

2.1 Comparison of HPOTP 45 MM Bearing Using 440C SS and Silicon Nitride Rolling Elements

The SINDA/SHABERTH thermomechanical model of the Rockedyne HPTOP pump end 45 mm ball bearing was used to perform a comparison of the bearings' steady-state operation using standard 440C stainless steel rolling elements and its operation with silicon nitride rolling elements. The simulation used an axial load of 3200 N (720 lb.), radial load of 11,120 N (2,500 lb.), applied at the main impeller which resulted in a radial reaction load of approximately5,000 N (approximately 1,125 lb.) at the test bearing. The operating speed and coefficient of friction were 30,000 rpm and 0.25, respectively. All other operating conditions were as per Phase II design.

The simulation with 440C rolling elements used curvatures of $f_i = 0.55$ and $f_o = 0.52$ (standard Phase II). The silicon nitride simulations used an outer race curvature of 0.52 and three inner races curvatures of 0.55, 0.53, and 0.52. A diametrical clearance of 0.1676 mm (0.0066 inches) was used for $f_i = 0.53$ and 0.52. The results of all the simulations are shown in **Exhibit 26 , 27** and **28**.

The resulting contact stresses for the maximum loaded rolling element are presented in **Exhibit 26**. Model predictions showed that the outer race stress would increase slightly by using silicon nitride. This increase is a result of two offsetting effects. One effect was the reduced outer race force resulting from a lower centrifugal force due to the lower density of silicon nitride (60% lighter than steel). The other effect is the reduced contact area as a result of the higher modulus of elasticity of silicon nitride (50% higher than steel). The outer race contact area was reduced by a larger percentage than was the outer race force resulting in a slightly higher outer race contact stress for silicon nitride at 30,000 rpm. The inner race stress with silicon nitride and the same inner race curvature of 0.55 was approximately 10% higher than with 440C balls. Using lower inner race curvatures reduced

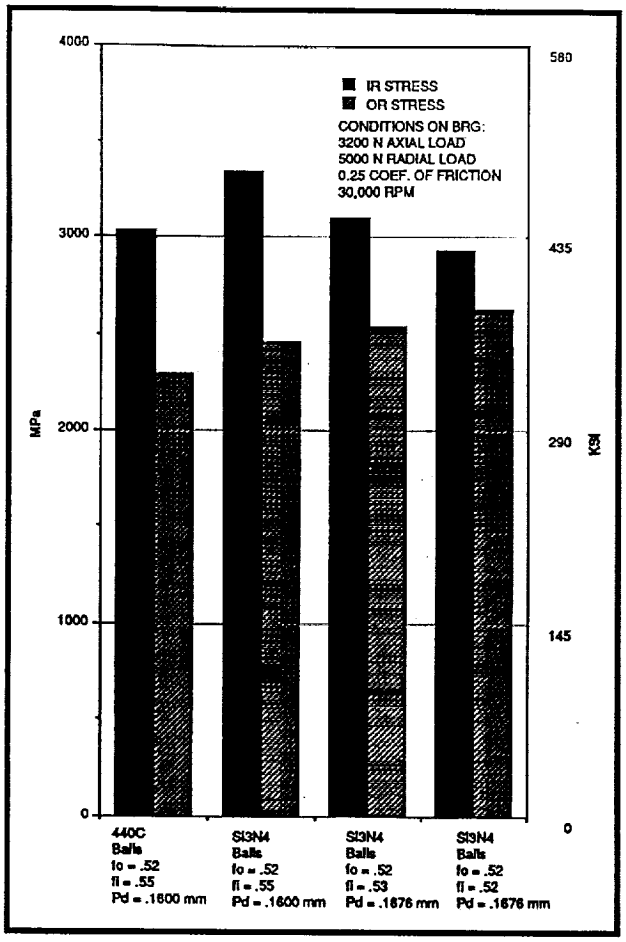

Exhibit 26 Comparison of Stress for 440C Stainless Steel Balls And Silicon Nitride Balls in Rockedyne HPOTP Pump End 45 mm Bearings

the stress by increasing the size of the contact ellipse. Thus, using an inner race curvature of 0.52 with silicon nitride, the inner race stress was predicted to be approximately4% less than that with 440C and fi = 0.55.

The heat generation, as shown in **Exhibit 27**, was about 30% less at the outer race with silicon nitride due to both the lower centrifugal load and smaller contact area. The inner race heat generation could be reduced approximately20% from the 440C value by using silicon nitride with fi = 0.55. If the inner race curvature of 0.52 was used with silicon nitride, the inner race heat would be increased 20% over the 440C inner race heat. This increase in heat generation was not believed to be detrimental to the bearing with silicon nitride rolling elements due to the low thermal expansion of silicon nitride (approximately25% of steel). The silicon nitride rolling elements would not thermally grow as much as the steel and, therefore, the bearing internal loading would not increase as much. Also, the lower thermal expansion would allow the ball size to remain more constant from ball to ball with different rolling element heating. This would aid in keeping the ball speed variation low which helps maintain low ball to cage loading.

The predicted component temperatures are provided in **Exhibit 28** for the 45 mm bearing

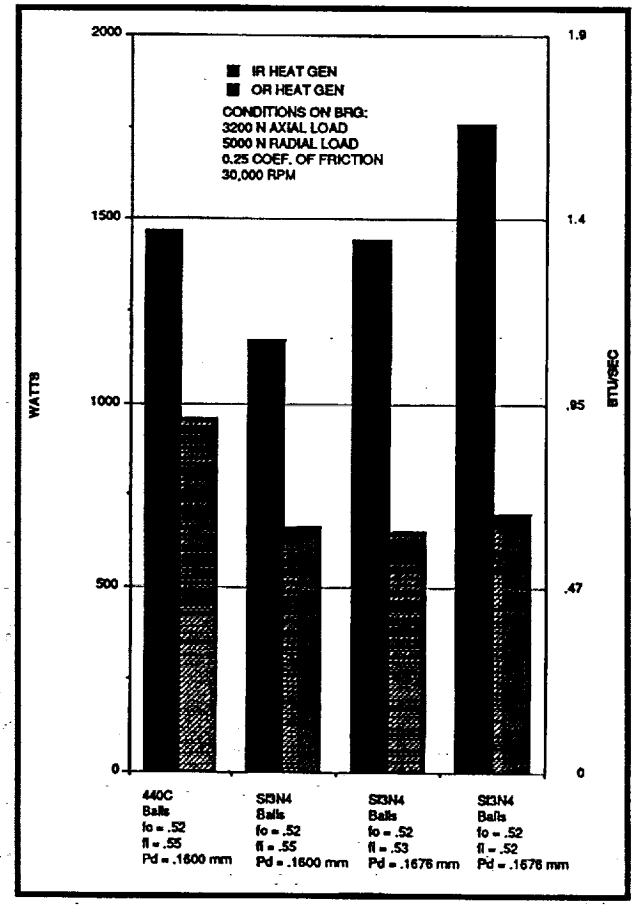

Exhibit 27 Comparison of Heat Generation for 440C Stainless Steel Balls and Silicon Nitride Balls in Rockedyne HPOTP Pump End 45 mm Bearings

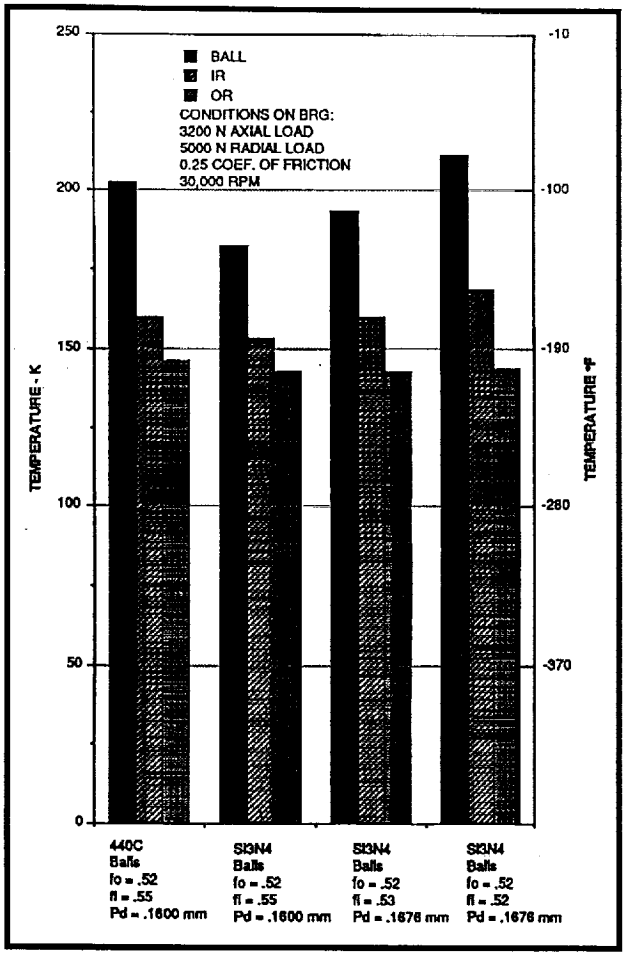

Exhibit 28 Comparison of Temperature for 440C Stainless Steel Balls and Silicon Nitride Balls in Rockedyne HPOTP Pump End 45 mm Bearings

with both 440C and silicon nitride rolling elements. As shown, the silicon nitride ball and outer race temperatures were lower than 440C predictions for all curvatures simulated. The inner race temperature with 440C balls for all curvatures except $f_i = 0.52$. Due to the increased heat generation with the larger contact area with $f_i = 0.52$, the inner race component temperature was slightly higher than the inner race with 440C rolling elements. It is believed however, that the benefit of reduced contact stress with $f_i = 0.52$ overcomes the disadvantage of the increase in heat generation. Thus, this limited study showed that bearings fitted with silicon nitride rolling elements and reduced curvatures should significantly improve the operation and extend the life of the 45 mm bearings in the pump end of the liquid oxygen turbopumps.

2.2 Further Analysis and Optimizatio of Rocketdyne 45mm Bearings with Silicon Nitride Rolling Elements

The High Pressure Oxider Turbopump (HPOTP) 45 mm pump end ball bearings were investigated to determine the optimum bearing geometry to be used with silicon nitride rolling elements. The SINDA/SHABERTH thermomechanical bearing analysis code was used to analytically simulate both bearings to determine thermal gradients, thermal expansion and its effect on radial load sharing and operating preload. The bearing geometries that were investigated were a Phase II configuration with variations in inner race curvature and internal diametrical clearance. The simulation used an inlet coolant temperature of 133K (-220°F), flow rate of 2.09 Kg/s (4.6 pps), coefficient of friction of 0.25 for the races and 0.2 for the cage. A preliminary comparison of the pump end bearings operating with silicon nitride balls was performed using radial load sharing, contact stresses, ball excursion, heat generation, and average component temperature. Also, the results for the bearings with standard Phase II geometry and standard 440C stainless steel balls were included for comparison.

The resultant operating loads for all the bearing configurations modeled are shown in **Exhibit 29**. As shown, the resulting axial preload was slightly less with the silicon nitride balls. This was expected due to the lower coefficient of thermal expansion of silicon nitride (approximately25% of steel). Thermal expansion in the pump end duplex pair bearings resulted in increased preload because the bearings are loaded

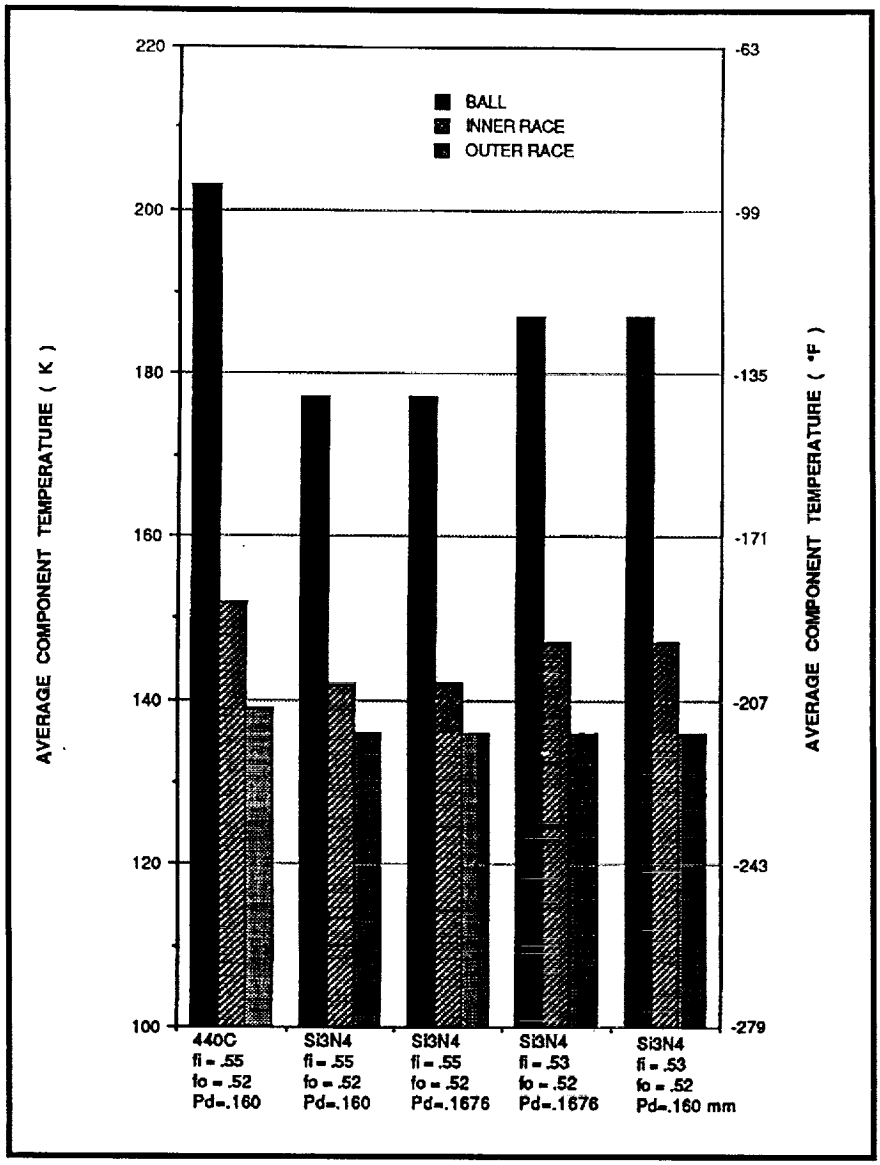

Exhibit 29 HPOTP Pump End Bearing Reaction Loads

against each other. Using silicon nitride balls would help maintain a more constant axial preload during operation. Since the thermal expansion of silicon nitride is significantly lower than steel, the preloading procedure during bearing/shaft assembly needed to be reviewed and needed to be modified to ensure the desired preload was obtained at both chilled static and operating conditions. The radial load sharing was only slightly different with the silicon nitride rolling elements as compared to 440C. Because the silicon nitride material is harder than steel (elastic modulus 50% higher than steel), the silicon nitride bearings are radially stiffer. Therefore, the inboard bearing (Bearing 2) with the Phase II geometry and silicon nitride balls would support a greater percentage of the total load on the pump end due to the slight shaft deflection between the pump end and the turbine end bearings. However, using an inner race curvature of 0.53 slightly reduced the bearing's radial stiffness which resulted in a slightly improved load sharing distribution. The change in bearing diametrical clearance studied had almost no affect on the operating loads.

The resulting contact stresses for Bearing 1 and Bearing 2 are shown in **Exhibit 30** and **31**, respectively. The result of changing only rolling element material to silicon nitride was approximately 10% high Hertzian contact stress for both bearings. The higher stress was due to the higher modulus of silicon nitride resulting in a smaller contact ellipse. Reducing the inner race curvature to 0.53 increased the contact area and decreased the inner race stress to only slightly greater than that for 440C Phase II. However, the outer race stresses increased slightly for this configuration due to the increased radial and

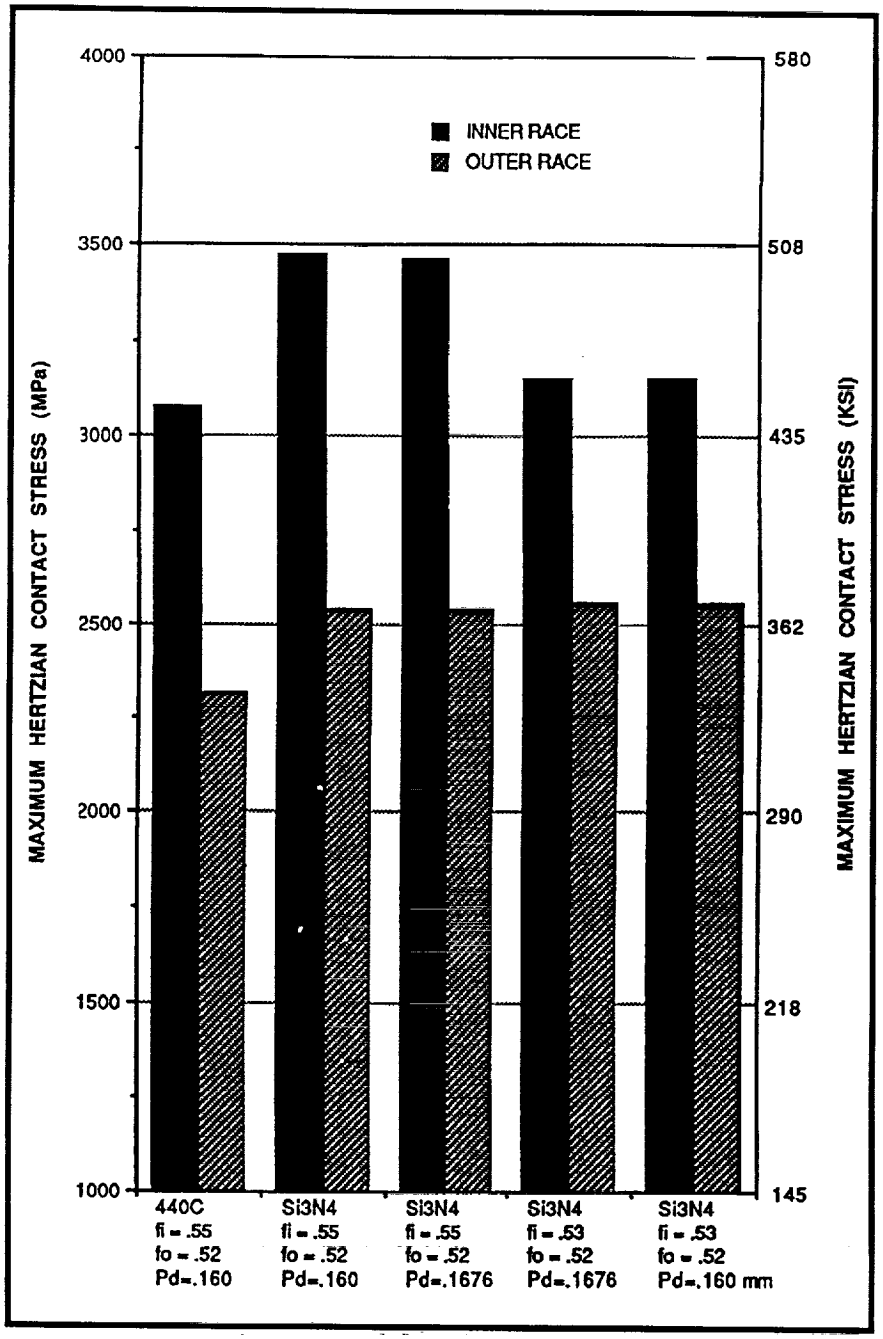

Exhibit 30 HPOTP Bearing 1 Contact Stress

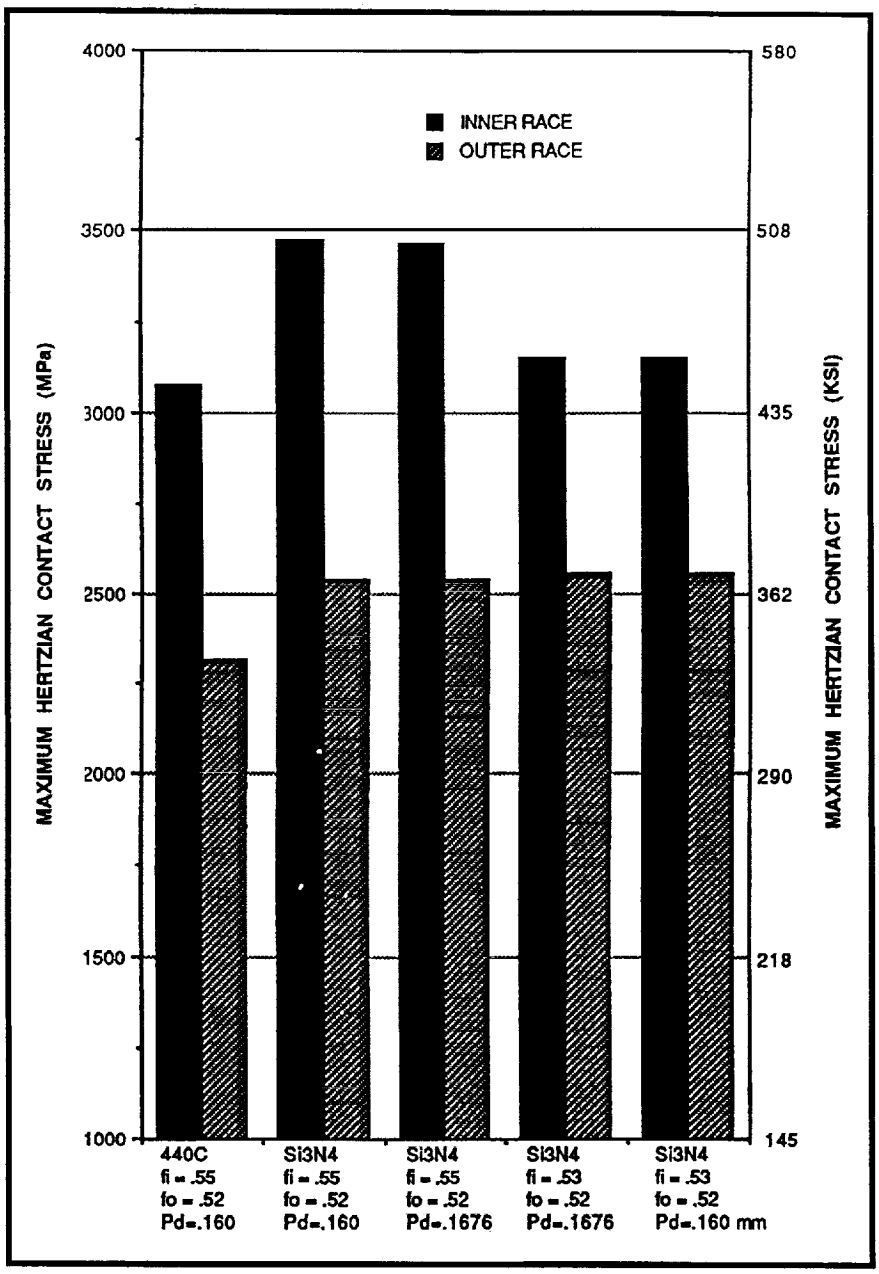

Exhibit 31 HPOTP Bearing 2 Contact Stress

axial loads. There was almost no difference in the stresses for the two clearances studied.

Ball excursion was significantly affected by the change in rolling element material and bearing geometry as shown in **Exhibit 32**. The ball excursion was reduced approximately25% for Bearing 2 and approximately55% for Bearing 1, by replacing the 440C balls with silicon nitride. This reduction was due to the lower inner race contact angles as a result of lower ball centrifugal force caused by the lower density of silicon nitride (60% lighter than steel). However, the ball excursion was increased approximately40% for Bearing 2 and approximately20% for Bearing 1 using silicon nitride and an inner race curvature of 0.53 as compared to the 440C Phase II bearings. Reducing the race curvature caused the contact angle variation from heaviest loaded to lightest loaded ball to increase which caused the ball speed variation or ball excursion to increase. The ball excursion was high for all of the cases due to the heavy radial load on the bearings. This is why the pump and bearings use cages with oval ball pockets to increase cage to ball clearance.

The frictional heat generation at the inner and outer raceway ball contacts was also significantly affected by the change in bearing geometry and ball material as shown in **Exhibit 33** and **34** for Bearings 1 and 2, respectively. The outer raceway heat reduction was also due to the smaller contact ellipse with silicon nitride. The smaller inner race curvature of 0.53 caused the contact ellipse to be larger and caused the contact angle to be higher which resulted in a higher ball spin

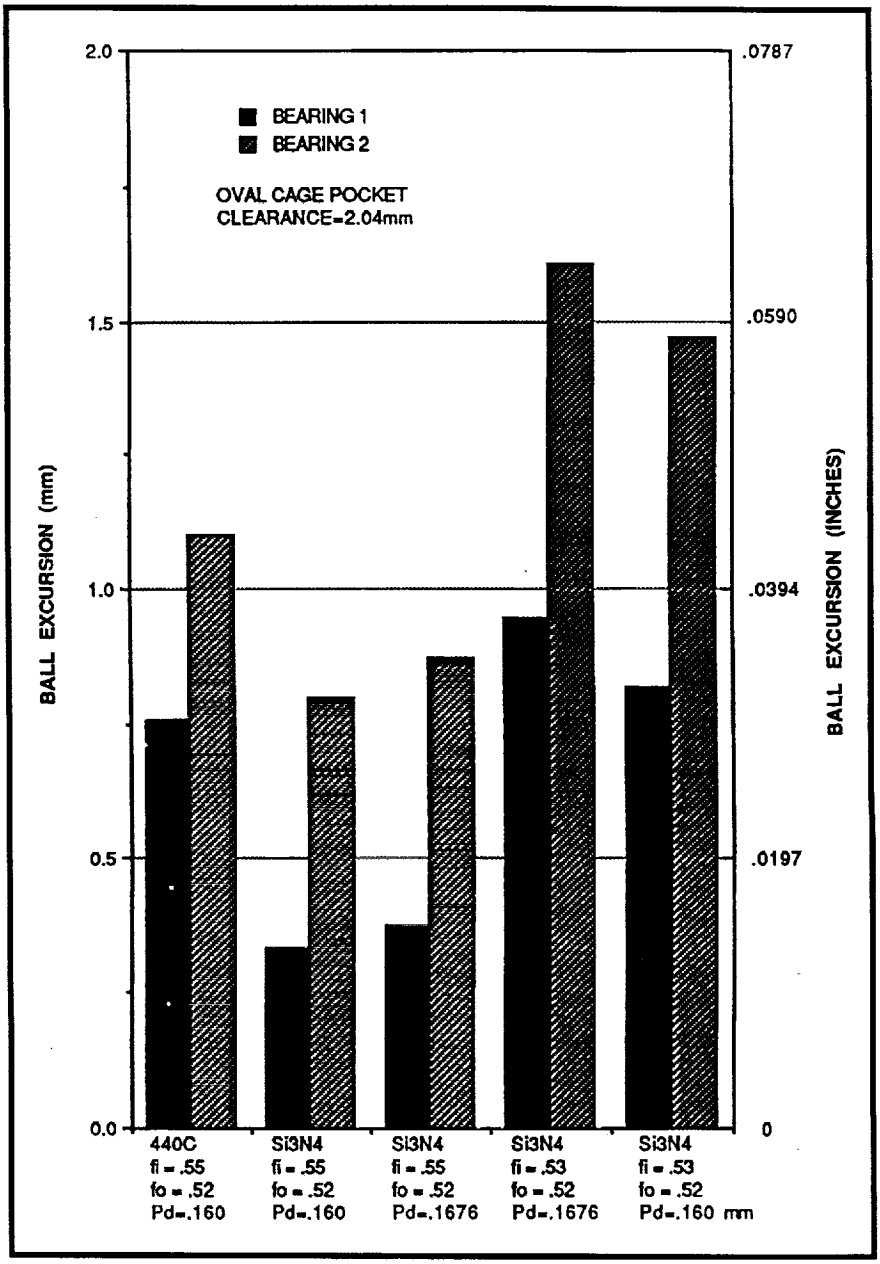

Exhibit 32 HPOTP Pump End Bearings Ball Excursion

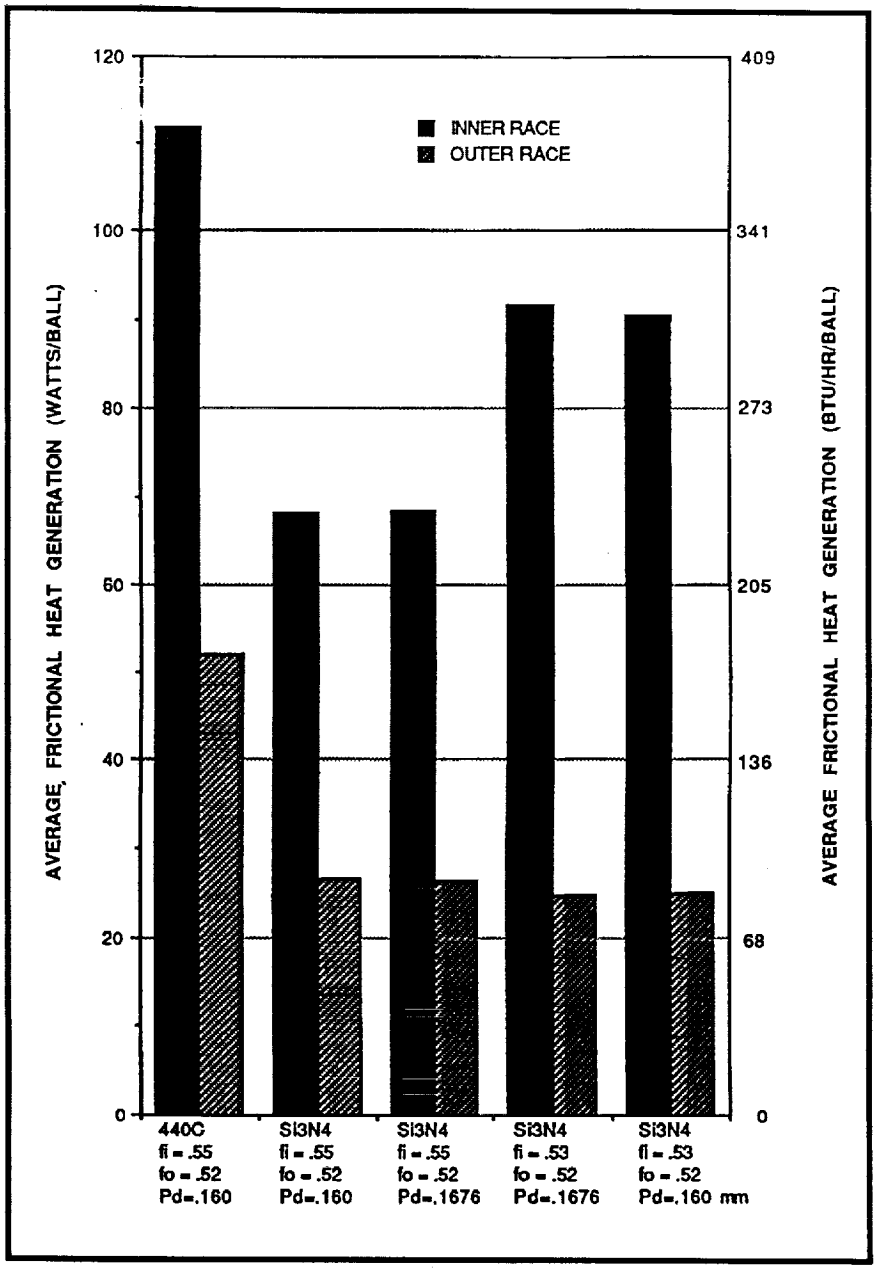

Exhibit 33 HPOTP Bearing 1 Frictional Heat Generation

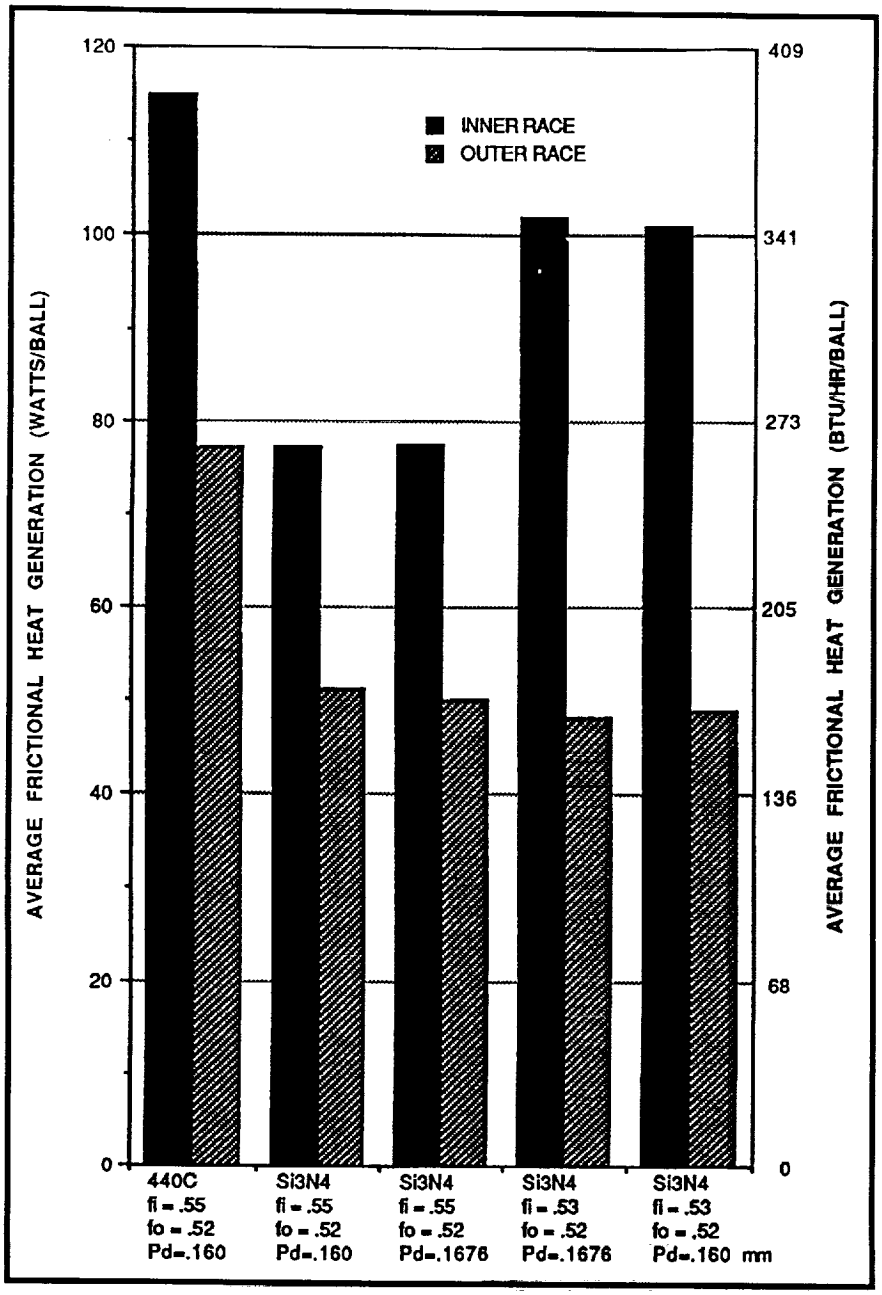

Exhibit 34 HPOTP Bearing 2 Frictional Heat Generation

giving the net result of only a 20% decrease in inner race heat as compared to 440C Phase I bearing.

In summary, the pump end bearings in the Space Shuttle Main Engine (SSME) high pressure oxidizer turbopump (HOPTP) were modeled to investigate the potential improvements to be gained by replacing the 440C steel balls with Si3N4 balls. Other factors, such as loads, friction and speeds being equal, the greater the ball spin normal to the contact surface, the greater the heat generated in the contact. The Phase II 440C 45 mm pump end bearings were modeled to provide a baseline for comparing the results of the Si3N4 bearing model. The Phase II bearing configuration was modeled with Si3N4 balls, and deviations from this configuration included reduced inner race curvatures and increased diametrical clearances. The results are shown in **Exhibit 35** for the Number 2 pump bearing which supported considerably more radial load than the Number 1 bearing.

Results from the Si3N4 modeling showed that an increase in diametrical clearance caused a slight increase in ball spin at the inner race. Since the bearings were radially loaded, each ball had different loads and speeds. The ball became unloaded at an aximuth angle of 120° and remained unloaded until it reaches an angle of 270°. The ball supported the greatest load at 0° azimuth and remained loaded until it passed 90° aximuth. The 90° position inner race contact angle was greater than the angle at zero position, causing an increase in ball spin. Increased clear-

MATERIAL	SILICON NITRIDE (Si3N4)				440C
INNER RACE CURVATURE	.55	.55	.53	53	.55
OUTER RACE CURVATURE	.52	.52	.52	.52	.52
DIAMETRICAL CLEARANCE (mm)	.16	.1676	.16	.1676	.16
SPIN/ROLL	*.128, **.372	*.13, **.39	*.141, **.529	*.145, **.592	*.16, **.447
GYROSCOPIC SLIP	*.0085	*.0088	*.0092	*.0094	**.0188

920417JC1521

* Heaviest Loaded Ball
**90° from Heaviest Loaded Ball

Exhibit 35 Spin/Roll and Gyroscopic Slip

ance also caused increased contact angle and increased ball spin relative to the inner race. Reduction in curvature increased the variation in contact angle within the ball complement, and produced a wider range of spin/roll values. The spin/roll values for the 440C balls were greater than for theSi3N4 balls for equivalent curvatures and clearances. The higher density steel balls produced larger centrifugal forces causing larger contact angles.

The gyroscopic slip, which is the ratio of the gyroscopic tangential force, at the ball surface, and the normal force exerted at the zero spin surface, was significantly larger for the 440C ball bearing. This was primarily caused by the higher density of the steel balls. The other parameters, ball angular speed and direction, and orbital speeds were not significantly different between the steel and Si3N4 ball bearings. The centrifugal loads, that were higher for the steel balls, were a small component of the normal force, compared to the applied radial load component.

The results from this investigation showed that the light Si3N4 balls provided potential for reducing the contact heat generation, caused by ball spin normal to the contact, and slip along the major axis of the contact caused by gryoscopic forces. These characteristics also reduced ball and raceway surface wear.

The resulting average component temperatures for each case simulated are shown in **Exhibits 36** and **37** for Bearings 1 and 2, respectively. The use of the silicon nitride rolling elements with all the bearing configurations modeled enabled the bearings to operate cooler than the 440C Phase II bearings. The increase in internal clearance had little affect on the operating temperatures since the bearing already had adequate clearance with 0.160 mm (0.0063 inches).

Based on preliminary comparisons of 440C Phase II bearings with bearings using silicon nitride rolling elements, it appeared that the best

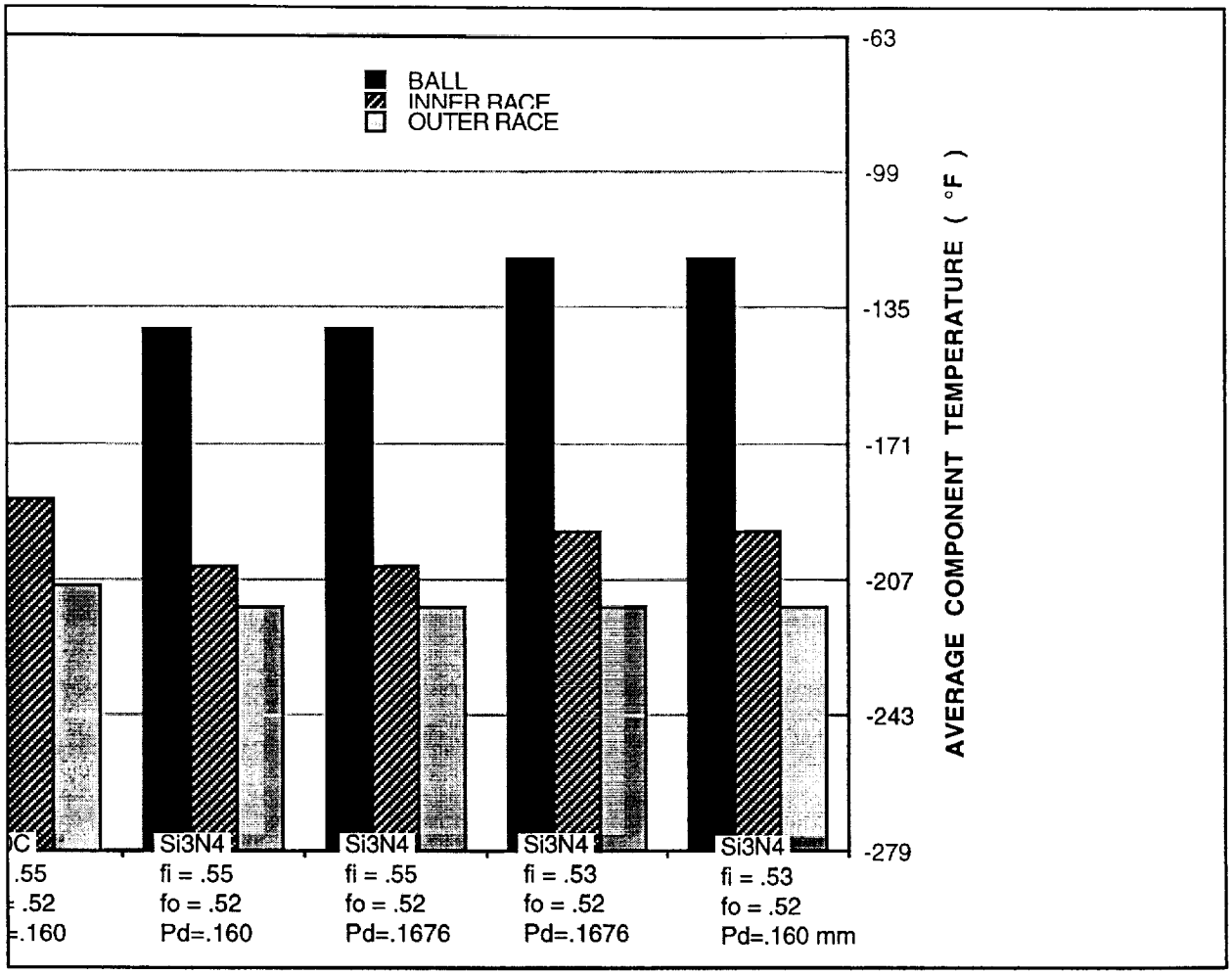

Exhibit 36 HPOTP Bearing 1 Component Temperature

bearing configuration to use with the silicon nitride balls would be the standard Phase II geometry of $f_i = 55$, $f_o = 0.52$, and $P_d = 0.160$ mm (0.0063 in). This configuration had the best results in all the parameters compared except for Hertzian contact stresses. However, it is believed that the stress levels for this configuration of 3,500 MPa (508 Ksi) are still acceptable for the 440C stainless steel races based on NASA rolling element fatigue contact data and is well within the capability of the silicon nitride material. The use of the silicon nitride balls in the HPOTP pump end bearings will significantly improve their performance based on this study and results of the silicon nitride rolling element testing in the MSFC Bearing and Seal Material Tester (BSMT).

2.3 Optimization of Additional Parameters for 45mm Rocketdyne Bearing with Silicon Nitride Bearings

The analysis to optimize the geometry of the 45mm pump end bearings with silicon nitride rolling elements was expanded to include variations in outer race curvature and an additional value for internal clearance. Previous analysis considered a single value of 0.52 for the outer race curvature, and two values, 0.16 mm (0.0063 in.), and 0.1676 mm (0.0066 in.), for internal clearance.

As shown in **Exhibit 38**, this required the evaluation of 13 configurations. The SINDA/ SHABERTH thermomechanical bearing analy-

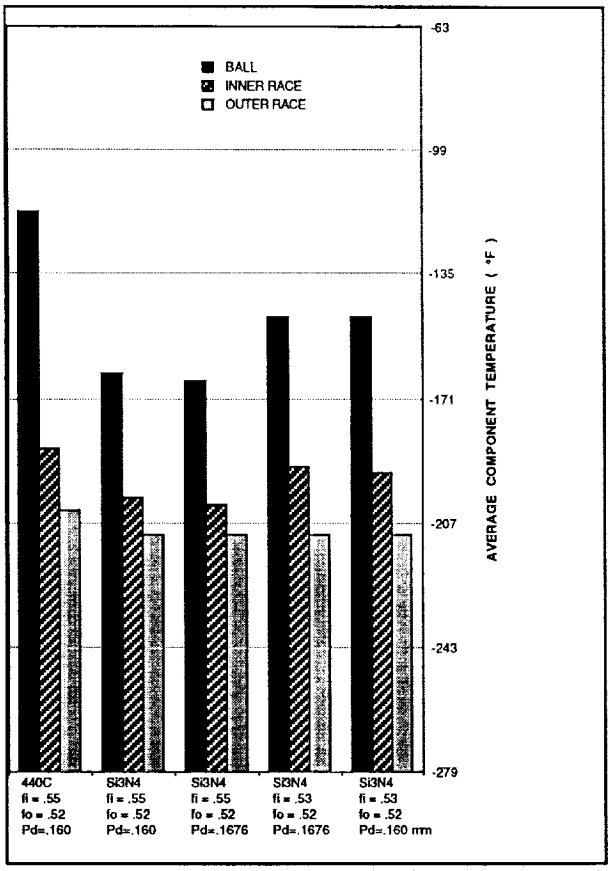

Exhibit 37 HPOTP Bearing 2 Component Temperature

sis code was used to model the pump end bearing pair. The model used an inlet coolant temperature of 133K (-220°F), a flow rate of 2.09 kg/sec (4.6 pps), and a coefficient of friction of 0.25 for the races and 0.2 for the cage.

Results from the analysis include ball excursions, reaction loads, contact stresses, heat generation, and component temperatures. These results are provided in **Exhibits 39** through **48**. Ball excursion is shown in **Exhibit 39** for the configurations evaluated. The bearings with silicon nitride rolling elements and Phase II configuration (fi = 0.55, fo = 0.51) had less ball excursion than the other configurations including the Phase II bearing with 440C rolling elements. For equivalent configurations, the bearings with silicon nitride balls had less ball excursion due to the lighter balls producing lower centrifugal loads and lower contact angles. Increasing the outer race curvature caused a decrease in ball excursions in the Number 1 bearing. With the lower outer race curvature of 0.52, some of the balls in the Number 2 bearing became unloaded which

Bearing	Clearances mm (in)	Inner Race Curvature	Outer Race Curvature	Number of Configurations
440C Phase II SI3N4 Rolling Elements	.16 (.0063)	.55	.53	1
	.102 (.004)	.53	.53	2
	*	.53	.55	3
	*	.55	.52	4
	*	.55	.55	5
	.16 (.0063)	.53	.52	6
	*	.53	.55	7
	*	.55	.52	8
	*	.55	.55	9
	*.1676 (.0066)	.53	.52	10
	*	.53	.55	11
	*	.55	.52	12
	*	.55	.55	13

*Completed during this reporting period

920514JC1439

Exhibit 38 Clearances and Curvatures Investigated

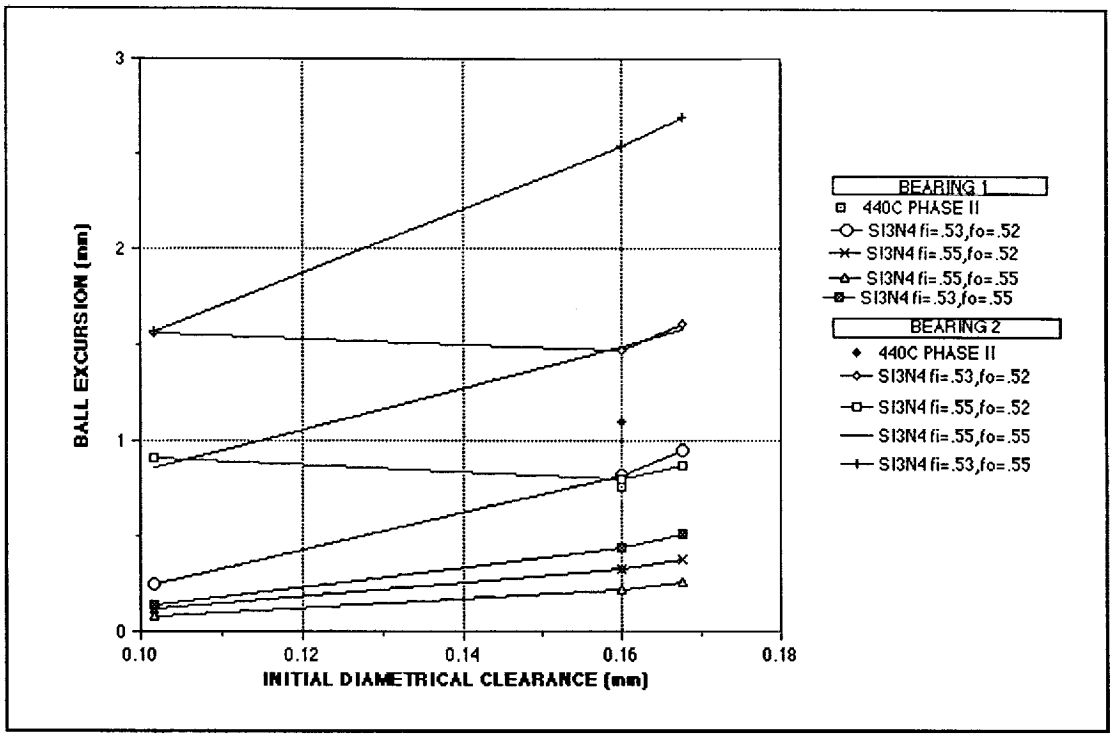

Exhibit 39 HPOTP Pump End Bearing Ball Excursion

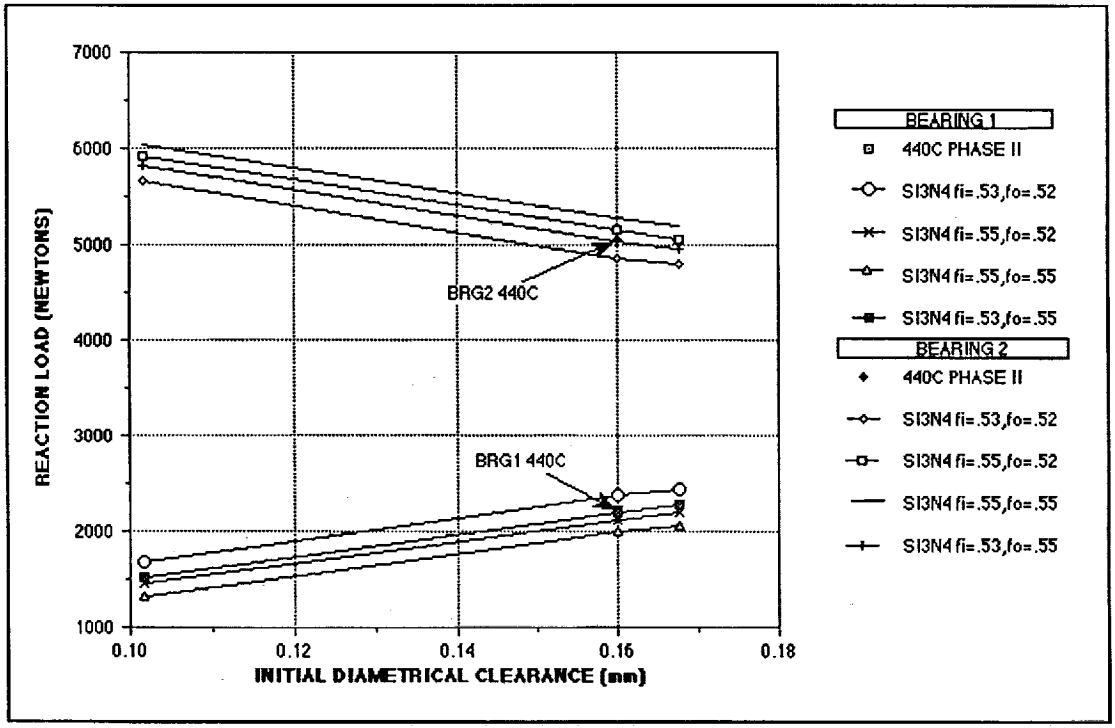

Exhibit 40 HPOTP Pump End Bearing Radial Load

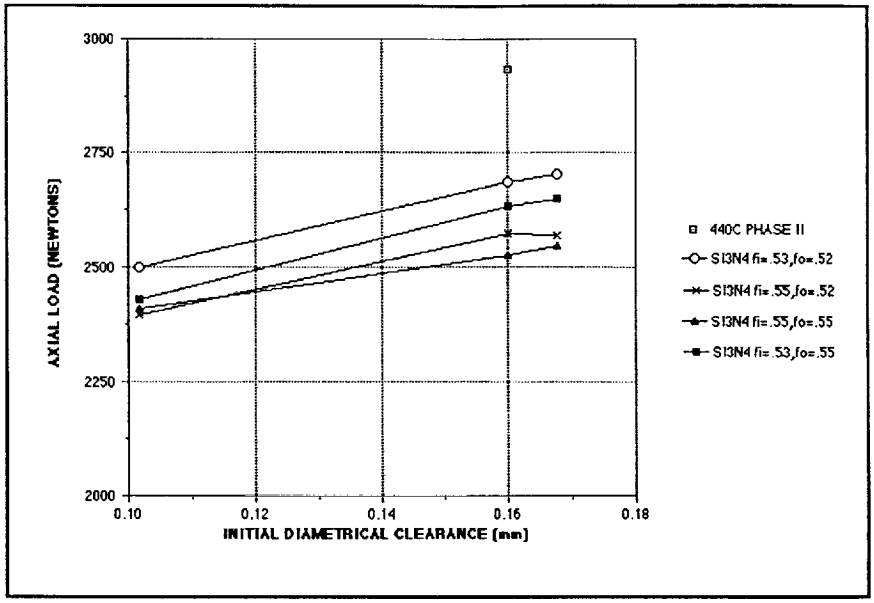

Exhibit 41 HPOTP Pump End Bearing Axial Load

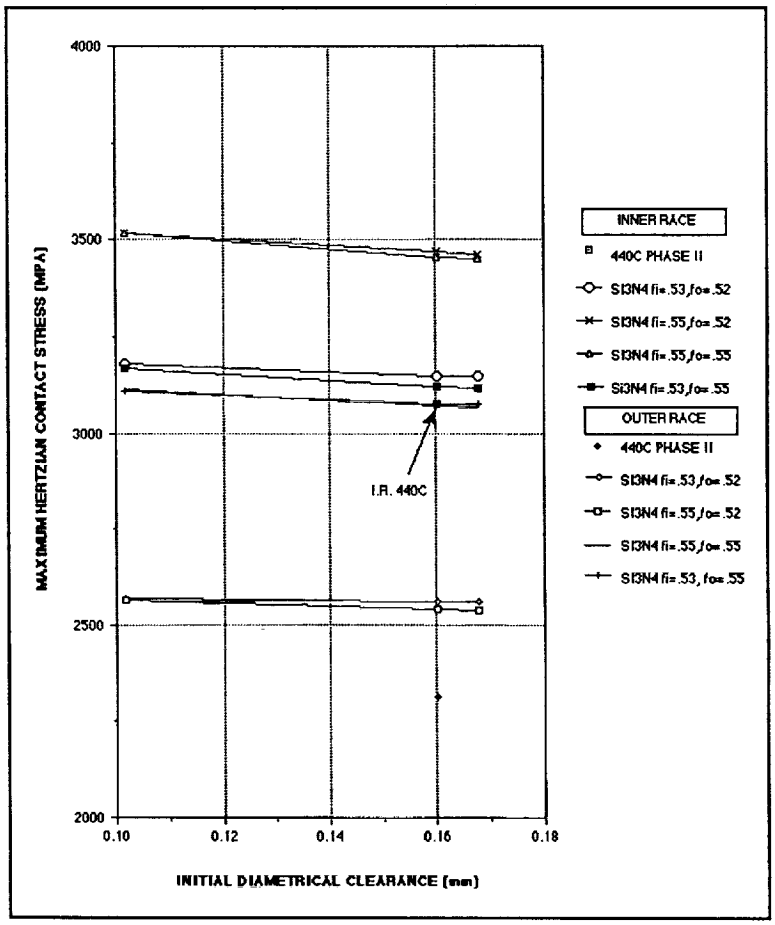

Exhibit 42 HPOTP Pump End Bearing 2 Contact Stress

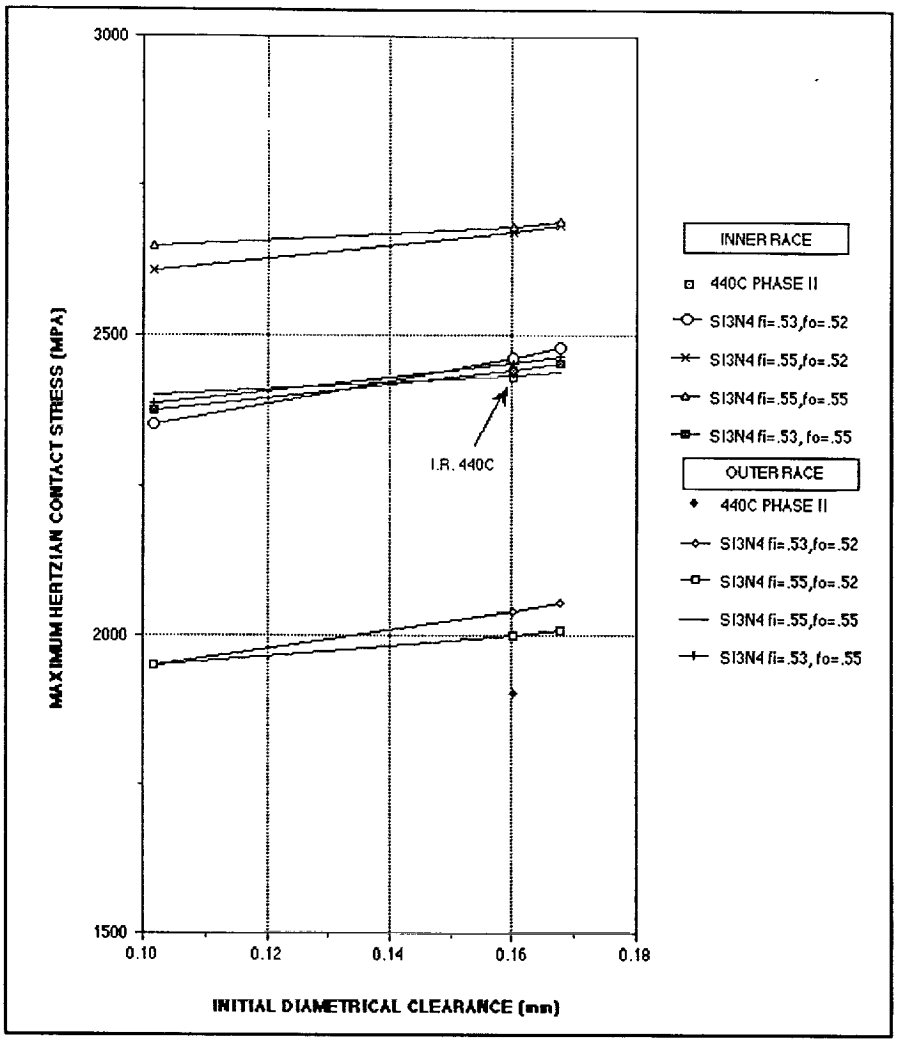

Exhibit 43 HPOTP Pump End Bearing 1 Contact Stress

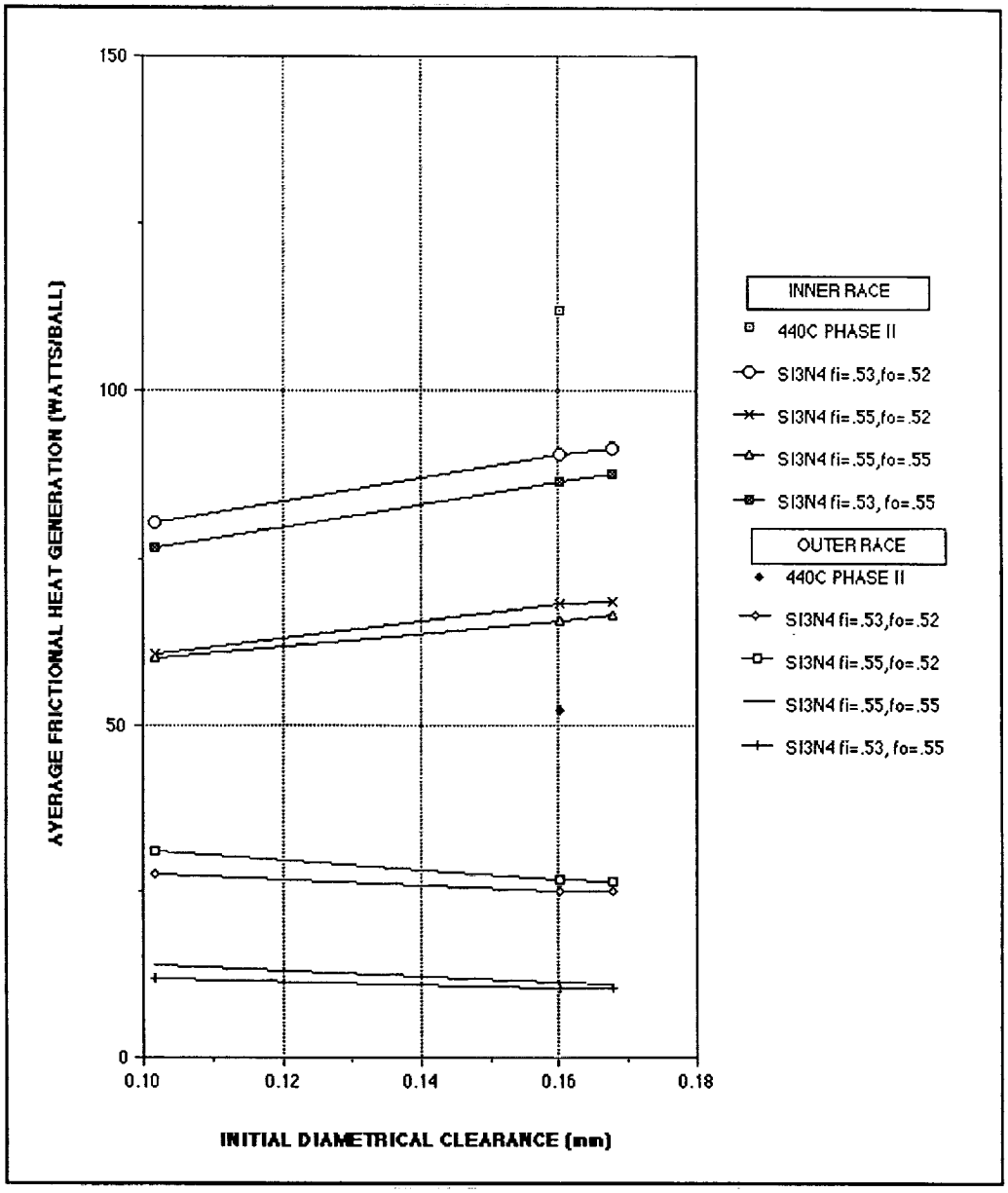

Exhibit 44 HPOTP Pump End Bearing 1 Frictional Heat Generation

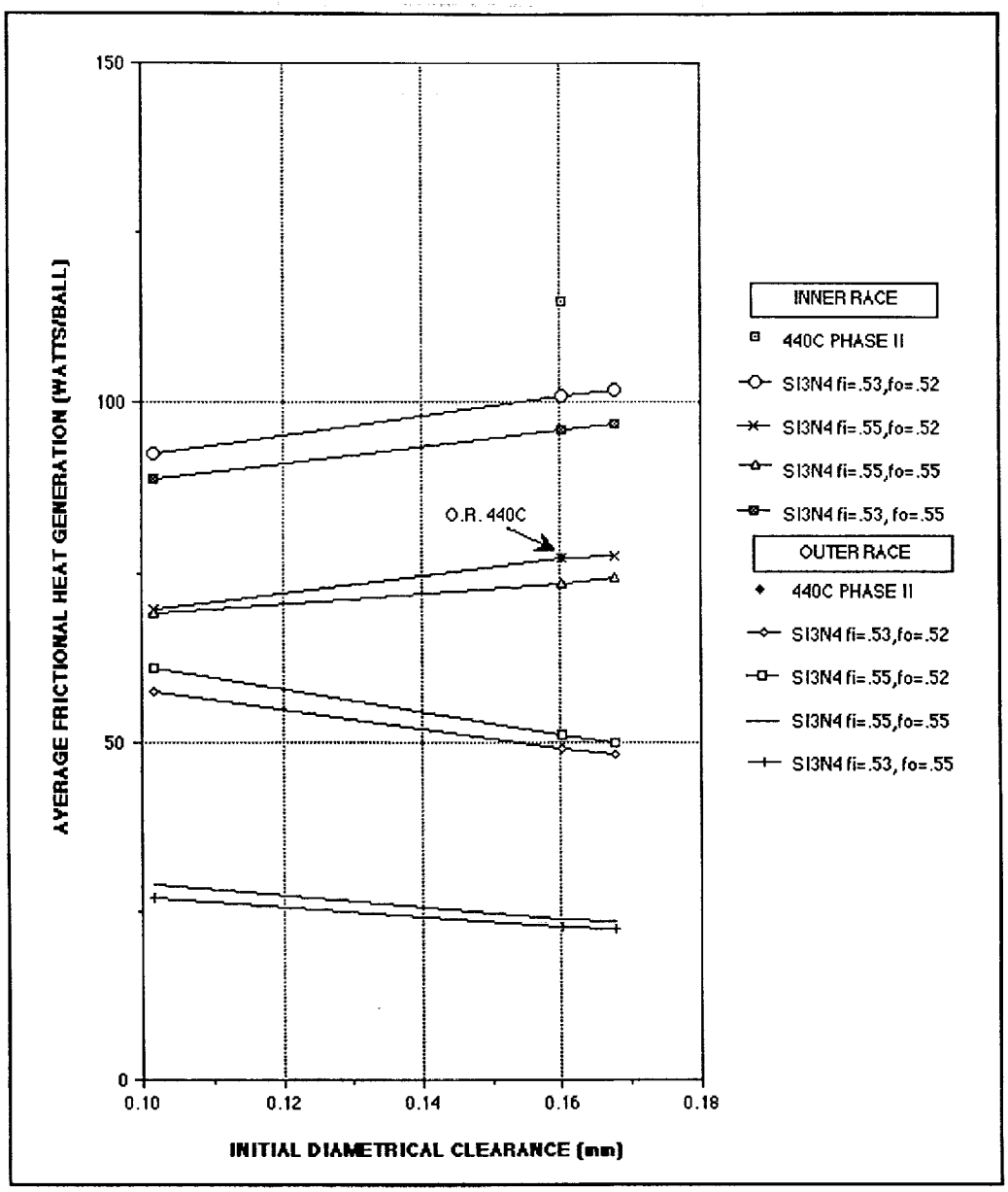

Exhibit 45 HPOTP Pump End Bearing 2 Frictional Heat Generation

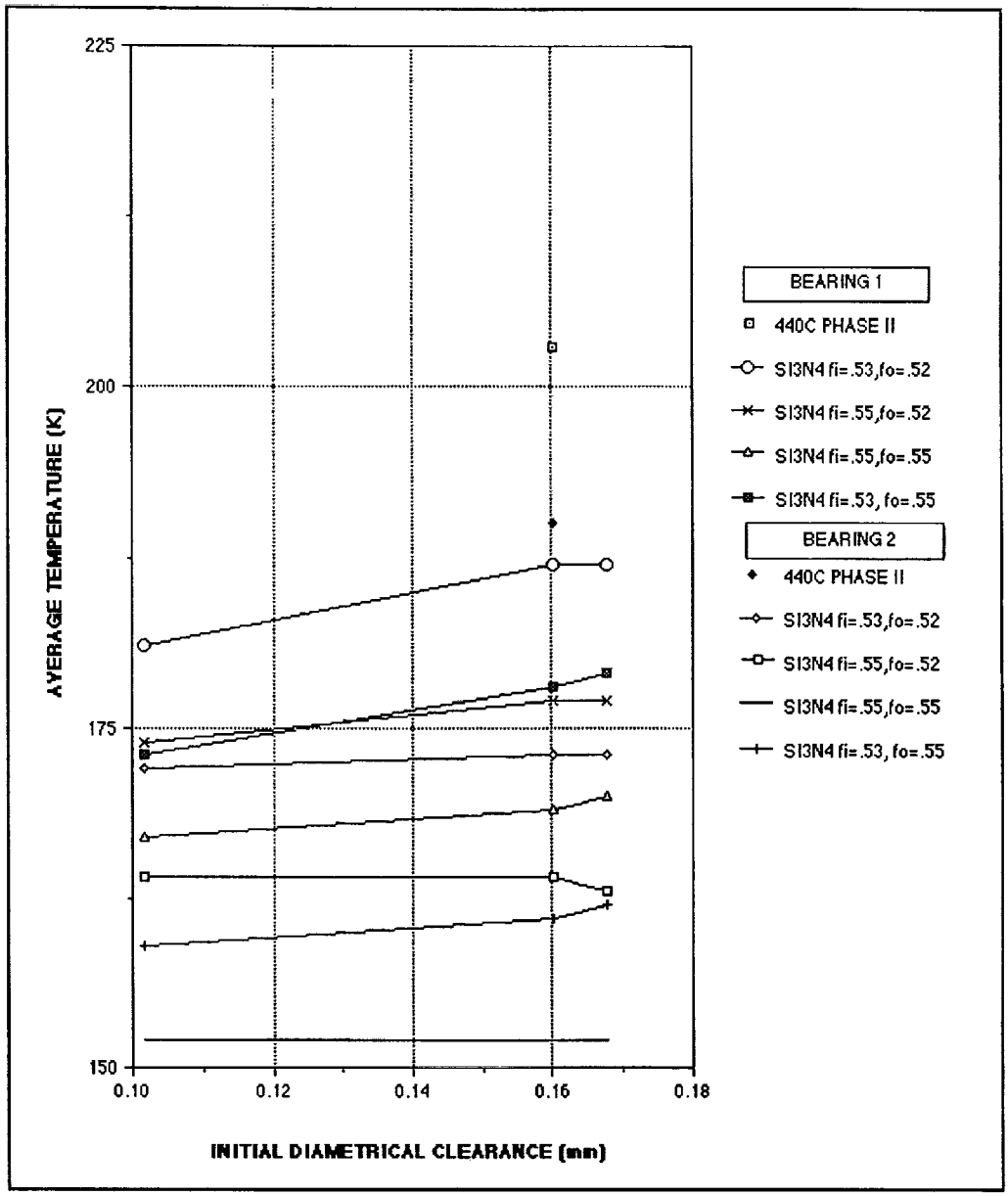

Exhibit 46 HPOTP Pump End Bearing Ball Temperature

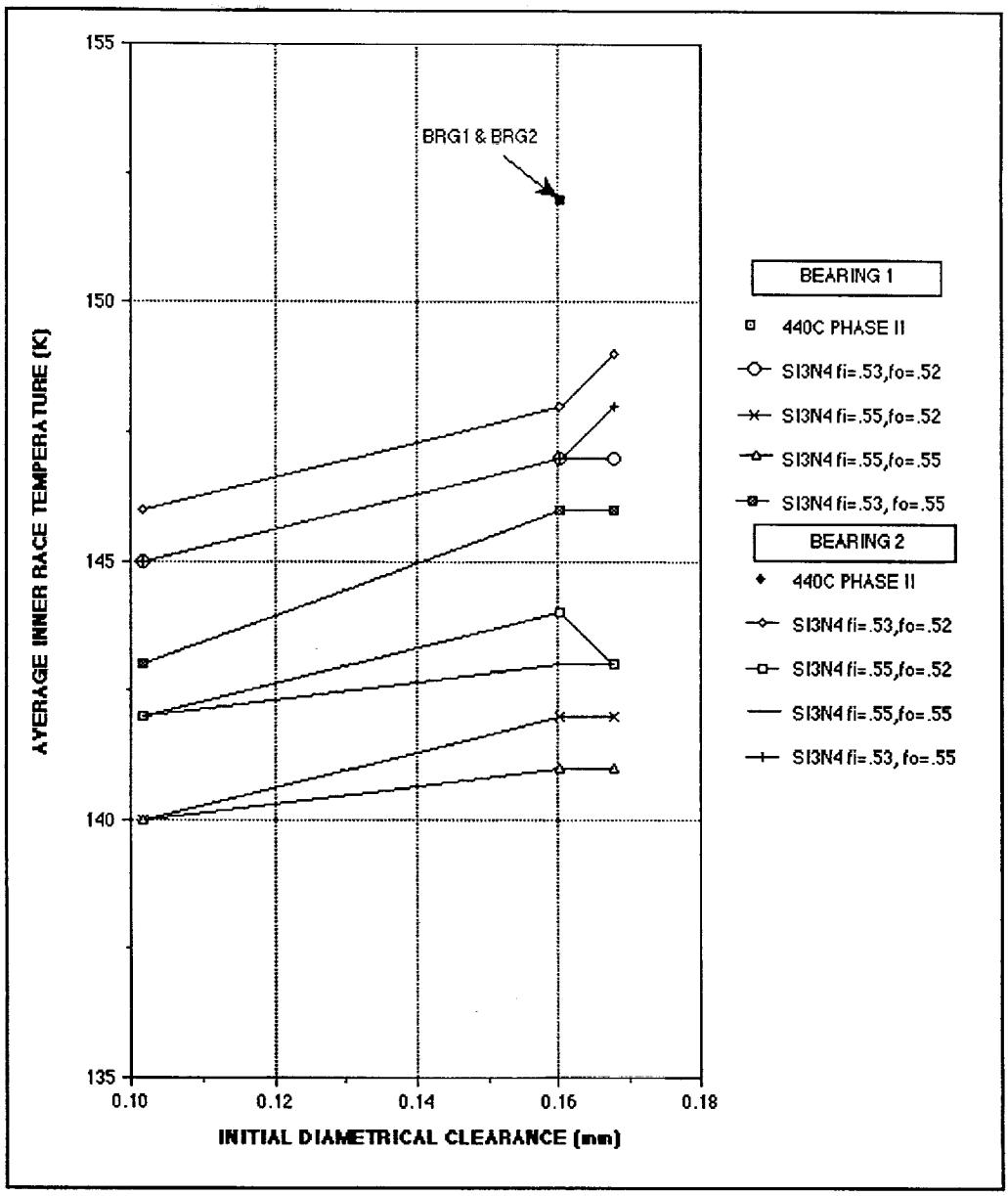

Exhibit 47 HPOTP Pump End Bearing Inner Race Temperature

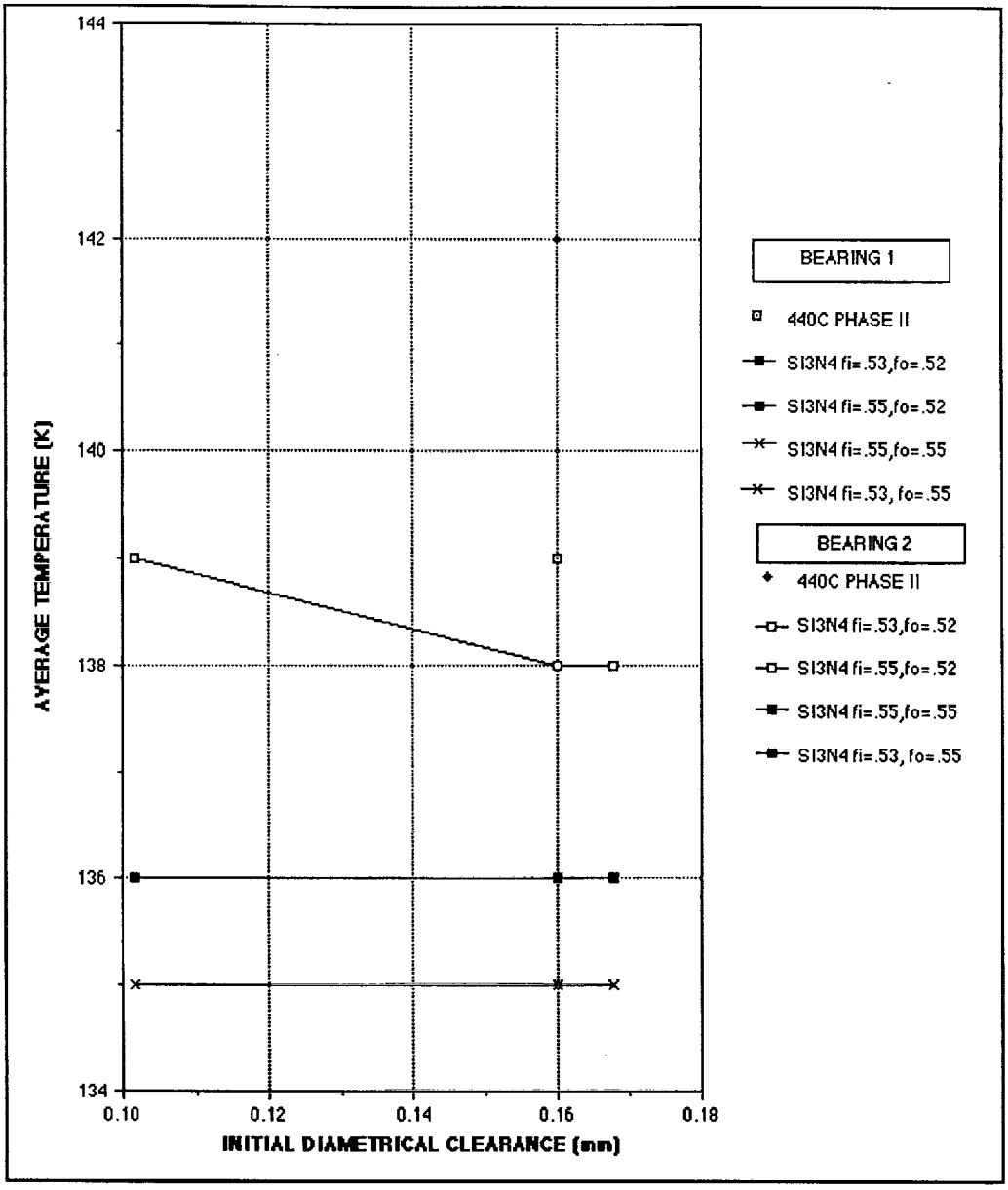

Exhibit 48 HPOTP Pump End Bearing Outer Race Temperature

reduced ball excursion. Increasing the outer race curvature to 0.55 prevented ball unloading and increased the ball excursion. The cage pocket clearance was 2.04 mm (0.08 in.). Ball excursions should be kept well below this value to prevent high ball/cage loads.

Bearing radial reactions are shown in **Exhibit 40** and axial reactions are shown in **Exhibit 41**. Increasing the outer race curvature of the Phase II configuration to 0.55 produced the highest radial reaction in Bearing 2 compared to the other configurations. Changing the outer race curvature from 0.52 to 0.55 had little effect on contact stresses as indicated in **Exhibits 42** and **43**. Heat generation as a function of initial clearance is shown in **Exhibits 44** and **45**. The outer race heat generation was reduced to approximately one-half when the outer race curvature was increased from 0.52 to 0.55. This produced about a 12-K (22°F) decrease in ball temperature in Bearing 2, as shown in **Exhibit 46**. The inner race temperature was not significantly changed as shown in **Exhibit 47**. Even though there was a two-fold decrease in outer race heat generation when the outer race curvature was increased from 0.52 to 0.55, the outer race temperature decreased only about 2-K (4°F) as shown in **Exhibit 48**. Half the heat generated at the outer race contact was assumed to go to the ball. The outer race was also effectively cooled with LOX which explained the weak temperature response to the change in heat generation.

Although increasing the outer race curvature of the Phase II configuration from 0.52 to 0.55 offered some small advantages in loads, inner race stresses, and component temperatures, these gains were not considered strong enough to support a recommended change because of extensive operating clearance with Phase II curvatures.

2.4 Assessment of Outer Race Tilt Effects on the 45 MM HPTOP Bearing Operating Characteristics

The HPOTP shaft/bearing thermomechanical model was used to investigate the influence of outer race rotation or tilt on the pump end bearings loads, stresses and thermal characteristics. The bearing configurations were Phase II with 440C rolling elements, and Phase II with Si3N4 rolling elements. Since there is a clearance or deadband between the outer race and bearing carrier, the bearing outer race is free to rotate or tilt within the constraints of this clearance. The nominal deadband was 0.1219 mm (0.0048 in.). This changes due to operating loads and temperatures to the values shown in **Exhibit 49**. The amount of outer race tilt that can be accommodated within this clearance is shown as the allowable tilt in Exhibit 49. Two estimates were made for operational outer race tilt. Tilt angles of Bearings 1 and 2 were varied until the reaction

Parameter	Phase II 45 mm Bearings with 440C Rolling Elements fi = 0.55, fo = 0.52, Pd = 0.16 mm				Phase II 45 mm Bearings with Si3N4 Rolling Elements fi = 0.55, fo = 0.52, Pd = 0.16 mm			
	Brg. 1	Brg. 2	Brg. 1	Brg. 2	Brg. 1	Brg. 2	Brg. 1	Brg. 2
O.R. Operating Dead Band (mm)	.0839	.084	.0869	.0869	.0877	.0874	.0884	.0885
Allowable Tilt (min.)	17.26	17.27	17.86	17.84	18.04	17.96	18.28	18.22
Operating Tilt (min.)	-5.16	11.0	-.344	5.16	-5.16	11.0	-.344	5.16
Ball Excursion (mm)	1.09	1.62	1.4	3.1	0.71	1.02	.842	2.16
Radial Reaction (N)	2,848	4,224	2,718	4,425	2,586	4,540	2,481	4,105
Axial Reaction (N)	4,652	4,652	3,311	3,311	4,053	4,053	2,887	2,887
Max. Hertz Stress (MPA)	2,770	3,000	2,567	2,909	3,082	3,405	2,799	3,283
Avg. Heat Generation watt/ball	I.R. 180 O.R. 97	I.R. 181 O.R. 109	I.R. 127 O.R. 63	I.R. 127 O.R. 79	I.R. 112 O.R. 55	I.R. 115 O.R. 71	I.R. 78 O.R. 33	I.R. 85 O.R. 50
Avg. Ball Temp. -K	252	235	213	194	204	186	182	165
Avg. IR. Temp. -K	174	173	156	156	152	152	144	145
Avg. O. R. Temp. -K	147	148	141	142	139	141	137	138

Exhibit 49 Bearing Operating Characteristics with Outer Race Tilt To Minimize Reaction Moments

moments were close to the opposing moments produced by the reactions to the radial loads. The unequal (circumferential) compression of the preload spring, due to outer race tilt was not considered in this case. Since the preload spring reacts to keep the two outer races parallel, neglecting the spring moments produced higher tilt angles in the moment balancing exercise. This method was expected to provide an upper limit on possible operational outer race tilt angles. The second estimate of tilt angles included the effects of the preload spring. As expected, the effect of the spring was to reduce the outer race tilt estimates, and required the outer races to become more in line or parallel. As shown in Exhibit 49, the estimated operational tilt angles were well within the capability of the deadband, and were no problems with the outer races binding or hanging up in the carrier due to loss of clearance. Other bearing operating characteristics such as stresses, ball excursion, and thermal are also shown in Exhibit 49. The Number 2 bearing with Si3N4 balls had higher radial reactions and higher contact stresses than the comparable 440C bearings. In all cases, ball excursion, axial reaction, and thermal characteristics were more favorable for the Si3N4 ball bearings. Reducing the tilt angles, reduces axial loads, contact heat generation, and bearing component temperatures.

Data from the analysis of these bearing configurations, with outer race tilt, were compared with those of a previous analysis with no outer race tilt. The results of this comparison are provide in **Exhibits 50** through **55**. Exhibit 50 compared radial and axial reactions. Allowing the outer races to tilt improved radial load sharing between Bearings 1 and 2, and increased the axial reaction. The maximum Hertz contact stresses for Bearing 2 were reduced when the outer races were tilted as shown in **Exhibit 51**. Bearing 2, for those cases without tilt, radially deflected such that some of the balls became unloaded. The bearing analysis code determined the speed of unloaded balls by assuming constant angular momentum, and that the ball travels in the outer race at zero contact angle. This causes the angular speed of the ball to decrease and remain constant until it becomes loaded. Unloaded balls therefore, reduce the average speed of the ball train. The ball excursions estimated for the Number 2 bearings, no outer race tilt, are based on the average ball train speed. Therefore, as balls become unloaded, the estimated ball excursion is reduced. As the outer race is tilted, all balls become loaded and the ball excursion increases. Further tilting of the outer race decreases the ball speed variation as shown in **Exhibit 52**. The average frictional heat generation is significantly increased when the outer races are tilted as shown in **Exhibit 53**. The loads are more uniformly distributed among the balls, increasing the average heat generation, which increases component temperatures, reduces operating clearance, and increases axial reaction. Bearing component temperature comparisons are shown in **Exhibits 54** and **55**.

Increasing outer race tilt significantly increases the bearing average heat generation. It was therefore concluded that an inner race curvature of 0.55 is preferred, to an inner race curvature of 0.53 because increasing race conformity would also increase heat generation in the contact. Allowing the outer races to tilt did not change the conclusion of the previous investigation, reported in the April 1992 progress report, that the Phase II curvatures are optimum for the Si3N4 ball bearings.

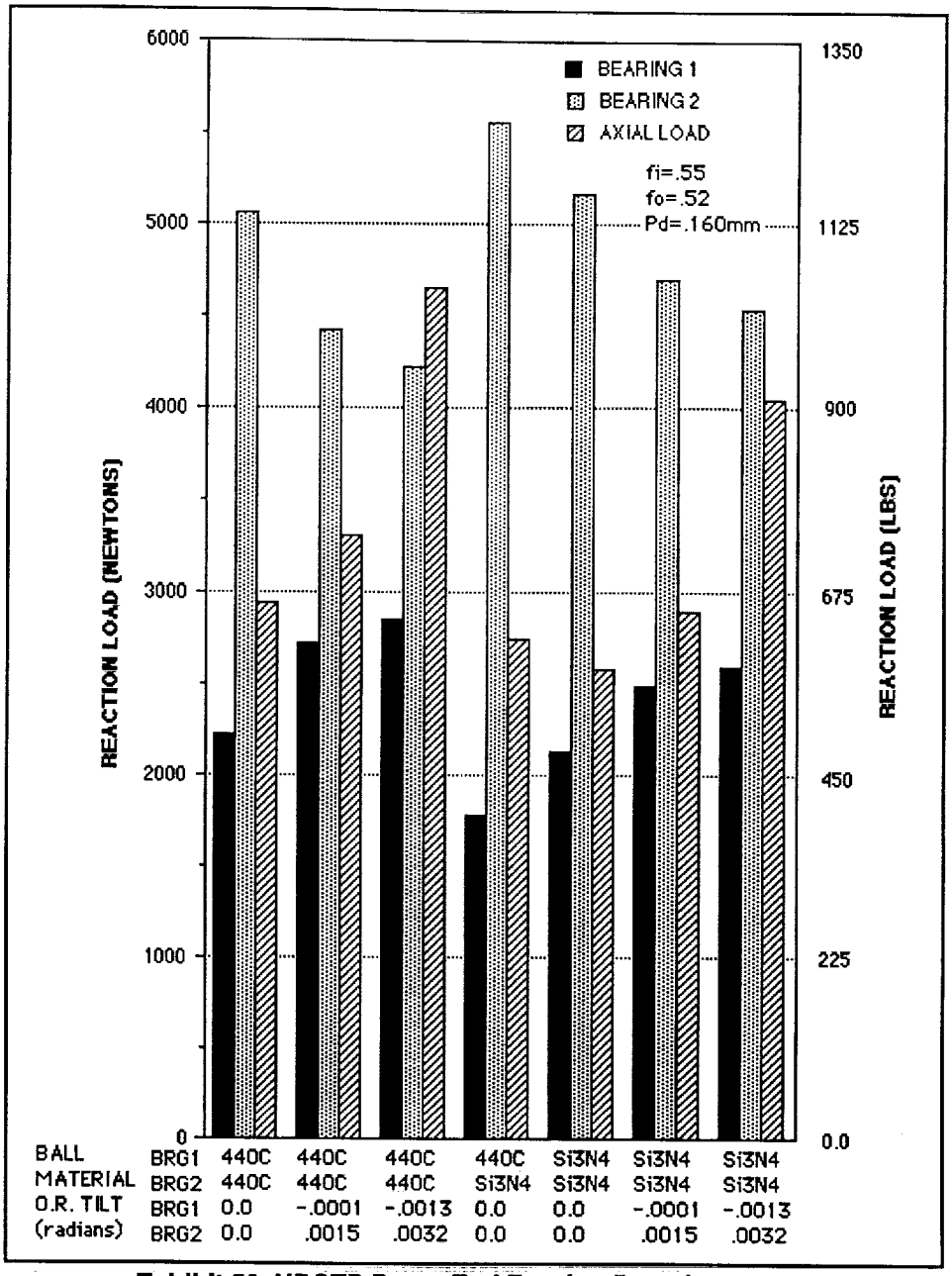

Exhibit 50 HPOTP Pump End Bearing Reaction Loads

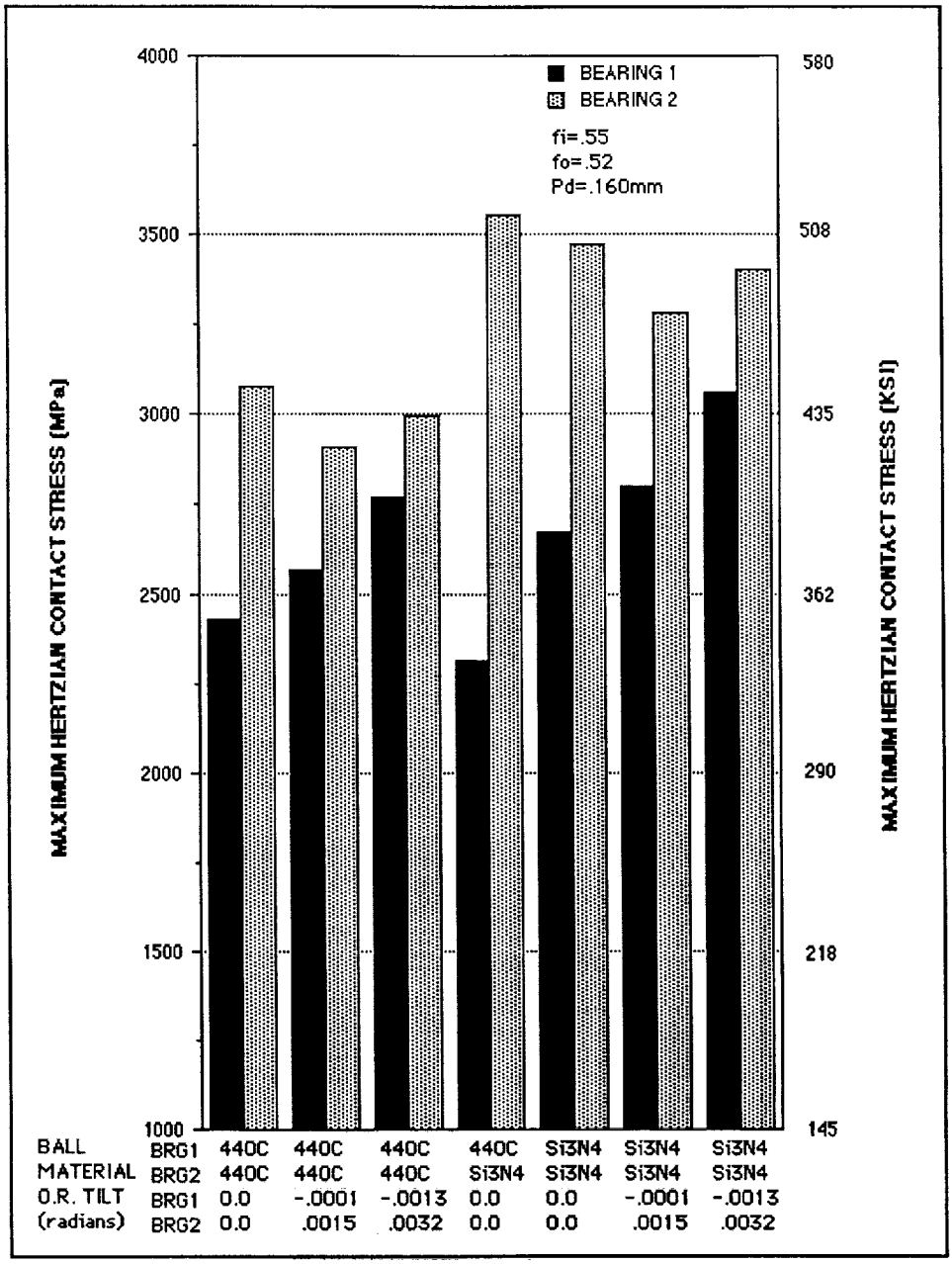

Exhibit 51 HPOTP Pump End
Bearing Inner Race Contact Stress

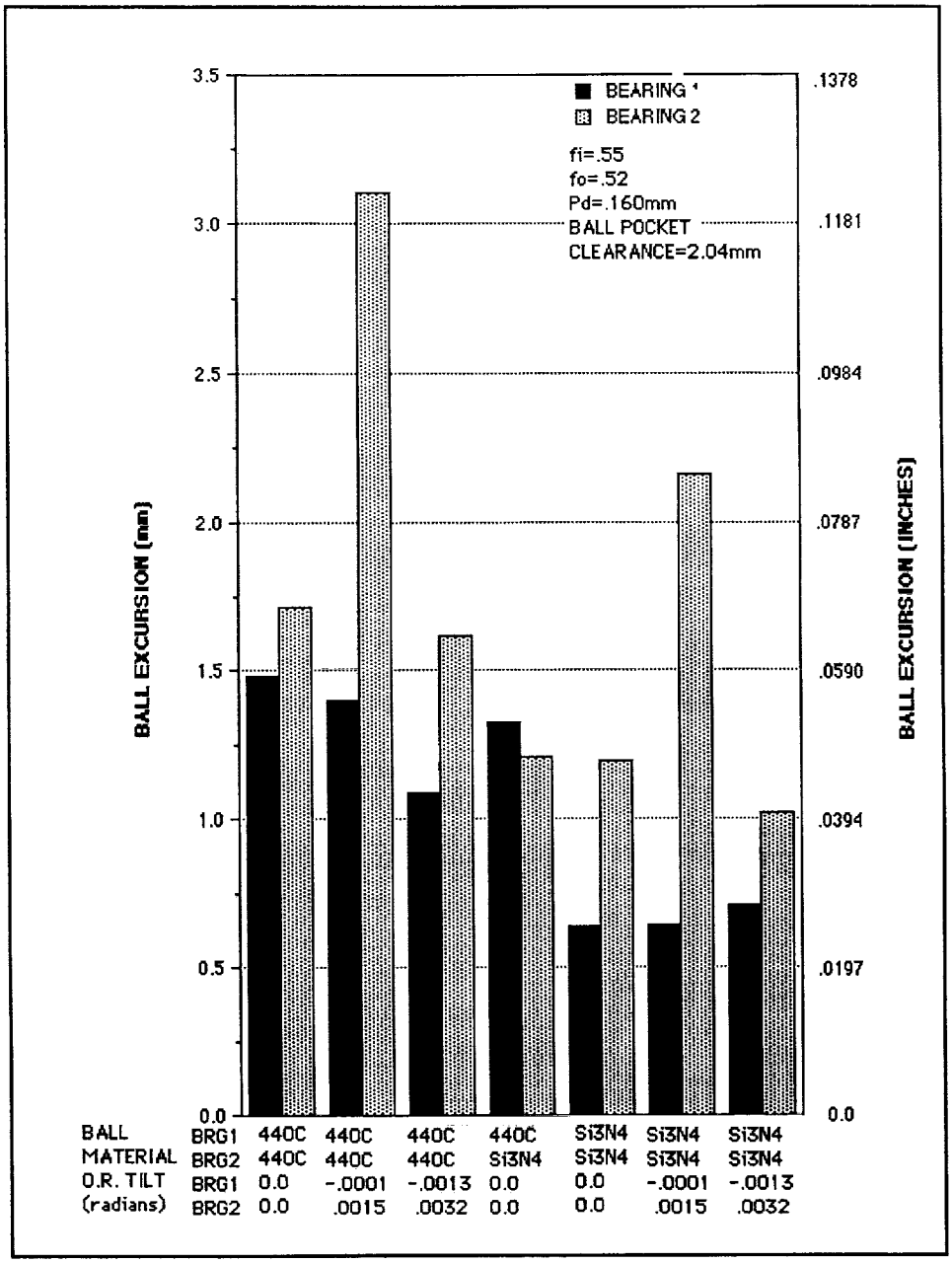

Exhibit 52 HPOTP Pump End Bearing Ball Excursion

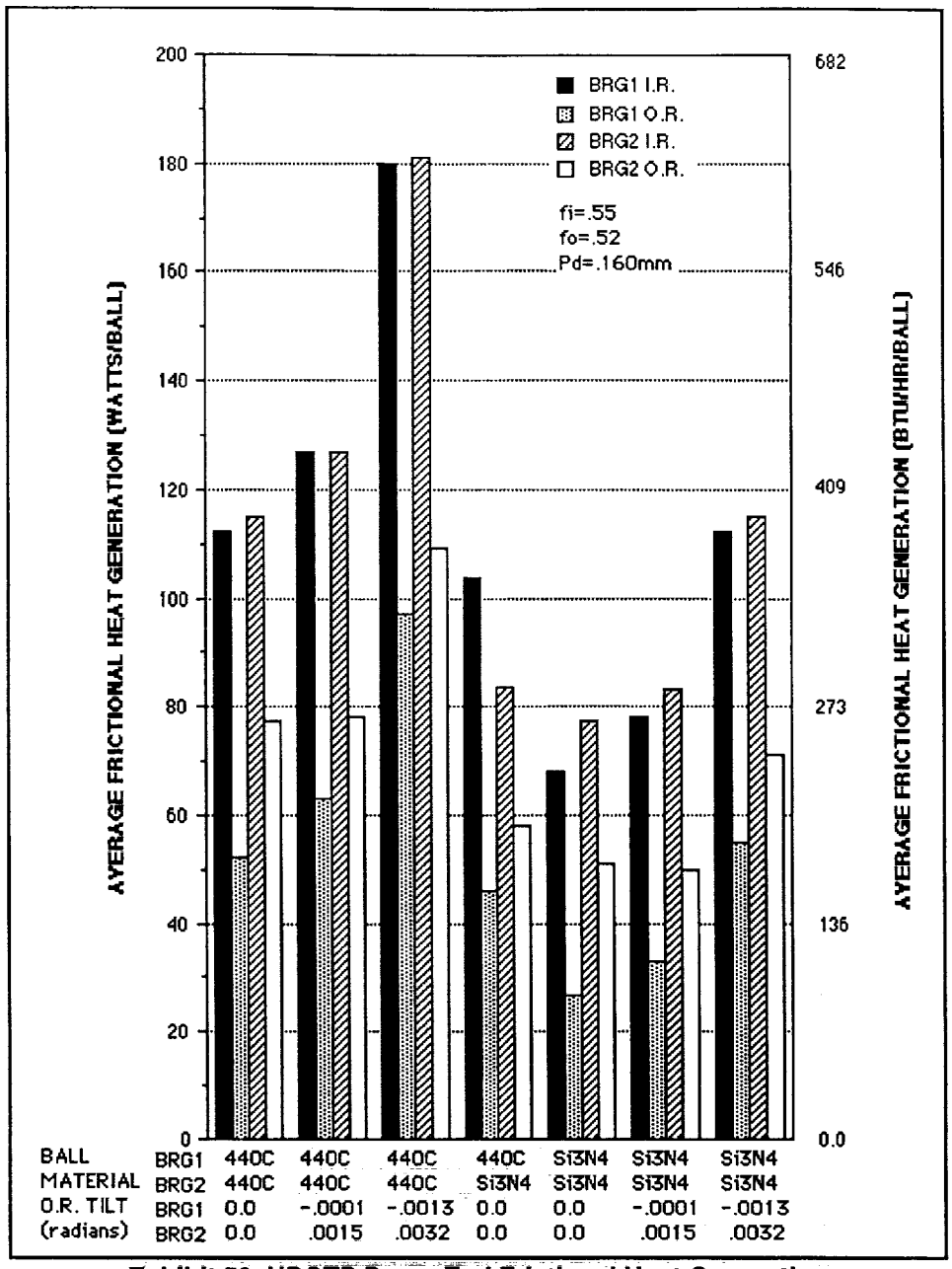

Exhibit 53 HPOTP Pump End Frictional Heat Generation

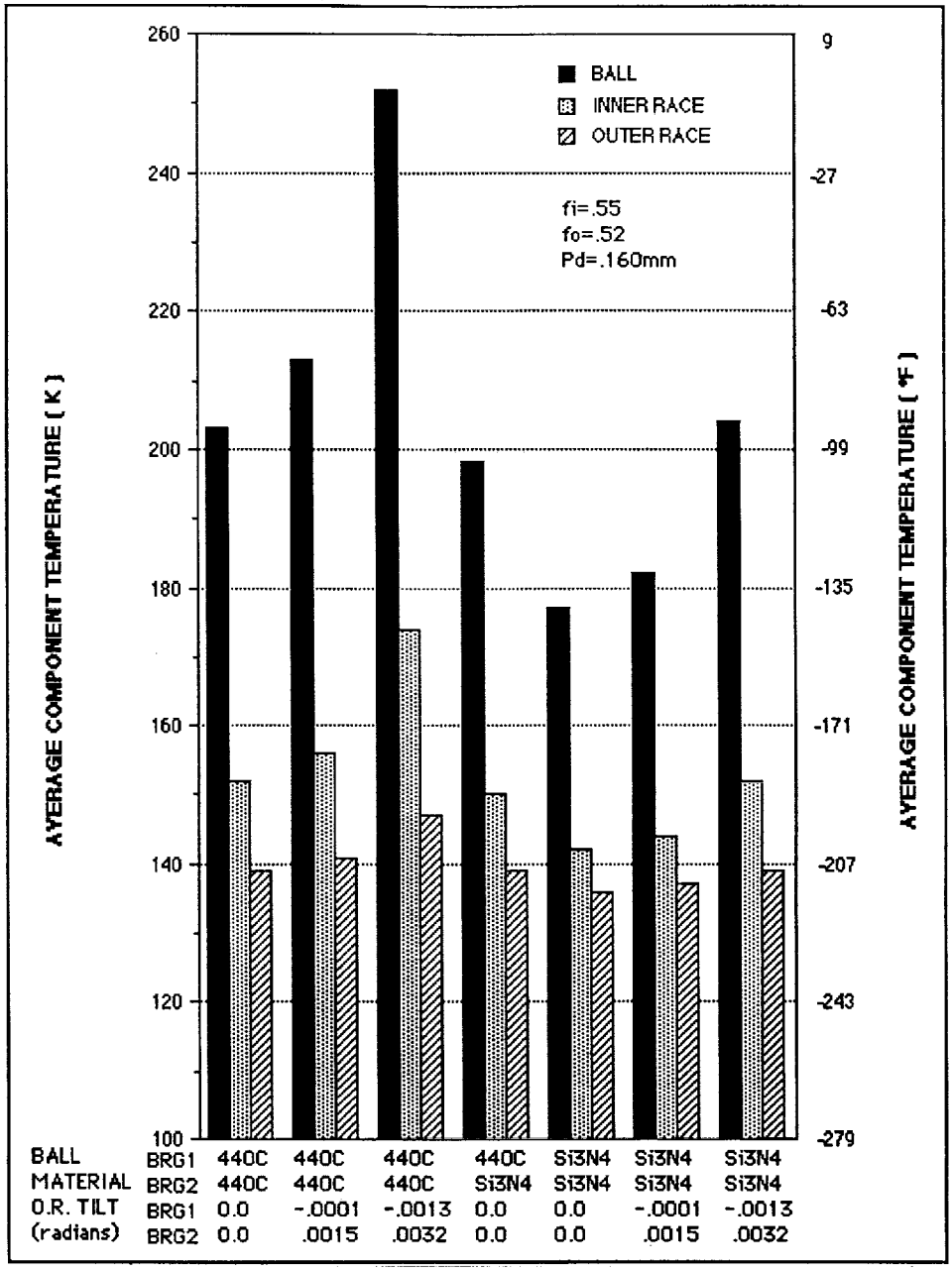

Exhibit 54 HPOTP Bearing 1 Component Temperatures

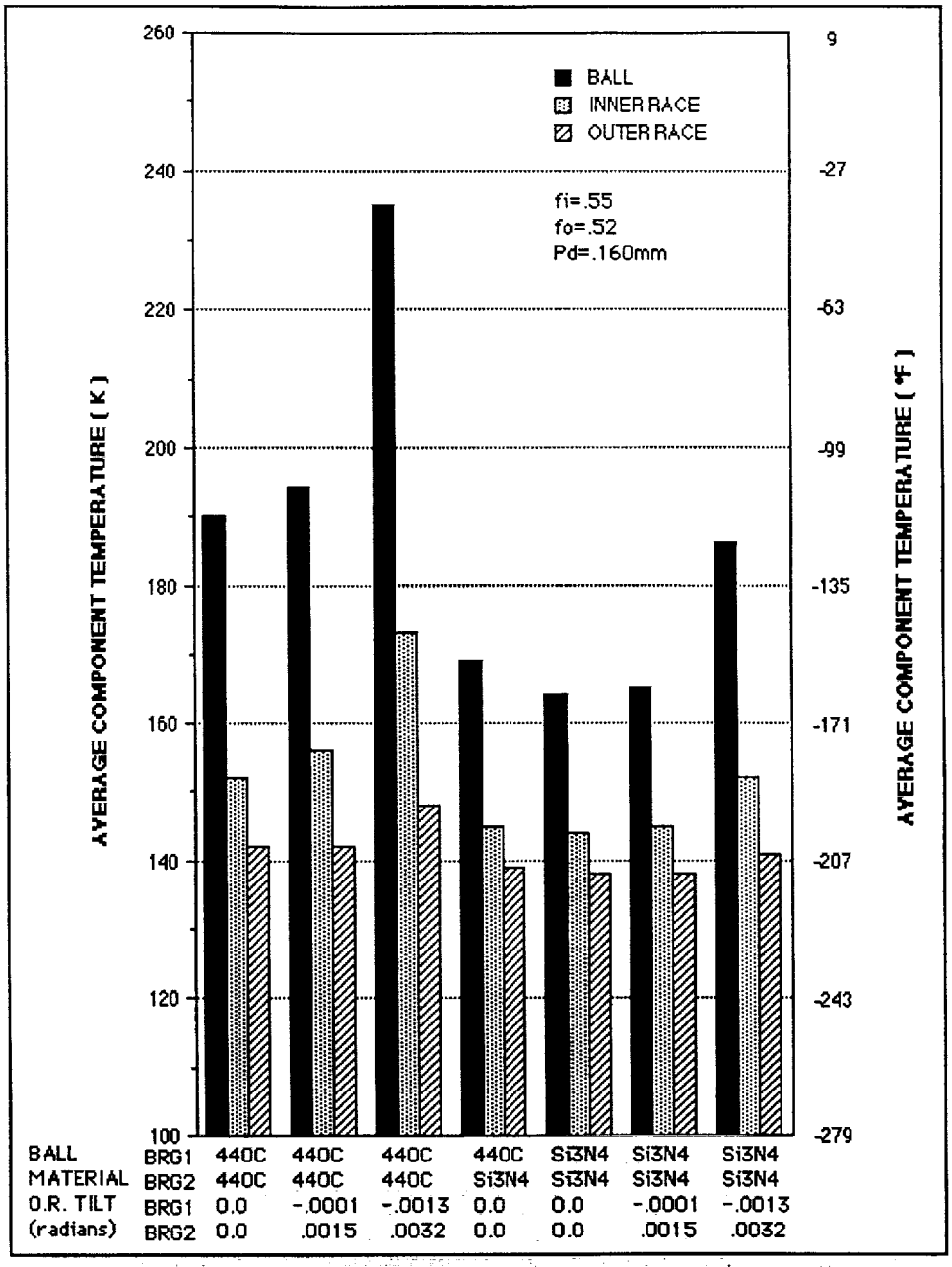

Exhibit 55 HPOTP Bearing 2 Component Temperatures

2.5 Investigation of Ball Pocket Clearances for 45 MM Bearings with Battelle Cages

Battelle cages were designed for the 45 mm bearings for use in the pump end of the SSME LOX turobpump. These cages provided a salox insert around each ball for film transfer lubrication. This required more space per ball, for the pockets, than the standard Armalon cage used in the Phase II 45 mm bearings. To increase the space per ball, one ball was deleted from the ball complement leaving eleven balls. With this modification, there was still not enough room to provide the Phase II cage pocket clearance of 2.04 mm (0.08 in.). The ball pocket clearance for the Battelle cages was 0.8 (0.031 in).

Bearing thermomechanical models were run to compare the operating characteristics of bearings with Battelle cages, and standard Phase II 45 mm bearings. The results of these runs are summarized in **Exhibit 56**. Two cases were run for each bearing configuration. One case allowed each bearing in the bearing pair to tilt (outer race) such that the resultant moment on the outer race was minimized. The second case constrained the outer race in the vertical position (zero tilt).

As shown in the exhibit, the most significant difference between the Phase II bearings, and those with Battelle cages was the difference in ball excursion and the pocket clearance to accommodate the excursions. The limited clearances in the Battelle cages could severely constrain ball movement causing increased ball pocket loads, heat generation, and ball skidding. The heat generation values shown do not include ball skidding, and consequently neither do the component temperatures. The ADORE program was used to determine the cage pocket loading for these conditions.

2.6 Investigation of Operating Stresses in the Fluoroloy-C Cage Design

Various analyses were performed to investigate and quantify operating stresses in the insert of the Fluoroloy-C cage design tested in the BSMT (Unit 2 Build 13). The tester was run for a cumulative time of 22 minutes at 30,000 RPM. This run time was approximately twice the baseline Phase II run time of approximately 10 minutes (Unit 3 Build 2). The test was terminated during the seventh rotational period due to the outer race temperature of Bearing 3 exceeding a redline of 136-K. Post test inspection of Bearing 3 revealed damaged ball pocket inserts. There were fractures and/or missing material in some of the inserts. Cage pocket to ball loads, as calculated with ADORE analysis, were not predicted to be large enough to cause the inserts to fail with the bearing operating under nominal conditions. Therefore, a study was performed to determine if the interaction of the shroud and inserts, caused

Parameter	45 mm Bearings fi = 0.55 fo = 0.52 Pd = 0.16 mm Battelle Cages, 11 Balls				Phase II 45 mm Bearings with 440C RollingElements fi = 0.55, fo = 0.52, Pd = 0.16 mm			
	Brg. 1	Brg. 2	Brg. 1	Brg. 2	Brg. 1	Brg. 2	Brg. 1	Brg. 2
Outer Race Tilt (min.)	-.344	5.16	0	0	-.344	5.16	0	0
Cage Pocket Clearance (mm)	0.8	0.8	0.8	0.8	2.04	2.04	2.04	2.04
Ball Excursion (mm)	1.4	3.06	1.41	1.36	1.4	3.1	1.48	1.36
Radial Reaction (N)	2,734	4,405	2,258	5,008	2,718	4,425	2,221	5,065
Axial Reaction (N)	3,292	3,292	2,900	2,900	3,311	3,311	2,920	2,920
Max. Hertz Stress (MPA)	2,637	2,979	2,500	3,146	2,567	2,909	2,429	3,076
Avg. Heat Generation watt/ball	I.R. O.R. 136.3 70	I.R. O.R. 139.3 87.4	I.R. O.R. 120 67	I.R. O.R. 125 86	I.R. O.R. 127 63	I.R. O.R. 127 78	I.R. O.R. 112 82	I.R. O.R. 116 77
Avg. Ball Temp. -K	220	202	207	196	213	194	203	190
Avg. I.R. Temp. -K	158	159	154	153	156	156	152	152
Avg. O.R. Temp. -K	142	143	140	139	141	142	139	142

Exhibit 56 Comparison of 45 MM Pump End Bearings and Bearings Equipped with Battelle Cages

by different coefficients of thermal expansion combined with centrifugal loading, could introduce residual stresses in the inserts which might add to ball impact induced stresses and cause the inserts to fail.

The approach used for this investigation consisted of two steps. First, a simple ANSYS model of the bronze phosphorous shroud was constructed to determine the amount of deformation of the shroud when subjected to thermal and centrifugal loads. **Exhibit 57** shows a plot of the cage geometry in room temperature, static, condition (dashed lines) overlaid by the deformed shape at speed and chilled (solid lines). The plot shows considerable shrinkage of the shroud in addition to bowing of the cross members under the spinning forces. The shroud was modeled using 3-D beam elements to represent the components of the shroud. Actual cross sectional dimensions were used to calculate section properties such as moment of inertia and product of inertia for the beam elements. The density of the beam elements representing the cross members/bend-over tabs was increased such that total centrifugal loading would represent the mass of the bronze phosphorous shroud material and also the mass of a cage insert. Each cross member sees the weight of half of an insert on either side. Modeling the cage shroud with beam elements allowed shroud displacements to be calculated accurately. However, the model needed to be further refined to solve for stresses in the shroud. For this analysis, the displacements were the critical parameter because the interference of the insert and shroud was being investigated. **Exhibit 58** lists the displacements in a cylindrical coordinate system, with the origin at the center of mass of the cage. The Z coordinate is perpendicular to the plain of the cage. The locations of the nodes are illustrated in **Exhibit 59**. The displacements were for a cage speed of 12,760 RPM and a bulk cage temperature of 116.3-K.

The second step in this investigation was to analyze the deformation of the inserts and to determine if interference occurred, and if so, how large are the induced stresses. The critical dimensions of the insert and shroud are shown in **Exhibit 60**. The coefficient of thermal expansion (CTE) of the insert is 1.044×10^{-4} mm/mm/K. This data is based on a manufacturers specification sheet for Fluoroloy-C. The CTE used in

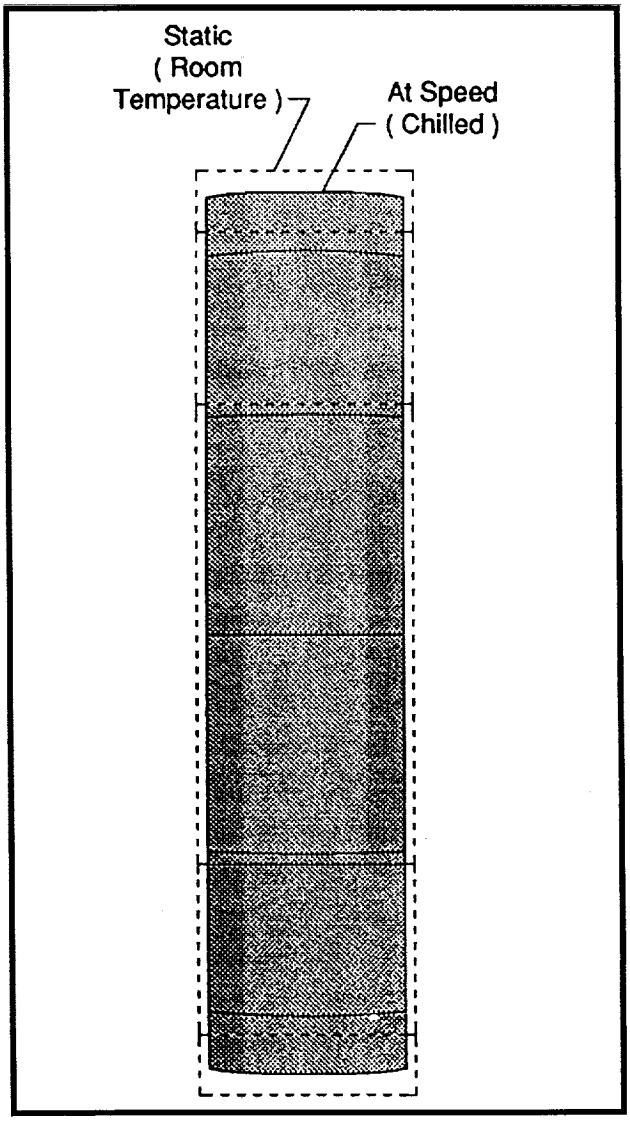

Exhibit 57 Cage Shroud Deformation at Speed and Chilled

the shroud analysis was 1.8 x 10^{-5} mm/mm/K. The shroud analysis indicated that under thermal and centrifugal loads the bendover tabs would circumferentially be 0.0541 mm closer together. Assuming that the insert shrinks by an amount of CTE* Delta Temp* L, the circumferential reduction of the insert was 0.348 mm. Therefore, the insert shrinks 0.2941 mm more than the shroud. This should cause no stress if the insert is not restrained by the bendover tabs. However, if the bendover tabs grip the insert and restrain the contraction of the insert then a circumferential tensile stress is introduced in the insert. The induced stress in the insert can be estimated by calculating the tensile force required to connect the two components if they are separated by a distance equal to the 0.2941 mm that is introduced by thermal and centrifugal forces. A simple analysis was performed assuming that the problem can be idealized as shown in **Exhibit 61**. Setting the total deflection equal to the differential deflection allowed the reaction forces to be solved by use of an equilibrium equation. Once the forces were calculated, the stresses in each component could be calculated. For this analysis, the web of area of the insert was used. This analysis yielded a tensile stress of 14.6 MPa in the insert. The tensile strength of the material is

Node	ΔR(inch)	ΔΘ(RAD)	ΔZ(inch)	ROT R (RAD)	ROT Θ (RAD)	ROT Z
18	-0.5685E-02	-0.1324E-02	-0.1127E-02	-0.1309E-10	-0.3034E-02	-0.1397E-08
22	-0.6040E-02	-0.1575E-08	-0.1127E-02	-0.2719E-10	-0.3034E-02	-0.5595E-09
23	-0.6100E-02	-0.1028E-02	-0.1128E-02	-0.4105E-05	-0.3018E-02	0.1041E-02
24	-0.6373E-02	-0.6852E-03	-0.1128E-02	-0.8549E-11	-0.3013E-02	-0.1548E-09
25	-0.6279E-02	-0.3304E-03	-0.1128E-02	0.4105E-05	-0.3018E-02	-0.1041E-02
66	-0.5685E-02	-0.1324E-02	0.1127E-02	0.1311E-10	0.3034E-02	-0.1397E-08
70	-0.6040E-02	-0.1575E-08	0.1127E-02	0.2720E-10	0.3034E-02	-0.5595E-09
71	-0.6100E-02	-0.1028E-02	0.1128E-02	0.4105E-0S	0.3018E-02	0.1041E-02
72	-0.6373E-02	-0.6852E-03	0.1128E-02	0.8558E-11	0.3013E-02	-0.1548E-09
73	-0.6279E-02	-0.3304E-03	0.1128E-02	-0.4105E-0S	0.3018E-02	-0.1041E-02
122	-0.5304E-02	-0.1324E-02	0.7513E-03	0.1114E-10	0.2586E-02	-0.1397E-08
123	-0.5036E-02	-0.1324E-02	0.3757E-03	0.6297E-11	0.1462E-02	-0.1397E-08
124	-0.4940E-02	-0.1324E-02	0.3399E-13	0.5894E-14	-0.9368E-14	-0.1397E-08
125	-0.5036E-02	-0.1324E-02	-0.3757E-03	-0.6285E-11	0.1462E-02	-0.1397E-08
126	-0.5304E-02	-0.1324E-02	-0.7513E-03	-0.1113E-10	-0.2586E-02	-0.1397E-08
Maximums						
Node	24	124	72	71	18	73
Value	-0.6373E-02	-0.1324E-02	0.1128E-02	0.4105E-05	-0.3034E-02	-0.1041E-02

Exhibit 58 Nodal Displacement of the Cage Shroud in Cylindrical Coordinates
The Coordinate System is centered at the cage geometric center with the Z axis normal to the cage.

Shroud

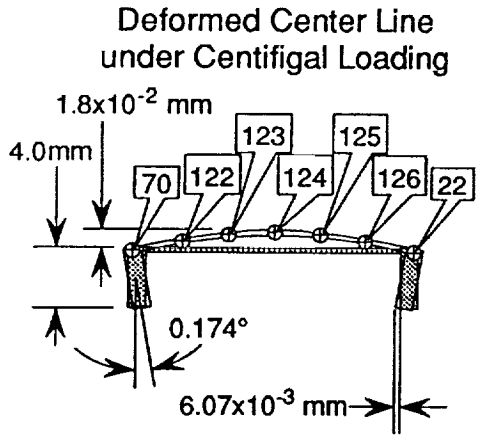

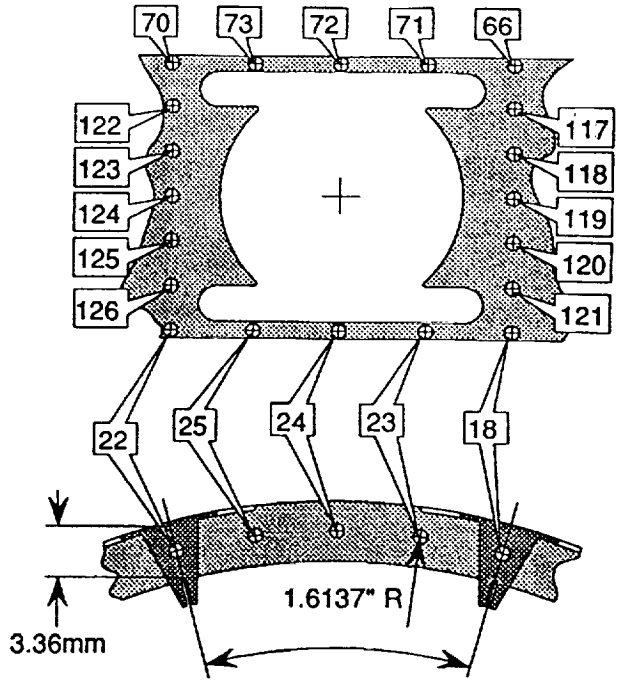

0.001324 rad / Δ Length 5.41×10^{-2} mm

Insert

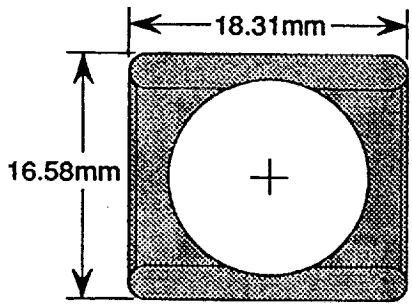

α Fluroloy-C

1.04×10^{-4} mm / mm / K T = 116K

Δ Length = 0.348 mm

Δ Width = 0.315 mm

Δ Cage Pocket Diameter = 0.299 mm

Change in Clamping Clearance $\alpha_B \Delta TL_B$ 1.8×10^{-5} (182) (3.36)

1.104×10^{-2} mm

$\alpha_F \Delta TL_F$ 1.104×10^{-4} (182) (3.36)

6.4×10^{-2} mm

Δ Clamping Clearance $6.4 \times 10^{-2} - 1.104 \times 10^{-2} = +5.29 \times 10^{-2}$ mm

Exhibit 59 Shroud Model Nodal Locations

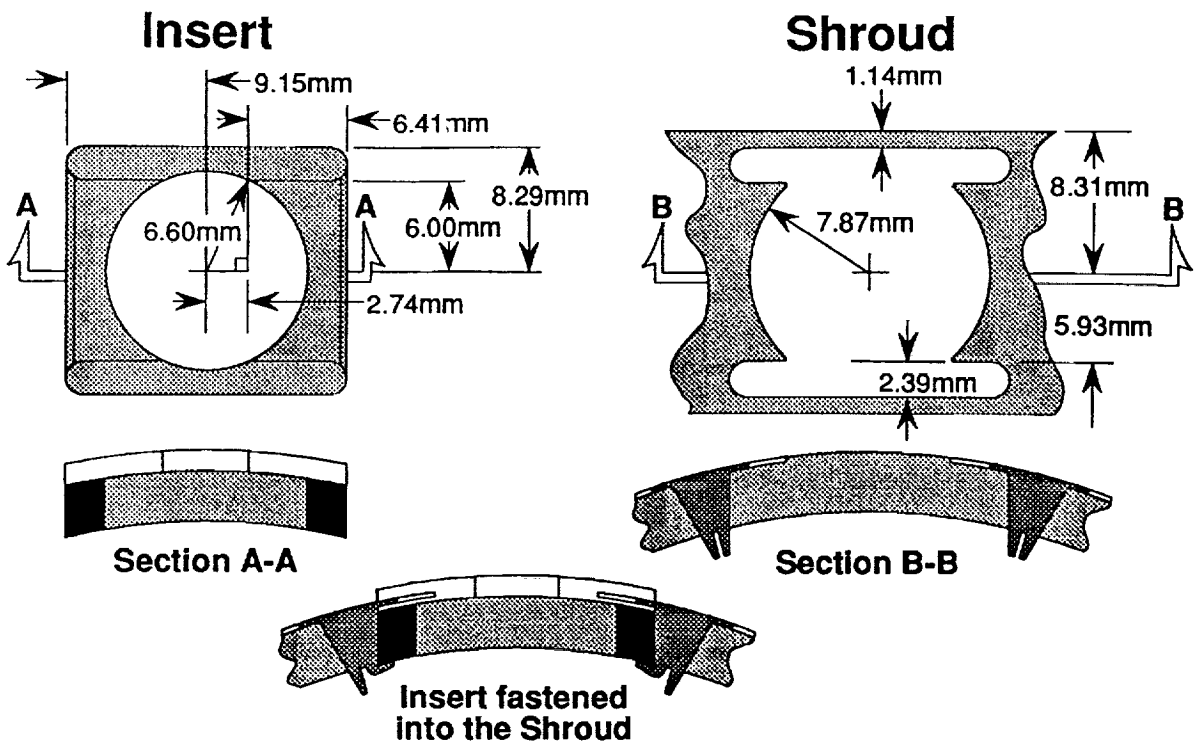

Coefficients of Thermal Expansion

Insert α 1.04×10^{-4} mm / mm / K

Shroud α 1.8×10^{-5} mm / mm / K

Interfacing Surface Thermal Deformations

Insert 1.04×10^{-4} (182) (6.00) = 0.1135mm

Shroud 1.8×10^{-5} (182) (5.93) = 0.0194mm

L_{ICOLD} = 5.8865mm

L_{SCOLD} = 5.9106mm

Interference 5.8865mm - 5.9106mm = -0.0241mm

Transverse Stresses assumming all deformation occurs in the Insert

$$S = \frac{PL}{A_{web} E_i} \qquad S = 0.0241\text{mm}$$

$$P = \frac{0.0241\ A_{web} E_i}{5.8865}$$

A_{web} = 0.1005 (0.1325) = 0.01331625"

E_i = 0.93GPa

P = 32.65 N

$\sigma = P/A_{web}$ = 3.9 MPa

σ for 3X stress concentration = 11.4 MPa

Exhibit 60 Cage Shroud and Insert Dimensions for Fluoroloy-C Cage

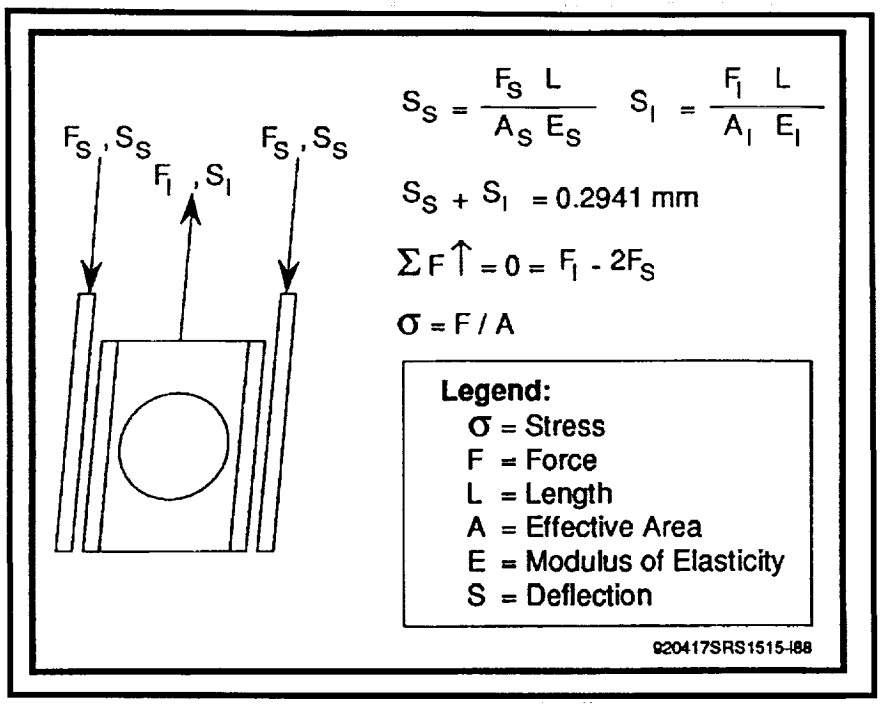

Exhibit 61 Idealized Model to Calculate Stresses Due to Bend-Over Tab Constraint

12.41 MPa to 15.16 MPa. These stresses were calculated based on using an elastic modulus of 0.93 GPa for the Fluoroloy-C which was the published value for room temperature modulus. The low temperature modulus would be higher resulting in higher insert stresses. On the other hand, this analysis assumed perfect claming of the insert with no cold flow. In actuality, perfect gripping will not be achieved, thus, from a displacement prospective, this is a worst case scenario. It should be noted that several new and previously tested cages were visually inspected to determine if the bendover tabs appeared to tightly grip the insert. The tabs appeared to be tight but not actually clamp into the material. Therefore, we do not believe that significant tensile stresses would be introduced through this phenomenon.

The potential for interference of the cage and shroud in the bearing axial direction was also investigated. This analysis determined that the guide land rails on the insert could interfere with insert retainers on the shroud. It was found that reducing the bulk cage temperature to 116.3-K would cause an interference of 0.0241 mm. Assuming a room temperature modulus for the Fluoroloy-C, then a stress of 3.9 MPa would be developed. Stress concentrations or a higher low temperature modulus could increase these stresses by as much as a factor of three. Evidence of these axial thermally induced was obtained by performing a static chill down test of the Fluoroloy-C cage design. In this t est, a cage was dunked into LN2 and allowed to chill down, then removed and inspected. Cracks were observed running in the circumferential direction in the fore and aft areas of several of the inserts. Based on the results, it was believed that the incorporation of additional clearances between the insert retainer and the insert or the development of stress relieving interfaces needed to be further investigated.

Two additional cage insert/shroud interference possibilities were investigated. First, the possibility of the side rails rotating and pinching the insert was investigated. The ANSYS analysis predicted that the side rails would rotate by 0.174 degrees each as indicated in Exhibit 59. This resulted in a loss of clearance of 0.012 mm at the inner radius of the cage. However, the differential thermal expansion of the insert exceeded this amount, therefore, there was no interference due to this rotation effect. The final deformation case

investigated was stresses developed due to bowing of the cage insert separators under centrifugal loading. The ANSYS model predicted that the centerline of the retainer would radially deflect 0.019 mm at a cage speed of 12, 769 RPM. A simple analysis was done to predict what stresses this bowing would introduce into the cage insert. The stresses predicted were negligible.

In conclusion, it appears that two sources of interference induced stress could contribute to failure of the inserts during operation. Stress can be created in the circumferential direction if the tabs exert a sufficient clamping force on the insert. However, inspection of the hardware indicated that this scenario was not probable based on the relatively light clamping observed in the cages examined. On the other hand, simple testing showed that axial stresses were introduced by chill down. Therefore, increasing the clearance between the insert retainer and insert or developing a stress relieving interface was considered.

2.7 Comparison of Cage Loads for BSMT Testing of Battelle Cages

The abrasive action of the glass fibers in ARMALON cages of the SSME LO_2 turbopump bearings was a contributor to rolling element wear in the bearings. Therefore, advanced cages using SALOX ball retainers were developed as an alternative to ARMALON cages. Traction testing has shown advantages of SALOX (Bronze/Teflon) over ARMALON (Teflon laminated glass fibers) in terms of transfer film development and traction coefficient. The advanced cages were manufactured specifically for the LO_2 pump bearing application by Battelle. Cages had been developed for the 45mm pump end bearing and for the 57mm turbine end bearings. The cages for the 57mm bearing have been tested in the BSMT and showed potential for improving bearing life. However, the BSMT as it was configured could not test the 45mm bearings. Testing of the 45mm bearing cages was planned for the Technology Testbed (TTB) engine at Marshall Space Flight Center. The 45mm bearing cage design was similar to the 57mm bearing cage with the exceptions of size and cage pocket geometry. The 45mm bearing cage used elongated cage pockets to accommodate large ball excursions caused by radial loads. Because of the difference in cage pocket geometry, it was desired to obtain some validation test data prior to live fire testing of the 45mm bearing cages in the TTB. Therefore, a set of 57mm bearing cages were modified to emulate the cage pocket clearances of the 45mm bearing cages. The modified cage pockets had a circumferential clearance of 2.03 mm (0.080 in) and an axial clearance of 0.066 mm (0.026 in). A BSMT test series was later conducted using 57mm bearings with the modified Battelle cages. The axial and radial loads applied to the BSMT test bearings were specified to emulate operating stresses, ball excursions, and cage loads that were anticipated for the 45mm bearings in the LO2 pump on TTB.

ADORE analysis was performed to compare the cage loads for the modified 57mm bearing cage in the BSMT to the 45mm bearing cage in the LO2 pump. It was found that the magnitude and nature of the cage loading was similar for the two cases modeled. **Exhibit 62** shows a comparison of cage guide land loads and cage mass center orbits for the 45mm and 57mm bearing cages. Both the upstream and downstream guide lands of both cages experienced peak loads of 222N to 266N (50 lbs to 60 lbs). The orbits of both cages were also similar indicating similar dynamic characteristics. Both cages tended to whirl with stable motion. The 45m bearing cage

orbit was slightly more erratic, however both cages interacted with the guide land only once during each orbit producing similar contact loads. **Exhibit 63** shows a comparison of cage pocket loads for the two cases modeled. The frequency and magnitude of cage loading is very similar for both cases. Both bearing cages showed occasional peak loads of up to 445N (100 lbs) with typical contact loads of 267N (60 lbs). The results of this analysis indicated that the BSMT testing of the modified 57mm bearing cage would produce loading very similar to the loading that would be experienced by the 45mm bearing cage in the HPOTP. Additional analysis was required to compare stresses in critical parts of the cage.

The SINDA/SHABERTH program was used to analyze the steady-state operation of the Battelle cage in the 45mm bearings. The pump end bearings were simulated with two operating tilt modes. One mode imposed no tilt of the outer races. The other mode balanced the moments on the outer races to estimate operating tilts of -0.0001 rad for the outboard bearing and 0.0015 rad for the inboard bearing. The results of the Battelle cage simulation for loads, contact stress, heat generation, and temperatures were compared to the standard Phase II 45mm bearings in **Exhibits 64** through **69**. The analysis showed that these parameters were only slightly increased with the Battelle cage due to the removal of the one rolling element. The simulation also investigated the use of the Battelle cage in the inboard position (Bearing 2) and a standard bearing in the outboard position (Bearing 1). The results were virtually identical to the previous results with Battelle cages in both bearings.

Ball excursions or ball to cage loads were the main concern for the Battelle cage design. It was desired to test the cage in the BSMT with 57mm bearings to the same level of cage loading as expected in the pump end bearings of the HPOTP. **Exhibit 70** shows the predicted ball excursion for the standard Phase II bearings and the bearings using the Battelle cage for both tilt scenarios in the HPOTP. The inboard bearing had the largest excursion because it had the larger radial load. The simulation predicted that with no outer race tilt, Bearing 2 excursion would be less than the pocket clearance but only because the balls opposite the high radial load became unloaded. However, when tilted, all the balls stayed loaded and the ball excursion was predicted to exceed the 2.03 mm (0.08 in) pocket clearance by approximately1.0mm (approximately0.04 inches) for both cage designs. Review of standard Armalon cages from Phase II 45mm bearings that had been run in HPOTPs was later performed in an effort to determine if the ball excursions were near the magnitude that the simulation predicted. One reason for the questioning of the predictions was that they were based on the best estimates of radial loads given by Rocketdyne.

Continuing under the assumption that the predicted ball excursion for the HPOTP bearing was reasonably accurate, the operating conditions for the BSMT needed to produce similar ball excursions in 57mm bearings with Battelle cages (12 balls) was determined. It was predicted, using the same analysis tools, that if the test bearings were loaded with 2890 N (650 lbs) axial and 3115N (700 lbs) radial load and run at 30,000 RPM, the ball excursion would be 1.83 mm (0.072 in) with no tilt (Case 1) and 2.18 mm (0.086 in) with 0.0010 rad of outer race tilt (Case 2) as shown in **Exhibit 71**. These values were very near the pocket clearance of 2.03 mm (0.08 in). To achieve the high values of ball excursion predicted for the HPOTP Bearing 2, the radial

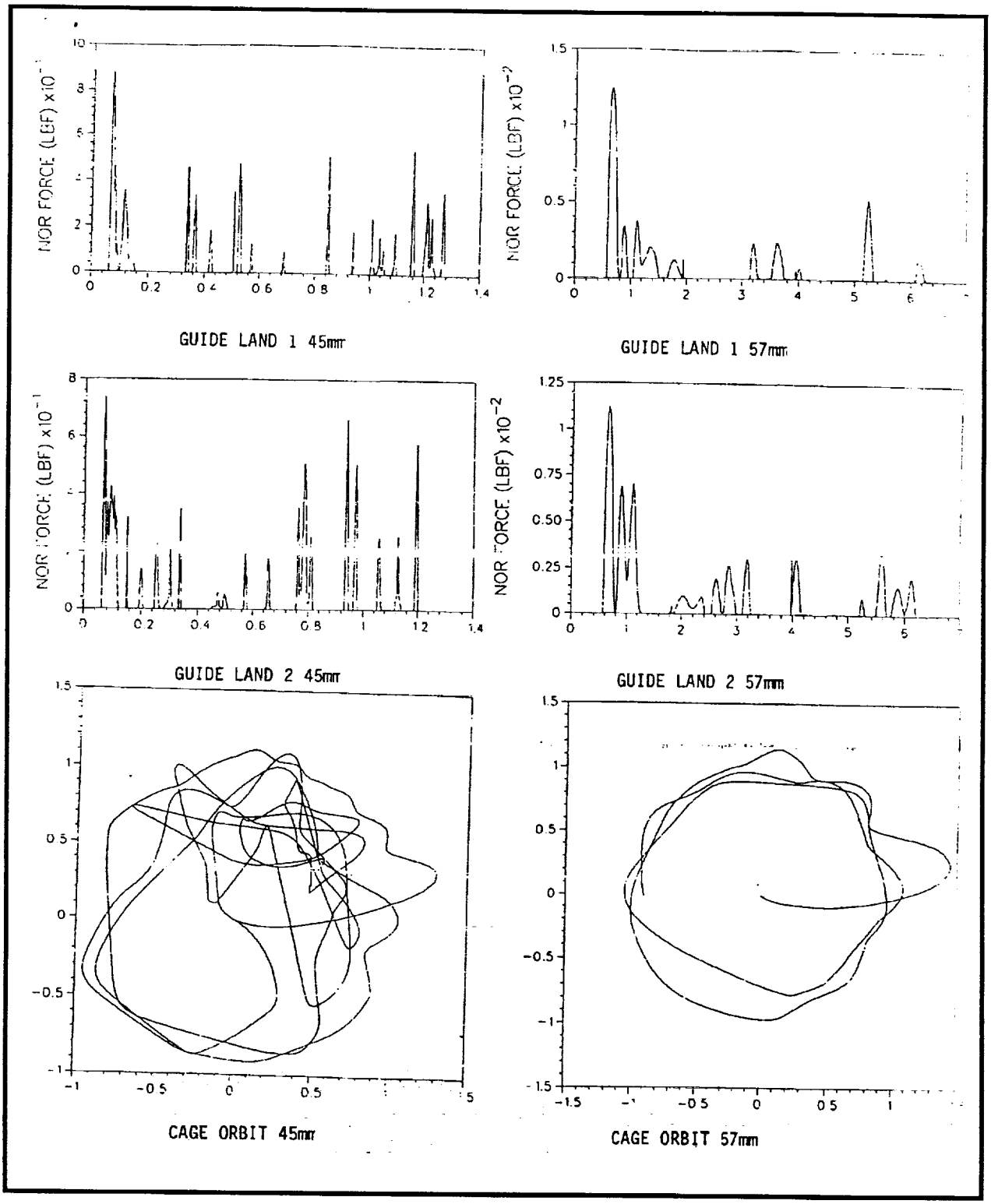

Exhibit 62 Comparison of Cage Guide Land Loads Versus Bearing Rotation and Cage Orbits for 45MM Bearing in Pump to 57MM Bearing in BSMT (Battelle Cages)

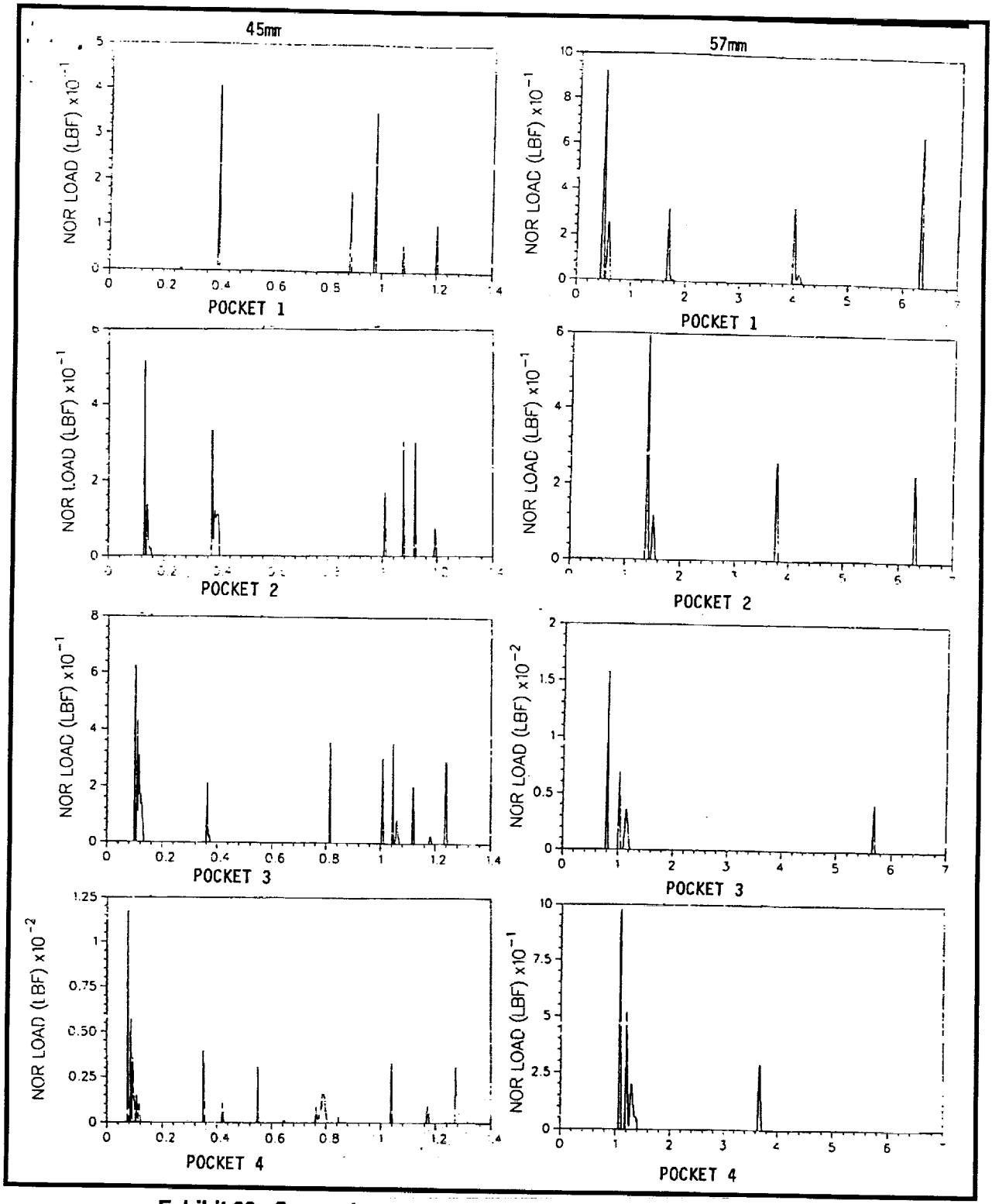

Exhibit 63a Comparison of Cage Pocket Loads for 45MM Bearing in Pump to 57MM Bearing in BSMT (Battelle Cages)

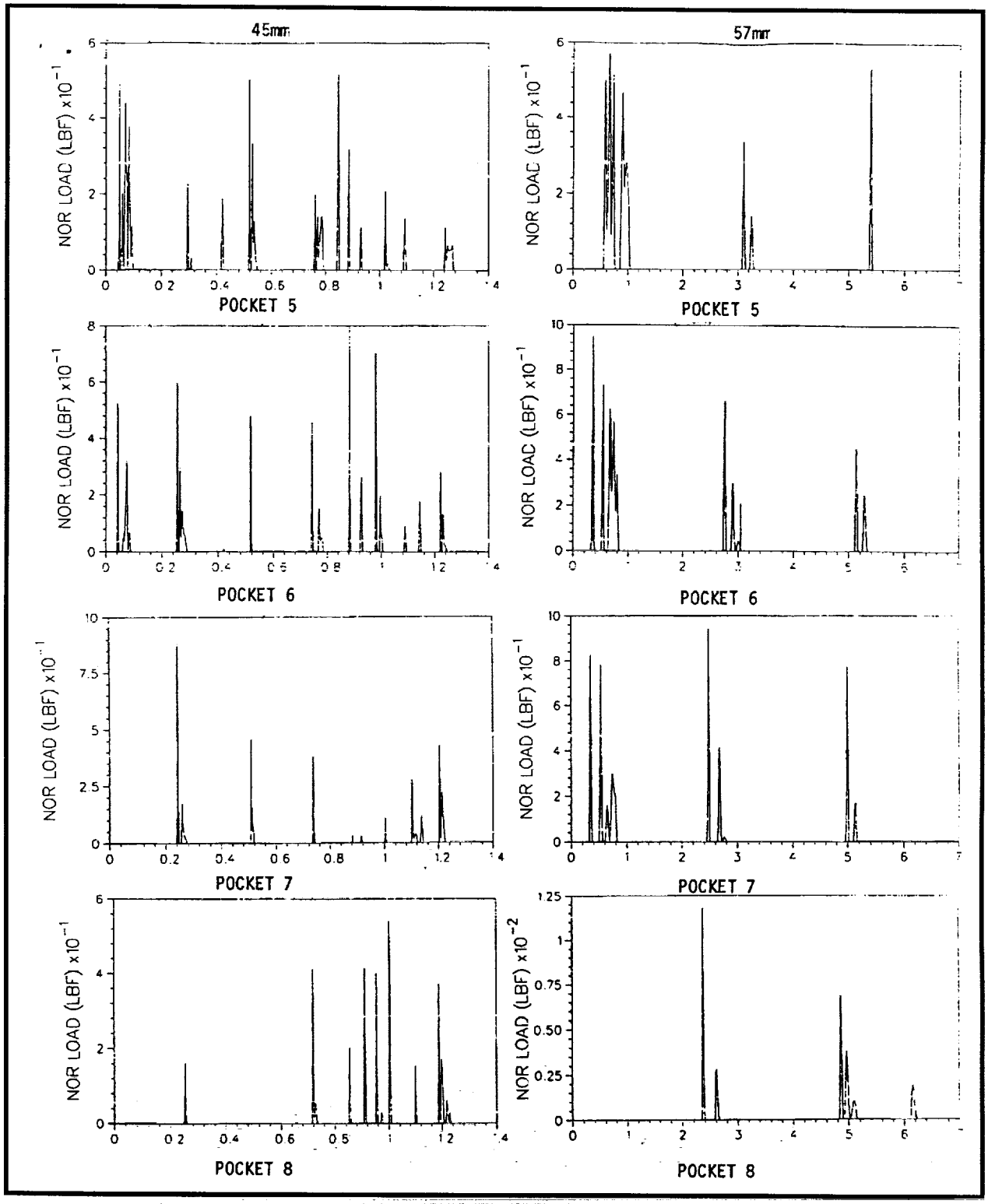

Exhibit 63b Comparison of Cage Pocket Loads for 45MM Bearing in Pump to 57MM Bearing in BSMT (Battelle Cages)

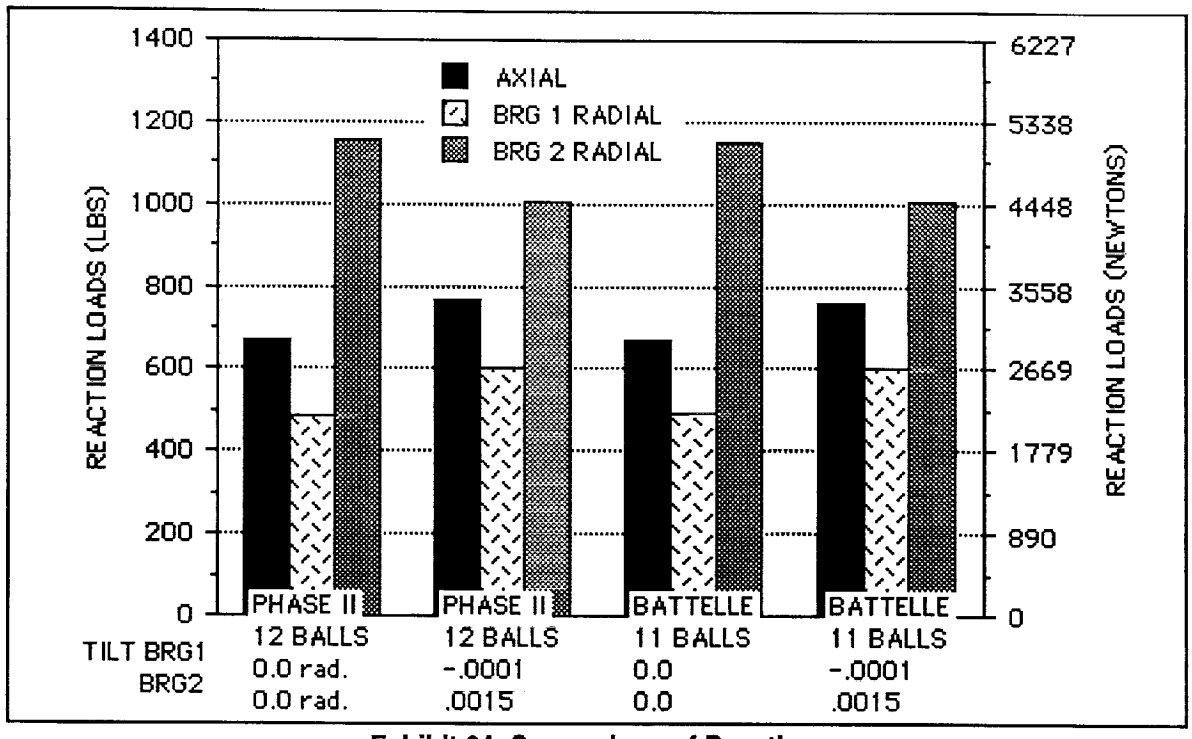

Exhibit 64 Comparison of Reaction Loads for HPOTP 45MM Bearings

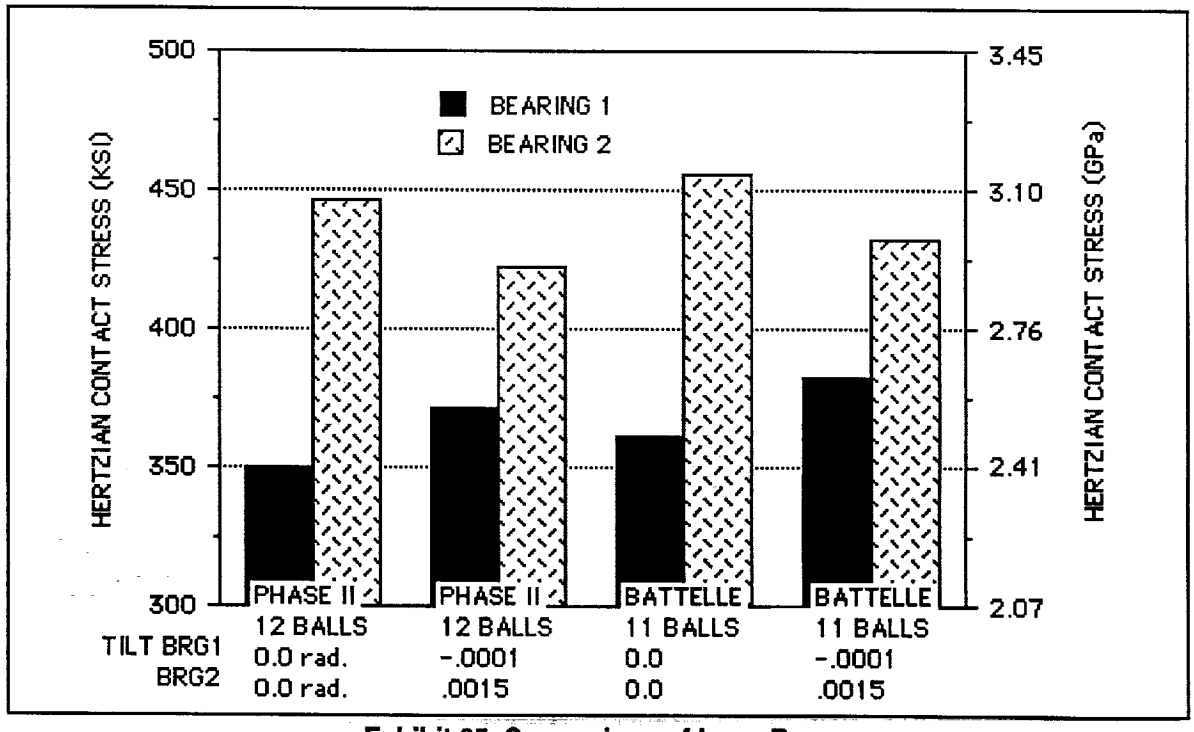

Exhibit 65 Comparison of Inner Race Contact Stress for HPOTP 45MM Bearings

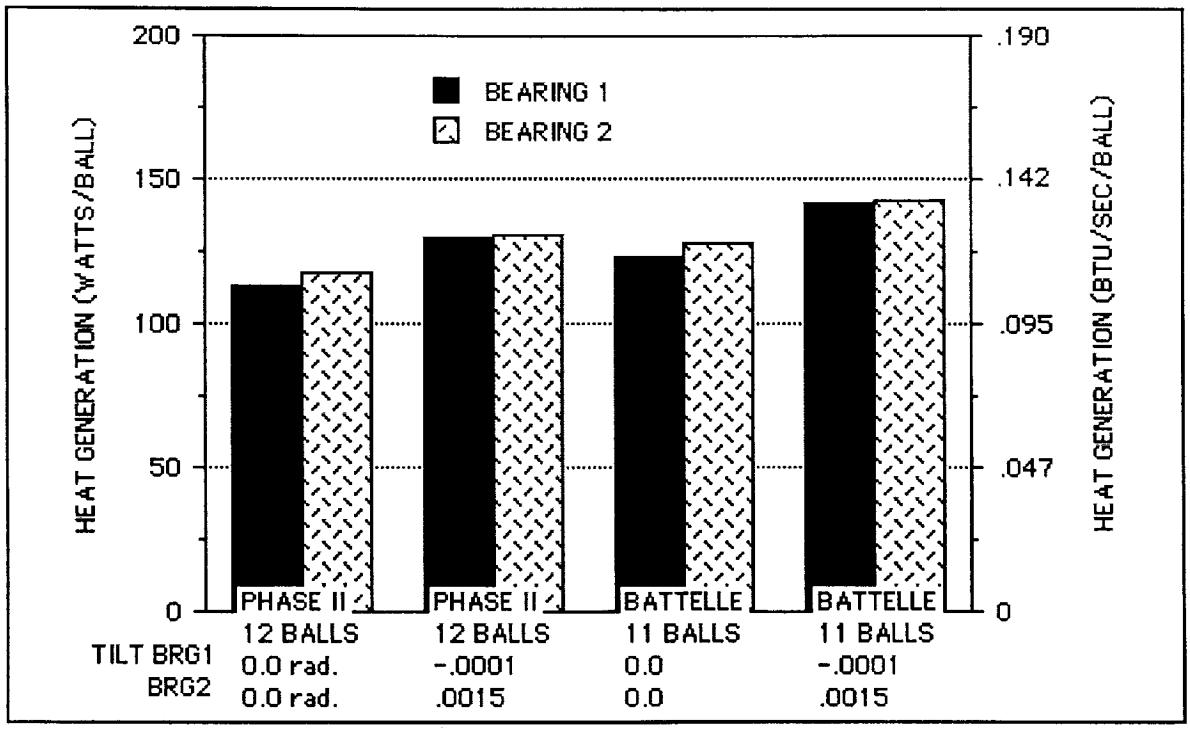

Exhibit 66 Comparison of Inner Race Heat Generation HPOTP 45MM Bearings

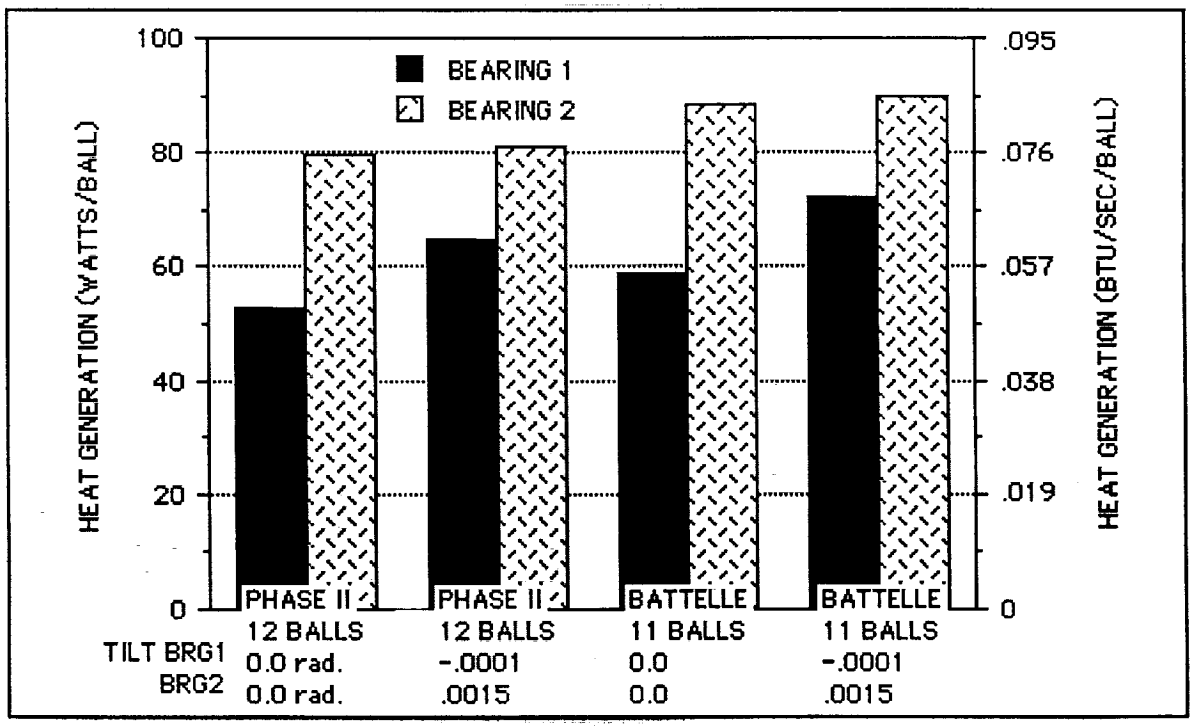

Exhibit 67 Comparison of Outer Race Heat Generation for HPOTP 45MM Bearings

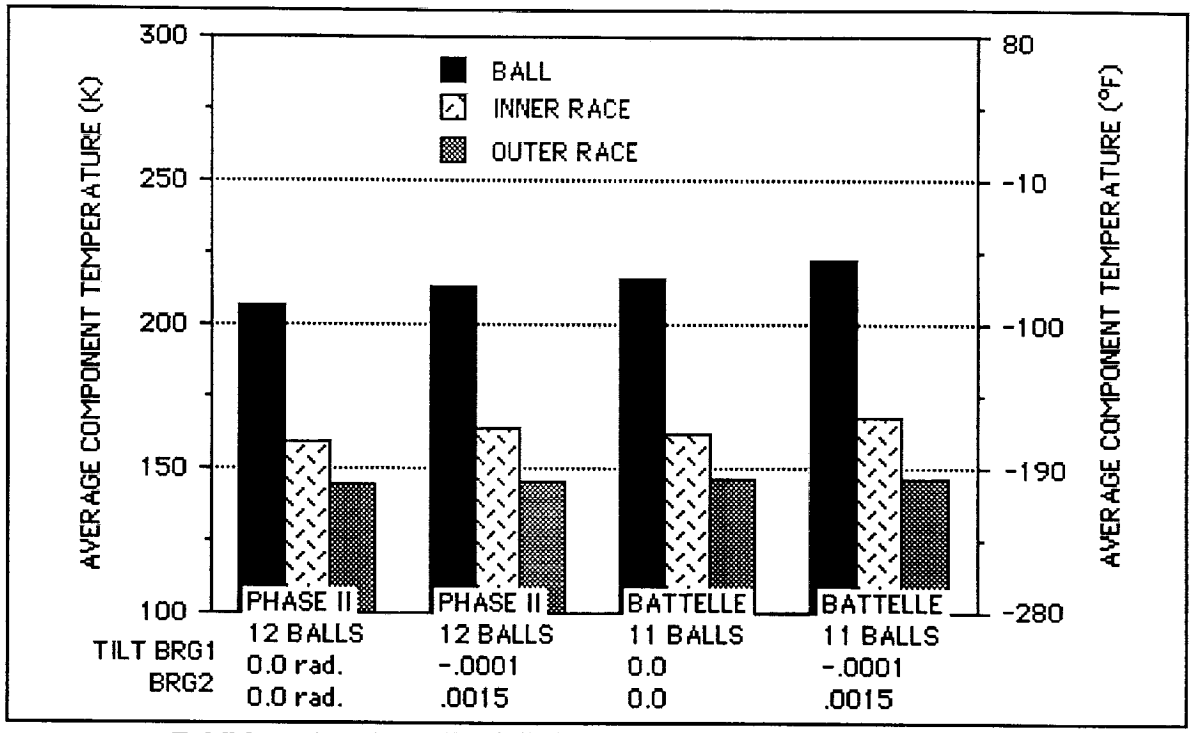

Exhibit 68 Bearing 2 Temperatures for HPOTP Pump End Bearings

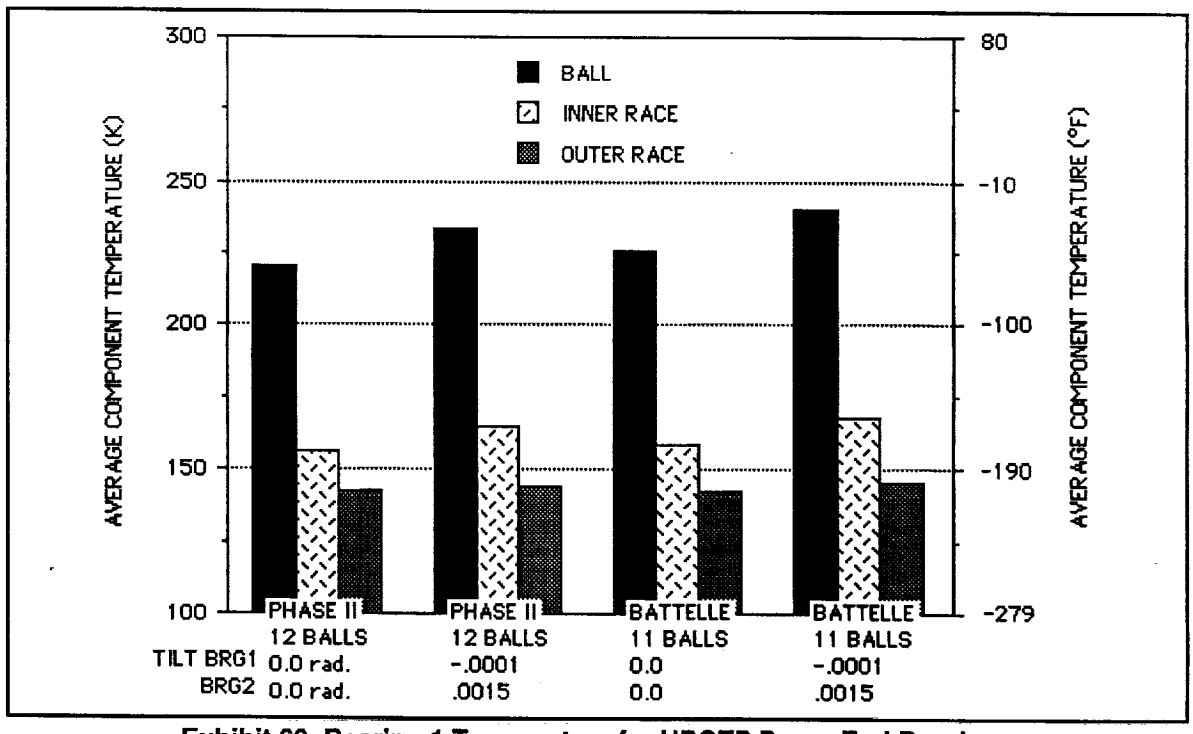

Exhibit 69 Bearing 1 Temperature for HPOTP Pump End Bearings

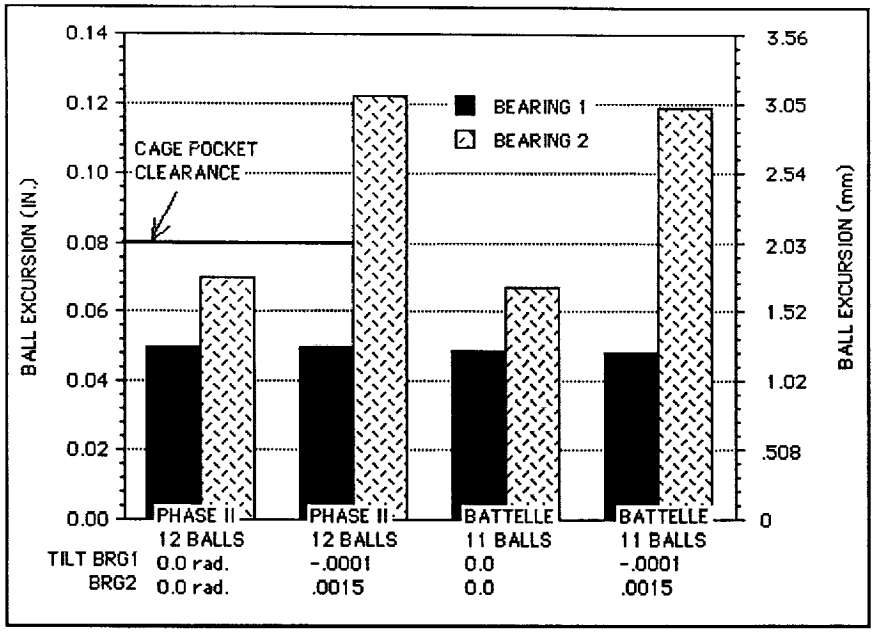

Exhibit 70 Comparison of Ball Excursion for HPOTP 45MM Bearings

load in the BSMT test bearing would need to be raised to approximately 4450N (1000 lbs) as shown in **Exhibit 72**. To obtain these load values in the BSMT requires that the test bearings be placed in the outboard positions. If Si_3N_4 rolling element bearings were used in the inboard positions and initially preloaded to 5780N (1300 lbs) the desired loads could be produced in the outboard positions. The maximum contact stress predicted for the Si_3N_4 bearing under these conditions was 3.6 GPa (522 ksi) which was only slightly higher than the 3.5GPa (508 ksi) value previously tested to in Unit 2 Build 14. The other operating parameters, such as contact stress and heat generation, for the 57mm test bearings in the BSMT were predicted to be less than those for the 45mm bearings in the HPOTP and are shown in **Exhibits 73** through **75**. This is because under the same load conditions the larger 57mm bearing has more capacity than the smaller 45mm bearing. Thus, cage loading will be the only comparable parameter in this test series.

2.8 P&W PEBB Operation with High Axial Preloads

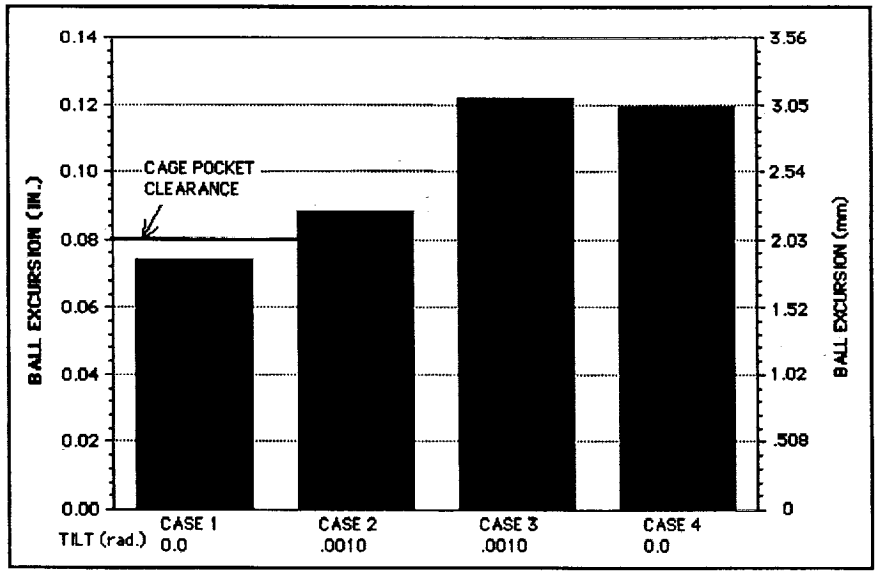

Exhibit 71 BSMT Outboard Bearing Ball Excursion

The PEBB of Pratt and Whitney ATD LOX turbopump operating with increased axial preload was investigated using the SINDA/SHABERTH thermomechanical computer program. The higher axial preload was desired to increase the bearing's radial stiffness and overcome any axial movement binding in the housing. The purpose of this analysis was to verify that the bearing would

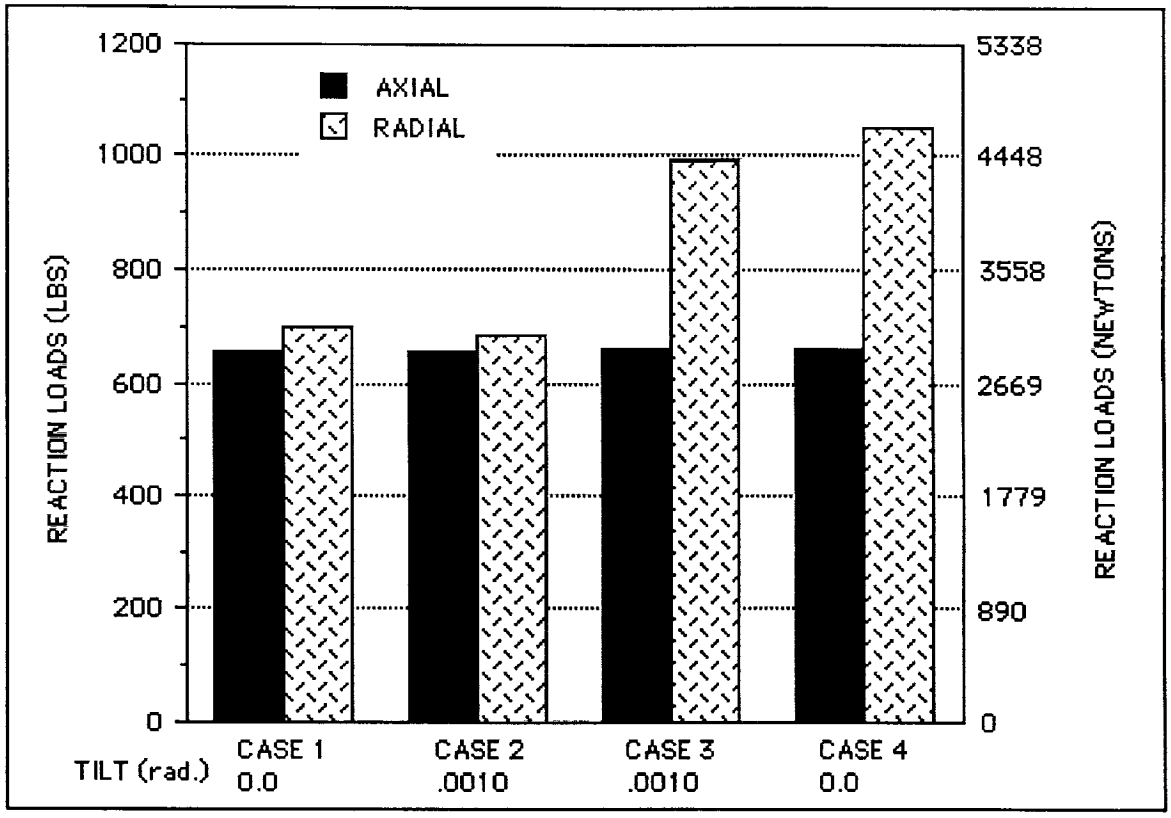

Exhibit 72 BSMT Reaction Loads for Outboard Bearings

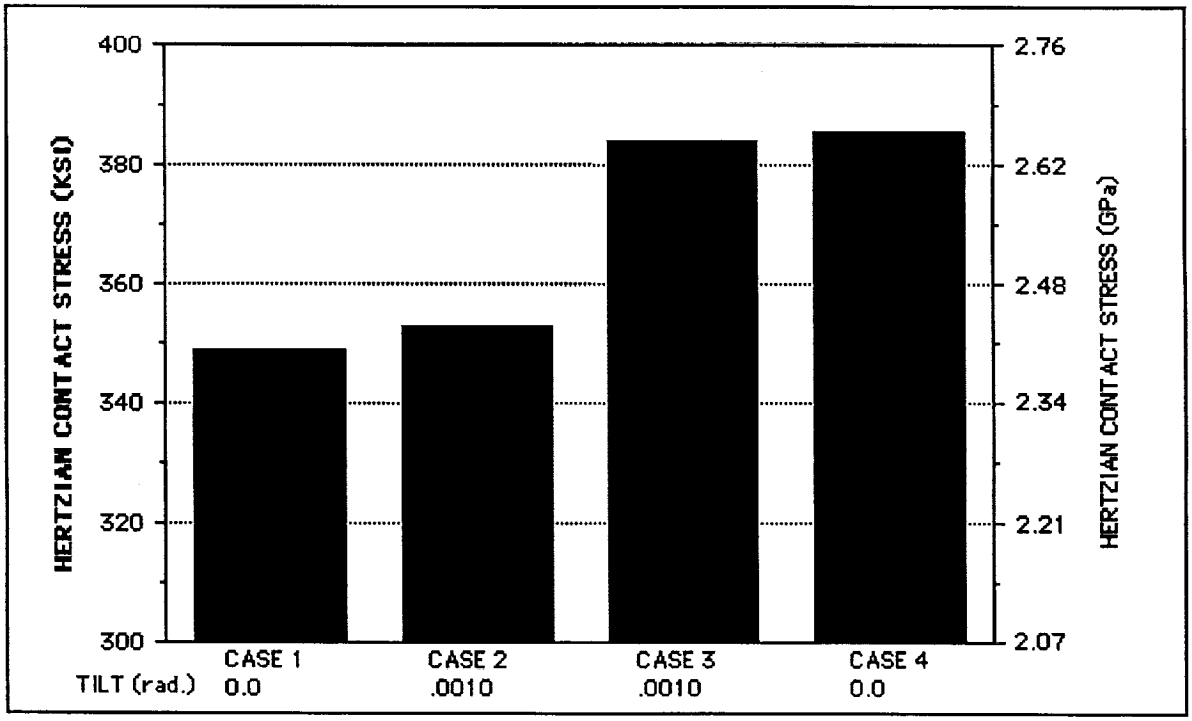

Exhibit 73 BSMT Outboard Bearing Inner Race Contact Stress

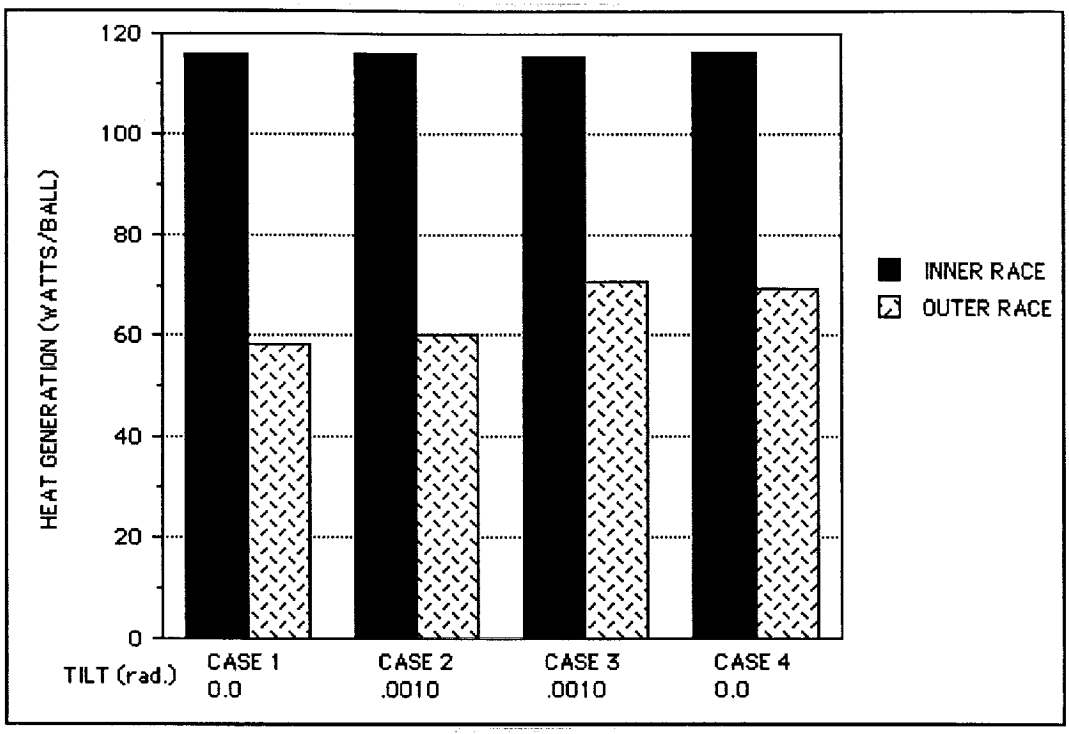

Exhibit 74 BSMT Outboard Bearing Contact Frictional Heat

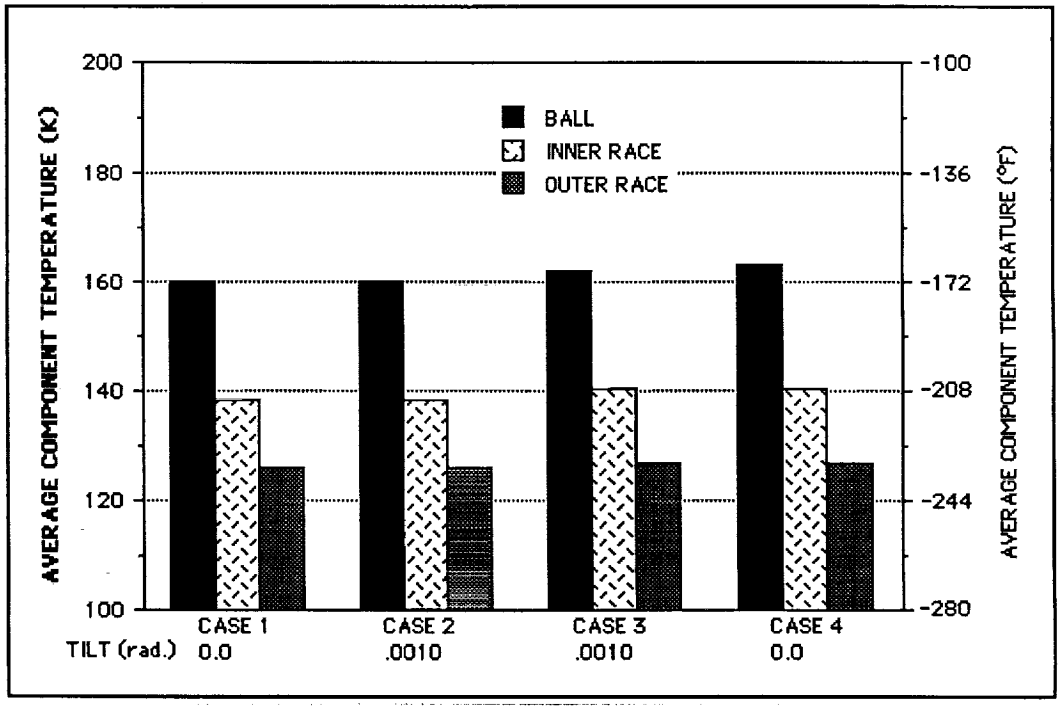

Exhibit 75 BSMT Outboard Bearing Component Temperatures

be thermally stable while operating under the increased axial load and that the radial stiffness would be increased.

The thermomechanical model simulated ATD pump end operating conditions of 3.6 kg/s (8.0 pps) LOX coolant flow, 119 K (215 R) inlet temperature, 10.62 MPa (1,540 psi) coolant pressure, 23, 750 rpm shaft speed, and 3,060 N (690 lbs) radial load. The axial load was varied from the original preload of 6,670 N (1,500 lbs) to an increased load of 40,000 N (9,000 lbs). The model was run for two different outer race positions. One position was with no tilting in the housing which meant that the inner race would be misaligned with the outer race due to shaft deflection. This position resulted in a high moment in the bearing. The second position simulated was a more realistic operating scenario in which the outer race would tilt to follow the inner race's tilt, thus reducing the misalignment between the inner and outer races and decreasing the moment in the bearing. The spring restoring moment, radial load moment and bearing internal moment on the outer race were resolved to determine the operating outer race tilt in the housing for the original preload condition. The resulting outer race tilt in the housing was determined to be 0.00085 radians which resulted in an outer race to inner race misalignment of only 0.00010 radians in which the outer race was tilted past the inner race. This tilt was then used in the increased axial load study.

The predicted steady-state component temperatures for the PEBB are shown in **Exhibit 76**. The coolant temperature rise across the PEBB is given in **Exhibit 77**. These results show the temperatures increasing rapidly with increasing axial load but they do not reach unreasonable limits. The internal clearance remaining in the bearing for these conditions is shown in **Exhibit 78** and illustrates that even at the highest load simulated there will be clearance remaining. These results are valid for both outer race tilt positions. The difference in the two tilt positions was so small that it made virtually no difference in the average heat generation, temperature or clearance. However, the tilt position did make a significant difference in the radial stiffness of the bearing as depicted in **Exhibit 79**. The stiffness was calculated using the secant method in which the total radial deflection from centerline was divided into the radial load. The radial stiffness

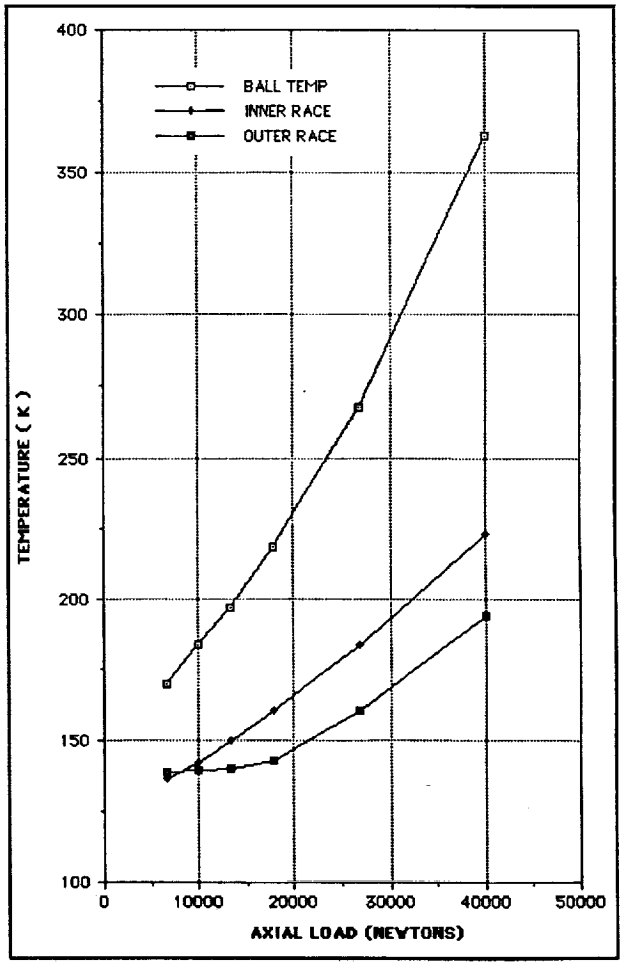

Exhibit 76 PEBB Average Component Temperatures for Steady-State Operation with Increased Preload

of the bearing for the case with 0.00085 radians of outer race tilt increased with axial load as expected. The case with zero outer race tilt produced a high radial stiffness at the original axial preload and decreased to a minimum at approximately 17,000 N (4,000 lbs) before increasing with axial load. The reason the radial stiffness was initially high was that when the inner race tilted due to shaft deflections the centerline of the inner race moved up against the radial load, thus decreasing the total radial movement and increasing the radial stiffness based on the secant method. This inner race movement toward the radial load was decreased as the axial load was increased, decreasing the radial stiffness. At 17,800 N (4,000 lbs) the inner race movement due to tilt was overcome at which point the stiffness began to increase with axial load.

2.9 ATD LOX Pump PEBB Radial Stiffness with Straight and Diverged Deadband

The radial stiffness of the PEBB in the Pratt and Whitney ATD LOX pump was predicted using the SINDA/SHABERTH program. This program was used to simulate the bearing operating under normal conditions at 109% RPL of approximately 25,000 rpm shaft speed, 10.3 MPa (1,500 psia) LOX coolant pressure, 136K (245°R)

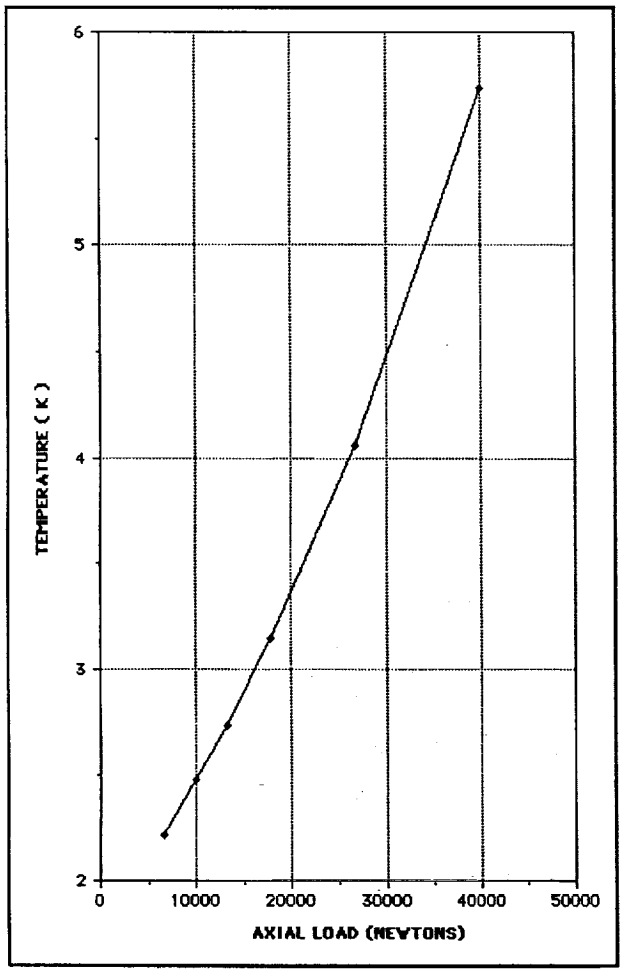

Exhibit 77 Coolant Temperature Rise Across PEBB Operating with Increased Payload

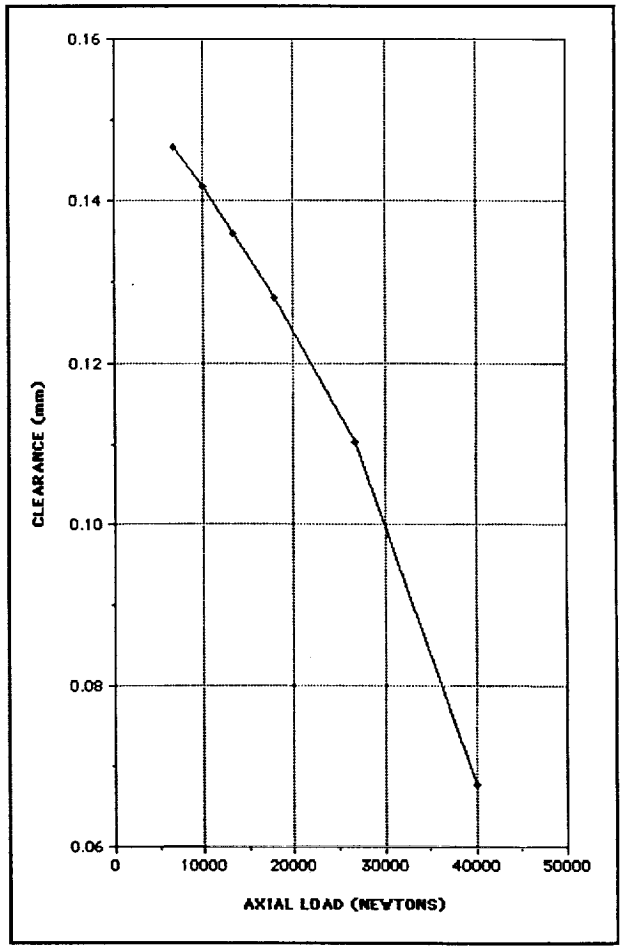

Exhibit 78 PEBB Internal Clearance Operating with Increased Preload

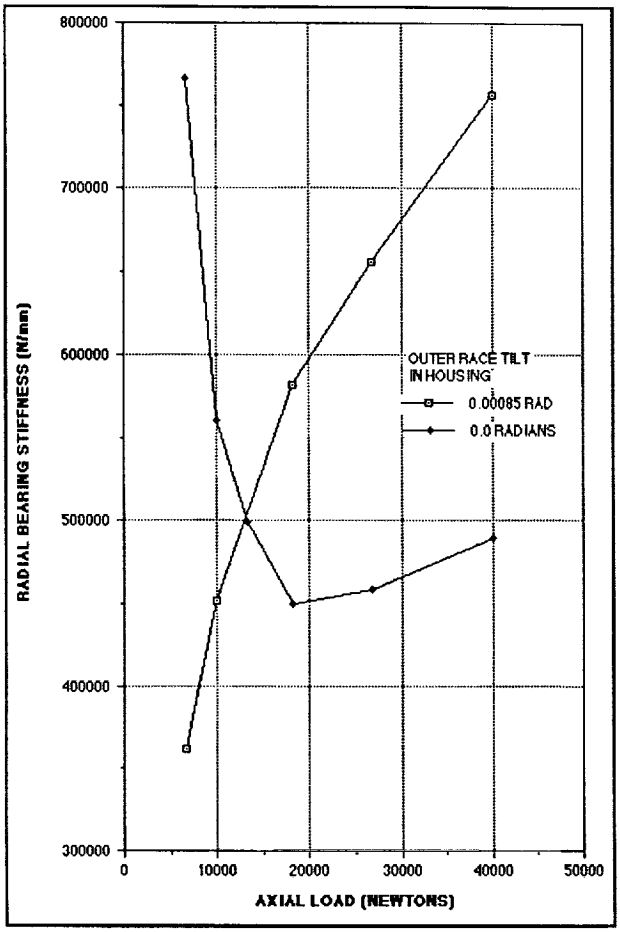

Exhibit 79 PEBB Radial Stiffness With Increased Preload Calculated Using Secant Methods

inlet temperature, and 3.6 Kg/sec (8.0 lbs/sec) coolant flow rate. The bearing was modeled with reaction loads of 6,672 N (1,500 lb) axial preload and radial loads of 1,223 N (275 lbs) fixed and 1,668 N (375 lbs) rotating. The two radial loads were varied from in-phase which resulted in a 2,891 N (650 lb) load to out-of-phase which gave a -445 N (-100 lb) load. The investigation simulated two housing deadband configurations: .002 rad. diverging radial taper towards the main impeller and a straight deadband. The outer race of the PEBB was tilted about its center to balance the moments on the bearing.

The moments that were being balanced were the internal moment in the bearing due to shaft deflection, restoring moment due to the preload spring tilt, and radial load moment due to the net radial reaction load multiplied by the moment arm which was from the center of the contact ellipse to the edge of the outer race. These moments are pictorially illustrated in **Exhibit 80**. The internal moment was calculated by the SHABERTH program and was a function of the operating loads and the outer race tilt angle specified. The preload spring moment was calculated using the equation for the PEBB preload spring moment that was previously derived. The moment on the outer race due to centrifugal loading of the rolling elements at different contact angles around the bearing was neglected because tilt angles and radial loading was so low that the contact angle variation was very small.

The moment balancing progress was a trial and error technique in which an outer race tilt angle was chosen, the program was run for a specified radial load combination, and the resulting moments were added to determine if they summed to zero. Titling the outer race toward the main impeller, where the main load was applied to the shaft, would reduce the internal moment and increase the spring restoring moment. Whereas, the magnitude of the radial load moment was relatively unchanged by outer race tilt. However, depending on which corner of the race inboard (main inpeller side) or outboard, the outer race was tilted, the radial load moment would resist the tilt or amplify the tilt. **Exhibit 81** shows the resulting balanced moments as a function of radial load. The moments shown as negative indicated that they are in the direction to resist tilting or straighten the outer race in the housing. The internal moment for the diverged deadband case changes signs at about 1,335 N (300 lbs). This is due to the radial load having increased enough to cause the outer race to sit

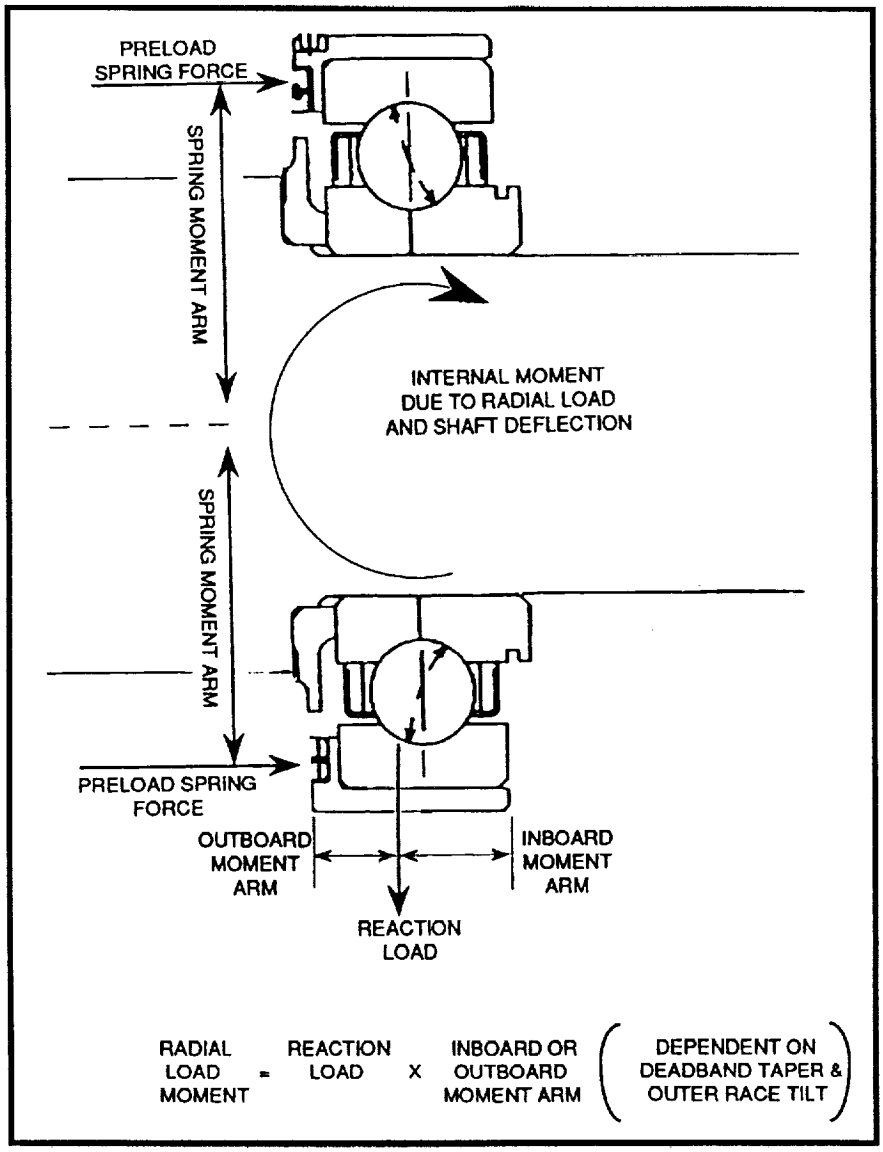

Exhibit 80 Tilting Moments Reacting on PEBB Outer Race

down on the diverged deadband as indicated in **Exhibit 82** which shows the tilt angles corresponding to the balanced moments. The magnitude of the radial load studied did not increase enough to cause the outer race to tilt more than the divergence of the housing deadband.

The reason the outer race tilts more with the diverged deadband is that the race will first contact on its outboard corner as shown in **Exhibit 83a**, thus the radial load moment was in the direction to tilt the race toward the main impeller. With a straight housing deadband the outer race will pivot about the inboard corner, shown in **Exhibit 83b**, and the radial load will resist the tilting of the race. However, the tilting of the outer race for any of these conditions did not have a significant effect on bearing rolling element to race heat generation or component temperatures because the tilt angles were so small. Additional analysis was being conducted to investigate the effects of tilt on cage to ball heat generation.

The radial deflection resulting from tilt was calculated as a function of radial load for both housing deadband tapers using the SHABERTH program. These deflections are shown in **Exhibit 84**. This deflection is not only due to the compression of the bearing material but also the movement of the inner race as they tilt relative to each other. Thus, for the diverged case above 1,110 N (250 lbs) radial load the total deflection

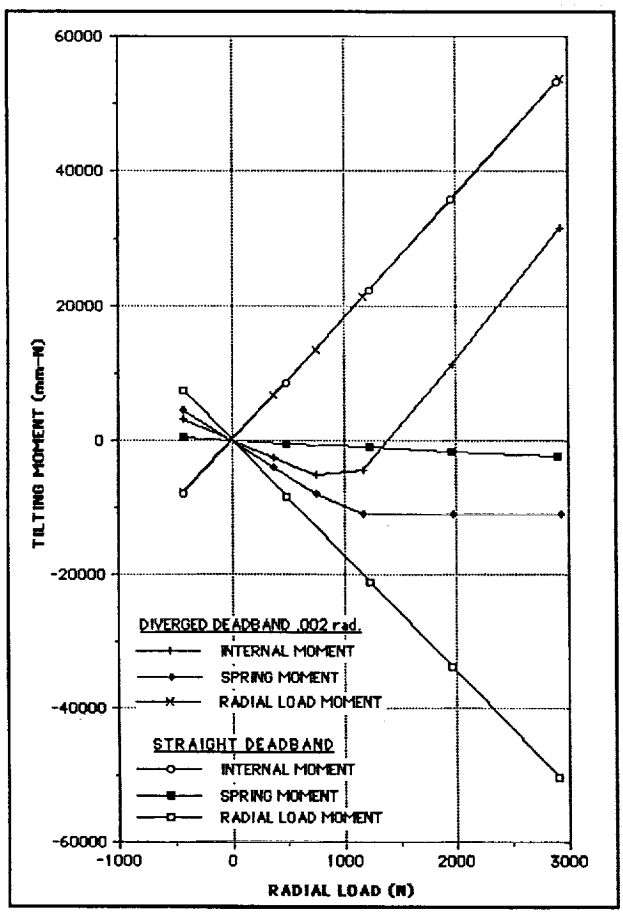

Exhibit 81 ATD LOX Pump
PEBB Reaction Moments on Outer Race

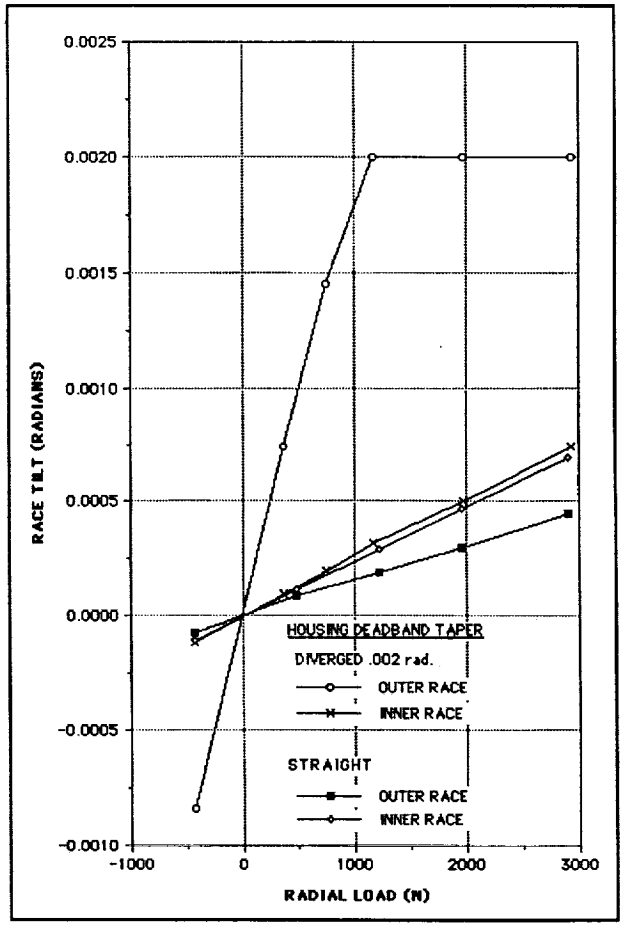

Exhibit 82 ATD LOX Pump
PEBB Reaction Moments on Outer Race

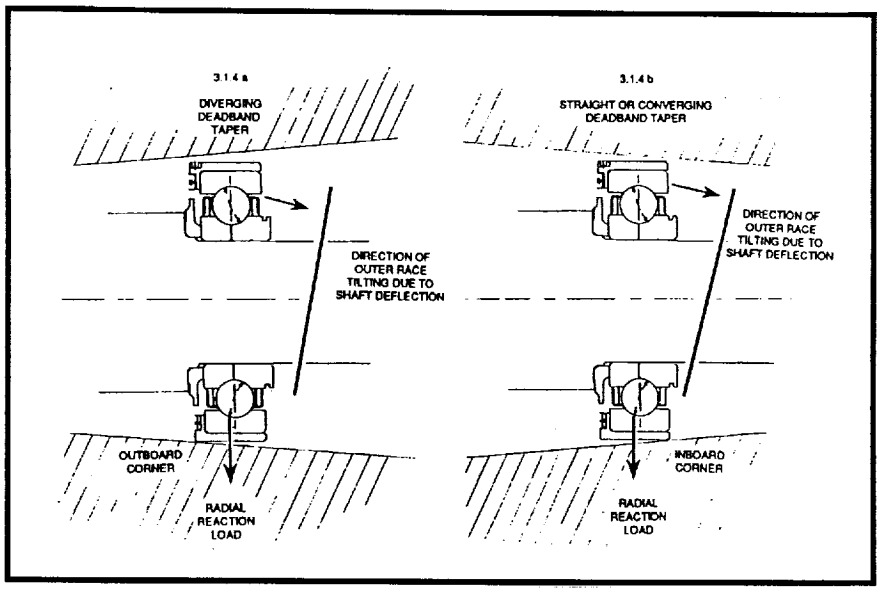

Exhibit 83 ATD LOX Pump PEBB Reaction Moments On Outer Race

2.10 ATD Pump End Ball Bearing Outer Race Tilt Analysis

The outer race of the ATD Pump End Bearing is enclosed in a sleeve which in turn is supported in a housing. There is a clearance between the sleeve and housing to allow the outer race/sleeve assembly to move in the axial direction. This clearance also permits the outer race to tilt. The amount of tilt is determined actually decreases because the outer race is now fixed (see **Exhibit 82**) but the inner race continues to tilt. This caused the contact angles in the bearing to increase which moves the inner race in the opposite direction to the radial load.

The radial stiffness was then calculated using the secant method of dividing the bearing radial reaction load by the total radial deflection at that load. The resulting stiffness for both housing deadband configurations are shown in **Exhibit 85** as a function of radial load. Because the deflection of the bearing with low relative tilt angles (straight housing deadband) was so small its radial stiffness was high. The decrease in stiffness plotted at 445 N (100 lbs) for the straight taper was probably due to the numeric accuracy of the program since the loads and deflections it is working with are very small. Thus, it is believed that the radial stiffness for the PEBB in a straight housing would be approximately 700,000 N/mm (4.0e +6 lbs/in) and with the diverged housing the stiffness would be 35,000 to 87,000 N/mm (200,000 to 500,000 lbs/in).

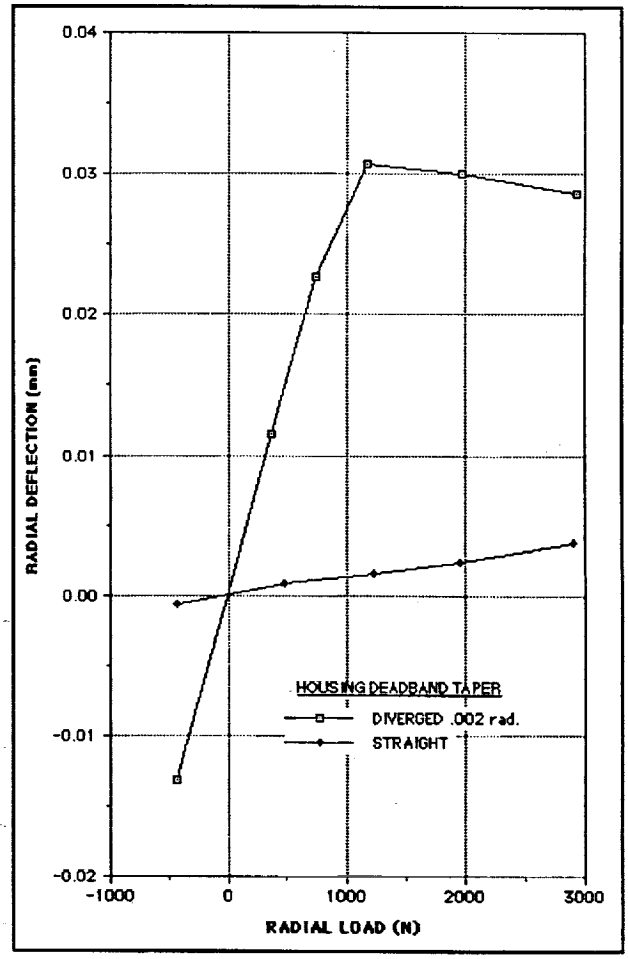

Exhibit 84 ATD LOX Pump PEBB Radial Deflection of Inner Race With Respect to Outer Race

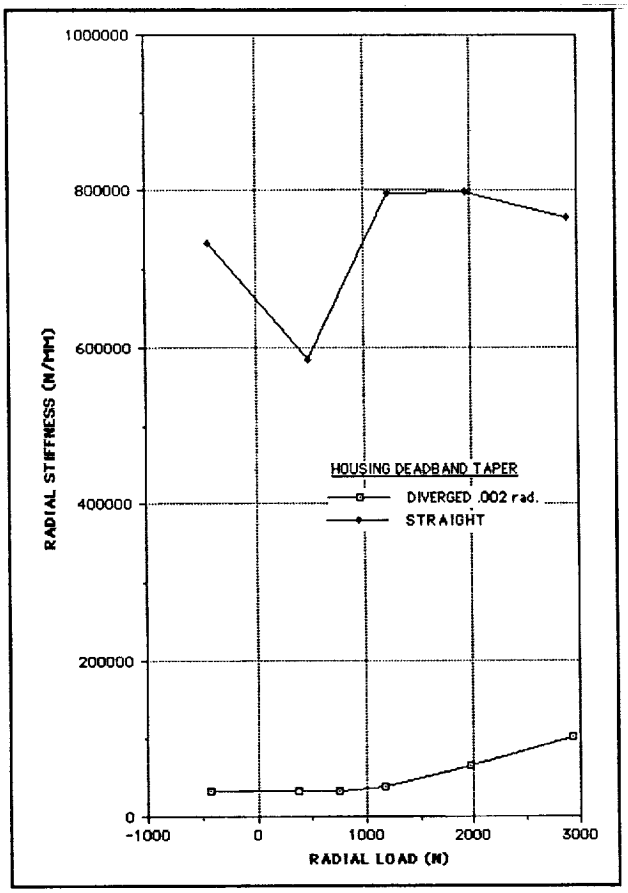

Exhibit 85 ATD LOX Pump PEBB Radial Stiffness of Bearing Using Secant Method

by the moments on the outer race but is limited by the sleeve to housing clearance. The housing bore may either be straight or tapered. If the housing bore diameter increases in the direction of the turbine the taper is designated as divergent. The amount of taper in the housing bore also affects the limiting value of outer race tilt.

The following analysis demonstrates the influence of clearance and taper on possible outer race tilt. A conceptual representation of the bearing sleeve/outer race in a tapered housing is shown in **Exhibit 86**. 1-A of the exhibit shows the assembly centered in the housing bore. It is assumed that the sleeve sticks out of the bore as shown. It is further assumed that the assembly sits down in the bore and rotates such that the outer surface of the assembly is parallel with the bore taper as shown by 1-B. The assembly then rotates until the upper edge contacts the bore as shown by 1-C.

From the exhibit the following relations were written.

1) $M = [(D + C + W_b\theta)^2 + W_b^2]^{1/2}$

2) $\text{Cos}\ _\beta = D/M$ (since M = 0)

3) $\text{Sin}\ \delta = \dfrac{Wb + D\theta}{M}$

4) $\tau = \beta - \delta$

5) $\alpha = \tau + \theta$

The maximum outer race tilt were estimated as a function of clearance and bore divergence angle. The maximum outer race tilt versus housing taper for the ATD pump end bearing is shown in **Exhibit 87** for a typical operating clearance. The amount of outer race rotation or tilt during operation is dependent on the moments acting on the outer race. Radial loads produce internal moments in the bearing, and the outer race contact with the housing and preload spring produces moments. The sum of these moments is zero at a particular value of outer race tilt. Another potential moment on the outer race is nonuniform fluid pressure produced by the bearing coolant flow.

Outer race tilt, increases ball excursion as shown in **Exhibit 88**. When ball excursion exceeds ball to cage pocket clearance excessive heat can be generated, and ball and cage wear dramatically increased. Estimated ball to cage pocket operating clearance was 0.762mm (0.030

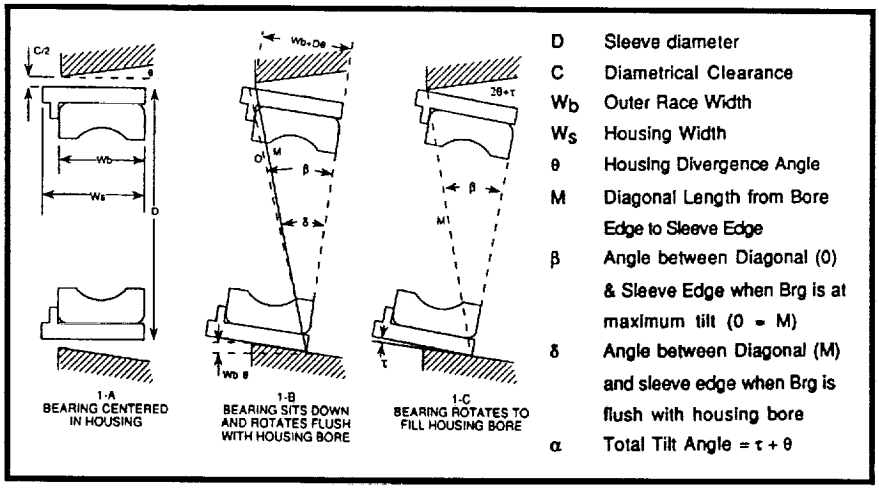

Exhibit 86 Configuration Description of Bearing Outer Race Tilt

2.11 Static Load Capacity of High Pressure Fuel Pump Ball Bearings

The static load capacity of 45 mm fuel pump bearings was calculated to evaluate handling load limits on the SSME high pressure turbopumps. The load capacity calculated was based on the ANSI stress criterion which states: It has been found that for all ball bearings suitably manufactured from hardened alloy steels deformations occurring under maximum contact stress of 4000 megapascals (N/mm2) in) for the ATD Pump End Ball Bearing. Since the limiting value of outer race tilt is strongly dependent on housing bore taper (**Exhibit 87**), this taper should be minimized or eliminated.

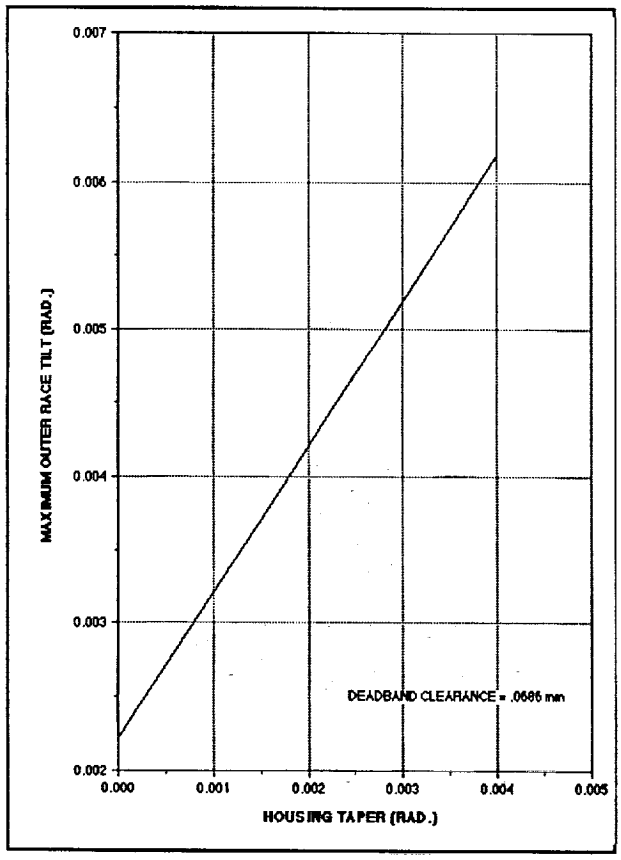

Exhibit 87 Outer Race Tilt Versus Housing Taper

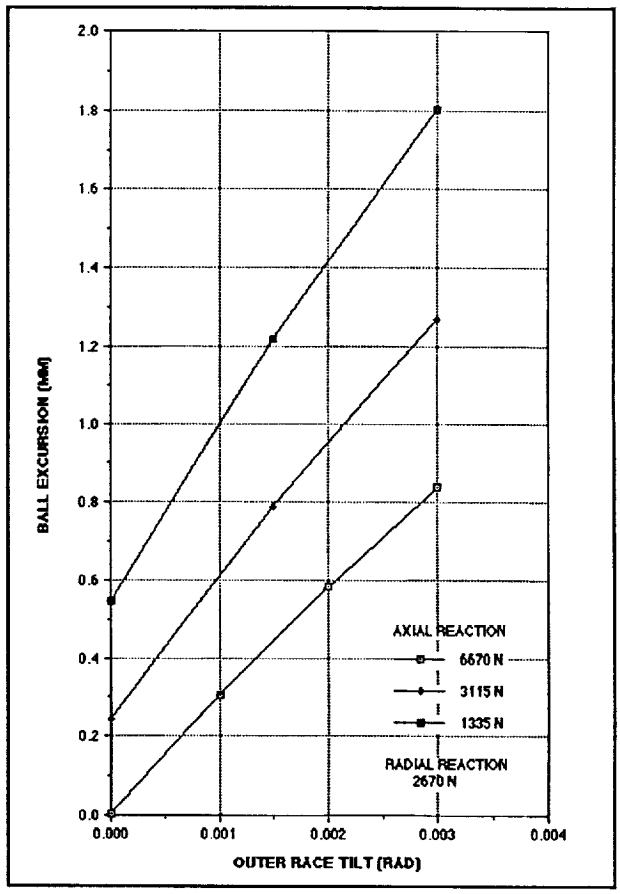

Exhibit 88 PEBB Ball Excursion

(580,000 psi) acting at the center of contact do not greatly impair smoothness or friction". An equation for this criterion can be found in Ref 1. This static load capacity (C's) is stated as shown in **Exhibit 89**.

Based on this criterion each duplex bearing pair in the pump has a static load capacity of 25,750 N (5789 lbs). Therefore, accelerations caused by handling should not exceed levels which cause inertial loads to exceed these levels.

These results were verified using SHABERTH which allowed the affects of preload to be included. The SHABERTH results were consistent with the results stated above. It was found that approximately 6000 lbs per bearing pair was required to induce stresses of 4000 megapascals.

2.12 Contact Geometry Characteristics for the Fuel Pump Ball Bearing

The SINDA/SHABERTH LH_2 bearing test rig model was used to simulate nominal ball bearing operation for normal pump operating conditions. The objective was to calculate the nominal Hertzian contact parameters to support independent investigations into the formation of "river-mark" features observed on silicon nitride balls that have been run in the rig or in the pump. The model was run in the thermal mode to determine the operating temperatures and axial preload. The following boundary conditions were used:

Fluid Inlet Temperature:	-240.0 C
Shaft Speed	35000 RPM
Static Ambient Preload	3781 N
Radial Load	889 N

The operating conditions were calculated to be as follows:

Ball Average Operating Temperature	-229.4 C
Maximum Ball Surface Temperature	-207.7 C
Inner Race Average Temperature	-233.0 C
Outer Race Average Temperature	-232.6 C
Operating Axial Load	3882 N
Operating Radial Load	360 N.

Selected ball to race contact parameters and other selected parameters for these conditions are shown in **Exhibit 90**.

Exhibits[1] 91 and 92 below illustrate graphically the ball to race contact parameters calculated. It should be noted that the contact stress at any point within the contact ellipse is given by the following relationship:

$$\sigma = ((3Q)/(2\Pi ab))\{1-(x/a)^2-(y/b)^2\}^{1/2}.$$

The slip velocity at any point within the contact ellipse can be obtained by vectorially subtracting the ball surface velocity from the race surface velocity using the velocity vectors provided.

Cs (ANSI) = $\varphi s \iota z D^2 COS\alpha$	
φs = 1980 in	(Tabulated value versus a (.13) from Table 11.1 Ref 1)
ι = 2	(number of rows of rolling elements - 2 for duplex bearing pair)
Z = 14	(number of rolling elements per row)
D = 0.34375 in.	(Ball diameter)
α - 27.9 deg	(Contact angle)
Cs = (1980) (2) (14) (0.34375)2 COS 27.9 = 5789 lbs)	

Exhibit 89 Static Load Capacity

Peek Inner Race Contact Stress		2193.3 (N/mm2)
Peek Outer Race Contact Stress		1804.2 (N/mm2)
Inner Race Contact Load		1246.4 N
Outer Race Contact Load		2759.4 N
Inner Race Contact Angle		17.3°
Outer Race Contact Angle		7.7°
Ball Orbital Velocity		1463.8 (rad/s)
Ball Angular Speed	WX	-8157.4 (rad/s)
	WY	911.3 (rad/s)
	WZ	0.0 (rad/s)
Inner Race Semi-Major Contact Axis		1.06985 mm
Inner Race Semi-Minor Contact Axis		0.25364 mm
Outer Race Semi-Major Contact Axis		2.25577 mm
Outer Race semi-Minor Contact Axis		0.32359 mm
Inner Race Spin-to-Roll		21
Outer Race Spin-to Roll		0

Exhibit 90 Ball to Race Parameters

2.13 Hydrostatic Bearing Test Review

SRS was asked to review the feasibility of using the LH_2 bearing test rig for hydrostatic bearing testing using water as the test fluid. The rig was originally designed for cryogenic hydrostatic bearing testing. Thus, hydrostatic test and reaction bearings were designed for LOX and LH_2. The rig was modified for rolling element bearing testing before any hydrostatic bearing testing was performed. However, the current configuration utilized an LH_2 bearing in the lower test bearing location. The cost of cryogenic fluids was a major cost component of cryogenic bearing tests. Therefore, testing with water significantly reduce the cost of future hydrostatic bearing tests. SRS modifyied existing rig hydrojet models to determine water pressure and flow rates needed to support a hydrostatic bearing test. Drawings were obtained for the LOX hydrostatic bearing designs. This bearing was evaluated for use with water. LOX has similar density to that of water thus; the required mass flow rates through the bearing orifices was predicted to be similar. Bearing stiffness versus pressure drop was calculated for the bearing design using water as the test fluid.

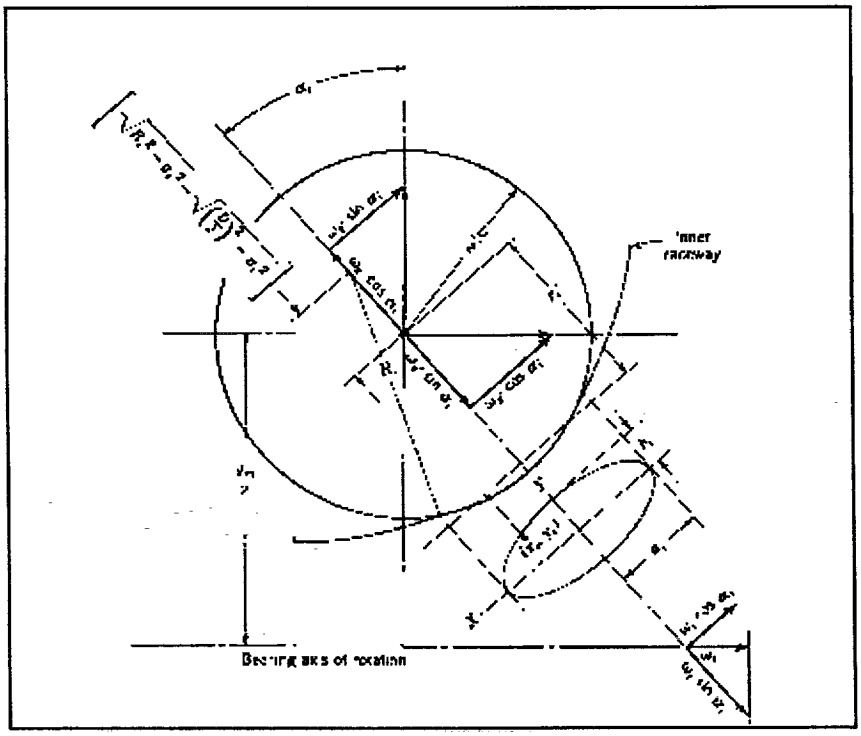

Exhibit 91 Inner Race Contact Geometry

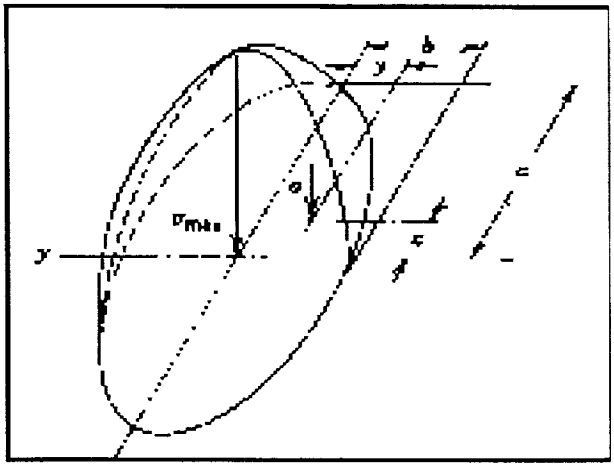

Exhibit 92 Compressive Stress Distribution in the Contact

results were normalized with respect to nominal values for 35K operation (K_{xx} = 1,224,316 lb/in; K_{yx} = =129,341 lb/in). Cross-coupled stiffness increased by a factor of 5 over the range while the primary stiffness was reduced to 66% of the nominal value. This decrease in the principal bearing system was a concern for rotor dynamic stability of the system. However, it should be noted that even at the highest speed the primary stiffness was 808,048 lbs/in, quite high. The stiffness trend should be noted and incorporated in rotor dynamic analysis of rig prior to very high-speed operation.

2.14 Fluid Film Bearing Tester Off Design Analysis

Hydroject, the hydrostatic bearing design code used to design the LH_2 bearing test rig hydrostatic bearing slave bearing, was transferred to and recompiled using a 32 bit FORTRAN compiler. The code had to be modified slightly to be compatible with the new compiler, however, performance was significantly improved. The modified code was used to evaluate hydrostatic bearing performance for off-design, over speed operating conditions. The hydrogen slave bearing was simulated with current rig pressures and flow rates, and speed was varied from 35,000 RPM up to 125,000 RPM. Bearing stiffness and cross-coupled stiffness was calculated for 75% bearing eccentricity. **Exhibit 93** shows the results of the bearing stiffness analysis. The

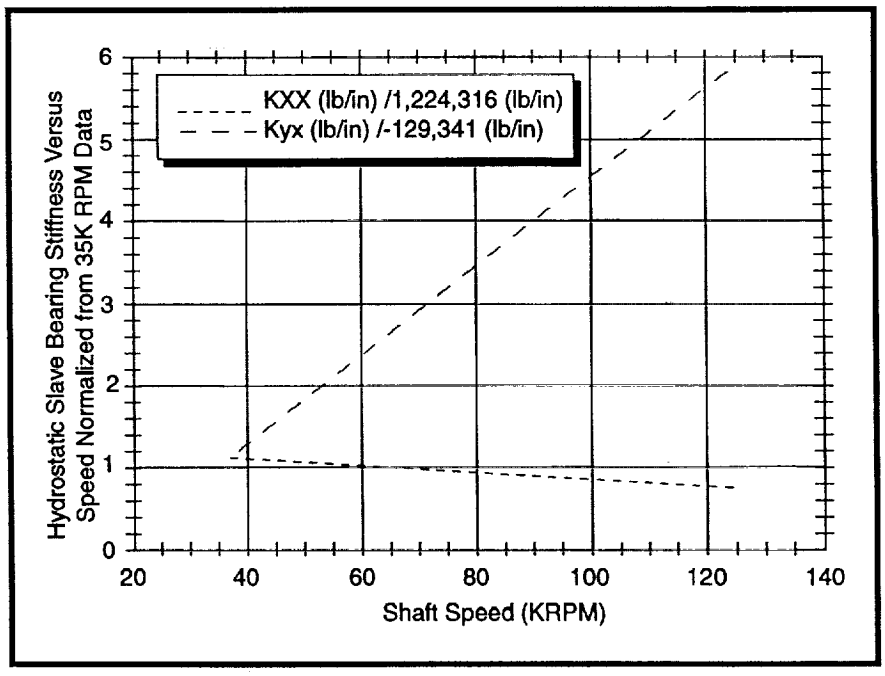

Exhibit 93 H2 Slave Bearing Stiffness Variation

3.0 — Design of Rolling Element Bearings for the Marshall Space Flight Center - Simplex Turbopump Design

The SRS bearing design team played a significant role in the design of the cryogenic bearings that were successfully developed for the Simplex Turbopump. The Simplex turbopump was being designed by MSFC to supply liquid oxygen to a solid fuel hybrid booster. The booster was not man rated and minimum cost and complexity were design goals. Rolling element bearings were used since their operating characteristics are well known and they provided the most cost effective approach for load support. One approach considered was to use standard off-the-shelf bearings. However, bearings constructed from LO_2 compatible materials such as 440C stainless steel were not available as off-the-shelf items from bearing manufacturers. Therefore, to continue the development work on the Simplex pump, preliminary analysis was performed using the 45mm bearings currently used for the pump end bearings of the Rocketdyne High Pressure Oxidizer Turbopump (HPOTP).

The Simplex Turbopump was designed to minimize the severity of the bearing operating conditions. Estimates of load conditions were 2670 N to 445O N (600 lbs to 1000 lbs) radial load and approximately 2200 N (500 lbs) axial preload at a shaft speed of 25,000 rpm. The liquid oxygen coolant conditions at the upstream bearing were expected to be 95 K to 110 K (170°R to 200°R) inlet temperature, 1.38 Mpa to 6.89 Mpa (200 psia to 1000 psia) inlet pressure and 0.9 kg/sec to 2.3 kg/sec (2 lbs/sec to 5 lbs/sec) flow rate. The downstream bearing had similar load conditions and its coolant came from the exit of the upstream bearing. **Exhibit 94** is a cross section of the Simplex pump showing the coolant path for the bearings.

Modeling of the Simplex bearings was performed using the SINDA/SHABERTH thermomechanical bearing program for steady-state simulations. This model consists of two 45mm bearings mounted on a common shaft and preloaded against each other. The model also simulates the compression of the preload springs due to thermal growth of the bearings to determine an operating axial load. The development of the thermal model was facilitated by making use of the previously developed thermal model for the 45mm bearings of the Rocketdyne HPOTP. The node configurations for the races and balls were used directly. The support structure nodes for the housing and shaft were developed specifically for the Simplex pump dimensions. The coolant flow path was also modeled specifically for the Simplex pump, but is basically the same as in the HPTOP pump end.

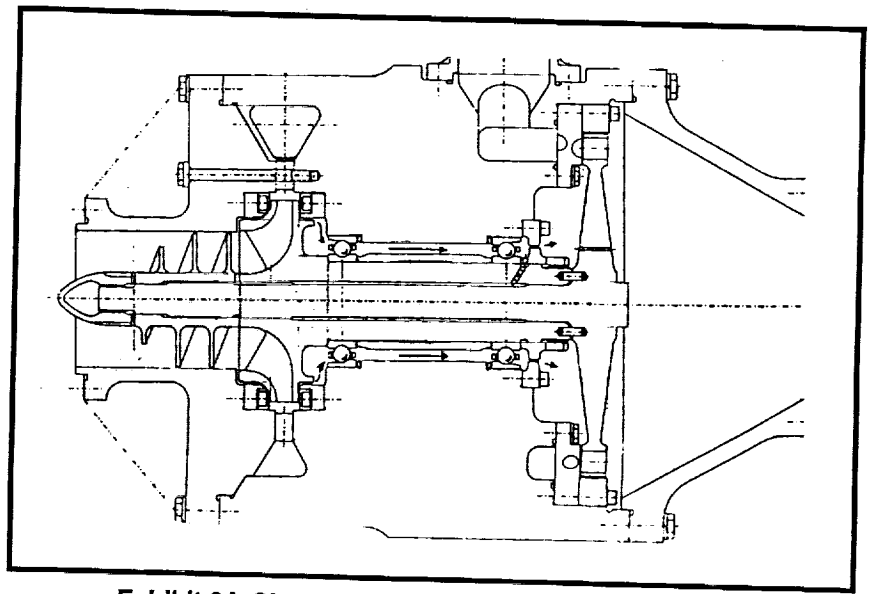

Exhibit 94 Simplex LO_2 Turbopump Cross Section

The SINDA/SHABERTH shaft, bearing, thermal model was used to perform a sensitivity study to evaluate axial preload requirements for the SIMPLEX pump bearings. The baseline bearing configuration evaluated consisted of two standard Phase II 45 mm SSME LOX pump bearings, one on the pump end and one on the turbine end, preloaded against each other. Si_3N_4 rolling elements were used and the material for both races was 440-C stainless steel. The objective of the study was to evaluate the effects of operating preload on the operating characteristics of the bearings for various radial load conditions. For this study, the outer races were constrained such that no outer race tilt was allowed. Curves were generated by varying the applied radial load on the pump from 2669 N (600 lbs) to 4448 N (1000 lbs). Axial preload was varied from 1780 N (400 lbs) to 3560 N (800 lbs). The parameters evaluated were radial reaction load, maximum contact stress, frictional heat generation, average component temperature, ball excursion, and bearing deflection.

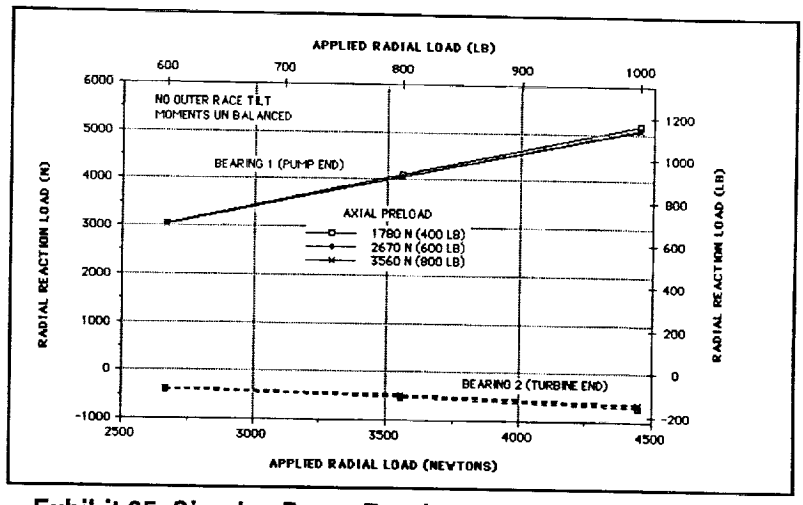

Exhibit 95 Simplex Pump Bearing Radial Reaction Loads

The bearing reaction loads for the cases modeled are shown in **Exhibit 95**. The curves show that bearing one acts as a fulcrum between the radial load applied to the shaft and the radial reaction at bearing two. This effect results in the reaction load on bearing one being greater than the radial load applied by the pump. The exhibit shows that preload has a negligible affect on the load sharing between the bearings. For the worst case scenario of 4448 N (1000 lbs) applied radial load, bearing one reacts 5025 N (1130 lbs) and bearing two reacts approximately 622 N (140 lbs). As a result of the location of the bearings, with respect to the applied load, bearing one must have a radial load capacity that exceeds the maximum anticipated radial shaft loading.

Maximum Hertzian contact stresses for the cases modeled are shown in **Exhibit 96**. The curves show that increased applied radial load results in increased maximum contact stress.

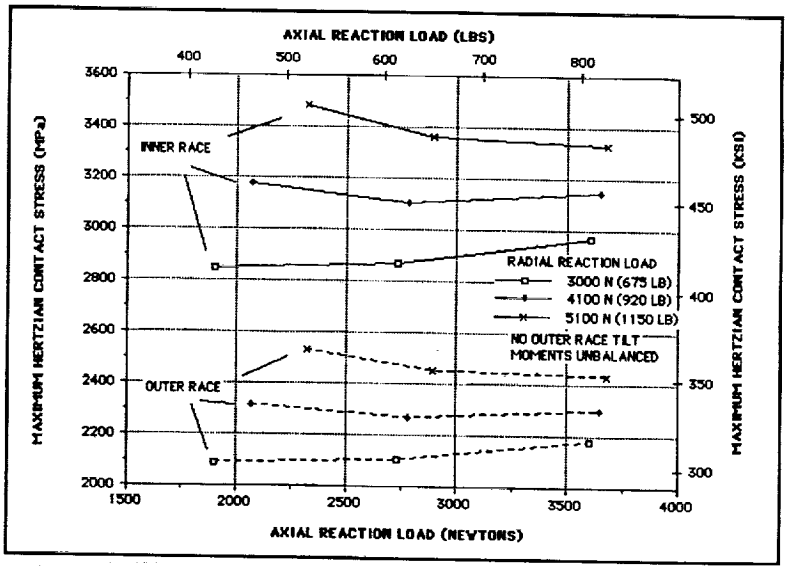

Exhibit 96 Simplex Pump Bearing 1 Race Contact Stress (45mm Phase II Bearing with Si3N4 Balls)

Inner race contact stress varies form 2850 Mpa (413 ksi) to 3490 Mpa (506 ksi) for the range of applied loads considered. These stresses are relatively high, however, BSMT test results have shown that the 440C bearings with Si_3N_4 rolling elements can operate at these stress levels for run times exceeding the design life of the SIMPLEX pump. It should be noted that for each case of radial reaction load there is an optimum value of axial preload in terms of contact stress. The optimum axial preloads for the radial reaction loads of 3000 N, 4100 N, and 5100 N are 1900 N, 2000 N, and 3700 N, respectively.

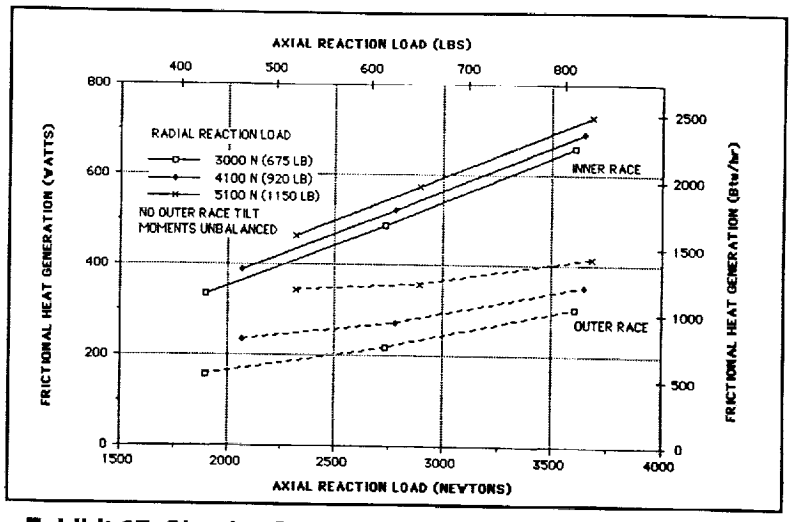

Exhibit 97 Simplex Pump Bearing 1 Race Heat Generation (45 mm Phase II Bearing with Si3N4 Balls)

Exhibits 97 and **98** show bearing one frictional heat generation and average component temperatures respectively. Inner race heat generation varies from 325 watts (1109 Btu/hr) to 740 watts (2525 Btu/hr) and the average ball temperature varies from 162K (292°R) to 183K (329°R). The curves show that in terms of heat generation and operating temperature, reducing preload improves bearing operating characteristics. The heat generation rates plotted do not include heat generated from ball excursions which exceed the ball pocket clearance in the cage pockets. **Exhibit 99**shows ball excursion, for each radial load case, as a function of axial preload. The curves show that the amount of axial preload required to prevent ball excursions from exceeding pocket clearance or unloading from the inner race, goes up with increasing radial reaction load. Based on the results of this study it appears that ball excursion and unloading drives the requirements for axial preload.

Exhibits 100 and **101** show the affects of axial preload on the load deflection characteristics of bearings one and two respectively. Increasing axial preload generally results in reduced radial deflection for a given radial load. These curves are presented to show the affect of preload on deflection. The absolute values of these curves should not be considered accurate because bear-

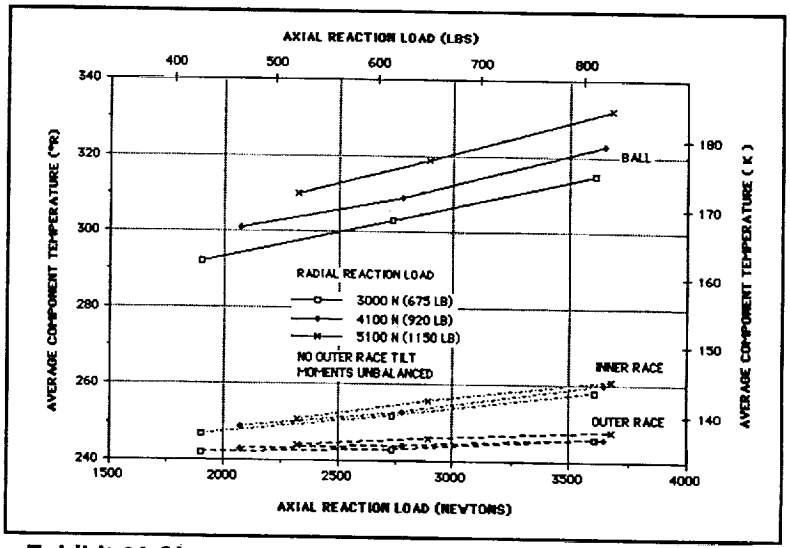

Exhibit 98 Simplex Pump Bearing 1 Component Temperatures

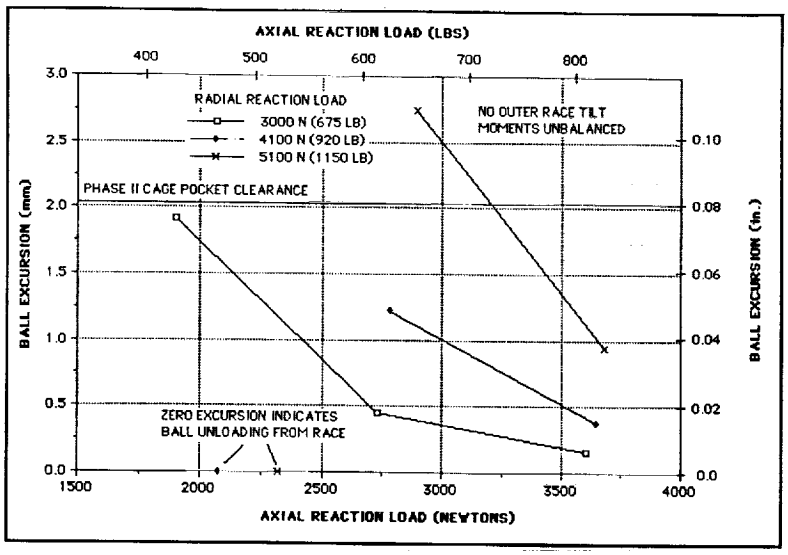

Exhibit 99 Simplex Pump Bearing 1 Ball Excursion (45mm Phase II Bearing with Si3N4 Balls)

ing moment and tilt have a significant influence on bearing stiffness. Additional analysis was performed to generate load deflection curves for specific cases of deadband and operating misalignment.

In summary, this preliminary analysis shows that the 45 mm Phase II bearings with Si_3N_4 balls can be used in the SIMPLEX pump for cases of radial loading on the impeller of up to 4448 N (1000 lbs). However, for large radial loads a relatively high axial preload is required to prevent ball unloading or excessive ball excursions. High radial and axial loading results in a relatively high stress operating environment which is approaching the limit of BSMT test experience.

Bearings of the Simplex pump were analyzed to determine their radial stiffness. The bearing configuration used in this study was very similar to the HPOTP pump end bearings. The bearing size is 45mm with inner race curvature of 0.55, outer race curvature of 0.52, and diametrical clearance of 0.0063 in. (0.16 mm). These bearings were modeled operating with silicon nitride balls and an axial preload of 600 lbs (2670 N). Radial loads on the shaft up to 1000 lbs (4.448 N) were applied. The bearing radial deflection was predicted for radial deadbands of 0.001, 0.002, and 0.003 in. (0.0254, 0.0508, and 0.0762 mm). For each condition the moments on the outer races were balanced to determine the operating tilt and it was assumed that the outer race would not slip radially on the preload spring. **Exhibit 102** shows the radial shaft deflection at Bearing 1 (pump end). The plot shows large deflections at low loads until the bearing outer race contacts the housing deadband at which point the slope of the curves change. **Exhibit 103** shows the deflection at Bearing 2 (turbine end). For the loads on the turbine end, Bearing 2 only touched the 0.001 in. (0.0254 mm) radial deadband. For the larger deadbands, the outer race will hang from the

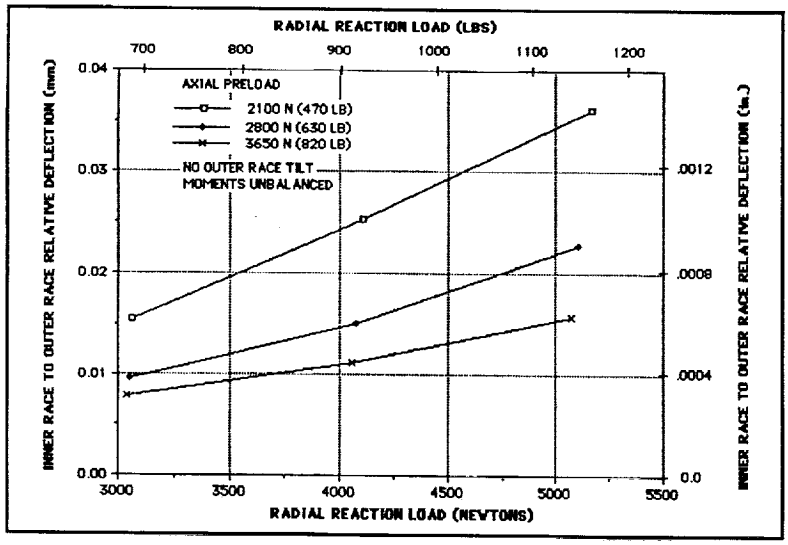

Exhibit 100 Simplex Pump Bearing 1 Radial Deflection (45mm Phase II Bearing with Si3N4 Balls)

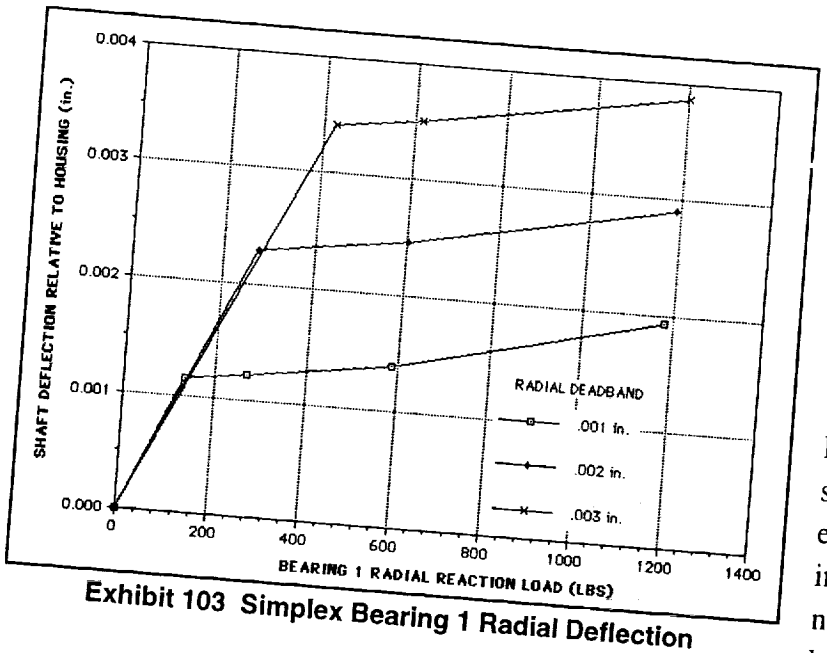

Exhibit 103 Simplex Bearing 1 Radial Deflection

spring be set to a minimum while maintaining sufficient travel to compensate for any further axial thermal expansion of the bearings. A value of 1780 N (400 lbs) was tentatively chosen for the minimum operating preload to perform the stiffness calculation and evaluation of remaining spring travel.

Once the operating and minimum preload values were chosen, the total spring travel was set. To have the bearings preloaded against each other with 2670 N (600 lbs) without external axial forces on the shaft and have 1780 N (400 lbs) on the unloading bearing when external forces are applied required that the preload spring of the loading bearing be totally compressed at 3560 N (800 lbs). This sets the total travel of the spring at 0.175 mm (.0069 in.). The spring would be compressed to .1321 mm (.0052 in.) with the 2670 N (600 lb) preload leaving .0432 mm (.0017 in.) of spring travel for shaft movement. Thus, when one spring is fully compressed due to shaft movement the other spring would be compressed .0889 mm (.0035 in.). Therefore, this configuration would allow for .0864 mm (.0034 in.) of spring compression by the bearings due to some anomalous thermal expansion. The spring can be easily modified to reduce the height of the pads to the .175 mm (.0069 in.) needed.

The bearings were simulated with falsely high frictional heating values to determine how much of an increase in heat would result in a loss of spring travel. The analysis showed that the frictional heat generated in the bearing would have to increase six times above the nominal value for the temperature of the bearing components to increase enough to thermally expand and fully compress the springs. Thus, the .0432 mm (.0017 in.) of remaining travel in each spring at nominal operation is believed to be sufficient margin for thermal expansion of bearings with silicon nitride rolling elements.

The radial deflection of the bearing was then calculated for both the nominal axial load of 2670 N (600 lbs) and the minimum load of 1780 N (400 lbs) as a function of radial load. A radial deadband of .025 mm (.001 in.) was used for this analysis. The analysis also simulated both the original shaft bearing spacing and the revised longer shaft spacing. The results are given in **Exhibit 104** and show that the reduced axial load of 1780 N (400 lbs) decreased the radial stiffness, but the shaft spacing did not significantly affect the radial deflections. It is believed that the minimum stiffness calculated would be sufficient.

In an effort to determine the radial stiffness value quickly for other analyses that were being performed, a simplistic view of the bearing was used in which the bearing was considered axially incompressible. Thus, axial movement was due only to preload spring compression. This did not

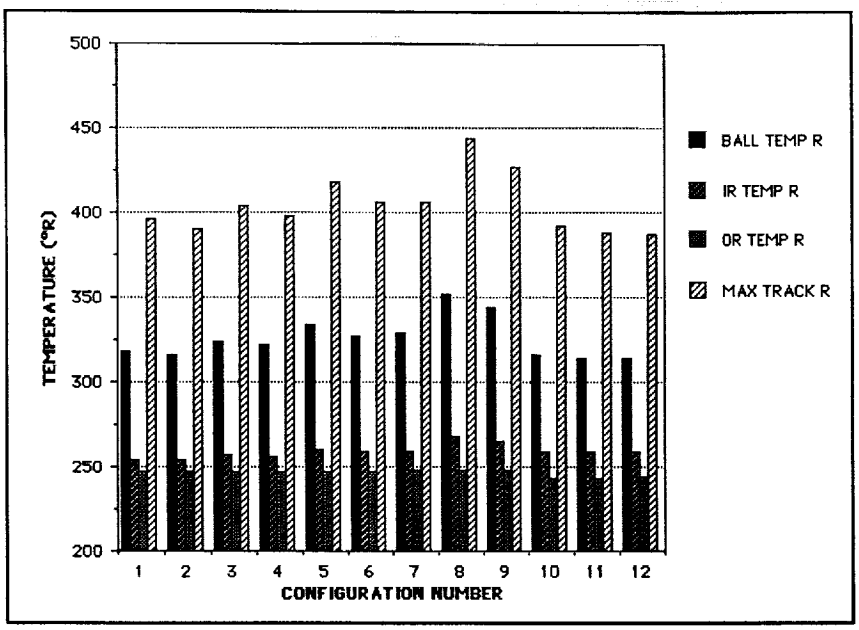

Exhibit 112 Simplex Pump 45mm Pump End Bearing Temperature

"stick out" changes and, thus, the axial preload changes as a function of press fit on the shaft, chill down, speed, and steady-state operation of the bearings. The analysis simulated preload springs with a stiffness of 20,314 N/mm (116,000 lb/in.), free height of 2.890 mm (0.1138 in.), and compression travel of 0.1753 mm (0.0069 in.). This spring was designed with a low travel so that one spring would completely bottom without unloading the opposing spring. The axial stiffness of the Simplex bearings with silicon nitride rolling elements was determined to be 103,550 N/mm (590,260 lb/in.). The equivalent axial stiffness of the bearing and the spring was calculated to be 17,010 N/mm (96,950 lb/in.).

The desired operating preload was determined to be 2670 N (600 lb.) from a previous analysis of the Simplex pump (August 1993 Progress Report). Thus, working backwards from this preload the amount of spring compression required during assembly was de-

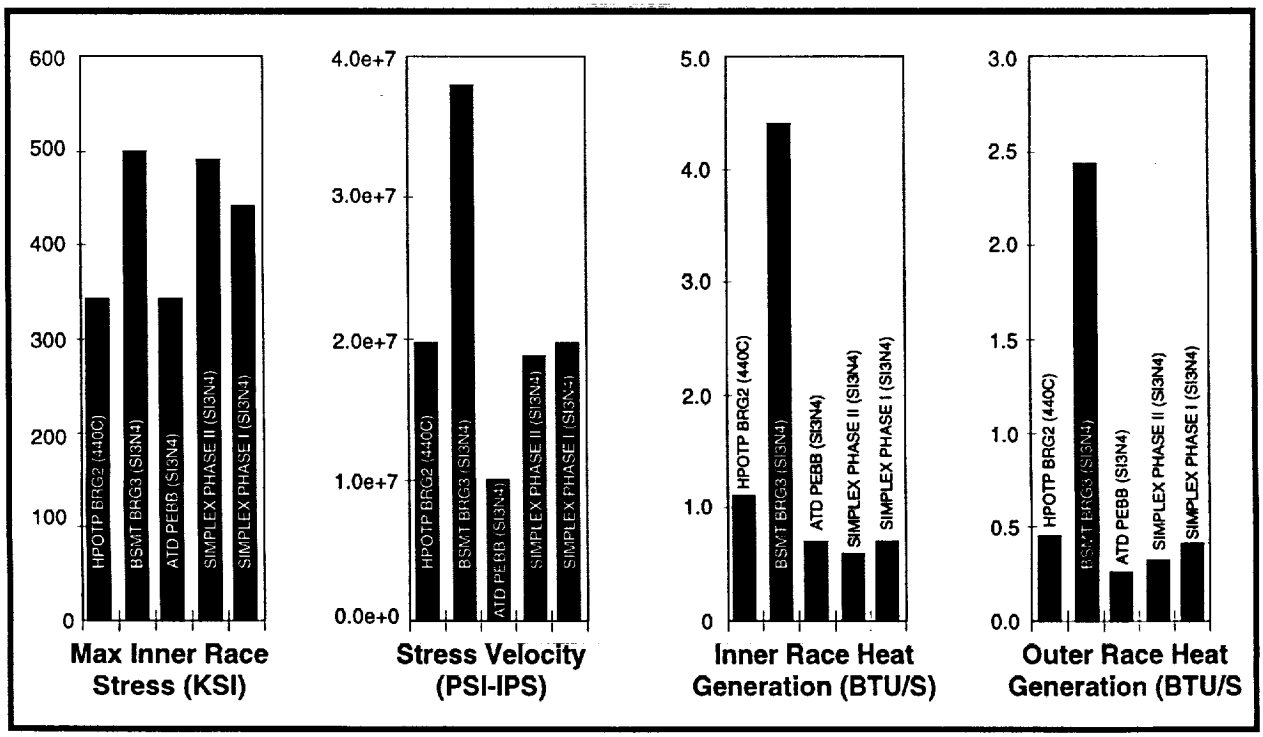

Exhibit 113 Simplex Bearing 1 Stress and Heat Compared to Other LO2 Bearings

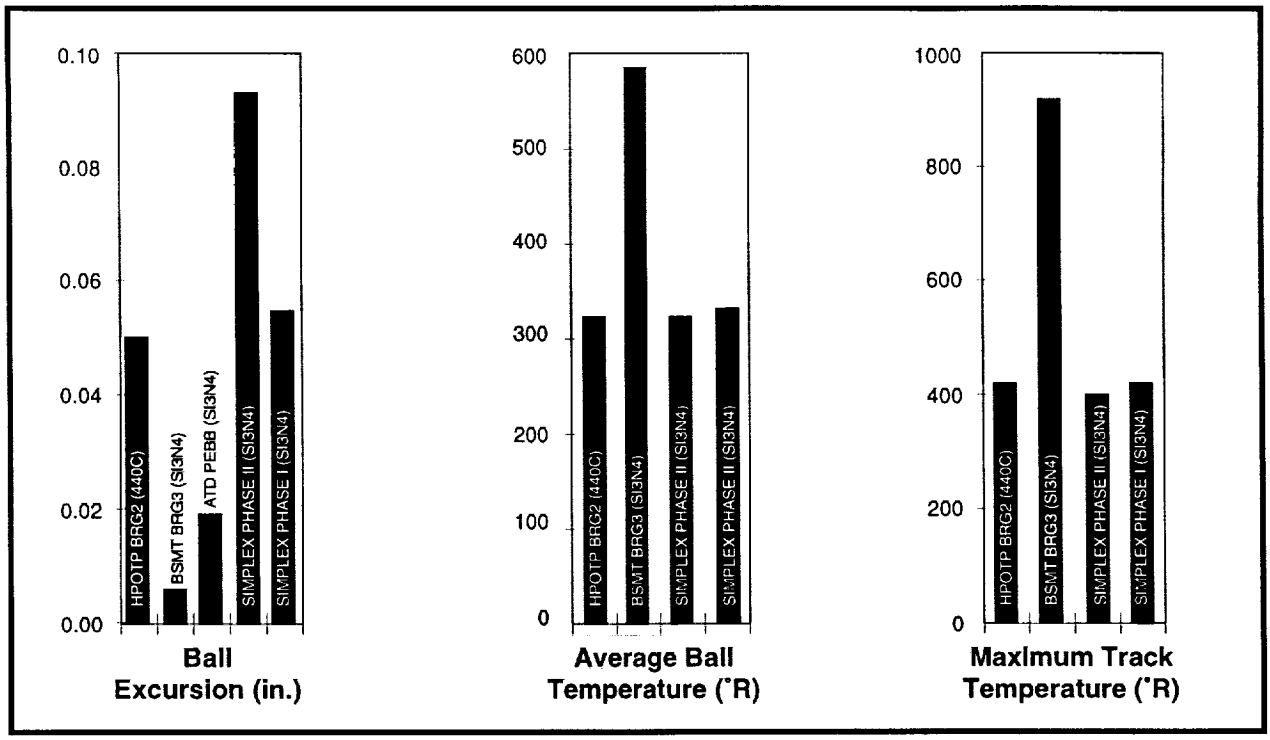

Exhibit 114 Comparison of Simplex Bearing 1 to Other LO2 Bearing Applications

termined. **Exhibit 115** illustrates the bearing preload of the Simplex pump at the different bearing conditions. As the exhibit shows, approximately 1650 N (370 lb.) of preload spring/bearing compression force is needed as the pump is assembled. Therefore, dividing this assembly preload by the equivalent spring/bearing stiffness gives the required compression of 0.0965 mm/bearing (0.0038 in/brg). This requires that the bearing inner race spacer be a total of 0.1930 mm (0.0076 in.) shorter than the two unloaded springs and housing spacing or 5.588 mm (0.220 in.) longer than just the housing spacing.

The preload increase due to press fitting the inner races on the shaft was determined using a .03556 mm (0.0014 in.) tight fit. The analysis also assumed that the inner and outer race faces were coplanar under a 220 N (50 lb) axial load. This analysis needs to be performed for each Simplex build and actual dimensions of the bearings and springs are verified. Also, a push-pull test after the shaft has been installed in the housing is desirable to verify the correctness

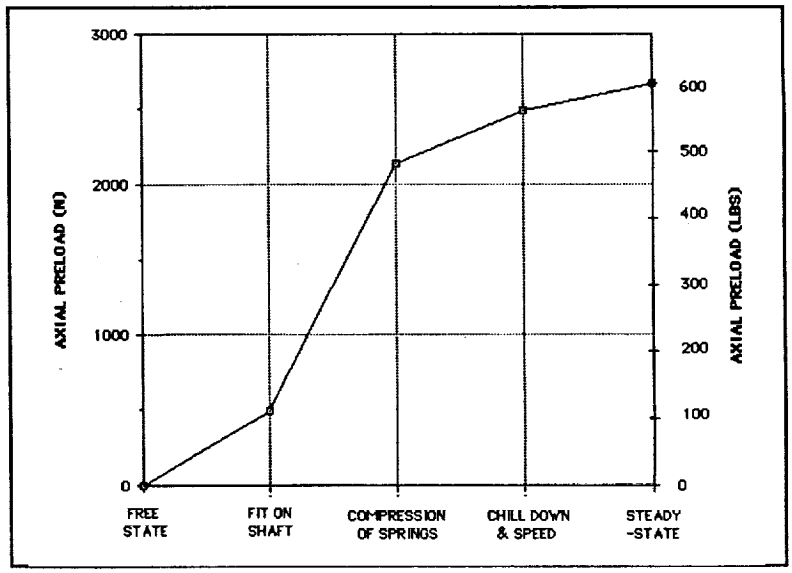

Exhibit 115 Simplex Preload at Different Bearing Conditions

of remaining spring travel. The remaining spring travel is crucial since it was set to a minimum to avoid bearing unloading during shaft axial transients.

The design trades performed under this effort were provided to NASA to support the in-house design of the SIMPLEX pump. This pump has now been successfully built and tested at MSFC.

4.0 — Hardware Anomaly Investigation

One of SRS Technologies support functions provided during the period of this effort was to provide analytical support and technical evaluation of various hardware anomalies that were encountered in SSME turbopumps or bearing rig testing. Many of the investigations of this type have been reported in other sections of this document. This section of the report documents the hardware anomaly studies that did not clearly fit in any of the other chapters of this document.

4.1 Investigation of Spiral Scarring on ATD Pump End Ball Bearing

Two ATD LOX turbopump tests were terminated prematurely due to excessive vibrations which occurred near the 88% power level. After the first test, Pratt & Whitney's post test inspection found that at least one rolling element had an unusual spiral scar. The scarring started with one mark at a relatively large radius and then a circular scarring with a tighter radius (~2.29 mm) was found inside of the larger radius scar. The scarring appeared to be located near 90° from the rolling track of the ball. Inspection of the bearing after the second test showed similar scarring on most of the rolling elements. However, there was significant variation in the sizes and locations of the scarring from ball to ball. Several possible scenarios were investigated to evaluate possible causes of the observed scarring.

The first scenario considered was that the bearing had become axially unloaded at some point in the test and the shafts axial position had shifted sufficiently to allow the spinning ball to come in contact with the shoulder on the load side of the inner race. However, investigation of the bearings geometry showed that in order for this to occur, the operating internal clearance of the bearing would have to be at least greater than 0.38 mm. No phenomenology could be identified which could account for the bearing operating with this much clearance. Therefore, this scenario was considered unlikely. However, it should be noted that it might be possible for the ball to contact the shoulder with a smaller clearance if there was significant misalignment of the inner and outer races due to outer race tilt or shaft bending.

An ADORE dynamic model of the bearing was used to investigate additional possible causes of the observed scarring. Various loading conditions were simulated and the orientation of the angular velocity vector was plotted on a scaled view of the bearing cross-section. The models were setup with an internal operating diametrical clearance of 0.127 mm. Several load cases were modeled to determine the effects of load on the orientation of the spin vector. **Exhibits 116, 117,** and **118** show the effects of axial load on the spin vector and contact angles. For these simulations,

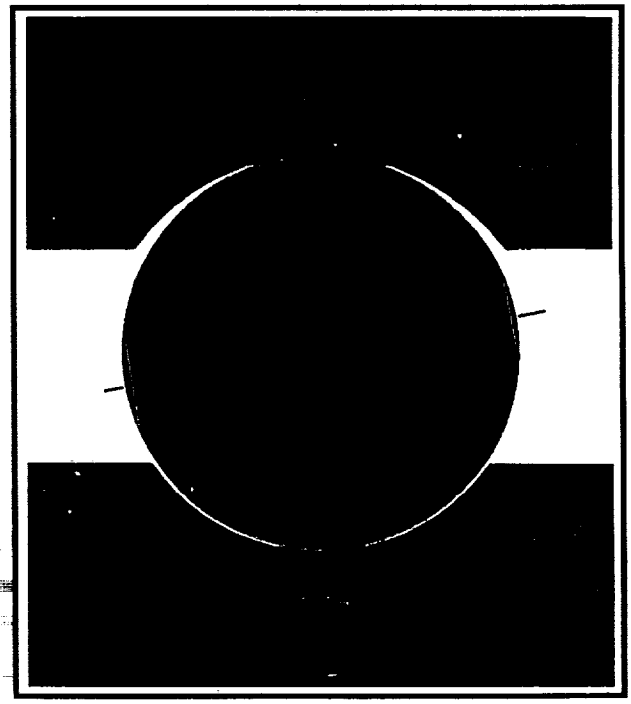

Exhibit 116 Spin Vector Orientation for ATD Pump End Bearing with 2,000 lbs Axial Load and 0 Radial Load

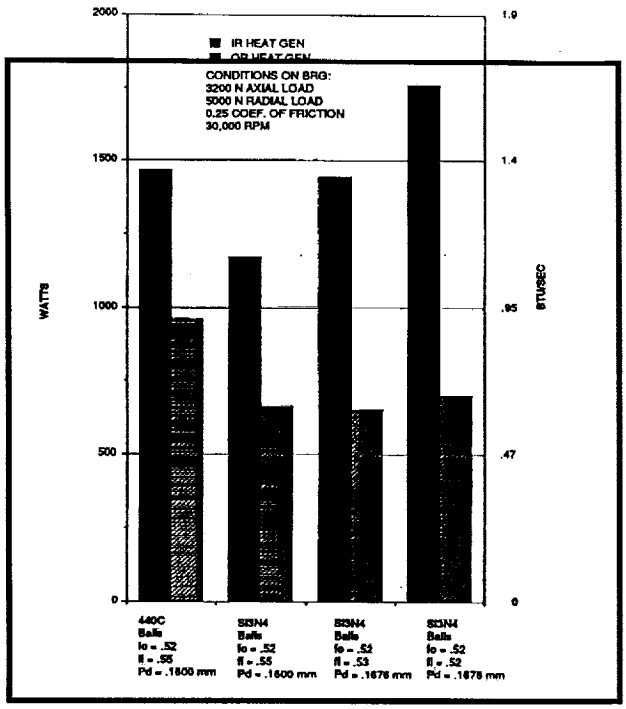

Exhibit 117 Spin Vector Orientation for ATD Pump End Bearing with 20,000 lbs Axial Load and 0 Radial Load

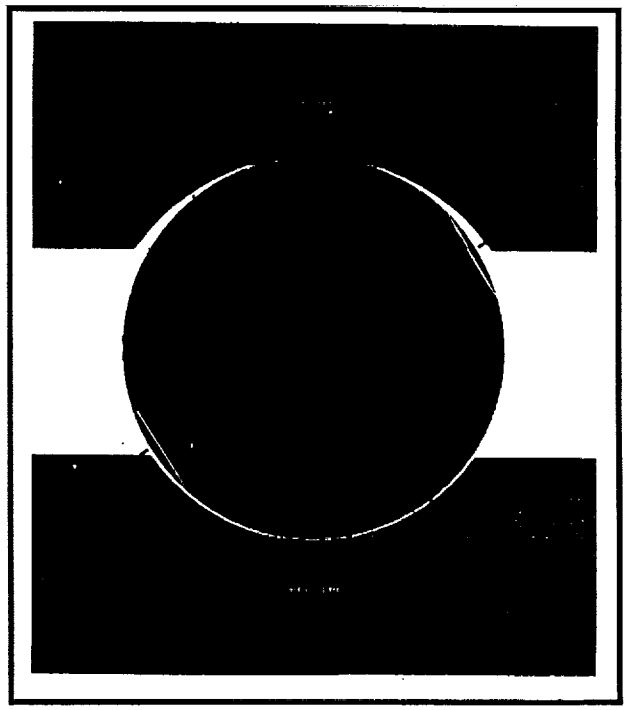

Exhibit 118 Spin Vector Orientation for ATD Pump End Bearing with 200,000 lbs Axial Load and 0 Radial Load

the applied radial load was 2,000 lbs, 20,000 lbs, and 200,000 lbs, respectively. The later axial loads are unrealistically high, and would result in failure of the bearing due to high stresses. However, the high loads illustrates the effect of radial load on the rolling element orientation. The illustrations have lines drawn near the spin poles which are scaled to the 4.57 mm diameter of the scarring seen after the first test. It can be seen from these plots that as the axial load increases the contact angles increase and the spin vector shifts towards the unloaded shoulder of the inner race. The analysis suggests that the scarring radius matches the unloaded shoulder for a load between 2,000 and 20,000 lbs. **Exhibit 119** shows the orientation of the rolling element for a bearing loading of 100 lbs axial load and 1,000 lbs radial load. The rolling element shown is for the heaviest loaded ball. The normal load on the inner race for this ball is 561 lbs. **Exhibit 120** shows the orientation of the same rolling element after the ball has rotated 100 degree's and has become unloaded on the inner race. Exhibits 119 and 120 show that with low axial loads the spin vector is nearly aligned with the shaft. The radius of the scarring is above the shoulders of the inner and outer races.

Reviewing the plots of the bearing with axial load only suggests that the most likely part of the bearing that could have caused the scarring is the unloaded side of the race grooves on the unloaded side race shoulders. It is possible to envision a scenario where the bearing is suddenly unloaded, due to axial vibration or an axial shift of the races for another reason, which causes the rolling element to contact the unloaded side of the race. The impact of the spinning ball on the race could possibly have caused the scarring. Pratt & Whitney reported finding some indications of contact with the unloaded side of the inner race. On the other hand, Exhibits 119 and

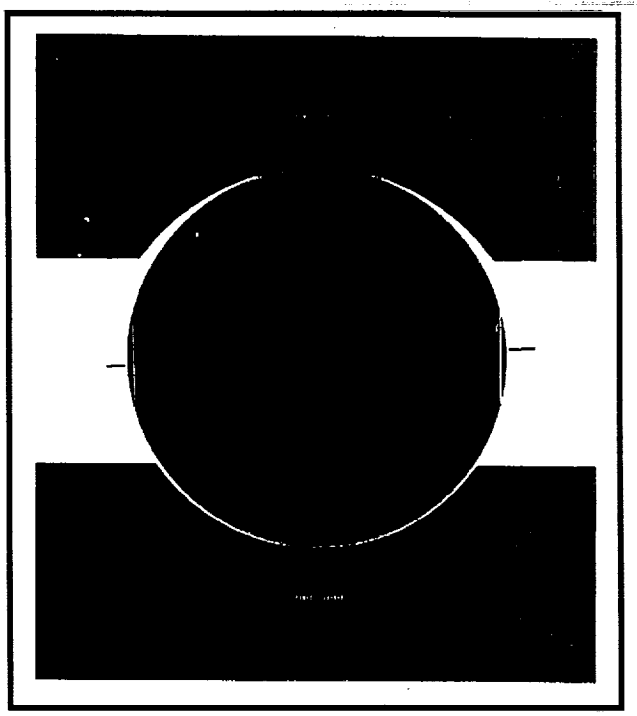

Exhibit 119 Spin Vector Orientation for ATD Pump End Bearing with 100 Lbs Axial Load and 1,000 Lbs Radial Load (Heaviest Loaded Ball)

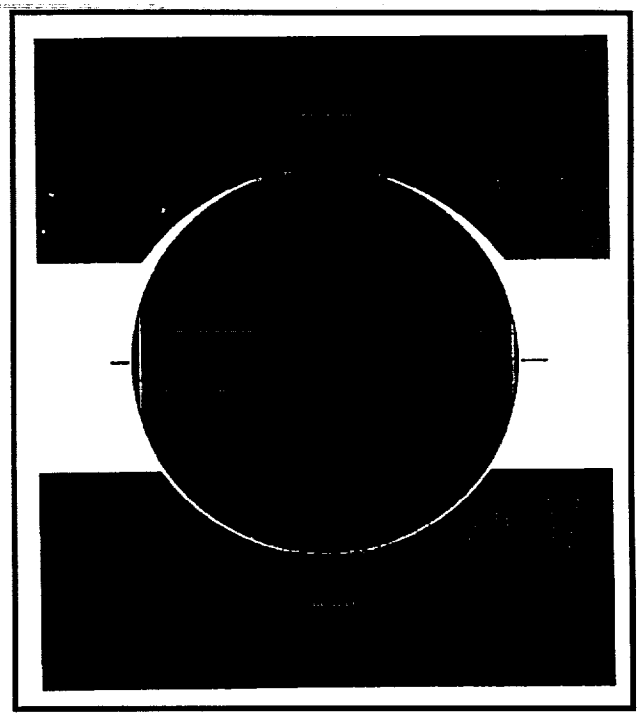

Exhibit 120 Spin Vector Orientation for ATD Pump End Bearing with 100 Lbs Axial Load and 1,000 Lbs Radial Load (Ball Unloaded on Inner Race)

120 show that as the ball becomes unloaded, the spin vector shifts to parallel with the shaft and the scarring seen has too small of a radius to have been caused by either of the races, for the ball spinning in this orientation. Therefore, if the scarring is caused by impacts with the unloaded side of the race, the phenomenon must occur due to the rapid shift of the races occurring so quickly that the ball does not have time to reorient its spin vector. This analysis does not predict the time period that would be required for the ball to reorient. Also, the analysis does not indicate the effect on ball orientation of the initial contact with the unloaded side of the race. Additional analysis is required to quantify these effects. However, based on the results of this analysis, it appeared that unloading of the bearing and contact unloaded side of the race was involved in generating the scarring.

4.2 ATD Pump End Ball Bearing Analysis Support

Analysis support was provided to aid the investigation of abnormal wear in the Pratt & Whitney ATD pump end ball bearing (PEBB). Tests were shut down prematurely due to the pump end ball bearing coolant delta temperature exceeding its redline value. There was a relatively gradual rise in coolant DT for about five seconds, and then a step increase of about 0.56K (1°R) followed by a gradual rise. The total temperature difference increased about 1.12K (2.5°R). This suggested at least two mechanisms for heat generation in the bearing. One, a relatively slow process which caused high local track temperatures degrading the contact lubrication followed by a step change in coolant temperature caused by a sudden increase in frictions (heat generation due to sudden loss of lubrication).

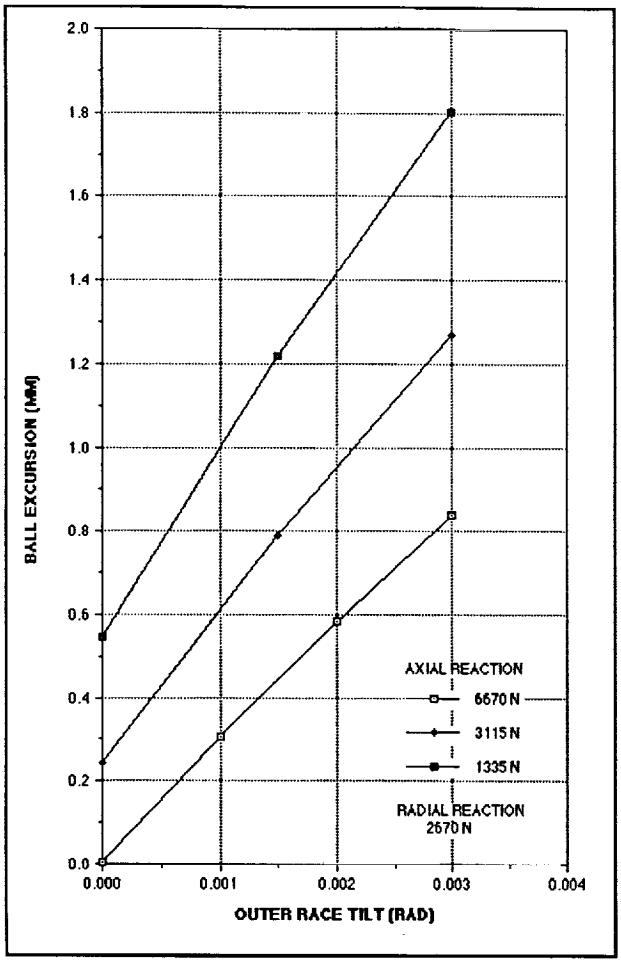

Exhibit 121 ATD PEBB Ball Excursion

The potential for cage/ball interaction to produce high ball heating was investigated with the quasi-static model, and later with the dynamic ADORE model. The quasi-static results are shown in **Exhibit 121** in which ball excursions are shown as a function of outer race tilt and axial load. The axial load was included because loss of preload would be consistent with ball track wear observed on the bearing outer race. This view is representative of bearing unloading, relative high fluid pressure levels on the cage and negative contact angles.

The diametrical cage pocket to ball clearance is 0.508mm (0.020 in) to 0.7112mm (0.028 in) at room temperature. It was estimated that the operating cage/ball clearance was about 0.762 mm (0.030 in). The operating clearance can be fully used to accommodate ball excursion for high tilt or loss of preload (axial load). When pocket clearances are lost there is a potential for rapid increase in cage heat generation, and accelerated cage pocket and ball wear.

The sensitivity of bearing coolant temperature rise to axial load, contact friction, and radial load was determined. The results are shown in **Exhibits 122** and **123**. As shown in Exhibit 122 the sensitivity of coolant temperature difference to axial load is amplified with increased contact friction. If the friction coefficient increased from 0.1 to 0.4, possibly by loss of Salox lubricant film, the coolant temperature difference can eas-

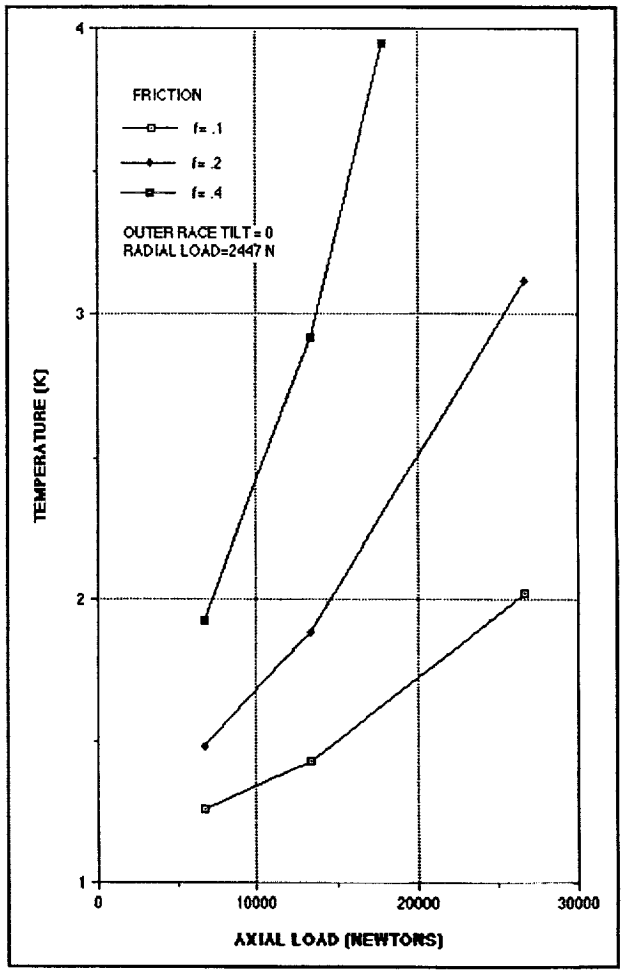

Exhibit 122 ATD PEBB Coolant Temperature Rise Versus Axial Load and Friction

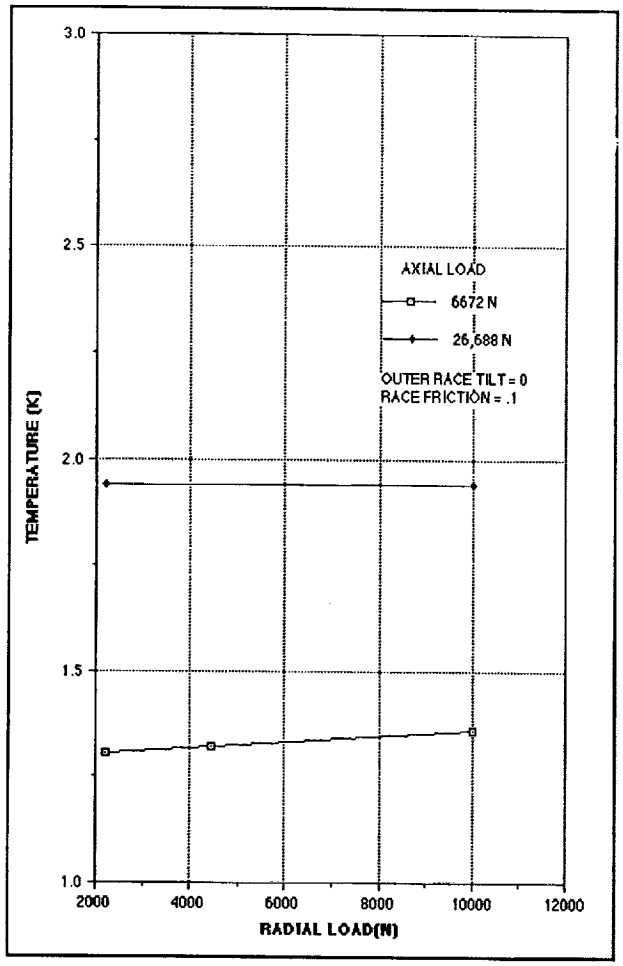

Exhibit 123 AFD PEBB Radial Load Versus Coolant Temperature Rise

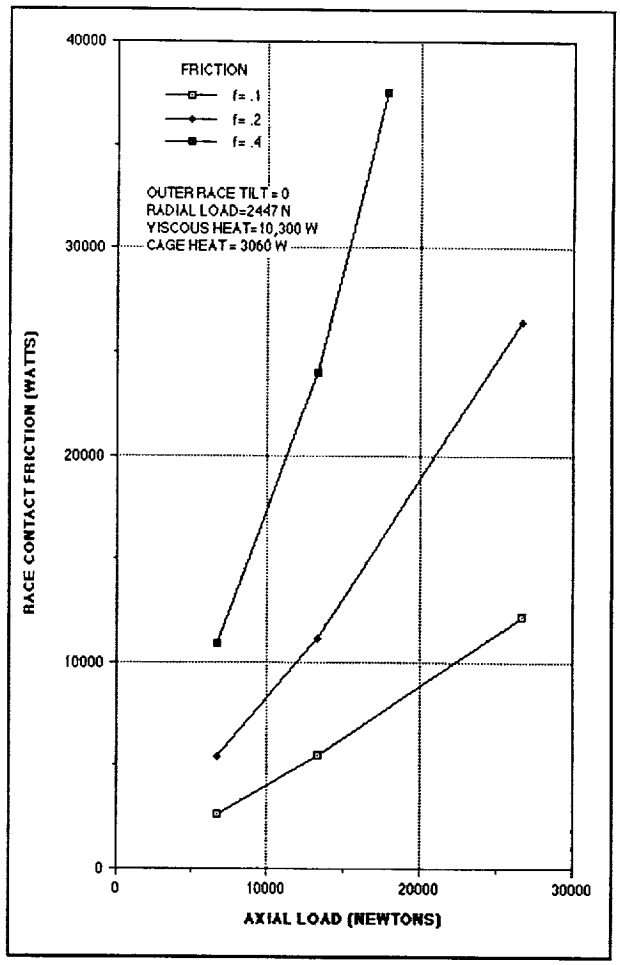

Exhibit 124 ATB PEBB Contact Friction Heat Versus Axial Load and Friction

ily double at moderate axial reactions (14,000N, (3150 lbs).). Coolant temperature rise was relatively insensitive to radial load changes as shown in Exhibit 123. The sensitivity of frictional heat generation to axial load and friction is shown in **Exhibit 124**. The maximum track temperature as a function of axial load and contact friction is shown in **Exhibit 125**.

These results showed that axial load and contact friction were the dominant parameters affecting bearing internal heat generation and coolant temperature. The other significant parameters affecting bearing internal heat generation are the ball/cage and cage/land heat generation. These parameters are affected by cage clearances and cage stability, and were investigated using the "ADORE" software.

An analysis was performed to estimate the magnitude of frictional cage heat generated in the LOX pump PEBB bearing. The SINDA/ SHABERTH thermomechanical model of the PEBB bearing was used to estimate circumferential ball excursions which occur in the bearing due to radial load and bearing misalignment (Exhibit 121). This analysis shows that for various combinations of axial load, radial load, and misalignment the ball excursions can exceed the estimated operating ball pocket clearance of .726 (30 mils). When ball pockets clearance is exceeded, large cage to ball loads occur and large

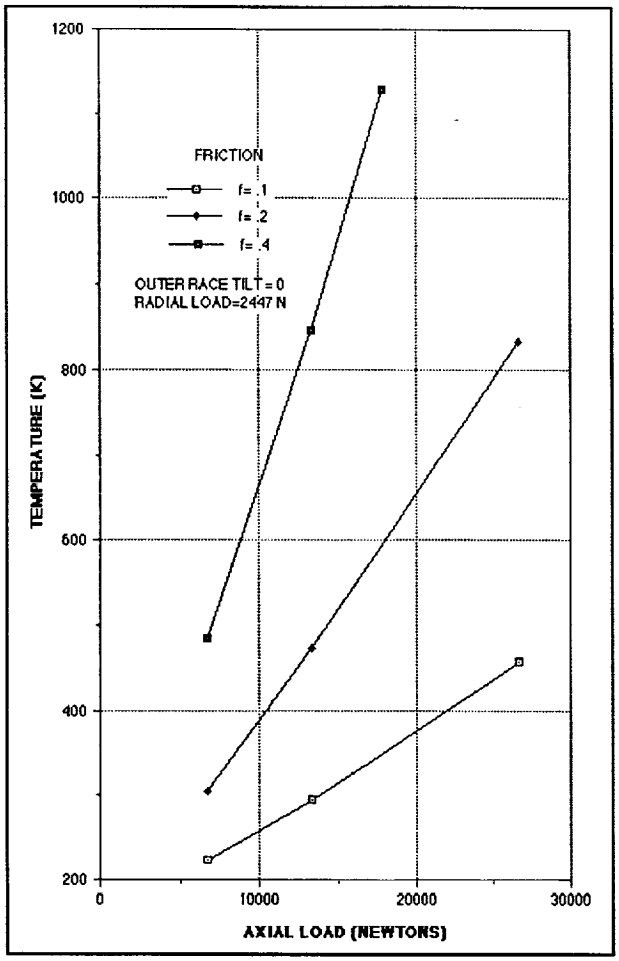

Exhibit 125 ATD PEBB Maximum Track Temperature Versus Axial Load and Friction

amounts of cage frictional heat are generated. To quantify the magnitude of cage heat generation a dynamic analysis was required. Therefore, the ADORE model of the PEBB was used to generate a curve of cage heat generation versus bearing misalignment. The bearing was modeled with a nominal axial load of 6672N (1500 lbs) and a nominal radial load of 2668N (600 lbs). The ball to cage heat generations predicted are shown in **Exhibit 126**. Only small changes in ball to cage heat generation rates were seen for misalignment angles of up to 0.0015 Rad. However, cage heat generation jumps by a factor of six for a misalignment angle of 0.003 Rad. This jump in ball to cage heat generation is caused by ball excursions exceeding the pocket clearance. For the flow conditions in the bearing, a heat generation of 6650 watts corresponds to a 0.56K (1°R) temperature rise across the bearing. ADORE also predicts a significant rise in cage heat generation between the cage and guide lands for cases where ball excursions exceed pocket clearance. Total cage to race heat generation versus misalignment is shown in **Exhibit 127**. The sum of cage to ball heat generation and cage to race heat generation is shown in **Exhibit 128**. These curves were provided to NASA for incorporation into in-house thermal analysis of various proposed failure scenarios.

Thus, the ADORE analysis showed the sensitivity of cage heat generation to misalignment. The sensitivity to ball speed variation caused by

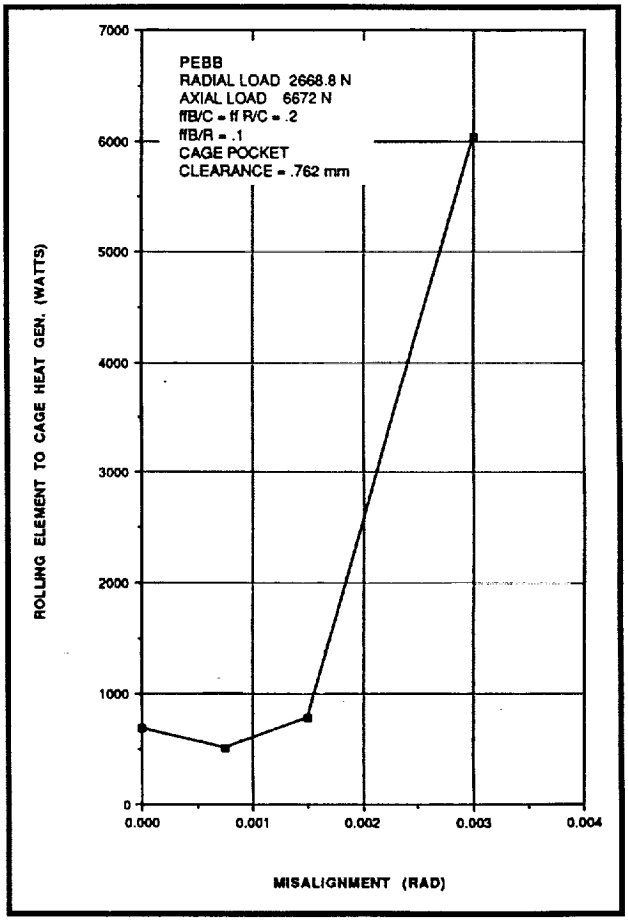

Exhibit 126 Total Ball To Cage Heat Generation

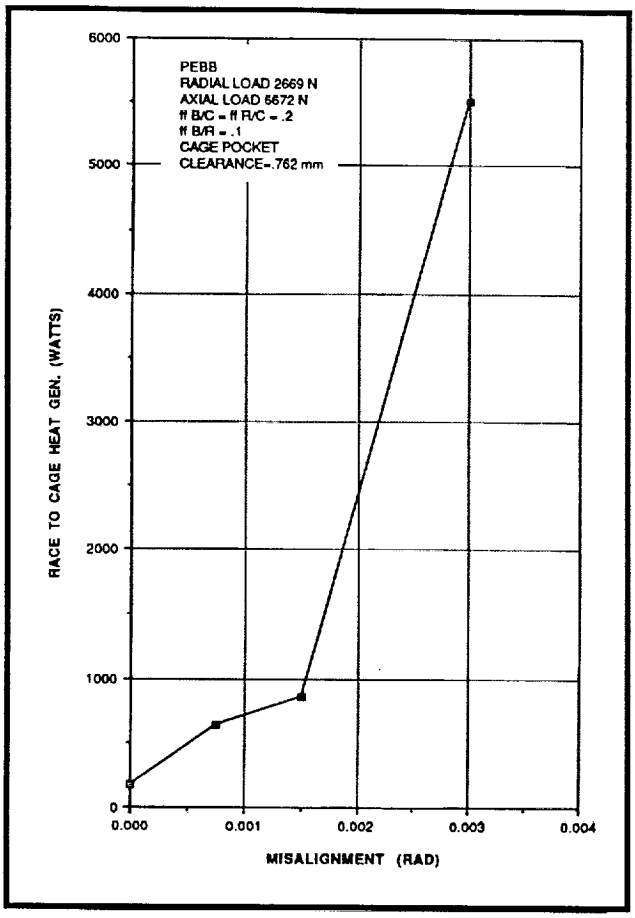

Exhibit 127 Total Cage To Race Heat Generation

misalignment or radial load could be reduced by opening the pocket clearance. Analysis has shown that bearing heat generation does not change significantly with misalignment until the ball excursions exceed the pocket clearance. The curves shown in Exhibit 121 can be used to calculate how much excursion the bearing can tolerate prior to exceeding pocket clearance. Opening the pocket clearance allows the bearing to operate at nominal heat generation rates with more misalignment. Therefore, opening the pocket clearance reduces the sensitivity of bearing heat generation to misalignment. However, changing pocket clearance can also affect cage stability. ADORE was used to evaluate the effects of ball pocket clearance on cage stability. For this analysis, the bearing was modeled with 6672N (1500 lbs) axial load, 2668N (600 lbs) radial load, and a misalignment of 0.015 Rad. For the initial analysis, the cage pocket clearance was increased from 0.76 mm (30 mils) to 1.27 mm (50 mils). The cage was found to be unstable with the larger pocket clearance. **Exhibit 129** shows a comparison of predicted bearing power loss (heat generation) and time averaged cage wear rate for the two cases modeled. Both power loss and wear rate increased by an order of magnitude for the larger pocket clearance. **Exhibit 130** shows the nature of the cage instability. The plots show the cage mass center orbital position as a function of bearing rotation. For the smaller cage pocket clearance, the cage tended to move towards one side of the bearing and didn't whirl significantly. For the larger clearance case, a backwards whirl instability

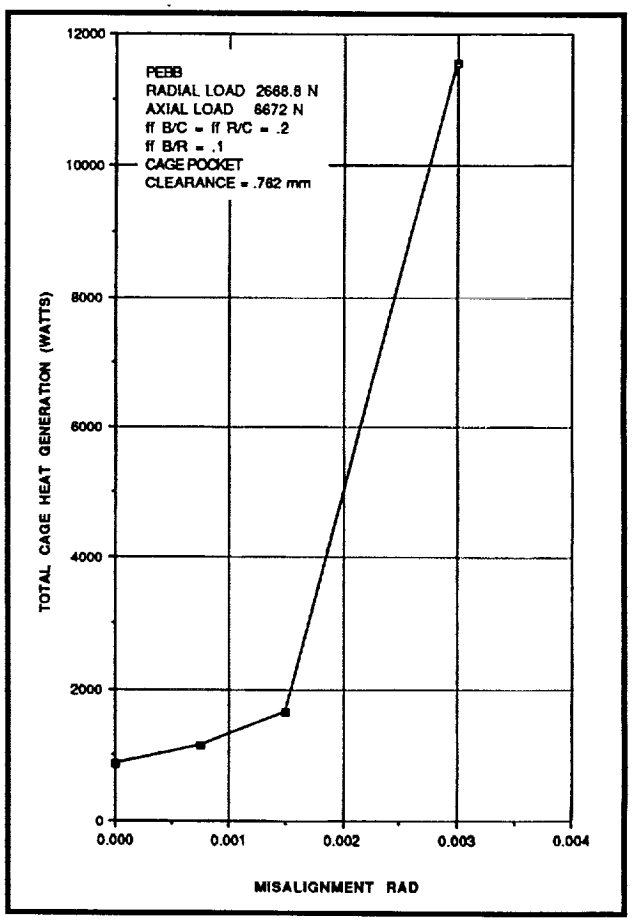

Exhibit 128 Total Cage Heat Generation

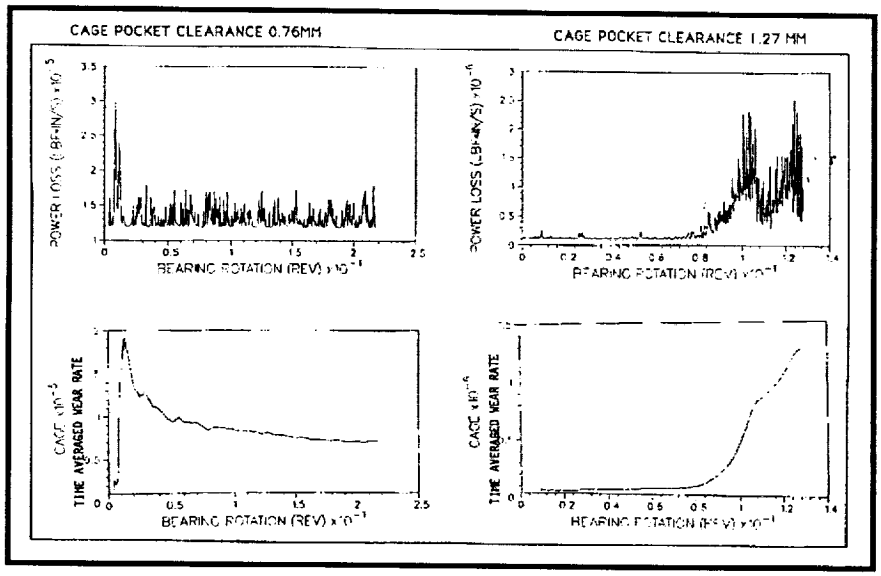

Exhibit 129 Effect of Cage Instability on Heat Generation and Cage Wear

occurs. This backwards whirl was indicated by the increasingly negative orbital position of the cage mass center and the large orbit of the cage.

Additional analysis was performed with ADORE to determine what forces were driving the instability. It was found that if the friction factor between cage and guide lands was reduced to 0.05 the instability would go away. The ADORE analysis included the journal bearing fluid forces between the guide lands and cage. However, the affect of axial flow through the bearing was not included. Inspection of PEBB cages after running in the pump seemed to indicate that very little rubbing was occurring between the cage and guide lands. If the cage was fully supported on a fluid film then the cage to race friction forces would be lower than indicated and the bearing should be able to operate with larger cage pocket clearances. However, it should be noted that opening the clearance increased the sensitivity of the cage to instability. Analysis was performed for various values of cage pocket clearance to find the threshold value of cage pocket clearance which would initiate the instability. The cage was predicted to operate stably with up to 1.07 mm (42 mils) pocket clearance. Therefore, this was a worse case stability limit and the bearing should have been able to operate stably even if the fluid film lift was lost at the cage guide lands. This analysis did not investigate the sensitivity of cage stability to other parameters such as radial load, axial load, internal clearance and misalignment. The values of these parameters were fixed at nominal values for each cage pocket clearance case studied.

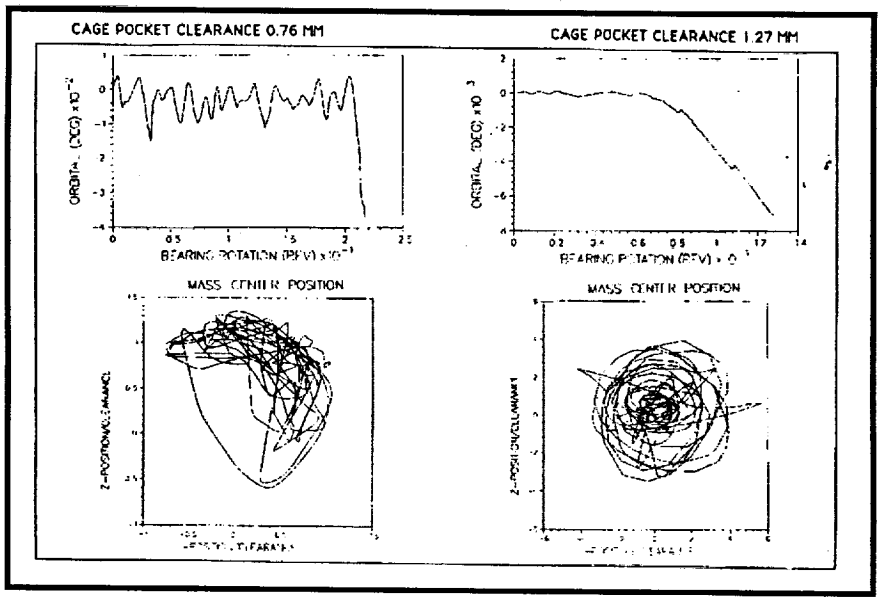

Exhibit 130 Effect of Cage Instability on Cage Motion

4.3 Investigation of Ball Size Variations Effects in ATD LO_2 Pumps

A preliminary investigation was conducted to evaluate the effects of ball size variation on heat generation and wear rate for the ATD pump end ball bearing. It was postulated that small ball to ball variations in surface finish, size, or heat transfer coefficient could cause a ball to ball temperature variation. Warmer balls would grow larger due to thermal expansion. A "boot strap" phenomenon could occur if a larger ball subsequently produced more heat. Bearings with 440C balls would be more susceptible to this phenomenon than would bearings with Si_3N_4 balls due to the lower coefficient of thermal expansion (CTE) of Si_3N_4. The CTE of Si_3N_4 is approximately 25% of the CTE of 440C.

Three cases were modeled with ADORE version 2.4 for an initial quick look at the sensitivity of heat generation and wear to ball size variation. Case number one was for nominal operating conditions at 104% power. Cases Two and Three were for the same loads and shaft speed. Case Two had one ball oversize by 0.0127mm (0.0005 in) and Case Three one ball oversize by 0.0254mm (0.0010 in). **Exhibit 131** shows a comparison of total bearing heat generation between Cases One and Two. Initially both bearings were generating approximately 13,600 in-lb/s (1540 watts) of heat. After approximately one shaft revolution, the total bearing heat generation for Case Two increases by a factor of two. This increased in heat generation occurred when the oversize ball, which had a lower orbital velocity, started rubbing the cage trying to slow the rest of the ball train. **Exhibit 132** shows the effect of this interference on component wear rates. The cage wear rate was increased dramatically while the race wear rates were increased only slightly.

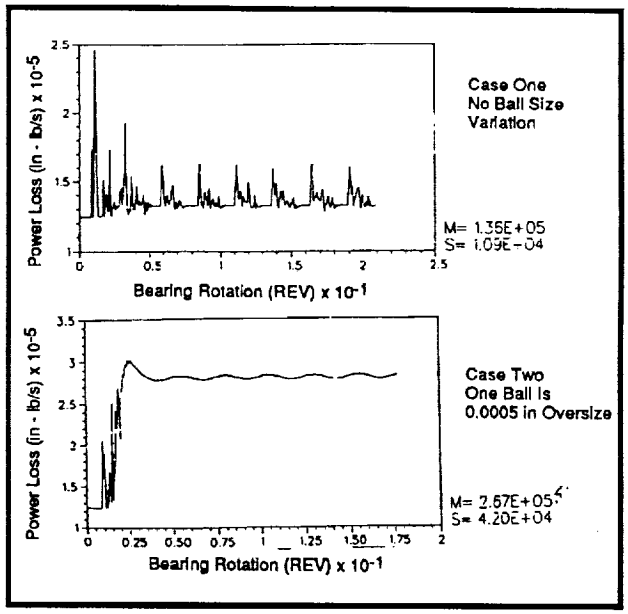

Exhibit 131 Affect of Ball Size Variation on Total Bearing Heat Generation

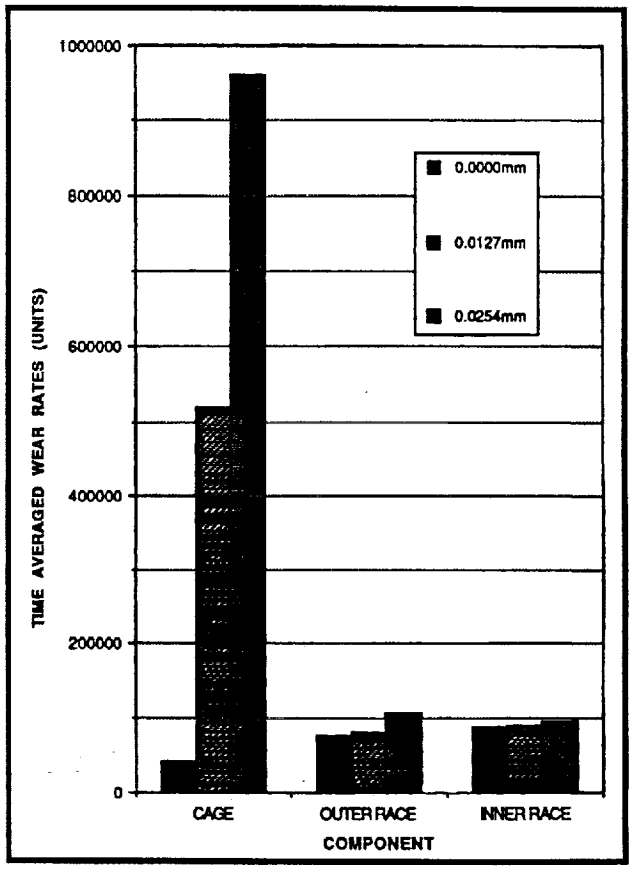

Exhibit 132 Time Averaged Wear Rates for Radial Loaded PEBB with One Oversized Ball

Exhibits 133 and **134** show the ball to ball variation in ball to race heat generation for the instant in time when the oversized ball was directly under the radial load. The chart shows that the heat generation increased significantly between the oversized ball and race. However, the heat generation of the other balls seemed to average out due to the change in load sharing caused by the oversized ball.

The results of this preliminary analysis showed that bearing heat generation could significantly increase as a result of ball size variation. A more thorough investigation was required before an attempt could be made to develop a viable bearing wear scenario based on ball size variation.

4.4 Evaluation of Bearing Stiffness Loss as a Function of Ball Wear for Rocketdyne SSME Fuel Pump Bearings. PC SHABERTH was used to evaluate bearing radial stiffness loss resulting from ball wear in the SSME fuel pump bearings. The objective was to provide a stiffness versus ball curvature to support further rotor dynamic analysis. A quick turn-around analysis was required, therefore a single bearing model was used to perform the study. The major limitation of a single bearing model is that the reaction moments supported by the bearing must be specified rather than calculated. A full shaft/bearing model was required to calculate the moments. For this study, two bounding cases of bearing reaction moment were considered.

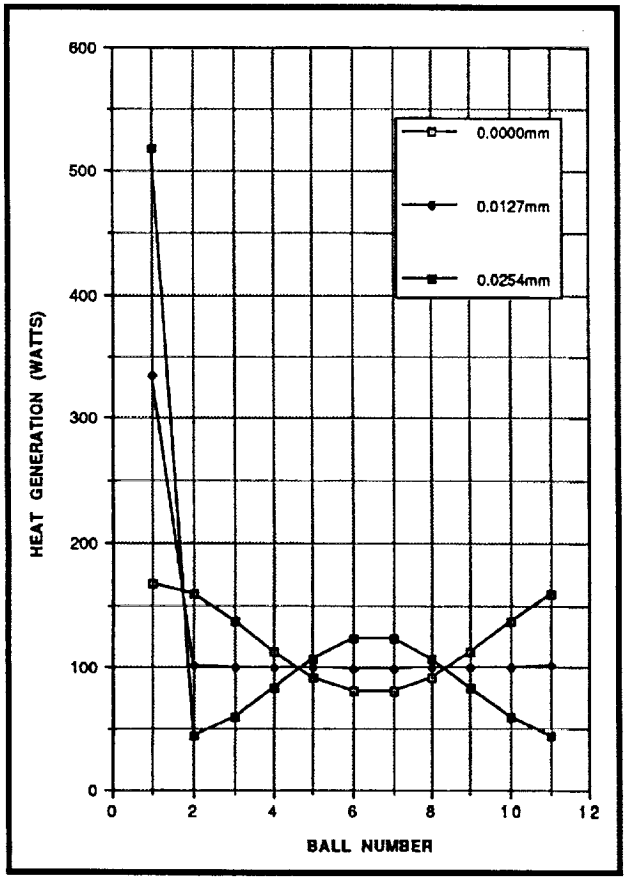

Exhibit 133 Inner Race Heat Generation With Oversized Ball Under Radial Load

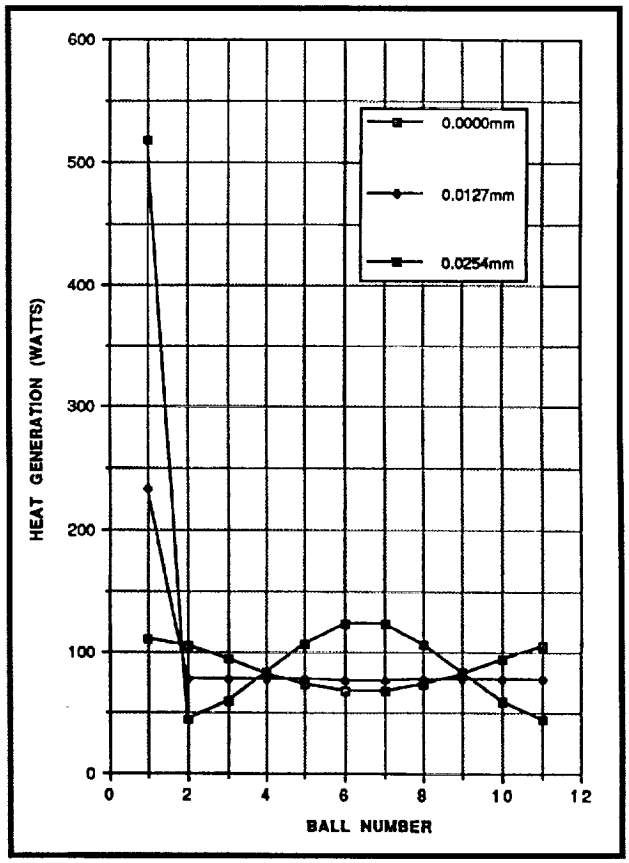

Exhibit 134 Outer Race Heat Generation With Oversized Ball Under Radial Load

For the first case, the outer race was assumed to be fully constrained so that no tilt relative to the inner could occur. The bearing was very stiff for the no tilt condition. **Exhibit 135** shows the calculated bearing stiffness for no tilt and diametrical ball wear up to 0.05mm (0.002 in.). The model includes the effects of bearing preload reduction which occurs as a result of ball wear. With no wear, radial stiffness was 2.01 x 10^5 N/mm (1.15 x 10^6 lb/in.). Diametrical ball wear of 0.05 mm (0.002 in) reduced bearing stiffness to 4.55 x 10^4 N/mm (2.6 x 10^5 in/lb.). **Exhibit 136** shows a plot of bearing deflection for the same cases of ball wear.

The second case modeled was the zero moment case. For this case, the outer race was not constrained, therefore it tilted until the reaction moment went to zero. The bearing was not radially stiff in this condition. **Exhibit 137** shows the secant radial stiffness for the zero moment case and diametrical ball wear up to 0.05 mm (0.002 in). With no wear, radial stiffness was 3.45 x 10^4 N/mm (1.97 x 10^5 lb/in.). Diametrical ball wear of 0.05 m (0.002 in) reduced bearing stiffness to 1.59 x 10^4 N/mm (9.10 x 10^4 lb/in.). **Exhibit 138** shows a plot of bearing deflection for the same cases of ball wear.

The results of this study showed that bearing stiffness is very sensitive to ball wear. Ball wear of 0.05 mm (0.002 in) reduced the stiffness by 77% for the no tilt case and 54% for the zero moment case. If the balls accumulated 0.05 mm of wear, the bearing stiffness was reduced by at least a factor of two.

4.5 Analysis of Rocketdyne HPOTP 2315R3 Pump End Bearings

The Rocketdyne High Pressure Oxygen Turbopump 2315R3 was tested on an engine at MSFC. This turbopump was assembled with the

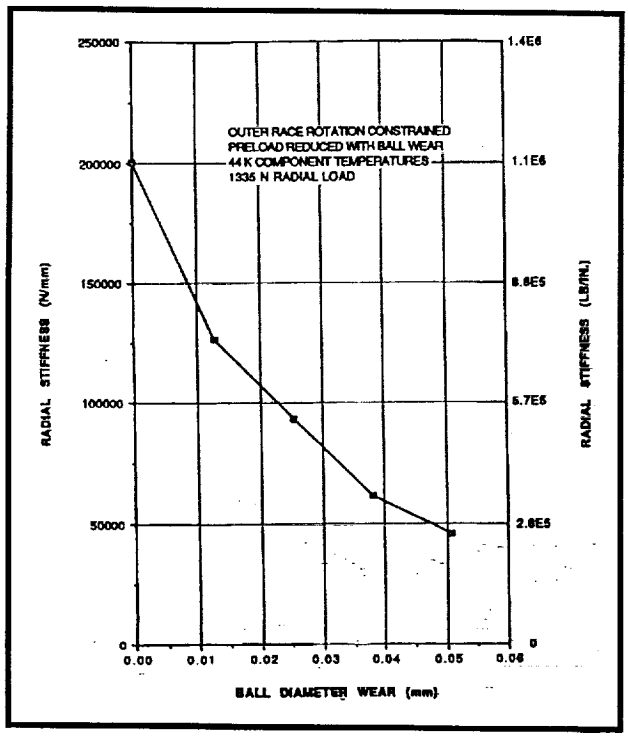

Exhibit 135 RKD HPFTP Bearing Secant Stiffness

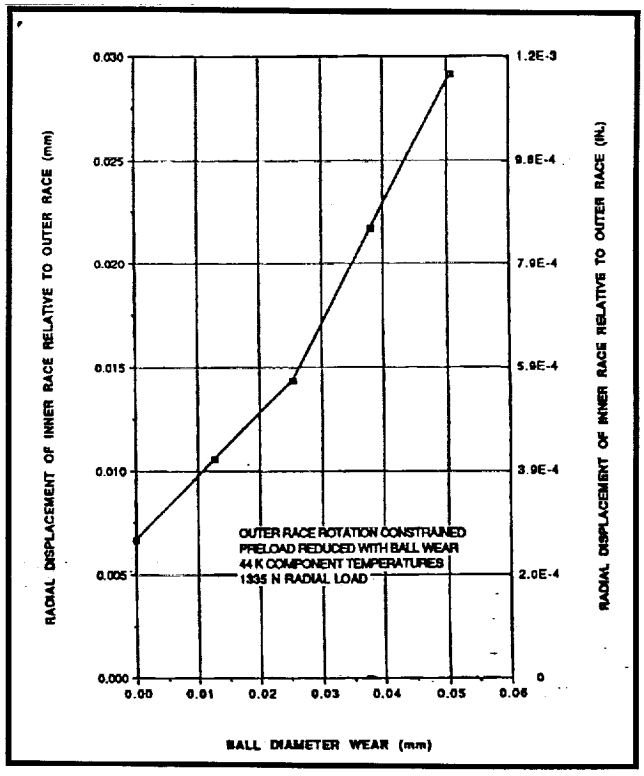

Exhibit 136 RKD HPFTP Bearing Radial Deflection

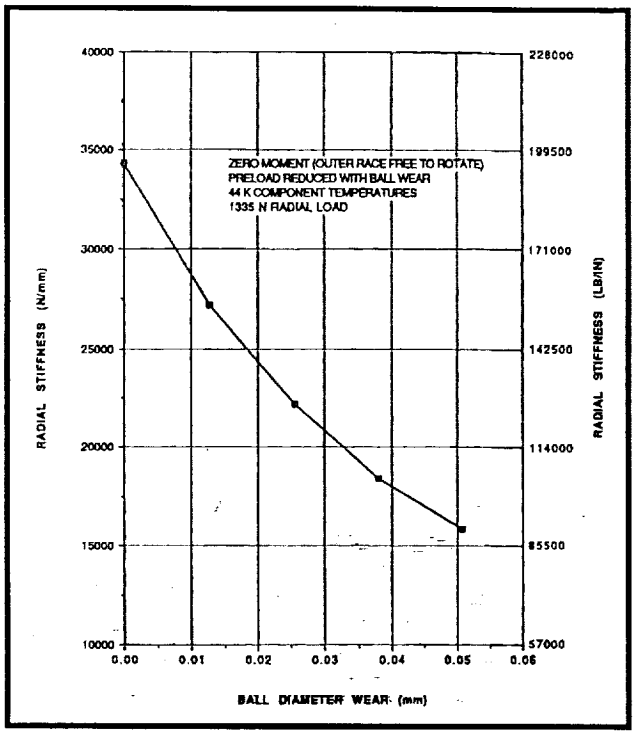

Exhibit 137 RKD HPFTP
Bearing Secant Stiffness (Zero Moment)

45mm pump end bearings containing silicon nitride balls. This application had previously been analyzed to determine the best bearing geometry and preloading configuration. The results of the previous analysis showed that the standard geometry and preload of Phase II flight bearings being used at that time with 440C steel balls were an acceptable configuration for the bearing using Si3N4 balls. However, during assembly of this pump an undersize bearing spacer was used between the pump end bearings. This spacer set the distance between the inner races of the bearings which set the axial preload. An error was made in the calculation of the required thickness of the bearing spacer needed for a bearing using Si3N4 balls. The error resulted in a bearing preload of 3385 N (761 lbs) instead of the target preload of 2135 N (480 lbs). Also, the internal clearance of the bearings was slightly off design as a result of the ball substitution. The internal clearance of each bearing was machined in the races using the average diameter of a specific set of steel balls, thus, creating a matched set of inner race, outer race, and balls. However, the steel balls used in these bearings were undersized by 0.00381 mm (0.00015 in.) for Bearing 1 and 0.01270 mm (0.00050 in.) for Bearing 2. Substituting the Si3N4 balls, which were 11.1125 mm (0.4375 in.) in diameter, resulted in a decrease of bearing internal clearance. The off design features of these bearings were simulated in the HPOTP application to determine if a problem in the operation of the bearings would result.

An analysis of the off design HPOTP pump end bearings with Si3N4 balls was performed using the SHABERTH/SINDA thermomechanical bearing program. With the exception of axial preload and bearing internal clearance, all other operating parameters were per Phase II specification. Two cases of radial load were used in the simulation. One case was

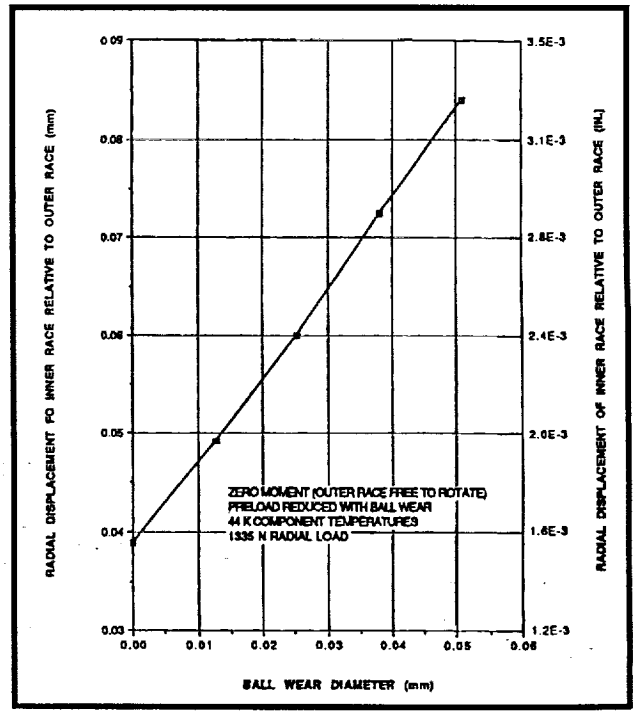

Exhibit 138 RKD HPFTP
Bearing Radial Deflection (Zero Moment)

considered nominal in which the pump end bearings supported approximately 3340 N (750 lbs). The other case used twice the nominal value and was considered worst case, although, radial loads in this range had been measured in instrumented pumps at MSFC. The results are shown in **Exhibit 139** and were compared to operating conditions for the HPOTP with 440C balls and the Bearing, Seal, and Materials Tester (BSMT) with 57mm bearings using Si3N4 balls. Comparing the flight configuration to HPOTP 2315R3 with nominal radial load showed that the only parameter that was not improved by using Si3N4 balls, even with the higher preload, was the maximum inner race contact stress. This fact would have been true even if the 2315R3 bearings had been assembled to specification. Previous analysis showed that the optimized 45mm bearing geometry with Si3N4 balls and nominal HPOTP parameters produced a maximum inner race stress of approximately 2.66 GPa (386 ksi). The higher contact stress was due to the modulus of the Si3N4 material. The high stress levels produced with Si3N4 balls had always been a concern, thus the BSMT had been used to test bearings with Si3N4 balls to very high contact stresses. Some of the results of the BSMT testing with silicon nitride balls are provided in Section 2 for comparison. The contact stress successfully tested to in the BSMT for over 126 minutes was well above the maximum contact stress predicted for HPOTP 2315R3 even using the worst case radial load configuration. Thus, based on this analysis and test experience it was believed that the off design clearance and preload of the HPOTP 2315R3 pump end bearings would not cause any bearing operational problems.

4.6 Analysis of 85mm LPOTP Bearing Ball Excursions

During prerun inspections of new SSME Low Pressure Oxidizer Turbopumps, technicians noticed that the torque required to rotate the shaft suddenly increased after the shaft rotated by some small angular amount. The torque increase was typically noticed after a rotation of approximately 270 deg. SRS was asked to investigate the possibility that this torque increase was caused by ball excursions resulting from the very small ball size variations which are present in all sets of ball bearings. For a new set of Grade 10 ball bearings, this variation is less than $\pm 10 \times 10^{-6}$ in. If ball excursion was the source of this phenomena, the torque increase would be noticed when one of the rolling elements begins to lead or lag the average ball train by an amount large enough to cause significant interference with the cage.

To investigate this scenario SRS developed a simple Mathcad spread sheet using equations presented in the text Rolling

	Flight HPOTP 440C Balls Nominal Radial Load		HPOTP 2315R3 Si_3N_4 Balls Nominal Radial Load		HPOTP 2315R3 Si_3N_4 Balls Worst Case RadialLoad		MSFC BSMT Si_3N_4 Balls (Turbine End Bearings)
	Brg 1	Brg 2	Brg 1	Brg 2	Brg 1	Brg 2	Inboard Bearing
Axial Load, N (lbs)	2780 (625)	2780 (625)	3434 (772)	3434 (772)	3443 (774)	3443 (774)	10480 (2356)
Radial Load, N (lbs)	1592 (358)	1793 (403)	1348 (303)	2100 (472)	2682 (603)	4270 (960)	3154 (709)
Maximum Inner Race Stress, GPa (Ksi)	2.26 (328)	2.31 (335)	2.67 (387)	2.81 (407)	2.92 (423)	3.19 (462)	3.44 (499)
Max SV,N/mm-s (psi-ips)	3.37E6 (1.92E7)	3.53E6 (2.01E7)	2.95E6 (1.68E7)	3.25E6 (1.85E7)	3.42E6 (1.95E7)	4.11E6 (2.34E7)	5.82E6 (3.32E7)
Inner Race Heat, W (Btu/s)	1266 (1.20)	1287 (1.22)	1097 (1.04)	1118 (1.06)	1129 (1.07)	1171 (1.11)	3788 (3.59)
Outer Race Heat, W (Btu/s)	562 (.533)	568 (.538)	479 (.454)	501 (.475)	536 (.508)	645 (.611)	2142 (2.03)
Ball Excursion, mm (in)	.965 (.038)	1.22 (.048)	.127 (.005)	.203 (.008)	.279 (.011)	.762 (.030)	.025 (.001)
Ball Temp, K (°R)	214 (385)	186 (334)	204 (367)	178 (320)	208 (374)	185 (333)	268 (482)
Max Track Temp, K (°R)	308 (554)	242 (435)	271 (488)	217 (391)	275 (495)	227 (408)	424 (763)

Exhibit 139 Comparison of HPOTP 2315R3 Pump End Bearings

Bearing Analysis , by Tedric A. Harris. The analysis involved solving for the average velocity of the ball train (cage speed) for an arbitrary shaft speed. The ball orbital speed for an off size ball was then determined for the same shaft speed. The relative velocity of the off size ball with respect to the cage could then be calculated. Using this relative velocity, the time required for a ball to travel the distance of the cage pocket clearance with respect to the cage could be determined as a function of shaft speed. Using the arbitrary shaft speed it was then possible to calculate the number of shaft revolutions required for the ball to traverse the pocket clearance and contact the cage. The torque increase would occur when the cage loading became sufficient to produce significant friction forces.

The analysis showed that for even relatively large ball size variations, a large number of shaft revolutions are required to cause cage interference. This analysis assumed that all of the balls were centered in the pockets initially. This is not a realistic assumption. However, for realistically small ball size variations the ball excursion are shown to be so small that multiple shaft revolutions would be necessary to produce significant cage force (friction) even if the off size ball were initially in contact with the cage. The Mathcad spread sheet and a plot of the number of shaft revolutions required to cause cage interference versus ball size variation is included in **Attachment C**.

Based on the results from the Mathcad model it did not appear that ball size variation was a reasonable explanation for the observed phenomena. A possible explanation is that the relatively high ball/race friction in the dry bearing causes the balls to try and roll up the race curvature causing the bearing to compress the preload spring. This loading would produce an increase in the torque required to rotate the shaft.

4.7 Space Shuttle APU Bearing Torque Investigation

A problem with the inner race of the bearings of an auxiliary power unit slipping and allowing the shaft to spin faster than the inner race was identified on a particular APU. It was desired to quickly determine the amount of torque the shaft needed to apply to rotate the bearing under nominal operating conditions. To address this quick response issue, the SHABERTH bearing program was used, without SINDA, to model the APU bearings at estimated temperatures and to calculate the torque required by each bearing. **Exhibit 140** shows a cross section of the unit depicting the location of the bearings. This unit had a nominal shaft speed of 72,000 rpm and used an oil mist to lubricate the bearings. The bearings had a 20 mm (0.787 in.) bore diameter with races and balls all made of M-50 steel. The axial preload simulated was 650 N (146 lbs.) with nominal radial loads of 188 N (42 lbs.) on the turbine end bearing and 625 N (140 lbs.) on the gear end bearing.

The model was run varying the radial load and inner race component temperature to determine the bearing torque sensitivity to these parameters. The resulting torque values for one bearing are shown in **Exhibit 141**. As shown, the inner race temperature has a much greater effect on bearing torque than does the radial load. This is because these bearings were well lubricated, thus providing low frictional work. However, the viscous fluid work is a significant portion of the total work and is greatly influenced by the inner race temperature which affects the bulk lubricant temperature. At the time of this study the exact

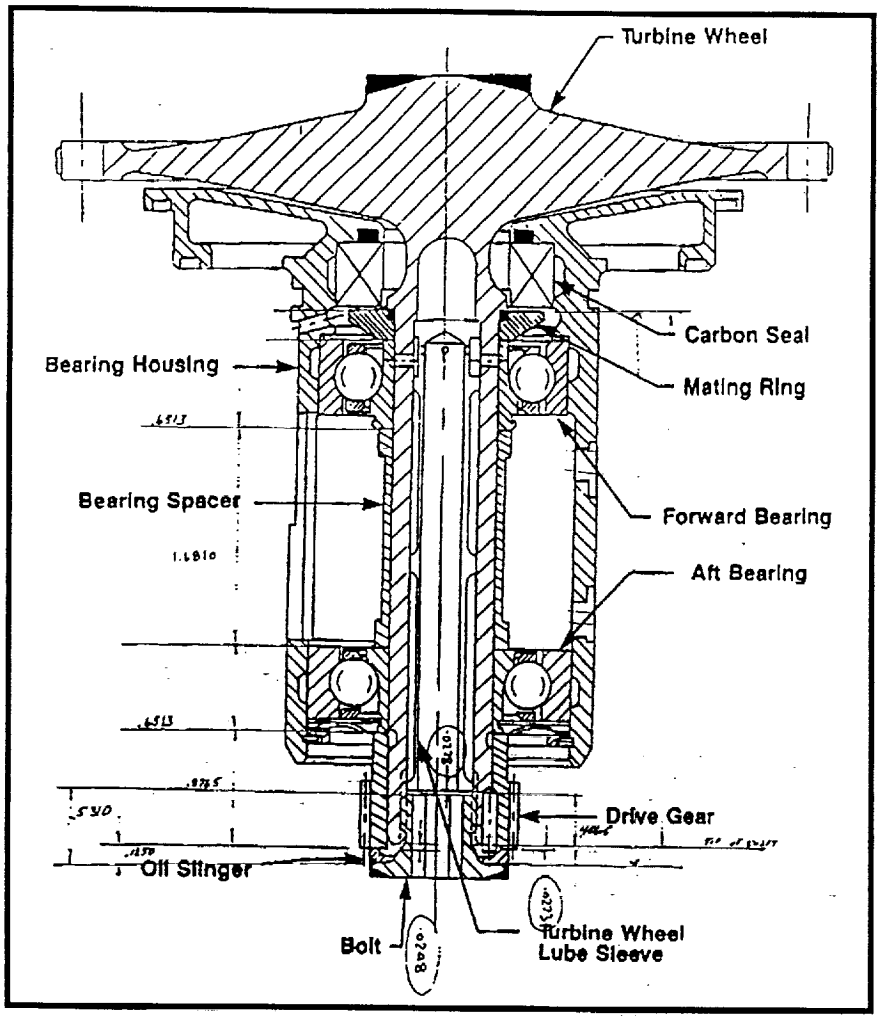

Exhibit 140 Space Shuttle Auxilliary Power Unit

characteristics of the lubricating oil were not known. Therefore, to expedite the analysis, a typical bearing oil was chosen for the study. After the curves of Exhibit 141 were generated, more was learned about the APU bearing oil. The oil chosen for the study was slightly more viscous than the actual APU oil. Thus, the results of Exhibit 141 at the low temperature are approximately 30% high and at the high temperature shown they are only 12% high.

4.8 ADORE Analysis of HPFTP/AT and HPOTP/AT Contact Traction Forces

A study was performed using the ADORE bearing dynamic simulation to evaluate traction forces in the ball to race contact zones of the HPFTP/AT and HPOTP/AT ball bearings. This study was part of the investigation of the "river-mark" surface distress phenomena that occurred in several sets of HPFTP/AT ball bearings. The objective of the study was to quantify the magnitudes and distributions of the traction forces in the contacts for the two applications. It was hoped that insight into the mechanisms involved in the formation of "river-marks" could be acquired by comparing traction forces in the LOX pump with traction forces in the fuel pump. The silicon nitride balls in the fuel pump proved to be much more susceptible to "river mark" formation than the identical balls used in the LOX pump.

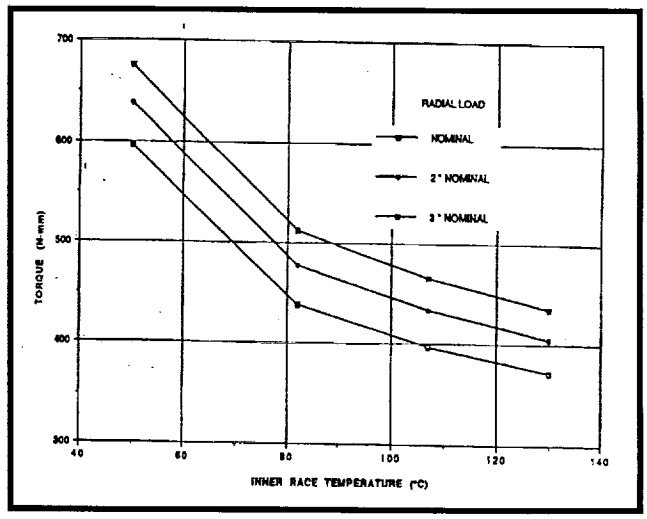

Exhibit 141 Torque By APU Turbine End Bearing at 72,000 RPM

A baseline LOX pump model was used to evaluate traction forces in the LOX pump application. The bearing was modeled with 1100 lbs axial load and 375 lbs radial load, shaft speed was 27,500 RPM. Three load cases were modeled for the hydrogen pump application. The shaft speed was 36,000 RPM for the fuel pump simulations. **Exhibits 142a - 142p** document the predicted traction forces for the various load cases requested. The predicted traction forces were plotted versus location in the contact ellipse. The traction vector plotted was calculated at various points along semi-major axis. The plots show the traction force (lbs) parallel to the semi-major axis in the upper left hand plot. The lower left hand plot shows traction force perpendicular to the semi-major axis (lbs). The plot in the upper right hand corner shows force in the direction of contact pressure. This force is not in engineering units. Curves were produced for both the inner race and outer race contacts and for the heaviest and lightest loaded ball for each load case.

The curves show that the rolling element motion is primarily outer race controlled for all of the bearing cases studied. The plots show two distinct points of pure rolling in the outer race contacts. The inner race contacts show a nearly anti-symmetrical traction force distribution about the center of the inner race contact ellipse. This pattern indicates ball spin relative to the inner race. It was noticed that for the case of high radial load, balls on the unloaded side of the bearing showed some spin relative to the outer race as well as the inner race.

One simulation was performed for the HPOTP/AT ball bearing for comparison with the HPFTP/AT cases. The loads for this model were 1100 lbs axial and 375 lbs radial. The distribution of traction forces in the LOX Pump ball contacts was similar to that predicted for the fuel pump bearings. However, the magnitude of traction forces was predicted to be slightly larger than in the fuel pump application. Two factors contribute to the higher predicted traction forces in the LOX pump. First, the applied loads used for the simulation were slightly larger than the loads used for the first two cases modeled for the Fuel Pump. The second factor is related to the traction curve used for the simulation. The traction model used for this analysis is as follows:

Traction coefficient = slip velocity * K or 0.1

This model produces a linear variation of traction coefficient as a function of slip velocity from zero, at zero slip, up to a maximum of 0.1. This type of traction model is representative of dry friction of many solid lubricants. The value of K used for the LOX Pump model is 0.0249. This value was based on available test data. The value of K used for the Fuel Pump model was 0.0012. This value was based on scaling the LOX value to comparable percent slip values. The difference in the traction curve slopes used also contributed to the magnitudes of the predicted traction forces.

The initial review of the analysis results suggested that increased local traction forces in the fuel pump application were not responsible for the formation of "river-mark" surface distress. However, it should be noted that the traction curve data for the hydrogen model was not supported by test data. Their was considerable uncertainty in the value used in the simulation. Parametric studies were later planned to evaluate sensitivity to this unknown.

A part of the river mark investigation, SRS participated in a visual inspection of silicon nitride balls from fuel pump Unit 6-5. The inspec-

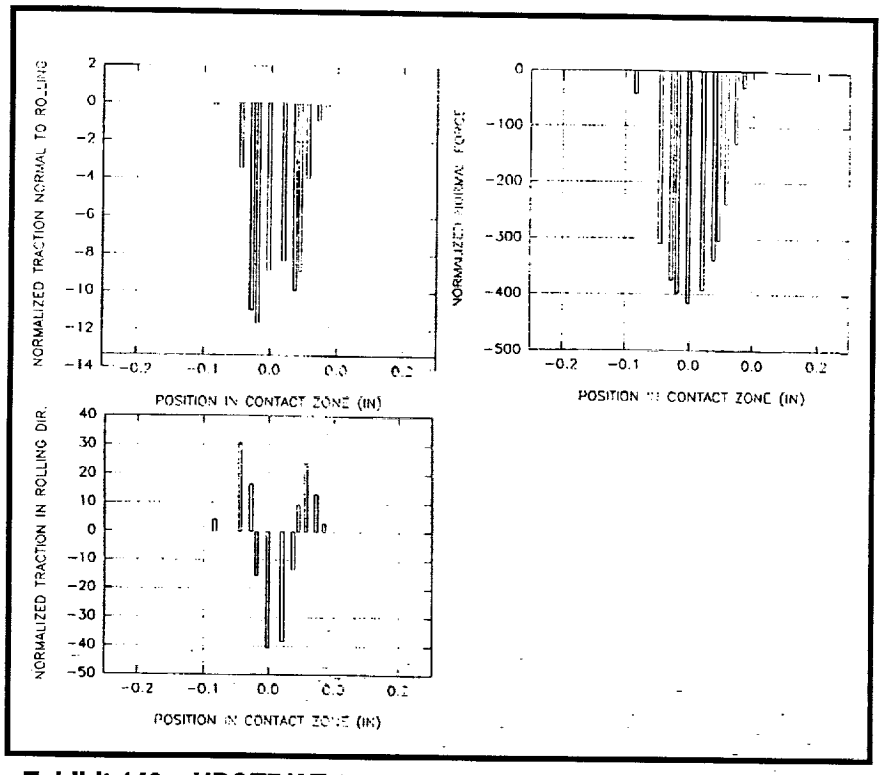

Exhibit 142a HPOTP/AT 1100 Lbs Axial Load 375 Lbs Radial Load Heaviest Loaded Ball, Outer Race

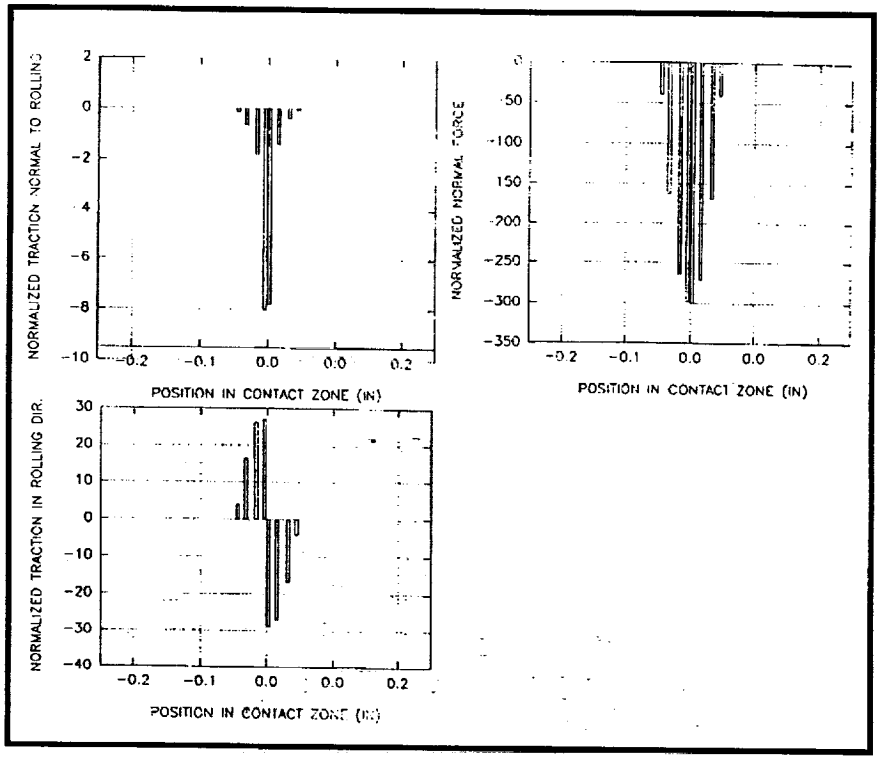

Exhibit 142b HPOTP/AT 1100 Lbs Axial Load 375 Lbs Radial Load Heaviest Loaded Ball, Inner Race

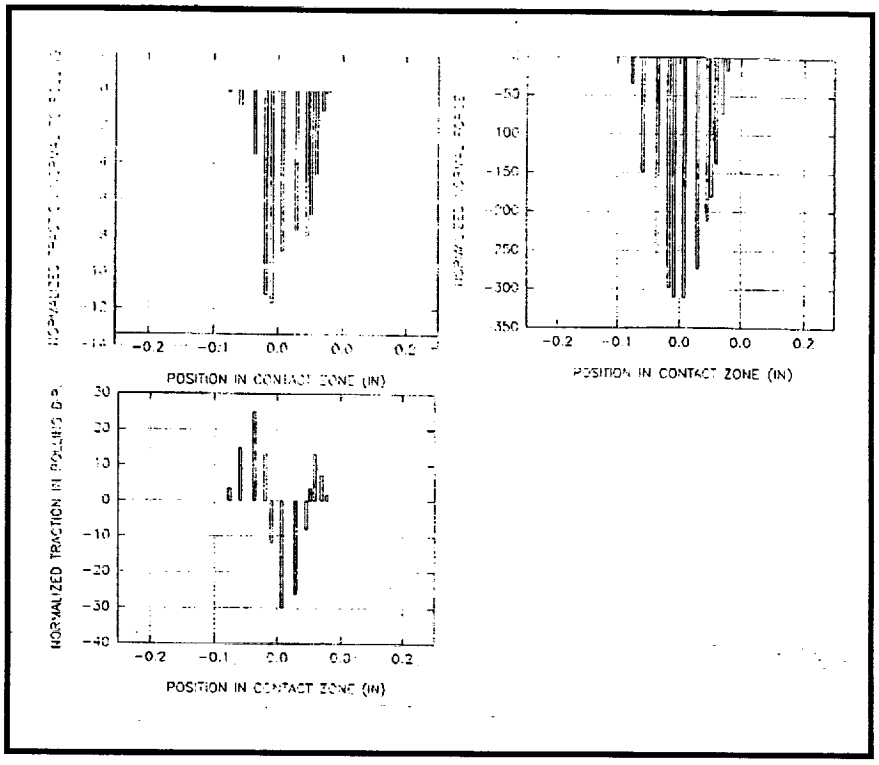

Exhibit 142c HPOTP/AT 1100 Lbs Axial Load 375 Lbs Radial Load Lightest Loaded Ball, Outer Race

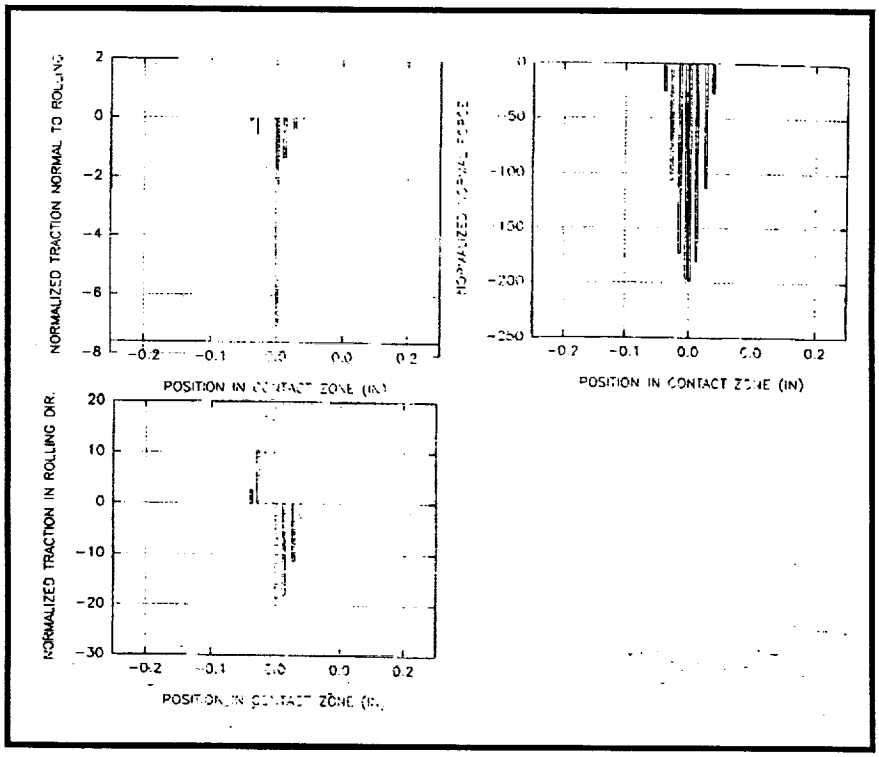

Exhibit 142d HPOTP/AT 1100 Lbs Axial Load 375 Lbs Radial Load Lightest Loaded Ball, Inner Race

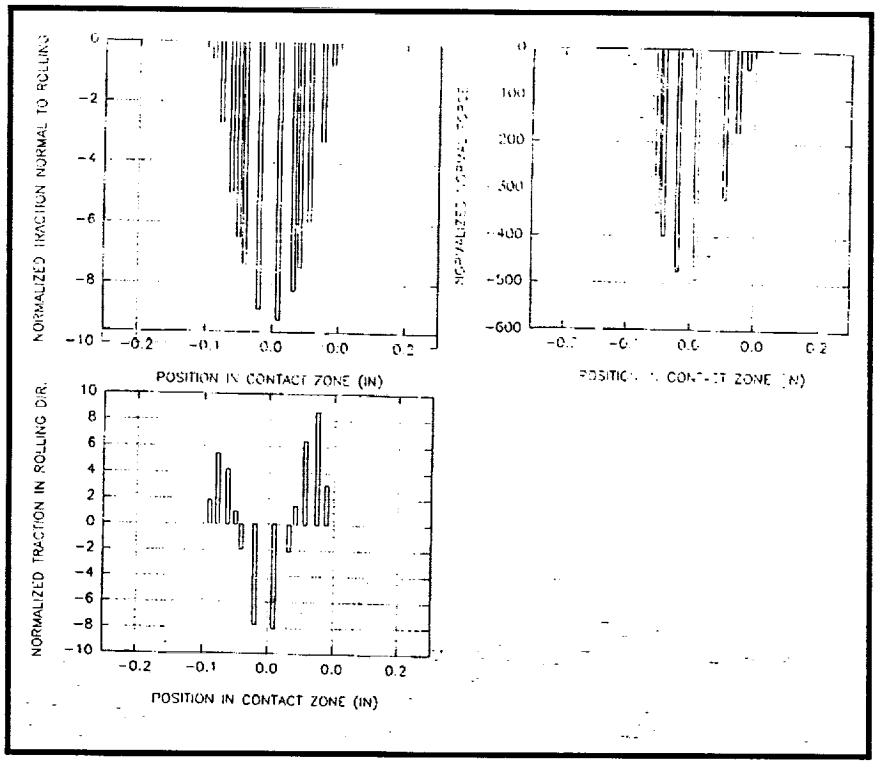

Exhibit 142e HPOTP/AT 875 Lbs Axial Load 125 Lbs Radial Load Heaviest Loaded Ball, Outer Race

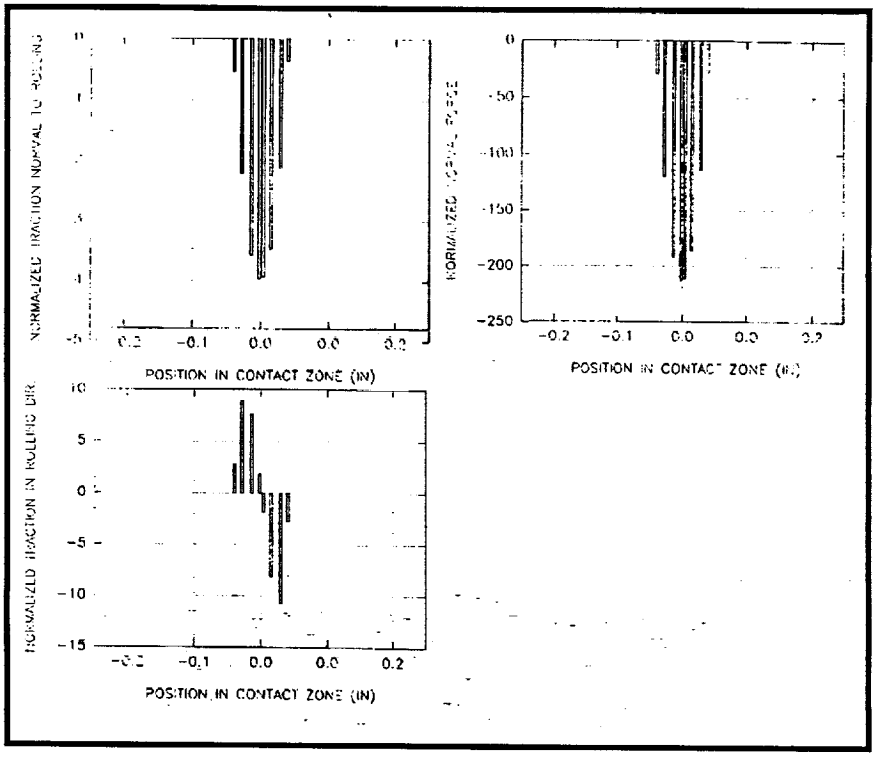

Exhibit 142f HPOTP/AT 875 Lbs Axial Load 125 Lbs Radial Load Heaviest Loaded Ball, Inner Race

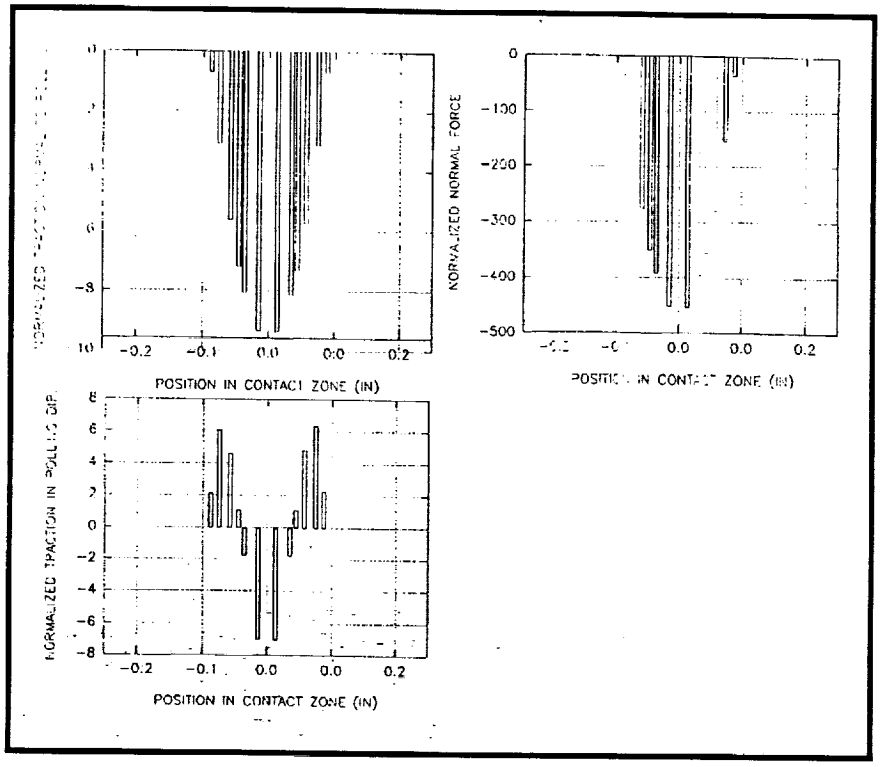

Exhibit 142g HPOTP/AT 850 Lbs Axial Load 125 Lbs Radial Load Lightest Loaded Ball, Outer Race

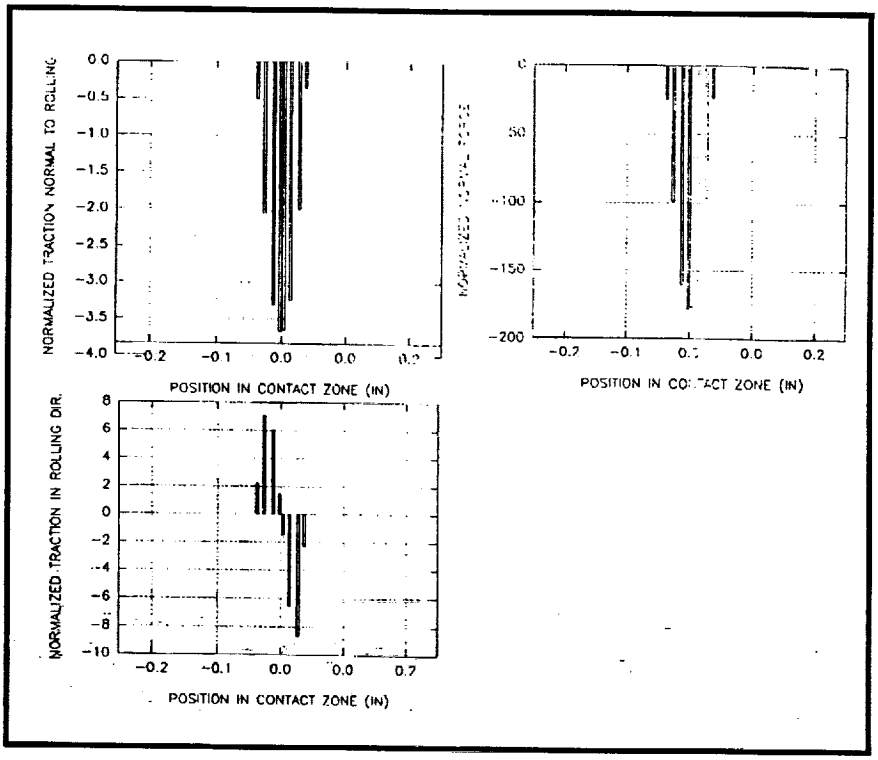

Exhibit 142h HPOTP/AT 850 Lbs Axial Load 125 Lbs Radial Load Lightest Loaded Ball, Inner Race

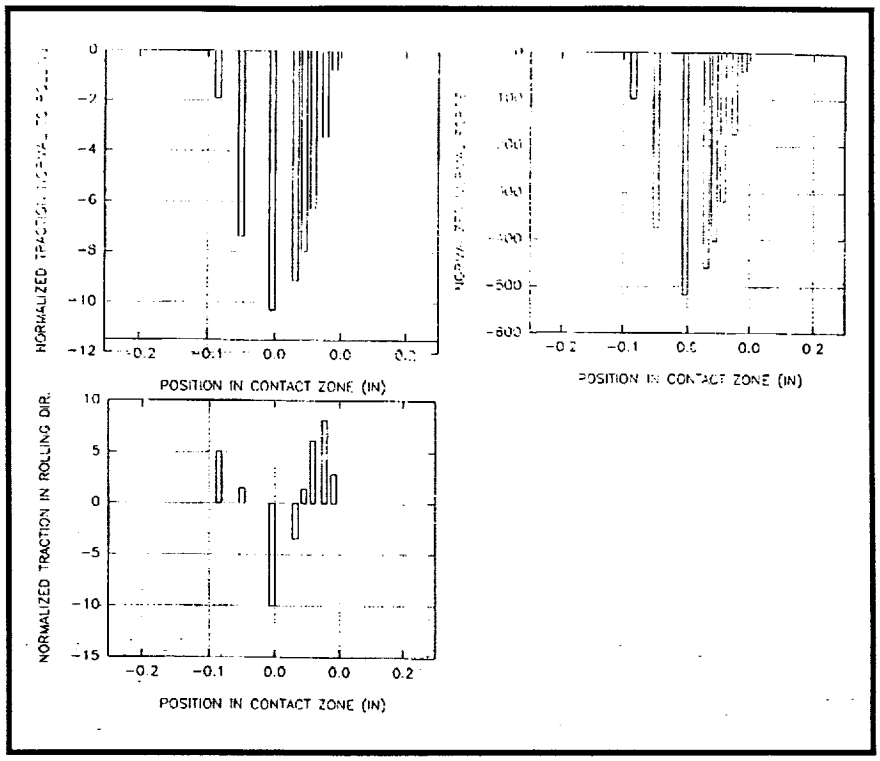

Exhibit 142i HPOTP/AT 950 Lbs Axial Load 125 Lbs Radial Load Heaviest Loaded Ball, Outer Race

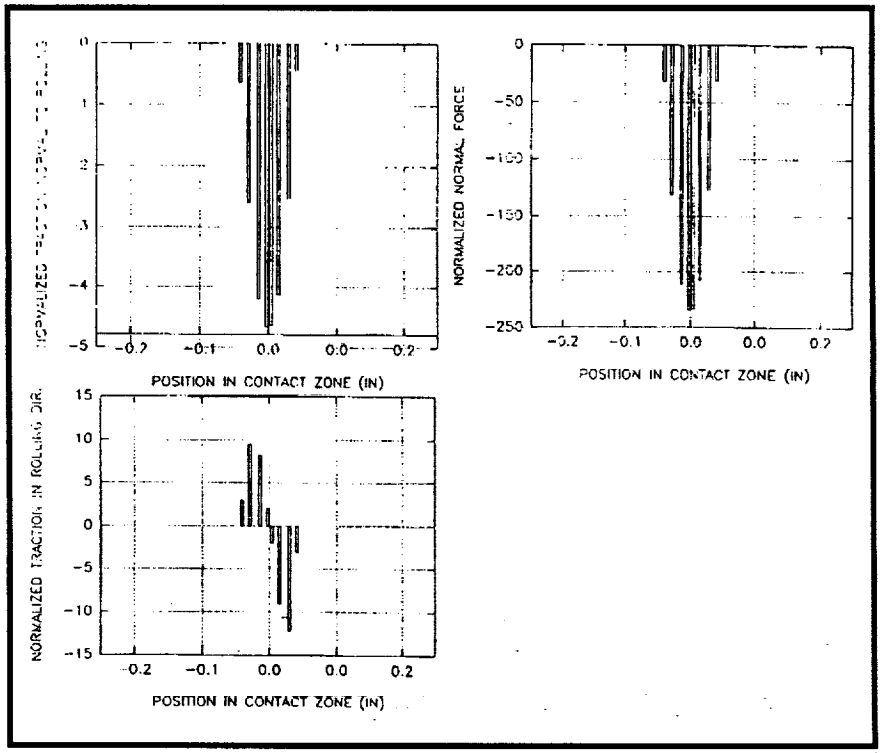

Exhibit 142j HPOTP/AT 950 Lbs Axial Load 125 Lbs Radial Load Heaviest Loaded Ball, Inner Race

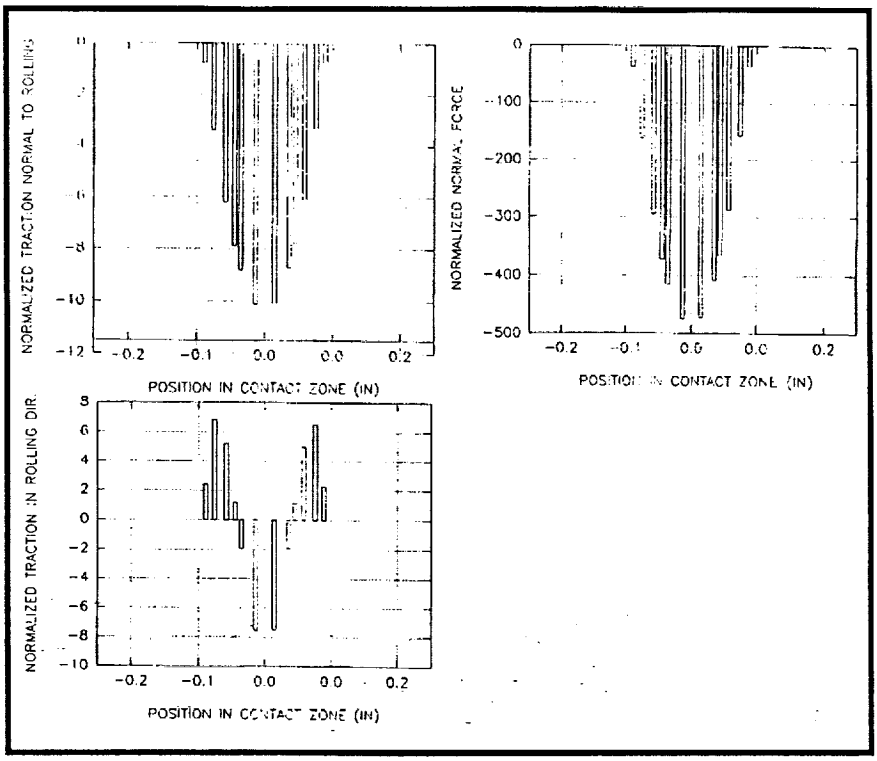

Exhibit 142k HPOTP/AT 950 Lbs Axial Load 125 Lbs Radial Load Lightest Loaded Ball, Outer Race

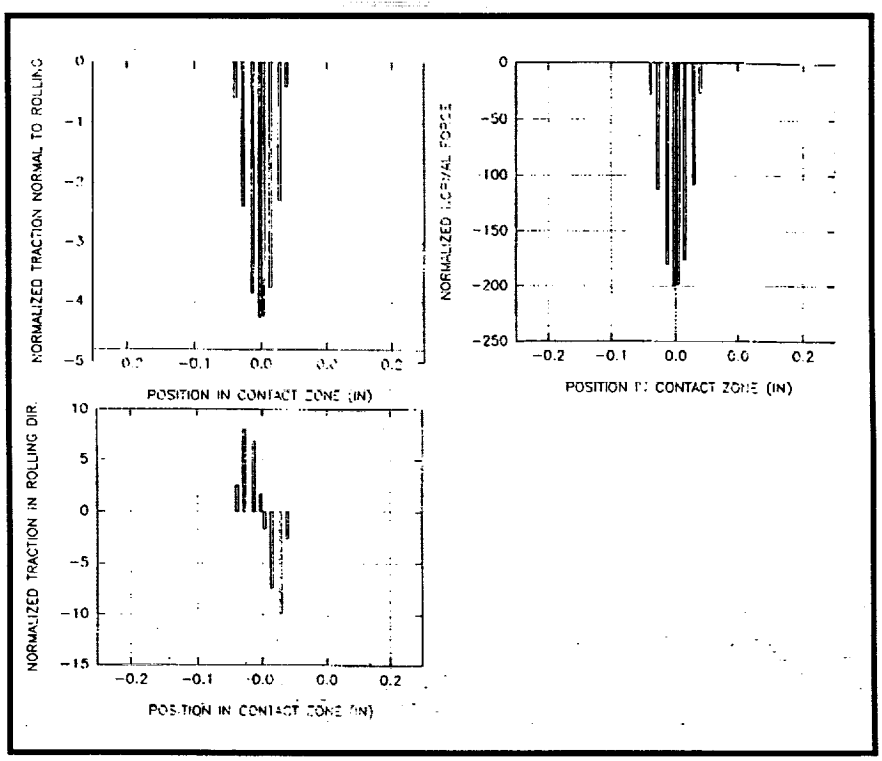

Exhibit 142l HPOTP/AT 950 Lbs Axial Load 125 Lbs Radial Load Lightest Loaded Ball, Inner Race

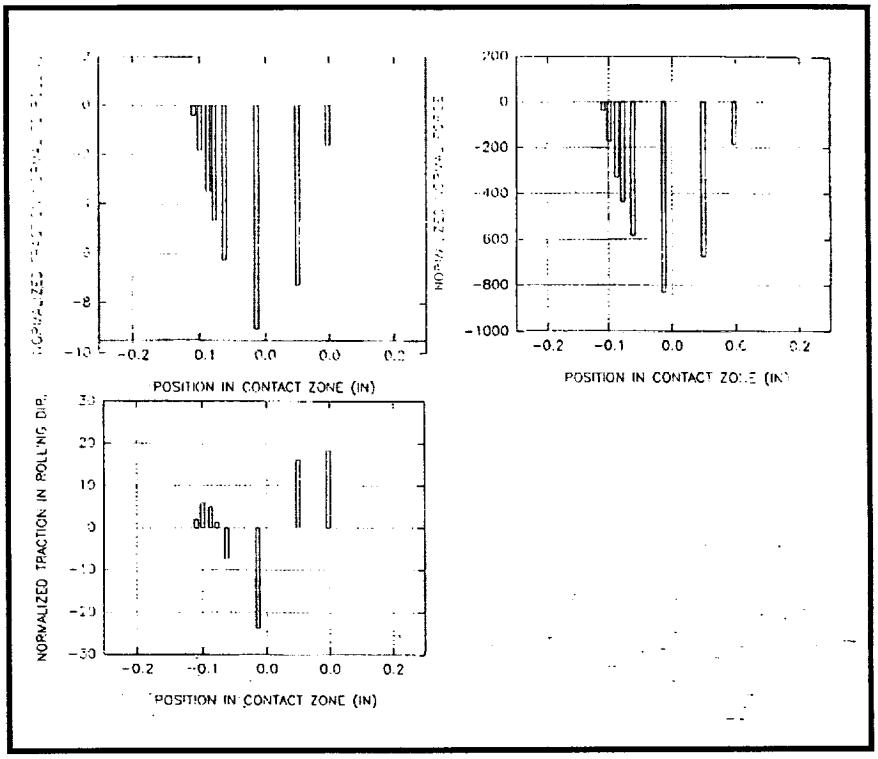

Exhibit 142m HPOTP/AT 950 Lbs Axial Load 2000 Lbs Radial Load Heaviest Loaded Ball, Outer Race

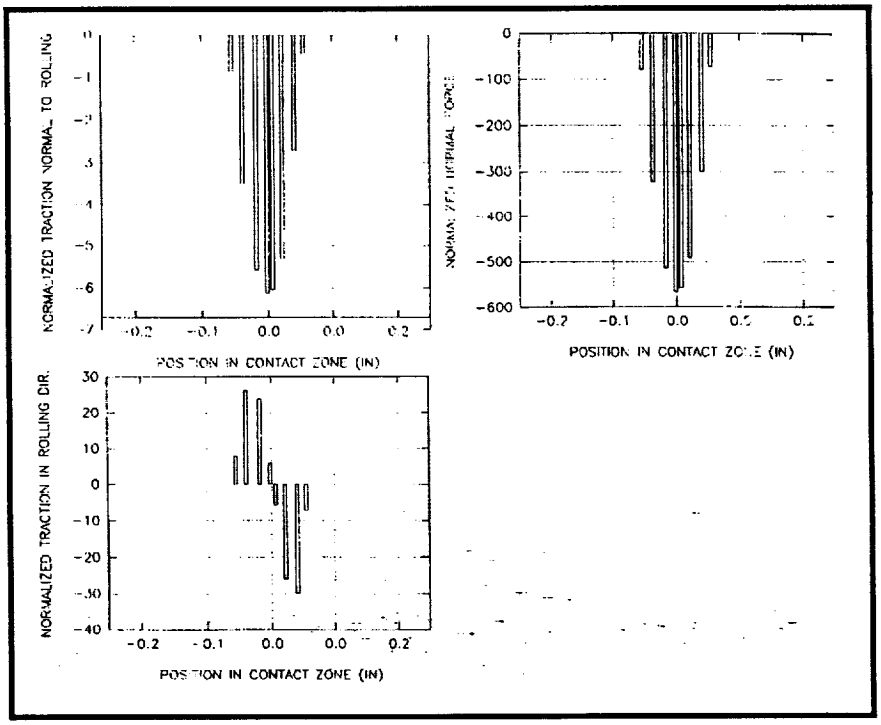

Exhibit 142n HPOTP/AT 950 Lbs Axial Load 2000 Lbs Radial Load Heaviest Loaded Ball, Inner Race

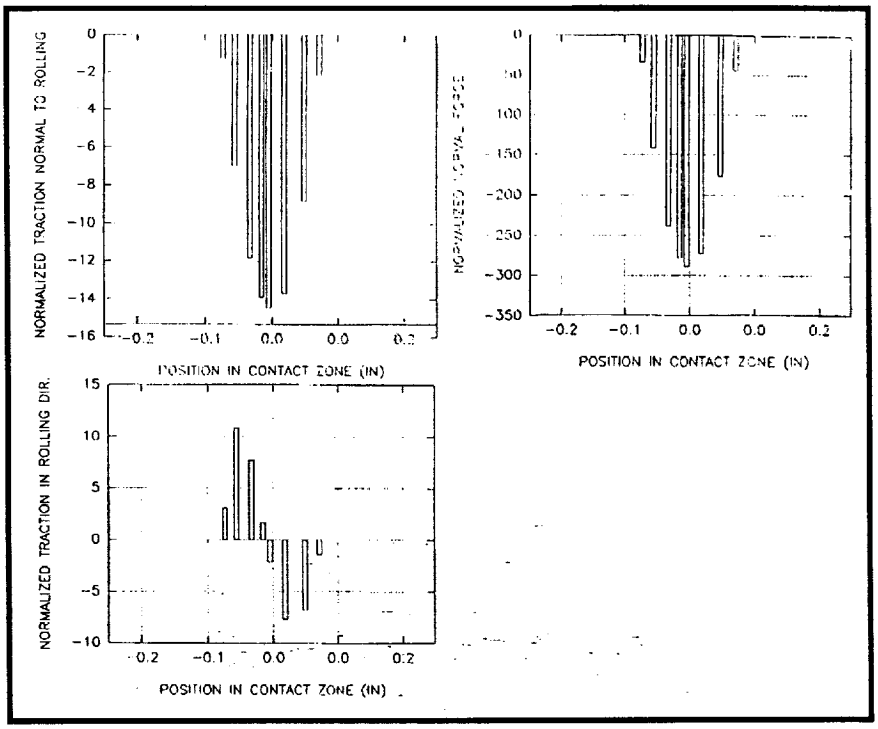

Exhibit 142o HPOTP/AT 950 Lbs Axial Load 2000 Lbs Radial Load Lightest Loaded Ball, Outer Race

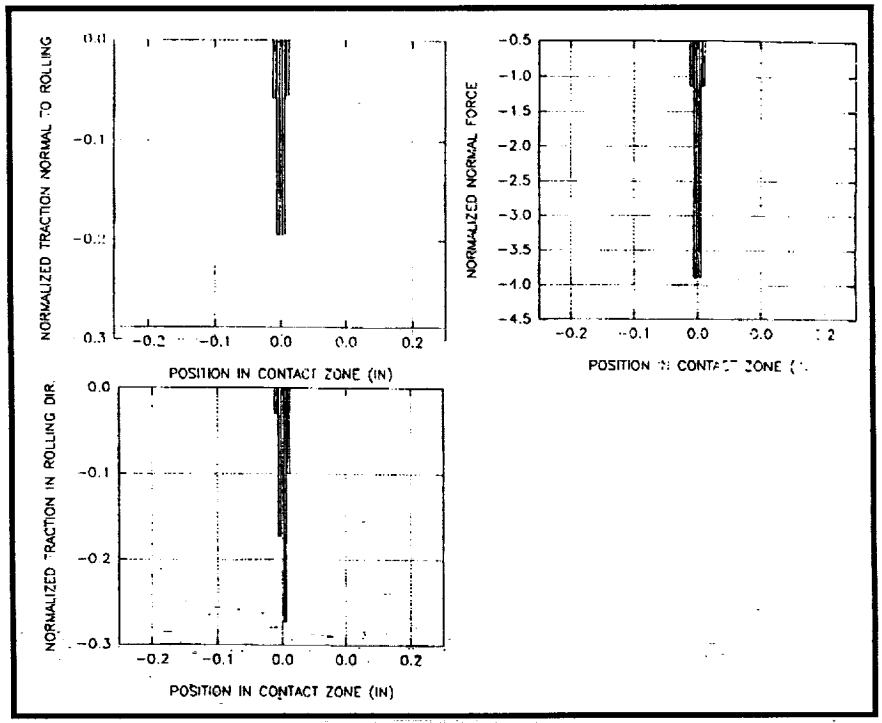

Exhibit 142p HPOTP/AT 950 Lbs Axial Load 2000 Lbs Radial Load Lightest Loaded Ball, Outer Race

tion was performed at MSFC. The bearings had been subject to 22 start cycles and 12,972 seconds run time. Mr. Chip Moore (MSFC) demonstrated use of the new stereo microscope and illumination tools which were available for this inspection. Mr. Moore had identified several "river-mark" locations that appeared to have sharper bottoms and be deeper than typical "river-marks". There was some concern because some of the observed features did not appear benign as typical "river-marks" observed in the past. Mr. Moore suggested that the difference in appearance could have been due mainly to the improved resolution of the stereo microscope. Previously inspected LH_2 rig bearings were retrived for comparison viewing with the stereo microscope. Balls from Rig build 3 were observed with the stereo microscope. These balls had over 30,000 seconds test time in the rig. With in a short period of time, some of the steeper "river-marks" were identified using the stereo microscope. Therefore, it was believed that the features observed in the Unit 6-5 balls were not atypical. The new viewing equipment only provided better resolution of the features. Identifying similar features in the Build 3 rig balls also reduced concerns about the nature of the rivermarks, because these bearings had been successfully tested for a full 30,000 second cycle.

4.9 ADORE Analysis Supporting FEP Coated Cage Debond Investigation. SRS was asked to develop dynamic bearing modes of the space shuttle engine low pressure oxider and fuel turbopump ball bearings. The objective of this modeling effort was to determine the magnitude of ball to cage impact forces. This data was needed to support fatigue testing of the FEP coated cages that had developed a visible debond in the ARMALON cage material. Loads predicted by ADORE analysis were used in the fatigue tester to demonstrate that the cage with the debond was still capable of meeting the fatigue life criteria of 10^7 cycles.

Baseline models were developed for both the LPOTP and LPFTP ball bearings. In general, the average value of all bearing parameters, based on drawing tolerances, was used in the models. However, bearing operating clearance was calculated assuming the loosest tolerance stack-up which resulted in maximum bearing internal radial clearance (IRC). The operating IRC for the oxidizer pump was 5.7×10^{-3} inches and the operating IRC for the fuel pump was 2.7×10^{-3} inches. Conversely, minimum values of cage pocket clearance were assumed. Maximum IRC and minimum pocket clearance represents the worse case scenario in terms of cage pocket loading. Worse case assumptions were also employed in determining bearing operating misalignment. The bearing models were misaligned as much as required to unload the bearing reaction moment. This misalignment increases ball excursion and potentially cage loads.

The LPFTP bearing model was used to perform three studies. The bearing was modeled with 2,000 lbs axial load and 550 lbs fixed radial load. The bearing was also modeled with 2,000 lbs axial load, 300 lbs fixed radial load, and 250 lbs synchronous radial load. Finally, a study was performed to compare cage loads for an FEP coated cage with loads in an uncoated cage. The results of these studies are shown in **Exhibit 143** through **144**. Selected results from the case with 550 lbs fixed radial load are shown in Exhibit 143. The cage to ball loads show the classic ball excursion loading scenario. Cage loads occurred cyclically twice per cage rotation. Cage loadings occurred during each ball orbit as the fast ball exceeded the pocket clearance and as the slow ball was overtaken by the cage. Peak cage

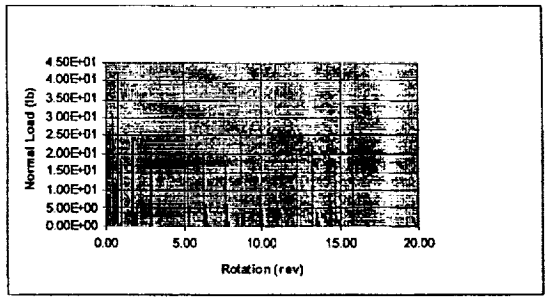

Typical Ball Cage Load

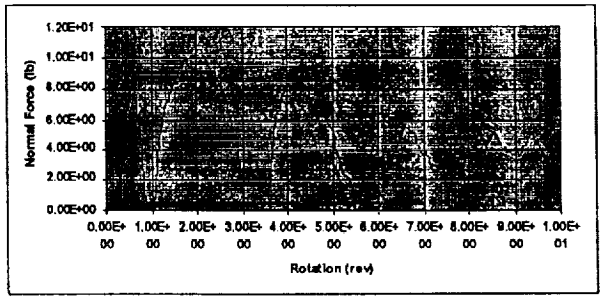

Cage to Race Load Per Land (Approximately 1/2 Total)

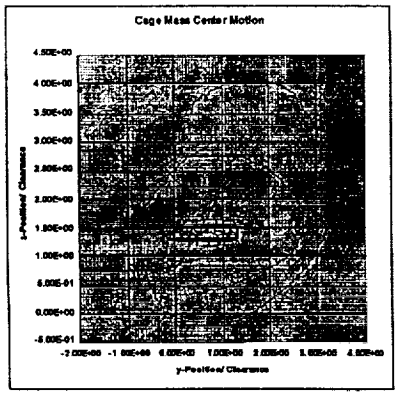

Cage Mass Center Orbit

16000 RPM, Fx=2000 lb,
Fy_{static}=550 lb IRC=2.7E-3 in
Gy=.0011rad
ffc=.075, ffr=.15

Exhibit 143 Predicted Cage Loads for SSME LPFTP

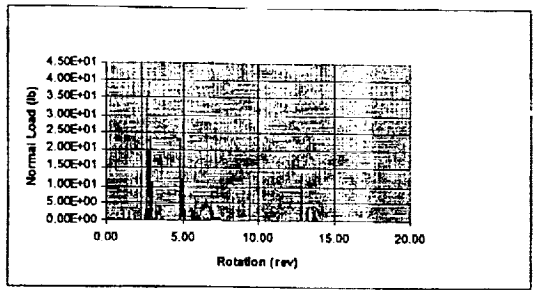

Typical Ball Cage Load

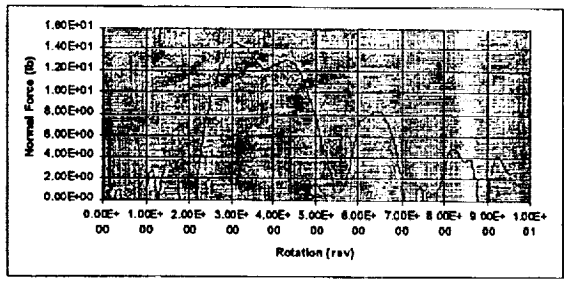

Cage to Race Load Per Land (Approximately 1/2 Total)

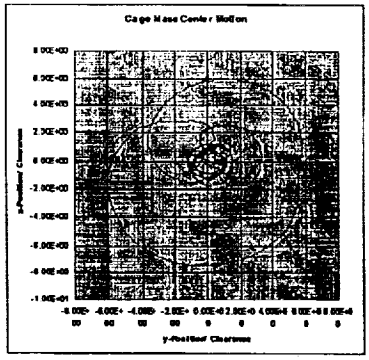

Cage Mass Center Orbit

16000 RPM, Fx=2000 lb, Fz_{static}=300 lb, Fz_{sync}=250 lb IRC=2.7E-3 in Gy=.000551rad ffc=.075, ffr=.15

Exhibit 144 Predicted Cage Loads for SSME LPFTP

loading predicted was approximately 35 lbs. The cage mass center orbit position plot showed that the cage moved to one side of the guiding clearance and stayed in approximately the same position This produced a cage to race load that was relatively constant and in a direction with a fixed orientation relative to the radial load. The average cage to race load was approximately 4 lbs per load or 8 lbs total. Of the cases modeled, this loading produced the largest cage loads. Exhibit 144 shows the same bearing with 250 lbs of the 550 lb radial load applied with a synchronous rotation rate. Peak cage to ball/load was approximately the same for this case (i.e., 35 lbs). However, the frequency of peak loading was less than for the case with all of the radial load fixed. **Exhibit 145** shows results from the final LPFRP bearing case modeled. This case is identical to the fixed radial load case shown in Exhibit 143. However, the ball to cage friction factor had been increased from 0.075 to 0.200. The objective of this study was to quantify the benefits of the FEP coating in terms of cage loading. The results generated were almost identical to the results shown in Exhibit 143. The fact that cage to ball loads in this baring were dominated by ball excursion loads minimizes the effect of the coating. The coating should produce more dramatic improvements for loading scenarios that do not cause excessive ball excursions.

The LPOTP ball bearing model results are shown in **Exhibit 146**. This bearing was modeled with 2,411 lbs axial load and 467 lbs fixed radial load. Worse case IRC and minimum pocket clearance were specified. This bearing cage had elongated ball pockets which afforded very large circumferential pocket clearance. No ball excursion loading was predicted for this

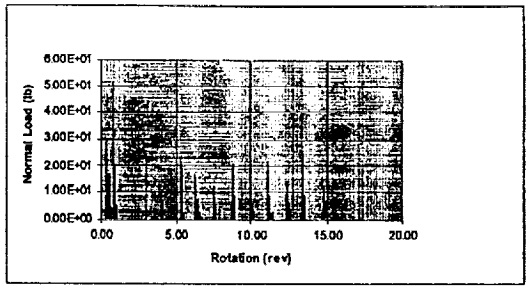

Typical Ball Cage Load

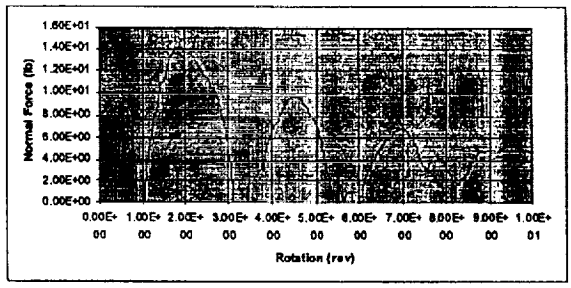

Cage to Race Load Per Land (Approximately 1/2 Total)

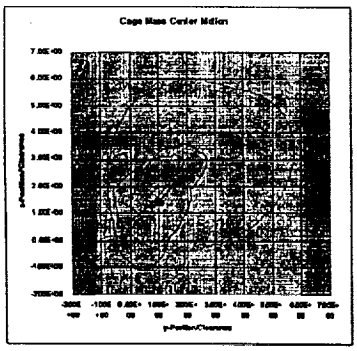

Cage Mass Center Orbit

16000 RPM, Fx=2000 lb,
Fy_{static}=550 lb IRC=2.7E-3 in
Gy=.0011rad
ffc=.075, ffr=.15

Exhibit 145 Predicted Cage Loads for SSME LPFTP

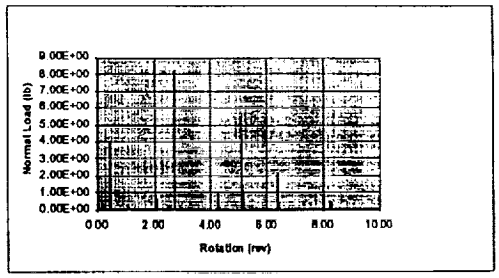

Typical Ball Cage Load

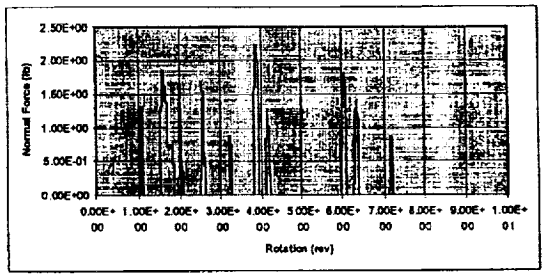

Cage to Race Load Per Land (Approximately 1/2 Total)

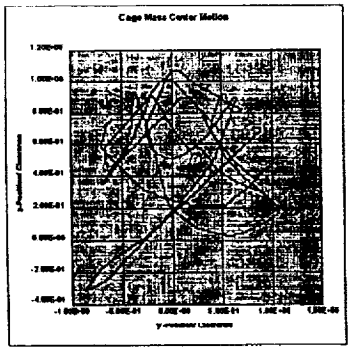

Cage Mass Center Orbit

5240 RPM, Fx=2411 lb,
Fz_{static}=467 lb, Fz_{sync}=0 lb
IRC=5.7E-3 in Gy=.0007rad
ffc=.075, ffr=.15

Exhibit 146 Predicted Cage Loads for SSME LPFTP

case. The cage dynamics were stable with quasi-randum motion of the cage in the clearance. Peak ball to cage forces were 8 lbs and peak cage to race forces were about 20 lbs on each side of the cage. There was no steady frequency for the loads in this bearing.

Based on the studies performed to date, it appeared that the LPFTP bearing with maximum radial load produced the worst case ball to cage forces. It appeared that a cyclical 35 lb pocket load would provide a conservative value for fatigue testing. In fact, it would be possible to argue for lowering the loading to 30 lbs because not all of the impacts reach the peak. The average peak loading was between 25 and 30 lbs. It may also be feasible to justify reducing the number of load cycles predicted in each engine firing by considering the effect of synchronous load. The model showed that synchronous loading did not reduce the magnitude of cage loads but did reduce the frequency of peak loading.

4.10 Stress Analysis for FEP Coated Cage Debond Investigation

SRS continued to support the FEP coated bearing cage debond issue utilizing the results from the ADORE analysis performed. As previously reported, ADORE models were run for both the space shuttle main engine low-pressure fuel and oxygen turbopump ball bearings. The ADORE analysis showed that the low pressure fuel turbopump bearing cage was more prone to cage loading and thus was the most appropriate cage for use in evaluating the effects of cage delamination on bearing safety margins. The fuel pump bearing had less cage pocket clearance and a higher ratio of radial to axial load. These factors caused increased cage loads relative to the low-pressure oxygen turbopump bearing.

The ADORE model of low pressure fuel pump ball bearing predicted the type of ball to cage loading associated with ball excursions exceeding the available cage pocket clearance. The magnitude of ball excursion loading was found to peek at approximately 30 lbs. Ball excursion loading occurs because of variations in ball orbital velocity as a function orientation relative to the bearing radial load. The radial load causes ball to race normal loads and contacts angles to change with ball position. The variation in contact angles results in the speed of individual balls to exceeding or lagging the cage rotational speed, which represents the average ball train speed. **Exhibit 147** shows a typical cage loading scenario typical of ball excursion loading. The loading shown in this exhibit is representative of the loading predicted for the low-pressure fuel turbopump.

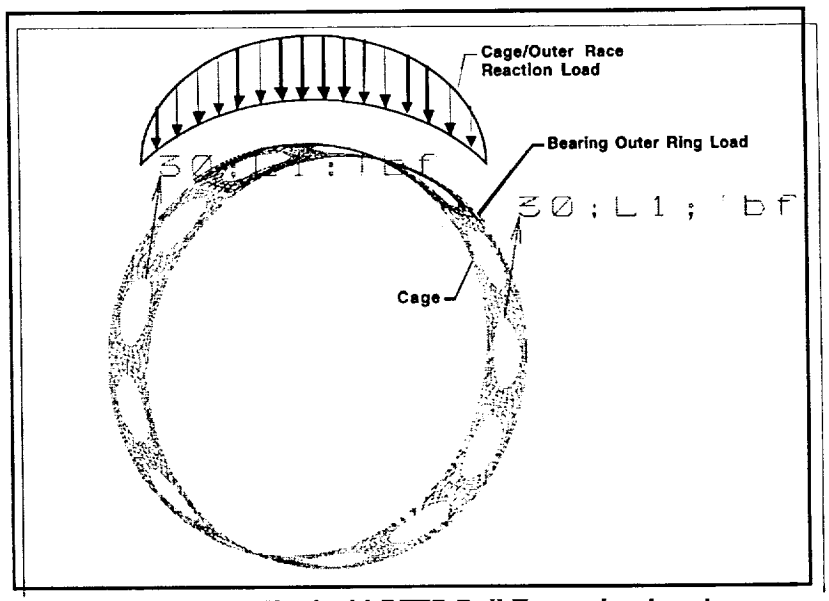

Exhibit 147 Typical LPFTP Ball Excursion Loads

The objective of the stress analysis performed was to determine the magnitude of cage stresses that result from this loading. The operating stresses can then be used to set loads for testing in the cage fatigue rig. However, the cage stress analysis was complicated by several factors. First, during operation, the cage is in dynamic equilibrium, but not necessarily in static equilibrium. Additionally, the cage loads are very transient in nature making it difficult to identify the worse case loadings. The loading that is shown in Exhibit 147 is derived from the ADORE analysis with assumptions that are conservative relative to stress. The main assumptions are that the loads are simultaneously peaking in the cage loading and cage lagging positions. Also, the location of the loads is in the two pockets displaced radially by the largest possible moment arm. Assumptions also had to be made relative to how the ball to cage loads were reacted by the cage/race contact. The most general and correct approach for accounting for the reaction load was to perform a non-linear FEM analysis of cage stress using gap elements to model the interaction of the cage with the race. This was the approach initially pursued in this investigation. A significant effort was expended pursuing development of a cage contact model. However, the model exhibited numerical stability problems. Examination of the problem lead to identification of a software glitch in the commercial ALGOR software which was used to develop the model.

An alternative analysis method had to be pursued in order to produce results within the time frame needed to support rig testing. SRS had several references on hand describing various approaches for modeling a flexible ring subjected to different loadings. The literature was collected as part of an effort to incorporate race flexibility into existing bearing analysis codes. During that study, several closed form solutions were evaluated and compared to non-linear FEM models. The closed form method consistently producing the most accurate results was found to be the method proposed by J.Y. Liu, and Y.P Chiu.[1] This method assumes that applied ring loads are reacted by a uniform external shear force. Although not intuitive, this method consistently produced results consistent with FEM. Linear super position can be used to calculate the cumulative effect of any number of individual loads. **Exhibit 148** illustrates the method as applied to the low pressure fuel turbopump ball bearing cage subjected to ball excursion loading. The chart quantifies the calculated magnitude of cage stress from bending moment, centrifugal force, and tensile forces. Centrifugal force produced a uniform 810 psi tensile stress. The P/A load was compressive between the loads and tensile in the area outside

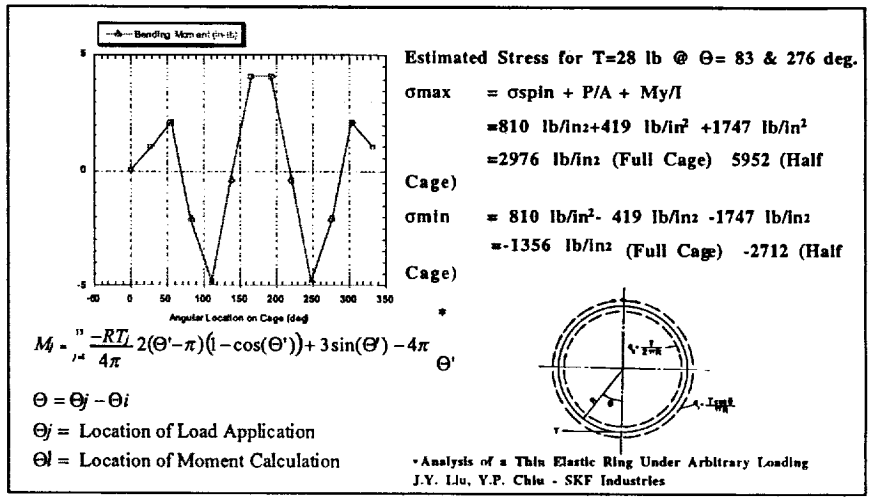

Exhibit 148 LPFTP Pump End Ball Bearing Estimated Cage Stress Based on ADORE Model Cage Loads and Liu Moment Solution

of the load zone. Cage bending moment varied symmetrically about the cage/housing reaction area. The bending stress was the largest contributor to cage stress. The bending moment is plotted in Exhibit 148. Each point on the diagram shows an angular location on the cage relative to the reaction load area. As the cage rotates, the bending moment varies per the displayed curve. Thus, a point on the cage is subjected to two major peaks in one bending direction; and one major and two minor peaks in the opposite bending direction. Only the centrifugal load is fixed and this becomes the mean stress. Each point on the OD and ID of the cage surface is subjected to 810 psi (centrifugal) ± 419 psi (P/A)± 1747 psi (bending) depending on the location of the point in the cage orbit. Based on this analysis, fatigue testing needed to be conducted with a mean stress of 810 psi and an alternating stress of ± 2166 psi. Any given point on the cage sees these stresses roughly two times per cage orbit. The cage rotates at 42% of the shaft speed. The cage orbit speed can be used to calculate the number of cycles required to meet a specified operational life.

These results were provided to MSFC for utilization in test planning. It should be noted that while no safety factors were used in the stress analysis worse case bearing loads and misalignment were assumed in the ADORE model used to calculate ball to cage loads. The actual operational cage loads will likely be considerably lower than calculated.

5.0 — Bearing Seals and Materials Test Support

The final three test series of the bearings seal and materials test program occurred during the period documented by the following sections. Unit 3, Build 6 was the first test series to occur in this period. This test build used standard Phase II Rocketdyne bearings and looked at the potential of Salox prelube to extend the life of the bearings. The prelube did have positive effects however, there was no dramatic life increase. Unit 2, Build 14 was the second rig test series covered in this report. This rig build demonstrated Si_3N_4 balls in Rocketdyne Phase II races. This was the first rig build that used both the radial and axial load capabilities of the BSMT. Over two hours of operation at speed in LOX, with some time at very high transient load levels was demonstrated with this build. This test series was one of the key milestones that ultimately resulted in adoption of the ceramic rolling elements that essentially solved the bearing wear and thermal stability problems experienced early in the Advanced Technology Turbopump Program.

Unit 3, Build 7 tested the use of the cages developed by Battelle Laboratories in combination with silicon nitride balls. The Battelle cages used Salox inserts and avoided the problems of fiber ends rubbing the balls as occurred with Armalon cages. However, the cage design had a larger web area necessitating removal of one of the balls from the bearing. This test series demonstrated the structural margins of the cage design and also resulted in the highest BSMT contact stresses ever experienced with silicon nitride balls. The high stresses resulted in fatigue spalling of the races. The robustness of the silicon nitride balls was demonstrated further because they were not damaged by continued operation or severely damaged races.

5.1 Summary of Unit 3 Build 6 Test Series

This test series accomplished 8 rotational tests with Phase II Rocketdyne LOX Pump Bearings. The bearings were prelubed with Salox to evaluate the potential for this process extending the useful life of the bearing. The prelube did seem to be beneficial in some ways, however, there was not a dramatic increase in bearing life.

Test 3060202. This was the first rotational test for Unit 3, Build 6. This build was fitted with LOX turbopump turbine end Phase II bearings. The races of Bearings 1 and 4 were used in a previous test. The balls were new. The balls and cages were dry film lubricated and the inner and outer races were prelubed with Salox. This provided immediate lubrication to the contacts which would otherwise have had to wait until the lubricant was transferred from the cage to the balls as the bearing is rotated. An objective of this test series was to evaluate potential bearing life improvement resulting from this lubrication technique.

Prior to a successful rotational test, there were two attempts that were cut due to instrumentation problems. These problems were corrected and the tester was rotated at 15,000 RPM for approximately 100 seconds. During the test, two temperature measurements behaved in an anomalous manner; Bearing 2 outer race temperature (T1005), and Bearing 4 outer race temperature (TA1007). Coolant temperature biases prior to rotation introduced uncertainty in the estimated heat generation throughout the tester.

A comparison of selected measurements and engineering data between this and previous tests is shown in **Exhibits 149** and **150**. Unit 2, Build 12 (212202) contained silicon nitride ball bearings, and Unit 3, Build 3 (3030101) contained

Test Parameter	TEST NUMBER		
	212202	3030101	3060202
Shaft Speed (RPM)	14,949	15,000	15,071
Time at Speed (sec)	115	90	100
Subcooling	58	56	
Flow Rate (lbs/sec)	6.4	6.5	6.3
Brg #4 Inlet Temp (°F) T1018	-263 biased	-262	-257
Between Brgs 3 & 4 (°F) T1024	-260 biased	-262 biased	-256 biased
Brg #3 Outlet Temp (°F) T1019	-260 biased	-260	-255
Brg #1 Inlet Temp (°F) T1021	-260	-262	-256
Temp Between Bgr 1 & 2 (°F) T1023	-259 biased	-262.5 biased	-256 biased
Brg 2 Outlet Temp (°F) T1022	-258	-260	-255
Tester Inlet Temp (°F) T1001 T1002	-259 biased -268	-270.5 biased -270 (est.) bas meas.	-263 -264
Tester Outlet Temp (°F) T1003	-261	-259.7	-255 biased
Tester Inlet Pressure (psig) PA1001 PA1002	445 444	447 445	442 445
Tester Outlet Pressure (psig) PA1003	430	433	433
Pressure Between Brg 3 & 4 (psig) P1006	427	433	436
Horsepower	67.7	N/A	72
Torque (in-lbs)	6,283	Lost	6,607
Brg #1 O.R. Temp (°F) T1004 (TA1004)	-264 (-264)	-273 (-265)	-260 (-260)
Brg #2 O.R. Temp (°F) T1005 (TA1005)	-250 (bad)	-258.8 (-257)	bad (-254)
Brg #3 O.R. Temp (°F) T1006 (TA1006)	-255 (-256)	-263 (-259)	-254 (-254)
Brg #4 O.R. Temp (°F) T1007 (TA1007)	-262 (-261)	-262 (-262)	-259 (bad)

920804JC1823

Exhibit 149 BSMT Test Conditions and Selected Data (Test 3060202)

PARAMETER	212202	3030101	3060202
• Delta Temp Across Brg Pair (°F)			
T1022-T1021	2	2	1
T1019-T1018	2	2	2
• Delta Temp Across Brg 1 (°F)			
T1023-T1021	1.0	-0.5	0.0
Brg 2			
T1022-T1023	1.0	2.5	1.0
Brg 3			
T1019-T1024	2.0	2.0	1.0
Brg 4			
T1024-T1018	0.0	0.0	1.0
• Brg Outer Race Temp - Fluid Inlet Temp (°F)			
Brg 1			
T1004-T1021	-4	-3	-4
Brg 2			
T1005-T1023	9	5.5	2
Brg 3			
T1006-T1024	8	3	2
Brg 4			
T1007-T1018	1	0	-2
• Heat Generated (btu/sec) Across			
Brg 1	2.71	-	0
Brg 2	2.71	6.72	2.65
Brg 3	5.41	5.38	2.65
Brg 4	0	0	2.65
• Heat Generated Across			
Brg 1&2	5.41	5.37	2.65
Brg 3&4	5.41	5.37	5.3
• Inlet Vortex			
Load	8.12	22.86	18.52
Drive	13.54	21.51	18.52
• Pressure Drop (psi)			
Brg 1	N/A	N/A	N/A
Brg 2	N/A	N/A	N/A
Brg 3	-3	0	9
Brg 4	17	12	3
Brg 1&2	15	14	9
Brg 3&4	14	12	12
• Flow (lbs/sec) through Brg pair	6.4	6.5	6.3
• H.P.	67.7	-	72
• Torque (in-lbs)	6,283	-	6,607
• Shaft Speed (rpm)	14,949	15,000	15,071

920605JC0813

Exhibit 150 BSMT Test Parameters Comparison LOX Tests (Test 3060202)

Phase II bearings. This allowed data from this test to be compared with those from silicon nitride ball bearings, and baseline Phase II 440C bearings. The horsepower and torque values from this test compared favorably with those from Unit 2, Build 12. The pressure loss through the tester was lower for this test compared to the other tests.

The temperature profiles for each of the measurements in the tester are shown in **Exhibit 151**. The Bearing 1 and Bearing 4 outer race temperatures were well below the coolant inlet temperature which indicated possible cold coolant leaking around the thermocouple housing and affecting the measurement.

The pressure profile through the tester is shown in **Exhibit 152**. Since the pressure between Bearings 3 and 4 was higher than the outlet pressure, Bearing 3 apparently did not act as a pump.

Following the rotational test, the bearings were examined through a borescope. The Number 1 bearing was in good condition. The balls were shiny with light gold bands. The Bearing 2 balls had wide bands of material that appeared to be teflon. The bands were crisscrossed and some were light gold in color. Bearing 3 balls were similar. The bands were not as pronounced as those in Bearing 2. Bearing 4 balls had light bands and streaks. There was an a occasional gold tinted band and some light colored specks on the ball surfaces.

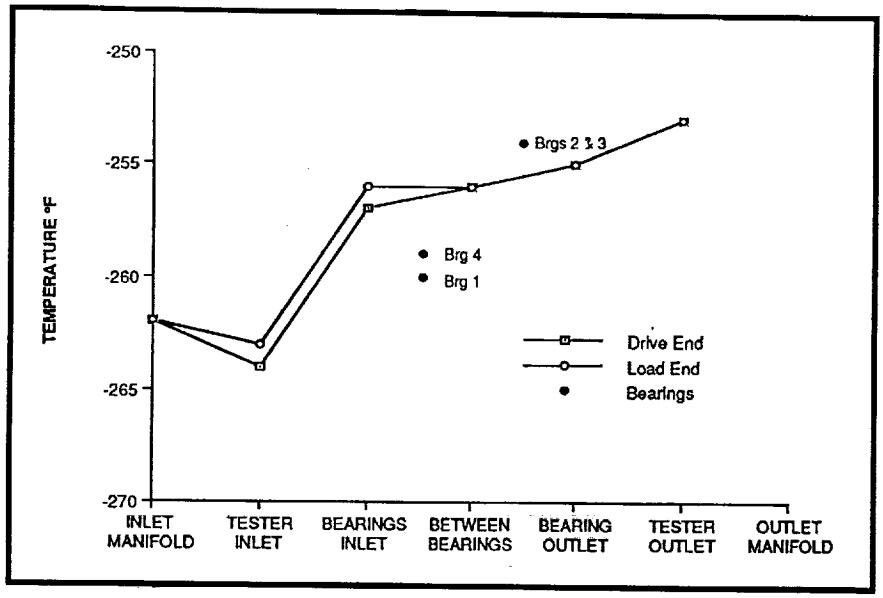

Exhibit 151 Temperature Profile Test 3060202

Test 3060301. This was the second rotational test for Unit 3, Build 6. Plans were for a rotational speed of 25,000 RPM for a duration of 120 seconds. These objectives were successfully accomplished. There was an overspeed to about 26,000 RPM. This was reduced during the run to 25,000 RPM. The outer race temperature of Bearing 2 (T1005) appeared erratic prior to tester rotation but performed correctly during the tester rotational period.

The torque and horsepower for this test were higher than those of comparable tests as shown in **Exhibits 153** and **154**. The average test speed was slightly higher for this test, which could in part account for the higher torque and power values. The temperature increase across the bearings was the same for this test and a previous test of bearings with Si_3N_4 balls. The drive end pressure loss, in this test, was greater than the load end. This was a reversal of the previous tests pressure characteristics which exhibited higher load end pressure losses. The outer race temperature measurements for this test were comparable with those of the previous tests.

The temperature profiles for each end of the tester are shown in **Exhibit 155**. Also shown are the bearing outer race temperatures.

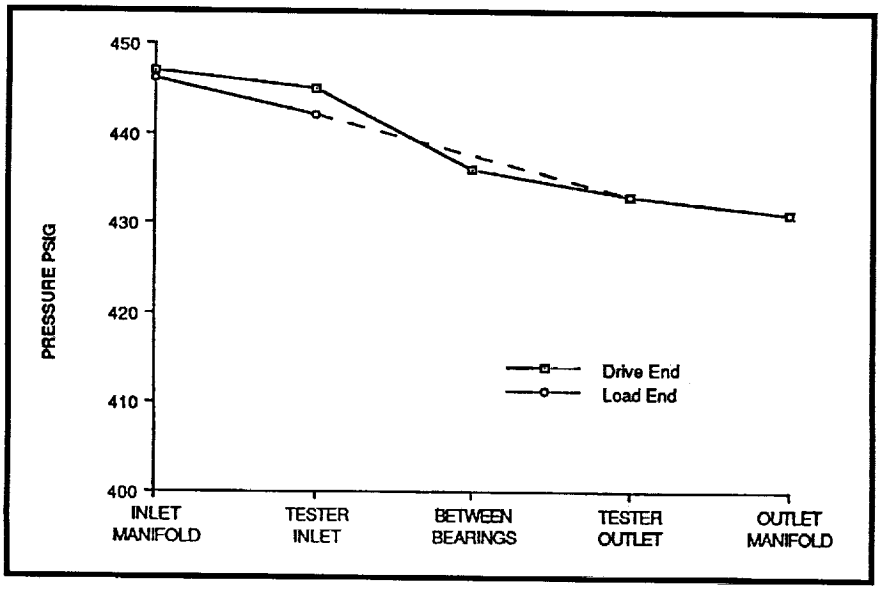

Exhibit 152 Pressure Profile for BSMT Test 3060202

The pressure profiles through the tester are shown in **Exhibit 156** . The pressure between the bearings, P1006, was erratic during the first part of the rotational test. The average value of this measurement was above the exit pressure; indicating little, if any, pumping of the Number 3 bearing.

Results of the borescope examination showed that the balls in the Number 1 bearing were shiny with light

Test Parameter	TEST NUMBER		
	2120302	3030301	3060301
Shaft Speed (RPM)	25,036	24,979	25,115
Time at Speed (sec)	120	140	130
Subcooling	41	40	40
Flow Rate (lbs/sec)	6.41	6.4	6.4
Brg #4 Inlet Temp (°F) T1018	-247	-246.4	-246
Between Brgs 3 & 4 (°F) T1024	-244	-242.5	-245
Brg #3 Outlet Temp (°F) T1019	-240	-238.6	-239
Brg #1 Inlet Temp (°F) T1021	-247	-244.9	-246
Temp Between Bgr 1 & 2 (°F) T1023	-245	-241.5	-243
Brg 2 Outlet Temp (°F) T1022	-240	-238.5	-239
Tester Inlet Temp (°F) T1001 T1002	-265 -262	-262 -257.2	-266 -264
Tester Outlet Temp (°F) T1003	-241	-238.8	-242
Tester Inlet Pressure (psig) PA1001 PA1002	449 446	449.6 447	444 449
Tester Outlet Pressure (psig) PA1003	413	414.2	412
Pressure Between Brg 3 & 4 (psig) P1006	410	417.5	419
Horsepower	212	226	242
Torque (in-lbs)	11,718	12,570	13,341
Brg #1 O.R. Temp (°F) T1004 (TA1004)	-258 (-248)	-267.6 (-248)	-236 (-249)
Brg #2 O.R. Temp (°F) T1005 (TA1005)	-239 (-244)	-239.2 (-239.5)	-245 (-240)
Brg #3 O.R. Temp (°F) T1006 (TA1006)	-240 (-241)	-241 (-241.5)	-240 (-240)
Brg #4 O.R. Temp (°F) T1007 (TA1007)	-249 (-254)	-258.1 (-247)	-245 (-256)

[illegible]

Exhibit 153 BSMT Test Conditions and Selected Data (Test 3060301)

PARAMETER	2120302	3030301	3060301
• Delta Temp Across Brg Pair (°F)			
T1022-T1021	7	6.4	7
T1019-T1018	7	7.8	7
• Delta Temp Across Brg 1 (°F)			
T1023-T1021	2.0	3.4	3.0
Brg 2			
T1022-T1023	5.0	3.0	4.0
Brg 3			
T1019-T1024	4.0	3.9	6.0
Brg 4			
T1024-T1018	3.0	3.9	1.0
• Brg Outer Race Temp - Fluid Inlet Temp (°F)			
Brg 1			
T1004-T1021	-1	-3.1	-3.0
Brg 2			
T1005-T1023	6	2	3.0
Brg 3			
T1006-T1024	4	1	5.0
Brg 4			
T1007-T1018	-2	-0.6	1.0
• Heat Generated (btu/sec) Across			
Brg 1	5.42	8.85	8.06
Brg 2	13.56	7.81	10.75
Brg 3	10.84	10.2	16.13
Brg 4	8.13	10.2	2.69
• Heat Generated Across			
Brg 1&2	18.98	16.7	18.81
Brg 3&4	18.98	20.3	18.81
• Inlet Vortex			
Load	48.8	44.53	53.76
Drive	40.67	28.12	48.38
• Pressure Drop (psi)			
Brg 1	N/A	N/A	N/A
Brg 2	N/A	N/A	N/A
Brg 3	-3	3.3	7
Brg 4	36	29.5	30
Brg 1&2	36	35.4	32
Brg 3&4	33	32.8	37
• Flow (lbs/sec) through Brg pair	6.41	6.4	6.4
• H.P.	212	226	242
• Torque (in-lbs)	11,718	12,570	13,341
• Shaft Speed (rpm)	25,036	24,979	25,115

92060BJC1650

Exhibit 154 BSMT Test Parameters Comparison LOX Test (Test 3060301)

bands of white material that was probably teflon. There were also some light bronze colored bands on some balls. Bearing 2 balls had light gray and bronze bands. Some of the bands were dark bronze. The different colored bands gave a marbled appearance in the surface. The balls in the Number 3 bearing were similar in appearance to those in the Number 2 bearing. The bands were slightly darker indicating somewhat higher operating temperatures for Bearing 3. The Bearing 4 balls had light gray and bronze colored bands. There were white specks of material on some of the balls.

Radial loading of the bearings in the BSMT was also investigated. The radial load would be used to increase the peak stress levels in 57 mm bearings with Si_3N_4 balls to 3.5 GPa which was the level predicted for 45 mm pump end bearings with Si_3N_4 balls and Phase II geometry. The thermomechanical model of the BSMT predicted that a radial load of approximately 6,000 N (1,350 lbs.) with an axial load of 8,900 N (2,000 lbs.) was required to produce this stress level. However, this radial load was also reacted by the outboard bearing which did not have much preload remaining due to the P.A. loading in the BSMT. Thus, another option to achieve this stress level

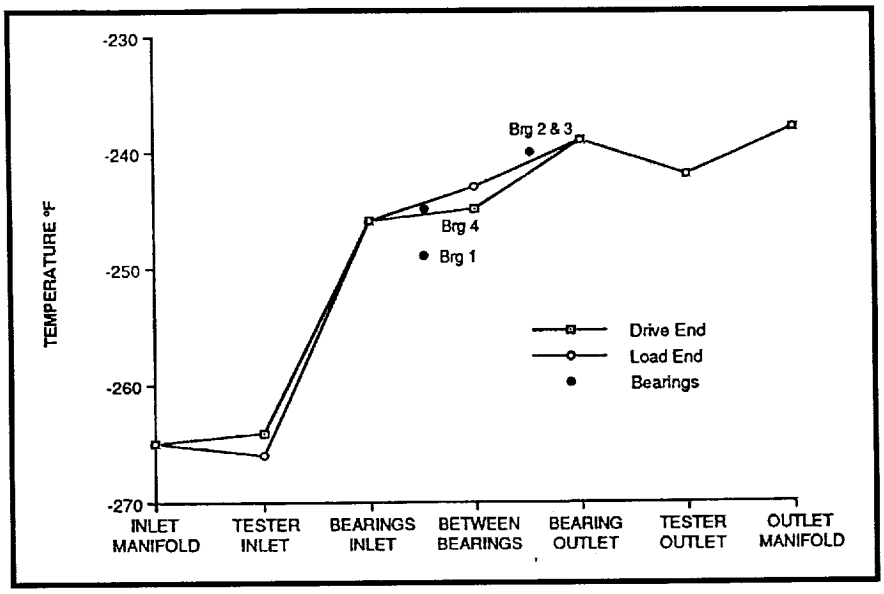

Exhibit 155 Temperature Profile Test 3060301

in the inboard bearings was to use an axial load "pulse" of a relatively short duration during the run. This pulse could be applied, in addition to the P.A. loads, by the axial load cell already in place. The computer model predicted an additional axial load of approximately 4,100 N (920 lbs.) would be needed to produce the 3.5 GPa contact stresses.

Analysis of the Battelle Salox/bronze cage design was performed using the thermomechanical model of the SSME LOX turbopump 45 mm bearings. Results predicted that the race heat generation per ball increased ~10% and contact stress increased only 2% for the 11 ball Battelle cage design as compared to the standard Phase II 12 ball Armalon cage. However, the Battelle cage ball pocket clearance would be exceeded by almost 4 times as compared to 1.5 times for the Phase II Armalon cage. This was due to the round ball pocket design of the Battelle cage which did not allow as much ball excursion as did the oval pockets of the Phase II cage. An ADORE analysis was later performed to determine the cage to ball loading for the Battelle cage operating under these conditions.

Testing of BSMT Unit 3 Build 6 was terminated due to the observed degraded appearance of the bearings. Approximately 51 minutes of test time at 30,000 RPM had been accumulated on the bearings which were using 440C balls, Armalon cage, and 440C races preburnished with Salox. The benefits of the preburnishing were later assessed after hardware disassembly and inspection.

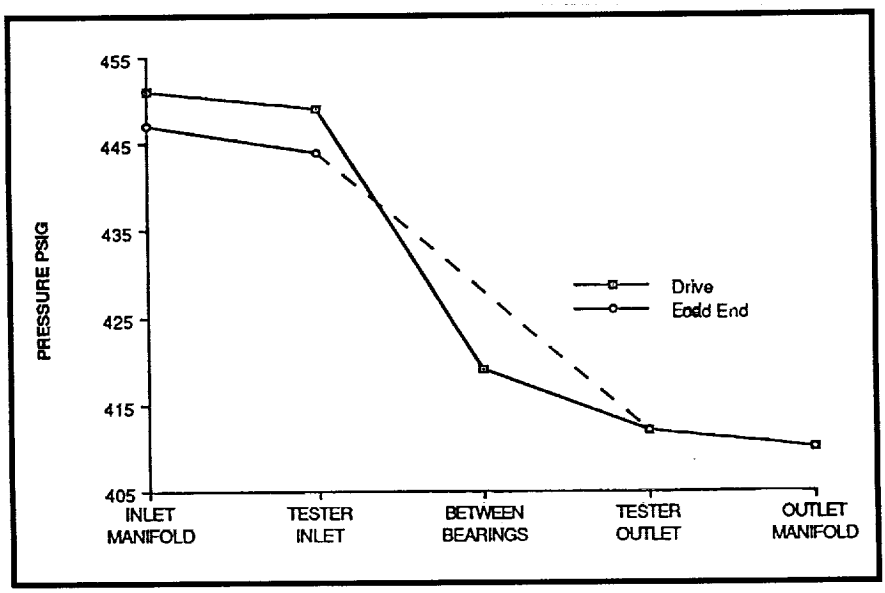

Exhibit 156 Pressure Profile for BSMT Test 3060301

Battelle cages were designed for the 45 mm bearings for use in the pump end of the SSME LOX turbopump. These cages provided a Salox insert around each ball for film transfer lubrication. This required more space per ball, for the pockets than the standard Armalon cage used in the Phase II 45 mm bearings. To increase the space per ball, one ball was deleted from the ball complement leaving eleven balls. With this modification, there was still not enough room to provide the Phase II cage pocket clearance of 2.04 mm (0.08 in.). The ball pocket clearance for the Battelle cages was 0.8 mm (0.031 in.).

Bearing thermomechanical modes were run to compare the operating characteristics of bearings with Battelle cages, and standard Phase II 45 mm bearings. The results of these runs are summarized in **Exhibit 157**. Two cases were run for each bearing configuration. One case allowed each bearing in the bearing pair to tilt (outer race) such that the resultant moment on the outer race was minimized. The second case constrained the outer race in the vertical position (zero tilt).

As shown in **Exhibit 157**, the most significant difference between the Phase II bearings, and those with Battelle cages was the difference in ball excursion and the pocket clearance to accommodate the excursions. The limited clearances in the Battelle cages could severely constrain ball movement causing increased ball pocket loads, heat generation, and ball skidding. The heat generation values shown did not include ball skidding, and consequently neither did the component temperatures. The ADORE program was later used to determine the cage pocket loading for these conditions.

Test 3060402. Test 3060402 was the third rotational test in this series. The test was planned for three speed levels; 26,000, 28,000, and 30,000 RPM. Planned duration at each speed was 120 seconds. The test was cut after about 30 seconds at 26,000 RPM, by coolant temperature measurement T-3 exceeding its redline. This was determined to be an instrumentation problem, and the redline was removed from this measurement and the test recycled. During the second attempt, a speed of 28,000 RPM was maintained for about 126 seconds and a speed of 30,000 RPM was maintained for about 110 seconds. The higher speed test was prematurely cut due to the outer race temperature T1006 of Bearing 3 exceeding its redline value of 133 K (-220°F). Bearing outer race temperatures are shown for test speeds of 28,00 and 30,000 RPM in **Exhibit 158**. As shown, the Bearing 3 outer race temperature "spiked" and exceeded the redline value. The Bearing 3 TA measurement, shown in **Exhibit 159**, did not exhibit this characteristic. The Bearing 2 measurement (TA1005) did, however, show tendency to become thermally unstable.

Test parameters and selected data from this test are compared with those of previous tests in

Parameter	45 mm Bearings fi = 0.55 fo = 0.52 Pd = 0.16 mm Battelle Cages, 11 Balls				Phase II 45 mm Bearings with 440C RollingElements fi = 0.55, fo = 0.52, Pd = 0.16 mm			
	Brg. 1	Brg. 2	Brg. 1	Brg. 2	Brg. 1	Brg. 2	Brg. 1	Brg. 2
Outer Race Tilt (min.)	-.344	5.16	0	0	-.344	5.16	0	0
Cage Pocket Clearance (mm)	0.8	0.8	0.8	0.8	2.04	2.04	2.04	2.04
Ball Excursion (mm)	1.4	3.05	1.41	1.35	1.4	3.1	1.48	1.36
Radial Reaction (N)	2,734	4,405	2,258	5,008	2,716	4,425	2,221	5,055
Axial Reaction (N)	3,292	3,292	2,900	2,900	3,311	3,311	2,920	2,920
Max. Hertz Stress (MPA)	2,537	2,979	2,500	3,146	2,567	2,909	2,429	3,076
Avg. Heat Generation watt/ball	I.R. 138.3 O.R. 70	I.R. 139.3 O.R. 87.4	I.R. 120 O.R. 67	I.R. 125 O.R. 88	I.R. 127 O.R. 63	I.R. 127 O.R. 78	I.R. 113 O.R. 62	I.R. 116 O.R. 77
Avg. Ball Temp. -K	220	202	207	196	213	194	203	190
Avg. I.R. Temp. -K	158	159	154	153	156	156	152	152
Avg. O.R. Temp. -K	142	143	140	139	141	142	139	142

Exhibit 157 Comparison of 45 mm Pump End Bearings and Bearings Equipped with Battelle Cages

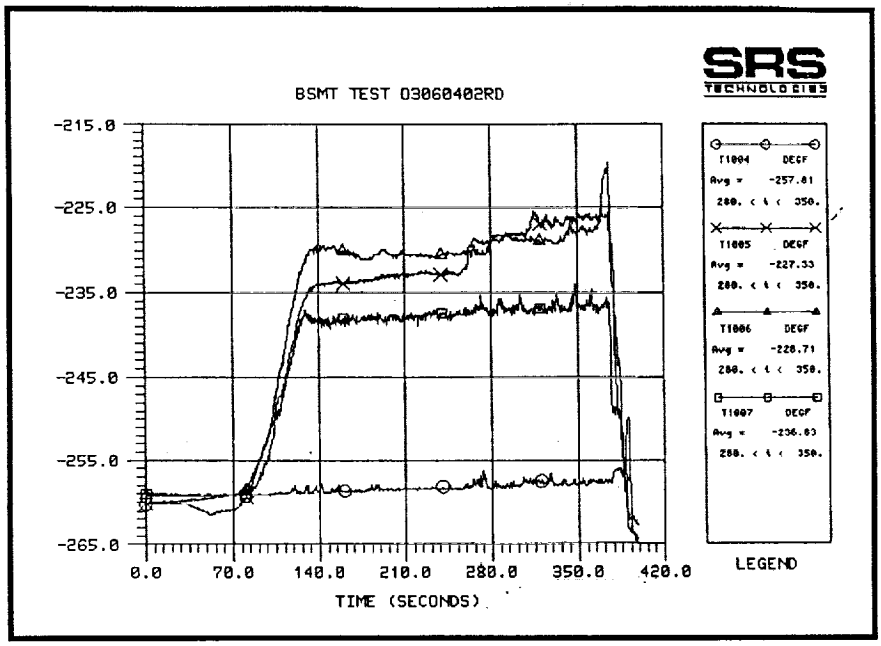

Exhibit 158 Bearing Outer Race Temperatures (T100-) (Test 3060402)

Exhibits 160 and **161**. The heat generated across the bearings was less for this test than the values determined from the previous test of 440C ball bearings (3030401). The values for this test were, however, higher than those determined from the Si_3N_4 ball bearing tests (2120401). The horsepower and torque values from this test also fell in between the values of the previous tests of 440C and Si_3N_4 ball bearings.

The temperature profiles through the tester are shown in **Exhibits 162** through **164**. Included are the bearing outer race temperatures.

The pressure profiles through the tester are shown in **Exhibits 165** through **167**. There was a decrease in pressure loss through the tester, as the speed was increased from 28,000 to 30,000 RPM. This could have been the result of increased pumping of the inboard bearings as speed increased, or a reduction in fluid rotation, due to vapor blanketing of the inboard bearings, as the temperature of the balls increased with speed.

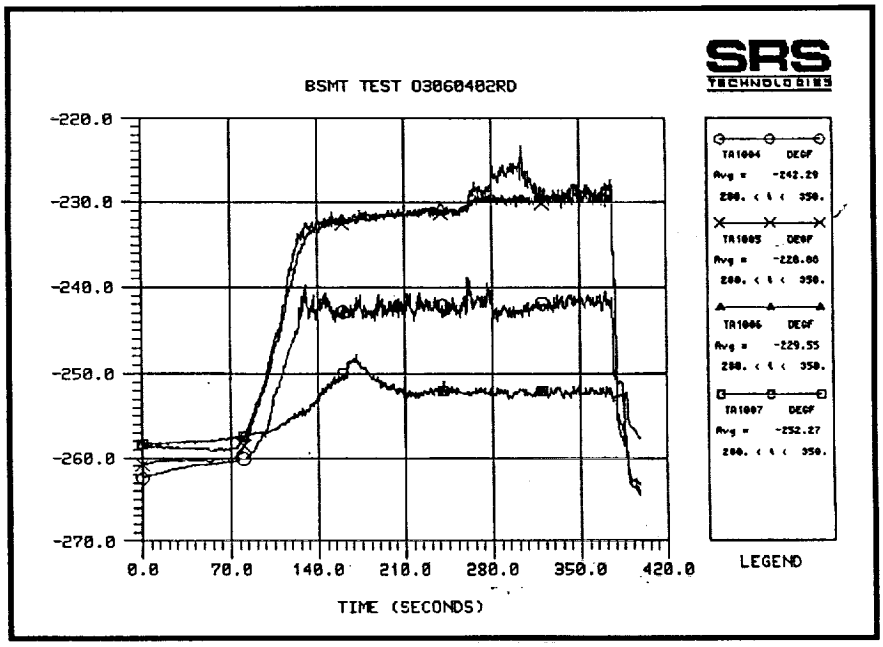

Exhibit 159 Bearing Outer Race Temperatures (TA100-) (Test 3060402)

The borescope inspection, following the rotation test, showed that the Number 1 bearing balls had wide bronze bands. The bronze color appeared to be darker after this test compared to the previous test. Bearing 2 balls had dark bronze bands. There were numerous scratches in the ball surfaces. The bearing appeared to be in good condition. The Number 3 bearing balls had dark bronze colored bands.

Test Parameter	TEST NUMBER		
	2120401	3030401	3060402
Shaft Speed (RPM)	29,995	30,231	30,031
Time at Speed (sec)	120	120	110
Subcooling	39	40	36
Flow Rate (lbs/sec)	6.4	6.45	6.4
Brg #4 Inlet Temp (°F) T1018	-245	-243	-240
Between Brgs 3 & 4 (°F) T1024	-242	-238	-237
Brg #3 Outlet Temp (°F) T1019	-235	-230	-228
Brg #1 Inlet Temp (°F) T1021	-243	-243	-239
Temp Between Bgr 1 & 2 (°F) T1023	-239	-236	-234
Brg 2 Outlet Temp (°F) T1022	-234	-229	-228
Tester Inlet Temp (°F) T1001 T1002	-265 -264	-264 -255	-262 -259
Tester Outlet Temp (°F) T1003	-235	-230	-231
Tester Inlet Pressure (psig) PA1001 PA1002	454 444	452.5 453.8	439 448
Tester Outlet Pressure (psig) PA1003	408	411	407
Pressure Between Brg 3 & 4 (psig) P1006	400	417	409
Horsepower	280	322	308
Torque (in-lbs)	12,933	14,768	14,238
Brg #1 O.R. Temp (°F) T1004 (TA1004)	-262 (-243)	-265 (-247)	-256 (-242)
Brg #2 O.R. Temp (°F) T1005 (TA1005)	-222 (-233)	-221.5 (-226)	-227 (-230)
Brg #3 O.R. Temp (°F) T1006 (TA1006)	-232 (-234)	-235 (-236)	-220 (-230)
Brg #4 O.R. Temp (°F) T1007 (TA1007)	-243 (-252)	-261 (-243)	-237 (-252)

920611JC1002

Exhibit 160 BSMT Test Conditions and Selected Data (Test 3060402)

PARAMETER	2120401	3030401	3060402
• Delta Temp Across Brg Pair (°F)			
T1022-T1021	9	13.6	11
T1019-T1018	10	13.7	12
• Delta Temp Across Brg 1 (°F)			
T1023-T1021	4	7.4	5
Brg 2			
T1022-T1023	5	6.4	6
Brg 3			
T1019-T1024	7	8.4	9
Brg 4			
T1024-T1018	3	5.3	3
• Brg Outer Race Temp - Fluid Inlet Temp (°F)			
Brg 1			
T1004-T1021	0	-4	-3
Brg 2			
T1005-T1023	17	10	10
Brg 3			
T1006-T1024	10	2	17
Brg 4			
T1007-T1018	2	0	3
• Heat Generated (btu/sec) Across			
Brg 1	10.84	20.04	13.44
Brg 2	13.54	17.33	16.13
Brg 3	18.95	22.75	24.19
Brg 4	8.12	14.36	8.06
• Heat Generated Across			
Brg 1&2	24.36	36.84	29.57
Brg 3&4	27.10	37.11	32.26
• Inlet Vortex			
Load	54.14	57.3	61.82
Drive	56.85	32.5	51.07
• Pressure Drop (psi)			
Brg 1	N/A	N/A	N/A
Brg 2	N/A	N/A	N/A
Brg 3	-8	6	2
Brg 4	44	36.8	37
Brg 1&2	46	41.5	32
Brg 3&4	36	42.8	39
• Flow (lbs/sec) through Brg pair	6.4	6.45	6.4
• H.P.	280	322	308
• Torque (in-lbs)	12,933	14,768	14,238
• Shaft Speed (rpm)	29,995	30,231	30,031

Exhibit 161 BSMT Test Parameters Comparison LOX Tests (Test 3060402)

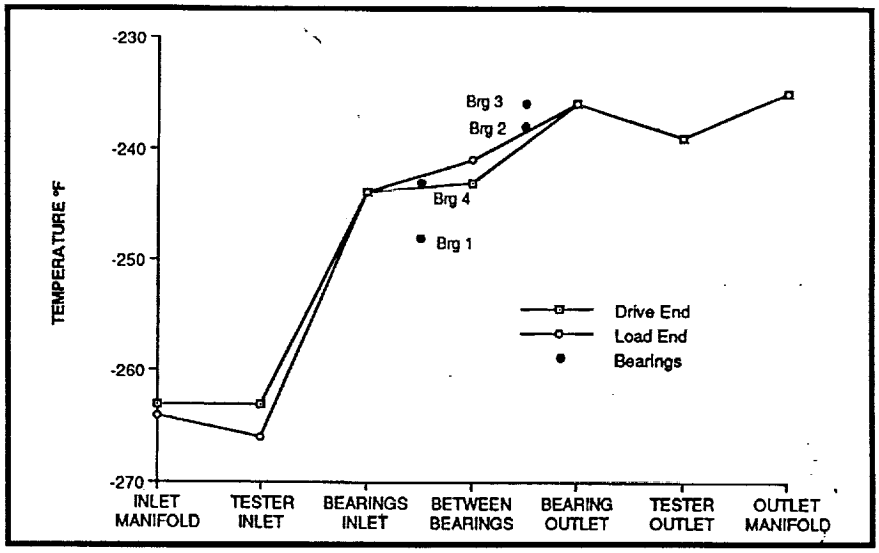

Exhibit 162 Temperature Profile Test 3060402
(Test Speed 26,000 RPM)

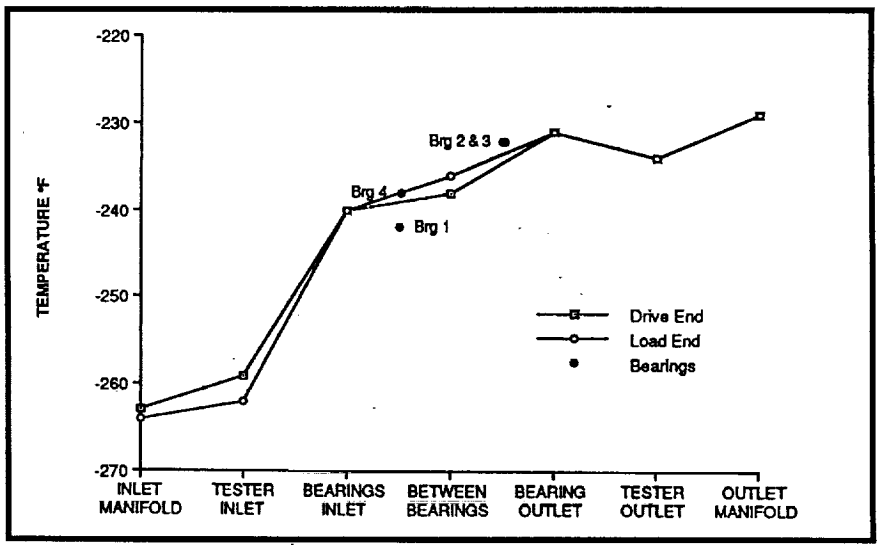

Exhibit 163 Temperature Profile Test 3060402
(Test Speed 28,000 RPM)

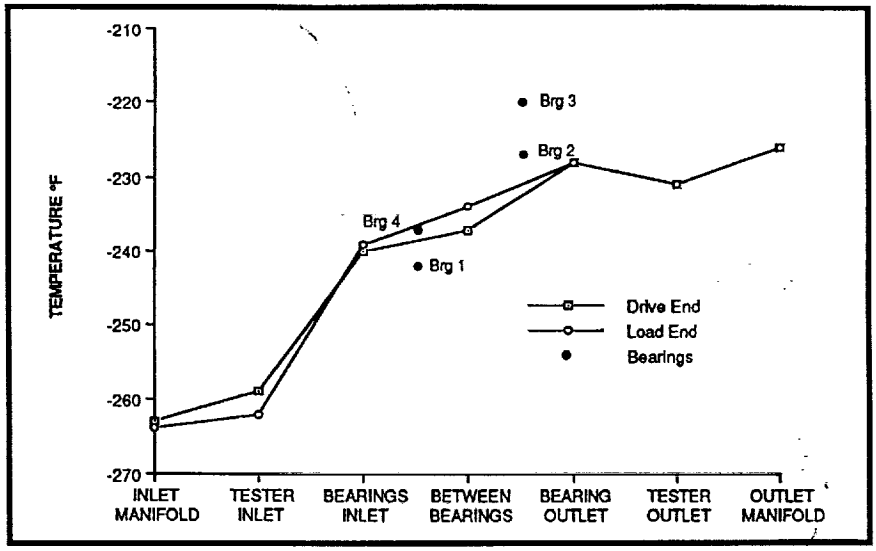

Exhibit 164 Temperature Profile Test 3060402
(Test Speed 30,000 RPM)

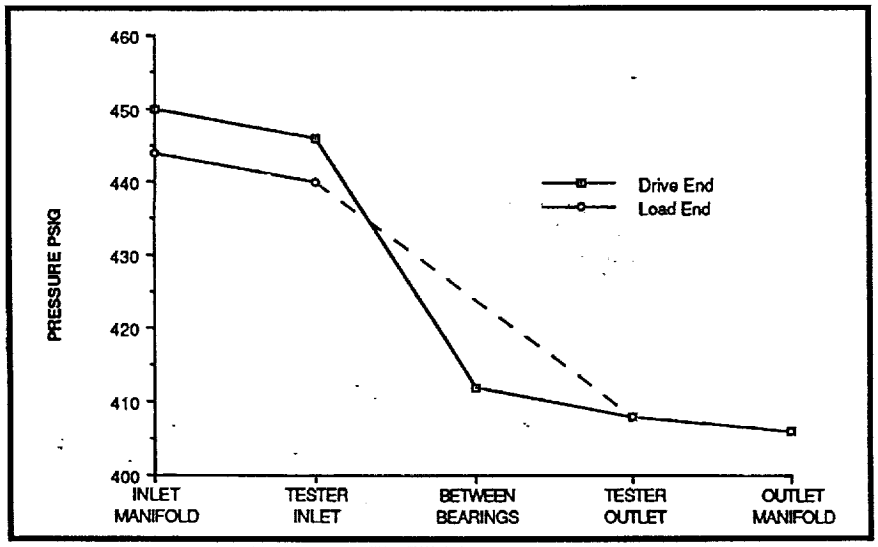

Exhibit 165 Pressure Profile Test for BSMT Test 3060402
Test Speed 26,000 RPM

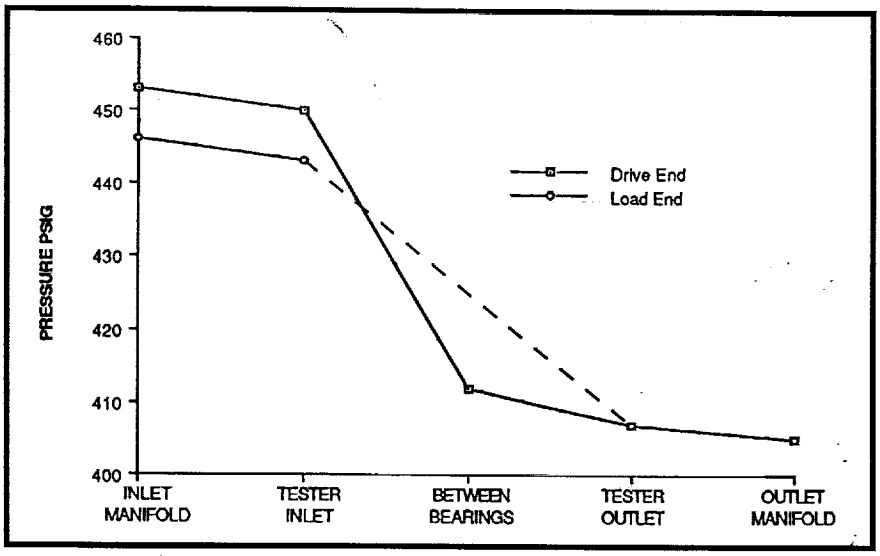

Exhibit 166 Pressure Profile Test for BSMT Test 3060402 Test Speed 28,000 RPM

Some bands were almost black. Areas within these bands were rough and frosty looking. The balls appeared to have reached a higher temperature than those in the other bearings. Bearing 3 had wide bands of white material that appeared to be teflon. There were numerous specks of material on the ball surfaces. Some of the bands had light bronze tint. The bearing appeared to be in good condition.

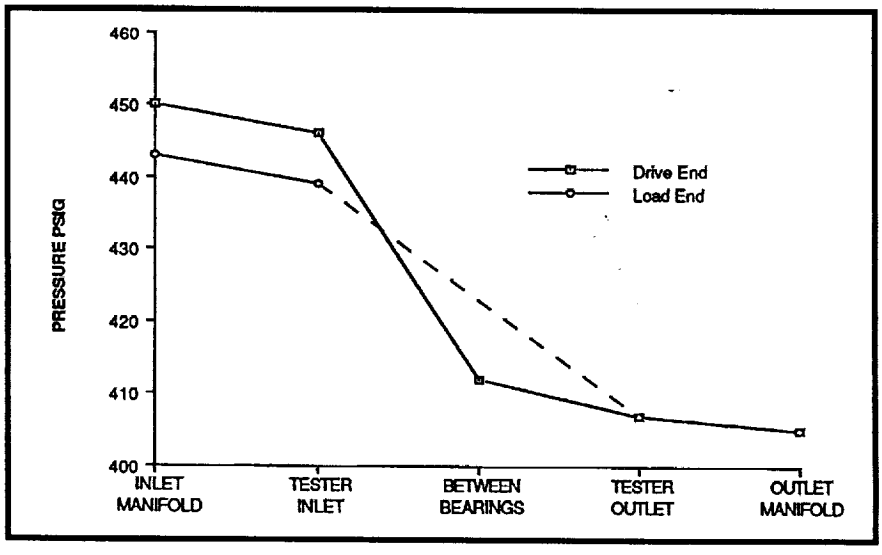

Exhibit 167 Pressure Profile Test for BSMT Test 3060402 Test Speed 30,000 RPM

Test 3060501. This was the fourth rotational test in this series. The redline on the Number 3 bearing outer race temperature was increased from 133 K (-220°F) to 135.8 K (-215°F). This was done because the previous test was cut due to the Bearing 3 temperature exceeding its redline, and subsequent borescope examination revealed the bearing to be in good condition. the planned duration of this test was 300 seconds at the test speed of 30,000 RPM. These objectives were successfully accomplished.

Test parameters and selected data from this test are compared with those of previous tests in **Exhibits 168** and **169**. Bearing 3 outer race temperature for this test reached 133 K (-220°F) compared to a Bearing 2 outer race temperature of 135.8K (-215°F) for Test 3030501, and 125.8K (-233°F) for Test 2120501. The maximum inboard bearing (Bearings 2 and 3) outer race temperatures were less for the Si_3N_4 bearings compared to the 440C ball bearings. Test 3060501 ran for 310 seconds compared to Test 3030501 which cut at 30 seconds due to the outer race temperature exceeding its redline value of 135.8 K (-215°F). Unit 2, Build 12 (2120501) load end pressure drop was greater than the drive end loss, and was about 0.0689 MPa (10 psi) higher than the other two

Test Parameter	TEST NUMBER		
	2120501	3030501	3060501
Shaft Speed (RPM)	29,954	30,177	29,997
Time at Speed (sec)	300	30	310
Subcooling	38	41	38
Flow Rate (lbs/sec)	6.4	6.4	6.4
Brg #4 Inlet Temp (°F) T1018	-243	-244.2	-242
Between Brgs 3 & 4 (°F) T1024	-237	-238.7	-240
Brg #3 Outlet Temp (°F) T1019	-232	-230.1	-230
Brg #1 Inlet Temp (°F) T1021	-241	-240.6	-242
Temp Between Bgr 1 & 2 (°F) T1023	-236	-234.2	-237
Brg 2 Outlet Temp (°F) T1022	-232	-229	-231
Tester Inlet Temp (°F) T1001 T1002	-266 -265	-264.3 -260.7	-265 -263
Tester Outlet Temp (°F) T1003	-236	-230.1	-233
Tester Inlet Pressure (psig) PA1001 PA1002	453 443	444.2 451.2	441 446
Tester Outlet Pressure (psig) PA1003	408	408.2	407
Pressure Between Brg 3 & 4 (psig) P1006	400	415.3	409
Horsepower	283	322	314
Torque (in-lbs)	13,087	14,789	14,528
Brg #1 O.R. Temp (°F) T1004 (TA1004)	-260 (-244)	-262.8 (-246.9)	-261 (-244)
Brg #2 O.R. Temp (°F) T1005 (TA1005)	-229 (-232)	-215 (-230)	-230 (-232)
Brg #3 O.R. Temp (°F) T1006 (TA1006)	-233 (-235)	-233 (-236.7)	-220 (-232)
Brg #4 O.R. Temp (°F) T1007 (TA1007)	-242 (-240)	-262.2 (-241.2)	-239 (-252)

920616JC0447

Exhibit 168 BSMT Test Conditions and Selected Data (Test 3060501)

PARAMETER	2120501	3030501	3060501
• Delta Temp Across Brg Pair (°F)			
T1022-T1021	9	11.6	11
T1019-T1018	11	14.1	12
• Delta Temp Across Brg 1 (°F)			
T1023-T1021	5	6.4	5
Brg 2			
T1022-T1023	4	5.2	6
Brg 3			
T1019-T1024	5	8.6	10
Brg 4			
T1024-T1018	6	5.5	2
• Brg Outer Race Temp - Fluid Inlet Temp (°F)			
Brg 1			
T1004-T1021	-3	-6.3	-2
Brg 2			
T1005-T1023	7	19.2	7
Brg 3			
T1006-T1024	4	5.7	20
Brg 4			
T1007-T1018	-1	3.0	3
• Heat Generated (btu/sec) Across			
Brg 1	13.5	17.34	13.44
Brg 2	10.8	14.1	16.13
Brg 3	13.5	23.3	26.88
Brg 4	16.2	14.9	5.38
• Heat Generated Across			
Brg 1&2	24.4	31.4	29.57
Brg 3&4	29.8	38.2	32.26
• Inlet Vortex			
Load	67.7	64.2	61.82
Drive	59.6	44.7	56.45
• Pressure Drop (psi)			
Brg 1	N/A	N/A	N/A
Brg 2	N/A	N/A	N/A
Brg 3	-8	7.1	2
Brg 4	43	35.9	37
Brg 1&2	45	36	34
Brg 3&4	35	43	39
• Flow (lbs/sec) through Brg pair	6.4	6.4	6.4
• H.P.	283	322	314
• Torque (in-lbs)	13,087	14,789	14,258
• Shaft Speed (rpm)	29,954	30,177	29,997

Exhibit 169 BSMT Test Parameters Comparison LOX Tests (Test 3060501)

load end test values. The other two tests involving Unit 3 had higher drive end pressure losses, compared to the load end. The test with Si_3N_4 ball bearings (2120501) had lower power and torque values compared to the other two tests.

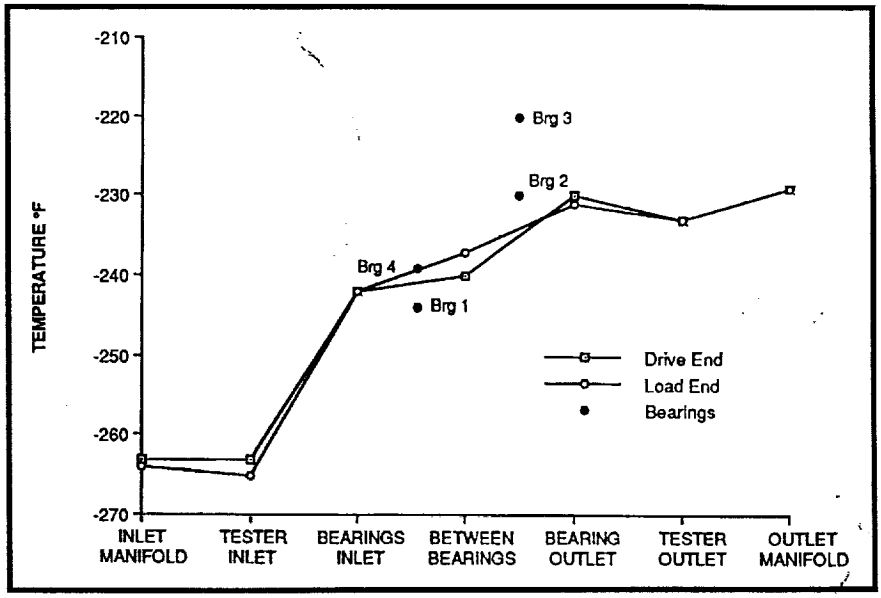

Exhibit 170 Temperature Profile for Test 3060501

The temperature profiles through the tester are shown in **Exhibit 170**. Included are the bearing outer race temperatures. It is believed that the tester outlet temperatures were less than the bearing outlet temperatures because of coolant flowing through the bearing outer race to housing deadband clearance.

The pressure profiles through the tester are shown in **Exhibit 171**. There was very little pressure loss across Bearing 3, which indicated that Bearing 3 was acting as a pump.

Bearing examination showed that Bearing 1 had light bronze bands on the balls. Some were darker than others. The bearing appeared to be in good condition. Bearing 2 balls had gray bands. There were no dark colored bands usually associated with elevated temperatures. This bearing was in good condition. Bearing 3 balls had dark bronze bands. Some streaks of rough frosty patches were in the surface of the balls indicating relatively high temperatures. The surface of Bearing 4 balls contained numerous crisscross scratches. The balls were shiny with some wide light gray bands.

Test 3060601. This was the fifth rotational test in this series. The test was planned for a duration of 600 seconds at a test speed of 30,000 RPM, and was successfully completed. The Number 3 bearing outer race temperatures (T1006, TA1006)

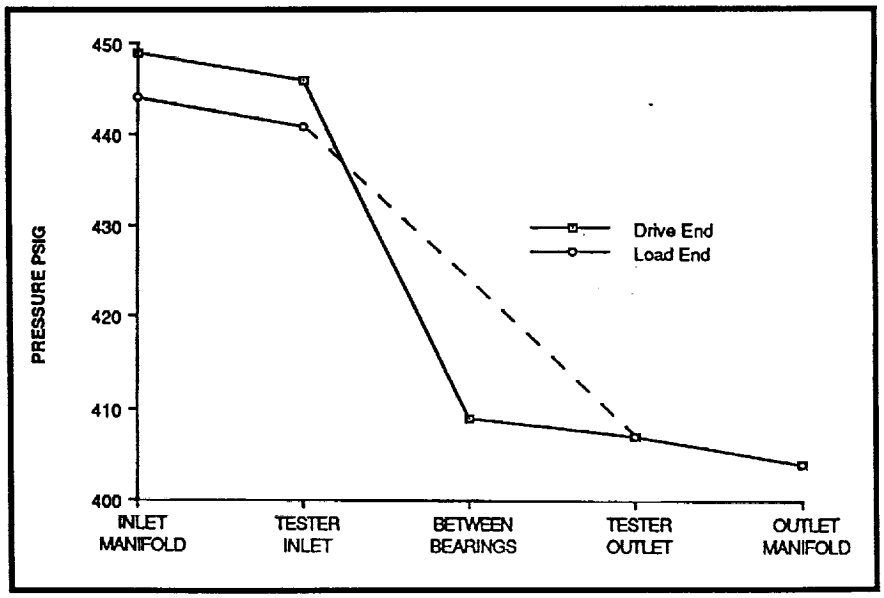

Exhibit 171 Pressure Profile for BSMT Test 3060501

redlines were increased from 133 K (-220°F) to 135.8 K (-215°F). During the test, the outer race temperature of Bearing 3 initially ran at about 133 K (-220°F), cooled to about 130.2 K (-225°F), and then rose to about 132.4K (-221°F) at the end of the test. This temperature history is shown in **Exhibit 172**. The outer race temperature of both Bearings 2 and 3 increased during the last 70 seconds of the test as shown in the exhibit. This characteristic was not exhibited by the other outer race temperature (TA1005 and TA1006). Raising the Bearing 3 outer race temperature redline 2.8 K (5°F) allowed the tester to run for 600 seconds at 30,000 RPM.

The outer race temperature of Bearing 2 (TA1005) did experience about a 2.8 K (5°F) "spike" at 600 seconds. The bearing outlet coolant temperatures (T1019, T1021) also increased slightly during the last 70 seconds of the test. This indicated that the heat generation in the bearings increased during this period. Test parameters and selected data from this test are compared with those of previous tests in **Exhibits 173** and **174**. Unit 2 Build 12 (2120602) used Si_3N_4 ball bearings and Unit 3 Build 3 (3030501) used standard Phase II bearings with 440C balls. Also shown is previous test data from Unit 3 Build 6. Test 3030501 was the last test for that build. The data from the previous run of Unit 3 Build 6 compares favorably with this run. The outer race temperatures of Bearing 3 were slightly less for this test. Horsepower was up slightly for this test due to a small increase in torque. Compared to Unit 3 Build 3, the power and torque were slightly less for this test. All the tests with 440C ball bearings, however, required higher power and torque than the tests with Si_3N_4 ball bearings.

The temperature profiles through the tester are shown in **Exhibit 175**. The bearing outer race temperatures are included. The pressure profiles through the tester are shown in **Exhibit 176**. There was only about 0.01379 MPa (2 psi) pressure loss across Bearing 3 indicating that the bearing was pumping. The measurement between Bearings 3 and 4 (P1006) was very noisy and fluctuated over about a 40 psi range.

Following the rotational test, the bearings were examined through a borescope. The balls in Bearing 1 had wide dark bronze bands and the bearing appeared to be in good condition. The Number 2 ball bearings had light and dark bronze areas giving a marbled appearance. This bearing also appeared to be in good condition. Some of the balls in Bearing 3 had small surface spalls. There were also light and dark bronze areas

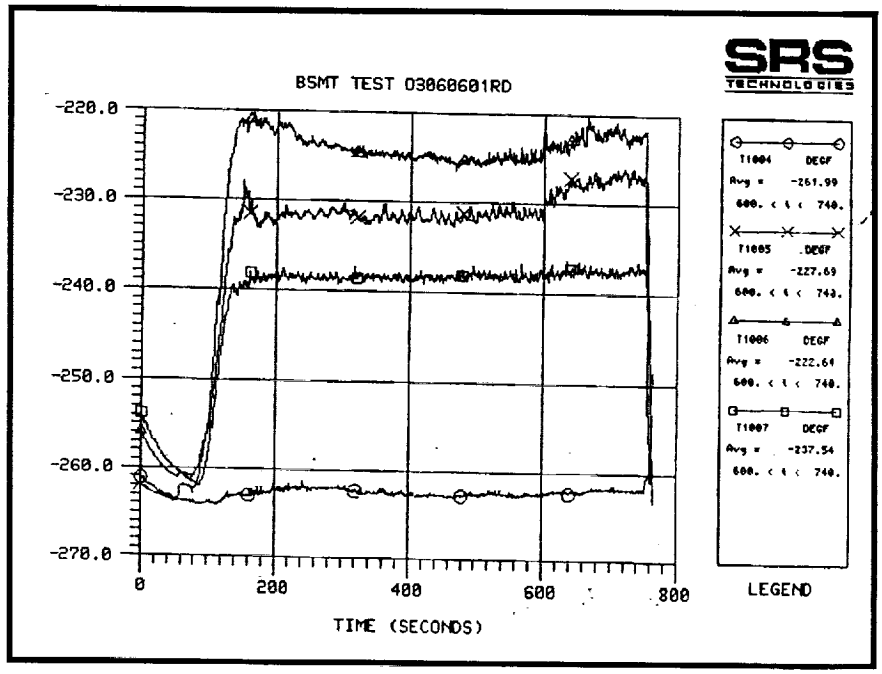

Exhibit 172 Bearing Outer Race Temperatures (Test 3060601)

Test Parameter	TEST NUMBER			
	2120602	3030501	3060501	3060601
Shaft Speed (RPM)	30,039	30,177	29,997	29,997
Time at Speed (sec)	600	30	310	605
Subcooling	36	41	38	38
Flow Rate (lbs/sec)	6.4	6.45	6.4	6.4
Brg #4 Inlet Temp (°F) T1018	-242	-244.2	-242	-242
Between Brgs 3 & 4 (°F) T1024	-236	-238.7	-240	-240
Brg #3 Outlet Temp (°F) T1019	-230	-230.1	-230	-231
Brg #1 Inlet Temp (°F) T1021	-240	-240.6	-242	-242
Temp Between Bgr 1 & 2 (°F) T1023	-235	-234.2	-237	-237
Brg 2 Outlet Temp (°F) T1022	-230	-229	-231	-231
Tester Inlet Temp (°F) T1001 T1002	-265 -263	-264.3 -260.7	-266 -263	-266 -264
Tester Outlet Temp (°F) T1003	-234	-230.1	-233	-234
Tester Inlet Pressure (psig) PA1001 PA1002	455 443	444.2 451.2	441 446	442 449
Tester Outlet Pressure (psig) PA1003	404	408.2	407	408
Pressure Between Brg 3 & 4 (psig) P1006	400	415.3	409	412
Horsepower	281	322	314	319
Torque (in-lbs)	12,957	14,789	15,428	14,760
Brg #1 O.R. Temp (°F) T1004 (TA1004)	-260 (-244)	-262.8 (-246.9)	-261 (-244)	-262 (-245)
Brg #2 O.R. Temp (°F) T1005 (TA1005)	-228 (-30)	-215 (-230.1)	-230 (-232)	-228 (-230)
Brg #3 O.R. Temp (°F) T1006 (TA1006)	-231 (-234)	-233 (-236.7)	-223 (-232)	-223 (-233)
Brg #4 O.R. Temp (°F) T1007 (TA1007)	-241 (-232)	-262.2 (-241.2)	-239 (-252)	-237 (-257)

Exhibit 173 BSMT Test Conditions and Selected Data (Test 3060601)

PARAMETER	2120602	3030501	3060501	3060601
• Delta Temp Across Brg Pair (°F)				
T1022-T1021	10	11.6	11	11
T1019-T1018	12	14.1	12	11
• Delta Temp Across Brg 1 (°F)				
T1023-T1021	5	6.4	5	5
Brg 2 T1022-T1023	5	5.2	6	6
Brg 3 T1019-T1024	6	8.6	10	9
Brg 4 T1024-T1018	6	5.5	2	2
• Brg Outer Race Temp - Fluid Inlet Temp (°F) Brg 1				
T1004-T1021	-4	-6.3	-2	-3
Brg 2 T1005-T1023	7	19.2	7	9
Brg 3 T1006-T1024	5	5.7	20	17
Brg 4 T1007-T1018	10	3.0	3	5
• Heat Generated (btu/sec) Across				
Brg 1	13.4	17.34	13.44	13.44
Brg 2	13.4	14.1	16.13	16.13
Brg 3	16.1	23.3	26.88	24.19
Brg 4	16.1	14.9	5.38	5.38
• Heat Generated Across				
Brg 1&2	26.9	31.4	29.57	29.57
Brg 3&4	32.2	38.2	32.26	29.57
• Inlet Vortex				
Load	67.2	64.2	61.82	64.51
Drive	61.8	44.7	56.45	59.14
• Pressure Drop (psi)				
Brg 1	N/A	N/A	N/A	N/A
Brg 2	N/A	N/A	N/A	N/A
Brg 3	-4	7.1	2	4
Brg 4	43	35.9	37	37
Brg 1&2	51	36	34	34
Brg 3&4	39	43	39	41
• Flow (lbs/sec) through Brg pair	64	6.4	6.4	6.4
• H.P.	281	322	314	319
• Torque (in-lbs)	12,957	14,789	14,258	14,760
• Shaft Speed (rpm)	30,039	30,177	29,997	30,000

Exhibit 174 BSMT Test Parameter Comparison LOX Tests (Test 3060601)

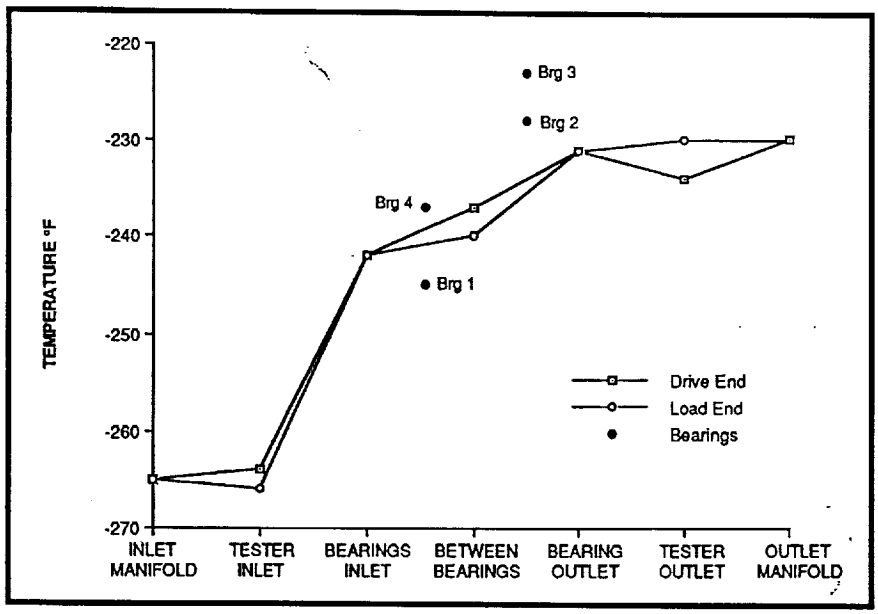

Exhibit 175 Temperature Profile For BSMT Test 3060601

giving a marbled appearance. Some balls had bands that were almost black. The Bearing 4 balls had shiny surfaces with numerous scratches. Some balls had light bronze bands. The bearing appeared to be in good condition.

Test 3060701. This was the sixth rotational test in this series. The test was planned to run until LOX tank depletion, which was about 25 minutes. The test was cut after about 204 seconds at a speed of 30,000 RPM. The cut was caused by the outer race temperature of Bearing 3 (T1006) exceeding its redline value of 135.8 K (-215°F).

Test parameters and selected data from this test are compared with those of previous tests in **Exhibits 177** and **178**. The measured temperature difference across Bearing 3 was greater, and the temperature difference across Bearing 4 was less for this test series, compared to the other tests. The apparent reason for this was that the temperature measurement (T1024) between these bearings was from 0.56 K (1°F) to 2.8 K (5°F) lower than in the previous tests. The heat generation for the drive end bearing pair (Bearing 3 and 4) for this test is comparable to that from Test 2120702 (Si_3N_4 balls) and the previous test (3060601) in this series. This value is much less than that observed in Test 3030501, which only ran for 30 seconds before being cut. The power and torque were less for this test than in the previous test in this series. There was also a slight decrease in RPM which could have accounted for the lower power and torque values.

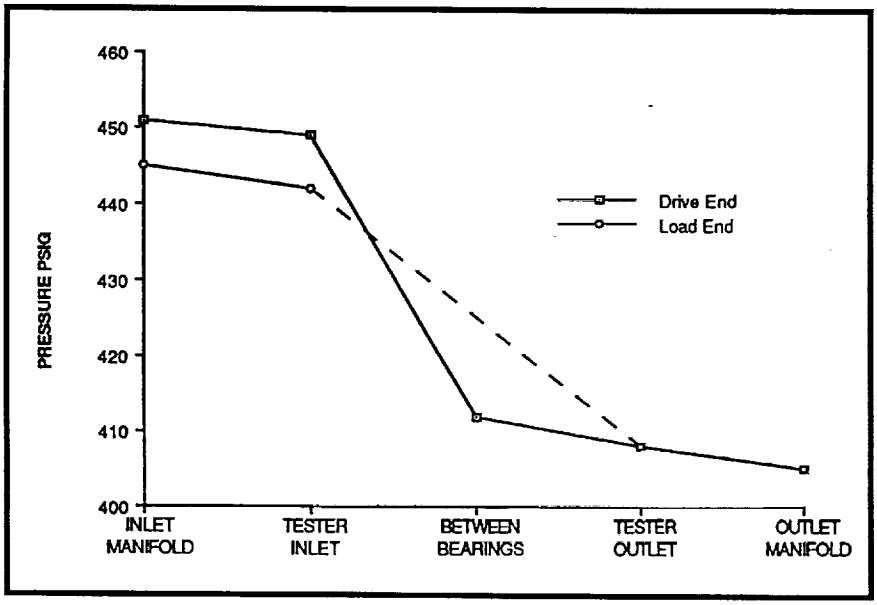

Exhibit 176 Pressure Profile For BSMT Test 3060601

The temperature profiles through the tester are shown in **Exhibit 179**. Included are the bearing outer race temperatures. The difference between the outer race tem-

Test Parameter	TEST NUMBER			
	2120702	3030501	3060601	3060701
Shaft Speed (RPM)	30,017	30,177	29,997	29,986
Time at Speed (sec)	600	30	605	204
Subcooling	35	41	38	37
Flow Rate (lbs/sec)	6.4	6.45	6.4	6.4
Brg #4 Inlet Temp (°F) T1018	-241	-244.2	-242	-241
Between Brgs 3 & 4 (°F) T1024	-235	-238.7	-240	-240
Brg #3 Outlet Temp (°F) T1019	-230	-230.1	-231	-231
Brg #1 Inlet Temp (°F) T1021	-239	-240.6	-242	-242
Temp Between Bgr 1 & 2 (°F) T1023	-234	-234.2	-237	-237
Brg 2 Outlet Temp (°F) T1022	-229	-229	-231	-231
Tester Inlet Temp (°F) T1001 T1002	-264 -263	-264.3 -260.7	-266 -264	-264 -263
Tester Outlet Temp (°F) T1003	-233	-230.1	-234	-234
Tester Inlet Pressure (psig) PA1001 PA1002	455 441	444.2 451.2	442 449	442 446
Tester Outlet Pressure (psig) PA1003	409	408.2	408	407
Pressure Between Brg 3 & 4 (psig) P1006	404	415.3	412	416
Horsepower	278	322	319	314
Torque (in-lbs)	12,821	14,789	14,760	14,507
Brg #1 O.R. Temp (°F) T1004 (TA1004)	-256 (-243)	-262.8 (-246.9)	-262 (-245)	-261 (-247)
Brg #2 O.R. Temp (°F) T1005 (TA1005)	-227 (-233)	-215 (-230.1)	-228 (-230)	-228 (-232)
Brg #3 O.R. Temp (°F) T1006 (TA1006)	-230 (-233)	-233 (-236.7)	-223 (-233)	-215 (-234)
Brg #4 O.R. Temp (°F) T1007 (TA1007)	-241 (-234)	-262.2 (-241.2)	-237 (-241.2)	-237 (-255)

Exhibit 177 BSMT Test Conditions and Selected Data (Test 3060701)

PARAMETER	2120702	3030501	3060601	3030701
• Delta Temp Across Brg Pair (°F)				
T1022-T1021	10	11.6	11	11
T1019-T1018	11	14.1	11	10
• Delta Temp Across Brg 1 (°F)				
T1023-T1021	5	6.4	5	5
Brg 2				
T1022-T1023	5	5.2	6	6
Brg 3				
T1019-T1024	5	8.6	9	9
Brg 4				
T1024-T1018	6	5.5	2	1
• Brg Outer Race Temp - Fluid Inlet Temp (°F)				
Brg 1				
T1004-T1021	-4	-6.3	-3	-5
Brg 2				
T1005-T1023	7	19.2	9	11
Brg 3				
T1006-T1024	5	5.7	17	25
Brg 4				
T1007-T1018	7	3.0	5	4
• Heat Generated (btu/sec) Across				
Brg 1	13.4	17.34	13.44	13.4
Brg 2	13.4	14.1	16.13	16.1
Brg 3	13.4	23.3	24.19	24.2
Brg 4	16.1	14.9	5.38	2.7
• Heat Generated Across				
Brg 1&2	26.9	31.4	29.57	29.6
Brg 3&4	29.6	38.2	29.57	26.9
• Inlet Vortex				
Load	67.2	64.2	64.51	59.13
Drive	59.1	44.7	59.14	59.13
• Pressure Drop (psi)				
Brg 1	N/A	N/A	N/A	N/A
Brg 2	N/A	N/A	N/A	N/A
Brg 3	-5	7.1	4	9
Brg 4	37	35.9	37	30
Brg 1&2	51	36	34	35
Brg 3&4	32	43	41	39
• Flow (lbs/sec) through Brg pair	6.4	6.4	6.4	6.4
• H.P.	278	322	319	314
• Torque (in-lbs)	12,821	14,789	14,760	14,507
• Shaft Speed (rpm)	30,017	30,177	30,000	29,986

Exhibit 178 BSMT Test Parameters Comparison LOX Tests (Test 3060701)

perature of Bearing 3 and bearing inlet coolant temperature was relatively high.

The pressure profiles through the tester are shown in **Exhibit 180**. The pressure loss across Bearing 3 increased in this test compared to the previous tests.

The following bearing examination showed that the balls in Bearing 1 were shiny with some light bronze colored bands. There were some areas with light scuffing on some balls. The balls in Bearing 2 were dull bronze colored. There were some light and dark colored areas giving a marbled appearance. The bearing appeared to be in good condition. The Bearing 3 balls were a dull dark brown. There were some dark bronze to black bands on some balls. One ball was sliding rather than rolling. One ball had a small surface spall. The balls in Bearing 4 were shiny with some light bronze bands. There were numerous surface scratches on the balls.

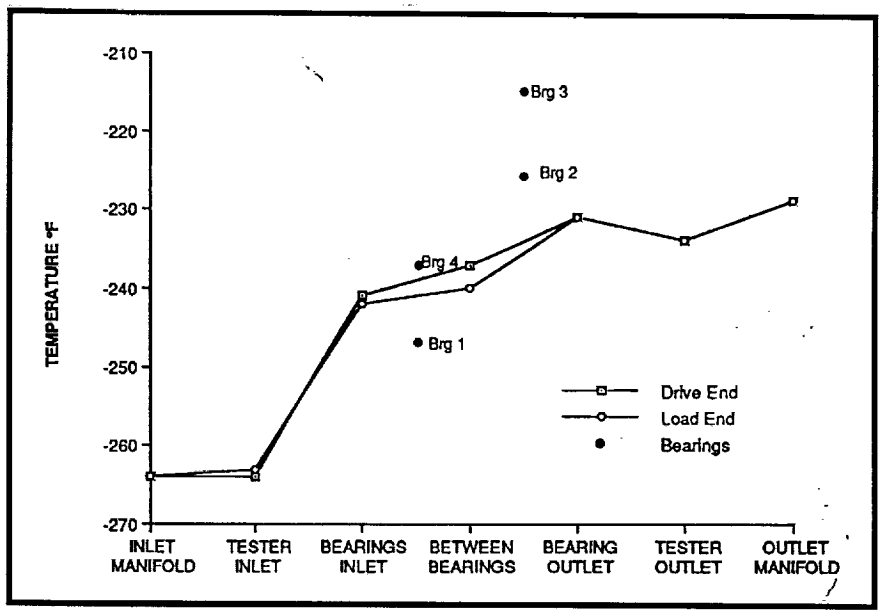

Exhibit 179 Temperature Profile for BSMT Test 3060701

Test 3060801. This was the seventh rotational test in this series. The test was planned to run with LOX tank depletion, and was successfully accomplished. The test ran for approximately 1,460 seconds at 30,000 RPM. The redlines on the bearings outer race temperatures were 135.8 K (-215°F). The run tank LOX temperature was the same for this test and the previous test (3060701). The temperature of the coolant entering the bearings was also approximately the same for this and the previous test. Although the previous test, 3060701, was cut due to Bearing 3 outer race temperature exceeding redline, it was decided to continue testing because of the apparent good condition of the bearings as seen through the borescope.

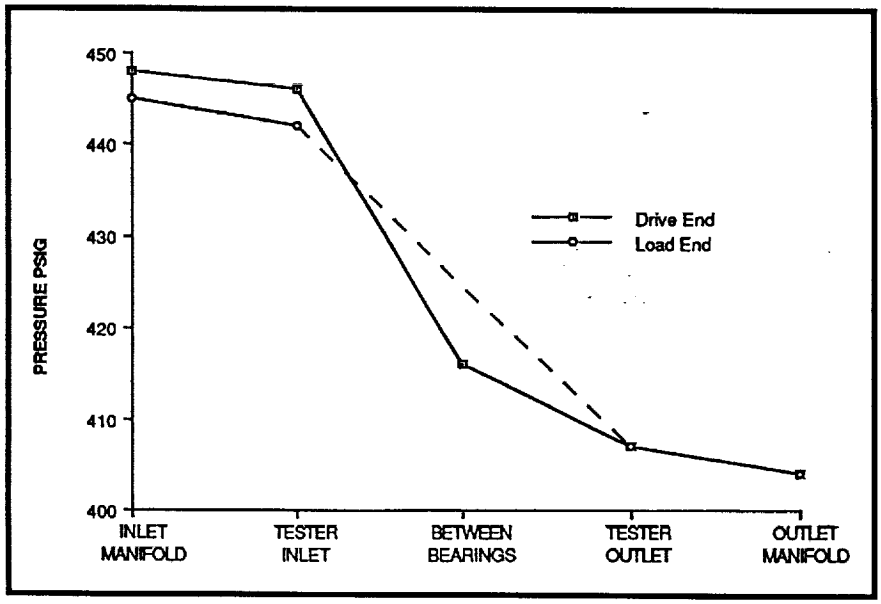

Exhibit 180 Pressure Profile for BSMT Test 3060701

Test parameters and selected data from this test are compared with those of previous tests in **Exhibits 181** and **182**. The outer race temperature of Bearing 4 (T1007) was significantly higher for this test compared to the other tests. Bearing 1 outer race temperature (T1004) did not follow this trend. Excessive wear in Bearing 3 may have been unloading Bearing 4 causing excessive ball sliding and heat generation. The anomaly was that the coolant temperature rise across Bearing 4 (T1024 - T1018) did not indicate higher heat generation. The temperature measurement between Bearings 3 and 4 (T1024) was believed to be biased low, or was influenced more in this test series by coolant bypass than in previous tests. Coolant flow around temperature probe TA1007 could have decreased the temperature in the cavity between the bearings and could have masked the temperature difference across the bearings.

The temperature profiles through the tester are shown in **Exhibit 183**. Included are the outer race temperatures. The temperature difference between the outer race temperature of Bearing 3 and inlet coolant temperature decreased about 3.3 K (6°F) compared to the previous test (3060701) which was cut because the temperatures of Bearing 3 outer race had exceeded redline. The pressure profiles through the tester are shown in **Exhibit 184**.

After examing the bearings through a borescope, the balls in Bearing 1 appeared to have light bronze areas. The balls were sliding

Test Parameter	TEST NUMBER		
	2121203	3030501	3060801
Shaft Speed (RPM)	30,029	30,177	29,902
Time at Speed (sec)	1,560	30	1,460
Subcooling	36	41	37
Flow Rate (lbs/sec)	6.4	6.45	6.4
Brg #4 Inlet Temp (°F) T1018	-242	-244.2	-241
Between Brgs 3 & 4 (°F) T1024	-237	-238.7	-239
Brg #3 Outlet Temp (°F) T1019	-230	-230.1	-230
Brg #1 Inlet Temp (°F) T1021	-240	-240.6	-241
Temp Between Bgr 1 & 2 (°F) T1023	-234	-234.2	-236
Brg 2 Outlet Temp (°F) T1022	-230	-229	-230
Tester Inlet Temp (°F) T1001 T1002	-264 -263	-264.3 -260.7	-266 -264
Tester Outlet Temp (°F) T1003	-234	-230.1	-234
Tester Inlet Pressure (psig) PA1001 PA1002	455 433	444.2 451.2	439 447
Tester Outlet Pressure (psig) PA1003	408	408.2	407
Pressure Between Brg 3 & 4 (psig) P1006	406	415.3	413
Horsepower	281	322	316
Torque (in-lbs)	12,956	14,789	14,662
Brg #1 O.R. Temp (°F) T1004 (TA1004)	-259 (-242)	-262.8 (-246.9)	-261 (-245)
Brg #2 O.R. Temp (°F) T1005 (TA1005)	-226 (-228)	-215 (-230.1)	-229 (-229)
Brg #3 O.R. Temp (°F) T1006 (TA1006)	-230 (-233)	-233 (-236.7)	-220 (-233)
Brg #4 O.R. Temp (°F) T1007 (TA1007)	-240 (-224)	-262.2 (-241.2)	-232 (-255)

920625JC1413

Exhibit 181 BSMT Test Conditions and Selected Data (Test 3060801)

PARAMETER	2121203	3030501	3060801
• Delta Temp Across Brg Pair (°F)			
T1022-T1021	10	11.6	11
T1019-T1018	12	14.1	11
• Delta Temp Across Brg 1 (°F)			
T1023-T1021	6	6.4	5
Brg 2			
T1022-T1023	4	5.2	6
Brg 3			
T1019-T1024	7	8.6	9
Brg 4			
T1024-T1018	5	5.5	2
• Brg Outer Race Temp - Fluid Inlet Temp (°F)			
Brg 1			
T1004-T1021	-2	-6.3	-4
Brg 2			
T1005-T1023	8	19.2	7
Brg 3			
T1006-T1024	7	5.7	19
Brg 4			
T1007-T1018	8	3.0	9
• Heat Generated (btu/sec) Across			
Brg 1	16.1	17.34	13.44
Brg 2	16.1	14.1	16.13
Brg 3	18.8	23.3	24.19
Brg 4	13.4	14.9	5.38
• Heat Generated Across			
Brg 1&2	26.9	31.4	29.57
Brg 3&4	32.2	38.2	29.57
• Inlet Vortex			
Load	64.5	64.2	67.2
Drive	56.4	44.7	61.82
• Pressure Drop (psi)			
Brg 1	N/A	N/A	N/A
Brg 2	N/A	N/A	N/A
Brg 3	-2	7.1	6
Brg 4	27	35.9	34
Brg 1&2	47	36	32
Brg 3&4	25	43	40
• Flow (lbs/sec) through Brg pair	6.4	6.4	6.4
• H.P.	281	322	316
• Torque (in-lbs)	12,956	14,789	14,662
• Shaft Speed (rpm)	30,029	30,177	29,902

Exhibit 182 BSMT Test Parameters Comparison LOX Tests (Test 3060801)

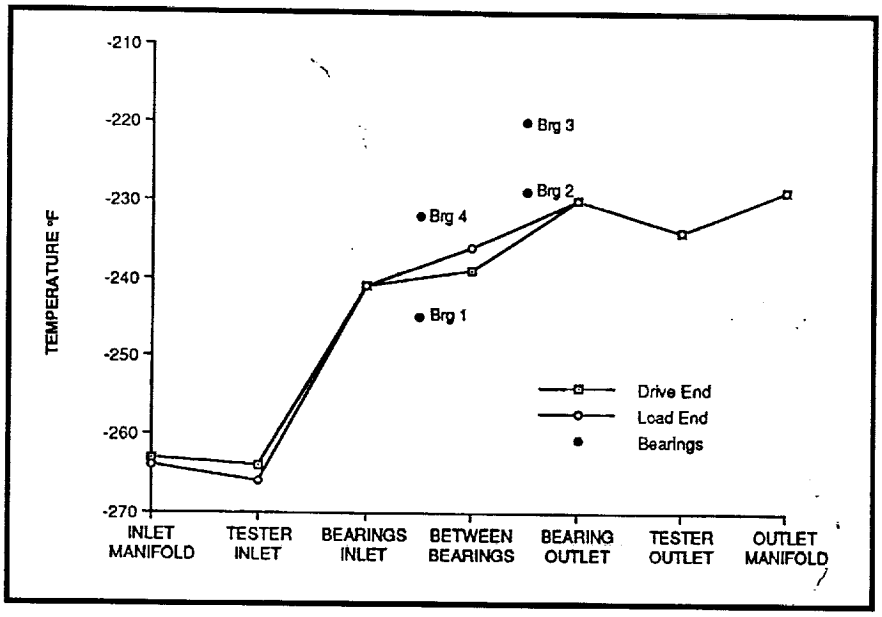

Exhibit 183 Temperature Profile for BSMT Test 3060801

rather than rolling, indicating ball wear or loss of preload. The bearing appeared to be in good condition. The balls in the Number 2 bearing had dark bronze areas and bands giving a marbled appearance. The bearing appeared to be in good condition. Some balls in the Number 3 bearing had surface spalls which appeared to be very shallow. Most of the balls slid when the shaft was rotated. The surface of the balls was relatively uniform in a dark bronze color. The Number 4 bearing balls had numerous deep scratches in their surfaces. The surfaces were shiny, and with the exception of the scratches, the bearing appeared to be in good condition.

Test 3060901. This was the eighth rotational test in this series. The test was planned for 360 seconds at 30,000 RPM, and was accomplished as planned. The test ran for approximately 375 seconds at 30,000 RPM. This test was run with a LOX tank temperature of about 100.8 K (-278°F). This was about 2.8 K (5°F) colder than the previous test value (Test 3060801). The bearing outer race temperature redlines were also lower from 135.8 (-215°F) to 134.7 K (-217°F). This was done to improve the thermal margin, and the response time for cutting the test in the event of a bearing failure. The bearing inlet coolant temperature was 1.7 K (3°F) lower for this test compared to the previous test (3060801).

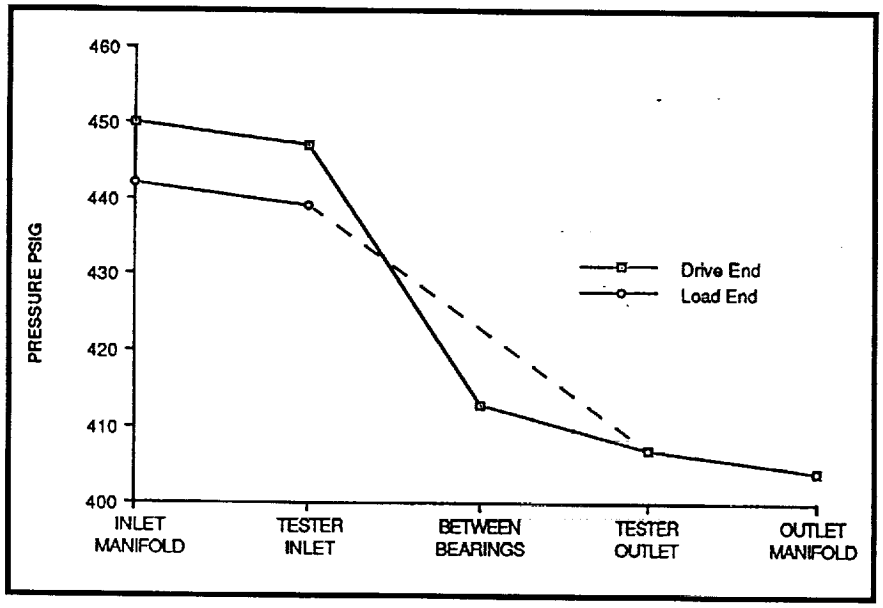

Exhibit 184 Pressure Profile for BSMT Test 3060801

Test parameters and selected data from this test are compared with those of previous tests in **Exhibit 185** and **186**. The outer race temperature of Bearing 4 (T1007) rose to the same level as the Bearing 3 temperature. The difference in the Bearing 4 temperature and the inlet cool-

Test Parameter	TEST NUMBER			
	2121203	3030501	3060801	3060901
Shaft Speed (RPM)	30,029	30,177	29,902	30,010
Time at Speed (sec)	1,560	30	1,460	375
Subcooling	36	41	37	40
Flow Rate (lbs/sec)	6.4	6.45	6.4	6.5
Brg #4 Inlet Temp (°F) T1018	-242	-244.2	-241	-244
Between Brgs 3 & 4 (°F) T1024	-237	-238.7	-239	-242
Brg #3 Outlet Temp (°F) T1019	-230	-230.1	-230	-233
Brg #1 Inlet Temp (°F) T1021	-240	-240.6	-241	-244
Temp Between Bgr 1 & 2 (°F) T1023	-234	-234.2	-238	-239
Brg 2 Outlet Temp (°F) T1022	-230	-229	-230	-233
Tester Inlet Temp (°F) T1001 T1002	-264 -263	-264.3 -260.7	-266 -264	-269 -268
Tester Outlet Temp (°F) T1003	-234	-230.1	-234	-236
Tester Inlet Pressure (psig) PA1001 PA1002	455 433	444.2 451.2	439 447	442 450
Tester Outlet Pressure (psig) PA1003	408	408.2	407	407
Pressure Between Brg 3 & 4 (psig) P1006	406	415.3	413	416
Horsepower	281	322	315	329
Torque (in-lbs)	12,956	14,789	14,662	15,212
Brg #1 O.R. Temp (°F) T1004 (TA1004)	-259 (-242)	-262.8 (-246.9)	-261 (-245)	-265 (-248)
Brg #2 O.R. Temp (°F) T1005 (TA1005)	-225 (-228)	-215 (-230.1)	-229 (-229)	-232 (-233)
Brg #3 O.R. Temp (°F) T1006 (TA1006)	-230 (-233)	-233 (-236.7)	-220 (-233)	-227 (-235)
Brg #4 O.R. Temp (°F) T1007 (TA1007)	-240 (-224)	-262.2 (-241.2)	-232 (-255)	-227 (-261)

Exhibit 185 BSMT Test Conditions and Selected Data (Test 3060901)

PARAMETER	2121203	3030501	3060801	3060901
• Delta Temp Across Brg Pair (°F)				
T1022-T1021	10	11.6	11	11
T1019-T1018	12	14.1	11	11
• Delta Temp Across Brg 1 (°F)				
T1023-T1021	6	6.4	5	5
Brg 2				
T1022-T1023	4	5.2	6	6
Brg 3				
T1019-T1024	7	8.6	9	9
Brg 4				
T1024-T1018	5	5.5	2	2
• Brg Outer Race Temp - Fluid Inlet Temp (°F)				
Brg 1				
T1004-T1021	-2	-6.3	-4	-4
Brg 2				
T1005-T1023	8	19.2	7	7
Brg 3				
T1006-T1024	7	5.7	19	15
Brg 4				
T1007-T1018	8	3.0	9	17
• Heat Generated (btu/sec) Across				
Brg 1	16.1	17.34	13.44	13.65
Brg 2	16.1	14.1	16.13	16.38
Brg 3	18.8	23.3	24.19	24.57
Brg 4	13.4	14.9	5.38	5.46
• Heat Generated Across				
Brg 1&2	26.9	31.4	29.57	30.03
Brg 3&4	32.2	38.2	29.57	30.03
• Inlet Vortex				
Load	64.5	64.2	67.2	68.25
Drive	56.4	44.7	61.82	65.52
• Pressure Drop (psi)				
Brg 1	N/A	N/A	N/A	N/A
Brg 2	N/A	N/A	N/A	N/A
Brg 3	-2	7.1	6	9
Brg 4	27	35.9	34	34
Brg 1&2	47	36	32	35
Brg 3&4	25	43	40	43
• Flow (lbs/sec) through Brg pair	6.4	6.4	6.4	6.5
• H.P.	281	322	316	329
• Torque (in-lbs)	12,956	14,789	14,662	15,212
• Shaft Speed (rpm)	30,029	30,177	29,902	30,010

Exhibit 186 BSMT Test Parameters Comparison LOX Tests (Test 3060901)

ant temperature was 1.1 K (2°F) higher than the comparable value for Bearing 3. This could have been caused by additional loss of preload, in the outboard bearing, causing ball skidding and/or allowing the outer race to rotate against the thermocouple. This condition appeared to grow as test time was accumulated. The temperature difference measured across the bearings was the same for this test and the previous test (3060801).

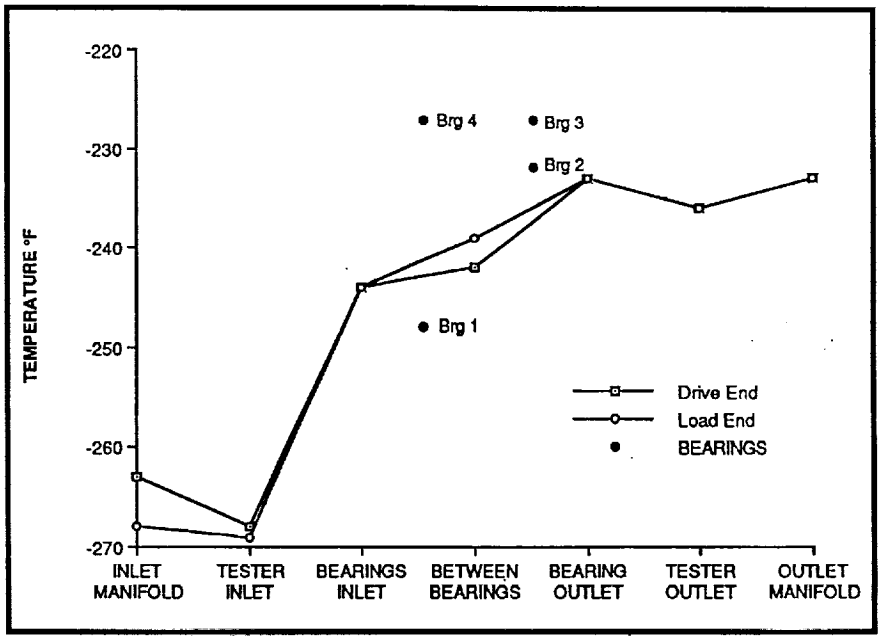

Exhibit 187 Temperature Profile for BSMT Test 3060901

The temperature profiles through the tester are shown in **Exhibit 187**. Included are the outer race temperatures. As shown, there was a large difference in the Bearing 4 and Bearing 3 outer race temperatures. The pressure profiles through the tester are shown in **Exhibit 188**.

The following bearing examination showed that the balls in Bearing 1 had grainy surfaces. Some balls had dark brown bands. Most of the balls would slide rather than roll when the shaft was rotated. The balls in the Number 2 bearing had light and dark areas giving a marbled appearance. There were dark bronze bands on many of the balls, and some balls had light specks in their surfaces. Most of the balls would slide with shaft rotation. The balls in Bearing 3 had dull surfaces and some of the balls had dark colored bands. One ball had a large shallow surface spall. Most balls would slide when the shaft was rotated. The Bearing 4 balls were shiny. They had numerous surface scratches and dents. All the balls appeared to be rolling when the shaft was rotated.

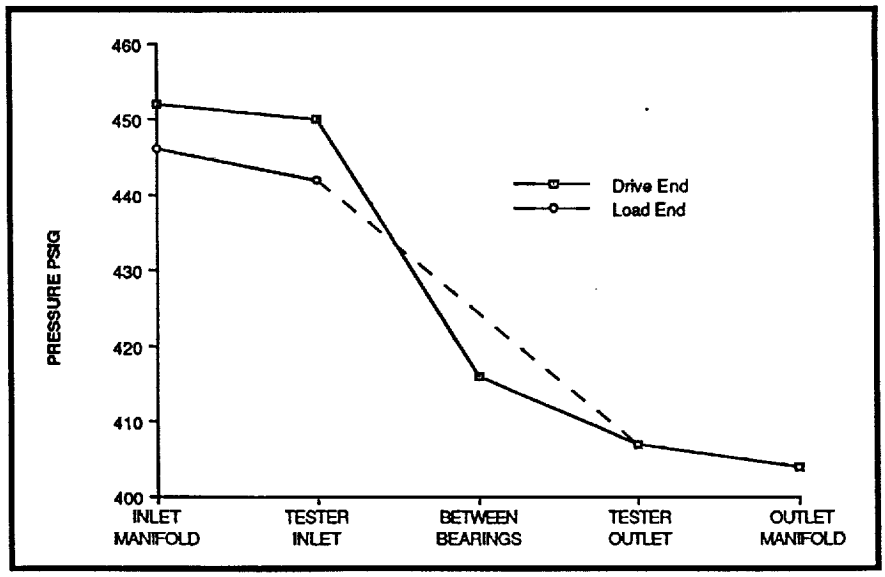

Exhibit 188 Pressure Profile for BSMT Test 3060901

Due to the observed condition of the bearings, it was decided to terminate testing of this build. A total of approximately 51 minutes of test time was accumulated at a speed of approximately 30,000 RPM.

5.2 Radial Loading of BSMT Bearings

The BSMT has the capability to load the test bearings radially and axially. In prior testing, the axial load was produced by the fluid pressure differential across the carriers, and no radial load was applied. Using the radial load actuator in the BSMT, to radially load the test bearings was considered. The combined radial and axial load could then be used to stress the test bearings to match levels predicted for the HPOTP pump end bearings, and Si_3N_4 rolling elements. It was then that we planned to run 57 mm Si3N4 ball bearings in the BSMT, to the stress levels predicted for the pump end bearings with Si_3N_4 balls, prior to testing Si_3N_4 rolling element bearings in the SSME test bed engine for ultimate use in the flight pumps.

The maximum stress level predicted for the Number 2 pump end bearing was about 3,500 MPa (507.6 ksi). This stress level was produced by axial preload and radially applied loads. The maximum stress level predicted for the 57 mm Si_3N_4 ball bearings in the BSMT with a nominal pressure induced axial reaction of 8,896 N (2,000 lbs.) was about 3,100 MPa (450 ksi). The required stress level in the BSMT inboard bearings could be achieved by increasing the axial load; all the balls were equally stressed to the highest level. This significantly increased the probability of fatigue failure; compared to a bearing subjected to higher radial load where a ball experiences the maximum stress only once during every approximately 2.3 shaft revolutions. Because of the potential of rapid bearing degradation with a steady high axial load, the method for producing the desired stress level with radial loading was also investigated.

The pressure differential across the BSMT carriers loaded the inboard bearings, and since the carriers were displaced toward the inboard bearings, the outboard bearing preload was reduced. Shown in **Exhibit 189** is the bearing reactions for the inboard (Bearings 2 and 3) and outboard bearings (1 and 4) as a function of carrier loads. This relationship was also dependent on bearing stiffness. The bearing deflection curve, used in estimating bearing reactions, is shown in **Exhibit 190**. The carrier load to produce a reaction of 8,896 N (2,000 lbs.) in Bearings 2 and 3 was about 8,229 N (1,850 lbs.). The preload remaining in the outboard bearings was about 667 N (150 lbs.). Consequently, the outboard bearings were very lightly preloaded when the tester was operating at a nominal speed of 30,000 RPM. As the bearings wore, this preload was reduced to zero. Thus, the preloading of the bearings needed to be assessed to determine a spring rate that would ensure the outboard bearings still had operating preload at full test speed through the duration of testing.

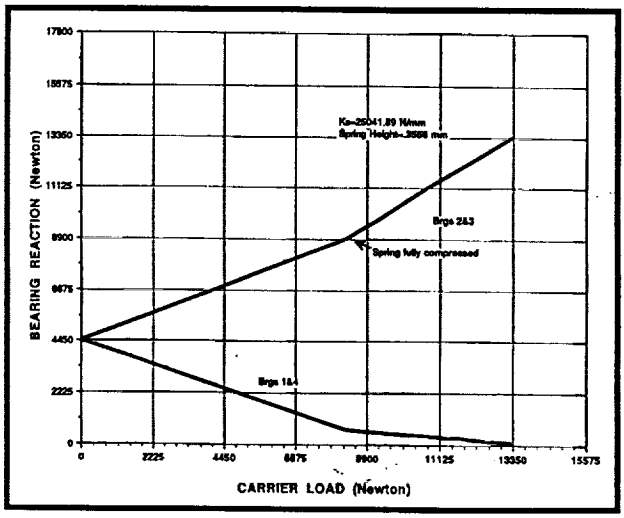

Exhibit 189 Bearing Reaction Versus Carrier Load

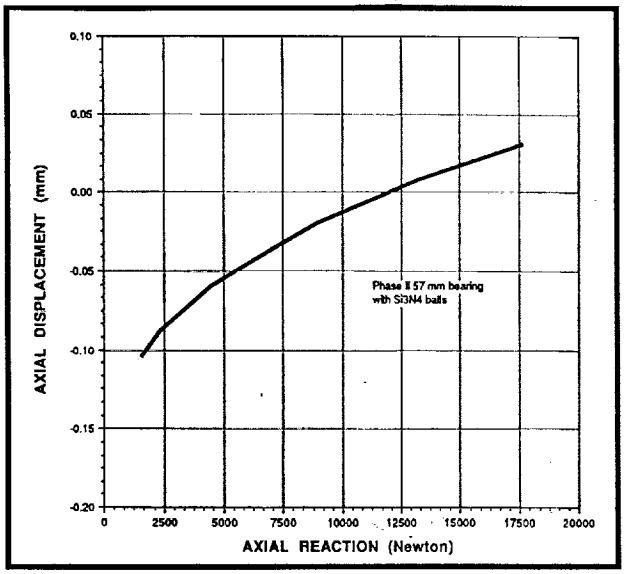

Exhibit 190 BSMT Axial Bearing Stiffness

It was determined from the thermomechanical model that a radial reaction of 5.949 N (1,337 lbs.) with 8,900 N (2,000 lbs.) was required on the bearing to produce a maximum contact stress of 3,512 MPa (5,092 kpsi). The tester thermomecha-nical model was run with axial and radial reactions shown in **Exhibit191**. In this case, Bearing 1 was preloaded about 1,344 N (302 lbs.). As shown, the ball excursion was very close to the pocket clearance for the Number 1 bearing.

There were six unloaded balls in the Bearing 1 ball complement. These runs were made assuming no outer race misalignment or tilt. Outer race tilt in the direction of inner race rotation, due to the radial load, caused more balls to become loaded and increased ball excursion. Although the predicted stresses, heat generation and component temperatures were not excessive, a dynamic simulation of these conditions, using the ADORE software, was needed to determine the effects of ball skid, and cage loads on heat generation and cage stresses.

An alternate approach to simulating the desired stress levels without radial loads and excessive stress cycles was to "pulse" the axial load to produce the desired load over a short period of time. Again, the preload spring rates used would have to ensure that the outboard bearings would have some minimum preload during this high axial load pulse.

BSMT Radial Loading. An analysis was done to investigate the merits of applying a radial load to test bearings in the Bearing Seal and Materials Tester (BSMT). The tester design had

PARAMETER	BEARINGS 1&4	BEARINGS 2&3
Radial Load N (lbs)	5821 (1309)	5949 (1337)
Axial Load N (lbs)	1344 (300)	8670 (1949)
Max I.R. Stress MPa (ksi)	3233 (469)	3512 (509)
Max O.R. Stress MPa (ksi)	2638 (382)	2851 (413)
Cage Pocket Clearance MM (in)	.635 (.025)	.635 (.025)
Ball Excursion MM (in)	.634 (.0249)	.1175 (.004626)
Heat Generated watts/ball	I.R 36 O.R. 34	I.R 236.7 O.R. 132
Component Temperature K (°F)	I.R 128 (-229) O.R. 128 (-229) Ball 132 (-222)	I.R 165 (-162) O.R. 132 (-222) Ball 193 (-112)
Number of Unloaded balls	6	0

Exhibit 191 BSMT Bearing Operating Characteristics Under Radial and Axial Loads

the capability to radially load the test bearings. However, this capability had not been used in prior testing because the pressure induced axial load unloaded the outboard bearings when they were preloaded to flight values (approximately 1,000 lbs preload), and because the operating characteristics of the bearings in the BSMT with a radial load had not been investigated in LN_2.

Analysis of the SSME HPOTP pump end bearings using Si_3N_4 rolling elements and pump design loads, gave a maximum Hertz stress of 3.5 GPa (507 Ksi) in the contacts. It was desirable to reproduce these stress levels in Si_3N_4 ball bearings in the BSMT to verify bearing operation at these stress levels. There were two loading options for producing the desired stress levels in the test bearings. One was to increase the axial load to about 13,344 newtons (3,000 lbs), and the other was to radially load the test bearings. However, high axial load increased the number of stress cycles, since all balls were equally loaded, compared to the combination of axial and radial loads.

The BMST design was unique in that bearing loads were induced by applying loads to the carriers rather than the shaft. Coolant flow through the tester produced an axial load on the carriers normally referred to as Pressure Area (PA) loads. The magnitude of the PA loads were somewhat uncertain due to the high rotation of the fluid upstream and downstream of the carriers. This load was estimated to be approximately 8,000 newtons (2,000 lbs) for 30,000 RPM and LOX coolant flow of 2.9 Kg/sec (6.5 lbs/sec).

Axial forces on the BSMT carrier loaded the inboard bearings and unloaded the outboard bearings. This design characteristic is illustrated in **Exhibit 192**. In the equilibrium position, the bearing reactions were equal, and equal to the preload. Displacement of the carrier by the PA load increased the Bearing 2 reaction and reduced the reaction at Bearing 1. The magnitude of the reactions depended on PA loads, preload spring characteristics, initial preload, and bearing load/deflection characteristics. **Exhibit 193** shows bearing reactions as a function of carrier loads for two initial preloads and the spring constant of 25,000 N/mm (143,000 lb/in). **Exhibit 194** provided similar information for a spring constant of 21,627 N/mm (123,500 lbs/in).

Exhibit 193 shows that the outboard bearings (1 and 4) had an axial reaction of about 445 N (100 lbs) when the carrier (PA) load was 8,900 N (2,000 lbs) and the initial preload was 4,448 N (1,000 lbs). Increasing the preload to 5,782 N (1,300 lbs) increased the outboard bearing reaction to about 2,891 N (650 lbs). The increased preload also increased the inboard bearings reac-

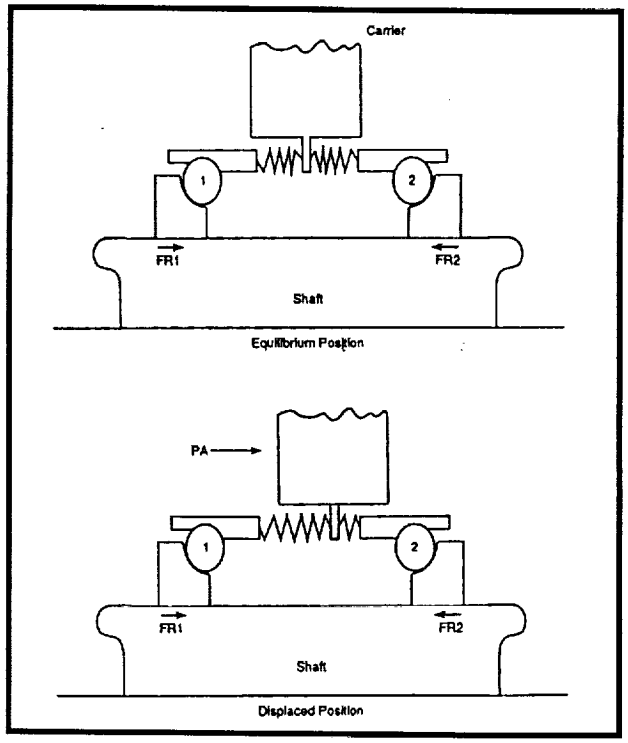

Exhibit 192 Bearing Reactions Versus Carrier Loads

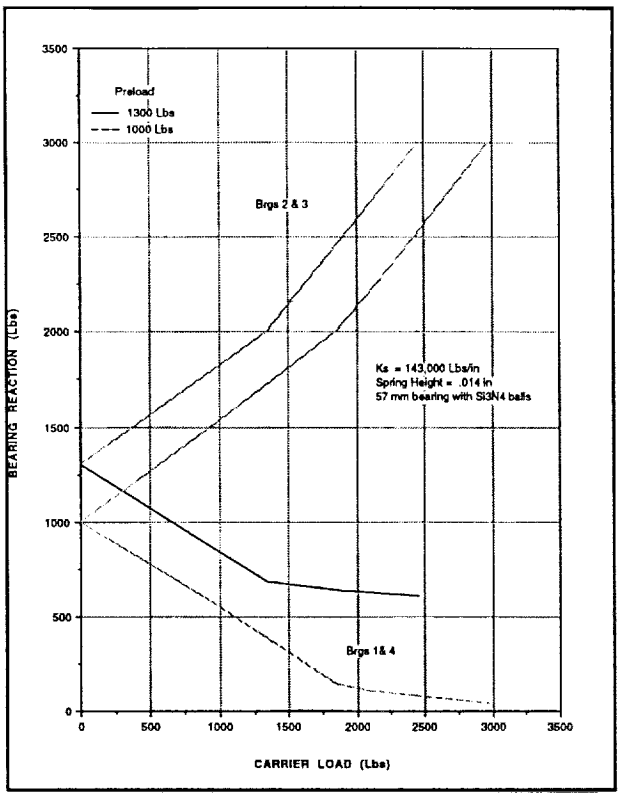

Exhibit 193 Bearing Reactions Versus Carrier (PA) Load

tion. A preload of 4,448 N (1,000 lbs) and a PA load of 8,900 N (2,000 lbs) produced a reaction of about 9,341 N (2,100 lbs) for the inboard bearings. Increasing the preload to 5,782 N (1,300 lbs) increased this reaction to 11,565 N (2,600 lbs).

Exhibit 194 shows the effects of reducing the preload spring constant on bearing reactions. The "softer" spring increased the bearings reactions at higher PA loading. **Exhibit 195** summarizes these comparisons at a specific carrier (PA) load of 8,900 N (2,000 lbs). Increased preload increased the axial reactions (preload) of the outboard bearings. The same trend could be accomplished with a softer spring. Increasing the preload and reducing the spring constant however, did reduce the remaining spring gap. The reduction in spring gap as a function of preload and spring constant is shown in **Exhibit 196**. Preloading the soft spring to 5,782 N (1,300 lbs) lefts an operating gap of about 0.0889 mm (0.0035 in). This reduced the margin for internal clearance reduction caused by internal dimensional changes in the bearings due to thermal effects.

The effects of ball or race wear on the initial preload and bearing reactions with the applied PA load were also investigated. Ball and/or raceway wear increased internal clearances, changed curvatures, and contact angles. This changed the bearing "stickout" and reduced the preload. Two cases of ball wear were investigated; 0.02154 mm (0.001 in) and 0.0508 mm (0.002 in). The loss of preload was determined by using the "SHABERTH" code to generate load deflection curves for the nominal ball size and the two conditions of ball wear. The curve for each wear case was displaced to account for the initial change in stickout caused by curvature

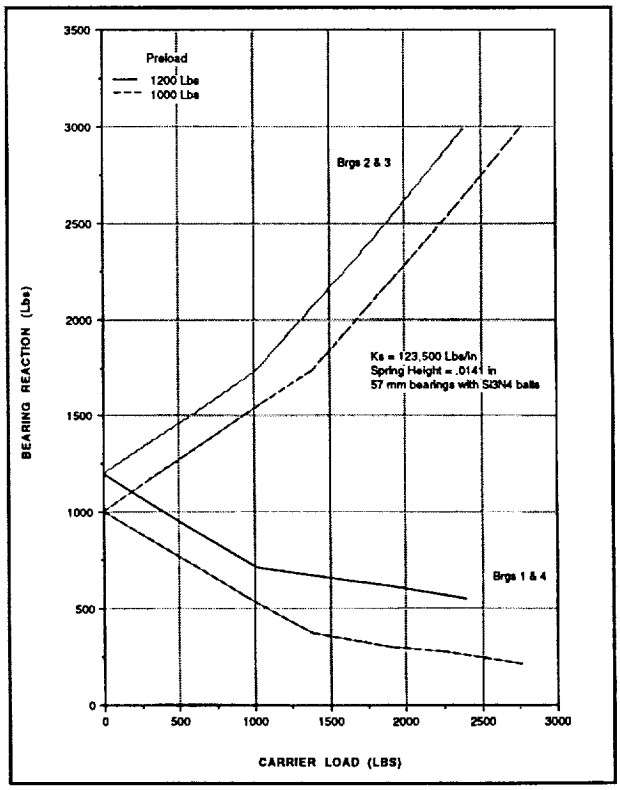

Exhibit 194 Bearing Reactions Versus Carrier (PA) Load

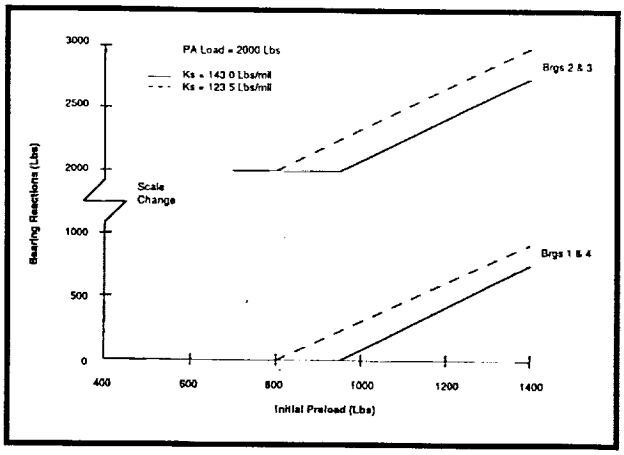

Exhibit 195 Bearing Reactions Versus Initial Preload with a PA Load of 2000 Lbs

and contact angle changes resulting from ball wear. The reduction in preload was determined by superimposing the spring curve on the bearing curves as show in **Exhibit 197**. The results are summarized in **Exhibit 198**. As an example, if the initial preload was 5,782 N (1,300 lbs) and ball wear was 0.0254 mm (0.001 in), and the spring constant was 25,042 N/mm (143,000 lbs/in) the preload would be reduced to about 4,448 N (1,000 lbs). Referring to **Exhibit 199**, for 4,448 N (1,000 lbs) preload spring constant of 25,042 N/mm (143,000 lbs/in), the outboard bearing reaction (1 and 4) would be about 444.8 N (100 lbs).

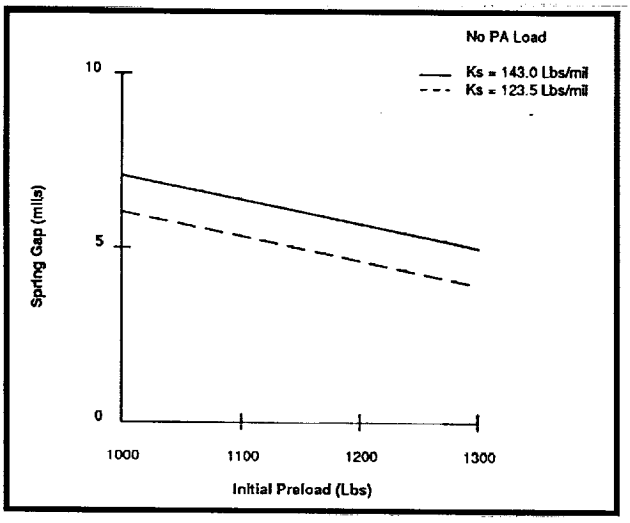

Exhibit 196 Spring Gap Versus Initial Preload

Based on this assessment, providing a preload of 5,782 N (1,300 lbs) with a spring constant of 25,042 N/mm (143,000 lbs/in), appeared to be the best compromise. The softer spring preloaded to 5,337 N (1,200 lbs) produced similar results, but had slightly lower gap height. Also, the 25,042 N/mm (143,000 lbs/in) spring was readily available; whereas acquiring a different spring would have been a problem.

5.3 Radial Load Analysis for Si_3N_4 Ball Bearings in the BSMT

Prior to testing Si_3N_4 ball bearings in the SSME Test Bed Engine LOX turbopump, bearings with Si_3N_4 balls were subjected to the same stress levels in the BSMT as expected in the engine

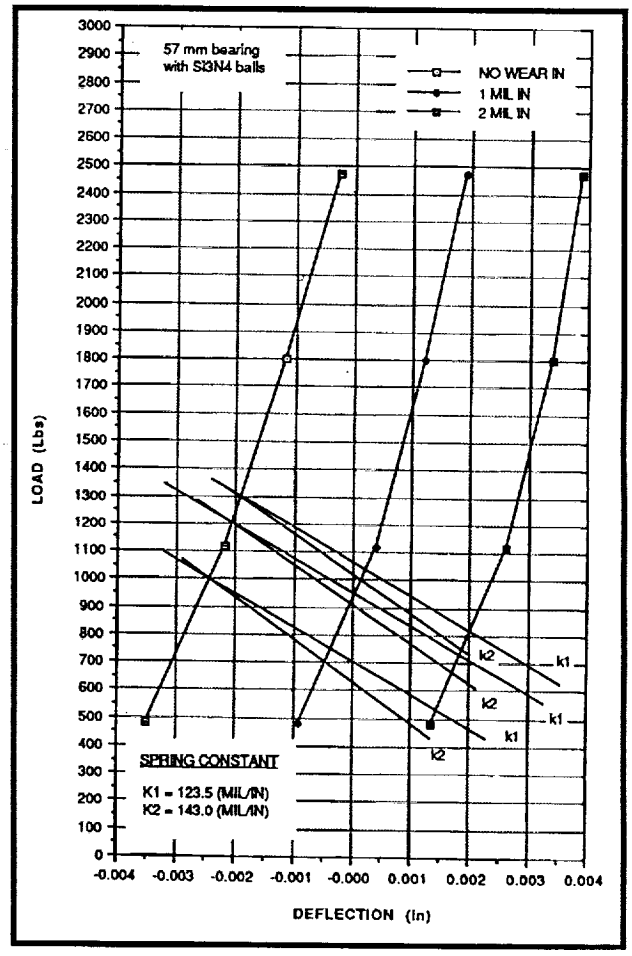

Exhibit 197 Bearing Axial Load Deflection

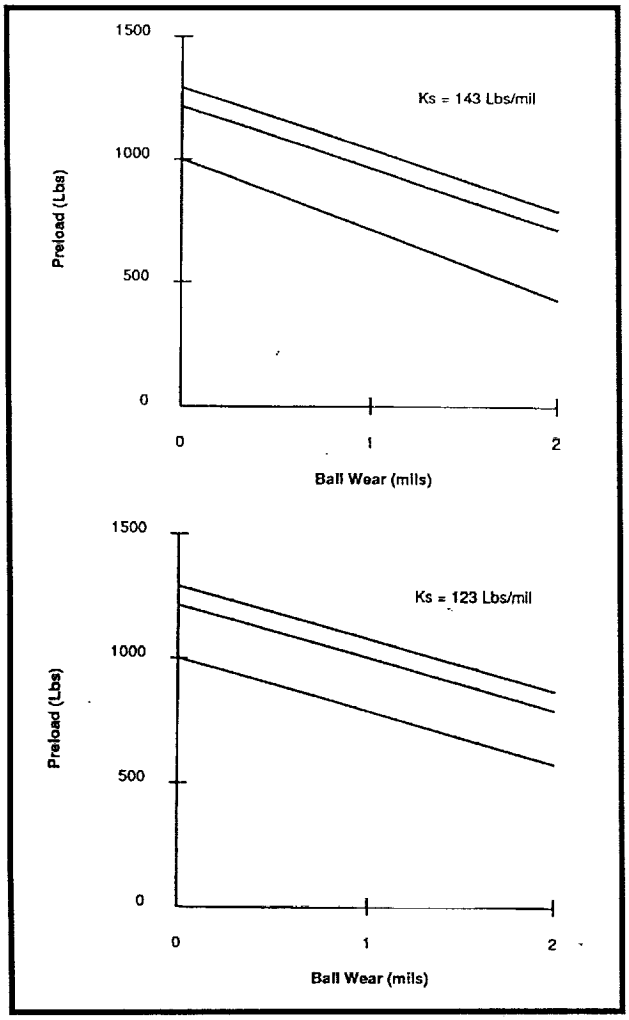

Exhibit 198 Preload Versus Ball Wear

turbopump. An analysis of the 45mm pump end bearings was done to establish stresses and other operating characteristics. The bearing model included Si_3N_4 rolling elements, and the shaft was loaded to produce representative flight bearing reaction loads. The results are provided in **Exhibit 200**. A radial load was required to produce similar stress levels in the BSMT bearings while maintaining sufficient preload on all the bearings. These bearings were 57mm phase II turbine end configuration with Si_3N_4 balls. This was necessary because the pressure load across the tester did not provide sufficient axial load to produce the required stress level in the ball/race contacts. The stresses and the operating characteristics for the desired load configuration are also shown in **Exhibit 200**. These loads produced a contact stress of 3.5 GPa (507 Kpsi) compared to the stress level of 3.3 GPa (476 Kpsi) estimated for the 45mm bearing in the turbopump.

Alternate tester load cases without radial load are shown in **Exhibit 201.** The only case producing stress levels, comparable to those in the pump, was the one with a 13344N (3000 lbs) axial load. This case however, produced a relatively high ball average temperature which reduced the thermal margin of the bearing.

The BSMT thermal and mechanical model results compared favorably with test results as shown in **Exhibit 202**. This provided reasonable confidence in predicting operating characteristics for loading conditions different from previous tester loads. Coolant temperature differences and outer race temperatures were mea-

No ball wear, 5782N (1300 Lb Preload), 8896 (2000Lb) PA Load
57 mm bearing SI3N4 balls

Bearings	Axial Load		Radial Load		Max Contact Stress		Ball Excursion		Ball Temperature		Balls Unloaded
	N	(Lbs)	N	(Lbs)	GPa	(ksi)	mm	(in)	K	°F	
184	2891	(650)	3114	(700)	2.7	(386)	.541	(.0213)	135	(-215)	0
283	11,565	(2600)	3114	(700)	3.5	(507)	~0		258	5.6	0

No ball wear, 4448N (1000 Lb Preload), 8896 (2000Lb) PA Load
57 mm bearing SI3N4 balls

Bearings	Axial Load		Radial Load		Max Contact Stress		Ball Excursion		Ball Temperature		Balls Unloaded
	N	(Lbs)	N	(Lbs)	GPa	(ksi)	mm	(in)	K	°F	
184	445	(100)	5338	(1200)	3.2	(463)	.262	(.0103)	130	(-225)	0
283	9,340	(2100)	5338	(1200)	3.5	(507)	~0		204	-92	0

Exhibit 199 Bearing Operating Characteristics

sured during test operation. These parameters are shown in **Exhibit 203** for several tester load conditions. The high axial load case produced an estimated outer race temperature of 132K (-222°F) which was within 1.0K (2°F) of the previous test redline value of 133K (-220°F). The redline temperature could have been increased, but the margin between the outer race temperature and the coolant saturation temperature would have decreased. The best approach for producing contact stress levels in the tester bearings comparable to stress levels expected in the turbopump, without significant increases in component temperature, was to increase preload to 5782N (1300 lbs) and apply a radial load on the tester of 6227N (1400 lbs). This produced an axial load of 11,565 N (2600 lbs) on the inboard bearings and a radial load of 3114N (700 lbs) on each bearing. For these conditions the outer race temperature was estimated to increase 2.1K (4°F) over the previously tested conditions.

PARAMETER	PHASE II 45mm PUMP END BEARINGS Si_3N_4 BALLS				PHASE II 57mm TURBINE END (tester bearings) Si_3N_4 Balls			
	Brg 1		Brg 2		Brg 1 & 4		Brg 2 & 3	
Axial Reaction N (Lbs)	2887	(650)	2887	(650)	2891	(650)	11,565	(2600)
Radial Reaction N (Lbs)	2481	(558)	4105	(923)	3114	(700)	3114	(700)
Max Hertz Stress MPA (K Psi)	2799	(406)	3283	(476)	2700	(386)	3500	(507)
Average Heat Generation Watts/Balls	I.R	O.R	I.R	O.R	I.R	O.R	I.R	O.R
	78	33	83	50	75	29	324	184
Average ball temp K (°F)	182	(-132)	165	(-163)	151	(-187)	258	(5.6)
Average O.R. temp K (°F)	137	(-213)	138	(-212)	125	(-235)	137	(-213)
Average J.RT. temp K (°F)	144	(-201)	145	(-199)	129	(-227)	188	(-121)

- Si_3N_4 Rolling Elements - LOX coolant.
- No Ball Wear
- 5782 N (1300 lb) Preload for Tester Bearings

Exhibit 200 45mm Pump End Bearings and 57mm Tester Bearings with Si3N4 Balls

Since the previous BSMT tests did not include the application of radial loads, initial tests with radial loads were planned to be run in LN_2 rather than LOX. The tester model was run with various radial reactions and a fixed axial reaction to estimate temperature, frictional torque, and contact stresses. The results are shown in **Exhibits 204, 205,** and **206**. It was noted that the torque was the contact friction torque and did not include the torque required to rotate the coolant fluid. Since the fluid torque was relatively independent of radial

PARAMETER	Brg 1 & 4		Brg 2 & 3		Brg 1 & 4		Brg 2 & 3		Brg 1 & 4		Brg 2 & 3	
Axial Reaction N (Lbs)	1067	(240)	8896	(2000)	2891	(650)	11565	(2600)	2670	(600)	13344	(3000)
Radial Reaction N (Lbs)	0		0		0		0		0		0	
Max Hertz Stress MPa (KPsi)	1542	(223.6)	3030	(439.3)	2160	(313.2)	3278	(475.3)	2160	(313)	3429	(497.2)
Avg Heat Generation Watts/Ball	I.R.	O.R.	I.R.	O.R.	I.R.	O.R.	I.R.	O.R.	I.R.	O.R.	I.R.	O.R.
	26	7	240	120	74	25	324	180	74	25	385	230
Avg Ball Temp K (°F)	143	(-203)	188	(-121)	150	(-189)	258	(5)	150	(-189)	305	(89)
Avg O.R. Temp K (°F)	124	(-236)	132	(-222)	125	(-235)	137	(-213)	125	(-235)	145	(-199)
Avg I.R. Temp K (°F)	127	(-232)	165	(-163)	129	(-227)	188	(-121)	129	(-227)	224	(-56)
Preload N (Lbs)	4448		(1000)		5026		(1300)		5026		(1300)	

- Si_3N_4 Rolling Elements - LOX coolant
- No Ball wear

Exhibit 201 Axial Load Cases for 57mm Bearings

	Coolant DT K (°F)	O.R Temp K (°F)
Test	5.3 (9.5)	126 (-233)
Model	4.7 (8.4)	125.5 (-234.1)

Exhibit 202 BSMT Model and Test Results

Tester Load Condition N (Lbs)	Coolant DT K (°F)	O.R. temp K (°F)	Max track tempK(°F)
Axial load 11,565 (2600) Radial load 3114 (700)	5 (9)	129.3 (-227.3)	425 (305)
Axial load 11,565 (2600) Radial load (0)	5 (9)	129.2 (-227.5)	421 (298)
Axial load 13,344 (3000) Radial load (0)	5.3 (9.5)	132 (-221.6)	519 (475)

Exhibit 203 Model Results for Alternalte Tester Loads

loaded to produce contract stresses comparable to those expected in the flight HPOTP pump end bearings. The bearings were preloaded to 5780 N (1300 lbs), rather than the 4450 N (1000 lbs). preload of prior tests. This was done to increase the outboard bearing's preload and reduce ball unloading when the radial load was applied. Approximately 2 hours and 7 minutes were accumulated in LOX at a test speed of 30,000 RPM.

load, the changes in friction torque were representative of torque changes with radial load. Torque versus radial load is shown in **Exhibit 205**. The contact stresses in LN_2 and LOX were very close. The difference was attributed to the difference in bearing component temperatures which affected the bearing operating internal clearance.

5.4 Unit 2, Build 14 Test of Si_3N_4 Ball Bearings with Axial and Radial Loads

Tests 2140801 - 2141401 Summary. The following section summarized six rotational tests that were completed. Five tests were run in LOX at a test speed of 30,000 RPM, and one was run in LN_2. The LN_2 test was a transient load test to simulate the transient levels during start and shut down of the flight LOX turbopump. This was done to demonstrate the capability of the Si_3N_4 ball bearings to accommodate high transient loads. A detailed report of the first six test was compiled under a separate test report. For completeness all tests in the Unit 2 Build 14 series are listed in **Exhibit 207**.

The purpose of this test series was to demonstrate the operation of the Phase II SSME HPOTP 57mm turbine end bearings, with Si_3N_4 balls,

Testing at steady runs of 30,000 RPM were stopped because the outer race temperature of

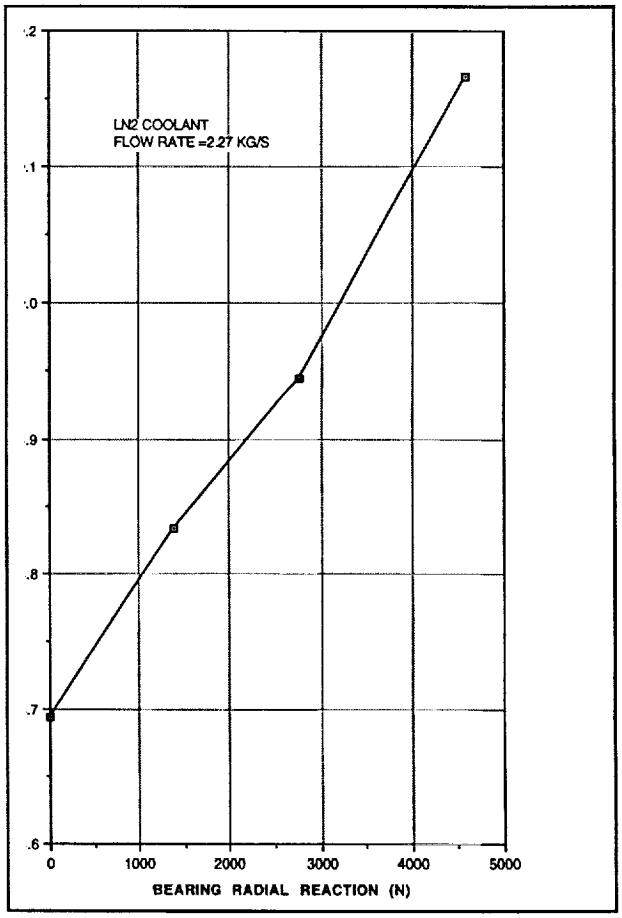

Exhibit 204 BSMT Outer Race Back Surface Temperature

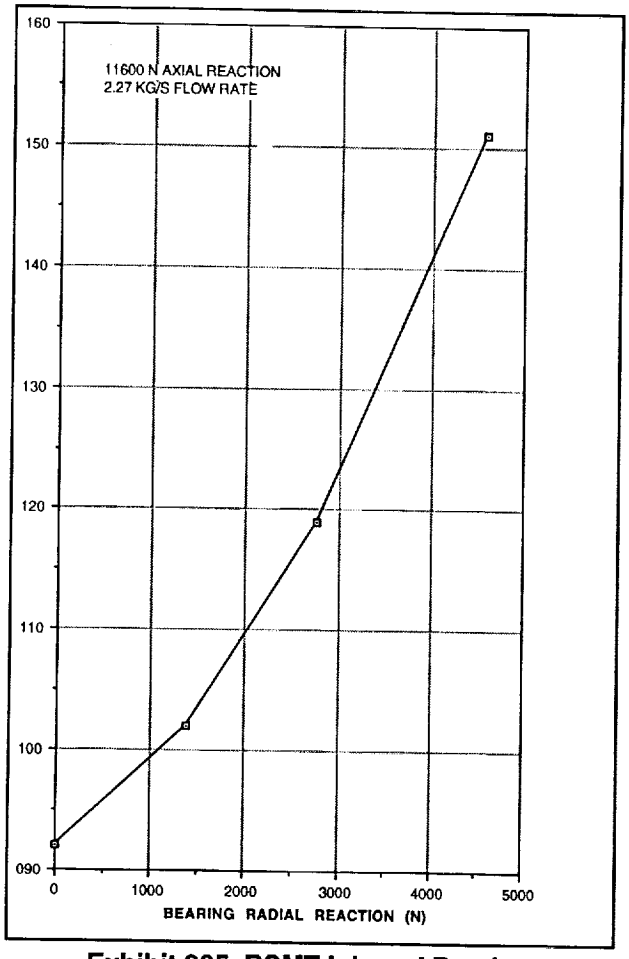

Exhibit 205 BSMT Inboard Bearing Torque with LN_2 Coolant

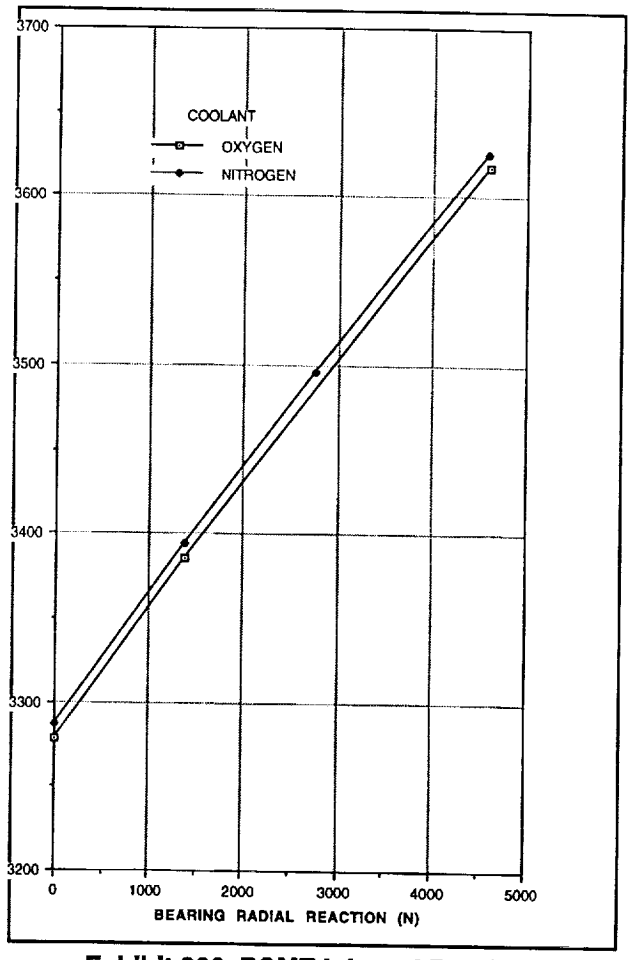

Exhibit 206 BSMT Inboard Bearing Race Contact Stress

Bearing 2 cut the ninth test after about 15 minutes at 30,000 RPM, and the inboard bearing's balls were severely discolored, although no spalls were observed through the borescope. Since an additional test objective was to perform a high load transient test, it was decided to terminate the steady speed tests before further bearing deterioration occurred. This allowed the high load transient test to be performed on bearings in relatively good condition (no spalled balls).

Test 2140801. This was the seventh rotational test in this series, and the sixth in LOX with an applied radial load. The axial load on the inboard bearings was estimated to be 10,230 N (2300 lbs), and the axial load on the outboard bearings was estimated to be 2800 N (630 lbs). These loads were estimated without accounting for ball and race wear. The radial load on each bearing was about 3030 N (681 lbs). The test ran until the LOX tank was depleted, which was about 21 minutes.

Test parameters and selected data from this test were compared with those of previous tests in this series, and a previous test on Si_3N_4 ball bearings with no radial load in LOX (test 2120501). These comparisons are shown in **Exhibits 208** and **209**. Torque and horsepower were higher for the current test. However, this was not reflected in the temperature differences across the bearings.

Test Speed (RPM)	Test Fluid	Estimated Loads Inboard Brg Axial (N)	Axial (lbs.)	Radial (N)	Radial (lbs.)	Time @ Speed (sec.)	Test No.
15,500	LN2	6230	1400	3260	733	155	2140202
25,000	LN2	7560	1700	3290	740	100	2140202
28,000	LN2	8230	1850	3670	825	67	2140301
30,000	LN2	8560	1925	3670	825	85	2140301
30,400	LOX	10,500	2360	3110	700	140	2140401
30,049	LOX	10,140	2280	3050	685	315	2140501
29,947	LOX	10,230	2300	3040	684	643	2140602
30,003	LOX	10,740	2415	3025	680	730	2140701
29,972	LOX	10,230	2300	3025	680	1280	2140801
30,000	LOX	10,140	2280	3010	677	1120	2140901
30,200	LOX	10,590	2380	3000	674	1350	2141001
30,200	LOX	10,410	2340	2990	672	1160	2141101
30,031	LOX	10,410	2340	3025	680	880	2141201
15,000	LN2	26,690*	6000*	710	160	95	2141401
30,000	LN2	8900	2000	3290	740	225	2141401

*(For one Sec)

Exhibit 207 Unit 2 Build 14 Test Summary

Temperature profiles through the tester are shown in **Exhibit 210**. Included are the outer race temperatures. The load end tester inlet temperature measurement (T 1001) was lost during the test. The value shown was estimated from previous test data. The pressure profiles through the tester are shown in **Exhibit 211**.

Following the rotational test the bearings were examined through a borescope. The Number 1 bearing balls were gray and shiny. There was some darker gray patches and scuff marks on the surfaces. One ball had parallel white streaks on its surface. The balls in Bearing 2 were dull metallic with some dark patches. There were some lighter areas and lighter gray bands. The balls in the Number 3 bearing were not as dull as those in Number 2. There were some dark patches and light gray streaks. The balls in the Number 4 bearing were gray and shiny. There were some light gray patches and streaks, and some scuff marks on the surfaces.

Test 2140901. This was the eighth rotational test in this series and the seventh in LOX with an applied radial load. The axial

Test Parameter	TEST NUMBER 2120501	2140501	2140602	2140701	2140801
Shaft Speed (RPM)	29,954	30,049	29,947	30,003	29972
Time at Speed (sec)	300	315	643	730	1280
Subcooling	37	39	40	40	40
Flow Rate (lbs/sec)	6.4	6.4	6.4	6.4	6.4
Brg #4 Inlet Temp (°F) T1016	-243	-244	-241	-243	-243
Between Brgs 3 & 4 (°F) T1024	-237	-240	-238	-239	-238
Brg #3 Outlet Temp (°F) T1019	-232	-233	-232	-232	-232
Brg #1 Inlet Temp (°F) T1021	-241	-243	-240	-242	-242
Temp Between Bgr 1 & 2 (°F) T1023	-236	-241	-237	-240	-240
Brg 2 Outlet Temp (°F) T1022	-232	-233	-231	-232	-233
Tester Inlet Temp (°F) T1001 T1002	-265 -258	-268 -267	-266 -263	-269 -266	-266 -268
Tester Outlet Temp (°F) T1003	-236	-236	-234	-235	-235
Tester Inlet Pressure (psig) PA1001 PA1002	453 443	449 444	449 441	453 446	450 445
Tester Outlet Pressure (psig) PA1003	408	408	406	408	408
Pressure Between Brg 3 & 4 (psig) P1006	400	420	419	421	421
Horsepower	283	309	304	310	342
Torque (in-lbs)	13067	14251	14063	14327	15820
Brg #1 O.R. Temp (°F) T1004 (TA1004)	(-244) -260	(-238) -262	(-237) -257	(-237) -262	(-237) -265
Brg #2 O.R. Temp (°F) T1005 (TA1005)	(-232) -229	(-236) -229	(-236) -220	(-235) -225	(-234) -228
Brg #3 O.R. Temp (°F) T1006 (TA1006)	(-235) -233	(-236) -233	(-235) -231	(-236) -232	(-235) -232
Brg #4 O.R. Temp (°F) T1007 (TA1007)	(-240) -242	(-246) -263	(-242) -265	(-245) -262	(-245) -263
Radial Load (Lbs) (Calculated from P-19)	0	1370	1368	1361	1361

Exhibit 208 BSMT Test Conditions and Selected Data (Test 2140801)

PARAMETER	Test No. 2120501	2140501	2140602	2140701	2140801
• Delta Temp Across Brg Pair (°F)					
T1022-T1021	9	10	9	10	9
T1019-T1018	11	11	9	11	11
• Delta Temp Across Brg 1 (°F)					
T1023-T1021	5	2	3	2	2
Brg 2					
T1022-T1023	4	8	6	8	7
Brg 3					
T1019-T1024	5	7	6	7	6
Brg 4					
T1024-T1018	6	4	3	4	5
• Brg Outer Race Temp - Fluid Inlet Temp (°F)					
Brg 1					
T1004-T1021	-3	5	3	5	5
Brg 2					
T1005-T1023	7	12	17	15	14
Brg 3					
T1006-T1024	4	7	7	7	6
Brg 4					
T1007-T1018	-1	-2	-1	-2	-2
• Heat Generated (btu/sec) Across					
Brg 1	13.5	5.6	8.4	5.6	5.6
Brg 2	10.8	22.5	16.9	22.5	19.6
Brg 3	13.5	19.7	16.9	19.7	16.8
Brg 4	16.2	11.3	8.4	11.3	14.0
• Heat Generated Across					
Brg 1&2	24.4	28.2	25.3	28.2	25
Brg 3&4	29.8	31.0	25.3	31.0	31
• Inlet Vortex					
Load	67.7	70.4	73.2	76	64.4
Drive	59.6	64.8	61.9	64.8	64.4
• Pressure Drop (psi)					
Brg 1	N/A	N/A	N/A	N/A	N/A
Brg 2	N/A	N/A	N/A	N/A	N/A
Brg 3	-8	12	13	13	13
Brg 4	43	24	22	25	24
Brg 1&2	45	41	43	45	42
Brg 3&4	35	36	35	38	37
• Flow (lbs/sec) through Brg pair	6.4	6.4	6.4	6.4	6.4
• H.P.	283	309	304	310	342
• Torque (in-lbs)	13087	14251	14063	14327	15820
• Shaft Speed (rpm)	29954	30,049	29947	30003	29972
• Radial Load (lbs)	0	1370	1363	1361	1361

Exhibit 209 BSMT Test Parameter Comparison LOX (Test 2140801)

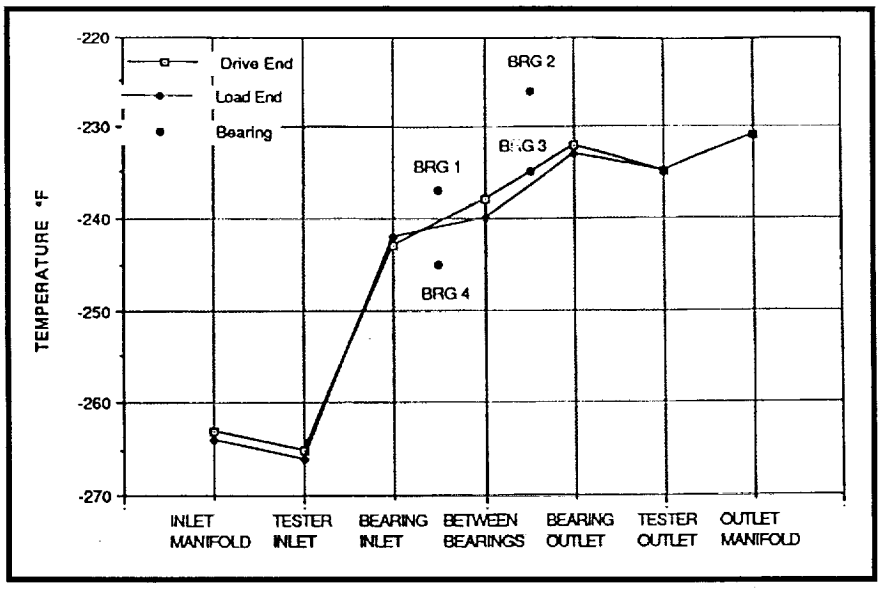

Exhibit 210 Temperature Profile for BSMT Test 2140801

load on the inboard bearings was estimated to be 10,140 N (2280 lbs), and the axial load of the outboard bearings was estimated to be 2870 N (645 lbs). These loads do not include effects of ball and race wear. The radial load on each bearing was about 3015 N (678 lbs). The test was planned to run until the LOX tank was depleted, which is about 21 minutes. An unplanned test cut occurred after about 19 minutes at a test speed of 20,000 RPM. The test was cut by the outer race temperature (T 1005) of Bearing 2 excluding its redline of 133K (-220°F). The increase of Bearing 2 outer race temperature was caused by an increase in shaft speed to about 31,500 RPM. The over speed was caused by a false display of a drop in shaft speed, which when compensated for by the operator, caused an increase in shaft speed of about 1500 RPM.

Since the outer race temperature of Bearing 2 was about 130K (-225°F) at nominal shaft speed, the increase in speed caused the temperature to exceed its redline and cut the test.

Test parameters and selected data from this test were compared with those of previous tests in this series and a previous test with Si_3N_4 ball bearings with no radial load (Test 2120501). These comparisons are shown in **Exhibits 212** and **213**. The torque was slightly higher for this test and had increased with the accumulation of test time.

Temperature profiles through the tests are shown in **Exhibit 214**. Included are the bearing outer race temperatures. The pressure profiles through the tester are shown in **Exhibit 215**.

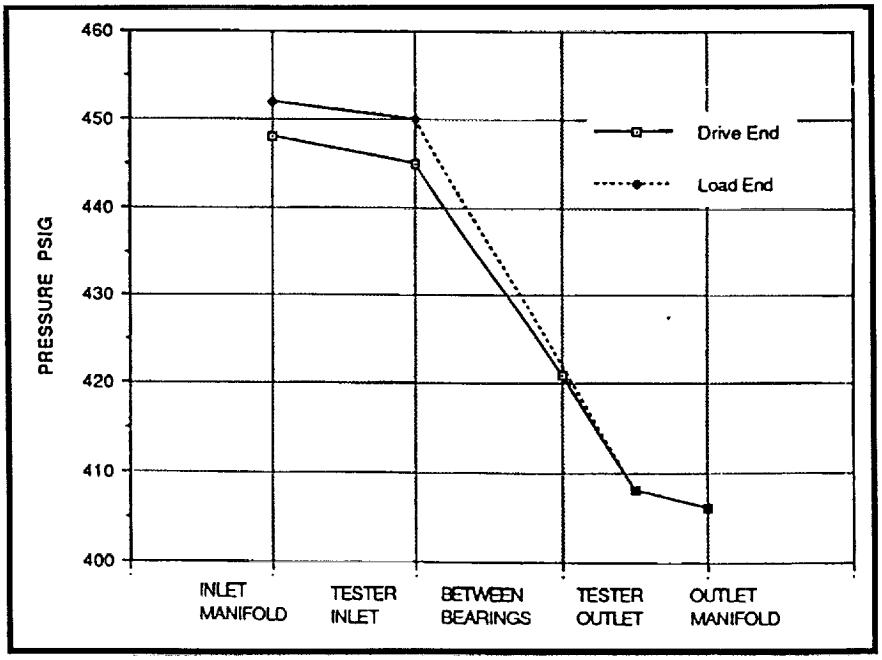

Exhibit 211 Pressure Profile for BSMT Test 2140801

Following the rotational test, the bearings were examined through a borescope. The balls in the Number 1 bearing were uniformly gray and shiny. There were some light scuff marks on some balls. There was no evidence of ball unloading and skidding. The balls in the Number 2 bearing were marbled in appearance. There were light and dark gray areas with patches of dark brown and black areas. This bearing appeared to be experiencing the highest temperature of the four bearings, which agreesd with the temperature measurements on the outer race. The balls in the Number 3 bearing were fairly uniform gray with some light brown patches. There were also some light gray areas and streaks. The Number 4 bearing had light gray shiny balls. There were a few white specks on some balls.

Test 2141001. This was the ninth rotational test in this series and the eighth in LOX with an applied radial load. The axial load on the inboard bearings was estimated to be 10,590 N (2380 lbs). The axial load on the outboard bearings was estimated to be 2780 N (625 lbs). The radial load on each bearing was 2990 N (673 lbs). The test was planned to run to LOX tank depletion. The test was cut a few seconds before tank depletion by the outer race temperature measurement (T 1005) of Bearing 2 exceeding its redline. Approximately 150 seconds before the test cut, RPM4 dropped about 1200 RPM. RPM2 remained fairly steady. There was an attempt to slightly increase speed which caused a slight increase in torque. These perturbations caused a small rise in the outer race temperature of Bearing 2 which cut the test.

Test parameters and selected data from this test were compared with those of previous tests in this series, and a previous test on Si_3N_4 balls bearings with no radial load in LOX (test 2120501). These comparisons are shown in

Test Parameter	TEST NUMBER					
	2120501	2140501	2140602	2140701	2140801	2140901
Shaft Speed (RPM)	29,954	30,049	29,947	30,003	29972	30000
Time at Speed (sec)	300	315	643	730	1250	1120
Subcooling	37	39	40	40	40	40
Flow Rate (lbs/sec)	6.4	6.4	6.4	6.4	6.4	6.4
Brg #4 Inlet Temp (°F) T1018	-243	-244	-241	-243	-243	-243
Between Brgs 3 & 4 (°F) T1024	-237	-240	-238	-239	-238	-239
Brg #3 Outlet Temp (°F) T1019	-232	-233	-232	-232	-232	-232
Brg #1 Inlet Temp (°F) T1021	-241	-243	-240	-242	-242	-242
Temp Between Bgr 1 & 2 (°F) T1023	-236	-241	-237	-240	-240	-240
Brg 2 Outlet Temp (°F) T1022	-232	-233	-231	-232	-233	-232
Tester Inlet Temp (°F) T1001 T1002	-266 -268	-268 -267	-268 -263	-269 -266	-266 -265	-267 -265
Tester Outlet Temp (°F) T1003	-236	-236	-234	-235	-235	-235
Tester Inlet Pressure (psig) PA1001 PA1002	453 443	449 444	449 441	453 446	450 445	450 446
Tester Outlet Pressure (psig) PA1003	408	408	408	408	408	408
Pressure Between Brg 3 & 4 (psig) P1006	400	420	419	421	421	421
Horsepower	283	309	304	310	342	343
Torque (in-lbs)	13087	14251	14063	14327	15820	16000
Brg #1 O.R. Temp (°F) T1004 (TA1004)	(-244) -260	(-238) -262	(-237) -257	(-237) -262	(-237) -265	(-237) -265
Brg #2 O.R. Temp (°F) T1005 (TA1005)	(-232) -229	(-236) -229	(-238) -220	(-235) -225	(-234) -226	(-229) -220
Brg #3 O.R. Temp (°F) T1006 (TA1006)	(-235) -233	(-236) -233	(-235) -231	(-236) -232	(-235) -232	(-232) -226
Brg #4 O.R. Temp (°F) T1007 (TA1007)	(-240) -242	(-246) -263	(-242) -265	(-245) -262	(-245) -263	(-245) -262
Radial Load (Lbs) (Calculated from P-19)	0	1370	1368	1361	1361	1355

Exhibit 212 BSMT Test Conditions and Selected Data (Test 2140901)

PARAMETER	Test No. 2120501	2140501	2140602	2140701	2140801	2140901
• Delta Temp Across Brg Pair (°F)						
T1022-T1021	9	10	9	10	9	10
T1019-T1018	11	11	9	11	11	11
• Delta Temp Across Brg 1 (°F)						
T1023-T1021	5	2	3	2	2	2
Brg 2 T1022-T1023	4	8	6	8	7	8
Brg 3 T1019-T1024	5	7	6	7	6	7
Brg 4 T1024-T1018	6	4	3	4	5	4
• Brg Outer Race Temp - Fluid Inlet Temp (°F)						
Brg 1 T1004-T1021	-3	5	3	5	5	5
Brg 2 T1005-T1023	7	12	17	15	14	20
Brg 3 T1006-T1024	4	7	7	7	6	11
Brg 4 T1007-T1018	-1	-2	-1	-2	-2	-2
• Heat Generated (btu/sec) Across						
Brg 1	13.5	5.6	8.4	5.6	5.6	5.6
Brg 2	10.8	22.5	16.9	22.5	19.6	22.4
Brg 3	13.5	19.7	16.9	19.7	16.8	19.6
Brg 4	16.2	11.3	8.4	11.3	14.0	11.2
• Heat Generated Across						
Brg 1&2	24.4	28.2	25.3	28.2	25	28
Brg 3&4	29.8	31.0	25.3	31.0	31	31
• Inlet Vortex						
Load	67.7	70.4	73.2	76	64.4	70
Drive	59.6	64.8	61.9	64.8	64.4	62
• Pressure Drop (psi)						
Brg 1	N/A	N/A	N/A	N/A	N/A	N/A
Brg 2	N/A	N/A	N/A	N/A	N/A	N/A
Brg 3	-8	12	13	13	13	12
Brg 4	43	24	22	25	24	25
Brg 1&2	45	41	43	45	42	41
Brg 3&4	35	36	35	36	37	37
• Flow (lbs/sec) through Brg pair	6.4	6.4	6.4	6.4	6.4	6.4
• H.P.	283	309	304	310	342	343
• Torque (in-lbs)	13067	14251	14063	14327	15820	16000
• Shaft Speed (rpm)	29954	30,049	29947	30003	29972	30000
• Radial Load (lbs)	0	1370	1363	1361	1361	1355

Exhibit 213 BSMT Test Parameter Comparison LOX Tests (Test 2140901)

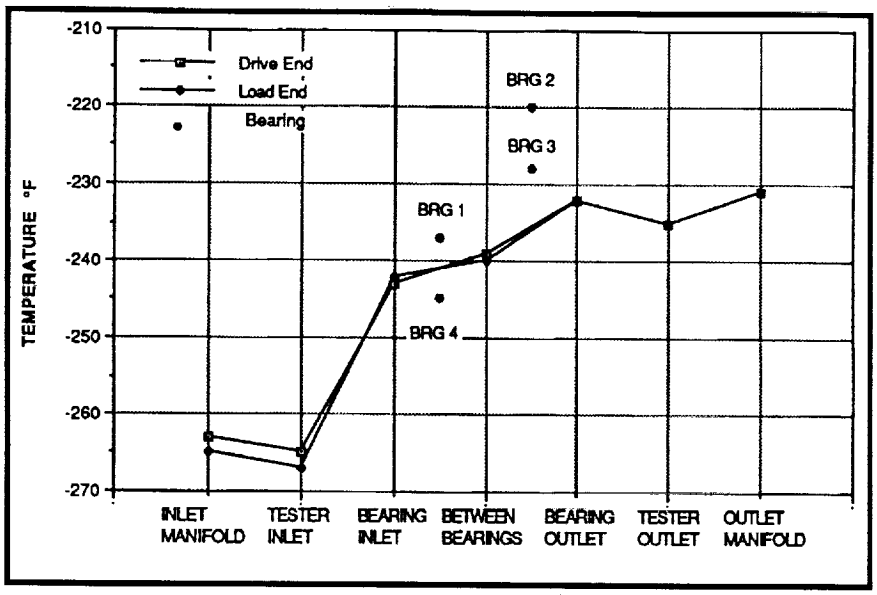

Exhibit 214 Temperature Profile for BSMT Test 2140901

Temperature profiles through the tester are shown in **Exhibit 218**. Included are the outer race temperatures. The pressure profile through the tester is shown in **Exhibit 219**. The inlet manifold pressure on the load end (P7) was erratic and the value shown was estimated.

The following bearing examination showed that the balls in Bearing 1 were shiny and gray. There were some light gray areas and streaks. The cages appeared to be in good condition. The balls in Bearing 2 were marbled in appearance. There were black and gray areas intermingled. This was probably caused by high temperature operation. The cages appeared to be in good condition. The Bearing 3 balls had a few dark areas. They were otherwise gray and shiny. This bearing was apparently running at a lower temperature than Bearing 2. The cage appeared to be in good condition. The Number 4 bearing was in like new condition. The balls were shiny and gray with light gray areas and streaks.

Exhibit 216 and **217**. Prior to this test, the torque measurement was checked and found to be reading about 20% high. The lower torque for this test was a result of re-calibration of the torque measurement. The high torque indicated for the previous test in this series was due to inaccurate torque measurement. The other data from this test compared favorably with those of previous tests.

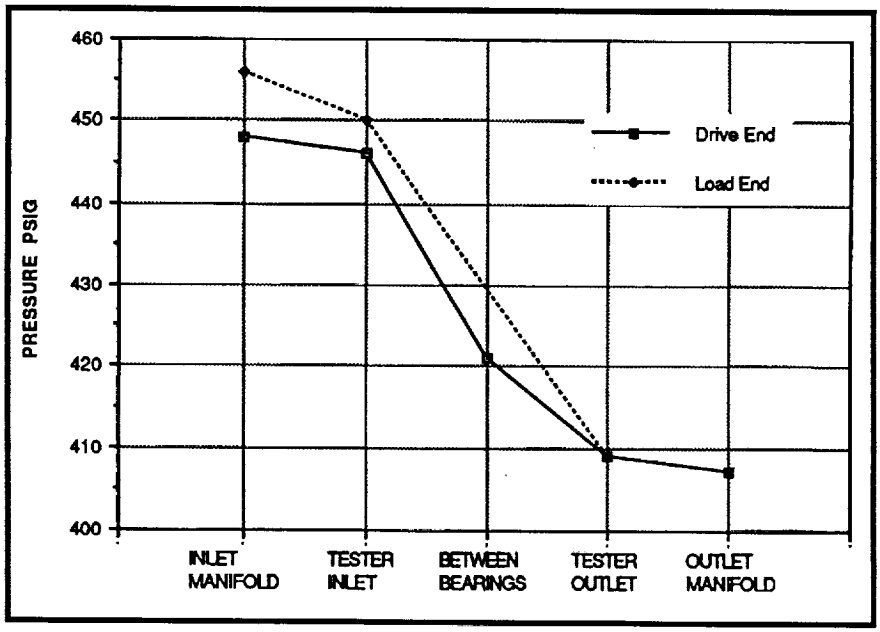

Exhibit 215 Pressure Profile for BSMT Test 2140901

Test 2141101. This was the tenth rotational test in this series and the ninth in LOX with an applied radial load. The axial load on the inboard bearings was estimated to be 10,400 N (2340 lbs), and the axial load on the outboard bearings was

Test Parameter	TEST NUMBER						
	2120501	2140501	2140602	2140701	2140801	2140901	2141001
Shaft Speed (RPM)	29,954	30,049	29,847	30,003	29972	30000	30200
Time at Speed (sec)	300	315	643	730	1260	1120	1350
Subcooling	37	39	40	40	40	40	39
Flow Rate (lbs/sec)	6.4	6.4	6.4	6.4	6.4	6.4	6.4
Brg #4 Inlet Temp (°F) T1018	-243	-244	-241	-243	-243	-243	-242
Between Brgs 3 & 4 (°F) T1024	-237	-240	-238	-239	-238	-239	-238
Brg #3 Outlet Temp (°F) T1019	-232	-233	-232	-232	-232	-232	-231
Brg #1 Inlet Temp (°F) T1021	-241	-243	-240	-242	-242	-242	-242
Temp Between Bgr 1 & 2 (°F) T1023	-236	-241	-237	-240	-240	-240	-238
Brg 2 Outlet Temp (°F) T1022	-232	-233	-231	-232	-233	-232	-232
Tester Inlet Temp (°F) T1001 T1002	-266 -266	-268 -267	-266 -263	-269 -266	-266 -265	-267 -265	-266 -264
Tester Outlet Temp (°F) T1003	-236	-236	-234	-235	-235	-235	-234
Tester Inlet Pressure (psig) PA1001 PA1002	453 443	449 444	449 441	453 446	450 445	450 446	451 444
Tester Outlet Pressure (psig) PA1003	408	408	408	408	408	409	407
Pressure Between Brg 3 & 4 (psig) P1008	400	420	419	421	421	421	420
Horsepower	283	309	304	310	342	343	285
Torque (in-lbs)	13087	14251	14063	14327	15820	16000	13,200
Brg #1 O.R. Temp (°F) T1004 (TA1004)	(-244) -260	(-238) -262	(-237) -257	(-237) -262	(-237) -255	(-237) -265	(-235) -264
Brg #2 O.R. Temp (°F) T1005 (TA1005)	(-232) -229	(-236) -229	(-238) -220	(-236) -225	(-234) -226	(-229) -220	(-230) -220
Brg #3 O.R. Temp (°F) T1006 (TA1006)	(-235) -233	(-236) -233	(-235) -231	(-236) -232	(-235) -232	(-232) -228	(-232) -228
Brg #4 O.R. Temp (°F) T1007 (TA1007)	(-240) -242	(-246) -263	(-242) -265	(-245) -262	(-245) -263	(-245) -262	(-242) -260
Radial Load (Lbs) (Calculated from P-19)	0	1370	1358	1361	1361	1355	1347

Exhibit 216 BSMT Test Conditions and Selected Data (Test 2141001)

PARAMETER	Test No. 2120501	2140501	2140502	2140701	2140801	2140901	2141001
• Delta Temp Across Brg Pair (°F)							
T1022-T1021	9	10	9	10	9	10	10
T1019-T1018	11	11	9	11	11	11	11
• Delta Temp Across Brg 1 (°F)							
T1023-T1021	5	2	3	2	2	2	3
Brg 2 T1022-T1023	4	8	6	8	7	8	7
Brg 3 T1019-T1024	5	7	6	7	6	7	7
Brg 4 T1024-T1018	6	4	3	4	5	4	4
• Brg Outer Race Temp - Fluid Inlet Temp (°F)							
Brg 1 T1004-T1021	-3	5	3	5	5	5	7
Brg 2 T1005-T1023	7	12	17	15	14	20	19
Brg 3 T1006-T1024	4	7	7	7	6	11	10
Brg 4 T1007-T1018	-1	-2	-1	-2	-2	-2	0
• Heat Generated (btu/sec) Across							
Brg 1	13.5	5.6	8.4	5.6	5.6	5.6	8.4
Brg 2	10.8	22.5	16.9	22.5	19.6	22.4	19.7
Brg 3	13.5	19.7	16.9	19.7	16.8	19.6	19.7
Brg 4	16.2	11.3	8.4	11.3	14.0	11.2	11.3
• Heat Generated Across							
Brg 1&2	24.4	28.2	25.3	28.2	25	28	28
Brg 3&4	29.8	31.0	25.3	31.0	31	31	31
• Inlet Vortex							
Load	67.7	70.4	73.2	76	64.4	70	67.6
Drive	59.8	64.8	61.9	64.8	64.4	62	61.9
• Pressure Drop (psi)							
Brg 1	N/A	N/A	N/A	N/A	N/A	N/A	N/A
Brg 2	N/A	N/A	N/A	N/A	N/A	N/A	N/A
Brg 3	-8	12	13	13	13	12	13
Brg 4	43	24	22	25	24	25	24
Brg 1&2	45	41	43	45	42	41	44
Brg 3&4	35	38	35	38	37	37	37
• Flow (lbs/sec) through Brg pair	6.4	6.4	6.4	6.4	6.4	6.4	6.4
• H.P.	283	309	304	310	342	343	285
• Torque (in-lbs)	13087	14251	14063	14327	15820	16000	13200
• Shaft Speed (rpm)	29954	30,049	29947	30003	29972	30000	30200
• Radial Load (lbs)	0	1370	1363	1361	1361	1355	1347

Exhibit 217 BSMT Test Parameter Comparison LOX Tests (Test 2141001)

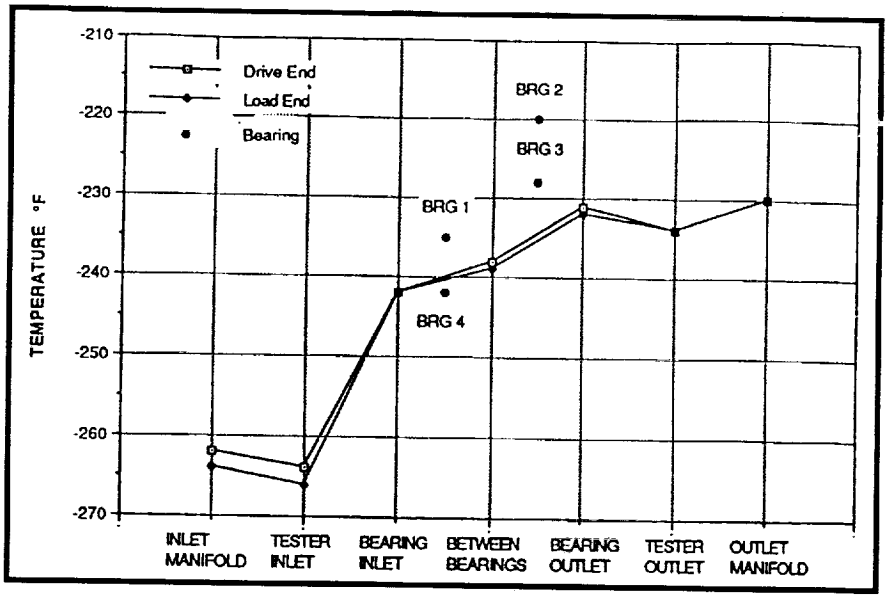

Exhibit 218 Temperature Profile for BSMT Test 2141001

estimated to be 2790 N (627 lbs). The radial load on each bearing was 2990 N (672 lbs). The test was planned to run to LOX tank depletion and successfully met this objective. Run time at 30,000 RPM was about 19.3 minutes.

Test parameters and selected data from this test were compared with those of previous tests in this series, and a previous test on Si_3N_4 ball bearings with no radial load in LOX (test 2120501). These comparisons are shown in **Exhibits 220** and **221.** The Number 2 outer race temperature was running about 1.7K (3°F) below redline. The carrier axial displacement probes showed movement during the test as shown in **Exhibit 222.** This was an indication of rapid bearing wear in the inboard bearings. Although the trend was significant, these measurements were not believed to be very accurate in absolute axial movement.

Including outer race temperature profiles, temperatures through the tester are shown in **Exhibit 223**. Pressure profiles through the tester are shown in **Exhibit 224**. No indication of bearing pumping was seen in this test series.

Following the rotational test, the bearings were examined through a borescope. The outboard bearings appeared to be in excellent condition. The Bearing 1 balls were gray and shiny with a few darker areas. The balls in the Number 2 bearing had light gray and dark brown to black patches in the surface giving a marbled appearance. One ball had a small indention in its surface. It did not appear to be a spall. Bearing 3 balls were approaching the appearance of those in Bearing 1. There was a mixture of gray, brown, and black in their surfaces. The balls in Bearing 4 were similar to those in Bearing 1.

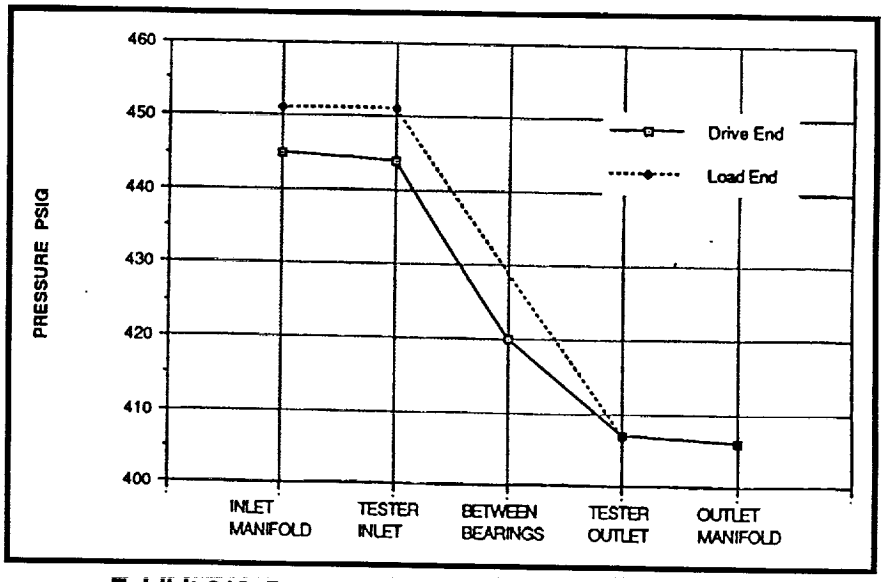

Exhibit 219 Pressure Profile for BSMT Test 2141001

Test 2141201. This was the eleventh rotational test in this series and the tenth in LOX with an applied radial load. The axial load on the inboard bearings was estimated to be 10,400 N (2340 lbs), and the axial load on the outboard bearings was estimated to be 2790 N (627 lbs). The radial load on each bearing was 3025 N (680 lbs). The test was planned to run to LOX tank depletion but was cut by the outer race temperature of Bearing 2 exceeding its redline. The tester ran for about 14.7 minutes at a speed of 30,000 RPM.

Test Parameter	TEST NUMBER							
	2120501	2140501	2140602	2140701	2140801	2140901	2141001	2141101
Shaft Speed (RPM)	29,954	30,049	29,947	30,003	29972	30000	30200	30200
Time at Speed (sec)	300	315	843	730	1260	1120	1350	1160
Subcooling	37	39	40	40	40	40	39	39
Flow Rate (lbs/sec)	8.4	8.4	8.4	8.4	8.4	8.4	8.4	8.4
Brg #4 Inlet Temp (°F) T1018	-243	-244	-241	-243	-243	-243	-242	-243
Between Brgs 3 & 4 (°F) T1024	-237	-240	-236	-239	-238	-239	-238	-239
Brg #3 Outlet Temp (°F) T1019	-232	-233	-232	-232	-232	-232	-231	-232
Brg #1 Inlet Temp (°F) T1021	-241	-243	-240	-242	-242	-242	-242	-242
Temp Between Bgs 1 & 2 (°F) T1023	-236	-241	-237	-240	-240	-240	-239	-240
Brg 2 Outlet Temp (°F) T1022	-232	-233	-231	-232	-233	-232	-232	-232
Tester Inlet Temp (°F) T1001 T1002	-264 -264	-268 -267	-266 -263	-266 -266	-266 -265	-267 -265	-266 -264	-267 -265
Tester Outlet Temp (°F) T1003	-236	-236	-234	-235	-236	-235	-234	-235
Tester Inlet Pressure (psig) PA1001 PA1002	453 443	449 444	449 441	453 446	450 445	450 446	451 444	451 445
Tester Outlet Pressure (psig) PA1003	408	408	406	408	408	409	407	406
Pressure Between Brg 3 & 4 (psig) P1006	400	420	419	421	421	421	420	420
Horsepower	283	308	304	310	342	343	285	286
Torque (in-lbs)	13087	14251	14083	14327	15820	15900	13,200	13,200
Brg #1 O.R. Temp (°F) T1004 (TA1004)	(-244) -260	(-238) -262	(-237) -257	(-237) -262	(-237) -265	(-237) -266	(-236) -264	(-237) -265
Brg #2 O.R. Temp (°F) T1005 (TA1005)	(-232) -229	(-236) -229	(-236) -229	(-236) -225	(-234) -228	(-229) -229	(-230) -229	(-233) -229
Brg #3 O.R. Temp (°F) T1006 (TA1006)	(-235) -233	(-236) -233	(-236) -231	(-236) -232	(-235) -232	(-232) -228	(-232) -228	(-235) -229
Brg #4 O.R. Temp (°F) T1007 (TA1007)	(-240) -242	(-246) -253	(-242) -256	(-245) -262	(-245) -263	(-245) -262	(-242) -260	(-245) -262
Radial Load (Lbs) (Calculated from P-19)	0	1370	1368	1361	1361	1358	1347	1345

Exhibit 220 BSMT Test Conditions and Selected Data (Test 2141101)

Test parameters and selected data from this test are compared with those of previous tests in **Exhibits 225** and **226**. The heat generation, horsepower and torque were fairly consistent throughout the test series. The disagreement in horsepower and torque values was due to the torque sensor measurement reading about 20% high. This was corrected for the last three tests in this series. The outer race temperature of Bearing 2 started high and remained high throughout the test series. The Bearing 3 outer race temperature increased the same amount of 2.8K (5°F) as Bearing 2 from Test 5 to Test 12. The outer race temperature of Bearing 3 was, however, about 2.8 to 5.6K (5°F to 10°F) lower than Bearing 2 and consequently never exceeded its redline. Comparing these tests with those of Unit 2 Build 12, which was not loaded radially, did not reveal any large differences that could be attributed to radial load. This was consistent with pretest model predictions.

Temperature profiles through the tester are shown in **Exhibit 227**. Included are the bearing outer race temperature. The pressure profiles through the tester are shown in **Exhibit 228**. There was an anomaly with the load end inlet pressure (P-7). The pressure was unrealistically low. The pressure transducer, however, did not exhibit a typical "off scale" characteristic of a failed measurement.

Following the rotational test, an examination of the bearings showed that the balls in Bearing 1 were shiny and gray with an occasional white streak. The balls in Bearing 2 were duller in appearance and had marbled surface color of

PARAMETER	Test No.							
	2120501	2140501	2140602	2140701	2140801	2140901	21401001	2141101
• Delta Temp Across Brg Pair (°F)								
T1022-T1021	9	10	9	10	9	10	10	10
T1019-T1018	11	11	9	11	11	11	11	11
• Delta Temp Across								
Brg 1 (°F)								
T1023-T1021	5	2	3	2	2	2	3	2
Brg 2								
T1022-T1023	4	8	6	8	7	8	7	8
Brg 3								
T1019-T1024	6	7	6	7	6	7	7	7
Brg 4								
T1024-T1018	6	4	3	4	5	4	4	4
• Brg Outer Race Temp - Fluid Inlet Temp (°F)								
Brg 1								
T1004-T1021	-3	5	3	5	5	5	7	5
Brg 2								
T1005-T1023	7	12	17	15	14	20	19	17
Brg 3								
T1006-T1024	4	7	7	7	6	11	10	10
Brg 4								
T1007-T1018	-1	-2	-1	-2	-2	-2	0	-2
• Heat Generated (btu/sec) Across								
Brg 1	13.5	5.6	8.4	5.6	5.6	5.6	8.4	5.6
Brg 2	10.8	22.5	16.9	22.5	19.6	22.4	19.7	22.4
Brg 3	13.5	19.7	16.9	19.7	16.8	19.6	19.7	19.6
Brg 4	16.2	11.3	8.4	11.3	14.0	11.2	11.3	11.2
• Heat Generated Across								
Brg 1&2	24.4	28.2	25.3	28.2	25	28	28	28
Brg 3&4	29.8	31.0	25.3	31.0	31	31	31	31
• Inlet Vortex								
Load	67.7	70.4	73.2	76	64.4	70	67.6	70
Drive	59.6	64.8	61.9	64.8	64.4	62	61.9	61.6
• Pressure Drop (psi)								
Brg 1	N/A	N/A	N/A	N/A	N/A	N/A	N/A	N/A
Brg 2	N/A	N/A	N/A	N/A	N/A	N/A	N/A	N/A
Brg 3	-8	12	13	13	13	12	13	12
Brg 4	43	24	22	25	24	25	24	25
Brg 1&2	45	41	43	45	42	41	44	43
Brg 3&4	35	36	35	38	37	37	37	37
• Flow (lbs/sec) through Brg pair	6.4	6.4	6.4	6.4	6.4	6.4	6.4	6.4
• H.P.	283	309	304	310	342	343	286	286
• Torque (in-lbs)	13087	14251	14063	14327	15820	16000	13200	13200
• Shaft Speed (rpm)	29954	30,049	29947	30003	29972	30000	30200	30200
• Radial Load (lbs)	0	1370	1363	1361	1361	1355	1347	1345

Exhibit 221 BSMT Test Parameter Comparison LOX Tests (Test 2141101)

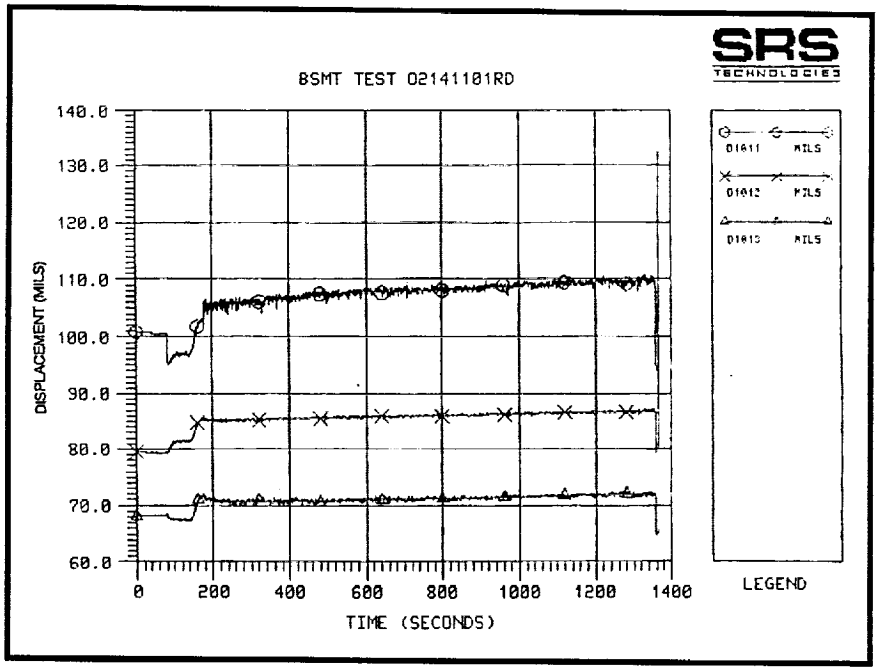

Exhibit 222 Carrier 2 Axial Displacement for Test 2141101

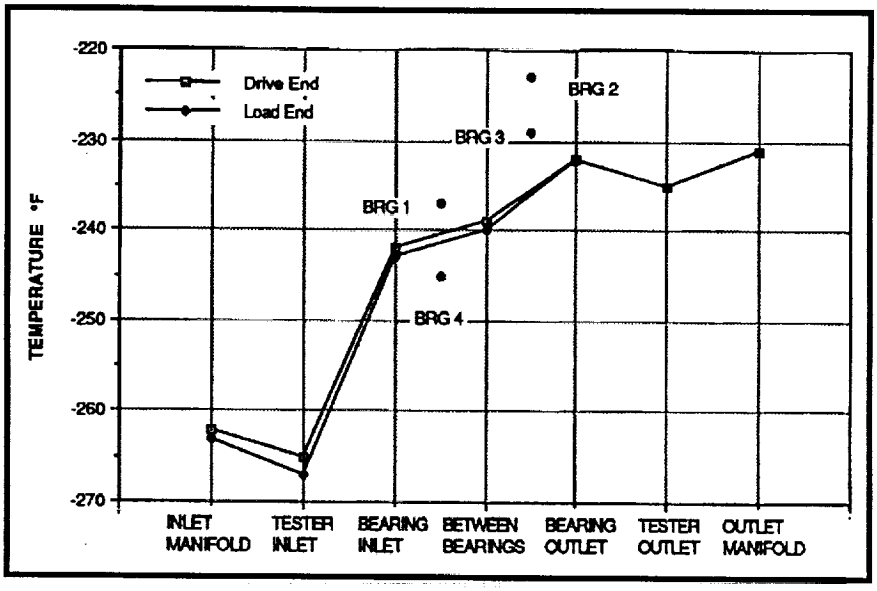

Exhibit 223 Temperature Profile for BSMT Test 2141101

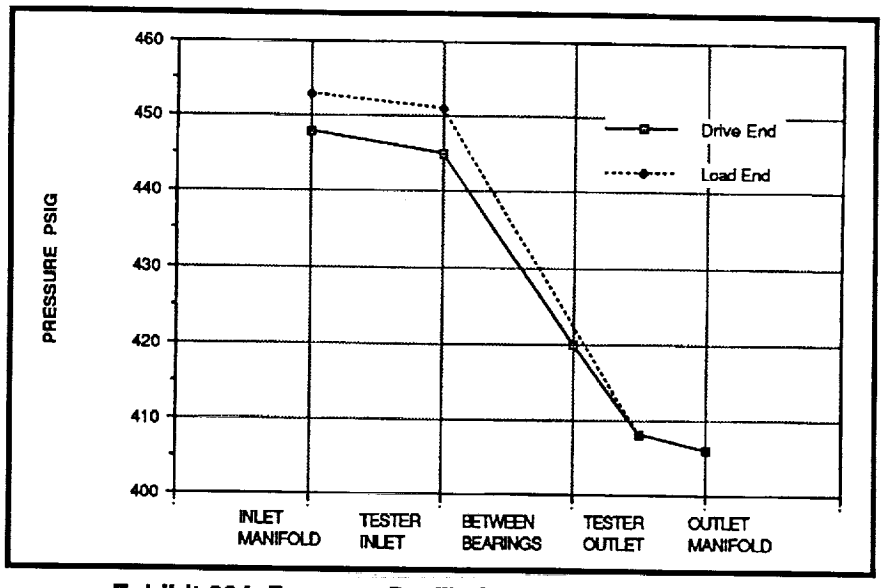

Exhibit 224 Pressure Profile for BSMT Test 2141101

Test Parameter	TEST NUMBER								
	2120501	2140501	2140602	2140701	2140801	2140901	2141001	2141101	2141201
Shaft Speed (RPM)	29,954	30,049	29,947	30,003	29972	30000	30200	30200	30001
Time at Speed (sec)	300	315	643	730	1380	1120	1380	1180	880
Subcooling	37	39	45	40	40	40	39	39	38
Flow Rate (lbs/sec)	8.4	8.4	8.4	8.4	8.4	8.4	8.4	8.4	8.4
Brg #4 Inlet Temp (°F) T1018	-243	-244	-241	-243	-243	-243	-242	-243	-242
Between Brgs 3 & 4 (°F) T1024	-237	-240	-238	-238	-238	-238	-238	-239	-238
Brg #3 Outlet Temp (°F) T1019	-232	-233	-232	-232	-232	-232	-231	-232	-231
Brg #1 Inlet Temp (°F) T1021	-241	-243	-240	-242	-242	-242	-242	-242	-241
Temp Between Bgr 1 & 2 (°F) T1023	-236	-241	-237	-240	-240	-240	-238	-240	-238
Brg 2 Outlet Temp (°F) T1022	-232	-233	-231	-232	-233	-232	-232	-232	-231
Tester Inlet Temp (°F) T1001 T1002	-264 -264	-268 -267	-266 -263	-269 -266	-266 -265	-267 -265	-266 -264	-267 -265	-268 -264
Tester Outlet Temp (°F) T1003	-236	-236	-234	-235	-236	-236	-234	-236	-234
Tester Inlet Pressure (psig) PA1001 PA1002	453 445	449 444	448 441	453 448	450 445	450 445	451 444	451 445	451 444
Tester Outlet Pressure (psig) PA1003	408	408	406	408	408	409	407	408	408
Pressure Between Brg 3 & 4 (psig) P1008	400	420	419	421	421	421	420	420	419
Horsepower	283	308	304	310	342	343	285	286	284
Torque (in-lbs)	13067	14251	14063	14327	15829	16000	13,200	13,200	13,208
Brg #1 O.R. Temp (°F) T1004 (TA1004)	(-244) -260	(-238) -262	(-237) -257	(-237) -262	(-237) -259	(-237) -266	(-236) -264	(-237) -266	(-236) -264
Brg #2 O.R. Temp (°F) T1005 (TA1005)	(-232) -229	(-234) -229	(-238) -229	(-236) -225	(-234) -228	(-229) -220	(-230) -220	(-233) -223	(-233) -220
Brg #3 O.R. Temp (°F) T1006 (TA1006)	(-236) -233	(-236) -233	(-235) -231	(-236) -232	(-236) -232	(-232) -228	(-232) -228	(-236) -229	(-232) -228
Brg #4 O.R. Temp (°F) T1007 (TA1007)	(-240) -242	(-246) -263	(-242) -256	(-245) -262	(-245) -263	(-245) -262	(-242) -260	(-245) -262	(-243) -251
Radial Load (Lbs) (Calculated from P-19)	0	1370	1368	1361	1361	1366	1347	1346	1360

Exhibit 225 BSMT Test Conditions and Selected Data (Test 2141201)

PARAMETER	Test No.								
	2120501	2140501	2140602	2140701	2140801	2140901	2141001	2141101	2141201
• Delta Temp Across Brg Pair (°F)									
T1022-T1021	9	10	9	10	9	10	10	10	10
T1019-T1018	11	11	9	11	11	11	11	11	11
• Delta Temp Across									
Brg 1 (°F)									
T1023-T1021	5	2	3	2	2	2	3	2	2
Brg 2									
T1022-T1023	4	6	6	8	7	8	7	8	8
Brg 3									
T1019-T1024	5	7	6	7	6	7	7	7	7
Brg 4									
T1024-T1018	6	4	3	4	5	4	4	4	4
• Brg Outer Race Temp - Fluid Inlet Temp (°F)									
Brg 1									
T1004-T1021	-3	5	3	5	5	5	7	5	2
Brg 2									
T1005-T1023	7	12	17	15	14	20	19	17	19
Brg 3									
T1006-T1024	4	7	7	7	6	11	10	10	12
Brg 4									
T1007-T1018	-1	-2	-1	-2	-2	-2	0	-2	-1
• Heat Generated (btu/sec) Across									
Brg 1	13.5	5.6	8.4	5.6	5.6	5.6	8.4	5.6	5.6
Brg 2	10.8	22.5	16.9	22.6	19.8	22.4	19.7	22.4	22.4
Brg 3	13.5	19.7	16.9	19.7	16.8	19.6	19.7	19.6	19.6
Brg 4	16.2	11.3	8.4	11.3	14.0	11.2	11.3	11.2	11.2
• Heat Generated Across									
Brg 1&2	24.4	28.2	25.3	28.2	25	28	28	28	28
Brg 3&4	29.8	31.0	25.3	31.0	31	31	31	31	31
• Inlet Vortex									
Load	67.7	70.4	73.2	76	64.4	70	67.8	70	70
Drive	59.6	64.8	61.9	64.8	64.4	62	61.9	61.6	61.6
• Pressure Drop (psi)									
Brg 1	N/A	N/A	N/A	N/A	N/A	N/A	N/A	N/A	N/A
Brg 2	N/A	N/A	N/A	N/A	N/A	N/A	N/A	N/A	N/A
Brg 3	-8	12	13	13	13	12	13	12	11
Brg 4	43	24	22	25	24	25	24	25	25
Brg 1&2	45	41	43	45	42	41	44	43	43
Brg 3&4	35	36	35	38	37	37	37	37	38
• Flow (lbs/sec) through Brg pair	6.4	6.4	6.4	6.4	6.4	6.4	6.4	6.4	6.4
• H.P.	283	309	304	310	342	343	285	286	286
• Torque (in-lbs)	13087	14251	14063	14327	15820	16000	13200	13200	13208
• Shaft Speed (rpm)	29954	30,049	29947	30003	29972	30000	30200	30200	30031
• Radial Load (lbs)	0	1370	1353	1361	1361	1358	1347	1345	1360

Exhibit 226 BSMT Test Parameter Comparison LOX Tests (Test 2141201)

gray, brown and black. There were some wide bands that appeared to be Teflon. The balls in the Number 3 bearing also had a marbled appearance. They did not appear to be as dull as the balls in the Number 2 bearing. The Number 4 bearing was similar in appearance to the Number 1 bearing. The outboard bearings (1 & 4) appeared to be in good condition.

Test 2141301. Test 13 was to be the LN_2 transient high axial load test but was terminated before shaft rotation due to axial load cylinder actuation problems. The wiring for the load cylinder solenoid was rewired for this test and was incorrectly installed, thus, causing the load cylinder to operate improperly.

Test 2141401. This was the twelfth rotational test in this series. It was a special test to demonstrate the capability of the Si_3N_4 ball bearings to withstand transient axial loads representative of those experienced in the SSME HPOTP during start and shutdown. Since this was a first for this type test, it was run in LN_2 for safety. The maximum transient axial load was 25,800 N (5,800 lbs), and the fluid (PA) load was estimated to be 1423 N (320 lbs), giving a maximum axial load of 27,223 N (6,120 lbs). The dwell time for the high load was approximately one second.

Torque and speed traces are shown in **Exhibit 229** for the time of axial load applications. The load was applied at approximately 133 seconds, and was released at 134 seconds, the axial load measurement (L1009) is shown in **Exhibit 230**. The other load measurement (L1010) was bad. The actuator pressures for the axial load (P0018) and the radial load (P0019) are shown in **Exhibit 231**. During the 15,000 RPM test phase, the radial load was 1423 N (320 lbs) and was 6580 N (1,479 lbs) during the 30,000 RPM test phase. The response of the outer race temperature measurements to the axial load pulse is shown in **Exhibit 232**. The Bearing 3 measurement (T1006) apparently lost contact with the outer race causing the dip in the measurement. Contact was regained as the measurement increased, and then

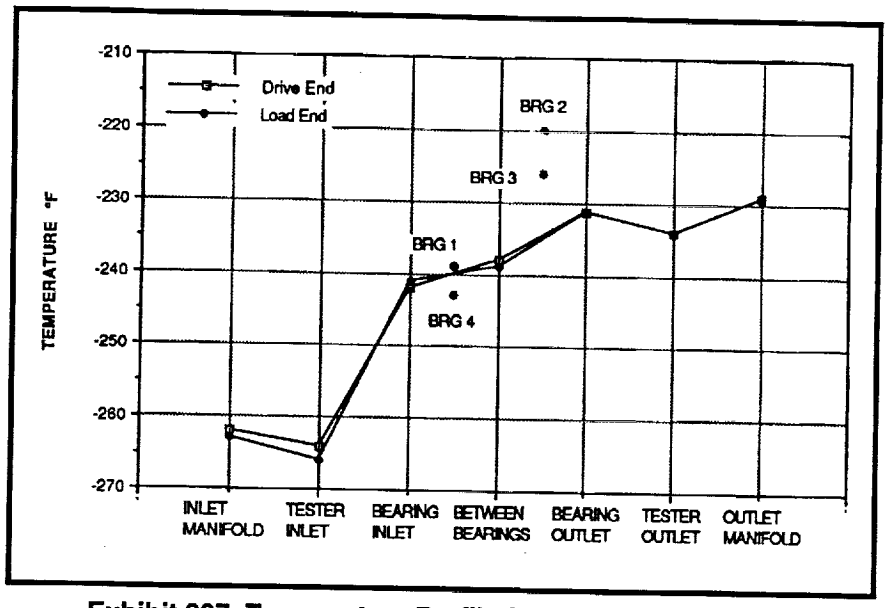

Exhibit 227 Temperature Profile for BSMT Test 2141201

decreased as the load was removed. The net increase was about 1.3K (2.3°F). This agreed with the model prediction of about 1.4K (2.5°F) rise caused by the load pulse. The behavior of the Number 2 bearing outer race temperature was not consistent. It also showed a small dip which could have been caused by loss of contact between the thermocouple and outer race. The relatively slow rise could have been caused by marginal contact, improving as the time increased.

The measured rise in bearing outlet temperature (T1019) due to the load pulse was about 0.6K (1°F). The predicted value was 0.33K (0.6°F). The predicted inner and outer race contact stresses are shown in **Exhibit 233**. The inner race stress increased from 3.2 GPa (470 ksi) to about 4.6 GPa (660 ksi) due to application of the axial load pulse. The temperature data correlated well with model predictions, and the load cell actuator pressure correlated well with load cell measurement (L1009), which verified that the bearings were loaded as planned.

Following the rotational test, the bearings were examined through a borescope. In general, the bearings appeared to be in good condition. There were no spalled balls, and all balls rolled when the shaft was rotated. The outboard bearing balls exhibited, for the first time, dark resin colored bands. These bands could have been caused by ball skid when the outboard bearings were axially unloaded with the application of the high axial load. The inboard bearings (Bearing 2 and 3) balls had dark brown to black patches in their surfaces giving a marbled appearance. There were no visible change in the bearings after the application of the high axial load.

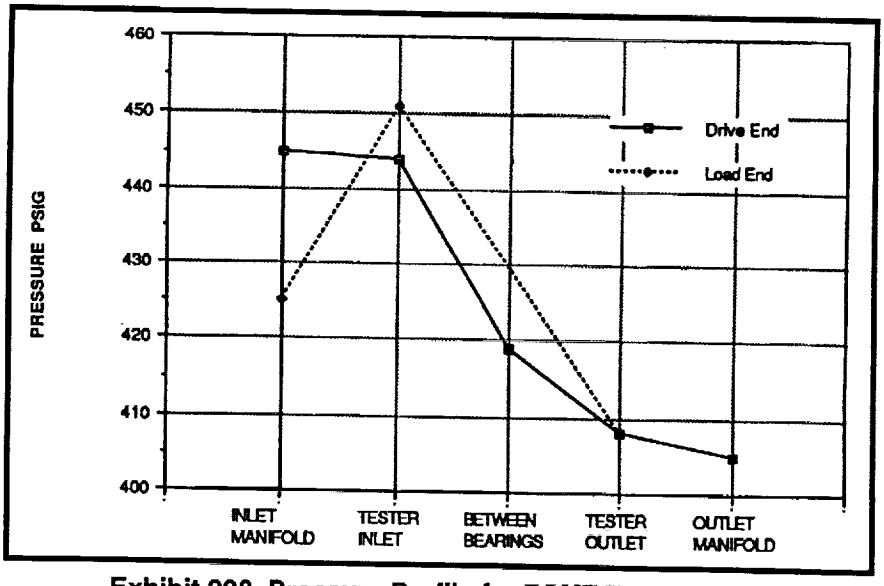

Exhibit 228 Pressure Profile for BSMT Test 2141201

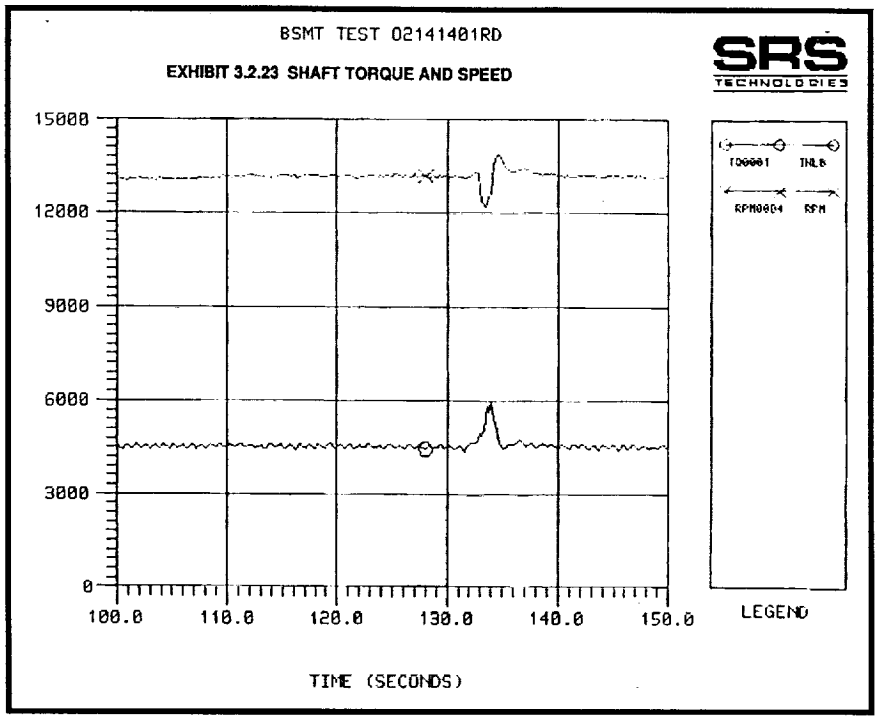

Exhibit 229 Shaft Torque and Speed for Test 2141401

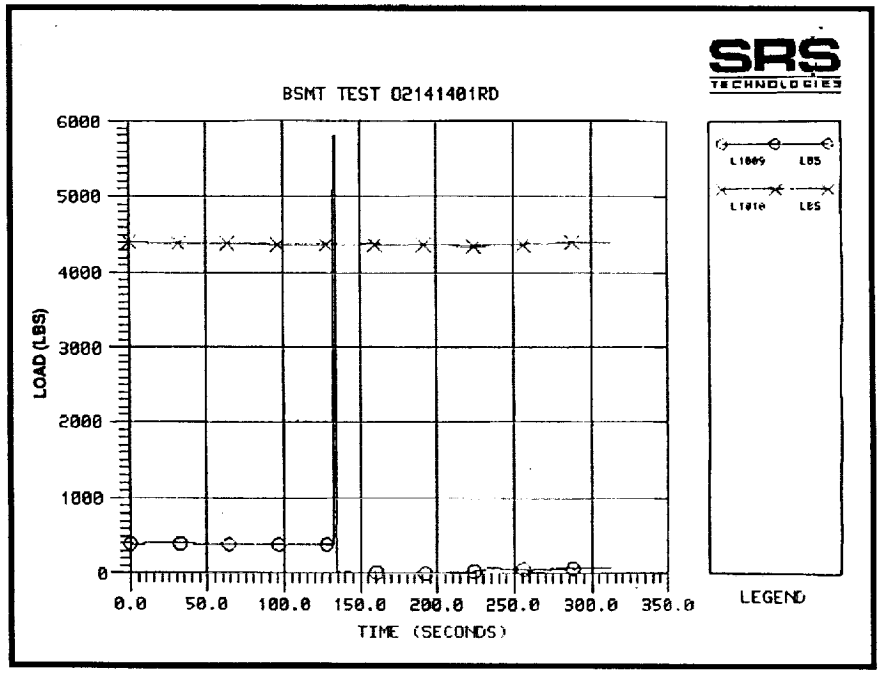

Exhibit 230 Inboard Bearings Axial Load for Test 2141401

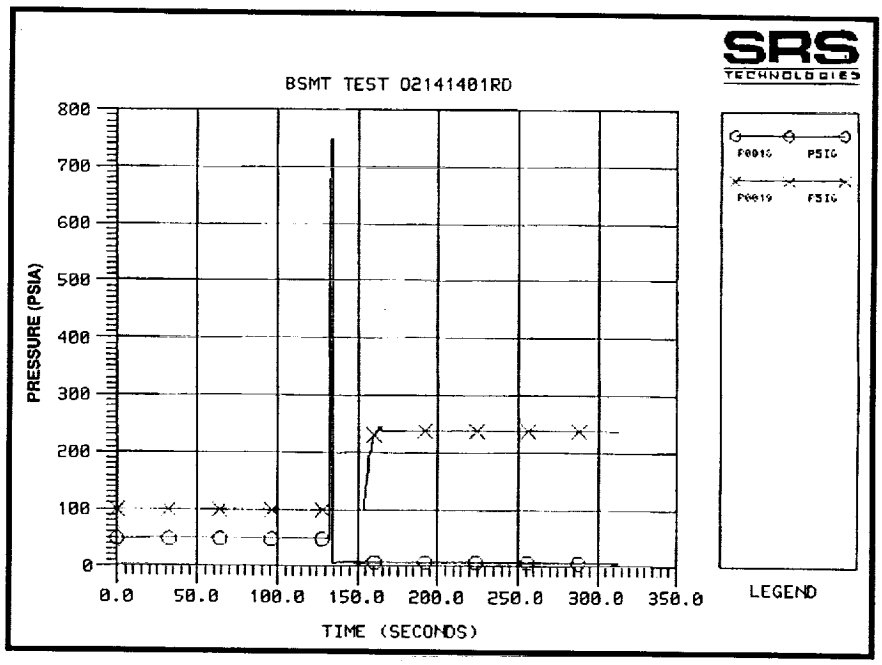

Exhibit 231 Axial and Radial Load Actuator Pressures for Test 2141401

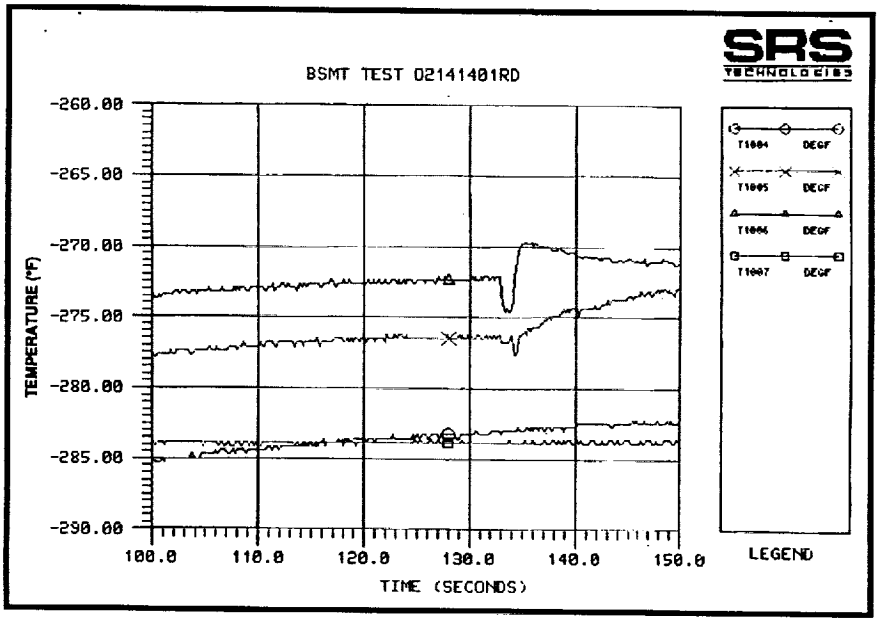

Exhibit 232 Outer Race Temperature Measurements for Test 2141401

The Si_3N_4 balls apparently survived the two hours and seven minutes of running in LOX at 30,000 RPM, and the application of high axial load without visible signs of spalling or other degradation.

Visual inspection of the Unit 2 Build 14 bearings was performed after tester disassembly. The Si_3N_4 rolling elements appeared to be in good condition with only surface discolorations of dark brown and black patches. The only degradation of the Si_3N_4 material that was observed was under high magnification and appeared as fine parallel cracks that were perpendicular to the rolling tracks on the balls. This degradation was termed "traction cracks" and one theory for its cause was the surface rubbing against the Armalon cage. The traction cracks were observed on the balls for all four bearings and was believed to be only a surface phenomenon posing no structural problems. The races of the outboard bearings looked in good condition with only moderate wear. The inboard bearing races did have expected surface spalls and wear due to the high contact stress levels and long run time imposed on them.

5.5 Testing of BSMT Unit 3 Build 7

The objective of this test series was to test the Battelle cage design under similar ball loading conditions as expected in the Rocketdyne HPOTP pump end 45mm bearings. The bearings tested in this series were 57mm bearings with inner race curvature fi = 0.55, outer race curvature fo = 0.53 and internal clearance Pd = 0.150 to 0.155mm (0.0059 to 0.0061 in). Bearings 1 and 4 (outboard bearings) used 440C stainless steel balls. Bearings 2 and 3 (inboard bearings) used Toshiba silicon nitride balls. All four bearings were fitted with the Battelle cage design with oval ball pockets giving a ball to cage clearance of 2.03 mm (0.080 in). This was the same ball pocket clearance as in the 45mm bearing cage design. The Battelle cage design used 12 balls instead of the standard 13 for the 57mm Phase II design and 11 balls for the 45mm bearing instead of the standard 12 balls. The elimination of one rolling element was necessary due to the web dimensions of the Battelle cage design being thicker than the web of the standard Armalon cage.

The tester used 5780N (1300 lbs) axial preload and 2890 to 3110N (650 to 700 lbs) applied radial load per bearing. At 30,000 RPM, it was estimated that the inboard bearings operated with approximately 10,230N (2300 lbs) and the

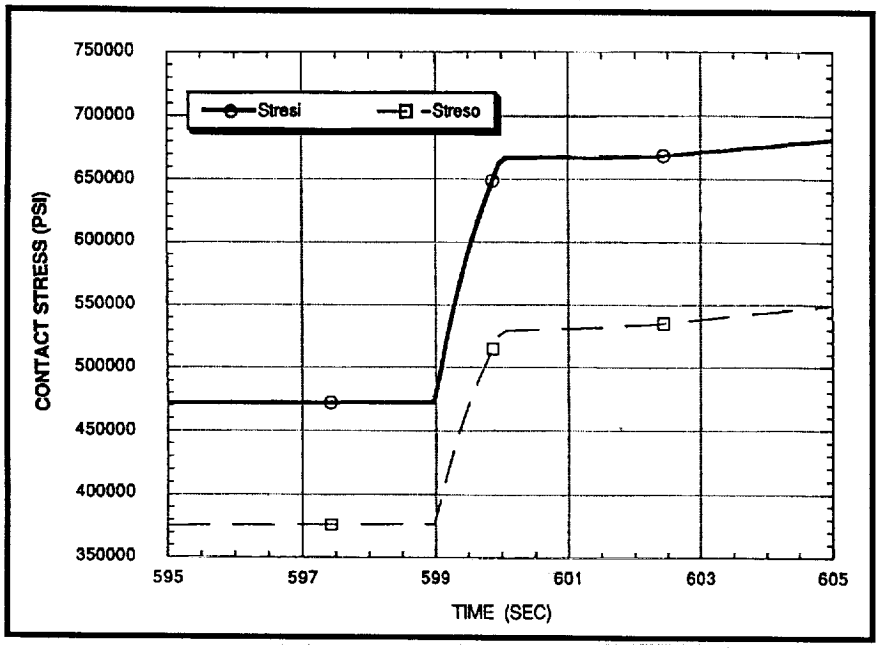

Exhibit 233 Predicted Inner and Outer Race Stresses for High Axial Load Test for Test 2141401

outboard bearings operated with 2890 N (650 lbs). With this loading configuration, the steel rolling element outboard bearings loaded the cage to approximately the level predicted for the HPOTP 45mm bearings due to the larger ball excursions of the steel balls. The specific operating conditions for each test run are given in **Exhibits 234** and **235**. The temperature and pressure profiles through the tester and post test borescope inspection observations for each test are provided in the following test summaries.

Test 3070201. This was the first rotational test of this series and was planned at four test speeds of 15,000, 25,000, 28,000, and 30,000 RPM for two minutes at each speed using LO_2 as the coolant. The test was successfully completed on the first attempt. The speed sensor RPM 0004 was reading 2000 RPM low but did not affect the test since the controller was able to use another sensor (RPM1004).

Test parameters and selected data from this test for each speed were provided in **Exhibits 234** and **235**, shown previously. The data were difficult to compare to previous tests due to this tester build being a hybrid setup with steel and silicon nitride rolling elements. The temperature profiles through each side of the tester at 30,000 RPM are shown in **Exhibit 236** and look similar to previous tests with steel or silicon nitride rolling elements. However, the pressure profiles through the tester at 30,000 RPM, shown in **Exhibit 237**, were anomalous due to the pressure between the bearings (P1006) reading only slightly above the exit pressure (PA1003). This indicated that most of the pressure drop was across the upstream bearing. The cause for the unusually low pressure reading was unknown.

Following the test, the bearings were inspected through a borescope. The Bearing 1 cage appeared to be in good condition with no excessive pocket contact visible. The balls of Bearing 1 had light gray tracks and one ball three slight scratches outside of the track area. The silicon nitride balls of Bearing 2 had several white streaks believed to be Teflon transferred from the cage. The balls also had a few black specks on their surface. Bearing 2 cage appeared to be in good condition. The Bearing 3 silicon nitride balls had slightly more black specks with a few balls displaying narrow black bands. Bearing 3 cage looked good. Bearing 4 steel balls had light brown tracks and Teflon transfer all over their surface indicating good cage contact. The cage looked in good condition with no signs of excessive pocket wear.

Test 3070302. This test was planned for only one speed of 30,000 RPM for five minutes. The first attempt was cut by T1006 (Bearing 3 outer race temp) exceeding the 133K (-220°F) redline shortly after reaching speed. The "quick look" data were reviewed and it was determined that T1006 was reading falsely high. T1006 was removed from the redline list and the test was rerun successfully.

The test parameters and selected data for this test were shown in **Exhibit 234** and **235**. The temperature and pressure profile through the tester are shown in **Exhibit 238** and **Exhibit 239**, respectively The operating parameters were about the same as the previous test values. The pressure between the bearings was again measuring abnormally low.

The bearings were inspected with a borescope after the test. The balls of Bearing 1 had light brown tracks and wide bands of Teflon transfer. Bearing 1 cage looked in good condition with no signs of ball pocket wear. Bearing 2 balls looked "cleaner" than after the previous test run. There was only a few balls with Teflon streaks and the

Test Parameter	TEST NUMBER									
	3070201				3070302	3070401	3070501	3070601	3070702	3070801
Shaft Speed (RPM)	15,000	25,000	28,000	30,000	30,000	30,000	30,100	30,100	30,100	30,000
Time at Speed (sec)	150	100	125	130	300	300	1320	700	360	1000
Flow Rate (lbs/sec)	6.4	6.4	6.4	6.4	6.4	6.4	6.4	6.4	6.4	6.4
Brg #4 Inlet Temp (°F) T1018	-259.5	-247.0	-243.5	-242.0	-243	-242	-242	-242	-242	-242
Between Brgs 3 & 4 (°F) T1024	-259.5	-246.5	-242.0	-239.0	-241	-240	-240	-239	-239	-239
Brg #3 Outlet Temp (°F) T1019	-257.0	-239.5	-234.5	-231.0	-233	-232	-231	-231	-231	-231
Brg #1 Inlet Temp (°F) T1021	-260.0	-246.0	-243.5	-241.0	-242	-242	-241	-241	-241	-241
Temp Between Brgs 1 & 2 (°F) T1023	-257.0	-242.5	-239.0	-236.0	-238	-237	-237	-237	-237	-236
Brg #2 Outlet Temp (°F) T1022	-257.5	-239.5	-234.5	-231.0	-233	-232	-231	-231	-232	-231
Tester Inlet Temp (°F) T1001 T1002	-267.0 -267.5	-266.0 -264.5	-265.5 -263.5	-265.5 -262.5	-268 -265	-267 -264	-266 -264	-268 -264	-267 -264	-267 -263
Tester Outlet Temp (°F) T1003	-250.0	-242.0	-237.0	-233.5	-236	-234	-234	-234	-234	-234
Tester Inlet Pressure (psig) PA1001 PA1002	442 442	444 442	442 444	444 444	444 444	444 446	445 444	445 446	447 442	445 446
Tester Outlet Pressure (psig) PA1003	432	411	407	407	405	406	406	406	406	406
Pressure Between Brg 3 & 4 (psig) P1006	431	413	409	409	408	411	409	411	409	411
Horsepower	56	218	252	280	300	300	300	300	300	300
Torque (in-lbs)	6600	13,000	13,400	13,800	13,880	13,800	13,800	13,800	13,770	13,730
Brg #1 O.R. Temp (°F) T1004 (TA1004)	-260 (-261)	-256 (-244)	-255 (-239)	-256 (-236)	-264 (-237)	-262 (-235)	-259 (-235)	-261 (-234)	-258 (-235)	-260 (-234)
Brg #2 O.R. Temp (°F) T1005 (TA1005)	-258 (-257)	-239 (-240)	-233 (-236)	-229 (-232)	-230 (-234)	-227 (-234)	-228 (-233)	-226 (-233)	-225 (-233)	-226 (-232)
Brg #3 O.R. Temp (°F) T1006 (TA1006)	-253 (-257)	-234 (-240)	-230 (-236)	-226 (-232)	-221 (-235)	-222 (-234)	-224 (-234)	-224 (-233)	-225 (-233)	-225 (-233)
Brg #4 O.R. Temp (°F) T1007 (TA1007)	-262 (-261)	-261 (-249)	-260 (-244)	-260 (-241)	-263 (-242)	-262 (-241)	-261 (-239)	-261 (-239)	-261 (-239)	-261 (-238)

Exhibit 234 BSMT Test Conditions and Selected Data

PARAMETER	3070201				3070302	3070401	3070501	3070601	3070702	3070801
• Delta Temp Across Brg Pair (°F)										
T1022-T1021	2.5	6.5	9.0	10.0	10.0	10.0	10.0	10.0	9.0	10.0
T1019-T1018	2.5	7.5	9.0	11.0	11.0	10.0	11.0	11.0	11.0	11.0
• Delta Temp Across Brg 1 (°F)										
T1023-T1021 Brg 2	3.0	3.5	4.5	5.0	5.0	5.0	4.0	4.0	4.0	5.0
T1022-T1023 Brg 3	-0.5	3.0	4.5	5.0	5.0	5.0	6.0	6.0	5.0	5.0
T1019-T1024 Brg 4	2.5	7.0	7.5	8.0	8.0	8.0	9.0	8.0	8.0	8.0
T1024-T1018	0.0	0.5	1.5	3.0	3.0	2.0	2.0	3.0	3.0	3.0
• Brg Outer Race Temp - Fluid Inlet Temp (°F)										
Brg 1 TA1004-T1021	-1.0	2.0	4.5	5.0	5.0	7.0	6.0	7.0	6.0	7.0
Brg 2 T1005-T1023	0.0	3.5	6.0	7.0	8.0	10.0	9.0	11.0	12.0	10.0
Brg 3 T1006-T1024 (TA1006-T1024)	6.5	12.5	12.0	13.0	20.0 (6)	18.0 (6)	16.0 (6)	15.0	14.0	14.0
Brg 4 TA1007-T1018	-1.5	-2.0	-0.5	1.0	1.0	1.0	3.0	3.0	3.0	4.0
• Heat Generated (Btu/sec) Across										
Brg 1	8.1	10.0	13.1	14.8	14.3	14.8	11.7	11.8	11.8	14.6
Brg 2	-1.3	8.6	13.1	14.8	14.3	14.8	17.5	17.7	14.7	14.8
Brg 3	6.8	19.7	21.6	23.3	23.1	23.2	26.2	23.3	23.4	23.8
Brg 4	0.0	1.4	4.3	8.8	8.7	5.7	5.8	8.8	8.8	8.7
• Heat Generated Across										
Brg 1&2	6.8	18.6	26.2	29.6	28.6	29.6	29.2	29.5	26.5	29.4
Brg 3&4	6.8	21.1	25.9	32.1	31.8	29.0	32.0	32.1	32.2	32.5
• Inlet Vortex Work (Btu/sec)										
Load	18.9	55.0	60.5	67.9	71.2	68.6	68.8	74.0	71.6	71.4
Drive	21.6	49.5	55.0	58.2	60.5	60.8	60.5	59.7	60.7	57.8
• Pressure Drop (psi)										
Brg 3	-1	2	2	2	2	3	3	3	3	3
Brg 4	11	29	35	35	37	35	35	35	33	35
Brg 1&2	10	33	37	37	39	36	39	37	41	37
Brg 3&4	10	31	35	37	39	38	38	38	36	38
• Subcooling °F	55	39	38	36	38	38	36	37	37	38
• Radial Load (lbs/brg)	650	650	650	650	650	700	700	700	700	700

Exhibit 235 BSMT Test Parameters Comparison

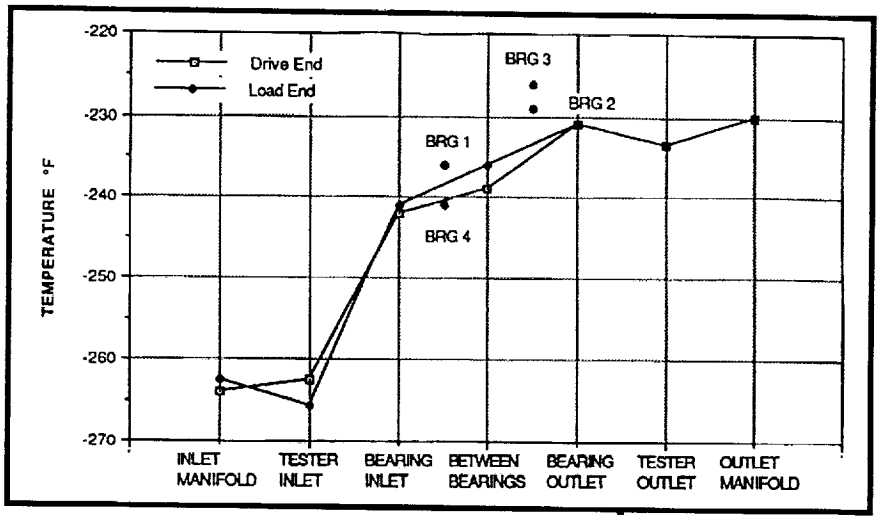

Exhibit 236 Temperature Profile for BSMT Test 3070201 (30,000 RPM)

black specks seen previously were much reduced. The cage showed no signs of wear. The balls of Bearing 3 had very wide bands of white Teflon transfer and the cage was in good condition. Bearing 4 balls had good Teflon transfer all over their surface but had no definite tracks. The Bearing 4 cage was in good condition.

Test 3070401. This test was planned for a five minute run at 30,000 RPM with an increased radial load of 700 lbs (3100N). A full duration run was successfully completed with a radial load of ~700 lbs (3100N) per bearing obtained. Bearing 3 outer race temperature measurement (T1006) was again reading high and was not placed on the redline list. No other anomalies were observed during this test run.

The test parameters and selected operating conditions were shown in **Exhibits 234** and **235**. The temperature and pressure profiles through each end of the tester are shown in **Exhibits 240** and **241**. The profiles and data are very similar to those of the previous run. Thus, no definite effect of the increased radial load was detected. This is understandable since the radial load was increased only 6%. However, this radial load should cause the ball excursions of the outboard bearings to be just under the pocket clearance which was the test goal. Examination of the cages after tester disassembly at the end of the test series was later performed to verify that cage pocket loading was as desired.

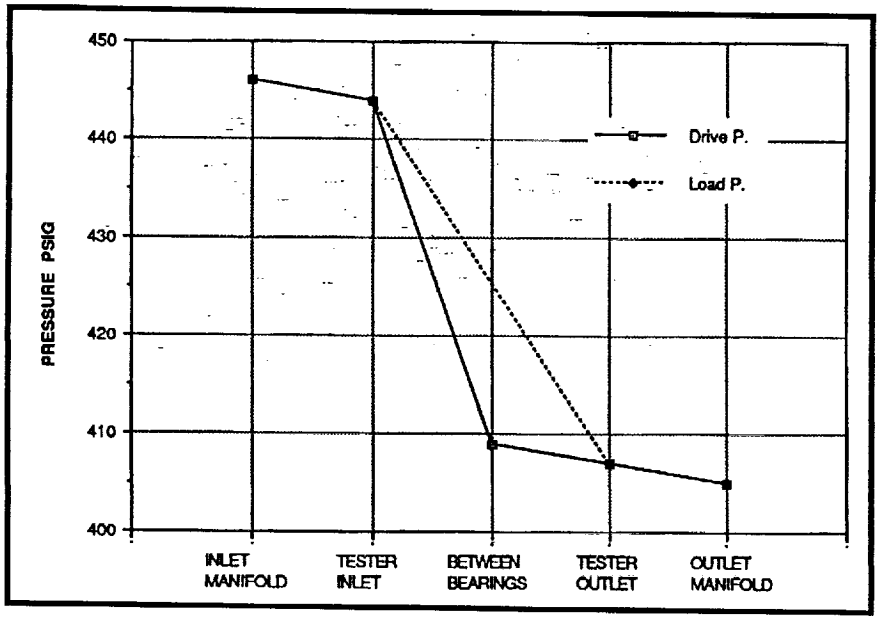

Exhibit 237 Pressure Profile for BSMT Test 3070201 (30,000 RPM)

The borescope examination of the bearings after the test showed that Bearing 1 balls had light brown tracks but no Teflon transfer bands as observed prior to this run. The cage of Bearing 1 was still in good

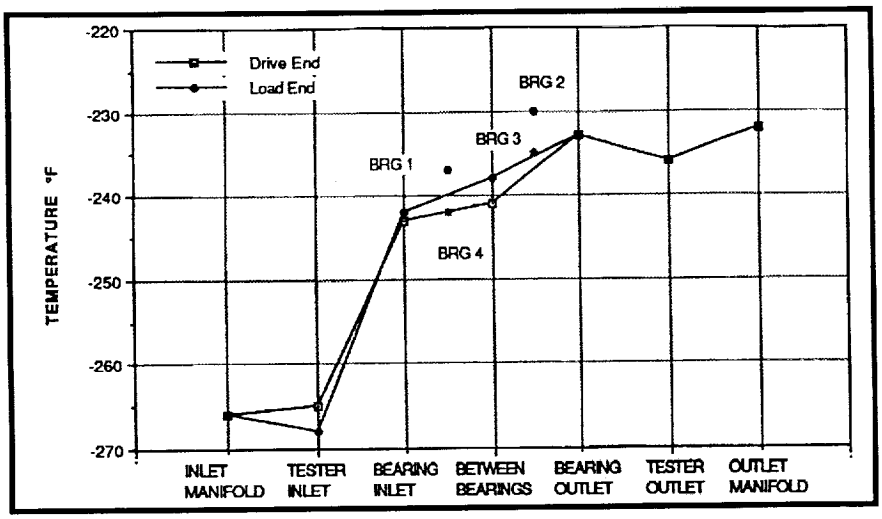

Exhibit 238 Temperature Profile for BSMT Test 3070302

condition with no visible signs of wear. Bearing 2 balls looked very clean with only light track marks and the cage pockets of this bearing also looked good. The balls of Bearing 3 had a few bronze metallic specks on their surface and one ball had a narrow dark track. The Bearing 3 cage looked in good condition. Bearing 4 balls had light brown tracks all over the ball surfaces indicating the balls had changed orientation during operation. The ball pockets of Bearing 4 cage showed signs of ball contact in the visible area but did not indicate high wear.

Test 3070501. This test was planned for LO_2 run tank depletion which is a long duration run of 20 to 25 minutes. The Bearing 3 outer race temperature measurement (T1006) was replaced and its redline was reactivated. The test was successfully completed on the first attempt and approximately 22 minutes of runtime at 30,000 RPM was obtained.

Test parameters and selected operating conditions were shown in **Exhibits 234** and **235**. Temperature and pressure profiles through the tester are shown in **Exhibits 242** and **243**. The temperature data was elevated about one degree above the temperatures of the previous run due to the LO_2 run tank warming up slightly during the long duration run as normal. The temperature trends through the bearings did indicate that the inboard bearings were generating approximately 15% more heat. This could have been caused by the bearing surfaces degrading and increasing the coefficient of friction.

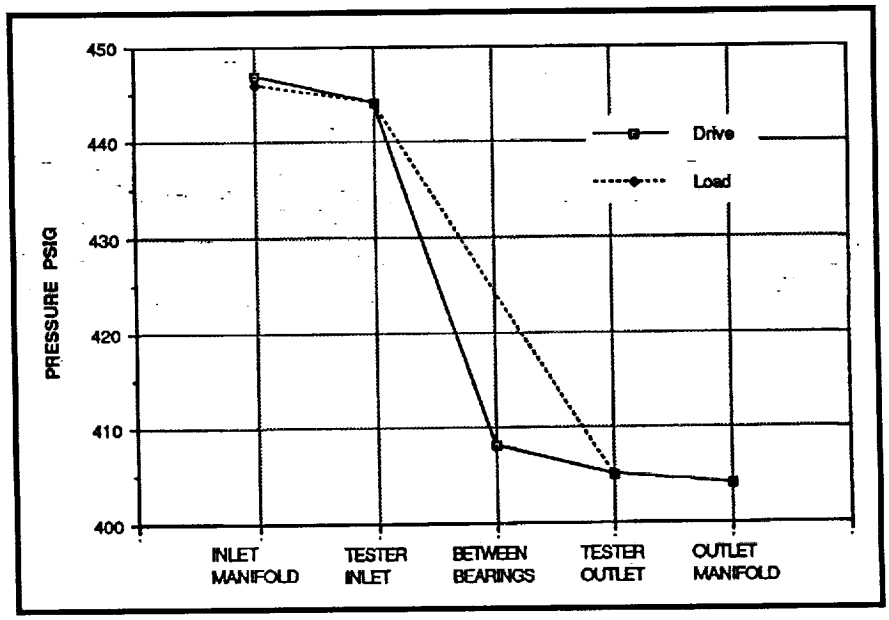

Exhibit 239 Pressure Profile for BSMT Test 3070302

The borescope examination of the bearings showed that Bearing 1 had balls with wide light brown load tracks

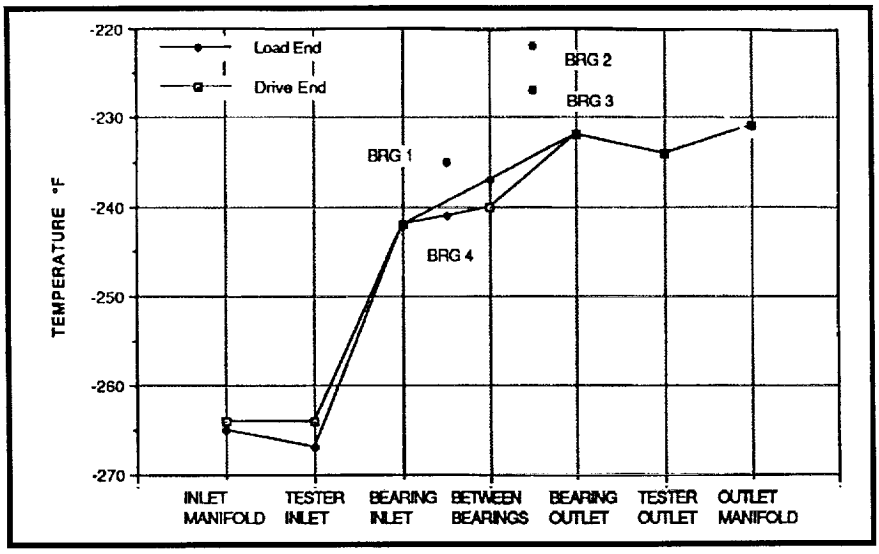

Exhibit 240 Temperature Profile for BSMT Test 3070401

but no evidence of Teflon transfer. The surface of the balls was still fairly smooth. The cage was in good condition with no evidence of wear in the pockets visible. The cage of Bearing 2 was also in good condition. The silicon nitride balls of Bearing 2 did have white smears of Teflon. Only two balls showed light narrow tracks on their surface. Bearing 3 balls, however, did show signs of the increased heat generation. They had dark splotches all over their surface but the surface was still smooth. It is believed that the race surfaces may be degraded but cannot be seen with the borescope. The cage of Bearing 3 still showed no signs of wear. The surface of Bearing 4 balls had a "frosty" appearance indicating a roughened finish. They also had medium brown tracks in random paths over the surface. No evidence of wear in the cage pocket was visible with the borescope.

Test 3070601. This test was planned for a LO_2 run tank depletion long duration run at 30,000 RPM. However, the test was cut early by speed sensor RPM2 reading high. It was determined that the sensor had gone bad after approximately 700 seconds at speed. Since the test lasted almost half the planned time it was decided not to recycle the test.

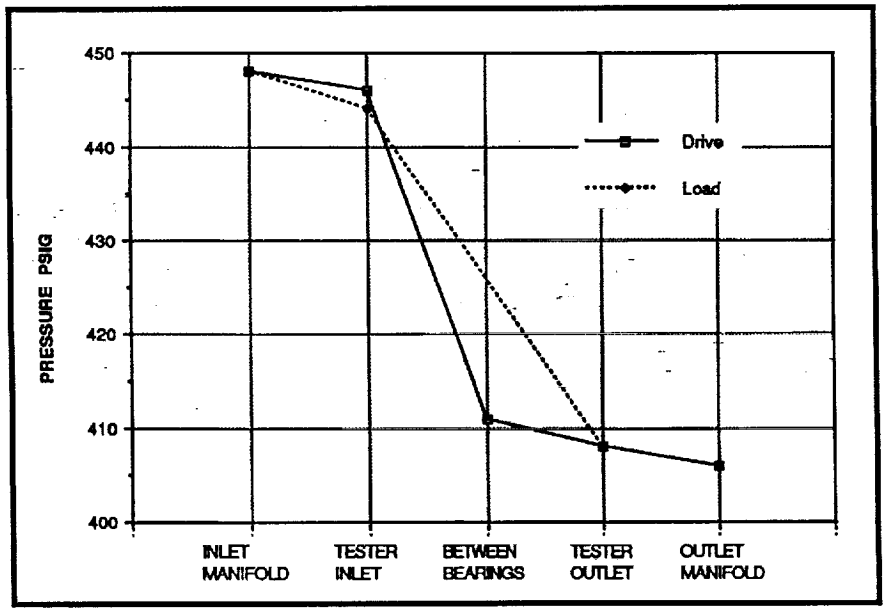

Exhibit 241 Pressure Profile for BSMT Test 3070401

The test parameters and selected data were provided in **Exhibits 234** and **235**. The temperature and pressure profiles through the tester are shown in **Exhibits 244** and **245**, respectively. The test results were very similar to the data from the previous test in which the heat generation across Bearing 2 was elevated slightly compared to earlier tests. The heat generation across Bearing 3 was

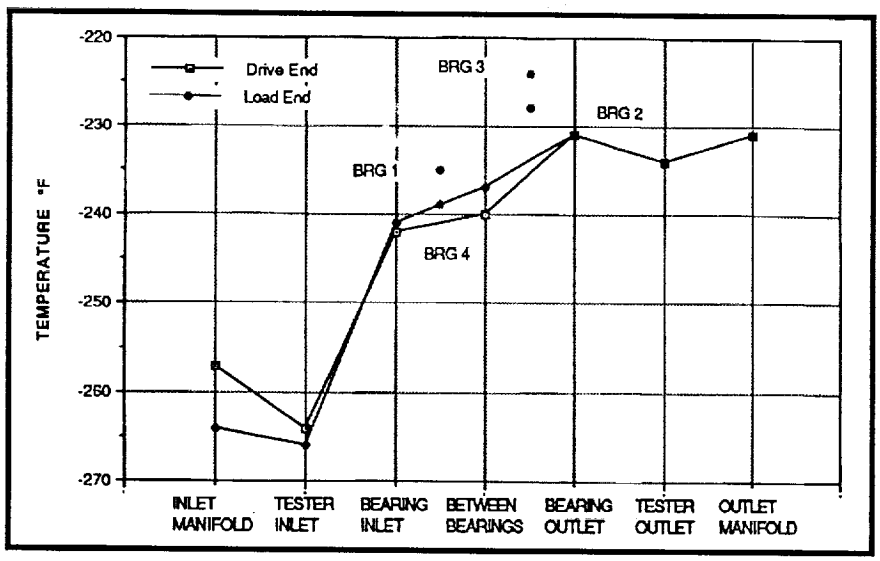

Exhibit 242 Temperature Profile for BSMT Test 3070501

back down to its previous level prior to Test 3070501. The viscous inlet vortex work on the load end of the tester was increased. This was due to T1001 reading 2°F lower than in previous runs. This measurement was suspect since it was reading 3°F colder than an upstream reading.

The borescope inspection showed that the bearings' appearance had not changed much from the previous inspection. Bearing 1 cage was still in good condition. The balls of Bearing 1 did show that the light brown track were getting a roughened "frosty" surface. The silicon nitride balls of Bearing 2 looked even cleaner than the previous run (3070501). The balls had only an occasional metallic speck on their surface. The cage of Bearing 2 showed no evidence of wear. Bearing 3 had dark brown to black splotches on the ball surfaces with no definite tracks. The cage, however, looked to be in good condition. Bearing 4 balls still had the "frosty" brown tracks but the cage was still in good condition.

Test 3070702. This test was planned for a full duration LO_2 run tank depletion run at 30,000 RPM. The first attempt (3070701) was cut after approximately 150 seconds at speed by RPM2 reading high. The instrument was judged to be faulty because all other instrumentation showed no anomalies. The redline was changed to RPM1002 and the test was recycled. The second attempt was successfully run to LO_2 depletion, but unfortunately at that time the run tank was less than half full. Only 380 second at speed was accumulated on the second run.

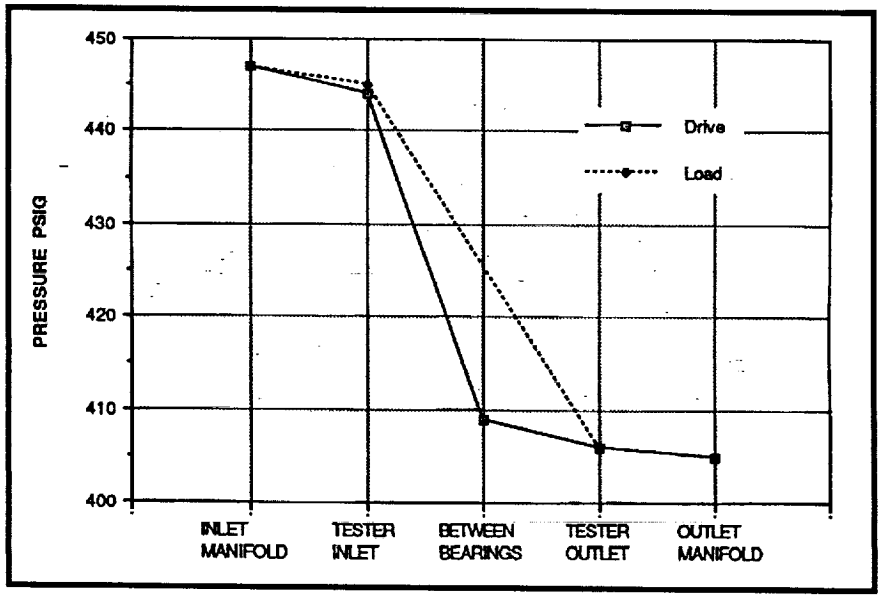

Exhibit 243 Pressure Profile for BSMT Test 3070501

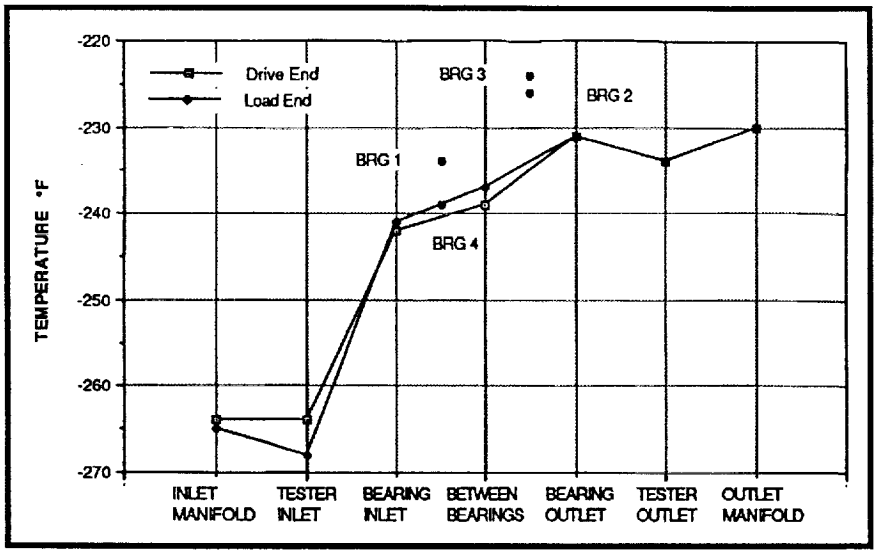

Exhibit 244 Temperature Profile for BSMT Test 3070601

Test parameters and selected data were shown in **Exhibits 234** and **235**. Illustrated in **Exhibit 246** and **247** are the temperature and pressure profiles through each end of the tester. The measured parameters were again very similar to the previous test except for the pressure drop and heat generation across the load end bearings. The load end pressure drop increased ~10% while the heat generation decreased by 10%. This phenomenon was not understood at the time since it was believed for the BSMT that higher pressure drops cause higher loads and more heat generation.

The borescope examination of Bearing 1 again showed the brown "frosty" tracks on the balls. The cage was in good condition. Bearing 2 components looked very good. The ball surface had almost no marks and the cage showed no wear. Bearing 3 balls, however, had dark brown bands or tracks over most of their surfaces but the cage was still in good condition. The balls of Bearing 4 had "frosty" brown tracks all over their surface. Evidence of ball to cage contact in the fore and aft position was visible on the Bearing 4 cage but was not excessive.

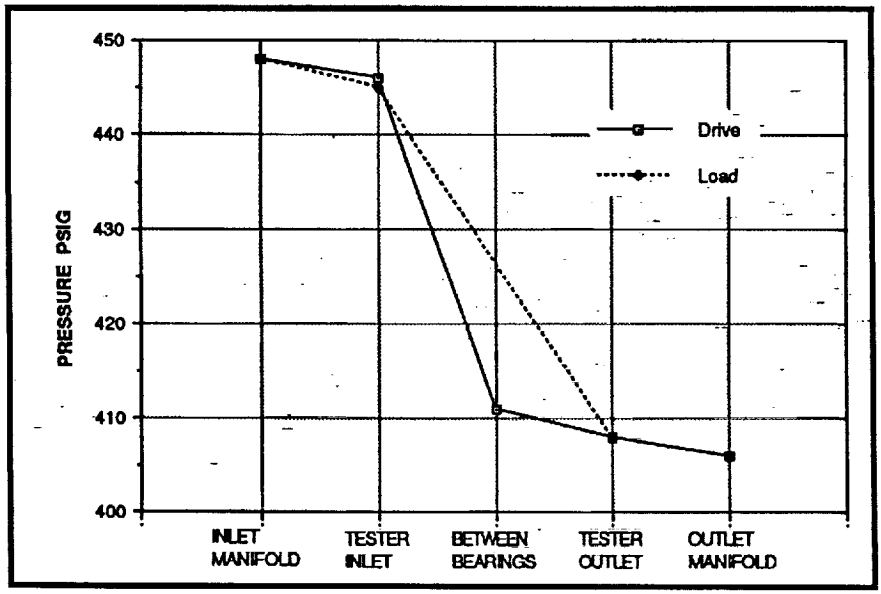

Exhibit 245 Pressure Profile for BSMT Test 3070601

Test 3070801. The test was scheduled for a full duration LO_2 run tank depletion at 30,000 RPM with 700 lb (3100N) radial load per bearing. The test was cut after approximately 1000 second at speed by T1005 (Bearing 2 outer race temperature) exceeding the -220°F (133K) redline. The data was reviewed and the temperature spike was judged to be real.

Shown in **Exhibits 234** and **235** were the test pa-

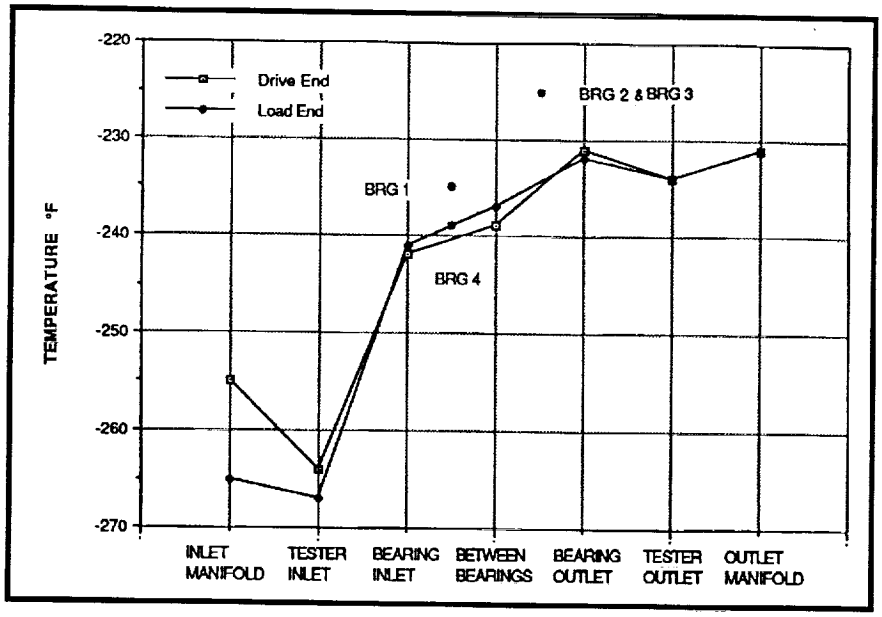

Exhibit 246 Temperature Profile for BSMT Test 3070702

rameters and selected data. The temperature and pressure profiles through both ends of the tester are shown in **Exhibits 248** and **249**, respectively. Comparison of this test data to the data of previous runs in this series showed virtually the same temperature and pressure trends. However, toward the end of the run the inlet fluid temperatures were increasing due to the fluid in the run tank warming up. This caused all of the other temperatures in the tester to increase correspondingly. The outer race temperature readings of the inboard bearings had risen to -222°F (132K) when Bearing 2 measurement spiked over the -220°F (133K) redline. The pressure reading between Bearings 3 and 4 was measuring fluctuations of 10 psi (70 KPa) early in the run but then stabilized to a gradual rise of about 5 psi (35KPa) over the remainder of the test. These pressure anomalies are indications of bearing degradation.

After the test, the bearings were inspected through a borescope. Bearing 1 cage was in good condition. The balls had brown tracks in random orientations. Bearing 2 balls had white to silver colored smears but the surfaces were still smooth. The discoloration of the silicon nitride balls could have been caused by wear debris from the races. It was reported by the test technicians that metallic particles were captured in the downstream fluid filters after this run. The cage in Bearing 2 had no visible signs of wear. The balls of Bearing 3 had the same dark brown tracks that were seen after the previous run. One ball had a small defect observed on the surface that is suspected to be a tiny spall. This defect was later verified after

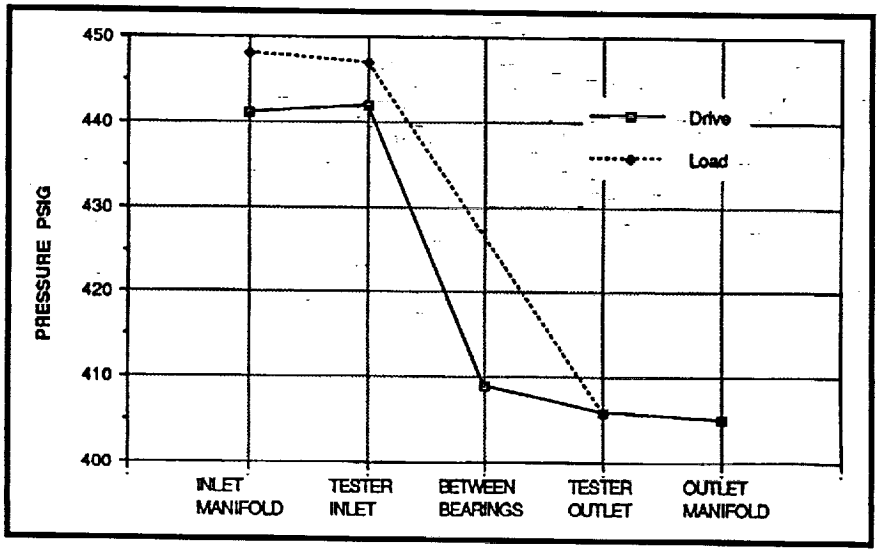

Exhibit 247 Pressure Profile for BSMT Test 3070702

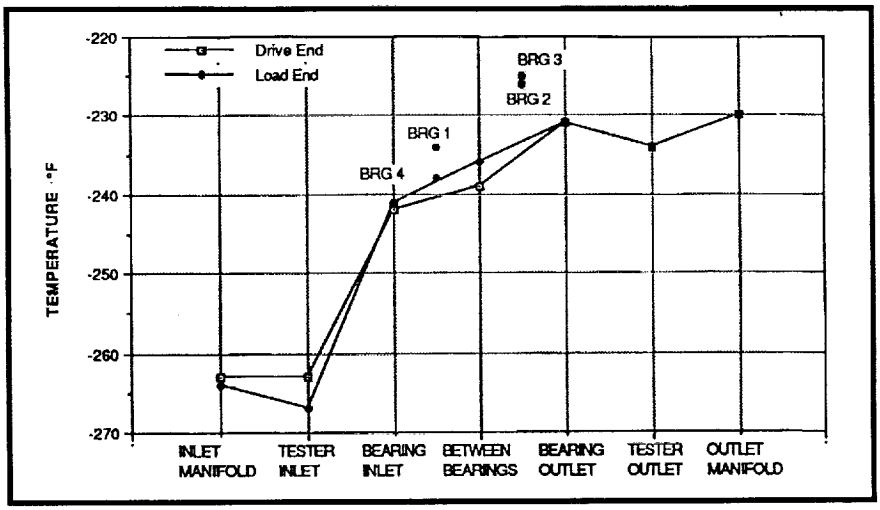

Exhibit 248 Temperature Profile for BSMT Test 3070801

tester disassembly. Bearing 3 cage showed no signs of wear. Bearing 4 looked much the same as after the previous run with brown tracks all over the surface of the balls and possibly only slight wear in the cage pockets.

Test 3070901. This test was planned for LO_2 run tank depletion. The test was cut by T1006 (Bearing 3 outer race temperature) exceeding the -220°F (133K) redline. Approximately 1130 seconds was accumulated at 30,000 RPM before the cut. The reason the race temperature exceeded the redline was because the LO_2 was getting low in the run tank and the inlet fluid temperatures were increasing.

The test parameters and selected data are shown in **Exhibits 250** and **251** along with data from previous runs in this test series. The temperature and pressure profiles through the tester are shown in **Exhibits 252** and **253**, respectively. The data trends were very similar to the previous run. However, the absolute value for most of the fluid temperature measurements were oscillating in a sine wave pattern with a peak to peak variation of approximately 2°F. This phenomenon was due to instrumentation problems and the fluid temperatures were not actually oscillating since not all the coolant temperatures in the flow path exhibited the oscillations.

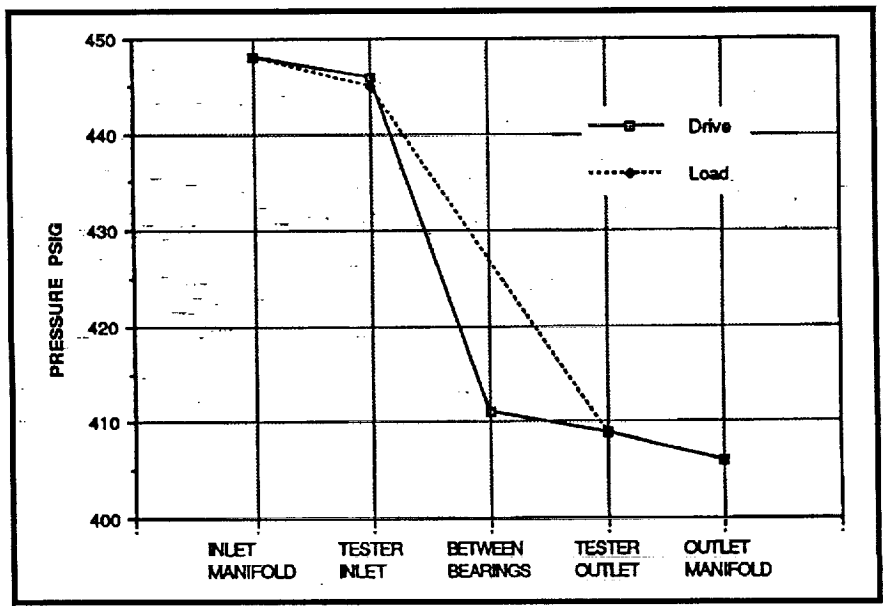

Exhibit 249 Pressure Profile for BSMT Test 3070801

After the test, the bearings were inspected through a borescope. Bearing 1 balls were a dark silver color with narrow brown tracks. The ball surfaces were still relatively smooth. The cage was still in good condition with no visible signs of degradation. The balls of Bearing 2 had either one or two wide brown tracks but the surface appeared to be smooth. No wear on the cage could

be seen. Bearing 3 ball had several narrow brown tracks in random patterns on their surface. The spall which was first seen after the previous run had not grown in size. The Bearing 3 cage was still in good condition. Beaing 4 balls looked much the same as previously with a "frosty" brown finish over the entire ball surface. The cage appeared to still be in good condition.

Test 3071001. This was the ninth rotational test in this series and was scheduled for LO_2 run tank depletion at 30,000 RPM with 700 lb radial load. The test was cut after about 730 seconds at speed by bearing 3 outer race temperature measurement (T1006) exceeding the -220°F (133K) redline. The T1006 measurement was averaging about -222°F (132K) but was erratic during the entire run. This erratic outer race measurement was an indication that the bearing was in degraded condition.

Test parameters and selected data for this test were shown in **Exhibits 250** and **251**. The test data showed that the coolant temperature across Bearing 3 were increased compared to previous runs. This trend can be seen in the coolant

	TEST NUMBER									
Test Parameter	3070302	3070401	3070501	3070601	3070702	3070801	3070901	3071001	3071101	3071201
Shaft Speed (RPM)	30,000	30,000	30,100	30,100	30,100	30,000	30,000	30,000	30,000	30,000
Time at Speed (sec)	300	300	1320	700	380	1000	1130	730	32	500
Flow Rate (lbs/sec)	6.4	6.4	6.4	6.4	6.4	6.4	6.4	6.4	6.4	6.4
Brg #4 Inlet Temp (°F) T1018	-243	-242	-242	-242	-242	-242	-242	-243	-243	-242
Between Brgs 3 & 4 (°F) T1024	-241	-240	-240	-239	-239	-239	-239	-240	-239	-239
Brg #3 Outlet Temp (°F) T1019	-233	-232	-231	-231	-231	-231	-231	-231	-232	-231
Brg #1 Inlet Temp (°F) T1021	-242	-242	-241	-241	-241	-241	-241	-242	-244	-242
Temp Between Brgs 1 & 2 (°F) T1023	-238	-237	-237	-237	-237	-236	-236	-237	-237	-237
Brg #2 Outlet Temp (°F) T1022	-233	-232	-231	-231	-232	-231	-231	-232	-232	-232
Tester Inlet Temp (°F) T1001 T1002	-268 -265	-267 -264	-266 -264	-266 -264	-267 -264	-267 -263	-267 -263	-267 -264	-267 -265	-267 -264
Tester Outlet Temp (°F) T1003	-236	-234	-234	-234	-234	-234	-233	-234	-235	-234
Tester Inlet Pressure (psig) PA1001 PA1002	444 444	444 446	445 444	445 445	447 442	445 446	444 444	446 448	476 444	444 445
Tester Outlet Pressure (psig) PA1003	405	406	406	406	406	406	406	406	406	407
Pressure Between Brg 3 & 4 (psig) P1006	408	411	409	411	409	411	412	420	410	409
Horsepower	300	300	300	300	300	300	300	300	300	300
Torque (in-lbs)	13,886	13,800	13,800	13,800	13,770	13,730	13,750	13,930	14,000	13,860
Brg #1 O.R. Temp (°F) T1004 (TA1004)	-264 (-237)	-262 (-235)	-259 (-235)	-261 (-234)	-258 (-235)	-260 (-234)	-260 (-233)	-262 (-235)	-261 (-245)	-260 (-233)
Brg #2 O.R. Temp (°F) T1005 (TA1005)	-230 (-234)	-227 (-234)	-228 (-233)	-226 (-233)	-225 (-233)	-226 (-232)	-225 (-232)	-224 (-233)	-227 (-234)	-223 (-233)
Brg #3 O.R. Temp (°F) T1006 (TA1006)	-221 (-235)	-222 (-234)	-224 (-234)	-224 (-233)	-225 (-233)	-225 (-233)	-224 (-233)	-222 (-234)	-225 (-234)	-219 (-232)
Brg #4 O.R. Temp (°F) T1007 (TA1007)	-263 (-242)	-262 (-241)	-261 (-239)	-261 (-239)	-261 (-239)	-261 (-238)	-261 (-238)	-261 (-237)	-262 (-241)	-261 (-236)

Exhibit 250 BSMT Test Conditions and Selected Data (Test 3071001)

PARAMETER	3070302	3070401	3070501	3070601	3070702	3070801	3070901	3071001	3071101	3071201
• Delta Temp Across Brg Pair (°F)										
T1022-T1021	10.0	10.0	10.0	10.0	9.0	10.0	10.0	10.0	12.0	10.0
T1019-T1013	11.0	10.0	11.0	11.0	11.0	11.0	11.0	12.0	11.0	11.0
• Delta Temp Across Brg 1 (°F)										
T1023-T1021	5.0	5.0	4.0	4.0	4.0	5.0	5.0	5.0	7.0	5.0
Brg 2										
T1022-T1023	5.0	5.0	6.0	6.0	5.0	5.0	5.0	5.0	5.0	5.0
Brg 3										
T1019-T1024	8.0	8.0	9.0	8.0	8.0	8.0	8.0	9.0	7.0	8.0
Brg 4										
T1024-T1018	3.0	2.0	2.0	3.0	3.0	3.0	3.0	3.0	4.0	3.0
• Brg Outer Race Temp - Fluid Inlet Temp (°F)										
Brg 1										
TA1004-T1021	5.0	7.0	6.0	7.0	6.0	7.0	8.0	7.0	1.0	9.0
Brg 2										
T1005-T1023	8.0	10.0	9.0	11.0	12.0	10.0	11.0	13.0	10.0	14.0
Brg 3										
T1006-T1024 (TA1006-T1024)	20.0 (6)	18.0 (6)	16.0 (6)	15.0	14.0	14.0	15.0	18.0	14.0	20.0
Brg 4										
TA1007-T1018	1.0	1.0	3.0	3.0	3.0	4.0	4.0	6.0	2.0	6.0
• Heat Generated (Btu/sec) Across										
Brg 1	14.3	14.8	11.7	11.8	11.8	14.6	14.7	14.7	19.9	14.3
Brg 2	14.3	14.8	17.5	17.7	14.7	14.8	14.9	14.8	14.6	14.6
Brg 3	23.1	23.2	28.2	23.3	23.4	23.8	23.3	26.2	20.3	23.2
Brg 4	8.7	8.7	5.8	8.8	8.8	8.7	8.7	8.6	11.4	8.8
• Heat Generated Across										
Brg 1&2	28.6	29.6	29.2	29.5	26.5	29.4	29.6	29.5	34.5	28.9
Brg 3&4	31.8	29.0	32.0	32.1	32.2	32.5	32.0	34.8	31.7	32.0
• Inlet Vortex Work (Btu/sec)										
Load	71.2	68.6	68.8	74.0	71.6	71.4	71.6	68.5	63.0	68.8
Drive	60.5	60.8	60.5	59.7	60.7	57.8	57.8	57.8	60.5	60.5
• Pressure Drop (psi)										
Brg 3	2	3	3	3	3	3	6	12	2	2
Brg 4	37	35	35	35	33	35	32	28	34	36
Brg 1&2	39	36	39	37	41	37	38	38	68	37
Brg 3&4	39	38	38	38	36	38	38	40	36	38
• Subcooling °F	38	38	38	37	37	38	38	38	40	38
• Radial Load (lbs/brg)	650	700	700	700	700	700	700	700	700	700

Exhibit 251 BSMT Test Parameters Comparison (Test 3071101)

temperature profile through the tester shown in **Exhibit 254**. There was also in increase in the pressure drop across Bearing 3 compared to the previous run. The pressure profile through the tester is shown in **Exhibit 255**.

The bearings were examined through a borescope after the test. Bearing 1 balls were a dull dark silver color on the surface with random brown tracks and the cage appeared to be in good condition. The balls of Bearing 2 had one distinct wide brown track with random narrow brown bands. Their surfaces were still smooth with no pits or spalls observed. The cage of Bearing 2 appeared in good condition. The appearance of the Bearing 3 balls was generally good. There were dark brown to black tracks with very fine shiny particles in the tracks. The tracks formed random patterns on the balls. The suspected spall that was observed after the two previous runs was not visible after this run. The Bearing 3 cage was still in good condition. The Bearing 4 balls were still "frosty" gray with no definite track patterns visible. The Bearing 4 cage showed no signs of degradation.

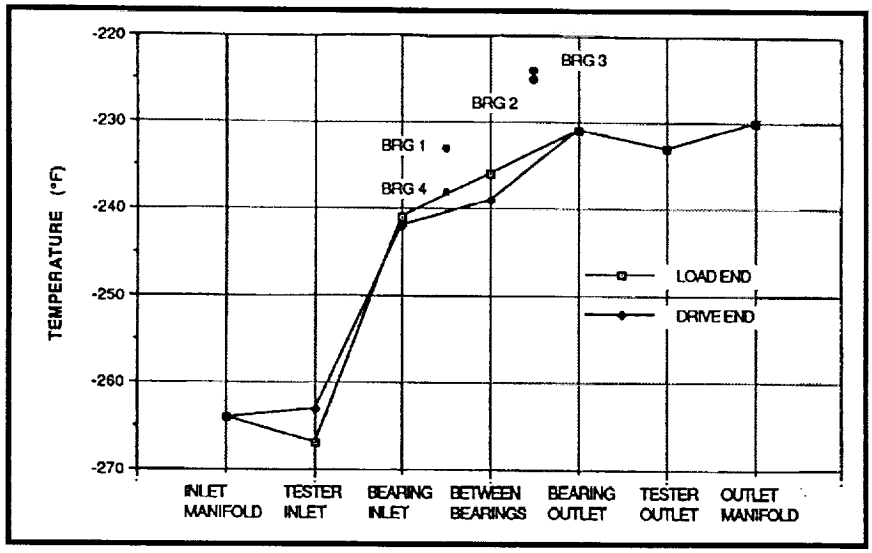

Exhibit 252 Temperature Profile for BSMT Test 3070901

Test 3071101. This test was scheduled for LO2 run tank depletion at 30,000 RPM and 700 lb (3114N) radial load per bearing. The test was cut prematurely after about 32 seconds at speed due to the pressure drop across the load end bearings (P33) exceeding the 80 psi (552 KPa) redline. The "quick look" data was reviewed and the high reading was verified to be real. The pressure drop across the drive end bearings was reading the normal value of about 40 psi (276 KPa). All temperature measurements were reading normal giving no indication of what the problem could have been. It was decided to attempt the test again.

The second attempt at this test (3071102) was cut before reaching speed by exit cavity pressure (PA1003) reading low. The cause of the low tester pressure was that Bearing 1 inlet coolant thermocouple (T1021) had blown out of its retainer allowing the coolant to escape the housing. The T1021 thermocouple was also the cause of the high pressure drop problem during the first attempt at this test. It was believed that the thermocouple had backed out from its proper position at the pitch diameter of the bearing. In its proper position, the thermocouple limits the amount of preswirl of the fluid in the inlet cavity before the coolant enters Bearing 1. When the thermocouple backed out of the inlet cavity, the vortex or preswirl was increased causing a higher pressure gradient between the inlet and exit pressure readings.

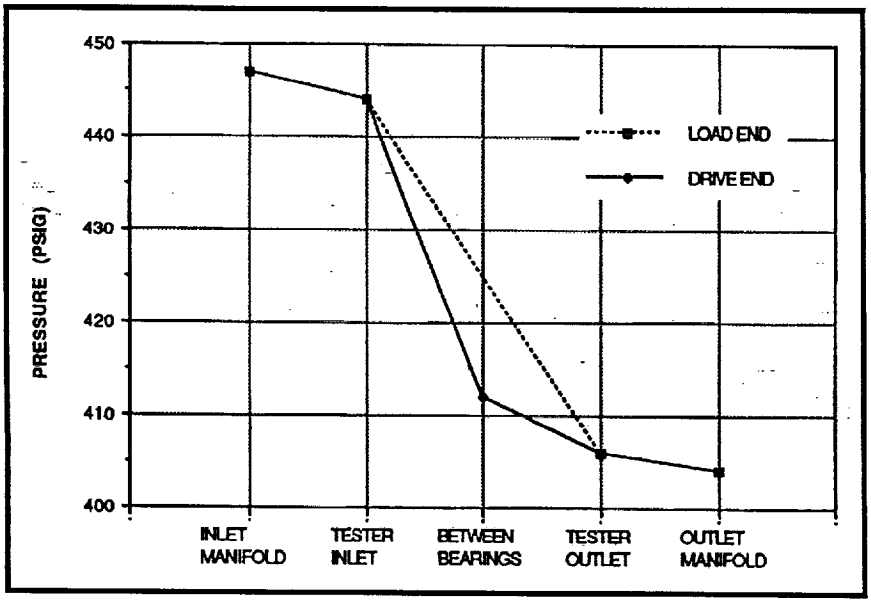

Exhibit 253 Pressure Profile for BSMT Test 3070901

The test parameters and selected data for this test at speed were shown in **Exhibits 250** and **251**. The temperature and pressure profiles for the first attempt at this test are provided in **Exhibits 256** and **257**, respectively.

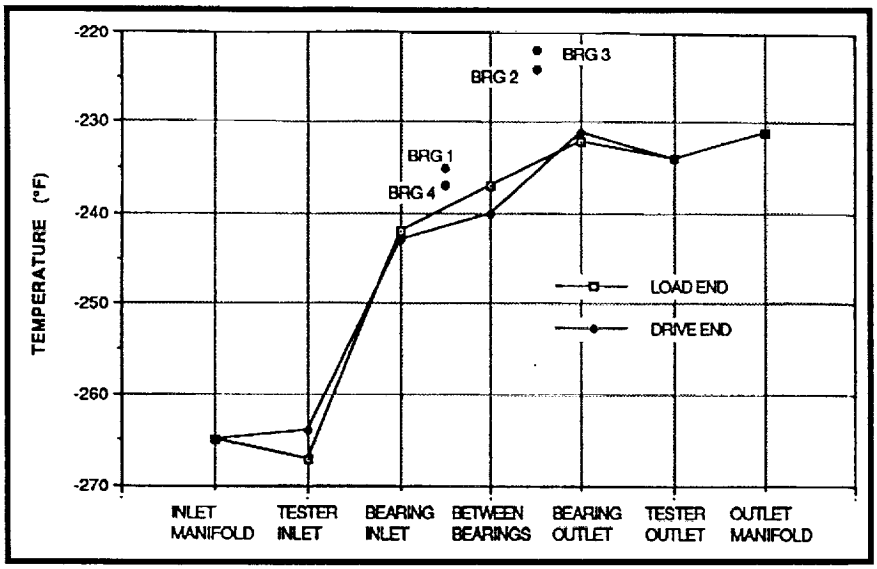

Exhibit 254 Temperature Profile for BSMT Test 3071001

The bearings were inspected through a borescope after the test. The bearings did not appear to be damaged by the anomalies of this test. Bearing 1 had random golden tracks on the balls. The cage was in good condition. The balls of Bearing 2 had dark brown tracks with silver to white splotches over the surface. It was speculated that the silver color was 440C material on the silicon nitride balls. Bearing 2 cage was in good condition. Bearing 3 balls only had dark brown tracks, no white material seen in Bearing 2. Bearing 3 cage also appeared to be in good condition. The balls of Bearing 4 still appeared "frosty" gray with only random light golden tracks. Bearing 4 cage looked in good condition.

This was the eleventh rotational test in this series. The test was planned for LO_2 run tank depletion at 30,000 RPM with 700 lbs (3114N) radial load per bearing. The test was terminated by Bearing 3 outer race temperature measurement (T1006) exceeding the new redline for this test of -215°F (136K). The amount of test time accumulated for this run was approximately 600 seconds. The T1006 measurement was erratic during the entire run which was an indication of a degraded bearing.

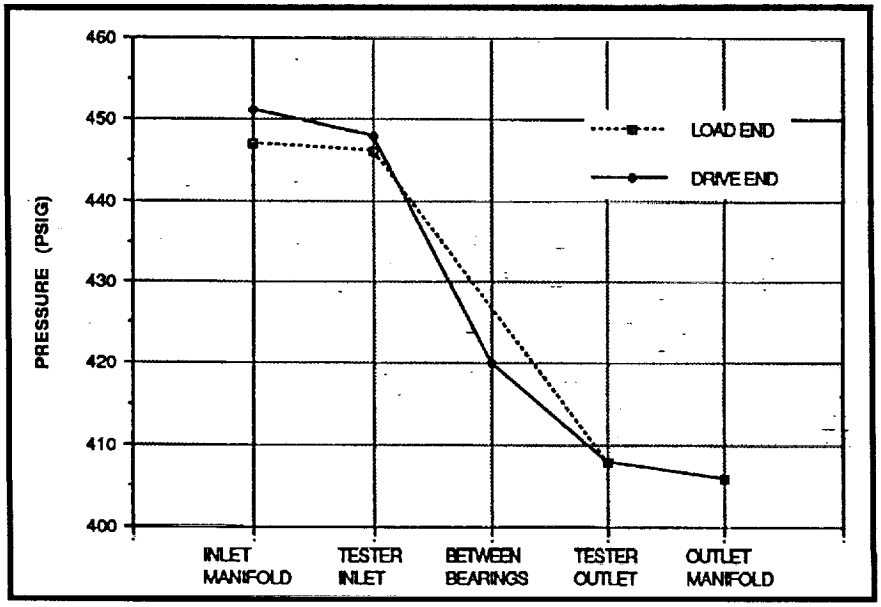

Exhibit 255 Pressure Profile for BSMT Test 3071001

The test parameters and selected data for this test were provided in **Exhibit 250** and **251**. The temperature and pressure profiles through the tester are shown in **Exhibits 258** and **259**, respectively. All the parameters looked normal for this test except for the elevated temperature of the Bearing 3 outer race.

The borescope inspection showed the bearings to be in much the same condition as after the previous

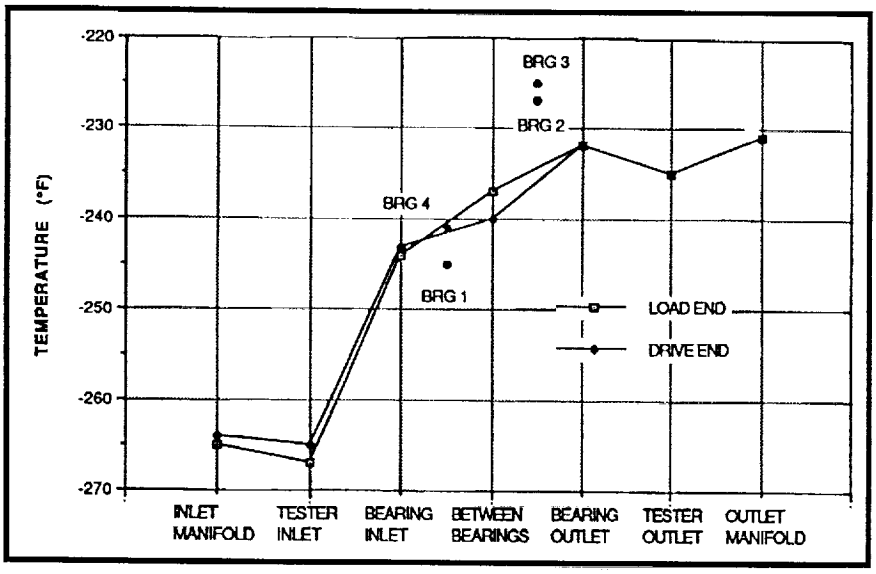

Exhibit 256 Temperature Profile for BSMT Test 3071101

test run. Bearing 1 still had the random golden tracks on the surface of the balls and the cage was in good condition. Bearing 2 had a dark brown track on each ball. A few metallic specks were also present on the ball surfaces. The cage of Bearing 2 appeared in good condition. The balls of Bearing 3 had no brown tracks but rather had dark gray to black smears and their surfaces appeared to have a "frosty" finish. The cage of Bearing 3 looked to be in acceptable condition. Bearing 4 looked much like Bearing 1 with random golden tracks on the balls and a good cage.

The following two tests were attempted with Unit 3 Build 7. The bearing configuration for this unit contained Battelle cages in all four bearings, silicon nitride balls in the inboard bearings and 440C stainless steel balls in the outboard bearings. The main objective of this test series was to verify the operation of the Battelle cage subjected to large ball excursions similar to those predicted for the SSME HPOTP pump end bearings. Radial load was applied to the tester to produce the desired ball excursion in the outboard bearings. Eleven rotational tests were previously completed and the accumulated run time at 30,000 RPM was more than twice the desired service life of the cage. The following tests addressed a second objective. This objective was to determine how much run time at 30,000 RPM the silicon nitride balls in the inboard bearings could accumulate, under the high contact stresses caused by the radial and parasitic pressure loads, before signs of degradation on the balls were visible.

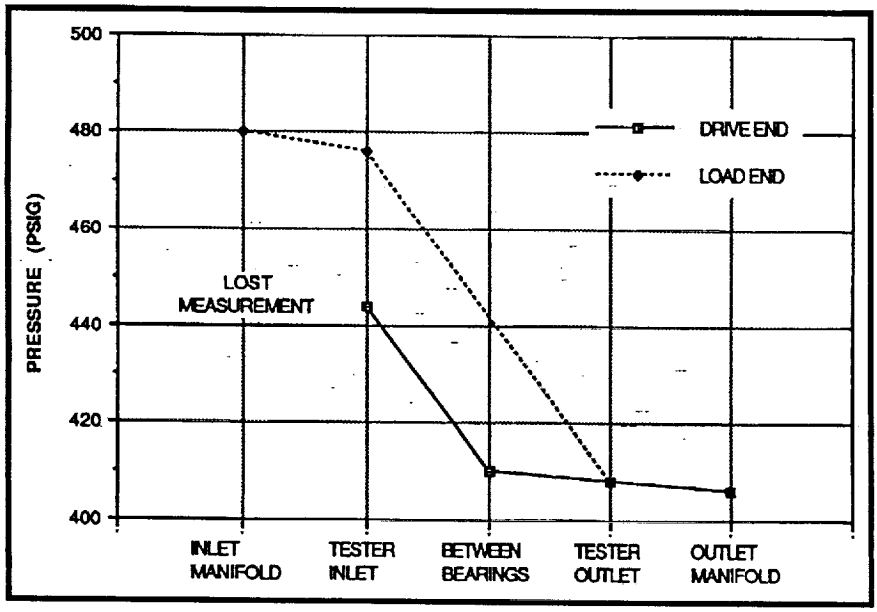

Exhibit 257 Pressure Profile for BSMT Test 3071101

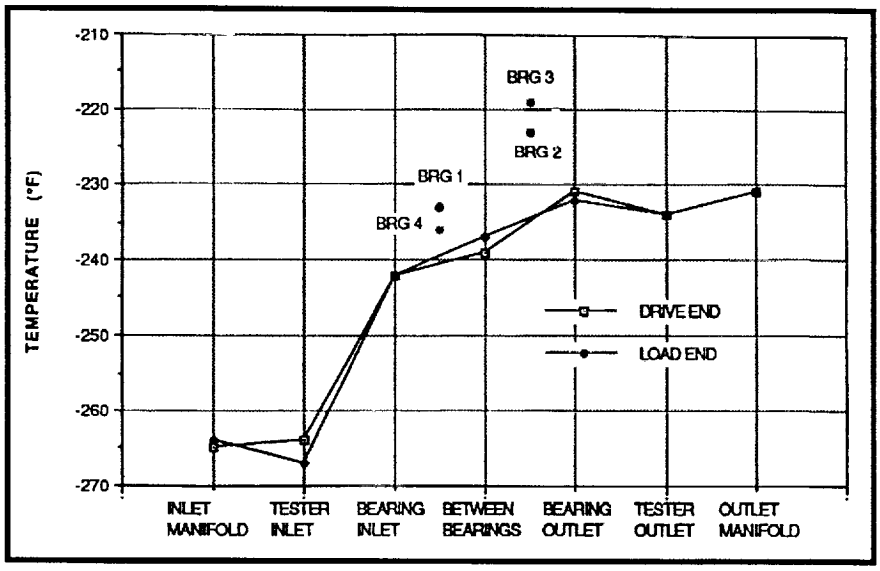

Exhibit 258 Temperature Profile for BSMT Test 3071201

Summary of Tests 3071301 and3071302

This test was planned for a speed of 30,000 RPM and a maximum time duration allowed by the run tank capacity which is approximately 20 minutes. A radial load of 700 lbs (3115N) per bearing was applied when the shaft speed reached 15,000 RPM. The first attempt was terminated by Bearing 3 outer race temperature exceeding the redline value of -215°F (136 K) before the test speed of 30,000 RPM was reached. The test was recycled and attempted again but with the same results. Studying the "quick look" data indicated that the Bearing 3 outer race temperature measurement was real and would not level off below the redline. It was decided to borescope the tester to visually inspect the bearings in an attempt to identify the reason for the rapid temperature rise of this bearing.

The borescope inspection after the test attempts showed all the bearings to be in relatively good condition. All of the Battelle cages were in excellent condition. The balls of Bearing 1 were smooth with random light golden tracks. Bearing 2 balls had dark brown tracks that formed a smeared pattern. The balls also had what appeared to be tiny metallic specks on their surface. The balls of Bearing 3 had wide dark brown tracks with a speckled texture. It appeared that this bearing did actually get hot, but the cause was not evident. Apparently the race surfaces were degraded causing a higher coefficient of friction. However, this could not be verified since the tracks of the races are not visible in the borescope. Bearing 4 balls had a "frosty" finish with a light golden color.

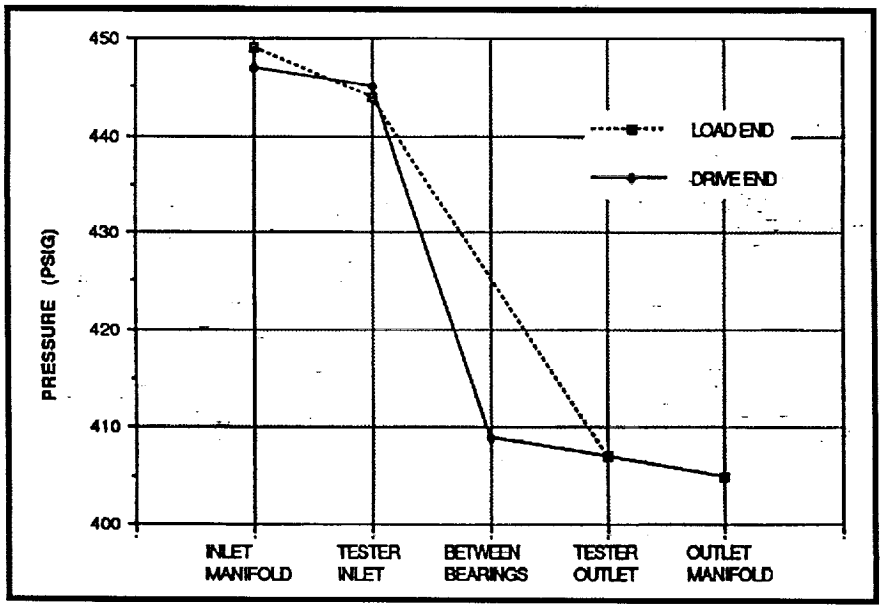

Exhibit 259 Pressure Profile for BSMT Test 3071201

Summary of Tests 3071401 and 3071402. Another test run was planned since the bearings still appeared to be in relatively good condition. This test was planned with colder coolant inlet temperature. The colder LO2 was used in an effort to lower the operating temperature of the Bearing 3 outer race below the redline value. All other operating parameters were the same as in the previous test. The first test attempt was cut after only a few seconds by the shaft torque (TQ1) breaking the high redline. Reviewing the data showed that the shaft speed measurement (RPM1004) did not indicate the speed increase. RPM1004 was used by the automatic speed controller and, since it showed no speed the controller kept increasing the speed until the torque required to turn the shaft exceeded the redline. The test technicians discovered that the sensor had become disconnected. The RPM1004 sensor was reconnected and the test was repeated. The speed controller worked properly and the radial load was applied at 15,000 RPM. Before the 30,000 RPM test speed was reached, the Bearing 3 outer race temperature (T1006) broke the high redline and cut the test. The tester was borescoped after the test but no visual differences were observed in the bearings' condition from the previous test. It was decided to conclude this test series and disassemble the tester. The bearings were later inspected after disassembly to assess their condition.

5.6 Unit 3, Build 7 Summary

The primary purpose of this test series was to demonstrate the successful use of the Battelle cage in a bearing operating with high ball excursions under environmental operating conditions similar to the HPOTP. These cages were designed and manufactured by Battelle Columbus Laboratories. This cage design utilizes a bronze/phosphorus structure with Salox ball pocket inserts. Due to the web structure thickness, the number of ball pockets for this cage design was reduced from 13 to 12. Also, the cages used in this test had oval ball pockets to simulate the pocket clearance of the HPOTP 45mm pump end bearings. The outboard bearings (Brgs 1 and 4) were the test bearings for cage pocket loading because the shaft loading on these bearings produced the most ball excursion. The outboard bearings were installed with 440C balls because they produce higher ball excursions than silicon nitride balls. The inboard bearings (Brgs 2 and 3) were installed with silicon nitride balls to withstand the severe loading on them which was required to produce the desired loading on the outboard bearings. The shaft loading was similar to the previous test series (Unit 2 Build 14), however, the maximum steady-state contact stress was slightly higher due to the reduced number of balls used with the Battelle cage. A complete description of the bearing configurations is provided in **Table 1**.

This was one of a series of tests conducted in the MSFC Bearing and Seal Materials Tester (BSMT) to evaluate rolling element bearings, seals, and advanced or alternate bearing and seal materials. Tests were conducted in environments similar to those in flight engine turbopumps. These tests were conducted in order to find the most promising designs and materials to be further demonstrated in a test bed engine and ultimately incorporated into flight engine turbopumps. A cross section of the BSMT is shown in **Exhibit 260**.

Highlights. This test series consisted of eleven rotational tests. Maximum run time for a test was limited to approximately 22 minutes due to the capacity of the LO2 run tank. Approximately

Position 1 (Load End):	P/N RS007955-261 S/N 14 Inner Race, 440C, Curvature 0.55 Outer Race, 440C, Curvature 0.53 12 Balls, 440C, Diameter 12.7 mm (0.5 in.) Cage, Bronze/Phosphorus with Salox Pocket Inserts Internal Clearance, 0.1549 mm (0.0061 in.)
Position 2 (Load End):	P/N RS007955-261 S/N 18 Inner Race, 440C, Curvature 0.55 Outer Race, 440C, Curvature 0.53 12 Balls, Si3N4, Diameter 12.7 mm (0.5 in.) Cage, Bronze/Phosphorus with Salox Pocket Inserts Internal Clearance, 0.1549 mm (0.0061 in.)
Position 3 (Drive End):	P/N RS007955-261 S/N 8687047 Inner Race, 440C, Curvature 0.55 Outer Race, 440C, Curvature 0.53 12 Balls, Si3N4, Diameter 12.7 mm (0.5 in.) Cage, Bronze/Phosphorus with Salox Pocket Inserts Internal Clearance, 0.1549 mm (0.0061 in.)
Position 4 (Drive End):	P/N RS007955-261 S/N 8687054 Inner Race, 440C, Curvature 0.55 Outer Race, 440C, Curvature 0.53 12 Balls, 440C, Diameter 12.7 mm (0.5 in.) Cage, Bronze/Phosphorus with Salox Pocket Inserts Internal Clearance, 0.1549 mm (0.0061 in.)

- All 440C components were dry film lubricated when new with Lubeco 905, which is a proprietary lubricant applied by the Lubeco Company.
- The Si_3N_4 balls were TSN-03H manufactured by Toshiba.

Table 1 BSMT Unit 3 Build 7 test Bearing Configuration

110 minutes of run time was accumulated at the nominal test speed of 30,000 RPM. The first rotational test was run with incremental speed increases to identify any tester assembly defects. The power required to rotate the shaft was increased approximately 7% from the previous test (Unit 2 Build 14). This was partly due to the increased ball excursion of the outboard bearings with the 440C balls. Between tests, the Battelle cages appeared to be in good condition as seen through the borescope. The inboard bearings, however, showed signs of degradation during the later tests. Outer race temperature of Bearing 3 was erratic and exceeded the redline cutoff terminating two tests. Borescope inspection showed that one ball of Bearing 3 had a slight spall. The run times, load configuration, and calculated Hertzian contact stresses are presented in **Table 2**.

Operating Summary. Unit 3 Build 7 test series experienced an unusually large number of instrumentation problems. Six test attempts were cut by instrumentation malfunctions. The Bearing 3 outer race temperature (T1006) caused the first cut. Based on the behavior of the reading it was judged that the thermocouple had gone bad. Two false test cuts were caused by a drive train speed sensor (RPM2) giving falsely high readings compared to other speed sensors. Two runs were cut by pressure readings. The pressure drop across the load end bearings (P33) cut high. The data were reviewed and no bearing problems could be detected, so the test was recycled. On the next attempt, the tester exit pressure (PA1003) cut low, because the inlet coolant temperature probe (T1021) had backed out of its retainer allowing coolant to escape. It was verified from further review of the data that T1021 had moved slightly in the previous test attempt allowing more inlet coolant preswirl causing the pressure drop across the bearings to be higher than normal. Another test attempt was cut by a high torque reading. The reading was real and the high torque was caused by the shaft being oversped due to the controller's speed sensor (RPM1004) being disconnected.

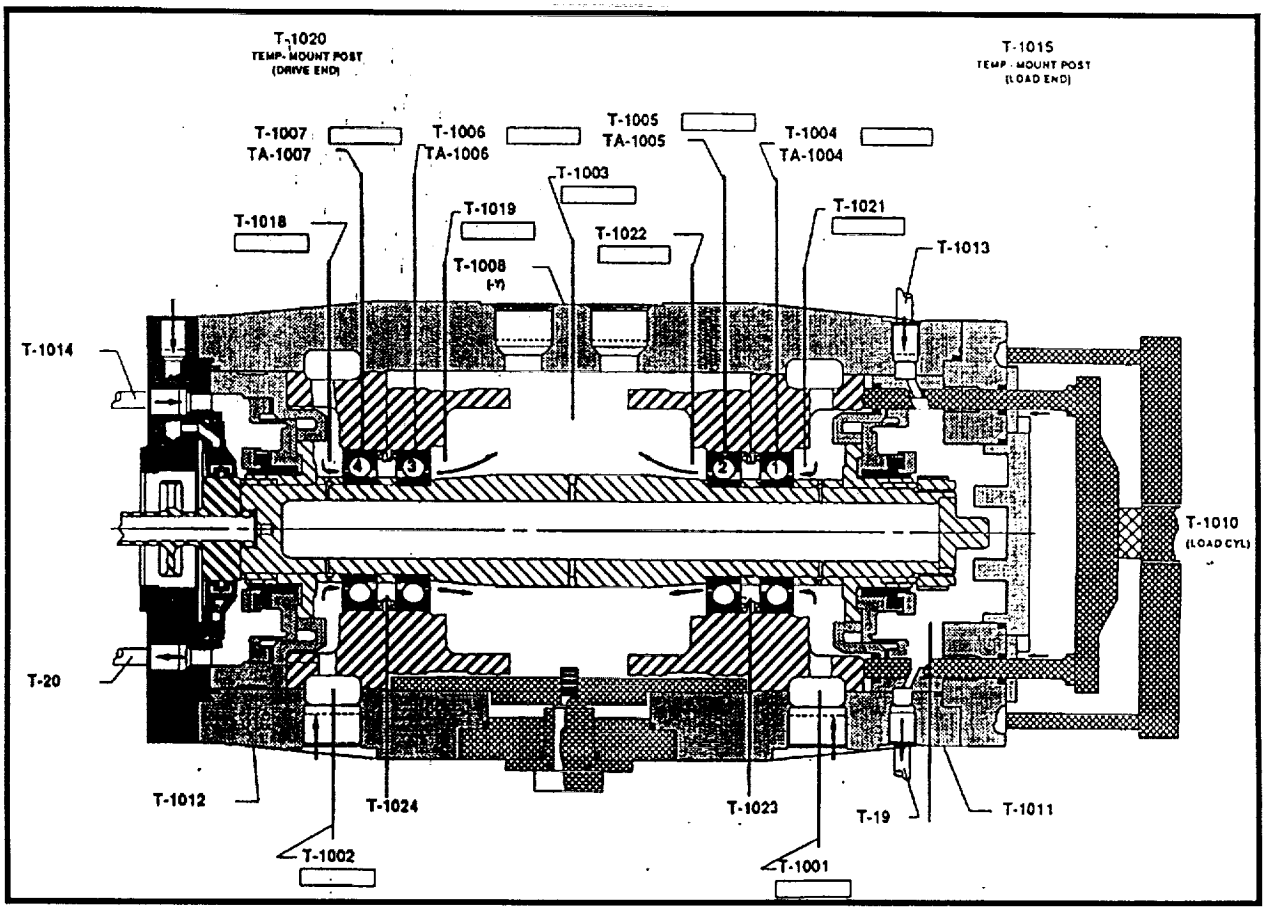

Exhibit 260 Tester Configuration with Temperature Instrumentation

Six test attempts were legitimately cut by bearing anomalies. During the seventh rotational test, Bearing 2 outer race temperature exceeded the -220 °F (133 K) high redline. Visual inspection of the bearing during post test borescope inspection indicated no bearing damage and testing was continued. During the ninth rotational test, Bearing 3 outer race temperature (T1006) exceeded the high redline. Borescope inspection showed only slight degradation of the bearing and testing was continued. However, no more successful runs were obtained due to T1006 exceeding the high redline before test speed was reached even when the value of the redline was increased to -215 °F (136 K) and 15 °F (8 K) colder inlet coolant was used.

Post Test Bearing Condition. Visual inspection of the bearings was performed after tester disassembly and their condition is graphically represented in **Exhibits 261** through **264**. Bearing 1 is represented in **Exhibit 261** and shows that the races were in very good condition. The inner race had a smooth contact path with good wide Salox transfer film. The outer race had a smooth track but only a narrow band of Salox transfer film. The cage was in excellent condition with no structural damage visible. The pockets showed moderate contact biased to the upstream side of the cage. The 440C steel balls of this bearing were in good condition with bronze Salox tracks covering most of their surface. Bearing 2 races, shown in **Exhibit 262**,

Test Number	Test Speed (rpm)	Time at Test Speed (sec)	Total Rotation Time (Sec)
O3070201	15,000	150	690
	25,000	100	
	28,000	125	
	30,000	130	
O3070302	30,000	300	450
O3070401	30,000	300	440
O3070501	30,100	1320	1440
O3070601	30,100	700	840
O3070702	30,100	380	540
O3070801	30,000	1000	1130
O3070901	30,000	1130	1300
O3071001	30,000	730	870
O3071101	30,000	32	180
O3071201	30,000	600	745
O3071302	30,000(planned)	0	140
O3071402	30,000(planned)	0	140
		TOTAL 6997	8905

- Total time at shaft speeds at and above 25,000 rpm was 8,385 seconds.
- Total time at speeds of approximately 30,000 rpm was 6,622 seconds.
- Preload was increased from the usual 4448 N (1000 lb) to 5800 N (1300 lb) to maintain axial loading on the outboard bearings while under radial load.
- The estimated average axial load on the inboard bearings (Brgs 2 and 3) operating in LO2 was 9785 N (2200 lbs) caused by the pressure differential across the load end bearing carriers and the remaining preload in the outboard bearings (Brgs 1 and 4). The resulting average axial load on the outboard bearings was 3000 N (675 lbs). A radial load applied to the bearings of approximately 3025 N (680 lbs) per bearing.
- The maximum estimated sustained contact stresses were:

	Brgs 1 and 4	Brgs 2 and 3
Inner Race	2.4 GPa (348 ksi)	3.5 GPa (508 ksi)
Outer Race	2.1 GPa (304 ksi)	2.9 GPa (420 ksi)

Table 2 Run Time and Test Speed of Unit 3 Build 7

were not in as good condition as the Bearing 1 races. The race distress was due to the high contact stresses caused by the heavy load and hard silicon nitride balls. The inner race had severe spalling of material in the contact tracks and the Salox film was a very dark bronze color. The outer race also had the dark Salox film and spalling appeared to be beginning. The outer race track had some eccentricity due to the radial load. Bearing 2 cage was in good condition with moderate ball contact. The silicon nitride balls had a smooth surface with dark bronze tracks. There were no "traction cracks" on their surface as was noted in the previous test series (Unit 2 Build 14) with silicon nitride against an Armalon cage. **Exhibit 263** depicts the inner race of Bearing 3 and shows the very severe spalling that occurred almost continuously around the race.

The outer race had minor spalling and heavy debris denting. The outer race also had a dark bronze track low in the raceway and a light bronze colored track up near the shoulder. The cage had very light wear in the pockets on the upstream side. The silicon nitride balls of Bearing 3 were in relatively good condition with dark brown bands and a spall or pit in one ball. Bearing 4 inner and outer races, shown in **Exhibit 264**, had a very similar appearance. The tracks had a matte surface finish with light bronze color low in the raceway and brass color on the upper edge. The cage had light contact in the pockets mostly on the upstream side. The steel balls of Bearing 4 were in good condition with dark bronze colored tracks all over their surface. **Table 3** provides the weight loss and dimensional changes of all the bearing components. However, wear losses were difficult to measure due to the Salox transfer film.

Test Data Summary. Test conditions and derived parameters for all tests in this series are provided in **Tables 4** and **5**. Typical coolant temperature and pressure profiles through each end of the tester are shown in **Exhibit 265** and **266. Exhibit 265** shows two anomalies that occur in the temperature measurements. These are the tester coolant outlet (T1003) reading below the bearing outlet temperature measurements (T1019 and T1022) and Bearing 1 and/or Bearing 4 outer race temperatures reading at or below their inlet coolant temperatures. These anomalies were believed to be caused by a slight coolant leak past the outboard carriers affecting the thermocouple readings of the outboard bearings and the tester outlet. Also, there may have

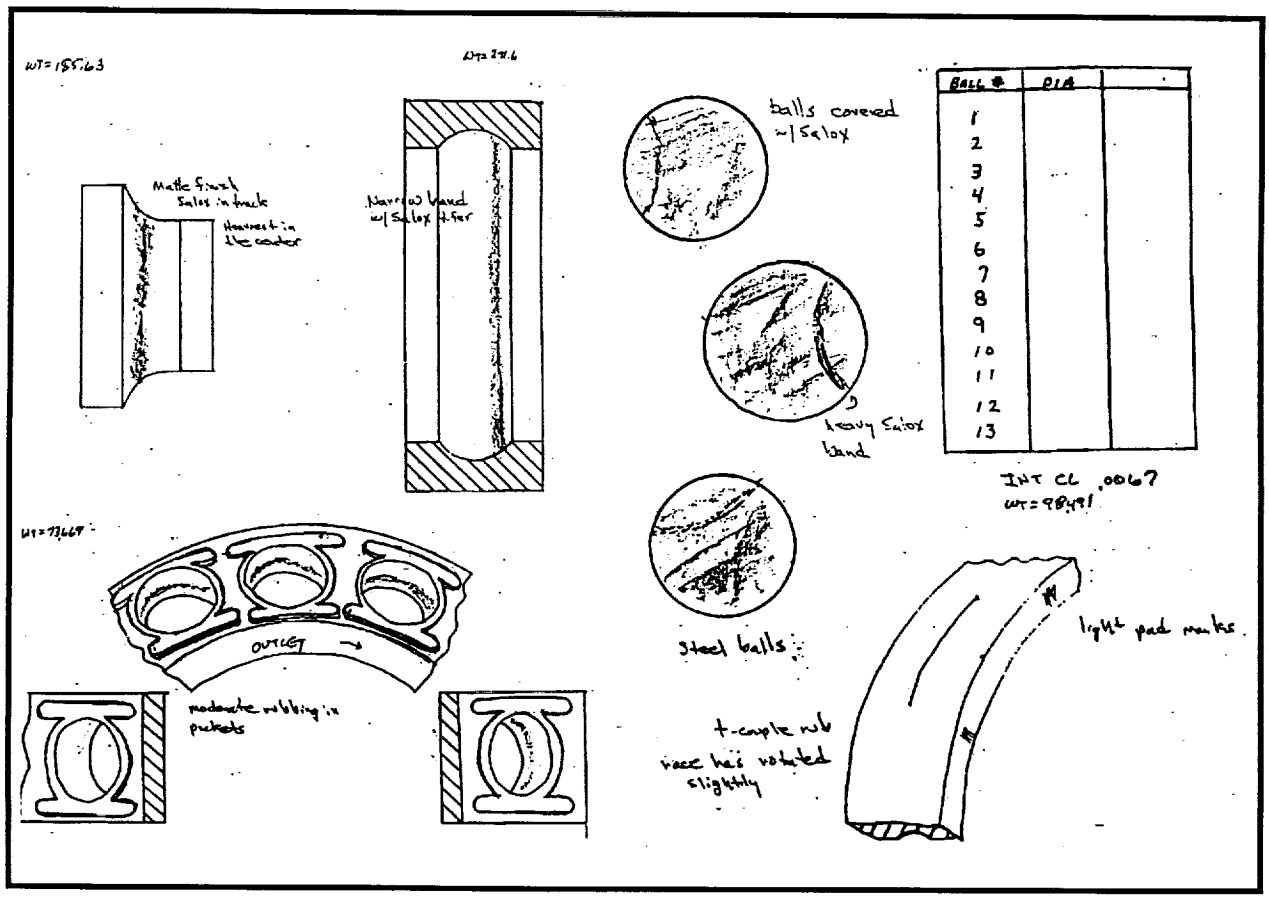

Exhibit 261 Visual Observation of Bearing 1 Components

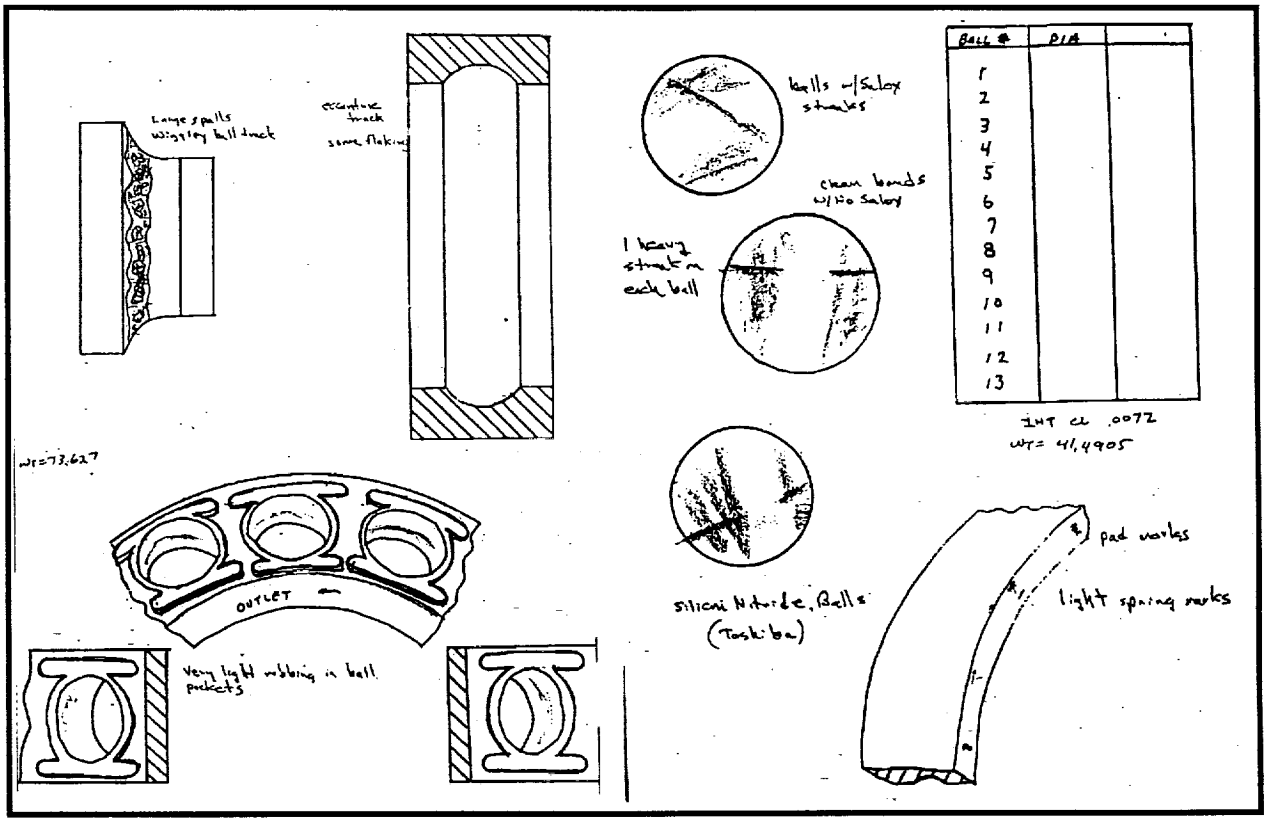

Exhibit 262 Visual Observation of Bearing 2 Components

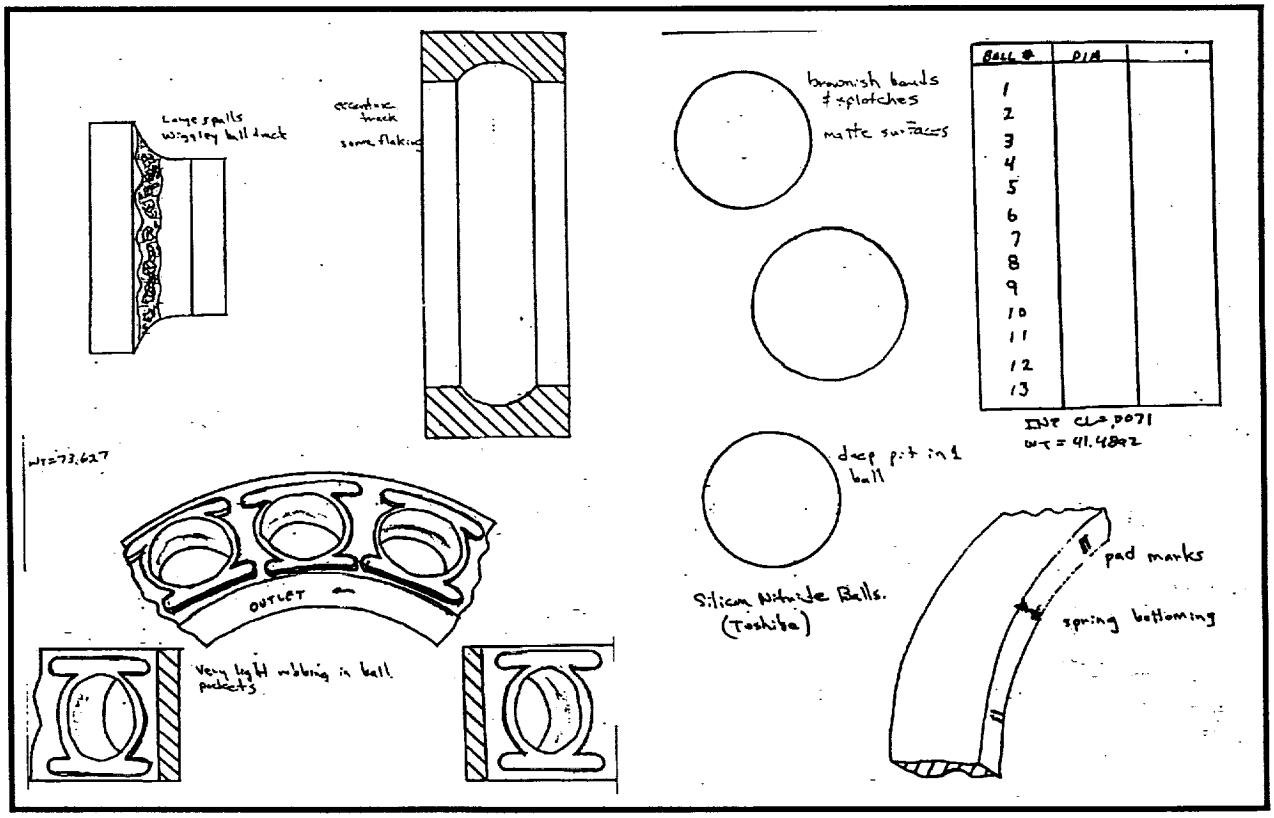

Exhibit 263 Visual Observation of Bearing 3 Components

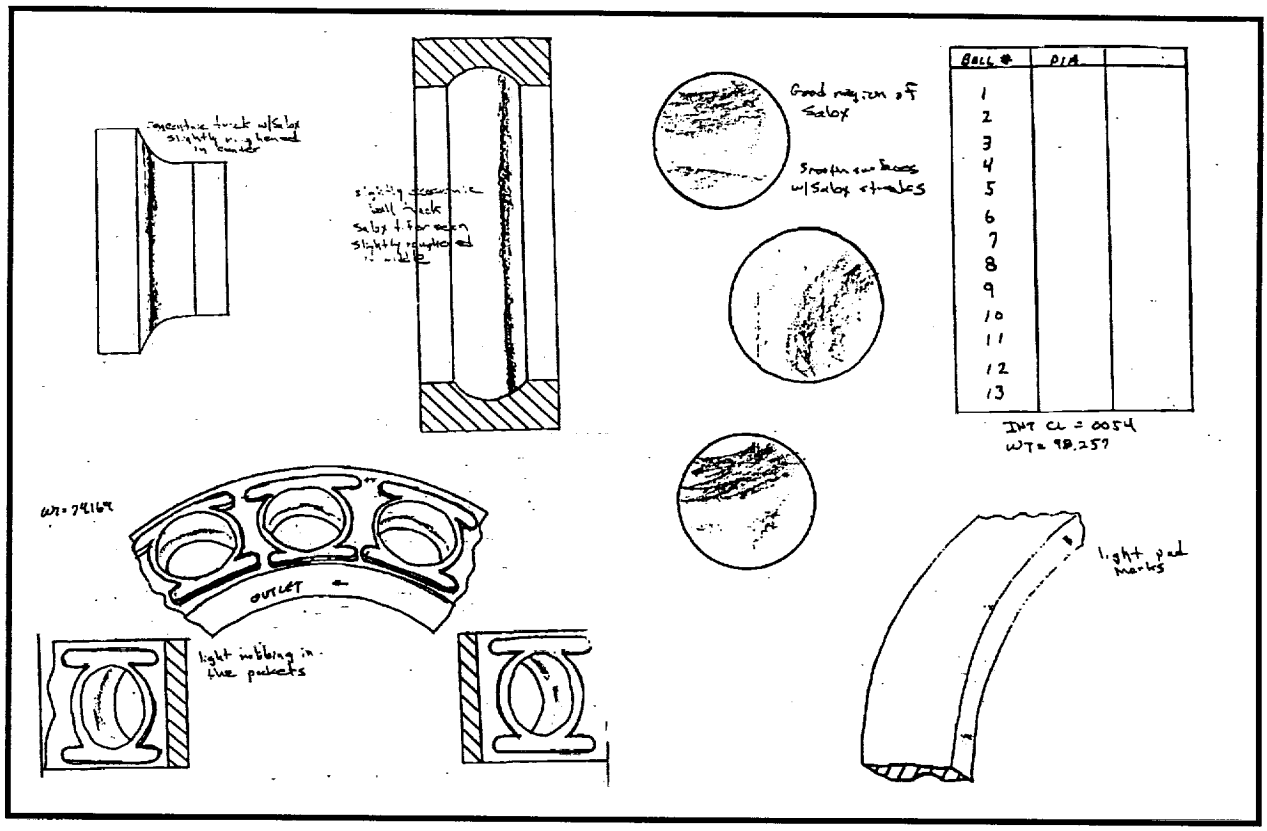

Exhibit 264 Visual Observation of Bearing 4 Components

been a 1 or 2 degree initial temperature bias in the readings that was not compensated for in the tables or profile plots.

The pressure profiles shown in **Exhibit 266** indicate that the total pressure drop across the bearing pair was near the normal level. However, the plot also shows that most of this pressure change occurred across the outboard bearing. This can only be confirmed for the drive end bearings since the load end bearings did not have a pressure measurement between their outer races. The large pressure change across the upstream bearing has been observed in other tester builds which used the Battelle cages. The reason for the upstream bearing higher pressure drop may have been that the fold over tabs of this cage design had a greater effect on the swirl of the coolant entering the bearing. Thus, the fluid was spun up closer to cage speed in the upstream bearing than with the standard Armalon cages.

The pressure drop across each bearing pair is plotted in **Exhibit 267** as a function of accumulated run time at 30,000 RPM. This plot shows that the pressure drops were relatively consistent from test to test except for Test 11 when the bearing inlet coolant temperature thermocouple backed out of position allowing a higher preswirl in the inlet cavity. **Exhibist 268** and **269** are plots of the torque and power required by the tester as a function of accumulated run time at 30,000 RPM. The torque and power required were very consistent and near the usual levels of previous tests.

Observations. The performance of the Battelle cages with the predicted increased ball excur-

BSMT ANSLYSIS SHEET									
PRETEST WT.						WT. LOSS			
						OR	IR	CAGE	BALLS
OR	IR	CAGE	BALLS		BRG1	0	0.03	0.011	0.009
291.6	185.66	73.68	98.5		BRG2	0	0.02	0.026	0.0474
291	185.8	73.58	41.5379		BRG3	0.2	0.2	0.043	0.0494
291.7	185.44	73.67	41.5386		BRG4	0.1	-0.27	0.031	0.243
292.2	184.98	74.2	98.5						
POSTTEST WT.									
291.6	185.63	73.669	98.491						
291	185.78	73.554	41.4905						
291.5	185.24	73.627	41.4892						
292.1	185.25	74.169	98.257						
NO. OF BALLS		12							
BALL DIA CAL.		NEW DIAS			FEDERAL MEAS.		PRETESTS		
					BRG1	BRG2	BRG3	BRG4	
BRG1	BRG2	BRG3	BRG4		66	58	-95	-4	
0.500062	0.500053	0.499894	0.499995		68	62	-96	-14	
					65	63	-95	-4	
	POST TESTS DIAS				65	56	-117	-16	
0.50005	0.499861	0.499841	0.499958		61	55	-114	-4	
					64	52	-114	-25	
WEAR					66	49	-117	-16	
1.2E-05	0.000191	5.27E-05	3.77E-05		68	46	-115	-22	
					63	48	-115	-15	
SPECIAL NOTES:					62	49	-118	-12	
					65	54	-115	-10	
THESE BALLS HAD SALOX ON THEM					63	52	-115	-5	
WEAR NOS. ARE NOT ACCURATE FOR THIS CAS					58	47	-108	-15	
BRG NO 3 DIAS ARE SUSPECT					60	45	-104	-7	
					64	49	-106	-3	
					66	50	-102	-2	
					57	50	-106	-7	
					56	49	-102	7	
					57	55	-91	-0.5	
					59	46	-109	-2	
					59	51	-105	-5	
					63	51	-110	3	
					64	52	-111	48	
					65	48	-111	-5	
					59	53	-105	-10	
					60	58	-108	-4	
					62	60	-109	-19	

Table 3 Unit 3 Build 7 Component Wear Losses

sions of the outboard bearings was excellent. The cages showed no structural damage. However, because the axial and radial loads on the bearings were not directly measured, the exact amount of ball excursion could not be determined. Moderate cage pocket contact in both the fore and aft positions of the pockets was experienced by all the cages as indicated by hardware observations.

This was the first test using the Battelle cage with silicon nitride rolling elements. It appeared that the Salox pocket inserts were less detrimental to the silicon nitride rolling elements than the standard Armalon material due to the absence of the "traction cracks" on the balls observed in previous silicon nitride tests. Also, because the Battelle cage required 12 balls instead of the normal 13 the steady-state contact stress on silicon nitride balls was the highest ever tested in the BSMT. As a consequence, there was only one small spall detected on one ball. Ball wear was near the usual silicon nitride level although the Salox transfer film made measurement difficult.

This test series proved that the Battelle designed cage is structurally sound for use in bearing applications with high ball excursions. Also, this test series showed that the Salox pocket inserts are beneficial for use with the silicon nitride rolling elements. Previous tests with Battelle cages have proven that the Salox transfer film is beneficial to bearings with steel rolling elements as proved by their extended test lives. However, this test series did not show a corresponding increase for silicon nitride bearing life when compared to silicon nitride bearings using an ARMALON cage.

Test Parameter	TEST NUMBER													
	3070 201				3070302	3070401	3070501	3070601	3070702	3070801	3070901	3071001	3071101	3071201
Shaft Speed (RPM)	15,000	25,000	28,000	30,000	30,000	30,000	30,100	30,100	30,100	30,000	30,000	30,000	30,000	30,000
Time at Speed (sec)	150	300	125	130	300	300	1320	700	380	1000	1130	730	32	600
Flow Rate (lbs/sec)	6.4	6.4	6.4	6.4	6.4	6.4	6.4	6.4	6.4	6.4	6.4	6.4	6.4	6.4
Brg #4 Inlet Temp (°F) T1018	-259.50	-247.00	-243.50	-242.00	-243.00	-242.00	-242.00	-242.00	-242.00	-242.00	-242.00	-243.00	-243.00	-242.00
Between Brgs 3 and 4 (°F) T1024	-259.50	-246.50	-242.00	-239.00	-241.00	-240.00	-240.00	-239.00	-239.00	-239.00	-239.00	-240.00	-239.00	-239.00
Brg #3 Outlet Temp (°F) T1019	-257.00	-239.50	-234.50	-231.00	-233.00	-232.00	-231.00	-231.00	-231.00	-231.00	-231.00	-231.00	-232.00	-231.00
Brg #1 Inlet Temp (°F) T1021	-260.00	-246.00	-243.50	-241.00	-242.00	-242.00	-241.00	-241.00	-241.00	-241.00	-241.00	-242.00	-244.00	-242.00
Temp Between Brgs 1 & 2 (°F) T1023	-257.00	-242.50	-239.00	-236.00	-238.00	-237.00	-237.00	-237.00	-237.00	-236.00	-236.00	-237.00	-237.00	-237.00
Brg #2 Outlet Temp (°F) T1022	-257.50	-239.50	-234.50	-231.00	-233.00	-232.00	-231.00	-231.00	-232.00	-231.00	-231.00	-232.00	-232.00	-232.00
Tester Inlet Temp (°F) T1001	-267.00	-266.00	-265.50	-265.50	-268.00	-267.00	-266.00	-264.00	-267.00	-267.00	-267.00	-267.00	-267.00	-267.00
T1002	-267.50	-264.50	-263.50	-262.50	-265.00	-264.00	-264.00	-264.00	-264.00	-263.00	-263.00	-264.00	-265.00	-264.00
Tester Outlet Temp (°F) T1003	-260.00	-242.00	-237.00	-233.50	-236.00	-234.00	-234.00	-234.00	-234.00	-234.00	-233.00	-234.00	-235.00	-234.00
Tester Inlet Pressure (psig) PA1001	442	444	442	444	444	444	445	445	447	445	444	446	476	444
PA1002	442	442	444	444	444	446	444	446	442	446	444	448	444	445
Tester Outlet Pressure (psig) PA1003	432	411	407	407	405	408	406	408	406	408	406	408	408	407
Pressure Between Brg 3 & 4 (psig) P1006	431	413	409	409	408	411	409	411	409	411	412	420	410	409
Horsepower	66	218	252	280	300	300	300	300	300	300	300	300	300	300
Torque (in-lbs)	6,600	13,000	13,400	13,800	13,880	13,800	13,800	13,800	13,770	13,730	13,750	13,930	14,000	13,860
Brg #1 O.R. Temp (°F) T1004 (TA1004)	-260 (-261)	-258 (-244)	-256 (-239)	-256 (-236)	-264 (-237)	-262 (-235)	-259 (-235)	-261 (-234)	-258 (-235)	-260 (-234)	-260 (-233)	-262 (-235)	-261 (-245)	-260 (-233)
Brg #2 O.R. Temp (°F) T1005 (TA1005)	-256 (-257)	-239 (-240)	-233 (-236)	-229 (-232)	-230 (-234)	-227 (-234)	-228 (-233)	-226 (-233)	-225 (-233)	-226 (-232)	-225 (-232)	-224 (-233)	-227 (-234)	-223 (-233)
Brg #3 O.R. Temp (°F) T1006 (TA1006)	-253 (-257)	-234 (-240)	-230 (-236)	-226 (-232)	-221 (-235)	-222 (-234)	-224 (-234)	-224 (-233)	-225 (-233)	-225 (-233)	-224 (-233)	-222 (-234)	-225 (-234)	-219 (-232)
Brg #4 O.R. Temp (°F) T1007 (TA1007)	-262 (-261)	-261 (-249)	-260 (-244)	-260 (-241)	-263 (-242)	-262 (-241)	-261 (-239)	-261 (-239)	-261 (-239)	-261 (-238)	-261 (-238)	-261 (-237)	-262 (-241)	-261 (-236)

Table 4 BSMT Test Colnditions and Selected Data

PARAMETER			3070 201			3070302	3070401	3070501	3070601	3070702	3070801	3070901	3071001	3071101	3071201
• Delta Temp Across															
Brg Pair (°F)															
T1022-T1021	9.00	0	6.50	9.00	10.00	10.00	10.00	10.00	10.00	9.00	10.00	10.00	10.00	12.00	10.00
T1019-T1018	9.00	0	7.50	9.00	11.00	11.00	10.00	11.00	11.00	11.00	11.00	11.00	12.00	11.00	11.00
• Delta Temp Across															
Brg 1 (°F)															
T1023-T1021	4.50	0	3.50	4.50	5.00	5.00	5.00	4.00	4.00	4.00	5.00	5.00	5.00	7.00	5.00
Brg 2															
T1022-T1023	4.50	0	3.00	4.50	5.00	5.00	5.00	6.00	6.00	5.00	5.00	5.00	5.00	5.00	5.00
Brg 3															
T1019-1024	7.50	0	7.00	7.50	8.00	8.00	8.00	9.00	8.00	8.00	8.00	8.00	9.00	7.00	8.00
Brg 4															
T1024-T1018	1.50	0	0.50	1.50	3.00	3.00	2.00	2.00	3.00	3.00	3.00	3.00	3.00	4.00	3.00
• Brg Outer Race Temp															
- Fluid Inlet Temp (°F)															
Brg 1															
TA1004-T1021	4.50	0	2.00	4.50	5.00	5.00	7.00	6.00	7.00	6.00	7.00	8.00	7.00	1.00	9.00
Brg 2															
T1005-T1023	6.00	0	3.50	6.00	7.00	8.00	10.00	9.00	11.00	12.00	10.00	11.00	13.00	10.00	14.00
Brg 3															
T1006-T1024 (TA1006-T102	12.00	0	12.50	12.00	13.00	20.0 (6)	18.0 (6)	16.0 (6)	15.00	14.00	14.00	15.00	18.00	14.00	20.00
Brg 4															
TA1007-T1018	-0.50	0	-2.00	-0.50	1.00	1.00	1.00	3.00	3.00	3.00	4.00	4.00	6.00	2.00	6.00
•Heat Generated (Btu/sec) Acros															
Brg 1	13.10	0	10.00	13.10	14.80	14.30	14.80	11.70	11.80	11.80	14.60	14.70	14.70	19.90	14.30
Brg 2	13.10	0	8.60	13.10	14.80	14.30	14.80	17.50	17.70	14.70	14.80	14.90	14.80	14.60	14.60
Brg 3	21.60	0	19.70	21.60	23.30	23.10	23.20	26.20	23.30	23.40	23.80	23.30	26.20	20.30	23.20
Brg 4	4.30	0	1.40	4.30	8.80	8.70	5.70	5.80	8.80	8.80	8.70	8.70	8.60	11.40	8.80
•Heat Generated Across															
Brg 1&2	26.20	0	18.60	26.20	29.60	28.60	29.60	29.20	29.50	26.50	29.40	29.60	29.50	34.50	28.90
Brg 3&4	25.90	0	21.10	25.90	32.10	31.80	29.00	32.00	32.10	32.20	32.50	32.00	34.80	31.70	32.00
• Inlet Vortex Work (Btu/sec)															
Load	60.50	0	55.00	60.50	67.90	71.20	68.60	68.80	74.00	71.60	71.40	71.60	68.50	63.00	68.80
Drive	55.00	0	49.50	55.00	58.20	60.50	60.80	60.50	59.70	60.70	57.80	57.80	57.80	60.50	60.50
• Pressure Drop (psi)															
Brg 3	2	1	2	2	2	2	3	3	3	3	3	6	12	2	2
Brg 4	35	1	29	35	35	37	35	35	35	33	35	32	28	34	36
Brg 1&2	37	0	33	37	37	39	36	39	37	41	37	38	38	68	37
Brg 3&4	35	0	31	35	37	39	38	38	38	36	38	38	40	36	38
• Subcooling °F	38	5	39	38	36	38	38	36	37	37	38	38	38	40	38
• Radial Load (lbs/brg)	650	0	650	650	650	650	700	700	700	700	700	700	700	700	700

940105DM1120

Table 5 BSMT Test Parameter Comparison

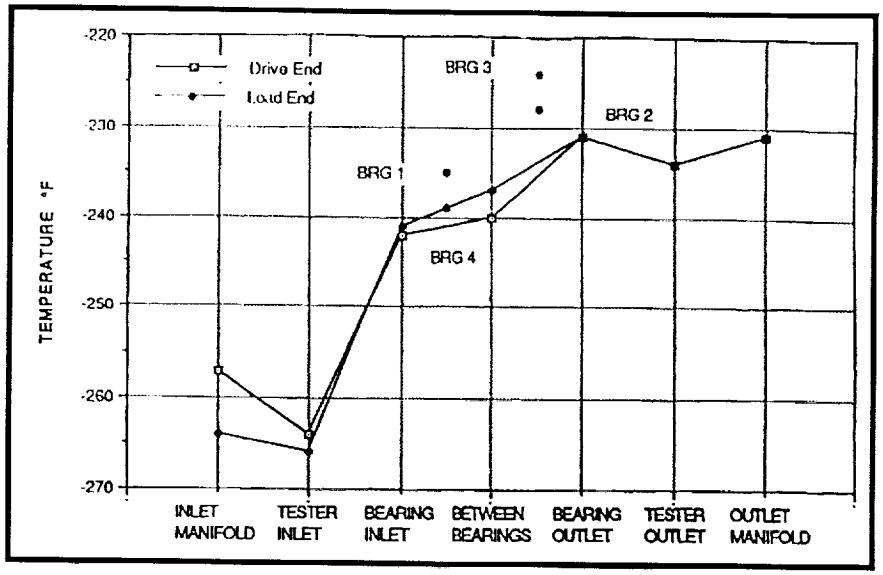

Exhibit 265 Temperature Profile for BSMT Test 3070501

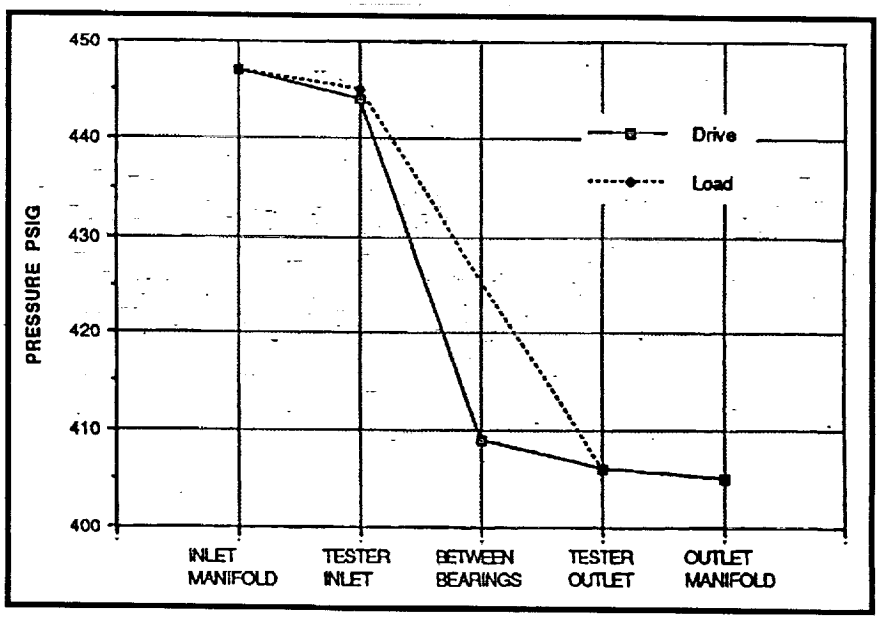

Exhibit 266 Pressure Profile for BSMT Test 3070501

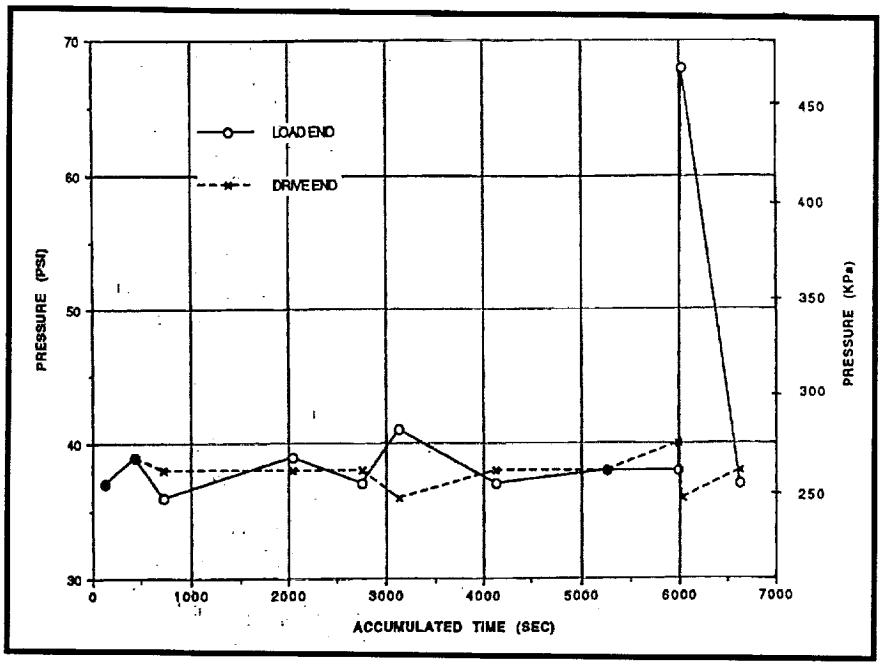

Exhibit 267 Pressure Drop Across Bearing Pair

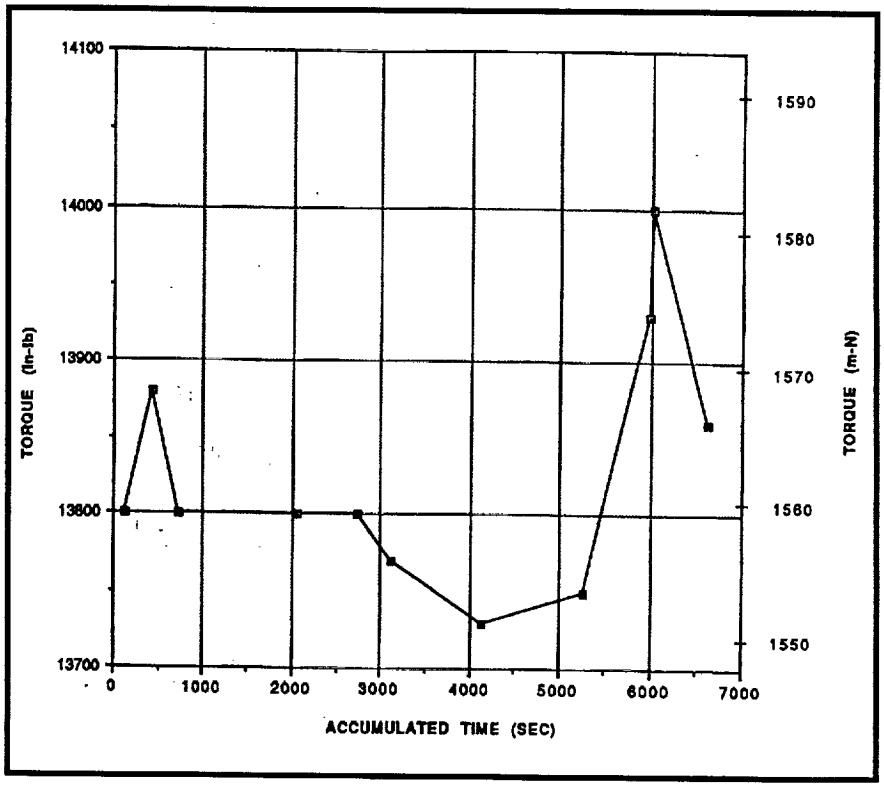

Exhibit 268 Unit 3 Build 7 torque Requirement at 30,000 RPM

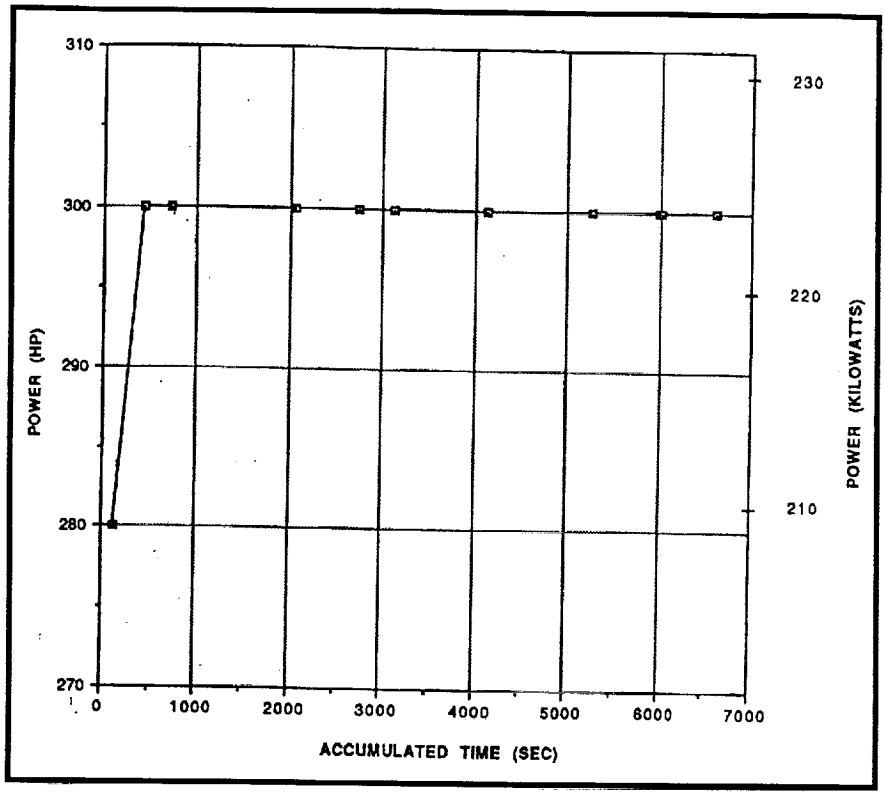

Exhibit 269 Unit 3 Build 7 Power Requirement at 30,000 RPM

6.0 — Liquid Hydrogen Bearing Test Rig Support

The bearing seals and materials tester demonstrated the value of actual cryogenic testing of rolling element bearings for turbopump applications. Without the test program, ceramic bearings would have never been considered as a safe and reliable fix for bearing wear problems. However, the rig also highlighted the need for a simpler test rig that reduced the logistics associated with bearing installation in the tester and rig installation in the facility. Concurrently, with the end of the BSMT program, MSFC was pursuing acquisition of a fluid film bearing test rig. The fluid film bearing tester was designed to operate at high speed using a gaseous nitrogen terry turbine. This is a very simple power source, compare to the diesel engine and 23 tol gear box required for the BSMT. The need for additional rolling element bearing testing, following completion of the BSMT program, prompted MSFC to investigate the feasibility of modifying the fluid film bearing tester to acquire rolling element bearing testing.

The investigation showed that it was feasible and practical to modify the rig to test ball and roller bearings in cryogenic hydrogen. Subsequently, the conversion of the rig to a rolling element bearing test rig was undertaken and completed. Later, testing was significantly more "user friendly" than the BSMT. Hardware builds could be accomplished by a two man crew, in-house in the tribology lab. Baring run time orders of magnitude more quickly than was ever demonstrated with the BSMT. The new test program was a resounding success and over 75,000 seconds of test time have been achieved as of January 2000.

Table 6 shows a summary of the various test configurations that have been tested under this program. Build zero was a shakedown build using 2 ball bearings. Approximately 35 minutes of rotational time was accrued during this build various procedures were addressed to improve axial load control on the bearings. Build 1 was the first attempt to run the rig with ball and roller bearings. Testing was terminated early due to axial rubbing in the thrust piston.

Builds two, three, and four achieved the objectives of the primary objectives of this test program. This objective was to investigate the safety and reliability issues associated with surface distress features, "river marks", that have been observed in silicon nitride bearings after removal from SSME turbopumps. The test accomplished under this program provided undeniable verification of the bearings to meet the 30,000 second design life with severe "river marks". In fact, the bearings used in Build 3 already had been subjected to significant engine tests time, including a high load event, prior to installation in the rig. These bearings had major "river marks" when installed in the rig. Build 3 demonstrated that these bearings still could achieve an additional 30,000 second life test cycle. In Build 4, an additional 30,000 second test cycle was achieved on a new set of bearings. Silicon nitride balls from a second manufacturer were tested in this build. These balls also developed "river marks" but survived the test series is in relatively good condition. Build 5 is the first successful rig build with a ball and roller bearing tested simultaneously. As of January 2000, approximately 14,000 seconds of run time has been demonstrated. Completion of this test series out to 30,000 seconds will demonstrate the robust-

Build Number	Bearing Manufac.	Element Config	IR w/PG Config	OR Config	Cage Config	Bearing Manufac.	Element Config	IR w/PG Config	OR Config	Cage Config
Build 0 (Shake-down Series)	MRC	440C Balls	9310 w/Salox p/l	440C	Armalon w/Salox Inserts	FAG	Toshiba TSN-03H Si3N4 Balls	Cr 30 w/Salox p/l	440C No AR tang	Armalon w/Salox Inserts
Build 1 RB: F5-2 PEBB LB: F6-4 TERB	FAG	Toshiba TSN-03H Si3N4 Balls	Cr 30 w/Salox p/l	440C w/Saloxp/l No AR tang	Armalon w/Salox Inserts	FAG	Toshiba TSN-03NH Si3N4 Balls	Cr 30 w/Salox p/l	Cr 30	Armalon
Build 2 RB: F5-2 PEBB LB: F5-3A PEBB	FAG	Toshiba TSN-03H Si3N4 Balls	Cr 30 w/Salox p/l	440C w/Saloxp/l No AR tang	Armalon w/Salox Inserts	FAG	Toshiba TSN-03NH Si3N4 Balls	Cr 30 w/Salox p/l	Cr 30 w/Saloxp/l No AR tang	Armalon w/Salox Inserts
Build 3 RB: F6-4 PEBB LB: F5-3A PEBB	FAG	Toshiba TSN-03H Si3N4 Balls	Cr 30 w/Salox p/l	CR 30 No AR tang	Armalon w/Salox Inserts	FAG	Toshiba TSN-03NH Si3N4 Balls	Cr 30 w/Salox p/l	Cr 30 w/Saloxp/l No AR tang	Armalon w/Salox Inserts
Build 3A RB: F6-4 PEBB LB: F5-3A PEBB	FAG	Toshiba TSN-03H Si3N4 Balls	Cr 30 w/Salox p/l	CR 30 No AR tank	Armalon w/Salox Inserts	FAG	Toshiba TSN-03NH Si3N4 Balls	Cr 30 w/Salox p/l	Cr 30 w/Saloxp/l No AR tang	Armalon w/Salox Inserts
Build 4 RB: F8-1A PEBB Rings LB: F7-1F PEBB Rngs	FAG	Cerbec NBD-200 Si3N4 Balls	Cr 30 w/Salox p/l	Cr 30 w/Salox p/l No AR tang	Armalon w/Salox Inserts (0.009 oz-in IMB)	FAG	Toshiba TSN-03H Si3N4 Balls	Cr 30 w/Salox p/l	Cr 30 w/Saloxp/l No AR tang	Armalon w/Salox Inserts (0.009 oz-in IMB)
Build 4A RB: F8-1A PEBB Rings LB: F7-1F PEBB Rngs	FAG	Cerbec NBD-200 Si3N4 Balls	Cr 30 w/Salox p/l	Cr 30 w/Salox p/l No AR tang	Armalon w/Salox Inserts (0.009 oz-in IMB)	FAG	Toshiba TSN-03H Si3N4 Balls	Cr 30 w/Salox p/l	Cr 30 w/Saloxp/l No AR tang	Armalon w/Salox Inserts (0.009 oz-in IMB)
Build 5 RB: F8-3 PEBB LB: F6-4 TERB	FAG	Toshiba TSN-034 Si3N4	Cr 30 w/Salox p/l	Cr 30 w/Salox p/l No AR tang	Armalon w/Salox Inserts Armalon	FAG	Toshiba TSN-034NH Si3N4	Cr 30 w/Salox p/l	Cr 30	Armalon

Table 6 HPFTP/AT LH2 Bearing Tester - Configuration Summary

ness of roller bearings with "river marks". This is considered critical by many people because the roller bearing geometry is consider worse than a ball with respect to propagation of surface flaws. Testing on Build 5 is anticipated to resume sometime in early 2000.

6.1 ALGOR Thermal Analysis of MSFC Hybrid Bearing Test Rig

An ALGOR finite element thermal model was developed to support test procedure development for the Hybrid Bearing Test Rig. The objective of the study was to determine the steady-state temperature distribution in the tester housing for the static, chilled down, condition. The resulting thermal map of the tester will be used to as a reference to evaluate the chill down period required prior to testing. The map will be checked against the three internal housing thermocouples to establish when the steady state chill down condition has been achieved.

The ALGOR results are shown graphically in **Exhibit 270**. The interior of the housing (left) is maintained at a constant temperature of 28 K (-410 °F) by contact with liquid hydrogen. The exterior of the housing (right) conducts to a frost layer on the exterior of the housing. The frost layer was estimated to be 13 mm (0.5 inch) thick. The frost layer is convecting to air at an ambient temperature of 283 K (50 °F). The analysis shows that the frost layer serves as an insulator. The temperature of the Inconel 718 housing increases to a maximum of about 136 K (-215 °F) at the frost/housing interface. There is a steep gradient within the frost layer, with the temperature increasing to about 260 K (8 °F) on the exposed frost surface. This analysis indicates that the frost layer may grow to an increased thickness until the temperature of the surface approaches the freezing point of water. Temperatures were predicted for each of the three thermocouple locations and used to determine when a chilled down condition has been established.

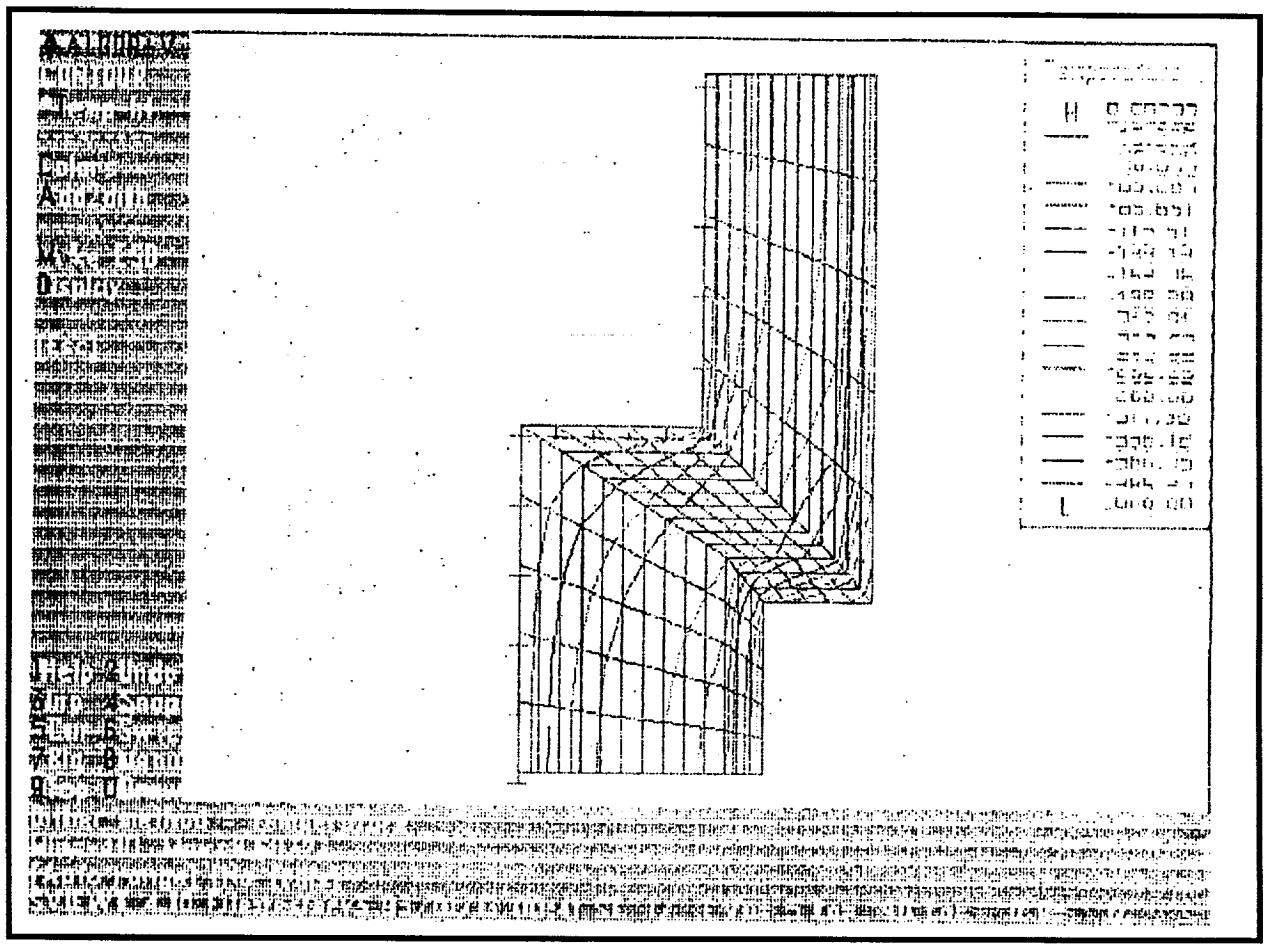

Exhibit 270 Steady State Temperatur Distribution for Chilled Down Condition

The model was developed using type 40 axisymmetric thermal elements. A non-linear solution was performed to allow for temperature dependent material properties. A four segment, piecewise linear, curve was used to specify the conductivity of Inconel 718. The conductivity of frost was estimated using the rule of mixtures. The frost was assumed to be 50% ice and 50% air. The convection coefficient for the frost to ambient air was based on an empirical relationship for free convection about a cylinder.

6.2 Development of SINDA/SHABERTH/ HYDROSEAL Model of MSFC Fluid Film Bearing Tester

Testing with the new Fluid Film Bearing Tester (FFBT) is described later in this report. In preparation for this testing, a computer model of the FFBT shaft/bearing system was developed using the SINDA/SHABERTH/HYDROSEAL (SSH) bearing code to predict pretest monitored and unmonitored bearing operating parameters. A cross section of the FFBT is given in **Exhibit 271** illustrating the location of the bearings. The FFBT is capable of testing fluid film bearings, ball bearings, and roller bearings. The first test series (Build 0) with the FFBT utilized two ball bearings and one fluid film bearing. The test bearing tested was designed for the Pratt and Whitney ATD fuel turbopump.

The test bearing for this series is the advanced design ball bearing utilizing silicon nitride balls and Cronidur X30 inner race. The reaction

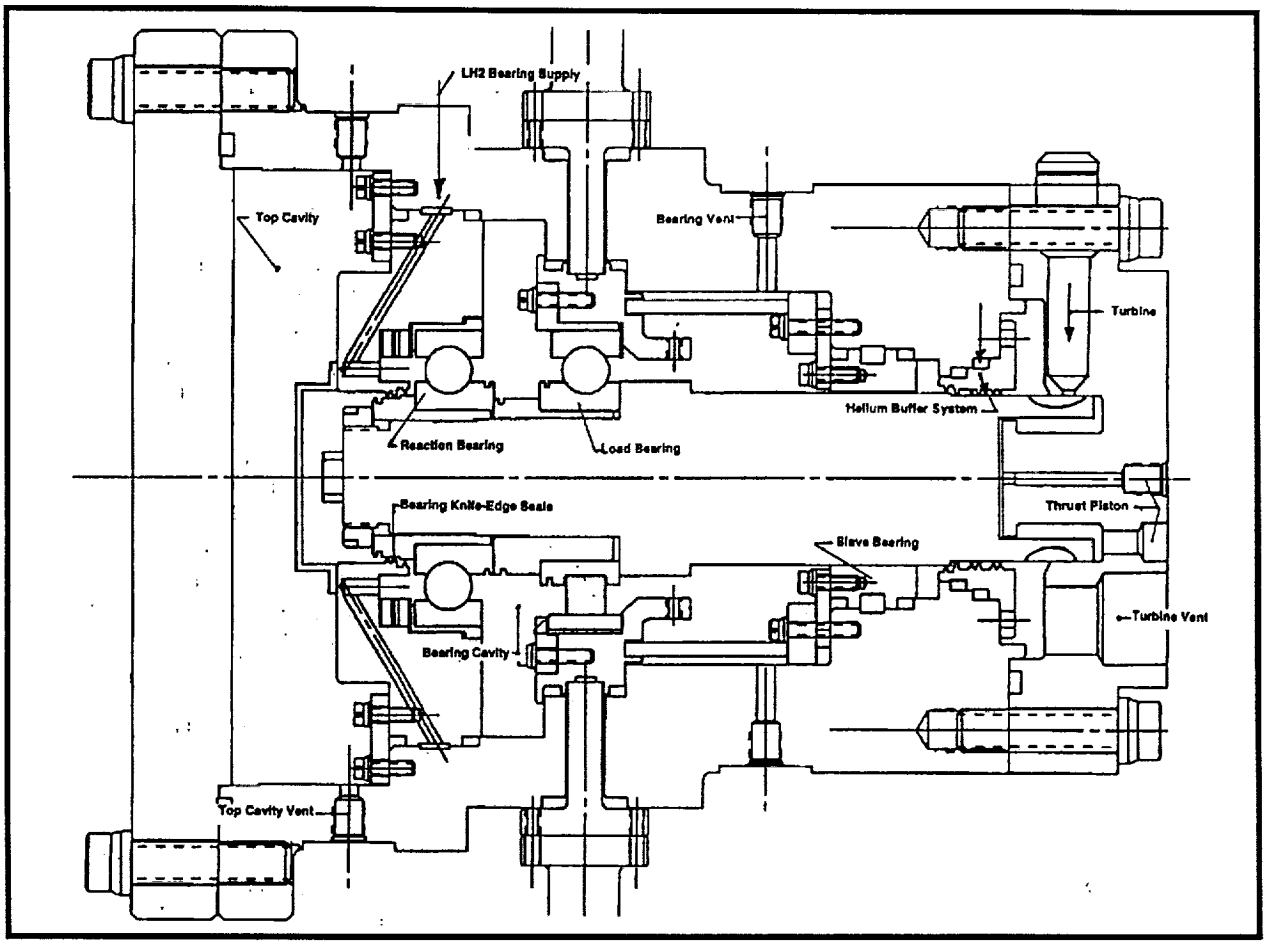

Exhibit 271 Fluid Film Bearing Tester Showing Optional Ball and Roller Bearing Installation

bearing is necessary to support the preload of the test bearing and will use the same race geometry but with baseline 440C balls, outer race, and a 9310 inner race. The slave bearing was a fluid film bearing of a hydrostatic design with eight square pocket recesses.

The development of the FFBT computer model was facilitated by making use of a previously developed thermal model of the AT HPFTP ball bearing. This thermal model is used to simulate the test bearing since it is the bearing being analyzed. Later, we modified the thermal model to also simulate the reaction bearing since its temperature will affect the operating preload of the ball bearings. The development of the mechanical portion of the computer model was very straight forward utilizing the SSH code in which conventional rolling element bearings and fluid film bearings can be modeled operating on a common shaft. Likewise, as with the thermal portion, most of the mechanical portion input for the ball bearings had been developed during past work.

The operation of the FFBT model was verified using assumed coolant fluid conditions and applied loads similar to those of the Pratt fuel turbopump. The results of the simulation were comparable to bearing results for the fuel pump, thus, the model appeared to function properly. The FFBT model then used to make pretest predictions for bearing and used to set redlines for automatic termination of tests.

6.3 Fluid Film Bearing Tester Redline Review

The FFBT facilities and internal flow paths were reviewed to determine instrumentation redline requirements. The objectives of the review were to ensure that the redline instrumentation was sufficient to detect a problem and terminate the test before serious damage of the hardware occurred and to limit the number of measurements that were on the redline list so as not to overburden the data collection system. The practice used in redline selection was: 1) ensure that proper coolant is delivered to the bearings and 2) detect problem close to bearing so that redline tolerances can be set tight. Thus, out of a total of 85 measurements in the facility and tester, 25 were determined as necessary for test termination and placed on the redline list.

During May 1995 the SINDA/SHABERTH/HYDROSEAL (SSH) computer model of the Fluid Film Bearing Tester (FFBT) was updated to reflect the modifications made to the hardware. The model then had the hollow shaft under the Top and Middle bearings and the "as measured" shaft-to-sleeve, sleeve-to-inner race, and outer race-to-sleeve fits. These dimensions are tabulated in **Exhibit 272**

Pretest predictions were made using the SSH model to determine the average component and maximum track temperatures. Also, predicted values for the measured parameters such as the outer race and sleeve temperatures at their outer diameters and the coolant temperature rise across the bearing were determined. Shown in **Exhibit 273** are the predicted values along with the estimates for inner and outer race maximum contact stress. The operating conditions used for this simulation of the FFBT were a shaft speed of 37,000 RPM, axial preload of 4448 N (1000 lbs), and a liquid hydrogen coolant flow rate of 0.3 kg/sec (0.7 lbs/sec) at 2.76 MPa (400 psia).

Once testing with the FFBT had begun and operating data obtained, the SSH model was calibrated using the coolant temperature changes across the bearings and the outer diameter temperature measurements of the outer race and sleeve. In general, the pretest predictions were very accurate. The accuracy of the model supported the redline limits used to detect the onset of a bearing problem.

CLEARANCE mm (in.)	TOP BEARING	MIDDLE BEARING
SHAFT/SLEEVE	.06579 (.00259)T	.06731 (.00265)T
SLEEVE/INNER RACE	.08661 (.00341)T	.09195 (.00362)T
OUTER RACE/SLEEVE	.03073 (.00121)L	.04318 (.00170)L
SLEEVE/HOUSING	.18034 (.00710)L	.22860 (.00900)T

Exhibit 272 FFBT Ball Bearing Diametrical Measured Clearanced

6.4 Rolling Element Bearing Tester Test Readiness Review

Joe Cody, Dave Marty, and Jim Moore attended the Bearing Tester Test Readiness Review in August 1995 to address any questions regarding pretest analysis. Pretest analysis results were presented by Mr. Gibson. Several areas of additional analytical support were identified. All of the analysis to date has addressed hydrogen testing. In discussions following the Test Readiness Review, it was decided to modify the thermal model to simulate the initial shakedown runs using liquid nitrogen as a

(35,000 RPM, 4448 N AXIAL PRELOAD, 0.3 KG/SEC COOLANT FLOW)

	FRICTION = 0.1		FRICTION = 0.2	
	TOP BRG	MIDDLE BRG	TOP BRG	MIDDLE BRG
AVG. BALL TEMP. K(F)	43.0 (-382.5)	35.7 (-395.7)	62.8 (-347.0)	42.5 (-383.5)
AVG. I.R. TEMP. K(F)	34.3 (-389.3)	31.7 (-403.0)	40.0 (-387.9)	33.3 (-400.1)
AVG. O.R. TEMP. K(F)	34.5 (-397.9)	31.5 (-403.3)	40.9 (-386.3)	33.2 (-400.2)
MAXIMUM TRACK K(F)	93.3 (-292.0)	59.4 (-353.0)	177 (-141.0)	97.8 (-284.0)
COOLANT DELTA K(F)	5.0 (9.1)	4.2 (7.6)	6.4 (11.6)	4.9 (8.8)
SLEEVE O.D. TEMP K(F)	33.2 (-400.3)	30.8 (-404.9)	38.9 (-390.0)	32.1 (-402.2)
O.R. O.D. TEMP K(F)	37.3 (-392.9)	32.4 (-401.6)	47.9 (-373.7)	35.3 (-396.4)
IR MAX. STRESS GPa(Ksi)	2.06 (299)	3.43 (497)	2.06 (299)	3.43 (497)
OR MAX. STRESS GPa(Ksi)	1.93 (280)	1.81 (262)	1.93 (280)	1.81 (262)

Exhibit 273 Fluid Film Bearing Tester Pretest Predictions

coolant. Comparison of analytical data with liquid nitrogen test data would provide an initial calibration point for the analysis prior to hydrogen testing. The tester SINDA/SHABERTH bearing model was also used to investigate several off-design operating conditions. A simulation was be performed to evaluate bearing performance for cases of elevated inlet coolant fluid temperature; addressing the effects of excessive run tank warming during a test. Additionally, the transient tester model was used to evaluate bearing performance and degradation that occurs in the event that coolant flow is stopped completely and the tester is required to spin down dry.

The SHABERTH/SINDA computer model of the MSFC LH2 Bearing Tester, also known as Fluid Film Bearing Tester (FFBT), was set up to simulate the rig operating with liquid nitrogen as the coolant for the initial shake-down tests. This modification is very simple and is done by setting the IFLUID flag in the SINDA file to select nitrogen as the coolant. The mass flow rate of coolant is specified as usual in the ARRAY DATA block. However, the mass flow rate for nitrogen had to be estimated since the orifices measuring flow were calibrated for hydrogen. This was done by assuming the same volumetric flow rate and multiplying by the ratio of the two fluid densities at the measured conditions. The flow rate was calculated to be approximately 8.6 kg/sec (19 lbs/sec) of liquid nitrogen flowing to the ball bearings.

The model was then run using the calculated nitrogen flow rate for both 20,000 and 37,000 rpm test shaft speeds with only the nominal axial preload of 4448 N (1000 lbs). The results for the simulations are given in **Exhibit 274** showing the coolant temperature rise across the bearings and the outer race back surface metal temperature.

6.5 Preparation for Hydrogen Testing of HPFTP/AT Ball Bearing

The first ball bearing test series for the HPFTP/AT bearings was first scheduled to begin in October 1995. Test stand scheduling and long lead time facility modifications resulted in pushing back the test schedule. The intervening time was utilized to review and prepare the analytical models to support the test series. The fluid properties program, which calculates fluid properties for heat transfer coefficients used in the SINDA simulation of the bearings, was updated to include the database for hydrogen. The up-

	REACTION BEARING		TEST BEARING	
SHAFT SPEED	Delta T	O.R. Temp	Delta T	O.R. Temp
20,000 rpm	1.7 K (3 °F)	93.3 K (-292°F)	0.33 K (0.6°F)	93.3 K (-292°F)
37,000 rpm	10 K (18°F)	217 K (-69°F)	1.1 K (2°F)	101 K (-279°F)

Exhibit 274 Model Predictions for LH2 Bearing Tester with LN2

dated routine was checked against tabulated properties to ensure accurate results. The hydrogen properties calculated correlated to the tabulated values. Tests were conducted to verify that the new preload spring model, developed specifically for the Hybrid Bearing Tester, was functioning properly. The tests showed that the new model accurately simulates the spring and also that the initial set up required to model a preload spring is more straightforward and simplistic than with the previous model.

6.6 Test Support for the MSFC LH2 Bearing Tester

The liquid nitrogen shake-down testing of the bearing test rig was initiated in _____. The objective of the initial tests was to verify instrumentation and test procedures prior to beginning the actual test series using liquid hydrogen. Two anomalies were identified during the first test. During the chill down period, tank pressures and line pressures did not respond as anticipated. In-situ inspection of the hardware revealed that a manual valve used for inspection had been left open. Verification of valve position was incorporated into the procedures. The second anomaly identified related to the delta pressure between the two ends of the bearing tester under test flow conditions. An automated control system is used to control flow to the lower cavity, thus controlling the delta pressure. During the run the control valve went to full open; however, the flow was not sufficient to maintain the correct pressure in the cavity. This anomaly was corrected with hardware modifications. The tester was rotated at speeds up to 20,000 rpm for a short period during the test. Bearing outer ring temperature rose to higher than expected values and rotation was terminated. Post test analysis showed that the temperature rise was consistent with larger axial loads caused by the pressure differential in the cavities. The analysis showed that the bearing was not over-stressed during the run. Hardware modifications to the lower cavity flow control later eliminated the additional loading.

The objective of the second test was primarily to verify the corrections to the lower flow cavity control. During the test, flow was brought up to test conditions and the pressure differential between the two cavities was monitored. The cavity pressures tracked as expected. Some modulation, on the order of +/- 50 psi, was observed as the valve controller modulated the valve to maintain the pressure differential. This magnitude of load change on the bearings was not a significant concern for the twin ball bearing test.

The Liquid Hydrogen Bearing Tester at MSFC Test Position 506 has successfully completed the LN_2 verification runs and was converted for testing with LH_2 during February 1996. This build of the LH_2 Bearing Tester utilized a Pratt & Whitney HPFTP/AT ball bearing with steel balls in the Reaction Bearing position (top bearing), an HPFTP/AT ball bearing with silicon nitride balls in the Test Bearing position (middle bearing), and a hydrostatic fluid film bearing in the Slave Bearing position (bottom bearing). The two ball bearings are preloaded against each other with a 1000 lbs of axial load.

Test P2026013. A non rotating cold flow test with LH_2, designated P2026013, was performed as a check of instrumentation function and for fluid leak detection. The LH_2 pressure was increased to the operating set point of 1500 psig and flow rates of 0.5 pps through the ball bearings and 0.75 pps through the fluid film bearing were established and maintained for approximately 700 seconds. The top cavity vent was closed to

prevent leakage flow through the shaft top seal, thus, the thrust piston was used to counter the pressure loading (PA) on the top end of the shaft. The pressure in the thrust piston was automatically controlled to maintain 200 psi higher than the top cavity pressure when tester pressure was at operating level. However, the thrust piston pressure fluctuated +/-150 psi about the desired level at a very high frequency. It was not known if the fluctuation anomaly was due to the controller or cavitating flow in the tubing. All other pressure and temperature measurements looked acceptable.

Test P2026014. The first rotational test in LH_2, designated P2026014, was then successfully performed at a shaft speed of approximately 7500 rpm for 220 seconds with 1000 lbs axial preload and no radial load. Steady speed was difficult to maintain in this low range and again the thrust piston pressure fluctuations were observed. The axial displacement photonic did indicate axial shaft movement of approximately +/-0.0005 inches with the same frequency as the thrust piston pressure fluctuations. Again, the cause of the pressure fluctuations was not known. The turbine drive supply pressure also exhibited high frequency fluctuations of +/-50 psi. The turbine pressure anomaly may have been caused by the thrust piston pressure fluctuations since the two pressure supplies shared a common exit. The tester supply and exit pressures were acceptable near their set points of 1500 and 1450 psig, respectively. Also, the hydrostatic bearing supply pressure was stable at 1860 psig. All other pressures were in the acceptable range.

The temperature data from Test P2026014 showed all the measurements were nominal except for T213 and T212 which are the Reaction Bearing outer race and turbine exit, respectively. The remaining outer race temperature measurement on the Reaction Bearing appeared to be functioning but not sensing the metal temperature since it did not respond to speed changes as did the measurements on the Test Bearing. The coolant flow rates looked good at 0.5 pps to the ball bearings and 0.8 pps to the hydrostatic bearing.

Test P2026015. This test was performed and successfully achieved a shaft speed of approximately 15,000 rpm with most operating parameters being the same as the previous test. The only exception being that the thrust piston pressure was placed in the manual control mode. This change was made in an effort to determine the cause of the thrust piston high frequency pressure fluctuations exhibited in the earlier tests. The result of the control change was a much improved behavior of the thrust piston supply pressure. Fluctuations were now in the acceptable range of +/-15 psi. Also, the axial displacement showed almost no vibration during this test as a result of the decreased pressure fluctuations. However, the turbine supply pressure still exhibited high frequency fluctuations of +/-50 psi. This did not seem to have a significantly detrimental effect on the shaft speed and may be normal for this type turbine drive.

The other temperature and pressure data showed no anomalies. The Test Bearing outer race temperatures indicated an 8 deg. F rise with shaft speed. However, the one remaining measurement on the Reaction Bearing did not respond with speed and actually showed a 5 deg. F decrease over the 300 seconds at speed. These outer race temperature measurements may be strongly influenced by coolant flowing in the bearing deadband. Also, the temperature rise and pressure drop across the ball bearings are diffi-

cult to determine due to the location of the measurements. The awkward location of the measurements are a consequence of retrofitting rolling element bearings to a tester that was initially designed to utilize fluid film bearings in all three positions.

Test P2026016. This test was not successfully completed due to a pressure control problem. The first attempt was terminated approximately 10 seconds after shaft rotation start due to a cut caused by T204 reading high. This is the temperature between the ball bearings and it was determined that the measurement was in error due to an instrument malfunction. The tester was quickly recycled for another attempt but was cut before rotation due to T215 reading high. At this point it was decided to shut down and review the "quick look" data for possible flow problems. The data review showed that the flow through the ball bearings had been shut off due to the EHV-3106 valve on the exit line closing. EHV-3106 is automatically controlled and was set up to maintain 1450 psig in the exit line. However, the inlet pressure drifted from its desired level of 1500 psig to just below 1450 psig. Thus, EHV-3106 tried to maintain the back pressure at 1450 psig and closed. As a temporary solution, EHV-3106 was manually set to 22% open position which is the nominal operating position for back pressures near 1450 psig if the inlet is at 1500 psig. This control change prevents EHV-3106 from shutting off the flow. As a more permanent solution, EHV-3106 was set to automatically control off of a delta pressure measurement across the tester to maintain a 50 psi drop.

Test P2026017. This test was successfully performed with a maximum speed of 37,000 rpm for a rotational time of approximately 780 seconds. This test was run to tank depletion as planned. The data showed that all the temperature measurements began to increase slightly at the end of the run, as expected, due to the last portion of the fluid in the run tank being heated by the ambient pressurization gas. Thus, an operational procedure was adopted to consider tank depletion to occur when the tank exit temperature reaches -400 deg. R. Two anomalies were observed in the test run. The tank pressure increased approximately 25 psi or 1.2% during the constant speed portion of the test. This pressure increase had no detrimental effect on the test. The second anomaly was an increase in required turbine power to maintain a constant speed for the last 150 seconds of the test. This power requirement increase coincided closely with the fluid temperature increase as the tank neared depletion. However, due to the limitations of the instrumentation around the bearings, the increased power could not be verified as increased heat generation in the bearings. The outer race temperatures of the Test Bearing increased 8 deg. F shortly before tank depletion while the inlet fluid temperatures increased 7 deg. F. This 1 deg. F net rise in outer race temperature may explain the power requirement increase. Also, the axial displacement data indicated that the shaft moved upward during the temperature increase near the end of the test. This movement could have been caused by a thermal expansion of the Test Bearing changing the bearing "stick out" and resulting in shaft movement.

Test P2026018. This test achieved the planned test speed of 35,000 rpm for approximately 90 seconds with radial load. However, the test was not run for the planned duration due to LH_2 run tank depletion. The liquid level sensor in the run tank malfunctioned prior to tank loading. Therefore, accurate measurements of LH_2 volume were not available. Estimates were made for the amount of liquid in the run tank. Apparently, the

tank level was at only 20% when it was thought to be full. After final tester chill down there was only enough hydrogen for 240 seconds of rotation time.

Test P2026018. This test was the first test with applied radial load. A 300-lb radial load was applied to the Test Bearing through Radial Load Cell #1. This load was reacted by the Reaction Bearing and the Slave (hydrostatic) Bearing. The SHABERTH computer model of the tester predicted 80% of the applied load would be reacted by the Reaction Bearing and 20% by the Slave Bearing. The shaft speed was first brought up to 20,000 rpm and then the radial load was applied before increasing the speed to the test goal of 35,000 rpm. However, the addition of the radial load was not discernible from the temperature measurements on or around the bearings. The application of the radial load was concurrent with a drop in shaft speed which may have masked the load's affect on the bearing temperature. The speed decrease was due to the controller allowing the turbine pressure to drop while the radial load was being adjusted. Also, the steady-state temperatures were not directly comparable to the previous test since the previous test speed was 37,000 rpm. Pretest analysis with the SINDA/SHABERTH thermomechanical model of the tester predicted that the small radial load would make no measurable difference in the coolant temperature rise across the ball bearings and only a 0.1 degree R increase in outer race temperature of the Test Bearing. This prediction was supported by the test results.

Test P2026019. This test was unsuccessful after three attempts. The first attempt was terminated by T204, fluid temperature between the ball bearings, reading high after only a few seconds into rotation. The reading appeared to be functioning properly as seen from the monitor output. However, the monitors are updated at approximately 2 second intervals and a spike in the reading caused by a thermocouple malfunction could have missed. Therefore, the test was recycled. The second attempt was cut by SP201, shaft speed, indicated high. This was an obvious instrumentation malfunction because the turbine drive pressure had not yet been increased at that time. Review of the speed reading on the monitor after the second cut showed normal and the test was recycled again. The third attempt was cut by SP201 and T206, fluid temperature between the Test and Slave Bearings, reading high. The controller reported that his speed indicator never showed a shaft speed higher than 10,000 rpm. The shaft speed redline was set at 40,000 rpm. Thus, it was decided that the speed indicator had a serious malfunction and the test was scrubbed.

Review of the high speed data for Test P2026019 showed that the turbine pressure had been increased to above 800 psig on the first and third attempts. Usually a turbine drive pressure of 800 psig would produce a shaft speed of approximately 35,000 rpm. The shaft speed data showed 3000 rpm for the first attempt and 13,000 rpm for the third attempt. Also, the speed data showed 23,000 rpm for the second attempt with zero turbine drive pressure. Based on this data it was obvious that the speed sensor had malfunctioned and that the first and third attempts had really overspeed causing the high fluid temperature readings. Speed sensor repairs were requested.

Test P2026020. This test was unsuccessful after one attempt. The run was terminated due to T206 high soon after rotation start. As in the previous test, the controller said he did not see the speed response expected for the corresponding

turbine drive pressure supplied. Thus, the shaft was again overspeed due to malfunction of the speed sensor. Work on the speed sensor was again requested.

Further testing was scrubbed due to a leak in the LH_2 run tank. The tester had been chilled and brought up to operating pressure when a leak at the top of the run tank was detected. Shut down and safety procedures were initiated. Testing will resume after run tank repairs are made.

Build 0 Summary. Testing of a set of Pratt & Whitney HPFTP/AT ball bearings in the liquid hydrogen bearing tester at MSFC was concluded and post-test inspection of the bearing components was performed during April 1996. This test series subjected the bearings to operation time in liquid nitrogen for the initial rig verification tests and liquid hydrogen for full speed bearing testing. The total rotational time accrued on the bearings was approximately 35 minutes with 27 minutes of the time utilizing LH_2. The rotational time at or above 35,000 rpm was 11.7 minutes. The ball bearings were preloaded with 1000 lbs of axial load and a 300 lbs radial load was applied for the last rotational test. However, early in the test series there was a problem with the thrust piston load oscillating rapidly which is believed to have caused the axial load on the Reaction Bearing to vary from 700 to 1300 lbs and on the Test Bearing to vary from 0 to 1300 lbs.

The Test Bearing (middle bearing) utilized silicon nitride balls, Cronidur 30 stainless steel inner race, 440C stainless steel outer race, and an Armalon cage with Salox pocket inserts. After disassembly and inspection the balls appeared to have "check" cracks over their entire surface. Also, cracks perpendicular to the tracks could be seen in the track path with minor surface spalling in this area. The spalls were not deep, almost as if the material in between cracks had flaked off. The appearance of the balls from the MSFC tester was much worse and not very similar to the observed condition of silicon nitride balls that had been run in the P&W fuel pumps. The outer race had a matte finish in the track with a bronze color indicating good Salox transfer. There were no spalls observed in the raceway and only minor debris denting. The inner race had surface distress on the lower portion of the track and there appeared to be Salox transfer in the remainder of the track. The cage had moderate ball to pocket contact in the fore and aft directions and only light contact side to side. The outer diameter guiding surface of the cage had moderate contact at two pocket positions indicating a slight imbalance.

The Reaction Bearing (top bearing) utilized 440C stainless steel balls and outer race, 9310 stainless steel inner race, and the Armalon/Salox cage. The balls have matte finish tracks that are bronze in color indicating Salox transfer. No spalls or other surface degradation was detected on the balls. The inner race track surface appeared similar to the ball surfaces with a light bronze matte finish. Also, the inner raceway had no surface degradation other than some light debris denting. The outer race track appearance was very similar to that of the inner race. There was some light scaring on the outside diameter of the outer race that could have been caused by the race spinning in the sleeve. The cage showed very light contact on the guide land surface and only fore and aft contact in the ball pockets.

The Slave Bearing (bottom bearing) was a hydrostatic bearing and the outer race portion was not removed from the tester housing but was visible from the open top of the housing while the shaft formed the inner race and was removed for inspection. The inner race had two light scratches

360 degrees around the race. The outer race had corresponding marks but on only one web in between two pockets. It was theorized that debris in the one pocket collected in the corners until it was thick enough to contact the shaft.

The shorter life of Build 0 has been determined to be a product of the poor axial load control during the test. The bearings were subjected to some severe axial load variations at high frequency. This resulted in development of an improved load control scheme for future builds.

6.7 Test Support for the MSFC LH_2 Bearing - Build 1

The next build of the MSFC LH_2 Bearing Tester utilized the ball bearing and the roller bearing from the Pratt & Whitney HPFTP/AT Units 5-2 and 6-4, respectively. This was the first LH_2 Bearing Tester build configuration to test a roller bearing. The silicon nitride ball bearing was placed in the Reaction Bearing (top) position with the silicon nitride roller bearing in the Test Bearing (middle) position. The Slave Bearing (bottom) position utilized the hydrostatic bearing as in the previous build.

The SINDA/SHABERTH computer model of the LH_2 Bearing Tester was modified to simulate the ball and roller bearing build configuration. The SHABERTH data deck for the P&W roller bearing was integrated into the SINDA/ SHABERTH model of the LH_2 Bearing Tester. The model was updated by substituting the preload spring routine, required when bearings are preloaded against one another, with a fixed axial load simulating the tester thrust piston. This modification provides better control of the simulated loads on the test bearings and allows improved simulation of dynamic axial load fluctuations caused by fluid pressure changes in the tester..

A SINDA thermal model of the P&W roller bearing, previously developed by SRS for Pratt & Whitney, was used in the LH_2 Bearing Tester model. However, it was determined during the analysis for Pratt & Whitney that the roller bearing generates such low heat rates for the HPFTP/ AT conditions that the average component temperatures rise less than 20 degrees above the coolant temperature. It was also shown that because the contact areas are large in roller bearings and slip velocities are low (compared to a comparable ball Bearing) maximum track temperatures also remain low. Therefore it was expected that thermally converging the roller bearing would not be required for every analysis. The updated tester model was executed once in the fully coupled mode to establish baseline operating temperatures for all of the components. The roller bearing thermal model was then be optionally turned off for subsequent analysis to reduce simulation time.

Build 1. SRS performed pretest scaling of flow rates and pressures for the first rotational test of the current bearing tester configuration. The tester utilized the ball bearing and the roller bearing from the Pratt & Whitney HPFTP/AT Units 5-2 and 6-4, respectively. Initial shake down runs were performed in liquid nitrogen. Data was reviewed from previous LN_2 runs to estimate turbine delta pressure requirements expected for initial rotational tests. It was determined that torque and coolant flow rates should not be significantly different from previous LN_2 tests performed with the tester in the two ball bearing configuration. Similarly, it was determined that tester fluid flow rates and coolant requirements would be similar to previous tests. SINDA/SHABERTH models were switched over from LH_2 to LN_2 in order to prepare for post test analytical support to the upcoming test series.

An improved method for post-test data processing was established. During the last test series, data review was based solely on review of the data plots provided by MSFC engineer Mr. H. N. Strong. It was determined that access to the raw data would improve review of the data by SRS and yield more useful information for correlation with the analytical models. Mr. Strong met with Dave Marty to review various options. It was determined that it was not practical for SRS to execute the MSFC data processing software over the then current modem-based connection to the MSFC EADSII computer system. The MSFC data processing software is not compatible with the terminals used for dial-in access. It was found that the best approach for SRS post test data processing is for SRS personnel to travel to MSFC and utilize the data processing package from the MSFC computer lab. Mr. Strong provided a short introduction to the software.

Test P2026021. The primary objective of the hydrogen bearing tester was to evaluate and quantify silicon nitride bearing rolling element wear modes under tightly controlled test conditions Defining the parameters influencing the formation o the "river mark" surface features observed in some HPFTP/AT ball and rolle bearings was of particular interest. The river marks hac been seen on most of the bal bearings inspected after extended engine testing and or roller bearings that have beer subjected to abnormally higl loads during engine tests. Fo the current test series, the tester was configured with one roller bearing and one ball bearing, as illustrated in the bottom half of **Exhibit 275**, in order to obtain test time for both bearing types. In this configuration an axial preload spring loads the outer race of the ball bearing which transmits the load to the shaft and forces the shaft towards the axial thrust piston illustrated on the right hand side of **Exhibit 275**. The roller bearing is not designed to carry an axial load, therefore, shaft position must be maintained by balancing the pressure loads on each end of the shaft. Axial load balance proved to be difficult with the tester in this configuration. Consequently, during testing the shaft contacted the housing portion of the thrust piston resulting in moderate rub damage to the shaft and thrust piston.

The test described above was the first shake down test of the liquid hydrogen bearing tester in the ball and roller bearing test configuration. The shake down test was conducted using liquid nitrogen to verify procedures and instrumentation prior to hydrogen testing. During test P2026021 the unit was chilled and the turbine

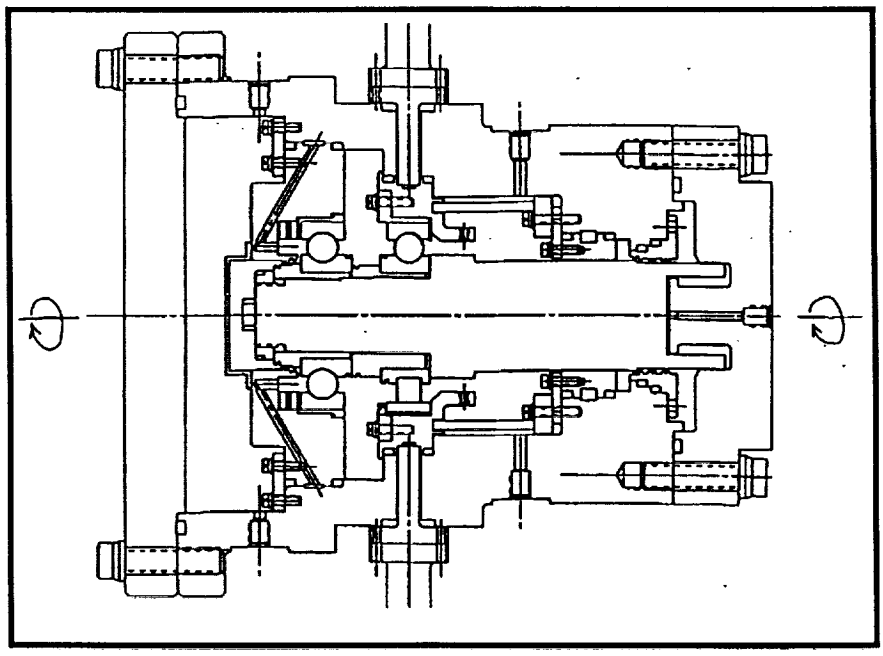

Exhibit 275 Liquid Hydrogen Tester Cross-Section

TP00-1017

pressure was increased three separate times to initiate rotation. The speed sensor indicated rotation during the first and second rotational attempts and rotation was confirmed audibly. Speeds of 36,000 and 40,000 RPM were indicated for the first and second rotations respectively. However, one of the shakedown test objectives was to obtain data required to calibrate the speed sensor, therefore, the magnitudes of speed detected were not considered valid.

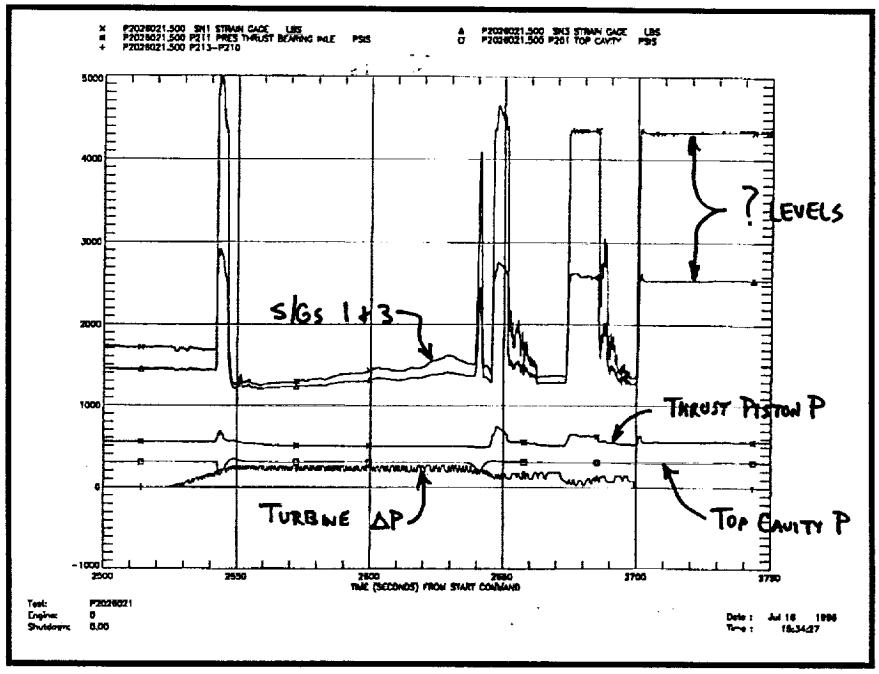

Exhibit 276 Selected Data from First Rotation

During, the first rotational period speed tracked relatively well with turbine delta pressure. However, during the turbine pressure ramp-up there was an unexpected change in the rig top cavity and thrust piston pressures. The thrust piston pressure increased while the top cavity pressure decreased. As expected the strain gages indicated a shaft motion toward the top cavity increasing the load on the ball bearing and increasing the clearance in the thrust piston. This motion occurred before the speed sensor indicated rotation. Selected data from this period can be seen in **Exhibits 276** and **277**. After the pressure anomalies peaked, the pressures returned to nearly the same values they had before turbine pressure was increased. The strain gauges showed shaft motion back toward the thrust piston as the pressures normalized. The stain gauges indicated the shaft moved back past the test start position to very near the position corresponding to bottoming the position. This would indicate rubbing in the thrust piston area.

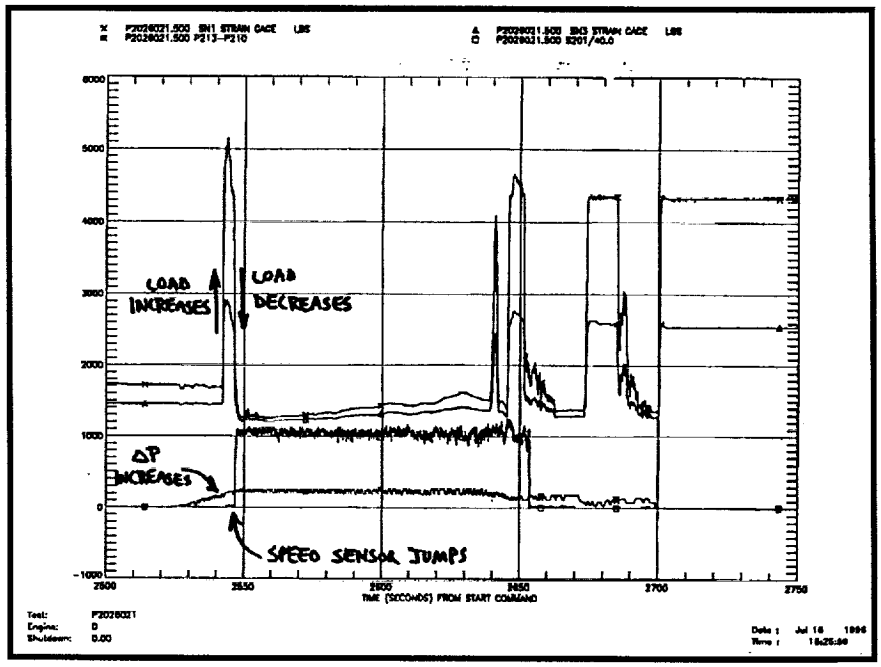

Exhibit 277 Selected Data from First Rotation

During the remaining rotational period the top cavity and thrust piston pressures remained relatively constant while the strain gauges indicated shaft motion slowly towards the top cavity. At the end of the rotational period the axial position of the shaft was approaching the pre-rotation axial position, based on the strain gauge data. As turbine pressure was decreased to stop rotation there were pressure spikes in the top cavity and thrust piston which were similar to the spikes that occurred as the turbine was pressurized. However, in this instance the spikes were slightly out of phase with the top cavity pressure decrease occurring prior to the thrust piston pressure increase. The strain gages indicated shaft motion toward the top cavity corresponding to both components of the shut down transient. It should be noted that the transient pressure variations did not seem to occur as a result of rotation. Shaft rotational break-away occurred as the start-up pressure transients subsided and rotation continued after the shutdown transient. The thrust piston transients occurred during turbine pressure ramp-up and ramp-down, however, reviewing the data did not show any correlation conclusively.

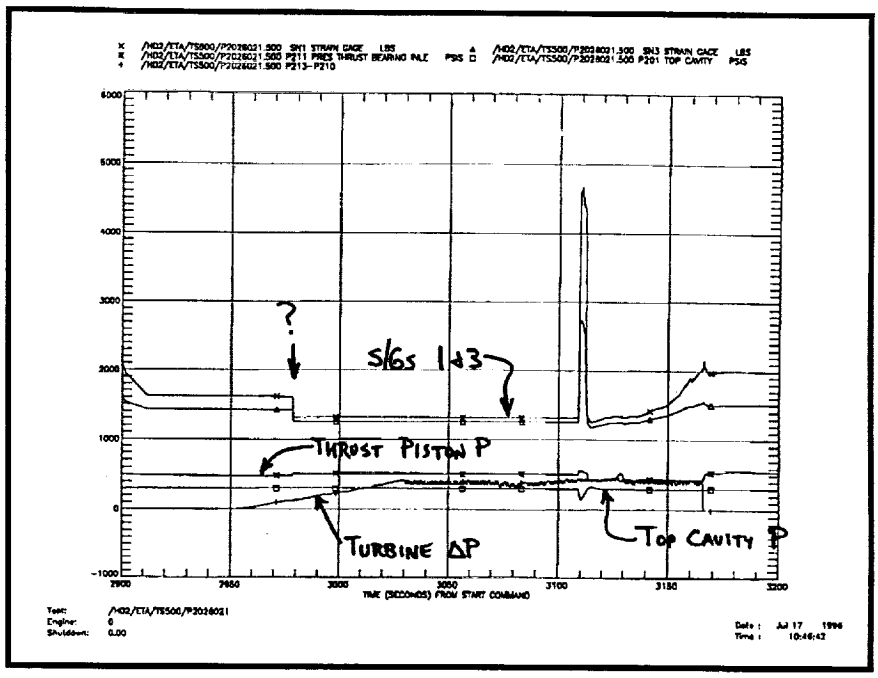

Exhibit 278 Selected Data from Second Rotation

Selected data from the second rotational attempt are shown in **Exhibits 278** and **279**. The second rotational attempt of Test 21 showed signs of possible binding or rub damage. As turbine pressure was ramped up, the strain gauges showed a shaft shift toward the thrust piston.

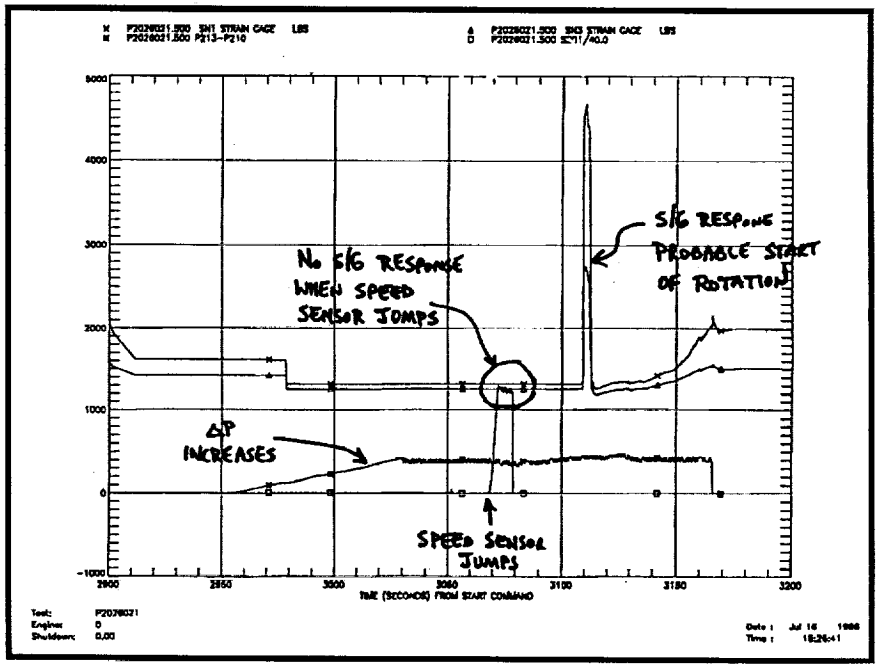

Exhibit 279 Selected Data from Second Rotation

Turbine pressure was increased gradually up to the nominal run value, however, shaft rotation was not indicated by the speed sensor. During the first 40 seconds of steady state turbine pressure the speed sensor showed only one very slow rotational movement that lasted for approximately five seconds. After 40 seconds the speed sensor indicated a jump in speed to near nominal values that lasted for approximately 10 seconds. After ten seconds the speed sensor indicated a sudden stop. The turbine pressure was relatively constant throughout the rotational periods. Shaft position did not change during any of the rotational events. The strain gauges indicated the shaft was slightly off the thrust piston. However, its possible that the shaft was contacting the thrust piston during this entire period because the data indicates a bias shift toward the top cavity occurred during the tests. There was one transient thrust piston and top cavity pressure event that occurred approximately 50 seconds after the 10 second rotation. The speed sensor data during this entire time frame is suspect because post-test inspection of the hardware showed the speed pickup was damaged at some point.

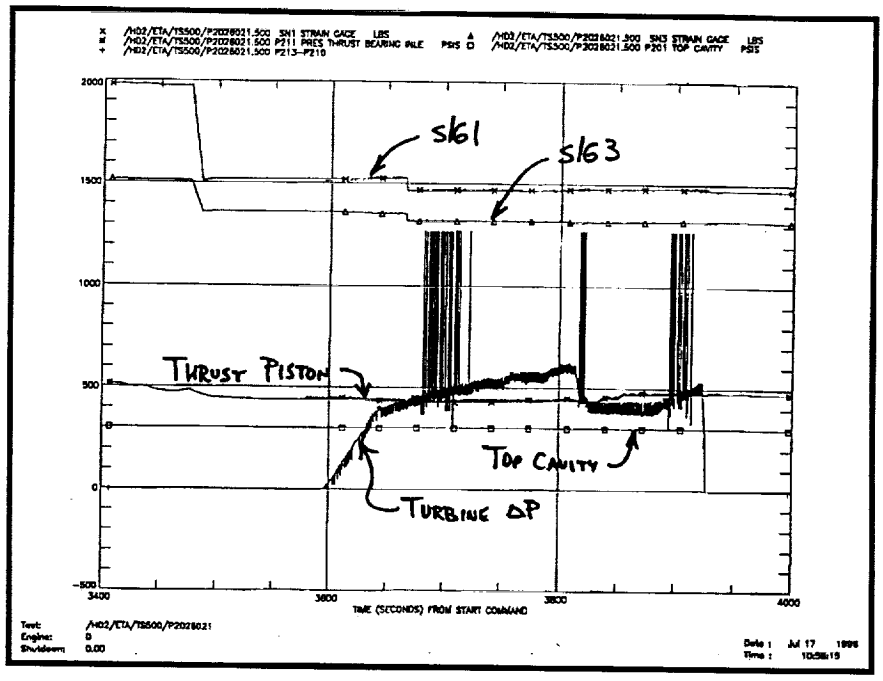

Exhibit 280 Selected Data from Third Rotation

The turbine was pressurized for a third attempt at rotation. Selected data from this attempt are shown in **Exhibits 280** and **281.** Again the strain gauges showed a shift toward the thrust piston as pressure was increased to the turbine. Turbine pressure was increased up to 600 psi, approxi-

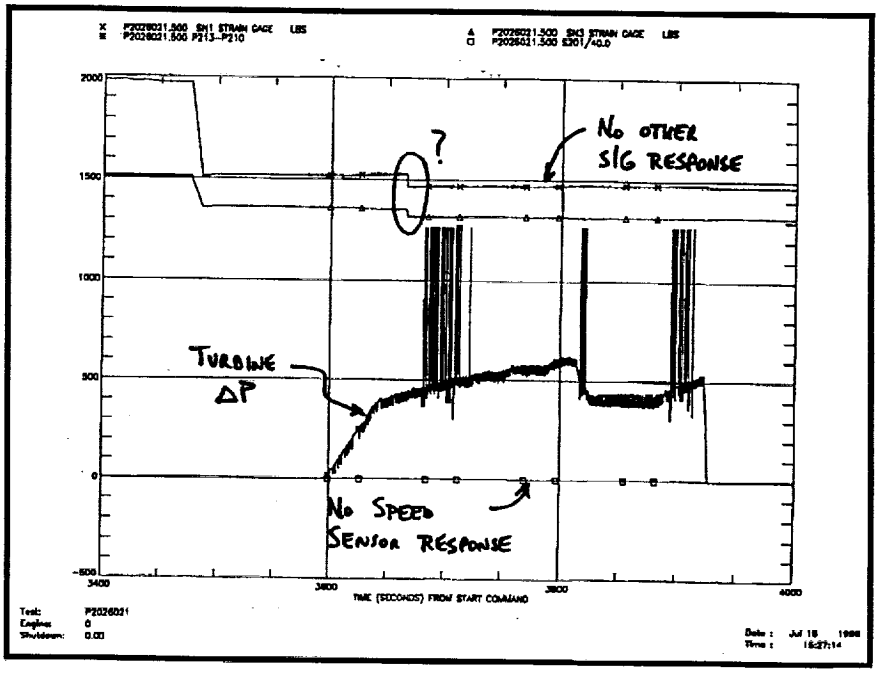

Exhibit 281 Selected Data from Third Rotation

mately 30% higher than required to rotate during rotation 1, but no rotation was detected by the speed sensor. Top cavity pressure remained constant during the entire period. Thrust piston pressure remained relatively constant, showing a slight increase toward the end of the time that the thrust piston was pressurized.

The bearing tester was disassembled after the LN_2 test to inspect for possible damage. The shaft and thrust piston both showed evidence of significant metal to metal contact during rotation. The damage was limited to the thrust piston cavity. Both bearings tested were previously used in engine tests. The ball and roller bearings did not appear to have been significantly affected by the test. The roller bearings had some river mark features but these were present when the bearing was installed. Mr. Roger Bursey, Pratt & Whitney, commented that the roller river marks might have grown slightly. The ball bearing appeared to be in near pristine condition. Mr. Chip Moore, from MSFC performed a detailed dimensional analysis to qualify the post test conditions of the bearings.

A post-test data review was conducted to discuss the test data, tester condition, and plans for the next tester build. It was concluded that fluctuations in the top cavity and thrust piston pressure balance allowed contact in the thrust piston during rotation. The tester build up resulted in less axial clearance than had been planed, thus reducing axial position margin. During testing the axial pressure balance was being controlled manually because earlier attempts to couple the top cavity and thrust piston pressures with an automated control resulted in high frequency oscillations and high loads. The possibility of reinstating automatic control based on the instrumented strain gauge or axial proximity probe was discussed. These measurements were not available during earlier tests. It was agreed that the tester would be reconfigured for the two ball bearing test configuration for the next test series. In this configuration the second ball bearing provides a relatively stiff axial position control to prevent rubbing in the thrust piston area. However, axial pressure balance is still important to prevent overloading the bearings. The instrumented preload spring was returned to Pratt & Whitney for re calibration prior to the next build.

6.8 Test Support for the MSFC LH_2 Bearing Tester Build 2

As reported in the previous section, Bearing Test P2026021 resulted in axial rub damage in the thrust piston area of the tester. The rub resulted from pressure transients which occurred when the turbine was pressurized to initiate rotation. During August 1996, several steps were taken to prevent this type of rubbing from occurring in future tests. First, it was decided that the tester would be repaired and then re configured to run with two ball bearings. This configuration was much stiffer, axially, than the ball and roller bearing configuration of test P2026021. The ball bearing in the test position reacts directly against the housing resulting in an axial stiffness of approximately 500,000 lbs/in for loads in the direction of the thrust piston. In this configuration, an extremely large pressure imbalance is required to cause rubbing in the thrust piston. Procedural changes were also implemented to minimize the start-up transients. The test procedure was modified to minimize pressure imbalances and an automated control circuit was installed to provide closed loop control to thrust piston flow based on feedback from the strain gauge on the bearing preload spring.

Build 2 Liquid Nitrogen Test. The tester was repaired and HPFTP/AT Pump End Ball Bearing (PEBB) F5-3A was installed in the test bearing location, HPFTP/AT PEBB F5-2 was installed in the reaction bearing location. The new tester build was installed on Test Stand 500 for the upcoming test series. An LN_2 cold flow / leak check was performed on August 30, 1996.

Test P2026022. The objective of the test was to verify the integrity of the rig plumbing prior to high pressure hydrogen testing. During the pressure test the top cavity was pressurized manually to 1500 psi. The thrust piston pressure did not track the top cavity pressure and this allowed a lager than expected axial load to be placed on the reaction bearing. Post processing of the data showed that the reaction bearing was statically subjected to an axial load of approximately 11,000 lbs. **Exhibit 282** shows the bearing loads for the test period. SHABERTH analysis predicts an inner race maximum contact of 687,000 psi for the bearing under the chilled test conditions. This exceeds the ANSI static load capacity rating which states that maximum contact stress should not exceed 609,000 psi. However, past experience has shown that the increased material yield strength at cryogenic temperatures allows the bearings to tolerate increased loads before detrimental Brinelling occurs, typically, up to 675,000 psi. Therefore, during this test the reaction bearing was slightly over stressed. The over stress could lead to reduced fatigue life for this bearing.

The LN_2 leak check verified the integrity of the rig and facility for high pressure hydrogen testing. The data review following the test provided insight for improvements to the test procedures and controls that were implemented to prevent a recurrence of the overload condition. Two options were identified for providing positive load control throughout the test profile. In future tests closed loop control would be provided between the strain gauge and the axial thrust piston or between the top cavity pressure and the axial thrust piston. Ultimately, the decision was made to control based on the delta pressures. With these modifications in place it was decided to proceed with hydrogen testing.

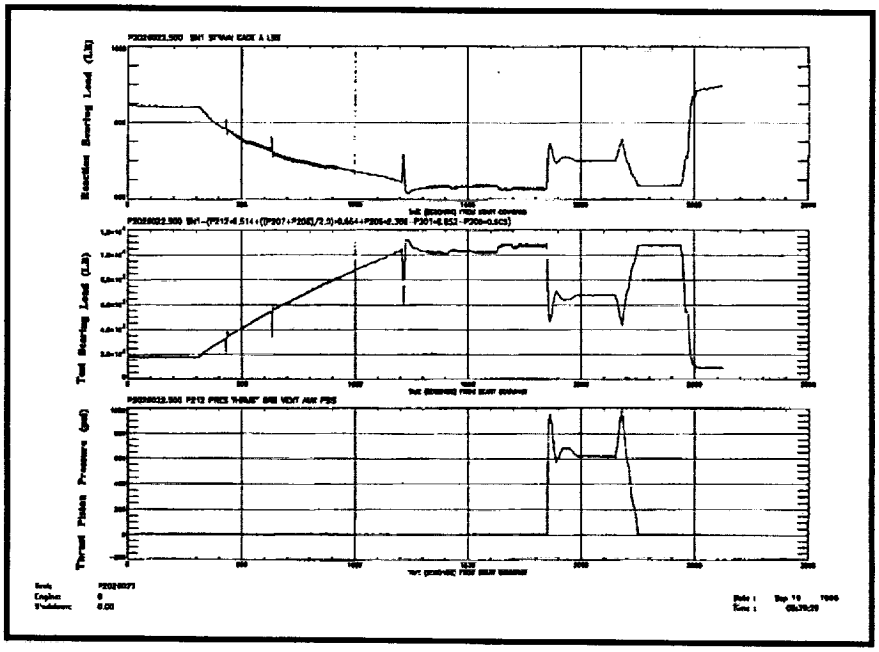

Exhibit 282 Bearing Loads During LN2 Leak Test

Build 2 Test Objectives. The overall objective of this LH_2 bearing test program was to support the SSME HPFTP/AT program by investigating the formation mechanisms and consequences of the "river mark" surface features observed in post engine test silicon nitride rolling elements. The river mark features appeared on the surface of the balls as

thin crack like marks often branching out like tributaries to a river. However, close inspection of the marks showed that they were typically flat bottomed troughs in the surface and that they were usually much wider than deep. The flat bottom suggested that they were more benign than a typical crack and not susceptible to propagation into the depth of the rolling element. Balls with known river marks have been successfully run in pumps; however, engine test time is limited and the long term durability of river-marked bearings has not been demonstrated. This LH_2 bearing rig test series was designed to evaluate the capability of severely river-marked bearings to continue to perform nominally throughout the complete design life of 8 hours.

The particular objectives of the Build 2 tests were to verify test procedures and instrumentation in order to demonstrate that the test rig could produce an operating environment similar to the turbopumps. This test series was a follow-on to the original shakedown series and subsequent Build 1 Series. During the shakedown test, which was the first time a rig of this design was used for ball bearing test, axial load control problems were experienced. The axial load is controlled by a preload spring and balancing the top cavity pressure with an axial thrust piston. Early in the test series the bearings were subjected to high frequency load variations of up to 5000 lbs. Post test inspection of the bearings revealed distress not typical of engine hardware. The Build 1 series involved using a roller bearing in the test bearing location. Again, axial load control proved difficult and the test was terminated due to axial rubbing. For Build 2 it was decided to return to the two ball bearing configuration and incorporate several procedural changes resulting from the experience of the previous runs. With the new procedures in place it was believed that axial load control could be achieved and the rig could successfully emulate the pump. To demonstrate this, Build 2 was assembled using two HPFTP/AT bearings that were known to be in good condition. The Build 2 test objective was to acquire approximately 30 minutes of simulated engine run time and then disassemble and inspect the bearings. The bearing inspection results would be used to determine if there were any anomalous rig test conditions that might introduce damage mechanisms not associated with the pump application. After accomplishing the Build 2 objectives, the rig would be reassembled and the reaction bearing would be replaced with a bearing with pre-existing heavy river mark formation. The rig would then be run with the goal of demonstrating 8 hours of operational time on the river-mark bearings.

Build 2 Test Series Highlights. This test series consisted of 11 cycles, as summarized in **Table 7**. The first cycle was performed using LN_2. The LN_2 cycle was conducted to leak-test the rig. No rotation was attempted. During the leak test the top cavity was pressurized but the thrust piston was not. Post Processing of the data showed that the bearing was axially loaded to approximately 11,000 lbs, resulting in contact stresses of approximately 687,000 psi. Therefore, slight brinelling of the bearing is expected. This is not expected to significantly affect the performance of the bearing. Following the leak check, four LH_2 cycles were performed to verify LH_2 cool down and to verify rig performance at low speed.

During the first three low speed rotation attempts, an axial load calibration of the tester was conducted but no rotation was attempted due to various instrumentation and facility problems. The first rotation of the tester occurred on the fourth LH_2 test cycle. After the chill down cycle

Table 7 Test Series Summary

Test#	Fluid	Time at Speed (Sec)	Nominal Test Speed (RPM)	Remarks
P2026022	LN_2	0	0	LH_2 leak
P2026023	LH_2	0	0	Axial load balance calibration
P2026024	LH_2	0	0	
P2026025A	LH_2	0	0	Load bearing unloaded
P2026026	LH_2	47	> 50,000	1 min dwell @ 10K, 20K and 30K
P2026027	LH_2	541	35,000	Static reverse axial load on load
P2026028	LH_2	61	Up to 45,000	bearing
P2026029	LH_2	209	35,000	165 lb radial load
P2027030	LH_2	104	35,000	125 lb radial load
P2028031	LH_2	555	35,000	125 lb radial load
P2028032	LH_2	309	35,000	155 lb radial load

- Total rotational test time on Build 2 was approximately 2,441 seconds.
- Total rotational test time at or above 35,000 RPM was approximately 1,826 seconds.
- Nominal axial load in the bearings for rotational tests was approximately 1,060 lbs.
- Radial loads were applied as noted above.
- The load bearing was statically axially loaded to 12,000 lbs, during test P2026022, resulting of maximum contact stresses of approximately 687,000 psi.
- High frequency turbine inlet pressure fluctuations were noted during rotational tests.
- Turbine pressure fluctuations produced speed fluctuations of approximately 500 RPM.
- Reaction bearing used was from Pump Build F5-2 and had 276 seconds of engine run time prior to being installed in Tester Build 1. The bearing acquired 230 seconds of low speed run time in tester Build 1 prior to being installed in the tester Build 2.
- Load bearing used was from Pump Build F5-3A and had 932 seconds of engine run time prior to being installed in tester Build 2.

of this test, the GN_2 turbine inlet pressure was increased to start rotation. Turbine inlet pressure was raised from 0 psi to approximately 1,100 psi. The speed sensor reported no rotation. This was the first rotational attempt and there was no baseline established for the expected breakaway torque and corresponding turbine inlet pressure. Engineers monitoring the data noted no speed indication, but did notice bearing temperature increasing. The test was cut and later evaluation of the data showed that the tester was actually rotating during the test. The estimated maximum speed was between 50,000 RPM and 65,000 RPM. Data analysis also showed that during the test period the reaction bearing was loaded axially to approximately 1,400 lbs and the load bearing was unloaded. This event lasted approximately 50 seconds.

The six remaining LH_2 tests produced approximately 2,382 seconds of rotational test time with approximately 1,238 seconds of rotation above 35,000 RPM. Load and speed control were maintained relatively well for these rotational tests. However, two anomalies were noted. During test P2026028 the speed sensor failed again, resulting in an overspeed to an estimated 45,000 RPM. The other noted anomaly was an inadvertent pressurization of the axial load piston which occurred after chill down but prior to rotation. This resulted in reverse axial loading of the test load bearing and possible slipping of the outer race in the housing. The top cavity of the tester was later pressurized to reseat the bearing. Strain gauge data showed that this procedure was successful.

The tests conducted during this Build resulted in calibration and verification of test rig operating parameters. The test procedures and load control mechanisms had now been optimized. The last four tests of this series demonstrated that the rig could be operated in a manner which closely emulates the load and speed conditions experienced by the bearings when installed on an engine. Based on these results, the test series was terminated so that the reaction bearing could be replaced with a river-marked bearing for continued testing.

Bearing Configurations. Bearing configurations for Build 2 are shown in **Table8**.

Axial Load Calibration. A test was performed during test P2026024 to provide data needed to calibrate the pressure balance on the shaft as required to control axial load. The rig is designed to axially load the bearings via a beam spring which reacts between the housing and the outer race of the reaction bearing (top bearing). The assembly preload is controlled by the thickness of a spacer between the housing and outer race. The reaction bearing transmits the axial load to the shaft. The load in the shaft is reacted through the load bearing to keep the shaft in equilibrium. Therefore, in the absence of any additional loads applied to the shaft, both bearings experience equal and opposite loads. This load can be measured from the output of the strain gauges mounted to the preload spring. However, during operation the end of the shaft and the inner rig are exposed to the high pressure hydrogen coolant flowing through the bearings.

Table 8 Bearing Configurations

Reaction Bearing (Top Bearing)	P/N4700318SK20 Inner Race, Cronidur 30, Curvature .58 Outer Race, 440C, Curvature. 52 11 Balls, Si3N4, diameter 0.8105 in Cage Armalon with Salox inserts Axial end play (60 lb load) 0.0278 in
Load Bearing (Bottom Bearing)	P/N4700318SK12 Inner Race, Cronidur 30, Curvature .58 Outer Race, Cronidur 30, Curvature. 52 11 Balls, Si3N4, diameter 0.8105 in Cage Armalon with Salox inserts Axial end play (60 lb load) 0.045 in

The bottom of the shaft is not exposed to this high pressure. The pressure load is reacted through the load bearing. The load bearing axial stiffness is very large (approximately 500,000 lbs/in) compared to the stiffness of the preload spring (13,333 lbs/in). The high stiffness of the bearing means that the shaft moves very little in response to axial load. The small shaft motion resulting from load applied to the load bearing causes very little force change in the soft preload spring and thus the load in the reaction bearing. To avoid overloading the load bearing, an axial thrust piston is pressurized during tests to offset the pressure load applied by the hydrogen. A small imbalance between the pressure times area load on the ends of the shaft can create large load variations in the load bearing. Detecting the imbalance with the preload spring strain gauges is difficult because of the small shaft position changes and softness of the preload spring. Thus, a test was performed to calibrate the tester and improve axial load control for the load bearing.

The pressure imbalance on the shaft can be calculated by summing the pressure times area values over all of the shaft surfaces exposed to fluid pressure. The exposed areas are easily determined from the drawings of the tester. However, determining the pressure acting on these surfaces depends on instrumentation which cannot always be located exactly on the affected surface. Therefore, calculation of the pressure loads is subjected to potential errors and must be calibrated.

The calibration test involved varying the thrust piston pressure and monitoring shaft displacement. During the test period the top cavity pressure was increased to the nominal test pressure of 1,170 psi. The thrust piston pressure was raised to approximately 1,100 psi. Before the test it was calculated that this configuration would produce a significant thrust imbalance in the direction of increasing the load on the load bearing (down). The thrust piston pressure was then increased over a range calculated to pass through equilibrium and produce a net upward thrust imbalance. The pressure profile from the test is shown graphically in **Exhibit 283**. During the test, shaft displacement (calculated by dividing the indicated strain gauge load by the stiffness of the preload spring) was recorded. The results from the test are shown in **Exhibit 284**. The test produced the expected nonlinear load deflection curve. The inflection point on the curve corresponds to unloading of the load bearing. At this point, the pressure imbalance is equal to the load

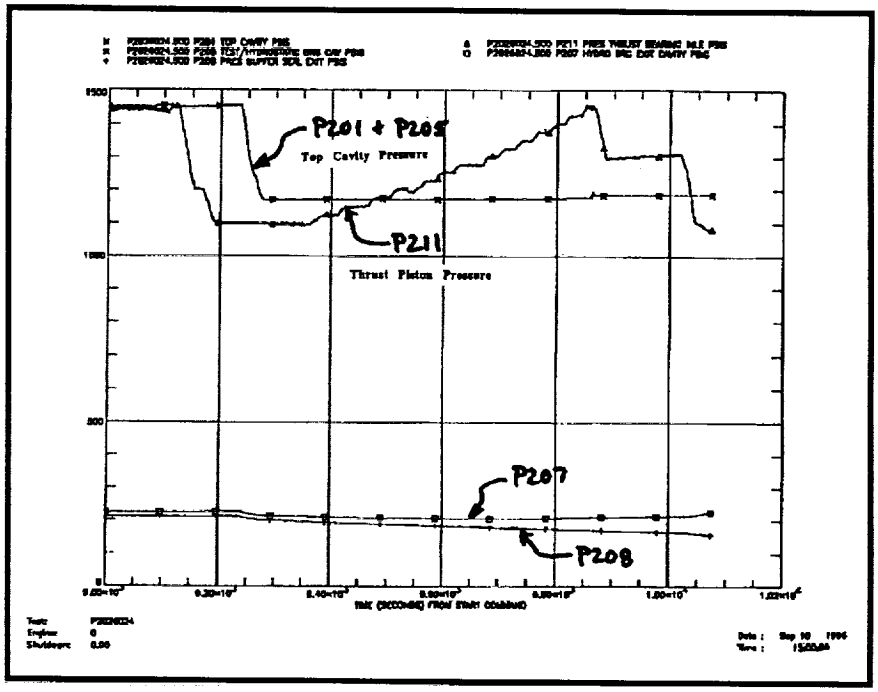

Exhibit 283 Pressure Profile for Axial Load Calibration Test

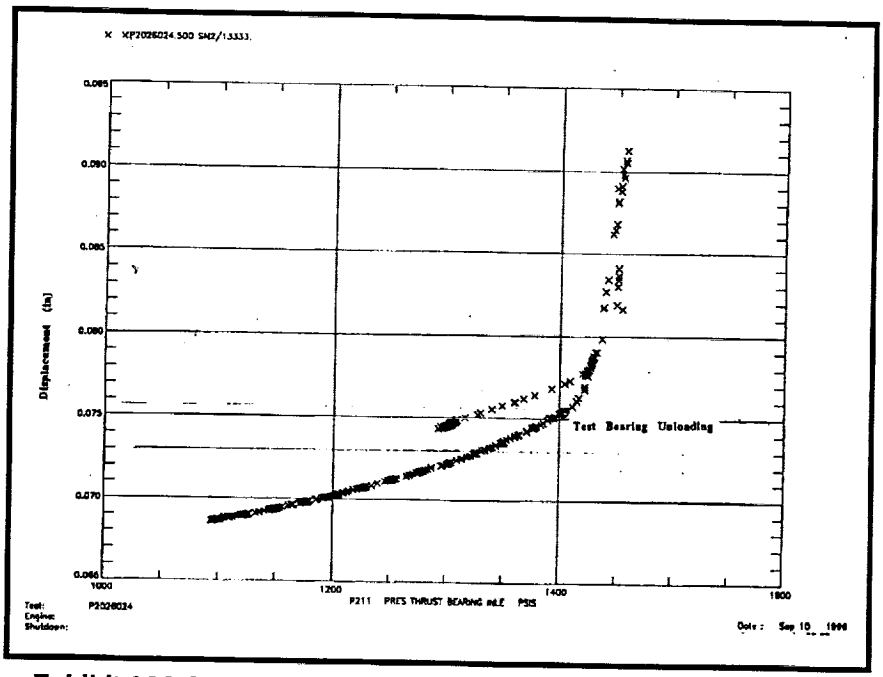

Exhibit 284 Load Deflection Test for Axial Load Calibration Test

in the preload spring. The soft preload spring is then the only restoring force for increased pressure imbalance toward the top of the tester. A small increase in the thrust piston pressure results in a relatively large compression of the spring. The data provided by this test was used to calibrate and verify the pressure load calculation for future testing. **Exhibit 285** shows a plot of the measured strain gauge load and the calculated value of pressure axial load (PAL).

Analysis of the data showed that the inflection point on the load deflection curve occurred at the same time that the calculated value of the PAL matched the measured strain gauge load. Thus the PAL calculation was verified and could be used with confidence as a control parameter for bearing axial load control. This approach provides significantly improved axial load control over load control based on the strain gauge measurements. The pressure measurements have much greater resolution than the strain gauges, in the region of interest.

Build 2 Test Series Summary. The objectives of tester Build 2 were accomplished. Test procedures were perfected and instrumentation was verified. The ability to operate the rig in a manner that consistently simulates pump operating conditions was demonstrated. The consensus of the project engineers was that the

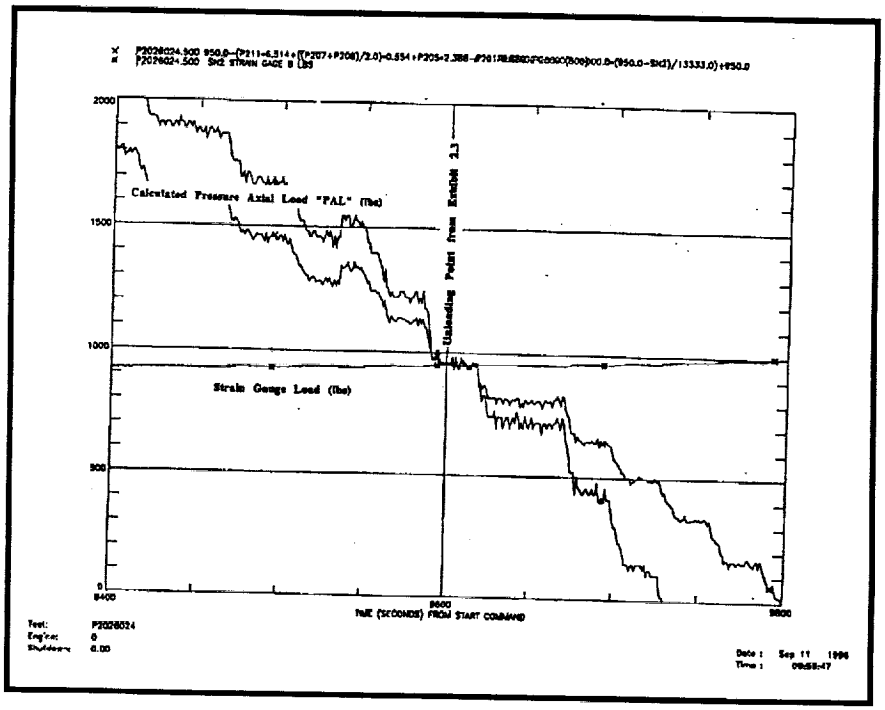

Exhibit 285 Calculated and Measured Loads for Axial Load Calibration Test

rig testing program was ready to proceed to the next phase designed to explore the robustness of river-marked bearings.

Build 2 Overspeed Analysis. The failure of the bearing rig speed sensor which occurred during rig test P2026026 resulted in an overspeed event. This test was the first test of this build in which the turbine was pressurized to attempt rotation. After chill down, turbine inlet pressure was increased to begin rotation. The inlet pressure was ramped up from zero to approximately 1,100 psi. The speed sensor and other instrumentation was monitored in real time. The speed sensor never indicated rotation. However, shortly after pressure was applied to the turbine, fluid temperatures began to increase. Turbine pressure was reduced and the test was terminated. A similar event occurred during test P2026028. However, during this event turbine pressure was limited to 800 psi based on revised redlines established after the previous successful test P2026027. After each event, the speed sensor was examined and problems were found which confirmed the speed sensor was not functioning.

A study was performed using the SINDA/ SHABERTH Model to estimate the maximum speed which occurred during the two overspeed events. Pratt and Whitney design data for the Terry turbine was used to estimate the power available to drive the rig as a function of turbine inlet pressure. The estimated power available is shown in **Exhibit 286**. SINDA/ SHABERTH was used to calculate rig power requirements for various speeds.

The model calculates frictional power losses for the rolling element bearings and viscous losses for the rolling element and hydrostatic bearings. A friction coefficient of 0.1 was used for the ball bearings. The calculated power requirements are shown in **Exhibit 287**.

The solid curve with circles represents the total power loss from the pair of ball bearings. The power requirement for the ball bearings grows exponentially. This is due to two factors. First, the cage and ball drag is a squared function of the velocity of the component with respect to the fluid. The second factor in the shape of the curve is a result of ball spin on the inner race which increases as speed and centrifugal force on the rolling elements increases. The power requirement for the hydrostatic bearing is shown

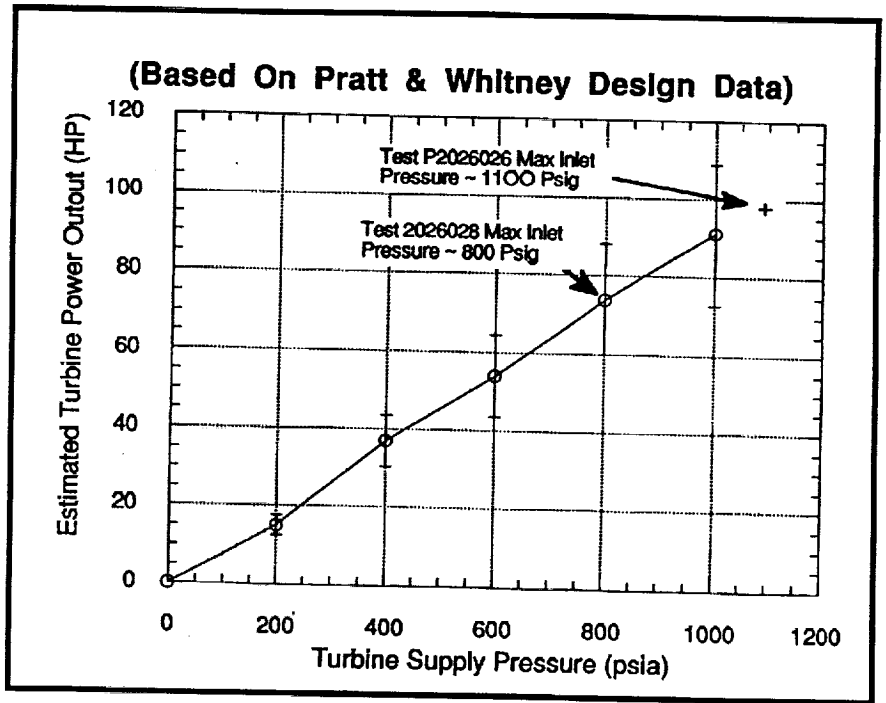

Exhibit 286 Power Available from Terry Turbine LH2 Rig Drive (Based on Pratt & Whitney Design Data)

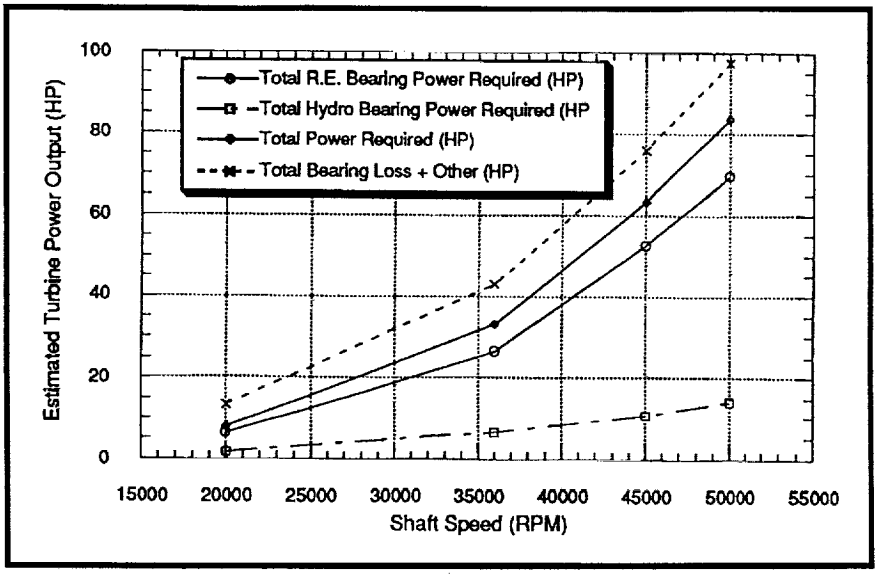

Exhibit 287 Calculated power Requirements for Driving LH2 Rig (Based on Pratt & Whitney Design Data)

by the dashed curve, with squares. The hydrostatic bearing power rises linearly and is largely a function of viscous shear forces in the fluid. Total power requirements, as predicted by the code, are shown by the diamond curve of **Exhibit 287**. This curve can be used to estimate the power required to drive the rig at a given speed. The calculated power should lie under the actual power requirement because there are additional losses in the system not accounted for by the model.

Build 2 experience showed that nominal operation of the rig at 36,000 RPM required a turbine supply pressure of approximately 500 psi. **Exhibit 286** shows that 500 psi corresponds to approximately 45 horsepower available. The SINDA model predicted 35 horsepower required. This point can be used to calibrate the model to account for additional losses in the system. It is assumed that the additional losses in the system will be mostly viscous shear losses and thus vary linearly with shaft speed. These additional losses were factored in to generate the top curve shown in **Exhibit 287**. This analysis predicted an estimated maximum bearing speed of 50,000 RPM for test P2026026 and 45,000 RPM for test P2026028. These results were significantly lower than the original speed estimates that were developed based on the quick look data alone. Analog strain gauge data was acquired during test P0206028 and was reviewed to determine if the calculated speeds could be confirmed by frequency analysis. The review was inconclusive.

Analysis of Speed and Thermal Effects on LH_2 Rig Operating Loads. SINDA/SHABERTH analysis was performed to investigate the effects of speed and temperature on the operating axial load of the HPFTP/AT ball bearings tested in the LH_2 rig. A single bearing model was used for this analysis. The bearing was modeled with nominal fits and clearances in order to produce generic results for reference during future rig builds. A baseline case was established by modeling the bearing in the static ambient condition. An axial load of 900 lbs was applied to the bearing for all cases studied. The static ambient shaft position, relative to the out race curvature center, was recorded for reference. The next case modeled was a static case with all components chilled to -400°F (-240°C). The shaft position was calculated to change 0.004 inches as a result of the bearing internal clearance change resulting from the chill-down process. The direction of the relative motion was such that each of the bearings would tend to contribute to increasing the preload on the bearings. The

preload spring constant is 13,333 lb/in. Therefore, the increased preload due to chill-down was calculated as follows: 2 X 0.004 in X 13,333 lb/in = 106 lbs.

The effect of speed on preload was calculated using a similar approach. The chilled static shaft position was used as a baseline. Runs were made for additional speed cases of 10K, 20K, 30K, and 36K (RPM). Shaft position was recorded for each case. The bearing change in stickout was then multiplied by the spring constant. The results from this study are shown in **Exhibit 288**. It should be noted that this chart represents load change contribution from each bearing. The curve shows that at 36,000 RPM each bearing contributes an additional 15 lbs to preload. Therefore, speed effects should increase preload by an additional 30 lbs.

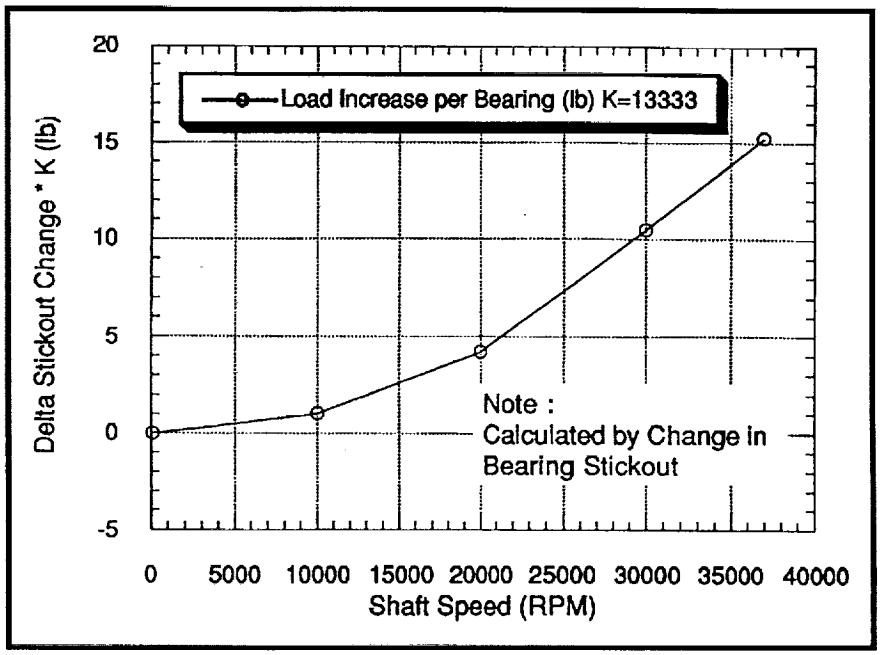

Exhibit 288 Speed Influence on Preload (Per Bearing)

A final study was performed to evaluate the effect of clearance loss due to bearing internal heat generation. In general, frictional heating results in a reduction of operating clearance resulting from heating of the balls and inner race to temperatures higher than the outer race. This effect was modeled by simply specifying a uniform ball and inner race temperature rise in the 36,000 RPM, chilled model. A 60°F delta temperature applied to the balls and inner race produced 8.5 lbs per bearing. This analysis is shown in **Exhibit 289.** The comprehensive thermal model of the bearings shows that the actual temperature rise is significantly less than 60°F. The ball temperatures are predicted to increase by approximately 10°F. Both the inner and outer races remain near fluid

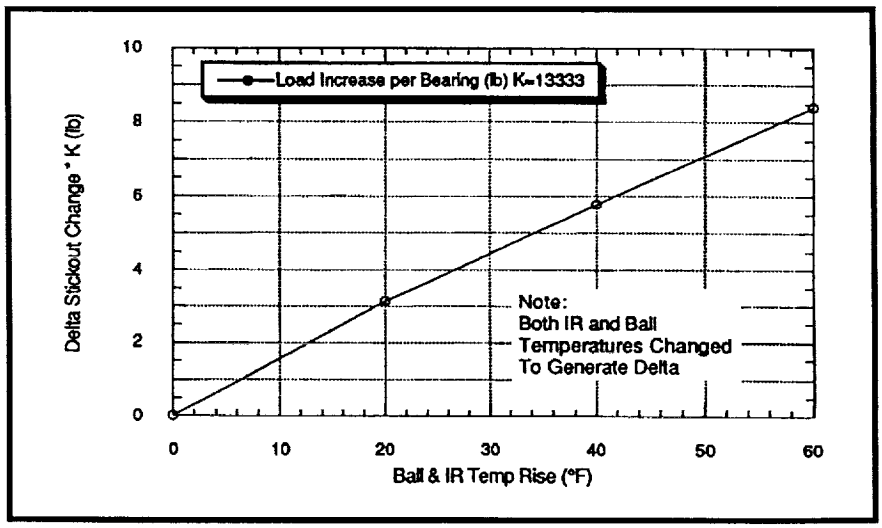

Exhibit 289 Temperature Influence On Bearing Preload (Per Bearing)

temperature. Based on the analysis of **Exhibit 289**, this temperature rise will have a negligible effect on operating preload.

The result of this loads analysis, was the finding that, for a generic LH_2 rig build, the operating axial preload on the bearings was approximately 136 lbs greater than the static ambient build preload.

Build 2 Hardware Tear Down and Inspection. Build 2 testing with the LH_2 rig was completed after achieving approximately 2,441 seconds of rotational time. Approximately 1,826 seconds of test time was at rotational speed above 35,000 RPM. The objectives of Build 2 were to refine test rig operational procedures and verify rig performance. A detailed report of Build 2 testing was presented in the September 1996 Progress Report. In October 1996, the rig was disassembled for inspection. Both the reaction bearing and load bearing were removed from the rig and disassembled. Visual inspection was performed on all of the rolling elements and races. Detailed surface measurements were performed on the races and on selected rolling elements.

Visual inspection of the reaction bearing revealed no significant changes from the pretest condition. This bearing was the bearing from HPFTP/AT Build F5-2. The bearing had acquired 276 seconds of engine run time and 230 seconds of low speed run time in tester Build 1 prior to Build 2 testing. The bearing rolling elements had minor river mark formations when installed in the rig. Visually, there was no apparent growth in the existing river marks. Also no increase in the number of river marks was noted. However, complete photographic records of the balls in the pretest condition were not available for comparison. Visual inspection of the cage showed no excessive wear areas. The cage did show more wear on one side of the outer race guide area than on the other. The eccentric wear was not excessive and was consistent with the wear pattern expected for a slight cage imbalance. Visually, the races appeared in excellent condition. Detailed surface measurements of the races, performed by Mr. Chip Moore, did show several dent marks on the inner race surface. The marks were similar to Brinell marks formed by statically overloading a bearing. However, the Brinelling was not uniform around the ring. There was one deep Brinell mark surrounded by less deep marks on either side. The spacing of the marks around the ring was consistent with the static spacing of ball contacts. The Brinell marks were not deep enough to be visible with the naked eye. The deepest mark was measured to be 7.5 microns (0.3 mils) deep. The Talyrond trace of the reaction bearing inner ring is shown in **Exhibit 290.** The Talyrond measurement indicated a maximum depth of approximately 3 microns, however, more accurate Talysurf measurements were used to determine the maximum depth. During assemble of Build 1 some binding of the bearing carrier was noted. The binding caused the bearing to misalign. Significant axial forces were applied to the bearing while in this misaligned condition.

The observed Brinell marks most likely occurred as a result of this anomaly during assembly. The minor Brinelling is not anticipated to significantly affect the expected life of the bearing.

The Load Bearing used for Build 2 testing was from HPFTP/AT Build F5-3A. This bearing had acquired previous run time of 932 seconds during engine tests prior to being installed in the rig for Build 2 testing. This bearing was in near pristine

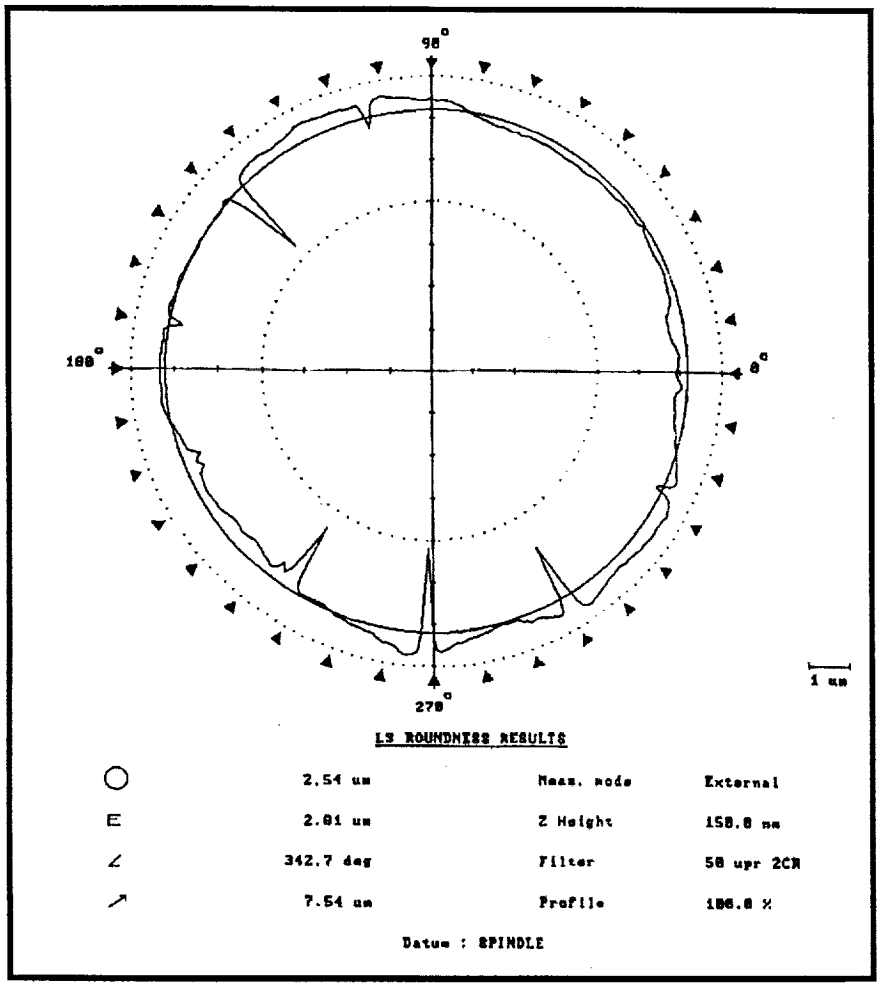

Exhibit 290 Talyrond Surface Trace of Reaction Bearing Inner Race

condition when installed in the rig. There were no visible river marks on the bearing when installed in the rig. Post Build 2 visual inspection of this bearing revealed that the bearing was still in near pristine condition after the completion of the Build 2 tests. The races showed no visible damage. The cage appeared in excellent condition. There were several dark streak marks observed on some of the rolling elements. It was found that these marks were deposits on the surface of the silicon nitride balls. The dark material could be easily removed from the surface by scratching with a dental pick. The material under the deposits did not appear distressed. The ease with which the material could be removed suggests that the deposits were probably SALOX deposits from the cage. This bearing was subjected to a static axial loading of approximately 12,000 lbs during testing. This load slightly exceeds the ANSI static load capacity of the bearing. Therefore, some Brinelling of the races was expected. A Talyrond trace of the bearing was performed on both the inner and outer races to determine the extent of the Brinelling. The outer race showed no sign of Brinelling. Uniform Brinelling of the inner race was detected with a typical depth of 2.5 microns (0.1 mil). The Talyrond trace of the load bearing inner race is shown in **Exhibit 291.** This magnitude of Brinelling is not expected to significantly reduce the life of the bearing. The silicon nitride rolling elements were examined at 10x and 40x for signs of river mark formation. One small surface feature was noted that appeared to be the possible initiation point of a river mark. It is believed that this feature was formed during Build 2 testing. The feature was photographed for documentation.

The results of the hardware inspection showed no evidence that the tester produces any anomalous wear modes not experienced in engine testing. The fact that the load bearing appears to be developing river marks also supports the similarity of the rig environment to the engine environment.

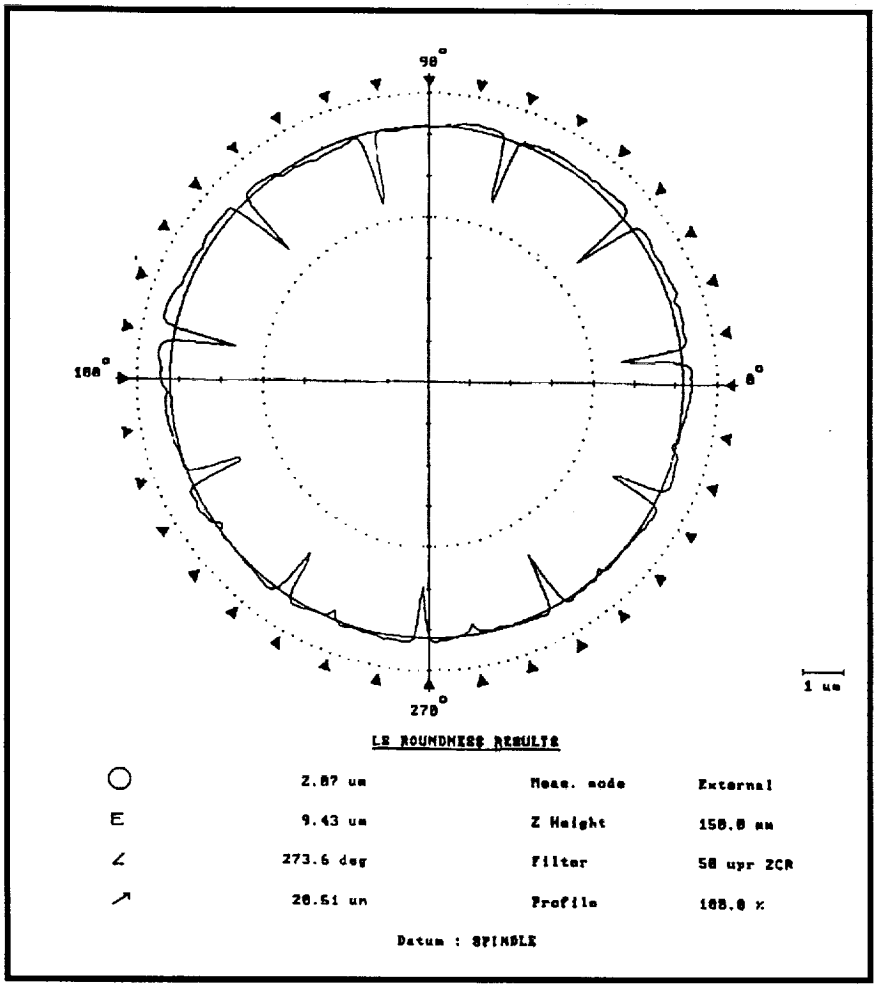

Exhibit 291 Talyrond Surface Trace of Load Bearing Inner Race

evaluated the ability of severely "river marked" bearings to safely meet the design life requirements of the HPFTP/AT application. The procedural revisions developed during the Build 2 seem to have eliminated many of the rig control problems experienced in the early tests. Two noteworthy anomalies were observed during the Build 3 test series. During tests P2026036 and P2026040 the rig break-away torque was higher than normal. On both occasions, the humidity was high and the rig was possibly left without a purge for some period of time. Therefore, ice formation was suspected as the cause of the increased break-away torque requirement. We began monitoring break-away torque with increased interest. Several pressure readings showed evidence of full or partial blockage of the hypo supply tubes during various tests. This phenomena also suggests the possibility of moisture in the system. Improved purge techniques were implemented.

6.9 Test Support for MSFC LH_2 Bearing Tester - Build 3

The LH_2 rig was reassembled after the test environment was confirmed by the Build 2 hardware inspection. The Build 2 Load Bearing was reinstalled in the Load bearing location. This bearing which is still in near pristine condition was used to track the formation and progression of river mark features via periodic inspection. The Bearing from HPFTP/AT Build F6-4 was installed in the reaction bearing location. This bearing has experienced three engine starts and was involved in a high load event during engine testing. This bearing has the most severe river mark features observed to date. Build 3 testing

Build 3 testing was temporarily suspended due to facility problems in October 1996. During preparation for Test P2026041, relief valves opened on the hydrogen run tank. Repair of the valves required the tank to be purged and warmed to facilitate removal of the valves for repair. Testing later resumed as Build 3A.

Test Objectives. The overall objective of the LH_2 bearing test program was to support the SSME HPFTP/AT Program by investigating the formation mechanisms and consequences of the "river mark" surface features observed in post engine test silicon nitride rolling elements. The river mark features appear on the surface of the balls as thin crack like marks often branching out like tributaries to a river. However, close inspection of the marks showed that they were typically flat bottomed troughs in the surface and they are usually much wider than deep. The flat bottom suggested that they were more benign than a typical crack and not susceptible to propagation into the depth of the rolling element. Balls with known river marks were successfully run in pumps; however, engine test time was limited and the long term durability of river-marked bearings was not demonstrated. The LH_2 bearing rig test series was designed to evaluate the capability of severely river-marked bearings to continue to perform nominally throughout the complete design life of 8 hours.

Build 2 of this test series was completed in September 1996. During Build 2, the rig was operated for 7 rotational cycles for a cumulative test time of approximately 2,441 seconds. Build 2 data was used to calibrate the rig and establish operating procedures used to assure that the rig test environment closely emulated the engine environment. The bearings installed in the rig for build 2 were low time bearings known to be in good condition. At the conclusion of Build 2 testing the bearings were inspected and found to be still in good condition. The only anomaly noted, post Build 2, was a small surface distress on one of the rolling elements which appeared to be the early formation of a river mark. These results indicated that the rig test environment was not introducing any additional failure modes on the bearings. Earlier rig testing with the Bearing Seals and Materials Tester (BSMT) in liquid oxygen and the LH_2 rig, prior to developing the current test procedures, had shown that rig test environments to be more aggressive than actual engine test experiences. It was found that the post test condition of the Build 2 bearings was consistent with bearings run in the engine for similar amounts of time. Based on the results of Build 2 it was decided to proceed with testing of a river marked bearing.

The objectives of Build 3 testing included establishing the robustness of river marked bearings by accumulating high speed long duration run time on a bearing with known river markings, and documenting formation of river marks. To address these objectives the rig was reassembled using the heavily river marked bearing from Pump Build F6-4. This bearing was installed on Pump F6-4 when the unit experienced a turbine and vane failure. This event caused increased loading on the bearing. The rolling elements from this bearing were the most heavily river marked bearings observed from engine tests. This bearing was installed in the reaction bearing position (top) of the LH_2 rig. The axial load on this bearing can be monitored directly from the strain gauges installed on the bearing preload spring. The load bearing (middle) from Build 2 was reinstalled in the rig for Build 3. The test plan called for acquiring approximately four hours of high speed (35k rpm) test time on the rig and then removing the rig for inspection of the bearings. This test plan was accomplished. Build 3 demonstrated four hours of life with bearings known to be heavily river marked. The load bearing, in good condition prior to Build 3 testing, developed heavy river marking during the four hours of testing.

Build 3 Test Series Highlights. This test series consisted of 24 cycles, as summarized in **Table 9**, and benefited extensively from test procedure optimization and calibration performed during Build 2 testing. Axial load and speed control problems experienced in Build 2 testing did not occur in this test series. A total of 15,595 seconds run time was accrued. The majority of the run time was accrued in the month of December 1996. The nominal test profile for the series

Table 9 Build 3 Test Series Summary

Test Number	Fluid	Time at Speed (Sec)	Nominal Test Speed (RPM)	Remarks
P202633	LN2	0	0	Coldflow and leak check
P202634	LH2	720	35,000	Axial load calibration performed
P202635	LH2	610	35,000	170 lb radial load
P202636	LH2	8	35,000	High break-away torque, P211 cut
P202637	LH2	813	35,000	295 lb radial load
P202638	LH2	0	0	Propellant depletion during chill
P202639	LH2	674	35,000	125 lb radial load, no speed sensor
P202640	LH2	314	35,000	125 lb radial load, high break-away torque, P201 cut
P202641	LH2	0	0	LH2 tank over pressurized
P202642	LH2	0	0	Relief valve failed
P202643	LH2	0	0	valve 3106 control problems
P202645	LH2	684	35,000	175 lb radial load, strain gauges erratic
P202646	LH2	808	35,000	175 lb radial load
P202647	LH2	937	35,000	175 lb radial load
P202648	LH2	978	35,000	175 lb radial load
P202649	LH2	905	35,000	175 lb radial load
P202650	LH2	919	35,000	175 lb radial load
P202651	LH2	825	35,000	175 lb radial load
P202652	LH2	1011	35,000	175 lb radial load
P202653	LH2	950	35,000	175 lb radial load
P202654	LH2	620	35,000	175 lb radial load, data system crash
P202655	LH2	980	35,000	175 lb radial load
P202656	LH2	1,050	35,000	175 lb radial load

Table 9 Build 3 Test Series Summary (Concluded)

- Total rotational test time on Build 3 was approximately 15, 595 seconds.
- Total rotational test time on Build 3 at 35,000 RPM was approximately 14,333 seconds.
- Nominal axial load in the bearings for rotational tests was approximately 875 lbs.
- Tests 02026036 and P2026040 had high break-away torque
- Reaction bearing used was from Pump Build F6-4 and had 1,594 seconds of engine run time prior to being installed in Tester Build 3. This bearing had acquired heavy river marks on all balls during engine tests. This bearing was heavily loaded during engine testing due to the Unit 6-4 2nd turbine vane failure.
- Load bearing used was from Pump Build F5-3A and had 932 seconds of engine run time prior to being installed in Build 2. The bearing acquired 2,441 seconds of rotational time in rig Build 2. Post Build 2 inspection found slight brinelling of the inner race and a small river mark type surface feature on one ball.

was as follows: static chill down, increase turbine pressure to start rotation, hold speed at 20,000 RPM, apply radial load, ramp speed to 35,000 RPM, run at speed until tank depletion. The typical bearing load was 875 lbs axial and 175 lbs radial load. A typical test duration was approximately 900 seconds at test speed.

The test series was divided into two groups of tests. The first group of tests (Tests P2026033 - Test P2026040) were performed in October 1996. The few anomalies that occurred in the test series occurred primarily in this group of tests. Test 33 was a non-rotational leak check with LN_2. Test 34 included an axial load calibration test similar to the test reported in September 1996. The test verified that our nominal operating axial load was approximately 875 lbs. Test 36 experienced a high break-away torque. It was necessary to bring the turbine inlet pressure up to approximately 300 psi to start shaft rotation. Typically, less than 100 psi turbine inlet pressure is required to start shaft rotation. Once the shaft rotated, running torque appeared normal. This test cut prematurely due to thrust piston pressure exceeding the redline. The thrust piston cut was linked to valve 3106 controlling erratically. The test was recycled and on the second start, break-away torque was normal. The rig was borescoped after this test and the bearings appeared normal. It was later learned that a purge may not have been immediately applied to the rig after the previous test. Therefore, internal ice may have contributed to the high initial break-away torque. A similar high break-away torque was experienced during rig test 40. During rig test 37 the radial load was intentionally increased form 175 lbs to 295 lbs to test a radial load sensor installed on the rig. This group of test resulted in approximately 3,139 seconds of high speed test time.

A facility problem occurred during chill down for Test 41. The LH_2 run tank became over pressurized while chilling the rig resulting in two relief valves opening on the tank. The rig was isolated from the tank and therefore not affected. However, repair of the valves required approximately two weeks. Test 42 was attempted after the valves were reinstalled, however, it was found that the relief valves still leaked.

The second group of tests in this test series occurred in December 1996. Very few anomalies occurred during this group of tests and approximately 12,456 seconds of test time were accrued. The first test in this group, Test 43, was stopped prior to rotation due to a fluid control valve problem. The only other anomaly in this group of tests happened during Test 54. During this test, the data acquisition system (DSU) crashed during the test. The DSU crash caused a loss of the speed sensor signal used to control the rig speed. This event could have resulted in an overspeed, however, post test inspection of valve position data did not indicate signs of an overspeed. Fail safe measures were implemented to avoid this problem in the future.

The four hour run time goal for this build was achieved. The rig was removed for tear down and inspection of the bearings. The rig was later reassembled with the same bearings for an additional four hours of testing.

Preliminary Bearing Inspection. The bearings were removed from the rig and subjected to visual and metric inspection. Visual inspection of the bearing races and cages showed no unusual wear. The races of both bearings had slight debris denting. Brinel marks from the Build 2 overload were still visible on the inner rig of the load bearing. Otherwise, the races and cages of both bearings appeared to be in good condition for the amount of run time incurred. The rolling elements from both bearings had heavy river marks. The reaction bearing (from Pump F6-4) had heavy river marking when installed in the rig. The river marks appeared to have widened slightly during the testing. It was also observed that the rolling elements had many finer marks covering a larger percentage of the surface area. These marks were less deep and more dense than the heavier river marks. The load bearing (from Pump F5-3 and Build 2) had heavy river marks on the majority of the rolling elements. Prior to Build 3, only one of the rolling elements from this bearing had any indication of river marking and that was very slight. The loads and speed were carefully controlled and measured during the Build 3 testing. Transient loads experienced during this test series were minimal. *Therefore, it appears that river mark formation occurs under nominal bearing operation in a LH_2 environment.* The load bearing rolling elements also had the finer pattern of light marks observed in the reaction bearing balls.

Mr. Chip Moore, MSFC, performed detailed metric measurements of the races, balls, and river marked bearings. Many of the rolling elements were also photographed for documentation. Mr. Moore attempted to develop a method for categorizing the severity of river marking so observable features can be related to bearing life.

Bearing Configuration. Bearing configurations for Build 3 are show in **Table 4**.

Test Series Summary. Build 3 testing demonstrated that heavily river marked bearings can continue to operate nominally for significant periods of time. Abnormal race wear or heat generation did not result from operating with the river marked bearings for the four hours of testing. The formation of river marks on the load bearing showed that river mark formation occurred under nominal pump operating conditions, which implies that the formation of river marks in engine tests are not necessarily the result of some peculiar load or environmental factor unique to the pump.

Table 10 Bearing Configurations

Reaction Bearing (Top Bearing)	P/N47003185J12 Inner Race, Cronidur 30, Curvature .58 Outer Race, Cronidur 30, Curvature .52 11 Balls, Si3N4, diameter 0.8105 in Cage Armalon with SALOX inserts Axial end play (60 lb load) .0455 in
Load Bearing (Bottom Bearing)	P/N 4700318SK12 Inner Race, Cronidur 30, Curvature .58 Outer Race, Cronidur 30, Curvature .52 11 Balls, Si3N4, diameter 0.8105 in Cage Armalon with SALOX inserts Axial end play (60 lb load) 0.045 in

6.10 Test Support for MSFC LH_2 Bearing Tester - Build 3A

In January 1997, the LH_2 bearing test rig was reassembled and prepared for continued testing. The LH_2 bearing rig Build 3 had been disassembled for inspection after accruing 15,595 seconds of rotational test time.

Hardware from rig Build 3 was reassembled, constituting rig Build 3A. Both the load and reaction ball bearings were reused in Build 3A. The only hardware changed from Build 3 was the bearing axial preload spring. The preload spring was replaced by a spring of identical design. The preload spring change was required because of strain gauge failures on the original spring. All three strain gauges on the new spring were verified after assembly in Build 3A. It was noted that the ambient static preload on the bearing was approximately 634 lbs after assembly. This static preload was slightly lower than observed from Build 3. Possible sources of this difference are errors in the spring calibration curves and/or increased bearing clearance resulting from previous testing. The metric studies from post Build 3 hardware showed very little wear.

Build 3A was transported to the test stand and installed during the third week of January 1997. An LN_2 coldflow and leak check test was performed to verify the installation (Test #: P2026057.500). The leak check verified the rig installation and instrumentation. A minor anomaly was noted during the leak test. It was noted that the thrust piston pressure was not immediately relieved when the thrust piston supply closed. This anomaly resulted in additional axial load on the reaction bearing of approximately 500 lbs. This amount of additional load did not result in exceeding any bearing or spring margins. The cause of the problem was identified and corrected.

LH_2 bearing test continued with Build 3A which ran with pump end ball bearings from HPFTP/AT F6-4 and F5-3A. These bearings had been subject to approximately 15,600 seconds of rotational time in the previous tester build (Build 3). Their post Build 3 condition was described in the December 1996 Progress Report and was judged acceptable for continued testing.

The test profile was modified for this build to include the application of high axial load cycles to the load bearing. These load cycles consisted of rapidly applying a shaft axial load to the bearing six times for a duration of 3 seconds each at a shaft speed of 20,000 rpm. After the load cycles were completed the shaft speed was ramped up to the test speed of 35,000 rpm. **Exhibit 292** shows the axial load cycles as measured for Test P2026068. This parameter (PAL1) was calculated based on various pressure acting on different areas of the shaft to produce a net axial load. The shaft axial load was produced by reducing the thrust piston pressure allowing the top cavity pressure to push the shaft down toward the load bearing. When the PAL1 load was added with the remaining preload from the reaction bearing, a total maximum load of approximately 5,000 lbs is supported by the load bearing. The axial load cycles were added to the test profile to simulate the transient loads in the HPFTP/AT during start up and shut down. Multiple cycles were executed for each test in order to obtain enough cycles to simulate 60 engines starts and stops in the remaining rotation time scheduled for this build.

The "cold flow, leak check" was successfully performed in January 1997 using LN_2. During February 1997, twelve tests were performed. The first (**P2026058**) was an axial load calibration test with no rotation to verify the correct preload spring compression and the operation of the automated load controls. Both conditions checked out satisfactorily. The next test (P2026059) was scheduled for a complete test profile, but was cut immediately after the axial load cycles due to DP239. DP239 is the measure of the pressure differential across the shaft and is used to determine the net axial load on the shaft. Its redline limits are broadened during the axial load cycles and are tightened after completion of the cycles. Unfortunately, the tighter limits were programmed to be enforced before the automatic controller could bring DP239 back to its normal level. Corrective measures were taken for the next test.

P2026060 was performed successfully completing all test objectives and obtaining 960 seconds at full speed before propellant depletion. The next test (**P2026061**) was aborted before rotation start due to P211 not responding. P211 is used for the thrust piston control and since it did not respond, the thrust piston was over-pressurized before the control personnel noticed the thrust piston pressure on another measurement. This over-pressurization resulted in an

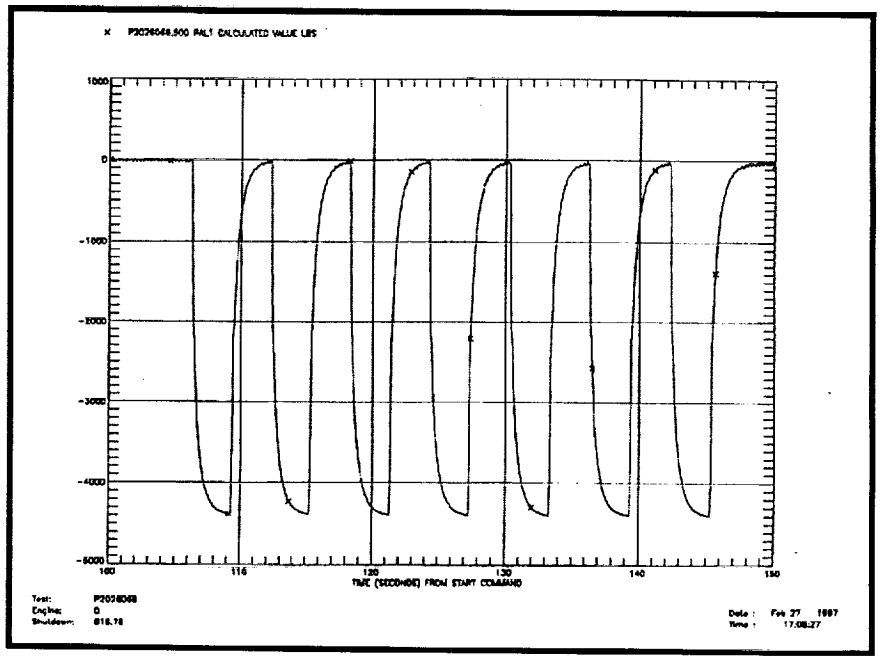

Exhibit 292 LH2 Bearing Tester Axial Load Cycles

axial load of approximately 7,800 lbs being applied to the reaction bearing. This load was well below the static axial load limit of this bearing which is about 10,000 lbs. Also, the reaction bearing housing is designed to permit the outer race to bottom on a ledge at 2,500 lbs before overloading the preload spring. Instrumentation inspection showed that a drop of moisture had collected and frozen in the line leading to the pressure sensor. The procedure was modified to manually observe P211 to verify its functionality before fully pressurizing the thrust piston.

P2026062 was cut on the first attempt during the axial load cycles due to a high DP239 reading. This pressure differential was high because the gain on the axial load cycle controller was changed to permit the load to reach the set point more rapidly. However, the gain change actually caused the load to over-shoot the desired level. The gain was reset and the test recycled. The second attempt was successful with six axial load cycles and approximately 660 seconds at test speed before run tank depletion.

Tests **P2026063** through **P2026069** were all run successfully with no anomalies observed in bearing data, instrumentation, or controls. At the end of Test P2026069 the bearings had completed 58% of the "time at full speed" goal.

Computer Modeling of Build 3A Test Profiles. The P&W HPFTP/AT pump end ball bearings being tested in Build 3 of the LH_2 bearing tester were simulated using the SINDA/ SHABERTH bearing modeling program. The SINDA/ code for these bearings had been developed previously during work for P&W. Thus, the SINDA model of these bearings needed only slight modification to simulate the bearing tester parameters and to be combined with the SHABERTH model of the tester. The complete model was then configured in the transient mode to simulate the axial load cycles on the tester bearing. Comparison of the model results with the test data for coolant temperature rise across the bearing, as well as outer race back surface temperature, provided valuable information for model calibration. Once the model had been calibrated, critical internal bearing operating parameters were predicted.

The axial load cycles provided an excellent opportunity to monitor a coolant temperature increase due solely to frictional heating in the bearing. Previously, coolant temperature changes across the bearing had been caused by speed increases. The coolant increase is caused by increased viscous work on the fluid and increased frictional heat generation in the bearing. This complicated modeling since there were two components of the heat increase to be predicted. Therefore, because the load cycles were performed at constant shaft speed, the frictional heat generation change can be isolated.

The measurements in the tester that monitor the load bearing frictional heat increased are the coolant exit temperature (T206) and the outer race back surface temperatures (T205 & T214). The data for T206 at the time of the axial load cycles is provided in **Exhibit 293** along with the load bearing and tester inlet coolant temperatures. Because the temperature change magnitude is close to the resolution of the thermocouple, the exact times of the axial load cycles were not definitively discernible. Therefore, the data for the thrust piston pressures are provided in **Exhibit 294** to indicate when the axial loads were applied. Thus, knowing the times when the high axial load was applied, the trends of increased temperature in the exit coolant measurement (T206) was detected. Unfortunately, the

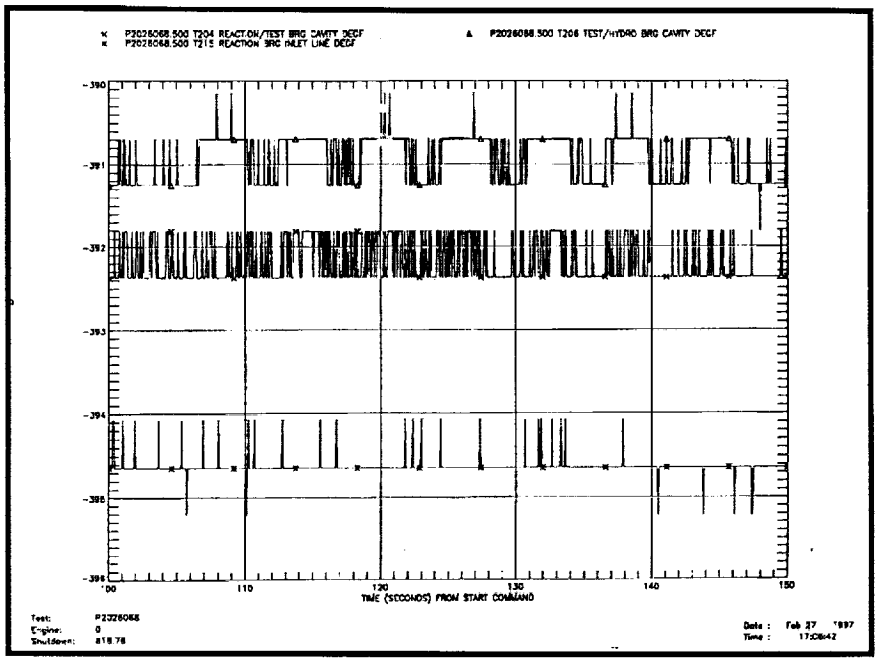

Exhibit 293 LH2 Bearing Tester Coolant Temperature Data

outer race measurements did not provide reliable data for this build and did not show any indication of temperature change due to the increased axial load. This necessitated that the modeling results could be compared with only coolant measurements for this tester build.

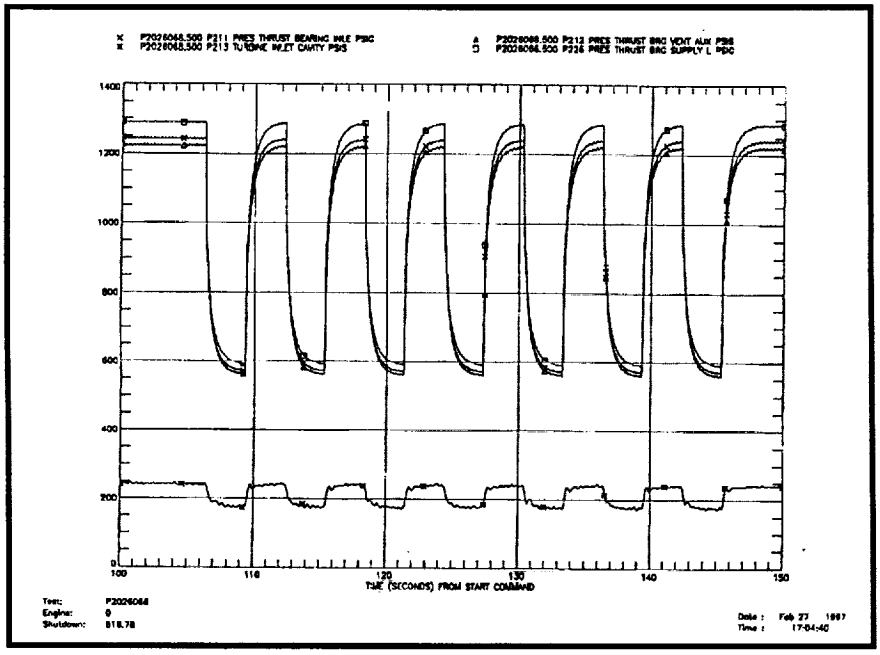

Exhibit 294 LH2 Bearing Tester Thrust Piston Pressures

The boundary conditions of Test P2026068 that affect bearing operation, such as speed, load, coolant temperature and pressure, and flow rate were programmed into the transient SINDA/ SHABERTH model to simulate the axial load cycles. The boundary conditions that changed the most and had the largest effect on the bearings operation were the shaft speed and axial load. **Exhibit 295** shows these two boundary parameters as programmed in the model.

The transient model results for coolant temperatures into and out of the load bearing corresponding to T204 and T206, are provided in **Exhibit 296.** The characteristic of most interest was the temperature change during the application of the high axial load to the bearing. As stated earlier, the change in delta temperature is caused by frictional heat changes due the increased axial load. The magnitude of the measurements is also affected by the viscous work done on the fluid by the bearing. As shown, the model predicted that the exit temperature would increase approximately 0.7 degrees Rankine. However, coolant mixing in the exit cavity from the hydrostatic slave bear-

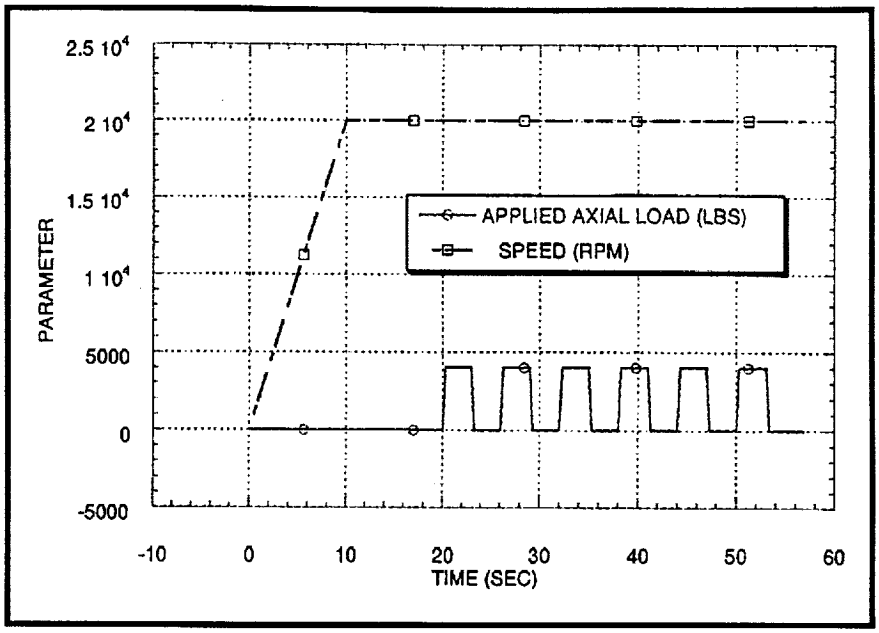

Exhibit 295 LH2 Bearing Tester Load Bearing Boundary Conditions (HPFTP/AT PEBB, F5-3A)

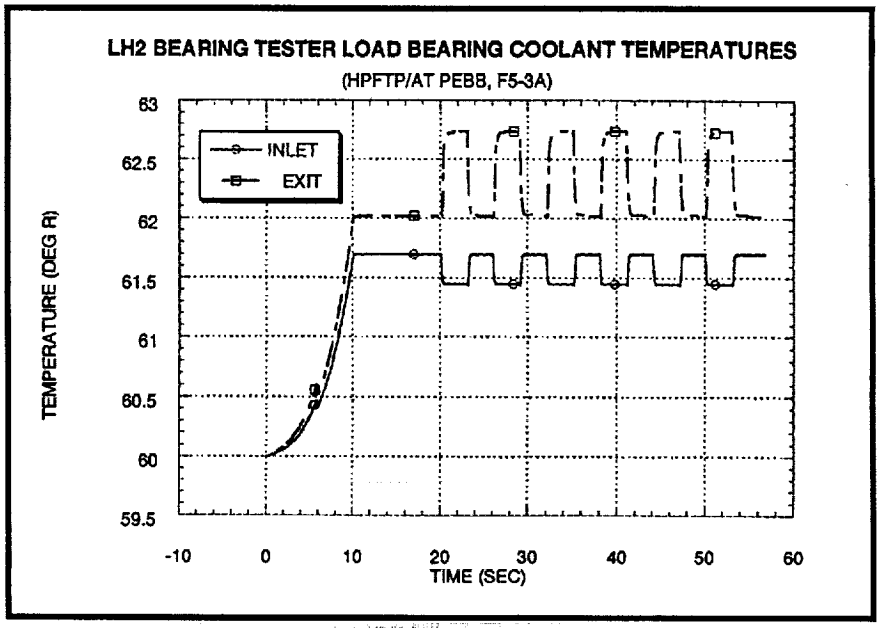

Exhibit 296 LH2 Bearing Tester Load Bearing Coolant Temperatures (HPFTP/AT PEBB, F5-3A)

ing, also affected the T206 measurement. The effect of mixing was calculated manually and indicated that the predicted temperature change was 0.6 degrees. This predicted delta temperature is very close to that measured with T206. This indicated high credibility for the friction heat calculations in the SHABERTH program. Also, the magnitude of the coolant temperature predictions were relatively close to the measured values, indicating that the viscous work calculations were fairly accurate as well.

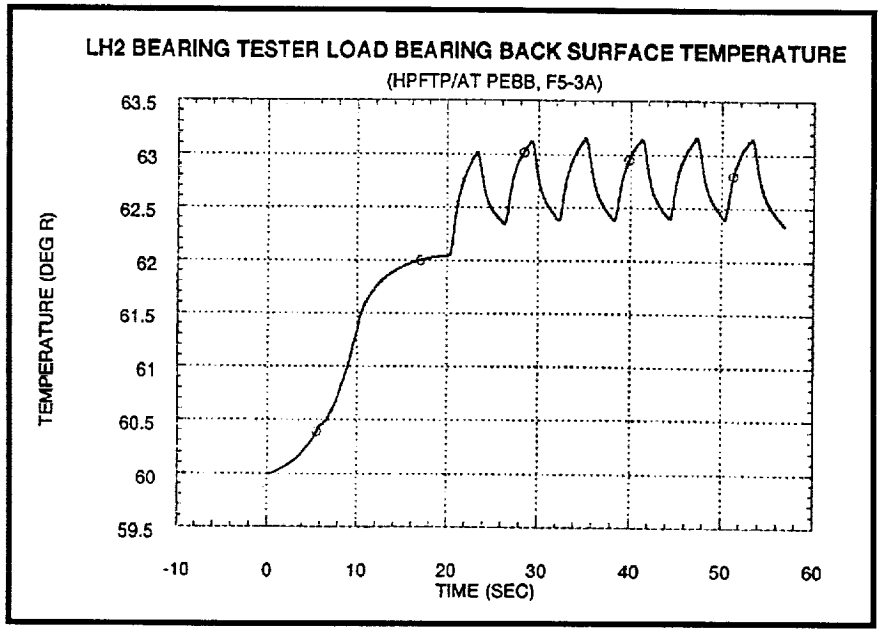

Exhibit 297 LH2 Bearing Tester Load Bearing Back Surface Temperature (HPFTP/AT PEBB, F5-3A)

It is interesting to note that the model predicted that the coolant between the reaction bearing and the load bearing would decrease by 0.25 degrees due to the load being slightly reduced on the reaction bearing during the axial load cycles. **Exhibit 297** shows the prediction for the outer race back surface temperature response and that it also should have about 0.7 degrees of change. However, this change was not seen in the data. In general, the outer race temperature measurements were not believed to be reliable.

The model predictions for the corresponding average bearing component and maximum track temperatures are provided in **Exhibit 298** and **299**, respectively. These temperature predictions indicate that this ball bearing operating with these coolant conditions is very thermally robust. The model also predicted, as shown in **Exhibit 300,** that even under the 5,000 lb axial load, the

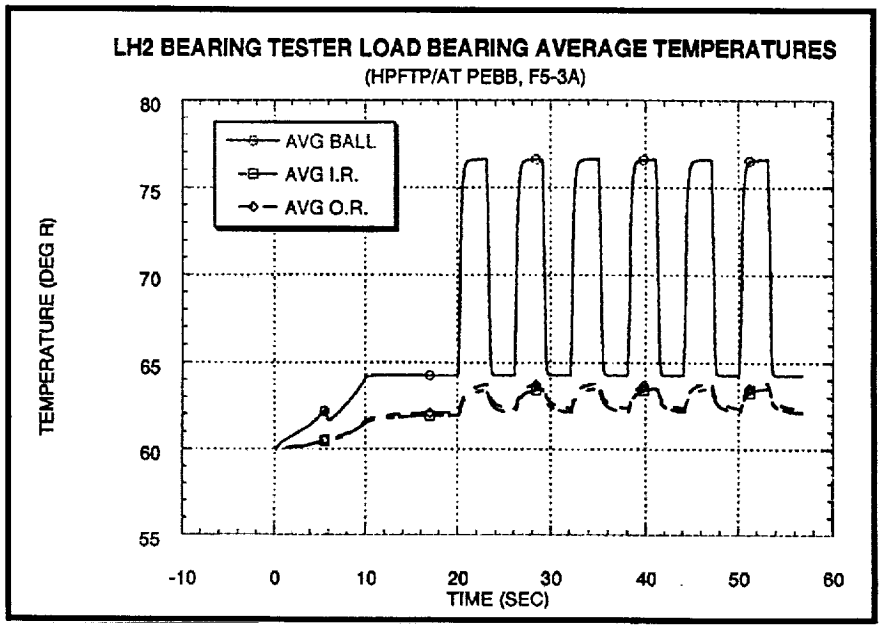

Exhibit 298 LH2 Bearing Tester Load Bearing Average Temperature (HPFTP/AT PEBB, F5-3A)

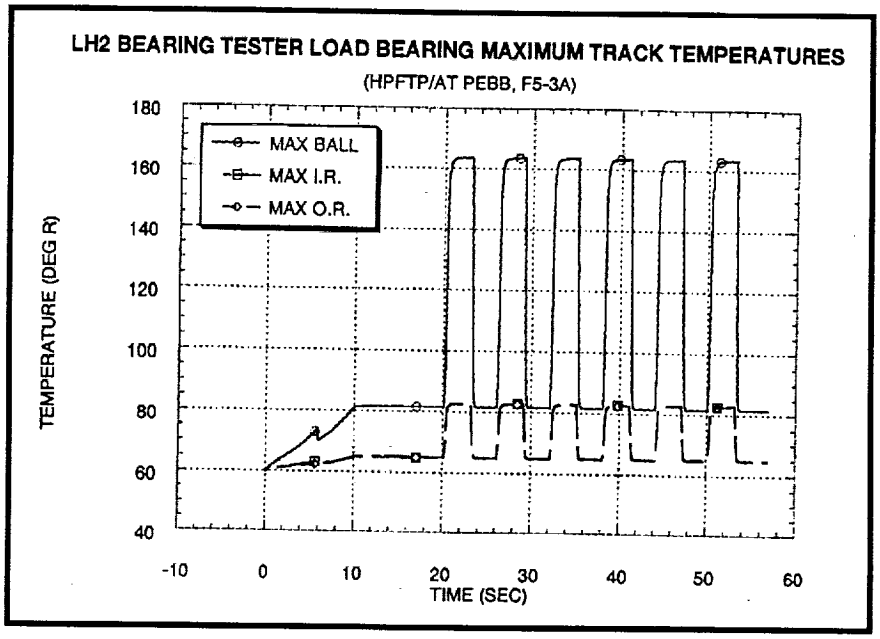

Exhibit 299 LH2 Bearing Tester Load Bearing Maximum Track Temperatures (HPFTP/AT PEBB, F5-3A)

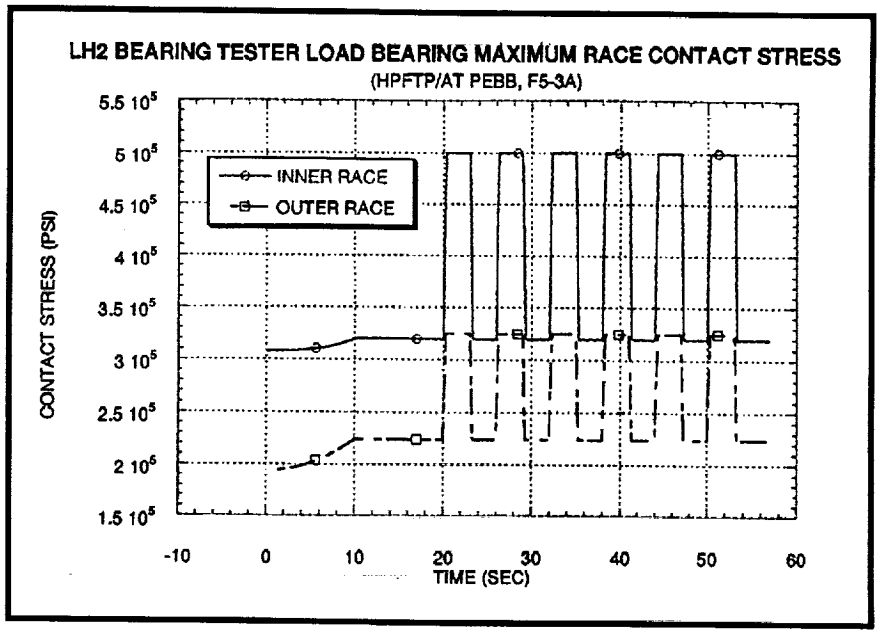

Exhibit 300 LH2 Bearing Tester Load Bearing Maximum Race Contact Stress (HPFTP/AT PEBB, F5-3A)

maximum contact stress is 23% below the maximum allowable contact stress for the Cronidur stainless steel races.

Build 3A Test Series Highlights. The test goals for Build 3A were achieved in March 1997. Eight rotational tests were successfully performed resulting in 96 minutes of time at 35,000 rpm and 129 minutes of total rotational time. Adding this time to the previous test times for Build 3A, yields a time of 201 minutes at 35,000 rpm and 260 minutes total rotational time on this build. Combining the time the bearings accumulated in Build 3A with the time previously accrued in Build 3 results in a total of 440 minutes of rotational time at 35,000 rpm and 520 minutes total rotation time. This time was in addition to the time the bearings were run in their respective HPFTPs and the time the load bearing was run in Build 2. The combined times the bearings experienced in both Build 3 and Build 3A met the endurance goals set for these bearings of 421 minutes at 35,000 rpm and 520 minutes total rotation time. These goals were based on simulating 60 missions of 8.67 minutes each with 81% of the time being run at 109% or 35,000 rpm for the HPFTPs.

The reaction bearing was also subjected to 120 high axial load cycles during testing with Build 3A. The axial load cycles were performed to simulate the transient loads in the pump during start up and shut down. The load cycles were accomplished by performing seven and later eight cycles at 20,000 rpm during the speed ramp up for each test. Each cycle consisted of allowing the pressure differential across the tester to push the shaft down thus increasing the load on the reaction bearing from the nominal 800 lbs preload to 5,000 lbs for three seconds.

Testing was accomplished without any anomalies of a serious nature. However, the data did reveal that the power required to maintain the tester shaft speed was decreasing slightly for approximately the last 20% of each test run. This phenomenon was initially thought to be due to the propellant warming as the tank neared depletion. The power decrease was studied further and is discussed.

At the conclusion of Test P2026077, the bearing rig was removed from the test stand and returned to the lab for bearing removal and inspection. Overall, the rolling element bearings were in sound condition. The cage from the reaction bearing (top position) was the most worn of the two cages and its wear was only moderate. Higher wear on the reaction bearing was expected because this bearing must do the majority of the fluid work on the entering bearing coolant. There was land contact on the other side of the cage at the outer diameter believed to be caused by a cage imbalance, but this contact was not serious. The cage pockets had contact 360 degrees around with the heaviest in the fore and aft directions. The pocket wear was fairly consistent from pocket to pocket, but was not excessive. The cage from test bearing (middle position) showed the same wear characteristics as the reaction bearing, but the magnitude of the wear was estimated to be only 33% as much. The races of both bearings did not seem to have degraded much since inspection after Build 3. The wear on the races appeared low and there was some debris denting in the tracks. The silicon nitride balls from the reaction bearing had micro-debris chipping that formed a continuous track around every ball. Some balls had signs of two of these debris tracks in different orientations. The load bearing balls did not show, to the naked eye, evidence of debris tracks.

Comparison of photos of the balls pre-Build 3, post Build 3, and post Build 3A showing the "river marks" on the surface was performed. The comparison illustrates that the original river marks on the balls did not substantially increase in area nor depth. However, the photos do show that the number of "tributaries" branching off the main "river" or fine cracks usually running perpendicular to the original flaw did increase with the run time on the bearings.

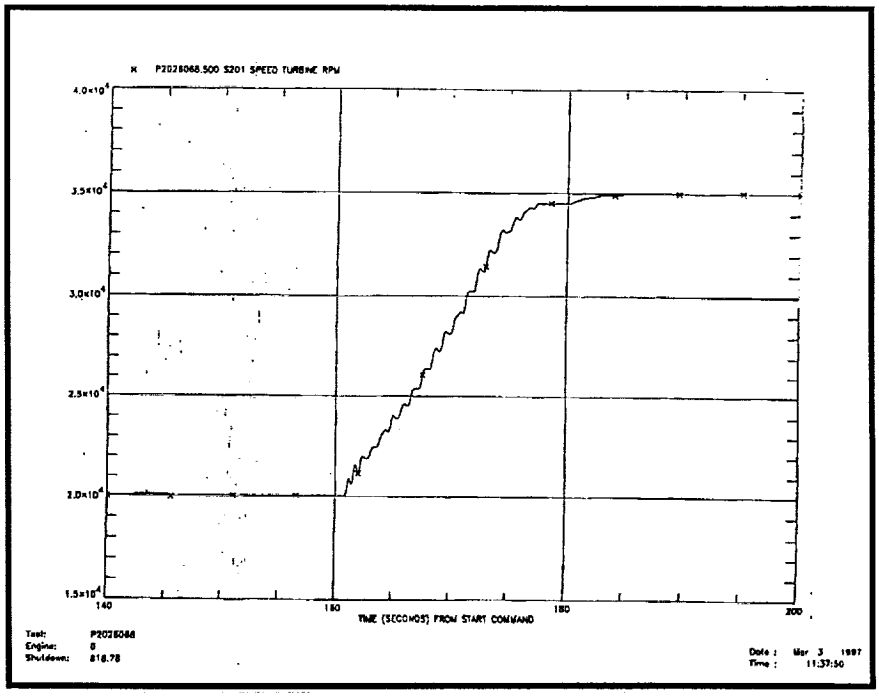

Exhibit 301 LH2 Bearing Tester Shaft Speed Increase

Additional Model Calibration from Build 3 and 3 A Test Data. Computer simulation of the MSFC liquid hydrogen bearing tester continued further enhancing the SINDA/SHABERTH program and calibrating the LH_2 bearing tester model. In February 1997, the high axial load cycles were studied in an effort to isolate and verify the frictional heating effects. The modeling results showed very good agreement with the measured data for the coolant temperature rise across the bearings. In March 1997, the viscous fluid work during shaft speed changes was studied. The speed change from the 20,000 rpm during the axial load cycles to the 35,000 test speed was simulated. **Exhibit 301** is a plot of the shaft speed data showing the speed ramp. **Exhibit 302)** is a plot of the coolant across the bearings showing the temperature increase during the speed increase.

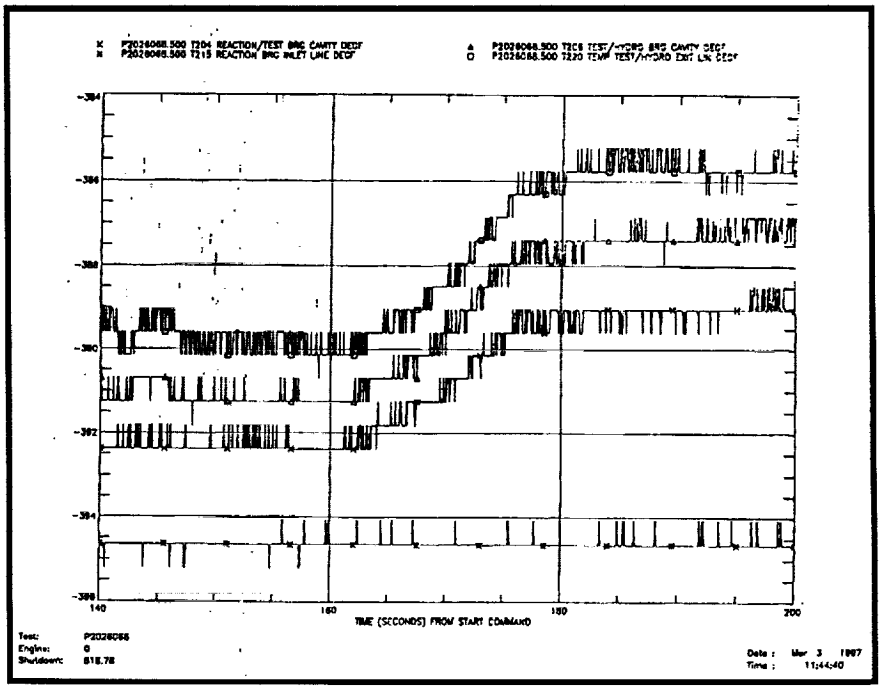

Exhibit 302 LH2 Bearing Tester Coolant Temperature Increase

The exit coolant temperature increase was due to both the frictional and viscous fluid heating. The model was calibrated very well for frictional heating as shown by the temperature comparisons during the high axial load cycles. Thus, any discrepancy in temperature comparisons between data and modeling results during the speed increase was probably due only to viscous heating from the fluid drag on the rotating components.

To simulate the LH_2 bearing tester shaft speed ramp from 20,000 to 35,000 rpm all of the measured boundary conditions for this portion of the test were programmed into the SINDA/ SHABERTH model of the tester. The model was then executed in the transient mode to simulate the speed ramp. The resulting coolant temperature predictions across the bearings are plotted in **Exhibit 303** for comparison with the measured data given in **Exhibit 302**. The measured temperatures in **Exhibit 302** were as follows: T215 is the reaction bearing inlet, T204 is between the bearings, and T206 is the load bearing exit. The model results were computed using coolant preswirl before the reaction bearing of 10% of shaft speed and before the load bearing of 25% of shaft speed. The comparison shows that the simulation under-predicted the coolant temperature rise at 20,000 rpm by approximately 0.6 degrees Rankine across the first bearing and 0.5 degrees across the second bearing. At 35,000 rpm, the simulation over-predicted the rise across the first bearing by about 1.7 degrees but across the second bearing, under-predicted by only 0.1 degrees.

Also as part of the viscous fluid work modeling, the power decrease with constant shaft speed phenomenon during the latter portion of each test, as shown in **Exhibit 304**, was simulated. The decreasing power requirement is probably real since the coolant is warming and density is decreasing toward the end of the test run as the run tank is nearing depletion. The coolant temperature increase is illustrated in the plot of coolant temperatures across the bearings for the last 300 seconds of Test P2026071 shown in **Exhibit 305**. The decreasing power measurement is substantiated by the coolant temperature rise across the bearings also decreasing during the last portion of the test shown in **Exhibit 306**.

6.11 Test Support for MSFC LH_2 Bearing Tester Build 4

Build 4 of the MSFC liquid hydrogen (LH_2) bearing tester was assembled in May 1997 using the same bearing configuration as the previous Build 3. This configuration placed a ball bearing in the load bearing position (middle position), a

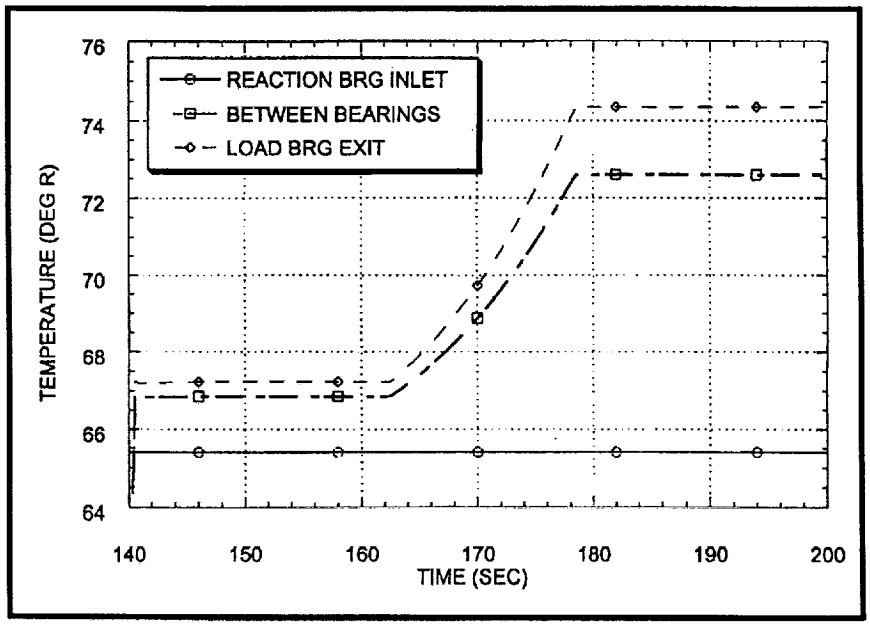

Exhibit 303 LH2 Bearing Tester Model Coolant Temperature Predictions

TP00-1017

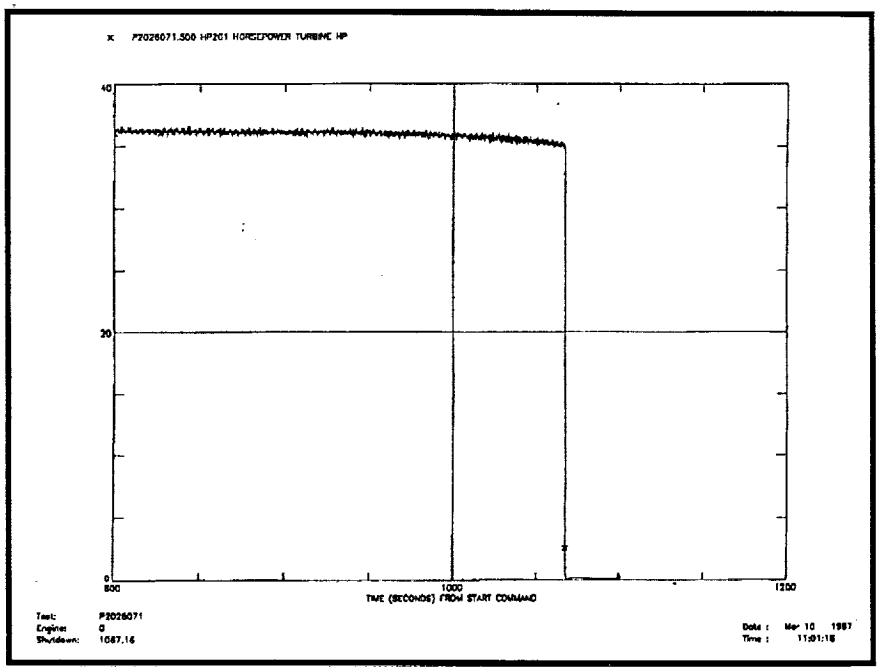

Exhibit 304 Example of Reducing Power Requirement Towards End of Test Run

shaft by a double beam spring on the outer race of the reaction bearing. The ball bearings of Build 4 were the Pratt & Whitney SSME High Pressure Fuel Turbopump (HPFTP) pump end ball bearing (PEBB) design. The bearing races were previously run in test pumps F8-1A and F7-1F. These races were fitted with new silicon nitride balls. The reaction bearing received Cerbec NBD-200 balls and the load bearing received the standard Toshiba TSN-03H balls.

ball bearing in the reaction bearing position (top position) and a hydrostatic bearing in the slave bearing position (bottom position). The two ball bearings are preloaded against each through the

The objective of this test series was to demonstrate the successful operation of the P&W HPFTP PEBB to exceed the design life, and to explore the effect of silicon nitride balls manufactured by different vendors on the formation of "river marks"; tiny surface defects detected on the Toshiba silicon nitride balls after nominal operation in the HPFTPs. A proposed explanation was that the fluorine present in pump assembly grease was reacting with the binder of the Toshiba silicon nitride balls. The rig was purposely assembled without using any Braycoat grease. This would provide a data point to evaluate the postulated correlation between fluorine in the grease, and the sili-

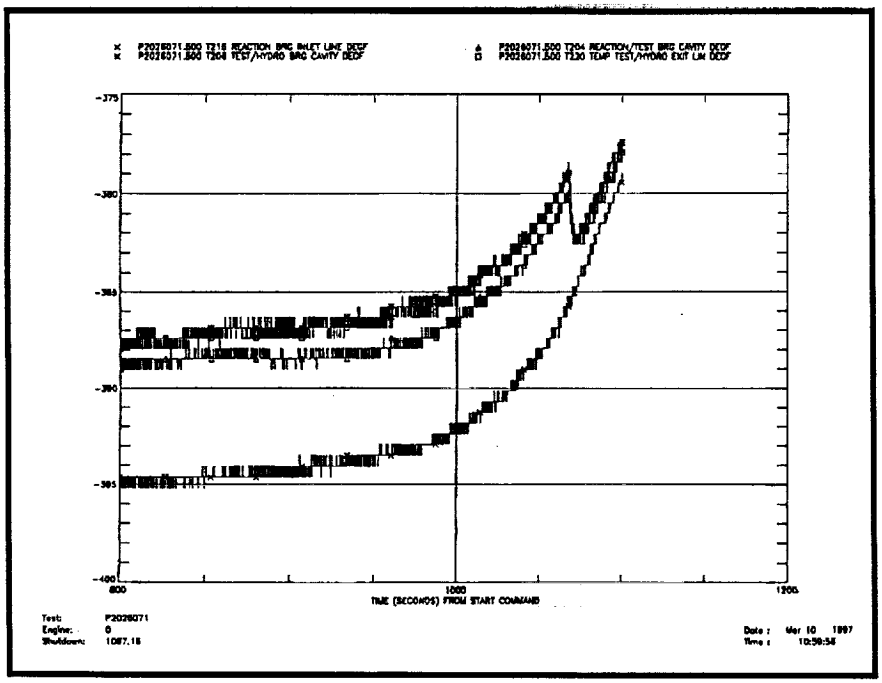

Exhibit 305 Coolant Temperature Warm Up During Later Portion of Test

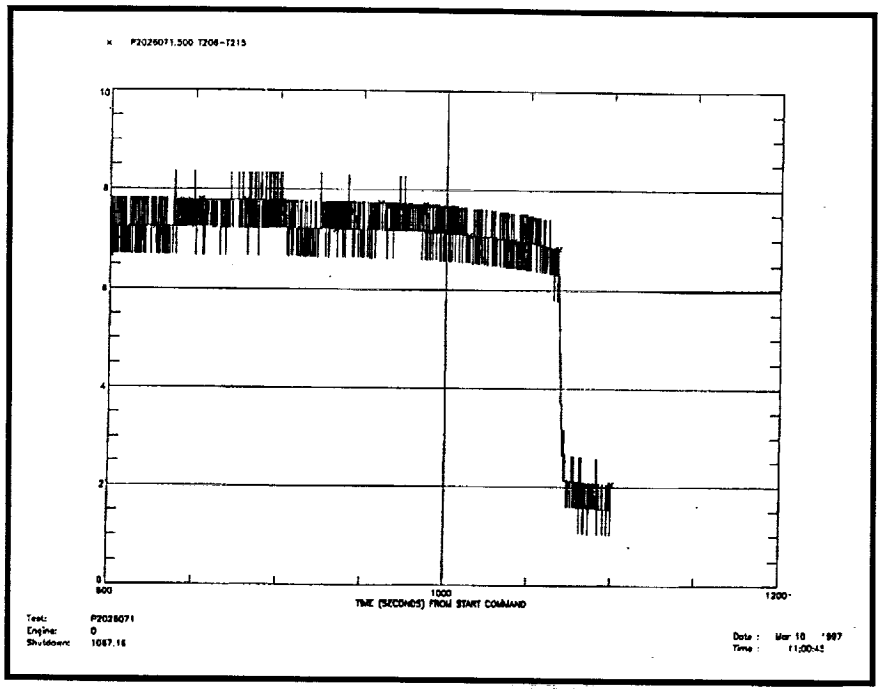

Exhibit 306 Coolant Temperature Rise Across Bearings Indicating Power Reduction

con nitride binder material. Test series investigated if the Cerbec silicon nitride balls were also susceptible to the formation of the river marks.

The LH_2 cold flow test and axial load calibration test were performed. No major leaks were detected in the tester assembly or in the supporting facilities. Proper axial preload on the ball bearings was verified through the use of the axial thrust piston and the instrumented preload spring. The three strain gages on the reaction bearing preload spring all read within 25 lbs of each other and average value was read to be 860 lbs which was only 10- lbs from the desired preload. The axial load calibration test collaborated the strain gage values by indicating what axial load on the shaft was needed to unload the load bearing. The axial load on the shaft was termed "PAL" and is a summation of all the pressure times area loads on the shaft including the thrust piston. When the PAL value is plotted versus the preload spring strain gage values as in **Exhibit 307**, the change in slope indicates when all the axial load has been removed from the load bearing and PAL is the only load reacting against the preload spring. As shown in the exhibit, this slope change occurred at approximately 900 lbs. When the spring constant of the load bearing (450,000 lbs/in) was considered, the calculations predicted that the

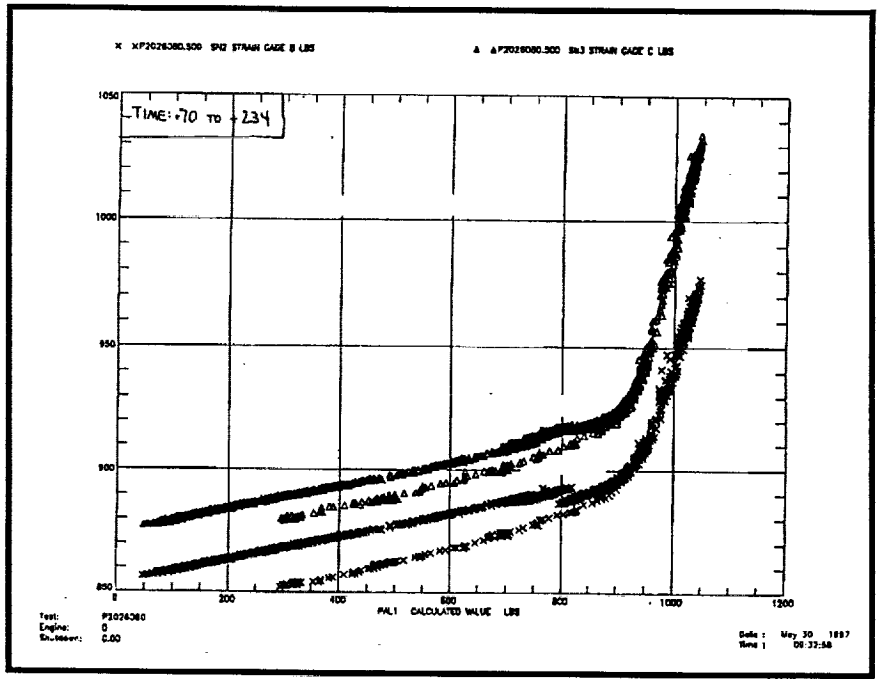

Exhibit 307 Axial Preload Calibration Test Results

change in slope should have occurred at 875 lbs which is very close to the measured value indicating that the preload was set correctly.

Build 4 Testing. Build 4 of the tester was configured with ball bearings in the reaction and load positions and a hydrostatic bearing in the slave position. The ball bearings were the Pratt and Whitney design for their SSME high pressure fuel pump. The bearing in the load position (test bearing) was fitted with new Toshiba TSN-03H silicon nitride balls which was the standard for the P&W design. The reaction bearing was fitted with new Cerbec NBD-200 silicon nitride balls. The major objectives of this tester build were to demonstrate the design life of the P&W bearings operating under conditions similar to those in a high pressure fuel pump, and to investigate the formation of the "river mark" surface defects on the different silicon nitride balls.

Test P2026081.500. First rotational test achieved 708 seconds of total rotational time with 582 seconds at 35,000 rpm. The test was nominal with test cut due to propellant depletion (T215 high). The data review showed that the tester operated normally, similar to Build 3 operation, with the exception of the thrust piston control having slightly more oscillation than normal. The thrust piston pressure oscillation resulted in a +/- 25 lbs variation in the test bearing load, which was judged to be undetrimental to the bearing performance. However, the test operator was asked to improve the response of the controller. Also, the strain gages on the preload spring indicated that the load on the reaction bearing increased approximately 8 lbs over the duration of the run. The reason for the gradual load increase was not known. Overall, conditions were acceptable for further testing.

Test P2026082.500. This test was terminated before rotation due to controller problems of the thrust piston pressure. The control valve EHV 3503 opened suddenly causing the thrust piston pressure to spike to approximately 1,500 psig without the tester being internally pressurized. This control anomaly resulted in about 10,000 lbs of axial load instantaneously applied to the reaction bearing. This load is believed to be within 10% of the static load capacity of this bearing. Thus, Bernelling of the reaction bearing races may have occurred and was later verified during the midpoint tear down and inspection. Investigation of controller problem was undertaken.

Test P2026083.500. This test was also terminated before rotation due to thrust piston control problems. Although no over pressurization of the thrust piston occurred, the automatic controller could not maintain the desired set point for the thrust piston pressure. The thrust piston pressure controller was again investigated.

Test P2026084.500. Thrust piston pressure control was improved by adjusting settings on the automatic controller and changing out the pressure transducer. Thus, 612 seconds of rotational time was obtained before test cut which was due to the propellant depletion. Data review showed nominal operation of the tester and bearings except for the thrust piston pressure which was still varying, but within the redline limits.

Test P2026085.500. The rotational time was cut during the ramp up to the test speed of 35,000 rpm by DP239 reading high. DP 239 is the pressure difference between the tester top cavity pressure and the thrust piston pressure and is to be maintained at a set point to provide low

resultant axial load on the shaft. The cause of the problems was again thrust piston pressure control.

Test P2026086.500. Non-rotational test to verify correction to thrust piston controls at operational pressures in the tester. Controller response was slow but was able to maintain pressure within redline limits.

Test P2026087.500. Attempted rotational test but was terminated due to propellant depletion before rotation start. The propellant depletion was caused by a facility relief valve opening and releasing the run tank contents to the burnstack. The test data was reviewed, but no over pressurization of the propellant system was detected. The relief valve was removed and rebuilt.

Test P2026088.500. Successful rotational test obtaining 616 seconds of rotation time before normal propellant depletion. The thrust piston pressure controller operation was acceptable although it was still was slow to respond to pressure changes in the tester. Temperature rise across the bearings was normal and all other operating parameters were within desired limits.

Test P2026089.500. Obtained 1,104 seconds of rotational time before test cut by T215 reading high due to normal propellant depletion. Data review showed normal operation very similar to the previous test. No anomalies were detected.

Test P2026090.500. Obtained 826 seconds of rotational time before test cut by T215 reading high due to tank depletion. Data review showed nominal operation.

Test P2026091.500. Obtained 822 seconds of rotational time before propellant depletion was detected by T215 reading high and terminating the test. Data review showed typical tester operation almost identical to the previous test operating conditions and results.

Test P2026092.500. Successful rotational test obtained 804 seconds of rotation time before normal propellant depletion. Depletion was detected by coolant temperature measurement T215. T215 indicated propellant temperature upstream of the tester had risen above the redline value of -385F due to a low level of LH_2 propellant in the run tank. No instrumentation or controller malfunctions were observed. The data from the test was reviewed and showed that all the operating parameters were within the normal range.

Test P2026093.500. Obtained 1,308 seconds of rotational time before test cut by T215 reading high and indicating normal propellant depletion. Again, the data review showed that instrumentation and operating parameters were in the normal range.

Test P2026094.500. Obtained 1,055 seconds of rotational time. The test experienced a nominal but by T215 reading high. The data review showed that the test was almost cut soon after the shaft speed had reached 35,000 rpm by the turbine drive pressure spiking to within 5 psi of the 650 psia high redline value. However, the pressure spike was so quick that the shaft speed did not significantly change. Shaft speed indicated a maximum speed of 36,200 rpm. The spike occurred before the shaft speed control had been placed on automatic. Thus, the spike was attributed to the manual operation. Once steady-state was achieved, the operation of the tester proceeded nominally.

The tester was borescoped after Test P2026094 to look for evidence of "river mark" formation. Because access to the shaft was not possible at this time, the shaft could not be rotated and only

four balls in each bearing were in view of the borescope. Of the visible balls in the load bearing, ball #3 had a definite river mark and balls #2, #5, and #6 were thought to also have river marks, but the view of these balls was not completely clear. The balls of the reaction bearing were not as visible making the identification of surface defects more difficult, but some kind of markings on the balls were observed. The other visible internal structure appeared to be in good condition allowing for the continuation of testing.

Test 2026095.500. Obtained 1,461 seconds of rotational time with a nominal cut due to propellant depletion as indicated by both T215 and T226 reading high. No anomalous control problems were observed during this test. However, the test profile was modified to include a radial load cycle to investigate the response of the three strain gages on the preload spring of the reaction bearing. These strain gages usually respond to the application of radial load by indicating the outer race has tilted slightly. This is nominal since it is known that a radial load on a ball bearing induces a rotating moment on the outer race. However, upon removal of the radial load after the speed cut, the strain gages did not show that the outer race moved back to the pre-radial load position. Thus, the test profile was modified to include a radial load cycle at 20,000 rpm to investigate if high speed shaft rotation would affect the outer race position restoration. The test data showed that, even at high speed, the outer race did not move back to the original pre-radial load position. It was then learned that the radial load actuator did not have an active return devise to remove the radial load. Thus, due to friction when cold, and the low magnitude of the radial load the load, on the shaft was not being removed explaining why the strain gage did not show a restoration of the outer race position. This was not a problem since when the tester warms to ambient conditions the radial load is relieved. All other data and operations were nominal.

Test P2026096.500. Obtained 867 seconds of rotational time. Test cut was due to propellant tank depletion as indicated by T215 high redline cut. The data showed that all parameters were operating at normal values except for SN3 which is a strain gage on the reaction bearing preload spring. The SN3 readings were approximately 200 lbs below the other strain gage readings and the erratic behavior of the measurement indicated that the strain gage or the connection had gone bad. This measurement was not critical to the tester operating and testing was continued.

Test P2026097.500. Obtained 1,111 seconds of rotational time before test cut due to T215 high. The SN3 strain gage measurement again indicated an instrumentation problem but all other data showed nominal operation.

The tester was again borescoped after this run to appraise the surface condition of the balls. During this borescope observation, ball #7, #8, and #9 of the load bearing were visible and appeared to have "river marks". The reaction bearing #2 and #1 balls were visible and showed very small "river marks". Nothing of a serious nature that would terminate testing was observed.

Test P2026098.500. The first attempt was cut due to DP239 high during rotation ramp up. DP239 is the pressure difference between the top cavity pressure and the thrust piston pressure. DP239 was normally held at 65 psi to maintain a zero net axial load on the shaft. However, during internal pressure changes, the automatic controller could not compensate or control fast enough and the pressure difference (DP239) exceeded the 100 psi redline. The test was recycled and the

thrust piston control was placed on manual. The second attempt was successful and obtained 435 seconds of rotational time before a cut on T215 high occurred. The DP239 pressure was maintained at the set point value with thrust piston control under manual operation. All other operating parameters appeared to be nominal.

Test P2026099.500. This test resulted in no rotational test time. The test was manually terminated during the initial pressurization of the rig. During pressurization of the rig, an automated control system is used to balance the axial pressure loads on the shaft. However, a test engineer noted that the thrust piston cavity pressure did not follow the upper cavity pressure normally, thus the test was terminated. A post test data review showed the probable cause of the anomaly was failure of the control system delta pressure transducer. Replacing the transducer corrected the problem in subsequent tests. Post test review of the data showed that the load bearing was subjected to an abnormally high axial load of approximately 4,500 lb as rig pressure increased. However, this load is well below the axial load capability of the bearing.

Test P2026100.500. This test resulted in 1,475 seconds of rotational time. The control system controlling shaft axial load performed smoothly verifying that the transducer replaced after Test 99 was responsible for the previous axial load control problems. The test was terminated by P208 low. P208 is the buffer seal exit pressure. Normal tests usually are cut by hydrogen temperature high. However, review of the data showed that the P208 usually starts dropping near hydrogen depletion. In this particular test, the rig was more thoroughly pre-chilled than normal. The chilled tank and rig resulted in the long test time and changed the normal slope of the fluid temperature warming rate at the end of the test. Therefore, the P208 shutdown was just an artifact of the abnormally long run and not cause for concern.

Test P2026101.500. This test produced 984 seconds of rotational test time. The test was terminated normally due to T215 (coolant inlet temperature) exceeding the redline. This cut is due to coolant depletion. No major anomalies were observed during this run. Turbine inlet pressure was observed to have some noise; however, the controller was able to maintain the desired 35,000 rpm shaft speed.

Test P2026102.500. 1,282 seconds of rotational test time was acquired during this test. No anomalies were noted in the test data. The test terminated normally due to propellant depletion.

Test P2026103.500. This test generated 1,300 seconds of rotational test time. This was a normal test to coolant depletion. The test was cut due to temperature T215 high. The midterm test goal of 15,000 seconds at speed was achieved during this test run. The only anomaly observed in this test was abnormal variations in the turbine inlet line pressure. Turbine inlet pressure spikes, similar to but larger than the spikes seen in Test P2026101.500, were observed in this test. It was not possible to absolutely determine the source of the pressure variations from the digital data. However, it appeared that the fluctuation occurred upstream of the turbine control valve. The automatic control system controlled correctly and attempted to maintain the speed set point of 35,000 rpm. Small deviations from the set point were caused by the fluctuations noted in this run.

Test 2026103.500. This test raised the total rotational test time on Build 4 to 16,883 seconds. This exceeds the goal for the midterm bearing

inspection (15,600 seconds). The rig was removed and disassembled for inspection of the bearings. Later the rig was reassembled and tested for an additional 15,600 seconds.

Build 4 Mid-Term Inspection. The midterm run time goal of 15,600 seconds was achieved with Build 4 of the liquid hydrogen bearing tester during July 1997. The bearing being tested in this build are the 60 x 130 mm ball bearings of the Pratt and Whitney design for use in their SSME high pressure fuel turbopump. The major goals of this build were to demonstrate the design life of the bearings under conditions similar to the HPFTPs and to investigate the formation of "river mark" defects in different silicon nitride ball materials in the absence of fluorinated grease in the flow path. In August 1997, the tester was removed from the stand and delivered to the Materials and Process Laboratory for disassembly and bearing inspection. The following observations were made during the "quick look" review of the ball bearings' condition.

The reaction bearing (top bearing) used Norton/ Cerbec NBD-200 silicon nitride balls and Cronidur races. Zero run time balls were installed for this build. The races had previous run time from engine test HPFTP F8-1A. However, in the tester, the races are loaded on the opposite side then they are in the pump, thus, they run on an unused surface. Visual inspection of the balls under low magnification showed that ball numbers 5, 7, and 10 had surface defects. Ball number 5 definitely had one "river mark" defect. The cage in this bearing was a test cage that slightly exceeded the maximum cage imbalance specification for flight hardware acceptance. The cage pockets had nominal fore and aft wear, but the outer diameter of the cage had moderate contact and wear on one side. However, the amount of wear was not excessive. The cage wear results were generally consistent with the ADORE cage imbalance studies performed earlier by SRS. The races of the reaction bearing were in overall good condition. They had moderately wide tracks with slight debris denting. The inner race did have very light Brinell marks, but they did not seriously degrade the running surface. There were eleven sets of Brinell marks, one for each ball, which consisted of about five indentations that trailed off to nothing in the direction opposite of race rotation. No corresponding Brinell marks could be found on the outer raceway track. The Brinell marks probably were produced during Test P2026083.500 in which the thrust piston control experienced an anomaly and overpressurized the thrust piston. This anomaly produced approximately 10,000 lbs of axial load on the reaction bearing. This load was very near the calculated static load capability of the bearing. However, these Brinell marks were not severe enough to deter further testing of the bearing.

The load bearing (middle bearing) used new Toshiba TSN-03H silicon nitride balls. The races were previously run in HPFTP F7-1F. As with the reaction bearing, the tester loading was on the previously unused side of the races. All of the balls had at least one "river mark" defect. Five of the eleven balls had two "river marks". The defects were long and narrow but appeared to be relatively shallow. These marks are typical of the defects seen previously on Toshiba balls from the HPFTP bearings. Thus, the formation of the "river marks" in a tester build that had no fluorinated grease present indicates that the fluorine was probably not the initiator of the defects. These "river marks" were not severe enough to terminate testing.

The races from the reaction bearing appeared in similar condition to the load bearing races, but without the Brinell marks. The tracks were moderately wide with some slight debris denting. The cage had very little wear on the outer diameter and the only wear in the pockets was in the fore direction which was also light.

One of the major objectives of this test series was to characterize any differences, with respect to river mark formation, between silicon nitride balls manufactured by Toshiba and balls manufactured by Norton. At the midterm inspection point the Norton balls did show fewer "river marks" than the Toshiba balls. However, "river marks" were observed on balls from both manufacturers. Additionally, it should be noted that while both bearings were subjected to approximately the same steady state loads, the test bearing (Toshiba balls) reacted directly against the housing while the reaction bearing reacted against the preload spring. This stiffer mounting may have resulted in a slightly more harsh environment. The test bearing also saw a slightly heavier radial load. More test time was required to determine if the resistance of the Norton material to "river mark" formation was significantly better than the current Toshiba material.

Tester Build 4 A Testing. During September 1997, the rig was reassembled as rig Build 4A. The rig was reassembled in the same configuration as Build 4. Several leak tests and cold flow runs were performed prior to attempting rotational testing. The cold flow tests were test P2026104.500, P2026105.500, and P2026106.500. Three tests were required due to leaky fittings and values that were identified during the initial cold flow tests. The cold flow tests were followed by two rotational tests. These tests are summarized below.

Test P2026106.500. Test was cut two times due to high turbine inlet pressure at start-up (P213). This test was the first attempt at rotation with Build 4A. Initially the test attempt proceeded normally, rig flow was established and the command was given to increase turbine pressure to start rotation. Turbine pressure was increased until it exceeded the 650 psi redline which caused an automatic shutdown of the rig. No rotation was indicated by the RPM sensor. However, strain gages and other instruments were noted to change in a manner consistent with rotation. Additionally, technicians noted that the rig audibly sounded as if it were rotating. Review of the data indicated that the rig had probably rotated and that the RPM sensor had probably failed. The rig was recycled and a second attempt at rotation was performed to confirm that the RPM sensor had failed. On the second attempt the turbine inlet pressure was increased to approximately 575 psi and held at this value while rotation was confirmed audibly. Following this second attempt, testing was terminated to investigate the RPM sensor problem. It was later found that a faulty connector caused the RPM sensor malfunction. Post test analysis of the data confirmed rotation and the turbine over pressure. The results of this analysis are shown in **Exhibit 308**. The curves show that approximately 55 horsepower was produced for a turbine inlet pressure of 650 psi. The predicted shaft speed for 55 horsepower is 39,000 rpm. This slight overspeed should have caused no damage of the rig. As noted on the chart, previous rig builds have been subjected to significantly higher overspeed events.

Test P2026107.500. Normal rotational test to propellant depletion. This test resulted in 1,318 seconds total rotational test time and 1,094 seconds of test time at 35,000 RPM. Seven axial

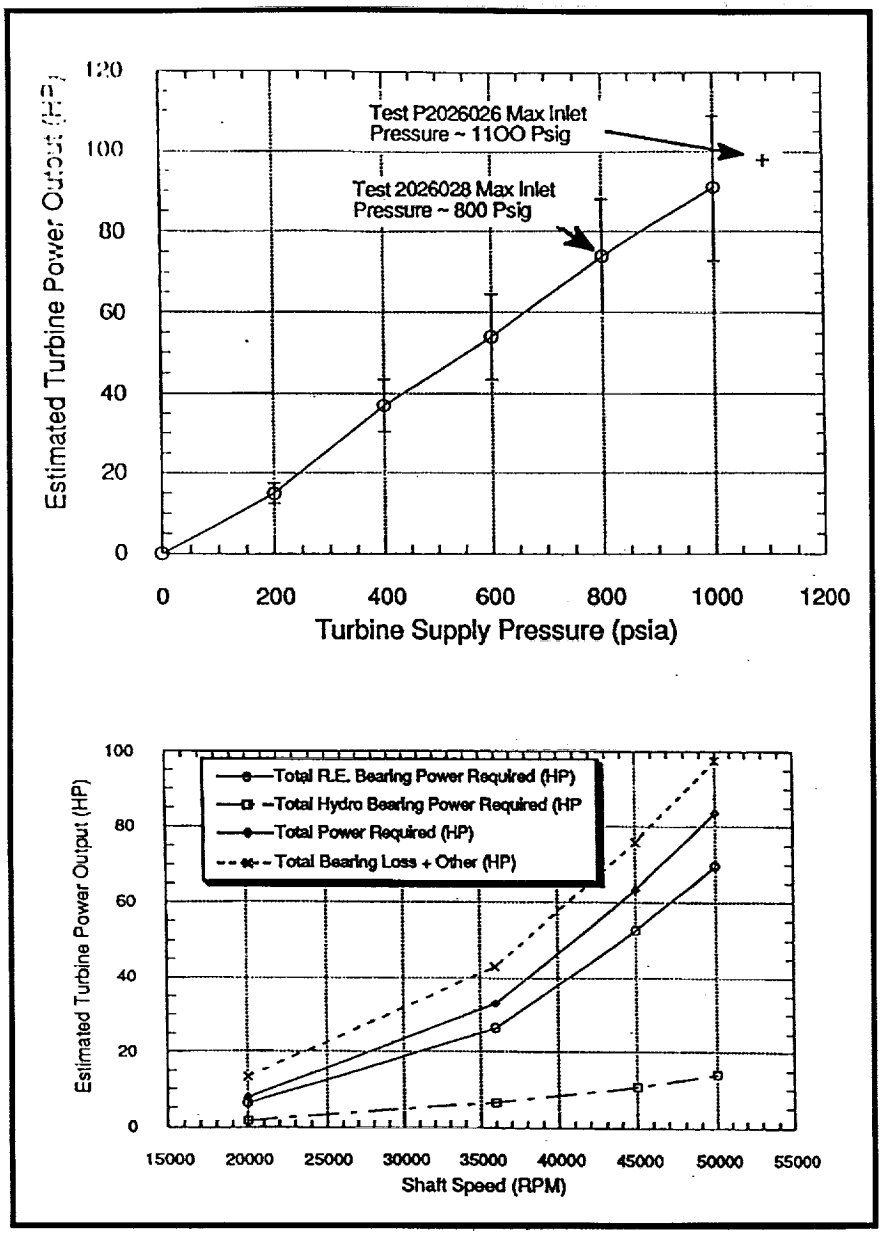

Exhibit 308 Rig Power Versus Shaft Speed Analysis

load cycles were performed at the shaft speed of 20,000 RPM prior to ramping the rig speed to 35,000 RPM. The axial load cycles were performed using the automated delta p controller. The objective was to cycle the thrust piston pressure delta p from 65 to -575 psi. This corresponds to a transient axial load on the load bearing of approximately 4,125 lbs. The controller slightly undershot the desired set point. Consequently, delta p was varied from 65 to -450 psi and the axial load cycles only went up to approximately 3,500 lbs. The autocontroller was adjusted to increase the transient load in future tests. The only anomaly observed in this test was a slight difference in the value positions required to maintain the desired flow across the rig. Post test analysis showed that some flow was leaking past the top cavity vent value that is normally closed during tests. The data indicated that the leak was relatively small. However, this problem was a concern because it is impossible to determine how much of the bearing coolant flow is exiting via this path. This problem was repaired prior to further testing.

Test P2026108.500. This was the second normal rotational test for rig Build 4A. This test produced 1,318 seconds total rotational time and 1,094 seconds of rotational time at 35,000 RPM. The test included seven transient axial load cycles applied at 20,000 RPM. The target transient axial load for each cycle was 4,125 lbs. This transient adds to the steady state load of approximately 875 lbs. However, the automated load control slightly undershot the desired set point

resulting in a transient axial load of only 3,500 lbs. The set points were adjusted for future tests. The test was cut normally due to propellant depletion.

Test P2026109.500. This test was the first test scheduled after a period of inactivity. Thus the rig and tank were initially at ambient temperature. The warm initial tank temperature and an incompletely filled run tank resulted in propellant depletion prior to rotation. No rotation time was accumulated during this test. A procedural change was implemented for this and subsequent tests. The target top cavity thrust piston delta pressure (DP239) was changed to increase the target transient axial load to 6,100 lbs during the test bearing axial cycles. This change was made to reflect the most recent engine test parameters.

Test P2026110.500. This test achieved 1,158 seconds of total test time and 1,007 seconds of test time at speed. Three transient axial load cycles were achieved. The test plan called for performing three cycles while reviewing the quick look data in real time to determine if the set points on the automatic load balance were accurate. The original plan was to make adjustments and then run 3 more axial load cycles. However, during the test, it was decided to proceed to high speed after the three cycles. The data showed that the transients load cycles peaked at approximately 5,600 lbs, just below the set point of 6,100 lbs. There were a couple of minor anomalies which occurred during this test. First, the radial load application step was inadvertently skipped while reviewing the axial load cycle. Consequently, the radial load was not applied until the rig was at full speed. Typically the load is applied during the 20,000 RPM dwell time. A slight discrepancy was also noted between the rig inlet/ exit pressure drop and the hydrogen flow rate. The flow rate was slightly low while the pressure drop was measuring nominal. It was later found that a bias in the pressure measurement was responsible for the discrepancy. The test ended normally with a cut due to propellant depletion.

Test P2026111.500. Two attempts were made to accomplish this test. Both attempts were terminated by a redline cut (P211 low) during the first cycle of the transient axial load cycle. It was later found that the redline was set improperly and did not correspond to the new axial load target of 6,100 lbs. The test achieved 2 axial load cycles and 112 seconds of total rotational time. No high speed test time was logged.

Test P2026112.500. This test was canceled due to a facility problem. The GN_2 supply pressure was too low to supply the thrust piston. A faulty regulator was responsible.

Test P2026113.500. A total of 728 seconds rotational time, 590 seconds at speed and seven transient axial load cycles were accomplished during this test. A redline cut was experienced due to the thrust piston balance exceeding tolerance after the transient load cycles were achieved. The problem was identified as an error in timing during the switch over from the axial load redline set to the high speed redline set. The rig was recycled and ramped up to speed to accomplish the high speed test time. The only anomaly noted in the data review was abnormally large biases in several of the pressure measurements. These biases were removed for the post test data review. The test was concluded normally due to propellant depletion.

Test P2022114.500. This test achieved 546 seconds total rotational time, 375 seconds at high speed and seven axial load cycles. This was a

normal test to propellant depletion. Large biases in pressures and temperatures were again noted in the data. The temperature bias was later traced to a faulty reference junction in the data acquisition system. The cause of the pressure bias is still under investigation.

Test 114 was the last test which occurred during November 1997. This brought the total Rig (Build 4 and 4A) run time on the bearings to 20,747 seconds.

Test P2026115.500. This test achieved 890 seconds total test time. The total high speed (35,000 RPM) test time was 756 seconds. A total of seven transient load cycles were applied to the test bearing. The transient load cycles were to a peak load of 6,100 lbs. The normal procedure for incorporation of transient cycles into the test was followed. The procedure called for ramping the shaft speed up to 20,000 RPM and then initiating the load cycles via the axial thrust balance controller. Once the load cycles were completed, speed was increased to 35,000 RPM. However, during this test the system experienced a redline cut after the last axial load cycle. Reviewing the quick-look data revealed that the problem was due to a timing error in switching from the liberal axial load (rig pressure balance) redlines in place for the transient cycles to the more stringent redlines used for high speed testing with steady state loads. After the cut, the rig was recycled and testing was resumed. Post test analysis of the test data showed no major anomalies. However, it was noted that the rig top cavity pressure (P201) appeared to have a bias of approximately +20 psi. Notes were made to check the transducer prior to additional testing.

Test P2026116.500. This test achieved 376 seconds of total test time with 210 seconds of test time at 35,000 RPM. Seven transient axial load cycles to 6,100 lbs were conducted on the test bearing. The previously noted bias in the rig top cavity pressure (P201) was absent in this test. The test terminated normally due to propellant depletion. The test time was low because a valve that is normally used only during chill down was not fully closed during the test allowing some flow to by-pass the tester.

Test P2026117.500. This test achieved 479 seconds of total run time and 313 seconds of test time at 35,000 RPM. Eight transient load cycles were conducted during the test. This was a normal test with cut due to propellant depletion. With the exception of a slightly shorter than average run time, no anomalies were noted. The reduced run time is believed to be due to the use of different hydrogen tankers being used to fill the run tank. The run tank was not completely full prior to testing.

Test P2026118.500. This test produced 925 seconds of total test time and 768 seconds at test time at 35,000 RPM. Eight transient load cycles were conducted to a peak load of 6,100 lbs on the test bearing. During the test run it was noted that the flow rate was generally lower than expected for our standard rig pressure profile. Post test analysis of the data showed that the rig back pressure (P217) was biased high by approximately 15 psi during the test. This bias resulted a reduced flow rate because of the incorrect delta pressure indication. However, all flows stayed within acceptable limits for the duration of the testing.

Test P2026118 was the final test conducted prior to the holidays. At the conclusion of this test the current bearings had been subjected to a total rig test time (Build 4 and 4A) of 23,417 seconds and 20,307 seconds at 35,000 RPM. Fifty-six transient load cycles have been applied

to the Toshiba TSN-03H bearing in the load position. Additionally, the rig has been subjected to 32 total starts.

The rig was borescoped after test P2026118 to verify the integrity of the bearings and to note the progression of river mark growth. During the inspection it was noted that rig torque's were low and rotation was relatively smooth. The rig was also borescoped after test P2026114. Therefore, there was 2,670 seconds total run time since the last borescope inspection. It was possible to see some river mark formation with the borescope. It was noted that the bearings appeared to have slightly more river marks than were noted in the previous inspection. However, the "river marking" still appeared to be relatively light.

Test P2026119.500. This test was the first rotational test after an extended down time for the holidays and facility sharing with other programs. The test achieved 472 seconds of total test time and 253 seconds at 35k RPM. A total of seven transient axial load cycles, to 6100 lb., were applied at a speed of 20k RPM. The relatively short test time accrued during this test was due to two factors. First, the run tank had not been thermally conditioned by recent testing which resulted in an abnormally high amount of propellant boil-off prior to testing. The second factor affecting run time was a facility redline cut that resulted in a protracted period of full flow no rotation. The redline cut was due to a data system off-line indicator. It was determined that this indication was faulty and the red line was removed so testing could proceed. The test terminated normally due to propellant depletion. No major anomalies were noted. It was noted that during the run, the thrust balance pressure difference (DP239) slipped from the set point of 65 (psi) to approximately 60 (psi). This small change resulted in a slight increase (approximately 25 lb.) in the reaction bearing load and a slightly greater decrease in the load bearing load.

Test P2026120.500. This test was aborted after two attempts were made to initiate rotation and begin testing. In both cases, the RPM measurement (S201) showed no indication of rotation when the turbine pressure was applied. However, indications of rotation were noted on other sensors (strain gauges and temperatures) and was confirmed audibly. Therefore, it was assumed that the speed sensor had failed. Post test inspection of the sensor confirmed that the speed sensor was inoperable due to a "patching error". The turbine inlet pressure reached 450 psi and 500 psi on the first and second tests, respectively. The normal turbine inlet pressure for high speed operation is approximately 550 psi. Therefore, the rig was not put in overspeed during these aborted starts. The test was credited with 71 seconds of rotational time.

Test P2026121.500. This test was conducted in the afternoon after the aborted test number P2026120. Consequently, the facility was very well pre-chilled and a large amount of test time was achieved. The total run time was 1441 seconds with 1305 seconds time at speed. Seven transient axial load cycles to 6100 lb. were applied to the load bearing. During this test, the LH_2 inlet flow measurement indicated a slightly lower than normal coolant flow rate with all other measurements normal. The measured flow rate was approximately 0.46 PPS compared to a nominal 0.50 PPS. SINDA/SHABERTH analysis had shown adequate cooling is provided at much lower flow rates, therefore the test was allowed to run to completion. The flow rate was controlled by maintaining inlet pressure and exit pressure by two independent valves. The valve positions

were controlled by adjusting to meet pre-specified values for P238 (inlet pressure) and P217 (exit pressure). Post-test data reviewed from this test found a slight bias in P217. The bias caused the P217 sensor to indicate a slightly higher pressure than the actual value. This resulted in closing the exit valve to a slightly more closed position than normal and reducing the flow. In the data review it was determined that the bias was not a major concern because of redundant redline cuts on both pressures and flow rates.

Test P2026122.500. This test achieved 1422 seconds of total run time with 1281 seconds at speed. Seven transient load cycles to 6100 lb. were performed on the load bearing. The test was complete to propellant depletion with a normal cut due to T215 high. Two Instrumentation errors were noted during the test. Data from T214 (load bearing outer race) dropped out several times and DP230 (bearing cavity exit flow orifice) drifted throughout the test. The instrumentation errors were checked prior to the next test.

Test P2026123.500. This test achieved 1199 seconds total rotational time with 979 seconds time at speed. A data review prior to the test showed that we needed to increase the number of transient cycles in order to meet the 120 cycle goal at approximately the same time as meeting our total run time and time at speed goals. Thus, it was decided to run the transient cycle program twice per test for the next few tests. During this test, 14 axial load cycles to 6100 lb. were applied to the load bearing. DP230 (bearing exit flow orifice) was still drifting in spite of repairs made after the last test. The reaction bearing outer race temperature (T213) dropped out during the test. The test terminated normally due to propellant depletion.

Test P2026124. This was the final test conducted in January. The test achieved 1106 seconds total run time and 892 seconds time at speed. Fourteen transient load cycles to 6100 lb. were applied to the load bearing. Several minor data problems were noted. However, the test was completed and terminated normally due to propellant depletion. The instrumentation anomalies included T202 (Reaction Bearing outer race temperature), T213 (Reaction Bearing outer race temperature), T214 (Load Bearing outer race temperature), and FC204 (Thrust Piston Flow) data dropouts.

Test P2026125.500. This test produced 743 seconds of total test time and 554 seconds of high speed test time at 35,000 RPM. Fourteen transient load cycles to 6100 lb. were applied to the load bearing while rotating at 20,000 RPM. The test terminated nominally due to propellant depletion. Prior to testing, the test engineer noted that there was a possibility that some pressure was in the rig top cavity when the instruments were zeroed for the test. This was later verified during the data analysis and was manifest as a top cavity pressure (P201) bias of approximately 10 psi. This bias was accounted for in post processing the data. During the tests the strain gauges started to diverge slightly at about 400 seconds from start. This divergence is consistent with outer race tilting and has been observed during several of the more recent tests. However, the tilt appeared to be about a different axis than has been observed in other tests. The turbine delta pressure, an indicator of horsepower into the rig, was noted to be slightly higher than the standard baseline (440 psi compared to 410 psi). Rig power required trended upward since Test 122. This could indicate increasing friction due to surface degradation on the balls or races. It should

be noted that slight fatigue spalling of the load bearing inner race was observed in the quick look data inspection conducted after the rig was disassembled. **Exhibit 309** shows a comparison of turbine pressure drop for tests 90, 102, 108, 122, 125, and 126. The three latter tests show the higher pressure drop required for operation at 35,000 RPM.

Test P2026126.500. This test achieved 1270 seconds total test time and 1127 seconds at high speed. Seven transient load cycles were conducted to 6100 lbs. This test was the final test required to meet the test time objectives. The cumulative run time statistics after this test are; 41 starts, 31,142 seconds rotational time, and 26,706 seconds time at high speed. The test terminated normally due to propellant depletion. No major anomalies were noted during the test. However, post test data review showed that pressure bias was still present with some of the instrumentation. In particular, the thrust piston pressure (P212) had a bias of almost 20 psi. The rig was removed from the stand at the conclusion of this test and the bearings were disassembled for inspection.

Build 4A Test Series Highlights. The test goals for this build were to achieve 31,200 seconds total run time, 25,272 seconds at 35,000 RPM, and 120 axial load cycles. These goals were based on simulating 60 engine run cycles. At the midterm inspection it was noted that the Toshiba TSN-03H balls in the load bearing had significant "river mark" features typical of high time pump bearings. The Cerbec NDB-200 balls in the reaction bearing position also had "river marks"; however, they were much lighter and only observed on some of the balls. It should be noted that the reaction bearing does not see the high axial loads that occur during the transient load test cycles. Completion of this test series completed the planned ball bearing tests and demonstrated the ability of four sets of ball bearings to meet the 60 mission design life goal in spite of known "river mark" formations existing on the balls.

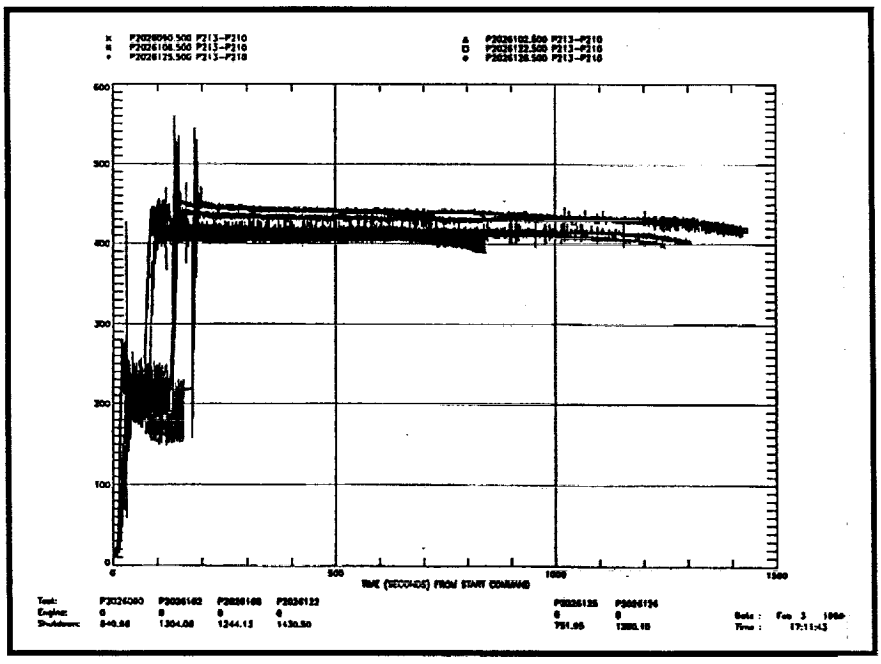

Exhibit 309 Turbine Pressure Drop for Selected Tests

After completion of Test 126, the bearings in the rig had accumulated 31,142 seconds of total test time and 26,706 of test time at 35,000 RPM simulating operation at 104% RPL. The ball bearings in the rig load position were also subjected to 126 transient load cycles from 870 lb. to 6100 lb. This test schedule was designed to simulate 60 engine run cycles. This test series successfully demonstrated, for a second time,

the ability of the hybrid ball bearings to meet the 60 mission design life in spite of the formation of the surface features that have been called "river-marks". Build 3 had demonstrated the life goal with bearings that had severe river-marks prior to being tested in the rig. New silicon nitride balls were used in the Build 4 bearings. Toshiba TSN-03H balls were used in the load bearing position and Cerbec NDB-200 balls were used in the reaction bearing.

The formation of "river marks" observed in Build 4 provided verification that the rig test simulated the pump environment sufficiently well to cause the same conditions which produce the river-marks in the pump. The new balls also provided the opportunity to observe the formation of river-marks as a function of run time and to compare the Toshiba material to the Cerbec material. As previously reported, river marks were observed on balls from both bearings at the mid test inspection. The Toshiba balls had more numerous and heavier marks than those observed on the Cerbec balls. However, the Toshiba balls were in the load bearing position which reacted directly through the housing instead of through a spring. Thus, this position can potentially produce a more severe load environment. The river-marks observed on the Cerbec balls seemed to be similar in form and feature to the ones observed in the Toshiba balls. Completion of this test series demonstrated the ability of four sets of ball bearings to meet the design life goals in spite of the river-mark surface features.

Post test inspection of the bearings after test 126 resulted in similar observations to those noted at the mid-term inspection. The load bearing had more heavy and more numerous river marking than was observed on the reaction bearing. However, both bearings did exhibit classical river mark formation. The load bearing, which was subjected the high axial load transients, did show some minor fatigue spalling damage on the inner race. Mr. Chip Moore (NASA/MSFC) performed detailed metric analysis of the hardware for documentation and identification of the effects of the extended service. The tests performed during this period are described below.

Post Build 4 Computer Modeling of Hydrostatic Bearing Flow Requirements. SRS was asked to investigate possible ways of reducing hydrogen consumption during bearing testing. The hydrogen supplied to the tester serves two functions. First, hydrogen flows across the bearings for cooling. Approximately one-half of a pound of H_2 per second is used for cooling. This flow emulates conditions in the pump. Therefore, it was decided not to try and modify this flow rate in the interest of similitude with the pump. The hydrostatic slave bearing was the second and largest consumer of hydrogen in the rig. For, our test conditions, the hydrostatic bearing used approximately one pound of H_2 per second.

The hydrostatic slave bearing was modeled using hydrojet to investigate the sensitivity of bearing stiffness and dampening to reduced hydrogen flow. The results of this study are summarized in **Exhibit 310**. Hydrojet was used to simulate the bearing under the design conditions. This case was labeled Case 2. The design conditions call for a 2,000 psi supply pressure with upstream and downstream vent pressures of 1,400 psi and 200 psi. The results from this baseline case were normalized and plotted for comparison with various other cases. Case 4 was analyzed to evaluate the effect of the lower rig speed (38,000 RPM). This small reduction had very little effect on the system stiffness an dampening. Therefore, all of the other analyses were performed at

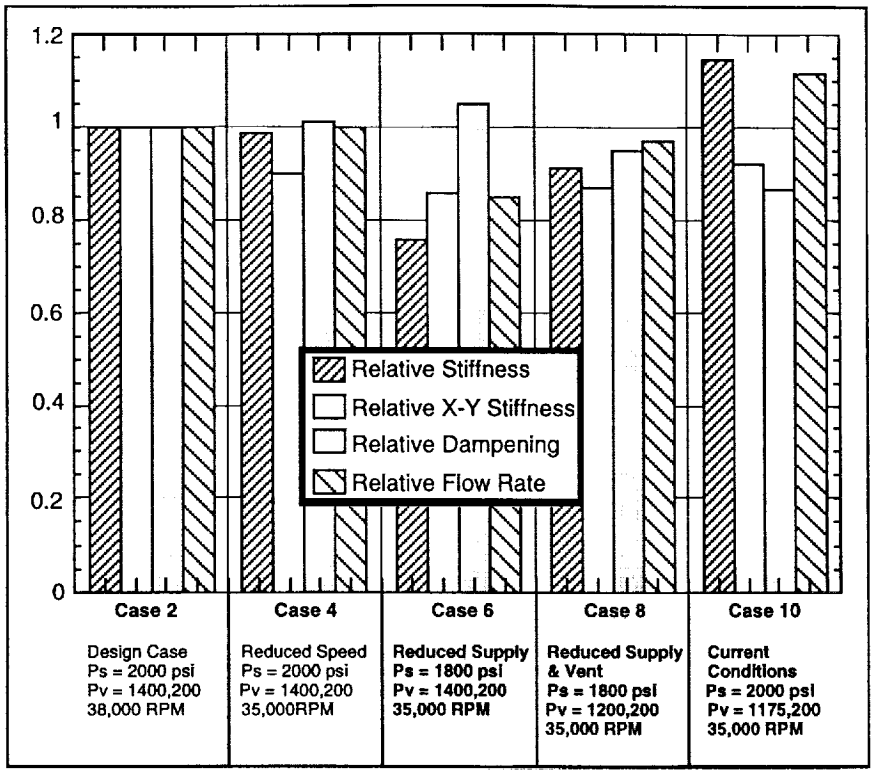

Exhibit 310 LH2 Rig Slave Bearing Flow/Stiffness Study

35,000 RPM. The next case modeled represents the current operating conditions at the time. This case is labeled Case 10. The results from this case show that we were operating with approximately 15% greater stiffness and approximately 15% less dampening than the design case. Case 8 was run to look at the effect of reducing both the supply and vent pressures while keeping the delta p across the supply and high pressure vent constant. The results from this analysis showed that this approach had little effect on flow or stiffness. Thus the analysis showed that delta p across the bearing was the primary parameter governing both stiffness and flow. The analysis labeled Case 6 illustrates this point. The delta p for Case 6 was reduced by 200 psi by dropping the supply pressure from 2,000 psi to 1,800 psi. This resulted in a flow rate savings of 15% relative to the design point and stiffness was reduced by 25%.

Based on the hydroseal analysis, it appeared that we could reduce the hydrostatic bearing supply pressure to approximately 1,800 psi. This would reduce the total rig H_2 consumption from approximately 1.5 lbs/second to approximately 1.35 lbs/second. Under these flow conditions we would be operating at approximately 95% of the design bearing stiffness. Thus, it appears that it would be relatively low risk to make this change and save approximately 10% of the LH_2 consumption per test. A minimum of one additional non-rotational test was planned to recalibrate the axial load balance in the rig for the new operating conditions. A minimum of 10 tests would be required to break even on LH_2 consumption because of the non-rotational test required for calibration.

6.12 Test Support for MSFC LH_2 Tester - Build 5

LH_2 rig testing prior to Build 5 quantified the characteristics of river-mark formation on ball bearings and has demonstrated the life capacity of river marked ball bearings. River-marks have also been observed on some HPFTP/AT silicon nitride roller bearings. The roller bearing geometry, a right cylinder with relatively sharp corners, may potentially be much more susceptible to propagation of surface defects such as river marks.

The roller bearing operational radial loads are much higher than the ball bearing loads. The typical roller bearing radial is 1,500 lbs compared to the nominal ball bearing radial load of 200 lbs. The LH_2 rig, configured for roller bearing testing, used one roller bearing and one ball bearing. The radial load was applied to the roller bearing and was reacted by a ball bearing and a fluid film bearing. The ball bearing was estimated to react approximately 65% of the load applied to the roller bearing. This resulted in a radial load on the ball bearing of 965 lbs for a roller bearing load of 1,300 lbs. Thus, the ball bearing is required to support approximately five times the nominal radial load. The SINDA/ SHABERTH software was used to evaluate the capability of the bearing to support these loads at the nominal operating speed and axial load (35,000 RPM, 890 lbs). Several load cases were evaluated and the results were plotted for review. The analysis showed that the ball bearing had sufficient capability for the testing.

Exhibit 311 shows the maximum predicted contact stress and minimum ball load as a function at radial load. The roller bearing test was estimated to result in an increased a maximum contact stress of 385,000 psi compared to 325,000 psi for a nominal ball bearing test. Ball unloading does not occur until the radial load reaches 2,100 lbs. Thus, unloading was not a concern for the proposed test. **Exhibit 312** shows that bearing B_{10} fatigue life decreased from 125 hours to 109 hours. Fatigue was not predicted to be a problem. However, the load bearing from the previous rig build did show some evidence of the initiation of fatigue damage. Therefore, bearing temperatures were closely monitored during the test series for signs of surface distress caused by fatigue spalling. **Exhibit 313** shows ball excursion versus radial load. The plot shows the bearing could accommodate radial loads of 1,300 lbs before the ball excursions exceed the available cage pocket clearance. Thus, we estimated that the test load of 965 lbs would not cause excessive cage wear or cage heating. Finally, **Exhibit 314** shows that bearing operating temperatures were not significantly affected by the proposed load increase.

In summary, the analysis performed demonstrates the capability of the ball bearing to meet testing requirements. This data is expected to contribute significantly to understanding the

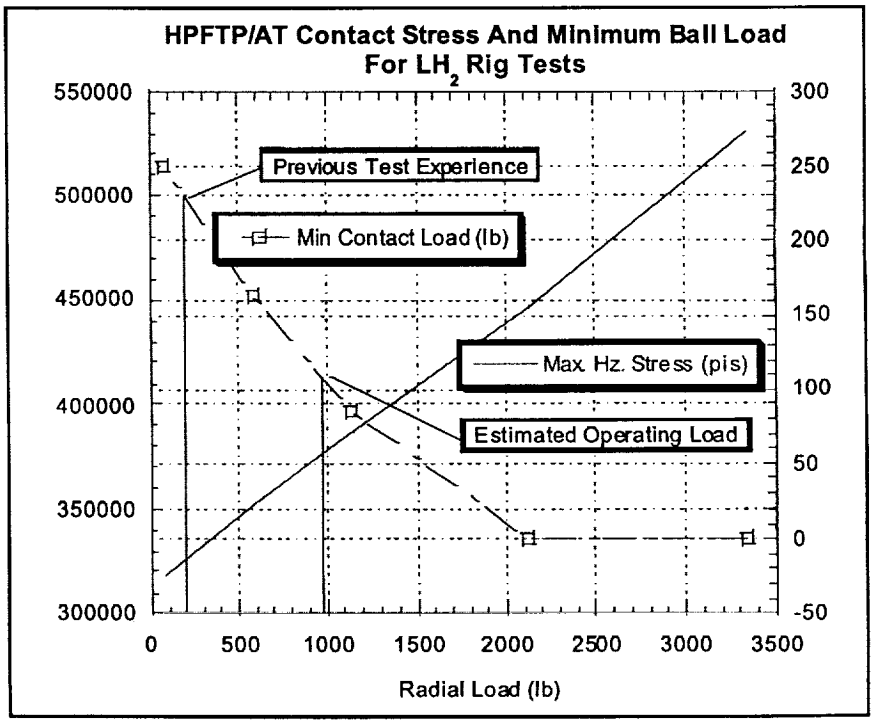

Exhibit 311 HPFTP/AT Contact Stress and Minimum Ball Load for LH2 Rig Tests

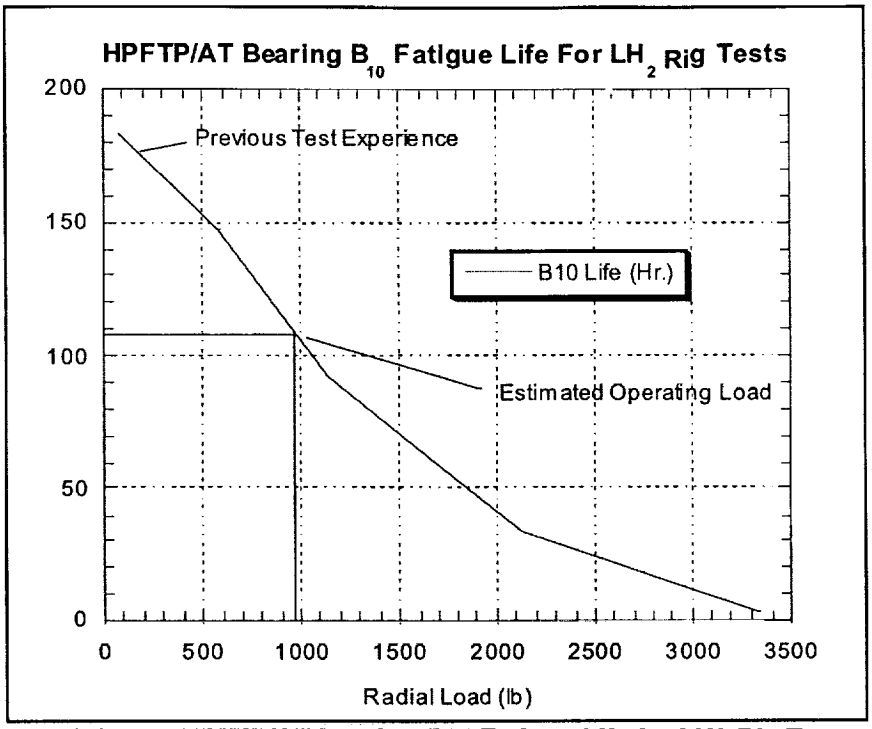

Exhibit 312 HPFTP/AT Bearing B10 Fatigue Life for LH2 Rig Tests

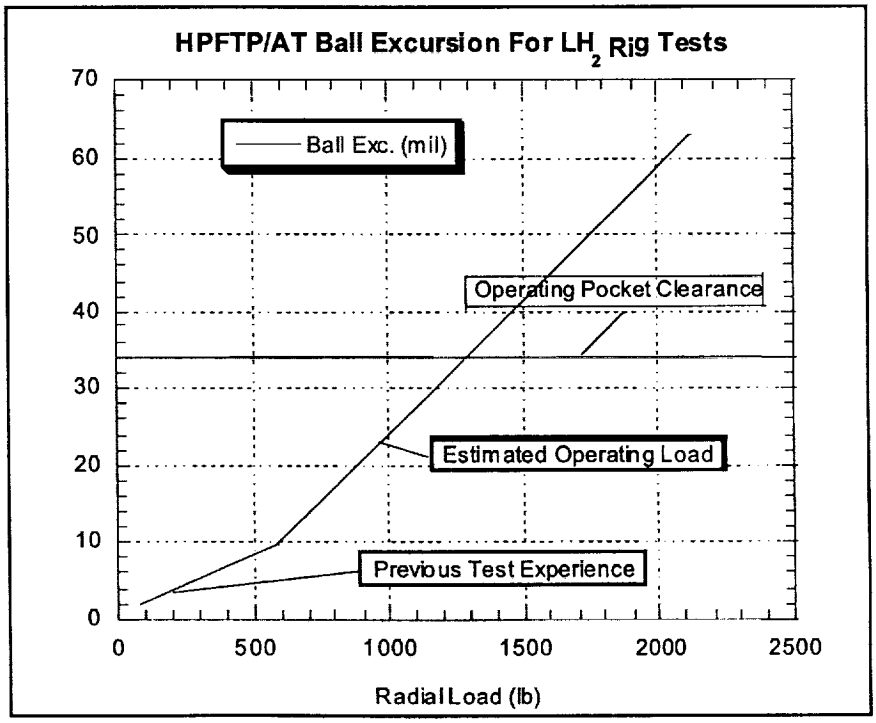

Exhibit 313 HPFTP/AT Ball Excursion for LH2 Rig Tests

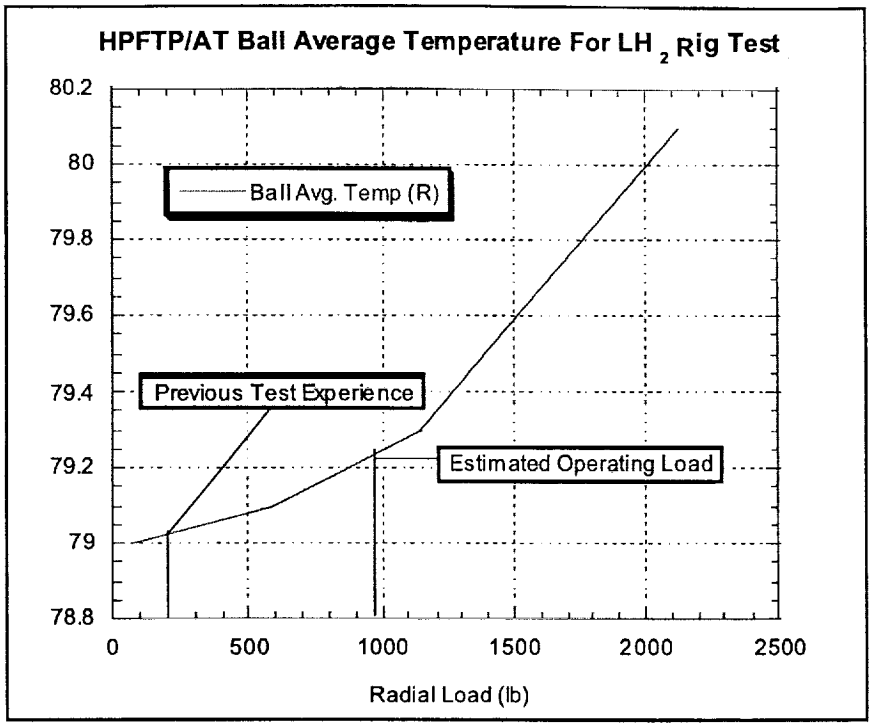

Exhibit 314 HPFTP/AT Ball Average Temperature for LH2 Rig Test

mechanism of river-mark formation and the consequences of operating river marked bearings.

Build 5 of the LH_2 rig was configured for hydrogen testing of fuel pump roller bearings. The build incorporated a ball bearing in the reaction bearing position and a roller bearing in the load bearing position. The roller bearing typically sees a radial load of approximately 1600 lb. during pump operation. The radial load cylinder in the rig imparted this type of load on the bearing. However, this load had to be reacted by the combined stiffness of the ball bearing and hydrostatic bearing. The load capability of the hydrostatic bearing was not clearly defined. Therefore, a Hydroseal model of the bearing was constructed to evaluate the load capability of this bearing. The results of this study are presented in **Exhibit 315**. Bearing reaction force in the load direction, cross direction, and total magnitude are plotted as a function of shaft eccentricity within the radial clearance. The analysis showed that a 1600 lb. load would utilize approximately 75% of the available radial clearance if operated with the same inlet pressure as currently used for ball bearing tests. This condition would provide adequate margin with respect to

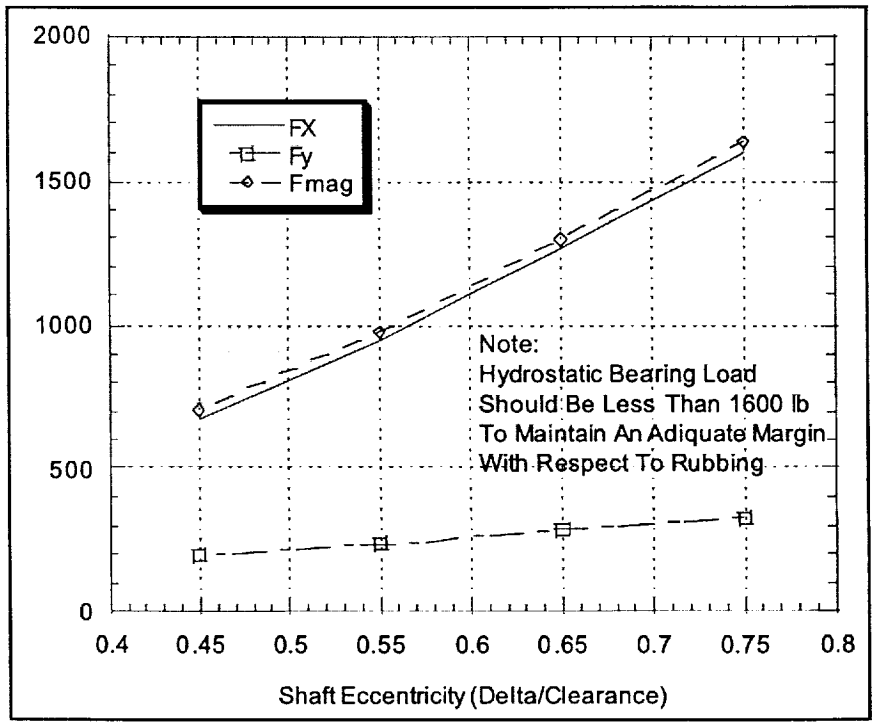

Exhibit 315 Hydroseal Analysis of LH2 Rig Hydrostatic Bearing

radial rubs. During testing the hydrostatic bearing load was on the order of 50% of the roller bearing load since the load is shared with the ball bearing. Thus, the Hydrostatic bearing stiffness was not a problem for the proposed tests. The exact load sharing was worked out using the SINDA/SHABERTH model once modifications to the model were completed to simulate the ball/roller test configuration.

The SRS SINDA/SHABERTH LH_2 rig model was updated in October 1998 to support the upcoming tests. The input data was updated to reflect actual measured hardware dimensions. The shaft bearing system model included the ball bearing, roller bearing, and a cylindrical bearing that simulated the hydrostatic bearing. Versions of the model were created to run in the SHABERTH only configuration. The SHABERTH only configuration allowed for quick turnaround analysis when the component temperatures were known from test data or previous coupled analysis. The current SINDA/SHABERTH input model is listed in **Exhibit 316**.

Build 5 Rotational Testing. The first hydrogen testing with rig build 5 was accomplished during November 1998. Build 5 had the HPFTP/AT Build F8-3 pump end ball bearing installed in the rig reaction bearing location. The HPFTP/AT Build F6-4 turbine end roller bearing was installed in the rig load bearing position. This build represented the first attempt to test roller bearings, with this rig, since the short lived first rig build that had been terminated early due to pressure control problems. The baseline conditions for this build were N = 35,000 RPM, roller bearing radial load = 1,1000 lbs, and ball bearing axial load = 700 lbs. The load sharing in the rig placed approximately 700 lbs radial load on the ball bearing.

There were two primary objectives of this build. First, the test would generate life data for the ball bearing with increased radial load. This data was needed to evaluate the effect of potential pump modifications to increase the PEBB radial load. The second objective was to demonstrate 30,000-second life capability for the hybrid silicon nitride roller bearing. Two leak checks (tests 001 and 002) and fifteen rotation tests (103 – 117) were accomplished. Details of the rotational tests are provided below.

Test P2096003. Test 3 was the first rotational test scheduled for this build and generated approximately 350 seconds of total rotational test time. A leaky value resulted in the loss of speed control during this test. Initially, the test progressed normally. Pressure was brought up in the rig and axial load balance was established. The test procedure then called for opening the turbine isolation valve (3501) to pressurize the turbine control valve (3502). At this point in the test, the turbine control valve 3502 was closed. However, when 3501 was opened, the shaft began rotating. No red line parameters were exceeded so the rig was allowed to continue spinning. Speed was approximately 30,000 RPM. The speed was fluctuating from 30,000 RPM to 20,000 RPM. However, there was no speed control available because the turbine control valve was commanded fully closed. The test was terminated. It was determined that the uncommanded rotation was due to a leaky turbine control valve. The maximum radial load applied during rotation was approximately 950 lbs. Zero time at speed was credited to this test because the speed never reached 35,000 RPM.

Test P2096004. Test 4, the second rotational test in the series, generated 920 seconds total test time and 68 seconds at speed. This test began normally, speed was increased to 10,000 RPM

```
P&W FLUID FILM BEARING / ROLLING ELEMENT TESTER (1 PEBB, 1 ROLLER & 1 FAKE FLD BRG)
    35000.     3     0  -25  -20    .00001                                                  11
B1          CRONIDUR 30          CRONIDUR 30          1.          1.          0.
     95.000          11      .0000   -20.31                      0
    20.5867
     0.5200        0.58
       .014        .014        .014         2.          2.          2.
         +1      84.176       3.556       0.241       0.610        .230          3
    0.04826     .058420     -.02540    -0.17780
     22.905       15.27       15.27       30.54       30.54      45.810
      25.40      51.450      60.000       79.22      111.13      130.00      135.64      165.10
    2.069E5     2.070E5     2.276E5     2.966E5     2.276E5     2.069E5     2.069E5
      0.270       0.270        .260        .300        .260        .270        .275
      8.218       8.218       7.833       3.211       7.833       8.218       8.218
   9.720E-6    9.720E-6    7.020E-6    0.630E-6    7.020E-6    9.720E-6    9.720E-6
                                        0.200       0.200
C2          CRONIDUR 30          CRONIDUR 30          1.          1.          0.
    103.000          14      .0724                                  0
    16.9469     16.9469     999999.         0.0      471.68        8.89
    27.9679     16.7132     999999.      999999.                                 20.
      90.00       0.333     999999.      1.2827          10.
      .1524       .1524       .0127         2.          2.          2.
      .2032       .2032       .0127         2.          2.          2.
         -1     119.405      4.8895       .5664       .5842        .140          3
    0.04851     .083820     .01270     -.17780
     34.610       34.61       34.61      32.512      32.512     32.5120
     25.400      52.421       73.00       88.90      119.97      133.00      136.98      186.94
    2.069E5     2.069E5     2.276E5     2.966E5     2.276E5     2.069E5     2.069E5
      0.270       0.270        .260        .300        .260        .270        .270
      8.221       8.221       7.833       3.211       7.833       8.221       8.221
   9.720E-6    9.720E-6    7.020E-6    0.630E-6    7.020E-6    9.720E-6    9.720E-6
                                        0.200       0.200
C3          DUMMY BRG            DUMMY BRG            1.          1.          0.
    103.000          14      .0965                                  0
    16.9469     16.9469     999999.         0.0      468.88        8.89
    27.9679     16.7132     999999.      999999.                                 20.
      90.00       0.333     999999.      1.2827          10.
      .1524       .1524       .0127         2.          2.          2.
      .2032       .2032       .0127         2.          2.          2.
         -1     119.405      4.8895       .5664       .5842        .140          3
    0.00000     .101600     .00000     -.12700
     0.0000       34.61       34.61      16.256      16.256     16.2560
     0.0000      19.304       73.00       88.90      119.97      133.00      137.11      186.94
    0.00000     2.236E5     2.207E5     2.966E5     2.207E5     2.103E5     2.072E5
      0.000       0.288        .260        .300        .260        .306        .270
     0.0000       7.861       7.833       3.211       7.833       7.944       8.221
   0.000000    8.618E-6    7.020E-6    0.630E-6    7.020E-6    11.97E-6    10.14E-6
                                        0.200       0.200
                                  1
-232.-232.-232.-232.-232.-232.-232.-232.-232.-232.-232.-232.-232.-232.-232.
-240.-240.-240.-240.-240.-240.-240.-240.-240.-240.-240.-240.-240.-240.-240.
-214.-214.-214.-214.-214.-214.-214.-214.-214.-215.-214.-214.-214.-214.  20.
     1              0         0.       25.40          0.       60.00    2.318E5
     1          130.90       25.40         0.       60.00       76.20    2.318E5
     1          308.20         0.       50.50       76.20       76.20    2.318E5
     1          351.80       50.50         0.       76.20         0.     2.318E5
```

Exhibit 316 SINDA/SHABERTH Input Model

```
    2          40.90        0.                  0.
    2         114.54       .0172              .00000
    2         248.18       .0000              .00000
    3          57.32        0.        0.
    3         114.54        50.0       0         0         0        0.0
    3         338.18         0.0      0         0         0     -4448.

    2    1                   0.                  0.
    2    2                  .0000              .00000
    2    3                  .0000              .00000
    3         114.54         0.        0.
    3

&BRGNUM
 HETRAN='NO '
&END
&CONDAT
 IDENT='SAT45',FILM=.TRUE.,XPCT=1.0
&END
&VISCO
 RIRC=.1218, RORC=.18989, RIRUS=.13808,RORLS=.1750,
 WIRS=.1155, WORS=.1004, COR=.1733,CIR=.1385, CPW=.0697,
 CW=.0958, CDCNF=1.2, CDCP=0.6, CAGEFF=.200, VFRU=0.10,
 VFRD=0.30,DELP1= 2.0,DELP2= 2.0,
&END
&OUTER
 HCODEO=1,
 VARO1= 1.,
 VARO2= 1.
&END
&INNER
 HCODEI=1,
 VARI1= 1.,
 VARI2= 1.
&END
&BALL
 HCODEB=3,
 VARB1= 1.,
 VARB2= 1.
&END
&JSPRG
 PREDEF=0.0137853 ,KSPRNG=82000., PLOAD=478.60, DELMX=15.5E-3,
 INTCL=.0063, TCRUV=.06125
&END
&FLGS
 FLAG='NOSPRG', SFLAG='S+S', AXLOAD= .TRUE.,.TRUE.,.TRUE.,.TRUE.,
 PRTHYDRO='YES', FFFLAG='NO '
&END
&FFBTSP
 FKSPRNG=11500., FPLOAD=1000., FINTCL=.0057, FTCRUV=.1625,
 FDELMX=0.13, SD0=0.001770
&END
```

Exhibit 316 SINDA/SHABERTH Input Model

and 50% of the radial load was applied (550 lbs). The speed was then ramped up to 35,000 RPM and the full radial load was applied. Automatic speed control was on for the high-speed time. Speed fluctuations from 35,00 RPM to 31,000 RPM were noted. After approximately 68 seconds at speed, a red line cut on the high side turbine pressure stopped the test. Review of the data showed that during the entire time at speed, the speed controller varied the turbine pressure wildly attempting to maintain constant speed. The rig was recycled and a second attempt at the test was begun. On the second attempt, speed was increased to approximately 30,000 RPM under automatic control. Once again large fluctuations in turbine pressure were noted. The speed was reduced to 11,000 RPM. It was decided to attempt a third speed ramp up with the speed controller off. The turbine pressure was manually increased to bring the speed up to approximately 27,000 RPM. In this mode the pressure was steady but turbine speed fluctuated wildly (27,000 RPM to 12,000 RPM). Speed control was varied to different set points trying to eliminate the speed fluctuations. However, no smooth operating point was identified. The test was terminated by the high side buffer seal exit temperature cut. Review of the data indicated that this was a normal shutdown, which occurred due to propellant depletion. Post test review of the strain gauge and pressure balance data showed that the shaft had experienced significant axial excursions during the torque excursion. The strain gauges showed a band approximately 100 lbs wide during the torque events. This 100 lbs variation equated to 7.5 mils axial travel.

The axial excursion anomaly had to be investigated. Two factors were considered. First, the fact that this build only had one bearing capable of carrying load resulted in high axial stiffness in one direction and low axial stiffness in the other direction. The other factor was uncertainly in the magnitude of the applied radial load. In previous tests, preload spring tilting was noted when the radial load was applied; no tilting had been observed in this build even though the radial load was much larger.

Test P2096005. This test was conducted in two parts, neither of which generated rotational time. The first part of this test was a radial load cylinder check-out performed at ambient temperature. A micrometer was set up on the load cylinder and the radial load actuator pressure was varied. No motion was noted during the test. Subsequently, the radial load cylinder was detached form the rig and exercised at higher pressures. At some unknown higher pressure the cylinder actuated. An abnormal fluid sound was noted. The cylinder was exercised several times until it appeared to operate smoothly. After the load cylinder was reinstalled, the rig was chilled for a rotational test. During the hydrogen test, the procedure was paused when the rig pressures were stabilized and the radial load cylinder was exercised. Spring titling was noted during this experiment. Hence it appeared that the radial load cylinder was hung up in the previous test and little or no radial load was applied. No rotation was attempted due to facility leaks observed from the control room.

A simple calculation was performed to see if the axial excursions noted during Test 4 could be due to exciting an axial vibration mode of the shaft. The system was modeled as a simple one degree of freedom spring mass system. The vibrational frequency for this system was simply the square root of the mass times the spring constant. The natural frequency was estimated to be 479 cycles/s (28,740 cycles/min).

This frequency was below synchronous for full speed operation. This axial mode was probably responsible for the observed axial excursions and torque variations. The rig would have been particularly sensitive to this mode if the radial load had not been applied.

P2096006. This test was the first fully successful test of Build 5. Previous rotational tests had all experienced abnormal axial vibrations and torque excursions. We had speculated that the radial load cylinder had not functioned properly on prior tests. After Test 005, the cylinder was removed and cycled. Exercising the cylinder showed evidence of fluid in the cylinder, possibly having caused freeze up. The fluid was purged by fully stroking the cylinder several times. In addition to purging the cylinder, the procedure was modified to allow a larger percentage of the radial to be applied at lower speed. The original procedure had called for incrementally applying the radial load as speed increased. This approach had provided the most margin relative to rubbing in the hydrostatic bearing. However, the previous runs had indicated that the radial load was not engaging the roller bearing in the deadband. The procedure adopted for Test 005 was to put 25% of the radial load on prior to rotation, then applying an additional 25% at 15,000 RPM, and the remaining 50% at full speed. This procedure was applied during the first attempt at rotation. During this attempt, the speed ramp was smooth and a speed of 35,000 RPM was obtained. The test cut, shortly after achieving full speed due to high turbine inlet pressure. The facility was recycled and the data was reviewed. We decided to apply the full radial load at 15,000 RPM on the next attempt. The second rotational attempt was successful and 401 seconds of test data at 35,000 RPM was obtained. Total rotational test time was 829 seconds. This new procedure greatly reduced the tendency of the rig to experience axial and torque excursions.

Test P2096007.500. Test 7 resulted in 903 seconds total test time and 522 seconds time at 35,000 RPM. This test used new procedures for radial loading (25% applied prior to rotation and the remainder of the load applied at 15,000 RPMs.) This test appeared to be normal. Shutdown was due to propellant depletion. Latter review of the data showed that there was actually some short duration torque anomalies (less than 1 second) that required the controller to ramp up the turbine pressure. On one occasion, turbine inlet pressure reached 630 psia, approaching the highside cut of 650 psi. The redline was raised to 700 psia for future tests. The speed and torque fluctuations seen during this test were much less than those experienced earlier in Build 5. Thus, the new radial load procedure seemed to have improved speed control, but some anomalies still occurred. The nature of the torque excursions was not fully understood but roller to race flange interactions were suspected. The configuration of this rig required significant axial movement to load the axial spring. This movement may have promoted the roller flange interactions.

Test P209608A.500. Test 8A produced 929 seconds total test time and 806 seconds at speed. A procedural change was made prior to this test to evaluate whether the speed fluctuations were being caused by the controller. For this test, the turbine pressure was manually dialed up until the shaft speed was measured to be 35,000 RPM. This procedure appeared to work well during the test; however, post test review of the data showed 30 to 40 speed drop outs of up to 4,000 RPM. This data showed that the speed variations were due to torque fluctuations and not an artifact of the controller. We decided that future tests would be run with the speed controller on.

Test P209609A.500. Test 9A produced 1,030 seconds total rotational time and 867 seconds at 35,000 RPM. This was a normal test with shutdown due to propellant depletion. One procedural change was implemented that involved lifting the shaft slightly higher than normal prior to applying the radial load. The radial load was then applied and speed was increased to 15,000 RPM. The axial load was then reduced from approximately 900 lb to 750 lbs. This axial load reduction shifts the shaft down by about 11 mils. We thought that this motion could help center the rollers which might be on the lower inner race guide flange after lifting the outer rig in the squirl cage. The effectiveness of this procedure was not clear. The run was smooth compared to earlier runs; however, some speed spikes on the order of 1,000 RPM were noted.

Test P209610A.500. This test was very similar to Test 09A described above. 935 seconds of total test time and 789 seconds of time at speed were obtained. The axial shift procedure described in the Test 09A paragraph was used again. This time the initial shaft position was slightly higher than it was in Test 09A. The axial shift imposed at 15,000 RMP was 25 mils. Once again, the effect of the shaft shift was not conclusive. The run progressed very smoothly with no speed excursions observed until about 800 seconds. At 800 seconds, speed and axial position excursions began. The excursions seemed to grow in amplitude reaching a peek of about 2,500 RPM at 950 seconds. At that point, the test terminated normally due to propellant depletion. The rig was borescoped after this test. The borescope inspection showed some shiny particles on various areas of the bearings. We believe these particles were generated by gauling of the anti-rotation tangs.

Test P2096011.500. Test 011 achieved 1,001 seconds total rotational time and 888 seconds time at 35,000 RPMs. This was a very clean test. Speed control was rock solid at high speed. Turbine inlet pressure was seen to increase at about 700 seconds. This increase occurred slowly over a period of about 100 seconds. This increase indicates a rise in rig torque. This did not appear to be related to the high frequency torque excursions seen in other tests. The test terminated normally due to propellant depletion. One procedural change was input for this test. The radial load applied prior to rotation was increase from 25% to 50% of the 1,100 lbs total load. The objective of this change was to ensure that the bearing was engaged radially prior to rotation. Breakaway turbine pressure was higher than normal for this test. The higher radial load may be responsible for the increased breakaway torque.

Test P2096012.500. No rotational time was accumulated on the rig during this test. Pretest a bias was noted on P201 the rig top cavity pressure. The procedure of test 011 was used for this test. Fifty percent of the radial load was applied prior to opening the turbine pressure. On the first attempt to rotate we got a redline cut on P201. This was diagnosed as being related to the pretest bias on the sensor. The rig was recycled for a second attempt. On the second attempt, turbine pressure was increased to the normal start-up valve but no rotation was noted by the speed sensor or thermocouples. The full radial load was applied and turbine pressure was further increased. No rotation was noted even though the turbine pressure was increased to 500 psi. The test terminated due to a second cut on P201 high. The high breakaway torque may have been related to the higher radial load being applied prior to rotation.

Test P2096013.500. Test 13 was conducted after Test 12 failed to break away. The rig was borescoped after Test 12 and appeared to have no anomalies. We believe that the procedure of applying a larger percentage of the radial load prior to rotation caused increased breakaway torque. For this test the radial load applied prior to rotation was reduced to approximately 220 lbs. Breakaway was slightly slower than nominal, but not out of family. The procedure of shifting the shaft during the run was omitted on this test. Axial load was raised to approximately 700 lbs and held for the duration of the test. The test produced 801 seconds total test time and 691 seconds at 35,000 RPM.

Test P2096014.500. Test 14 produced 1,103 seconds total test time and 1,026 seconds at 35,000 RPMs. This test had an anomaly on start-up. Only one strain gauge, SN3, was working for this test. The single working strain gauge showed that the shaft did not shift to the normal pretest position when the shaft delta pressure was increased to a nominal valve of 185 psi. It appeared that the outer bearing ring was hanging in the deadband preventing free axial travel. A decision was made to proceed with the test attempt and the turbine inlet valve was opened to 10%. No rotation was noted initially, however, while reviewing the data the shaft broke away with the turbine inlet valve still at 10%. The test then proceeded as normal. On shut down, the strain gauge response was normal indicating that the roller bearing was no longer hanging up. Some speed fluctuations were noted during the test. No action was taken during the test to try and moderate the speed fluctuations.

Test P2096015.500. This test produced 1,160 seconds total test time and 1,061 seconds at 35,00 RPMs. SN3 was the only functional strain gauge during this test. The test start was normal. The test ended due to propellant depletion. During the test, speed fluctuations were slightly worse than average. One anomaly occurred during the shut down procedure. The thrust piston pressure was relieved while we still had approximately 220 lbs radial load on the roller bearing. The strain gauges never showed the bearing fully unloading. The axial movement coupled with the radial load probably caused the roller bearing to hang up in the squirl cage.

Test P2096016.500. Test 016 accrued 1,328 seconds of total run time and 1,238 seconds at speed. Prior to this test, work was performed on the stand to restore malfunctioning strain gauges and verify the function of the radial load piston. Strain gauges SN2 and SN3 both functioned for this test. The radial load piston function was verified visually prior to the test. Additionally, the roller bearing outer race appeared to be free after apparently hanging up on shut down of the previous run. Speed fluctuations were noted during the 15,000 RPM portion of the test. Operation at 35,000 RPM appeared smoother than normal with one major exception. At approximately 250 seconds into the test, the speed suddenly dropped out to approximately 20,000 RPMs and then recovered overshooting to approximately 37,000 RPMs before resuming a steady 35,000 RPM. The rig continued to operate nominally for the remainder of the test. This was the longest test of the series.

Test P2096017.500. Test 017 was unsuccessful due to high breakaway torque and severe torque fluctuations once rotation started. Normal start-up procedures failed to produce breakaway on the first attempt. A decision was made to reduce the radial load in an attempt to induce breakaway. The radial load was reduced from

250 lbs to approximately 50 lbs, but the rotor did not breakaway. Turbine inlet pressure was increased to 100 psi, still the rotor did not breakaway. The test rig remained in this condition for approximately 20 seconds while discussions about alternatives were occurring. During the discussion, the rotor became free and accelerated to approximately 31,000 RPMs. The speed was then dialed back to 15,000 RPMs. Several severe speed drop outs occurred at this speed. An attempt was made to ramp the speed up, however, severe speed drop outs continued to occur and the test was manually terminated. The reason for the anomaly was not apparent at the time.

Build 5 Test Series Highlights. Five rotational tests were accomplished during February 1999. Total test time accrued was 4,392 seconds and time at 35K RPM was 4,016 seconds. Total cumulative test times for Build 5 at this point were 11,089 seconds rotational time and 8,330 seconds at 35K RPM. These summaries do not include any time for Test P2096017.500, which did not obtain steady state. This testing generated results similar to previous testing of this ball roller bearing build configuration. The rig operated nominally for the majority of the time; however, the rig experienced occasional severe speed fluctuations accompanied by axial vibrations. The source of these speed dropouts was not fully understood. The low axial stiffness of the rig was suspected of contributing to the problem. Test P2026017.500 had excessive breakaway torque and speed fluctuations. Testing was stopped after this run for a mid-term inspection. The initial look at the bearing hardware after disassembling the rig showed no significant anomalies.

6.13 Mid-term Inspection Results

A decision was made after test P2026107.500 to perform the mid-term inspection. Normally, two or three more tests would have been run prior to the mid-term inspection. The anomalies experienced in test 17 prompted the slightly early mid-term inspection. Mr. Chip Moore, MSFC, performed a detailed metric inspection of the ball and roller bearings. Visually, all of the hardware looked normal. The roller bearings did have some burnishing on the roller ends, however, the burnishing was very light. The end burnishing was heavier on the roller end that corresponded to the down direction on the stand. This was expected because this is the side that corresponds to reacting the axial load if the outer race hangs in the deadband. In general, the ball bearing cage pocket wear was slightly heavier than would have been expected for the amount of operation. Heavier pocket wear was expected due to the higher radial load. In summary, all of the bearing hardware appeared to be in excellent shape.

This tester build was the last conducted during the period of this contract. As of the date of this report, a Build 5A is anticipated. Build 5A will enable the goal of demonstrating 8 hour life from severely river marked roller bearings to be achieved. This data will greatly increase the confidence level associated with using the silicon nitride rollers in the ATD high pressure fuel turbopumps.

Reference

1. San Andres, L., "Thermohydrodynamic Analysis of Cryogenic Liquid, Turbulent Flow Fluid Film Bearings," Hydroseal Manual, NASA Grant NAG3-1434.

2. Cody, J.C., Marty, D.E., and Moore, J.D., "Evolution and use of Combined Mechanical and Thermal Codes for Cryogenic Turbopump Bearings", NASA Conference Publication 3012, VOL 1, 1988.

3. Marty, D.E., Moore, J.D., and Cody, J.C., "Development of Transient Thermo/Mechanical Bearing Analysis Methodology and Subsequent Software Implementation on a Personal Computer," NASA Conference Publication 3174, Vol. II, 1992.

4. Crecelius, W.J., and Pirvics, J., "Computer Program Operation Manual on 'SHABERTH' A Computer Program for the Analysis of Steady State and Transient Thermal Performance of Shaft-Bearing Systems", Technical Report AFAPL-TP-79-90, 1776.

5. San Andres, L., 1993, "An Introduction to the Analysis of Barotropic Fluid, Turbulent Flow, Fluid Film Bearings," Research Progress Report to NASA Lewis Research Center, Grant NAG3-1434, Texas A&M University, Mechanical Engineering Department, July 1993.

ATTACHMENT A

INPUT AND OUTPUT FILES USED FOR SHABERTH/HYDROSEAL ANALYSIS OF THE EH-14 FLUID FILM BEARING TESTER AS MODIFIED FOR ROLLING ELEMENT BEARING TESTER

```
P&W FLUID FILM BEARING / ROLLING ELEMENT TESTER (WITH 2 PEBBS & 1 FLUID BRG)
    37000.    3    0    5  -20     .001                                        11
B1        9310              AMS 5618           3.        3.        0.
     95.000        11     .0635    18.61                  0
   20.6375
       .52        .55
       .014       .014       .014        2.        2.        2.
          1    94.176     3.556     0.241     0.610      .230        3
   .045720   -.15240     70.18     19.80     30.54     30.54
     00.00     60.00     79.22    109.00    139.55    222.7
   2.07015   2.1345    3.1025    2.0895    2.0695
      .270      .270      .260      .270      .270
     8.218     7.831     3.200     7.665     8.218
  11.05E-6  9.973E-6  0.810E-6  9.761E-6  10.89E-6
                                  0.100     0.200
B2        9310              AMS 5618           3.        3.        0.
     95.200        11     .0635   -18.61                  0
   20.6375
       .52        .58
       .014       .014       .014        2.        2.        2.
          1    94.176     3.556     0.241     0.610      .230        3
   .045720   -.15240     70.18     19.80     30.54     30.54
     00.00     60.00     79.22    109.00    139.55    222.7
   2.0705    2.1345    3.1025    2.0895    2.0695
      .270      .270      .260      .270      .270
     8.218     7.831     3.200     7.665     8.218
  11.05E-6  9.973E-6  0.810E-6  9.761E-6  10.89E-6
                                  0.100     0.200
F3       AMS 5619           AMS 6265
             1          8          5          3          3          3
             0          1          2          1          0
             8
   0.1371600000000000-003   0.1371600000000000-003   0.7633716000000000-001
   0.3810000000000000-001   0.1270000000000000-001   0.5080000000000000-003
   0.0000000000000000       0.1905000000000000-001
   0.0000000000000000        360.000000000000
   0.0000000000000000
    5.000000000000000        50.00000000000000        95.00000000000000
   140.0000000000000         185.0000000000000        230.0000000000000
    275.0000000000000        320.0000000000000        19.00000000000000
    19.00000000000000        19.00000000000000        19.00000000000000
    19.00000000000000        19.00000000000000        19.00000000000000
    19.00000000000000       0.1320800000000000-002   0.1320800000000000-002
   0.1320800000000000-002   0.1320800000000000-002   0.1320800000000000-002
   0.1320800000000000-002   0.1320800000000000-002   0.1320800000000000-002
   0.1905000000000000-001
   0.1371600000000000-003
   0.0000000000000000       0.0000000000000000       0.0000000000000000
   0.0000000000000000       0.1905000000000000-001   0.0000000000000000
   0.0000000000000000
   0.2820139000000000-004    77.2526000000000        0.1014952000000000-004
    66.6754700000000        0.1790000000000000-003
    37000.0000000000         13739520.0000000         3447380.00000000
    517125.000000000
    3447380.00000000         66.6754700000000        0.1014952000000000-004
   0.0000000000000000
    3447380.00000000         66.6754700000000        0.1014952000000000-004
   0.0000000000000000
    13769520.0000000         3447380.00000000        0.2820139000000000-004
   0.1014952000000000-004    77.2526000000000         66.6754700000000
   3.360000000000000        0.1320800000000000-002   0.2500000000000000
   0.5000000000000000       0.1088664850000000
```

```
  0.250000000000000         0.640000000000000
   27.0000000000000          9.07475378149485        0.5000000000000000-001
  0.4400000000000000-001    0.1375000000000000-002    500000.000000000
  0.377360000000000
            1           1         199          10          12           1
            0           0           1
  0.700000000000000         0.600000000000000        0.9999999776482580-002
  0.1000000000000000-002    0.6000000000000000-002
  0.000000000000000         0.000000000000000
            1           1           0           0
                                    1
-133.-120.-138.-133.-133.-120.-120.-138.-137.-120. -64.-133.-138.-145.
-133.-122.-137.-133.-133.-122.-122.-137.-138.-122. -95.-133.-138.-145.
    1             0         0.        0.        0.     60.00   2.31BE5
    1         130.90        0.        0.     60.00     76.20   2.31BE5
    1         308.20        0.     50.50     76.20     76.20   2.31BE5
    1         351.80     50.50        0.     76.20        0.   2.31BE5
    2          40.90        0.                  0.
    2         114.54     .0000               .00000
    2         248.18     .0000               .00000
    3          57.32        0.        0.
    3         114.54    1800.0         0         0         0         0.
    3         338.18       3.0         0         0         0         0.

    2    1                 0.                  0.
    2    2                .0000               .00000
    2    3                .0000               .00000
    3         114.54        0.        0.
    3

 &GRGNUM
  METRAN='NO '
 &END
 &CONDAT
  IDENT='SAT45',FILM=.TRUE.,XPCT=1.0,PRESSR=2000.,TFZ=100.,IFLUID=1
 &END
 &VISCO
  BALLN=11., RIRC=.1218, RORC=.18989, RIRUS=.13808,RORLS=.1750,
  WIRS=.1155, WORS=.1004, COR=.1733,CIR=.1385, CPW=.0697,
  CW=.0958, CDCNF=1.2, CDCP=0.6, CAGEFF=.100, VFRU=0.10,
  VFRD=0.10,DELP1=-10.,DELP2=-10.,
 &END
 &OUTER
  HCODEO=1,
  VARO1= 1.,
  VARO2= 1.
 &END
 &INNER
  HCODEI=1,
  VARI1= 1.,
  VARI2= 1.
 &END
 &BALL
  HCODEB=3,
  VARB1= 1.,
  VARB2= 1.
 &END
 &JSPRG
  PREDEF=0.0137853 ,KSPRNG=82000., PLOAD=478.60, DELMX=15.5E-3,
  INTCL=.0063, TORUV=.06125
 &END
 &FLGS
  FLAG='NOSPRG', SFLAG='S+S', AXLOAD= .TRUE.,.TRUE.,.TRUE.,.TRUE.
 &END
```

*** S H A B E R T H / B R L ** TECHNOLOGY DIVISION S K F INDUSTRIES INC. ** S H A B E R T H / B R L ***

P&W FLUID FILM BEARING / ROLLING ELEMENT TESTER (WITH 2 PEBBS & 1 FLUID BRG)

THIS DATA SET CONTAINS 3 BEARINGS

BEARING NO. (1) - BALL BEARING

BEARING NO. (2) - BALL BEARING

BEARING NO. (3) - FLUID FILM BEARING

SOLUTION LEVEL = 1

THE MAXIMUM NUMBER OF MAIN LOOP ITERATIONS ALLOWED IS 20 AND THE RELATIVE ACCURACY REQUIRED IS 0.00010

*** S H A B E R T H / B R L ** TECHNOLOGY DIVISION S K F INDUSTRIES INC. ** S H A B E R T H / B R L ***

P&W FLUID FILM BEARING / ROLLING ELEMENT TESTER (WITH 2 PEBBS & 1 FLUID BRG)

UNLESS OTHERWISE STATED, LINEAR DIMENSIONS ARE SPECIFIED IN MILLIMETERS, TEMPERATURES IN DEGREES CENTIGRADE, FORCES IN NEWTONS, WEIGHTS IN KILOGRAMS, PRESSURES AND ELASTIC MODULI IN NEWTONS PER SQUARE MILLIMETER, ANGLES AND SLOPES IN DEGREES, SURFACE ROUGHNESS IN MICRONS, SPEEDS IN REVOLUTIONS PER MINUTE, DENSITY IN GRAMS PER CUBIC CENTIMETER, KINEMATIC VISCOSITY IN CENTISTOKES AND THERMAL CONDUCTIVITY IN WATTS PER METER-DEGREE CENTIGRADE.

B E A R I N G D A T A

BEARING NUMBER	NUMBER OF ROLLING ELEMENTS	AZIMUTH ANGLE ORIENTATION	PITCH DIAMETER	DIAMETRAL CLEARANCE	CONTACT ANGLE	INNER RING SPEED	OUTER RING SPEED
1	11	0.000	95.000	0.064	18.610	37000.	0.
2	11	0.000	95.000	0.064	-18.610	37000.	0.

C A G E D A T A

BEARING NUMBER	CAGE TYPE	CAGE POCKET CLEARANCE	RAIL-LAND WIDTH	RAIL-LAND DIAMETER	RAIL-LAND CLEARANCE	WEIGHT
1	INNER RING LAND RIDING	0.610000	3.5560	84.1760	0.241	0.230000
2	INNER RING LAND RIDING	0.610000	3.5560	84.1760	0.241	0.230000

S T E E L D A T A

BRG.NO.	INNER RING TYPE	LIFE FACTOR	OUTER RING TYPE	LIFE FACTOR
1	9310	3.000	AMS 5618	3.000
2	9310	3.000	AMS 5618	3.000
3	AMS 5618	3.000	AMS 6265	3.000

*** S H A B E R T H / B R L ** TECHNOLOGY DIVISION S K F INDUSTRIES INC. ** S H A B E R T H / B R L ***

P&W FLUID FILM BEARING / ROLLING ELEMENT TESTER (WITH 2 PEBBS & 1 FLUID BRG)

R O L L I N G E L E M E N T D A T A

BEARING NUMBER (1) TYPE - BALL BEARING

BALL DIAMETER	OUTER RACEWAY CURVATURE	INNER RACEWAY CURVATURE
20.6375	0.520	0.580

BEARING NUMBER (2) TYPE - BALL BEARING

BALL DIAMETER	OUTER RACEWAY CURVATURE	INNER RACEWAY CURVATURE
20.6375	0.520	0.580

BEARING NUMBER (3) TYPE - FLUID FILM

*** S H A B E R T H / B R L ** TECHNOLOGY DIVISION S K F INDUSTRIES INC. ** S H A B E R T H / B R L ***

P&W FLUID FILM BEARING / ROLLING ELEMENT TESTER (WITH 2 PEBBS & 1 FLUID BRG)

S U R F A C E D A T A

BEARING NUMBER	CLA ROUGHNESS OUTER	INNER	ROLL. ELM.	RMS ASPERITY SLOPE OUTER	INNER	ROLL. ELM.
1	0.01	0.01	0.01	2.000	2.000	2.000
2	0.01	0.01	0.01	2.000	2.000	2.000

L U B R I C A T I O N A N D F R I C T I O N D A T A

BEARING 1 IS OPERATING DRY WITH FRICTION COEFFICIENTS OF, RACE/R.E. 0.100 CAGE/R.E. AND CAGE/RING 0.200

BEARING 2 IS OPERATING DRY WITH FRICTION COEFFICIENTS OF, RACE/R.E. 0.100 CAGE/R.E. AND CAGE/RING 0.200

*** S H A B E R T H / B R L ** TECHNOLOGY DIVISION S K F INDUSTRIES INC. ** S H A B E R T H / B R L ***

P&W FLUID FILM BEARING / ROLLING ELEMENT TESTER (WITH 2 PEBBS & 1 FLUID BRG)

F I T D A T A A N D M A T E R I A L P R O P E R T I E S

BEARING NUMBER	COLD FITS (MM TIGHT) SHAFT	HOUSING	EFFECTIVE WIDTHS SHAFT	INNER RING	OUTER RING	HOUSING
1	0.0457	-0.1524	70.1800	19.8000	30.5400	30.5400
2	0.0457	-0.1524	70.1800	19.8000	30.5400	30.5400

BEARING NUMBER	SHAFT I.D.	BEARING BORE	EFFECTIVE DIAMETERS INNER RING AVE. O.D.	OUTER RING AVE. I.D.	BEARING O.D.	HOUSING O.D.
1	0.000	60.000	79.220	109.000	139.550	222.700
2	0.000	60.000	79.220	109.000	139.550	222.700

BEARING NUMBER (1)	SHAFT	INNER RING	ROLL. ELEM.	OUTER RING	HOUSING
MODULUS OF ELASTICITY	207000.0	213400.0	310200.0	208900.0	206900.0
POISSONS RATIO	0.2700	0.2700	0.2600	0.2700	0.2700
WEIGHT DENSITY	8.218	7.831	3.200	7.665	8.218
COEFF. OF THERMAL EXP.	0.00001105	0.00000997	0.00000081	0.00000976	0.00001089

BEARING NUMBER (2)	SHAFT	INNER RING	ROLL. ELEM.	OUTER RING	HOUSING
MODULUS OF ELASTICITY	207000.0	213400.0	310200.0	208900.0	206900.0
POISSONS RATIO	0.2700	0.2700	0.2600	0.2700	0.2700
WEIGHT DENSITY	8.218	7.831	3.200	7.665	8.218
COEFF. OF THERMAL EXP.	0.00001105	0.00000997	0.00000081	0.00000976	0.00001089

UNLESS OTHERWISE STATED, INTERNATIONAL UNITS ARE USED

GIVEN TEMPERATURES

BRG	O.RACE	I.RACE	BULK OIL	FLNG.1	FLNG.2	FLNG.3	FLNG.4	CAGE	SHAFT	I.RING	ROLL.EL.	O.RING	HSG.
1	-133.00	-120.00	-138.00	-133.00	-133.00	-120.00	-120.00	-138.00	-137.00	-120.00	-64.00	-133.00	-138.00
2	-133.00	-122.00	-137.00	-133.00	-133.00	-122.00	-122.00	-137.00	-138.00	-122.00	-95.00	-133.00	-138.00

*** S H A B E R T H / B R L ** TECHNOLOGY DIVISION S K F INDUSTRIES INC. ** S H A B E R T H / B R L ***

P&W FLUID FILM BEARING / ROLLING ELEMENT TESTER (WITH 2 PEBBC & 1 FLUID BRG)

SHAFT GEOMETRY, BEARING LOCATIONS AND SHAFT LOAD, PLANE X - Y.

4 GEOMETRIC SECTIONS 3 LOAD SECTION(S), 3 BEARINGS. MODULUS OF ELASTICITY = 2.318E+05

	POSI-TION	INNER DIAM. LEFT	INNER DIAM. RIGHT	OUTER DIAM. LEFT	OUTER DIAM. RIGHT	POINT FORCE	POINT MOMENT	LOAD INTENSITY LEFT	LOAD INTENSITY RIGHT		BEARING SEAT POS.ERR	BEARING SEAT DEFL/FOR	BEARING SEAT ANG.ERR	BEARING SEAT DEFL/MOM
1	0.0	0.0	0.0	0.0	60.0					1				
2	40.9	0.0	0.0	60.0	60.0					2	0.000	0.00E+00	0.0000	0.00E+00
3	57.3	0.0	0.0	60.0	60.0					3				
4	114.5	0.0	0.0	60.0	60.0	1800.0				4	0.000	0.00E+00	0.0000	0.00E+00
5	130.9	0.0	0.0	60.0	76.2					5				
6	248.2	0.0	0.0	76.2	76.2					6	0.000	0.00E+00	0.0000	0.00E+00
7	308.2	0.0	50.5	76.2	76.2					7				
8	338.2	50.5	50.5	76.2	76.2					8				
9	351.8	50.5	0.0	76.2	0.0					9				

*** S H A B E R T H / B R L ** TECHNOLOGY DIVISION S K F INDUSTRIES INC. ** S H A B E R T H / B R L ***

P&W FLUID FILM BEARING / ROLLING ELEMENT TESTER (WITH 2 PEBBS & 1 FLUID BRG)

SHAFT GEOMETRY, BEARING LOCATIONS AND SHAFT LOAD, PLANE X - Z.

4 GEOMETRIC SECTIONS 2 LOAD SECTION(S), 3 BEARINGS. MODULUS OF ELASTICITY = 2.318E+05

THRUST LOAD = 0.000E+00

POSI-TION	INNER DIAM. LEFT	INNER DIAM. RIGHT	OUTER DIAM. LEFT	OUTER DIAM. RIGHT	POINT FORCE	POINT MOMENT	LOAD INTENSITY LEFT	LOAD INTENSITY RIGHT	BEARING SEAT POS.ERR	BEARING SEAT DEFL/FOR	BEARING SEAT ANG.ERR	BEARING SEAT DEFL/MOM
1 0.0	0.0	0.0	0.0	60.0				1				
2 40.9	0.0	0.0	60.0	60.0				2	0.000	0.00E+00	0.0000	0.00E+00
3 114.5	0.0	0.0	60.0	60.0				3	0.000	0.00E+00	0.0000	0.00E+00
4 130.9	0.0	0.0	60.0	76.2				4				
5 248.2	0.0	0.0	76.2	76.2				5	0.000	0.00E+00	0.0000	0.00E+00
6 308.2	0.0	50.5	76.2	76.2				6				
7 351.8	50.5	0.0	76.2	0.0				7				

############ BRG NO. 1 ##############

(O.R./HOUSING CLEARANCE REMAINING) MILS DF34+FTH34 = 0.237591E-02

############ BRG NO. 2 ##############

(O.R./HOUSING CLEARANCE REMAINING) MILS DF34+FTH34 = 0.237591E-02

############ BRG NO. 3 ##############

(O.R./HOUSING CLEARANCE REMAINING) MILS DF34+FTH34 = 0.270079E-02

RESULTS FOR BEARING PAD # 1

ZEROTHth 0 SOLN CONVERGENCE: 1its on REC press, & 50TOTAL its on lands

SOLN FOUND IN Iter= 50, Iterp=10 ISYM= 0
Ex=-.009,Ey=0.004; Ec=0.010; Ax=-0.2681E-05,Ay=-0.2817E-04 Z0= 0.1120E-01
rpm= 0.37000E+05 Ps= 0.13790E+08 PL= 0.34474E+07 PR= 0.34474E+07 N/m2
Dorif= 0.13208E-02 m, Cd= 0.8600; Seals (L)= 0.00000E+00,(R)= 0.00000E+00

Rec: 1 -> Prec: (0.80087E-01) 0.42757E+07 N/m2 Flow: 0.42156E-01 Kg/s
Rec: 2 -> Prec: (0.11244E+00) 0.46102E+07 N/m2 Flow: 0.41491E-01 Kg/s
Rec: 3 -> Prec: (0.11713E+00) 0.46587E+07 N/m2 Flow: 0.41571E-01 Kg/s
Rec: 4 -> Prec: (0.11818E+00) 0.46696E+07 N/m2 Flow: 0.41671E-01 Kg/s
Rec: 5 -> Prec: (0.11888E+00) 0.46769E+07 N/m2 Flow: 0.41660E-01 Kg/s
Rec: 6 -> Prec: (0.11915E+00) 0.46797E+07 N/m2 Flow: 0.41536E-01 Kg/s
Rec: 7 -> Prec: (0.11706E+00) 0.46580E+07 N/m2 Flow: 0.41421E-01 Kg/s
Rec: 8 -> Prec: (0.10210E+00) 0.45033E+07 N/m2 Flow: 0.41633E-01 Kg/s

```
|   (Left Flow)= 0.16669E+00 Kg/s  (Right Flow)= 0.16675E+00 Kg/s
+-------------------------------------------------------------------------------+
|   FX=-0.47426E+03 N     FY= 0.13122E-01 N
|   MX= 0.12748E-01 Nm    MY= 0.53492E+01 Nm
+-------------------------------------------------------------------------------+
|   Pressure at film lands, MAX 0.46797E+01 MPa  MIN= 0.33851E+01 MPa
|   Torque on Film Lands= 0.12646E+01 N-m
+-------------------------------------------------------------------------------+
 For Pad# 1 WRITE DATA TO TEMP File:TEMPPAD1.

  ############  BRG NO.          1  ###############
 ------------------------------------
 (O.R./HOUSING CLEARANCE REMAINING) MILS DF34+FTH34 =   0.226703E-02
 ------------------------------------


  ############  BRG NO.          2  ###############
 ------------------------------------
 (O.R./HOUSING CLEARANCE REMAINING) MILS DF34+FTH34 =   0.226859E-02
 ------------------------------------


  ############  BRG NO.          3  ###############
 ------------------------------------
 (O.R./HOUSING CLEARANCE REMAINING) MILS DF34+FTH34 =   0.150704E-02
 ------------------------------------


+-------------@-----------------------------------------------------------------+
|  RESULTS FOR BEARING PAD # 1
|.....
-------------------------------------------------------------------------------
ZEROTHth O SOLN CONVERGENCE:  1its on REC press, &  50TOTAL its on lands
+-------------------------------------------------------------------------------+
|   SOLN FOUND IN Iter=  50, Iterp=10 ISYM= 0
|   Ex=-.008,Ey=0.004; Ec=0.009; Ax=-0.2731E-05,Ay=-0.2877E-04 ZO= 0.1120E-01
|   rpm= 0.37000E+05  Ps= 0.13790E+08  PL= 0.34474E+07 PR= 0.34474E+07 N/m2
|   Dorif= 0.13208E-02 m, Cd= 0.8600; Seals (L)= 0.00000E+00,(R)= 0.00000E+00
|
|   Rec: 1  -> Prec: ( 0.80001E-01) 0.42748E+07 N/m2  Flow: 0.42158E-01 Kg/s
|   Rec: 2  -> Prec: ( 0.11239E+00) 0.46097E+07 N/m2  Flow: 0.41494E-01 Kg/s
|   Rec: 3  -> Prec: ( 0.11719E+00) 0.46593E+07 N/m2  Flow: 0.41572E-01 Kg/s
|   Rec: 4  -> Prec: ( 0.11831E+00) 0.46709E+07 N/m2  Flow: 0.41670E-01 Kg/s
|   Rec: 5  -> Prec: ( 0.11901E+00) 0.46782E+07 N/m2  Flow: 0.41656E-01 Kg/s
|   Rec: 6  -> Prec: ( 0.11921E+00) 0.46802E+07 N/m2  Flow: 0.41533E-01 Kg/s
|   Rec: 7  -> Prec: ( 0.11700E+00) 0.46574E+07 N/m2  Flow: 0.41419E-01 Kg/s
|   Rec: 8  -> Prec: ( 0.10198E+00) 0.45021E+07 N/m2  Flow: 0.41635E-01 Kg/s
+-------------------------------------------------------------------------------+
|   Mass  Flow= 0.33344E+00 Kg/s =  0.20007E+02 Kg/min
|   (Left Flow)= 0.16669E+00 Kg/s  (Right Flow)= 0.16675E+00 Kg/s
+-------------------------------------------------------------------------------+
|   FX=-0.47702E+03 N     FY= 0.10119E+01 N
|   MX= 0.24189E-01 Nm    MY= 0.53809E+01 Nm
+-------------------------------------------------------------------------------+
|   Pressure at film lands, MAX 0.46802E+01 MPa  MIN= 0.33848E+01 MPa
|   Torque on Film Lands= 0.12646E+01 N-m
+-------------------------------------------------------------------------------+
 For Pad# 1 WRITE DATA TO TEMP File:TEMPPAD1.

  ############  BRG NO.          1  ###############
 ------------------------------------
 (O.R./HOUSING CLEARANCE REMAINING) MILS DF34+FTH34 =   0.226941E-02
 ------------------------------------


  ############  BRG NO.          2  ###############
```

```
(O.R./HOUSING CLEARANCE REMAINING) MILS DF34+FTH34 =   0.226995E-02
-------------------------------------


 ############  BRG NO.          3  ###############
-------------------------------------
(O.R./HOUSING CLEARANCE REMAINING) MILS DF34+FTH34 =   0.193127E-02
-------------------------------------


+---------------- ----------------------------------------------------------------+
|  RESULTS FOR BEARING PAD # 1                                                     |
|..................................................................................|
--------------------------------------------------------------------------------
ZEROTHth O SOLN CONVERGENCE:  1its on REC press, &  50TOTAL its on lands
+--------------------------------------------------------------------------------+
|   SOLN FOUND IN Iter=  50, Iterp=10 ISYM= 0                                    |
|   Ex=-.008,Ey=0.004; Ec=0.009; Ax=-0.2840E-05,Ay=-0.2914E-04 Z0= 0.1120E-01    |
|   rpm= 0.37000E+05  Ps= 0.13790E+08  PL= 0.34474E+07 PR= 0.34474E+07 N/m2      |
|   Dorif= 0.13208E-02 m, Cd= 0.3600; Seals (L)= 0.00000E+00,(R)= 0.00000E+00    |
|                                                                                |
|   Rec: 1  -> Prec: ( 0.79965E-01) 0.42744E+07 N/m2  Flow: 0.42159E-01 Kg/s     |
|   Rec: 2  -> Prec: ( 0.11234E+00) 0.46092E+07 N/m2  Flow: 0.41495E-01 Kg/s     |
|   Rec: 3  -> Prec: ( 0.11717E+00) 0.46592E+07 N/m2  Flow: 0.41573E-01 Kg/s     |
|   Rec: 4  -> Prec: ( 0.11834E+00) 0.46713E+07 N/m2  Flow: 0.41671E-01 Kg/s     |
|   Rec: 5  -> Prec: ( 0.11907E+00) 0.46788E+07 N/m2  Flow: 0.41656E-01 Kg/s     |
|   Rec: 6  -> Prec: ( 0.11926E+00) 0.46808E+07 N/m2  Flow: 0.41532E-01 Kg/s     |
|   Rec: 7  -> Prec: ( 0.11702E+00) 0.46576E+07 N/m2  Flow: 0.41418E-01 Kg/s     |
|   Rec: 8  -> Prec: ( 0.10196E+00) 0.45019E+07 N/m2  Flow: 0.41634E-01 Kg/s     |
+--------------------------------------------------------------------------------+
|   Mass  Flow= 0.33344E+00 Kg/s =  0.20007E+02 Kg/min                           |
|   (Left Flow)= 0.16669E+00 Kg/s  (Right Flow)= 0.16675E+00 Kg/s                |
+--------------------------------------------------------------------------------+
|   FX=-0.47814E+03 N      FY= 0.47011E+00 N                                     |
|   MX= 0.18402E-01 Nm     MY= 0.53940E+01 Nm                                    |
+--------------------------------------------------------------------------------+
|   Pressure at film lands, MAX 0.46808E+01 MPa  MIN= 0.33847E+01 MPa            |
|   Torque on Film Lands= 0.12646E+01 N-m                                        |
+--------------------------------------------------------------------------------+
 For Pad# 1 WRITE DATA TO TEMP File:TEMPPAD1.
ENTER=   -1.00000
```

FRICTIONAL HEAT GENERATION FOR EACH ROLLING ELEMENT

BEARING NO. 1

BALL NO.	OUTER RACE	INNER RACE	FLUID DRAG	CAGE/RE
1	88.489	119.00	0.00000	0.88470E-01
2	86.853	115.68	0.00000	681.36
3	83.179	108.16	0.00000	1144.4
4	78.905	99.132	0.00000	1246.5
5	75.421	91.521	0.00000	951.57
6	73.584	87.474	0.00000	354.18
7	73.584	89.208	0.00000	354.16
8	75.421	96.286	0.00000	951.56
9	78.905	105.59	0.00000	1246.5
10	83.179	114.26	0.00000	1144.3
11	86.853	119.37	0.00000	681.34

ENTER= 1.00000

BEARING NO. 2

BALL NO.	OUTER RACE	INNER RACE	FLUID DRAG	CAGE/RE
1	85.834	114.71	0.00000	0.10113
2	85.067	113.07	0.00000	604.96
3	82.633	107.79	0.00000	1036.6
4	79.480	100.74	0.00000	1150.3
5	76.671	94.273	0.00000	894.90
6	74.985	90.283	0.00000	337.82
7	74.985	88.619	0.00000	337.84
8	76.671	89.764	0.00000	894.92
9	79.480	94.703	0.00000	1150.3
10	82.633	102.10	0.00000	1036.7
11	85.067	109.62	0.00000	604.98

ENTER= 1.00000

*** S H A B E R T H / B R L ** TECHNOLOGY DIVISION S K F INDUSTRIES INC. ** S H A B E R T H / B R L ***

P&W FLUID FILM BEARING / ROLLING ELEMENT TESTER (WITH 2 PEBBS & 1 FLUID BRG)

B E A R I N G S Y S T E M O U T P U T METRIC UNITS

LINEAR (MM) AND ANGULAR (RADIANS) DEFLECTIONS REACTION FORCES (N) AND MOMENTS (MM-N)

BRG.	DX	DY	DZ	GY	GZ	FX	FY	FZ	MY	MZ
1	-1.403E-02	2.805E-03	-1.108E-04	-2.825E-06	4.414E-06	3.866E+03	755.	-5.873E-04	-1.172E-02	-1.343E+04
2	-1.403E-02	2.543E-03	9.749E-05	-2.835E-06	-1.617E-05	-3.867E+03	568.	-5.488E-04	1.069E-02	1.053E+04
3	-1.403E-02	-9.516E-04	4.770E-04	-2.840E-06	-2.914E-05	0.000	478.	-0.470	-18.4	-5.393E+03

	FATIGUE LIFE (HOURS)			H/SIGMA		LUBE-LIFE FACTOR		MATERIAL FACTOR	
BRG.	O. RACE	I. RACE	BEARING	O. RACE	I. RACE	O. RACE	I. RACE	O. RACE	I. RACE
1	830.	330.	250.	0.000	0.000	1.00	1.00	3.00	3.00
2	964.	416.	299.	0.000	0.000	1.00	1.00	3.00	3.00

TEMPERATURES RELEVANT TO BEARING PERFORMANCE (DEGREES CENTIGRADE)

BRG	O.RACE	I.RACE	BULK OIL	FLNG.1	FLNG.2	FLNG.3	FLNG.4	CAGE	SHAFT	I.RING	ROLL.EL.	O.RING	HSG.
1	-133.00	-120.00	-138.00	-133.00	-133.00	-120.00	-120.00	-138.00	-137.00	-120.00	-64.00	-133.00	-138.00
2	-133.00	-122.00	-137.00	-133.00	-133.00	-122.00	-122.00	-137.00	-138.00	-122.00	-95.00	-133.00	-138.00

*** S H A B E R T H / B R L ** TECHNOLOGY DIVISION S K F INDUSTRIES INC. ** S H A B E R T H / B R L ***

P&W FLUID FILM BEARING / ROLLING ELEMENT TESTER (WITH 2 PEBBS & 1 FLUID BRG)

B E A R I N G S Y S T E M O U T P U T METRIC UNITS

FRICTIONAL HEAT GENERATION RATE (WATTS) AND FRICTION TORQUE (N-MM)

BRG.	O. RACE	O. FLNGS.	I. RACE	I. FLNGS.	R.E.DRAG	R.E.-CAGE	CAGE-LAND	TOTAL	TORQUE
1	884.	0.000	1.146E+03	0.000	0.000	8.756E+03	43.8	1.083E+04	2.795E+03
2	884.	0.000	1.106E+03	0.000	0.000	8.049E+03	43.7	1.008E+04	2.602E+03

EHD FILM THICKNESS, FILM REDUCTION FACTORS AND HEAT CONDUCTIVITY DATA FOR THE OUTER AND INNER RACEWAYS RESPECTIVELY

BRG.	FILM (MICRONS)		STARVATION FACTOR		THERMAL FACTOR		MENISCUS DIST. (MM)		CONDUCTIVITY (W/DEG.C)	
1	0.000	0.000	0.000	0.000	0.000	0.000	0.000	0.000	37.4	13.6
2	0.000	0.000	0.000	0.000	0.000	0.000	0.000	0.000	37.1	13.0

	FIT PRESSURES (N/MM2)				BEARING CLEARANCES (MM)			SPEED GIVING ZERO FIT PRESSURE
BRG.	SHAFT-COLD,	OPER.	HSG.-COLD,	OPER.	ORIGINAL	CHANGE	OPERATING	SHAFT-INNER RING (RPM)
1	37.5	0.000	0.000	0.000	6.350E-02	-0.104	-4.096E-02	3.094E+04
2	37.5	22.8	0.000	0.000	6.350E-02	-8.177E-02	-1.827E-02	3.094E+04

C A G E D A T A METRIC UNITS
(CAGE HAS ONE DEGREE OF FREEDOM)

	CAGE RAIL - RING LAND DATA				CAGE SPEED DATA					
BRG.	TORQUE (MM-N)	HEAT RATE (WATTS)	SEP.FORCE (NEWTONS)	ECCENTRICITY RATIO	EPICYCLIC SPEED (RAD/SEC)	(RPM)	CALCULATED SPEED (RAD/SEC)	(RPM)	CALC/EPIC RATIO	CAGE/SHAFT RATIO
1	19.0	43.8	2.30	2.19	1.564E+03	1.494E+04	1.564E+03	1.494E+04	1.00	0.404
2	19.0	43.7	2.30	2.19	1.570E+03	1.499E+04	1.570E+03	1.499E+04	1.00	0.405

*** S H A B E R T H / B R L ** TECHNOLOGY DIVISION S K F INDUSTRIES INC. ** S H A B E R T H / B R L ***

P&W FLUID FILM BEARING / ROLLING ELEMENT TESTER (WITH 2 PE88S & 1 FLUID BRG)

R O L L I N G E L E M E N T O U T P U T FOR BEARING NUMBER 1 METRIC UNITS

AZIMUTH	ANGULAR SPEEDS (RADIANS/SECOND)				SPEED VECTOR ANGLES (DEGREES)		
ANGLE (DEG.)	WX	WY	WZ	TOTAL	ORBITAL	TAN-1(WY/WX)	TAN-1(WZ/WX)
0.00	-8672.893	1030.941	0.000	8733.951	1561.093	173.22	-180.00
32.73	-8678.185	1016.043	0.000	8737.461	1561.650	173.32	-180.00
65.45	-8690.856	980.825	0.000	8746.028	1563.020	173.56	-180.00
98.18	-8707.052	936.014	0.000	8757.219	1564.823	173.86	-180.00
130.91	-8721.621	895.868	0.000	8767.512	1566.494	174.14	-180.00
163.64	-8729.829	873.436	0.000	8773.415	1567.458	174.29	-180.00
196.36	-8729.829	873.436	0.000	8773.415	1567.458	174.29	-180.00
229.09	-8721.621	895.868	0.000	8767.512	1566.494	174.14	-180.00
261.82	-8707.052	936.014	0.000	8757.219	1564.823	173.86	-180.00
294.55	-8690.856	980.825	0.000	8746.028	1563.020	173.56	-180.00
327.27	-8678.185	1016.043	0.000	8737.461	1561.650	173.32	-180.00

*** S H A B E R T H / B R L ** TECHNOLOGY DIVISION S K F INDUSTRIES INC. ** S H A B E R T H / B R L ***

P&W FLUID FILM BEARING / ROLLING ELEMENT TESTER (WITH 2 PEBBS & 1 FLUID BRG)

R O L L I N G E L E M E N T O U T P U T FOR BEARING NUMBER 1 METRIC UNITS

AZIMUTH	NORMAL FORCES (NEWTONS)			HZ STRESS (N/MM**2)		LOAD RATIO QASP/QTOT		CONTACT ANGLES (DEG.)	
ANGLE (DEG.)	CAGE	OUTER	INNER	OUTER	INNER	OUTER	INNER	OUTER	INNER
0.00	-0.005	2806.846	1147.841	1772.472	2132.429	0.0000	0.0000	8.2483	20.5374
32.73	37.814	2778.166	1117.459	1766.414	2113.446	0.0000	0.0000	8.1253	20.5724
65.45	63.449	2713.232	1048.457	1752.543	2069.017	0.0000	0.0000	7.8350	20.6598
98.18	69.022	2636.194	965.945	1735.797	2013.253	0.0000	0.0000	7.4663	20.7727
130.91	52.630	2571.804	896.633	1721.548	1963.897	0.0000	0.0000	7.1367	20.8752
163.64	19.576	2537.751	859.762	1713.916	1936.600	0.0000	0.0000	6.9528	20.9341
196.36	-19.575	2537.751	872.049	1713.916	1945.782	0.0000	0.0000	6.9528	20.9359
229.09	-52.629	2571.804	930.123	1721.548	1988.050	0.0000	0.0000	7.1367	20.8799
261.82	-69.021	2636.194	1010.975	1735.797	2044.062	0.0000	0.0000	7.4663	20.7789
294.55	-63.448	2713.232	1090.870	1752.543	2096.548	0.0000	0.0000	7.8350	20.6655
327.27	-37.813	2778.166	1143.108	1766.414	2129.494	0.0000	0.0000	8.1253	20.5758

*** S H A B E R T H / B R L ** TECHNOLOGY DIVISION S K F INDUSTRIES INC. ** S H A B E R T H / B R L ***

P&W FLUID FILM BEARING / ROLLING ELEMENT TESTER (WITH 2 PEBBS & 1 FLUID BRG)

R O L L I N G E L E M E N T O U T P U T FOR BEARING NUMBER 2 METRIC UNITS

AZIMUTH	ANGULAR SPEEDS (RADIANS/SECOND)				SPEED VECTOR ANGLES (DEGREES)		
ANGLE (DEG.)	WX	WY	WZ	TOTAL	ORBITAL	TAN-1(WY/WX)	TAN-1(WZ/WX)
0.00	-8708.143	-1027.747	0.000	8768.581	1567.249	-173.27	180.00
32.73	-8711.301	-1020.033	0.000	8770.817	1567.613	-173.32	180.00
65.45	-8721.511	-994.226	0.000	8777.997	1568.776	-173.50	180.00
98.18	-8735.622	-958.308	0.000	8788.028	1570.408	-173.74	180.00
130.91	-8749.204	-923.555	0.000	8797.813	1572.007	-173.97	180.00
163.64	-8757.859	-901.201	0.000	8804.104	1573.038	-174.12	180.00
196.36	-8757.859	-901.201	0.000	8804.104	1573.038	-174.12	180.00
229.09	-8749.204	-923.555	0.000	8797.813	1572.007	-173.97	180.00
261.82	-8735.622	-958.308	0.000	8788.028	1570.408	-173.74	180.00
294.55	-8721.511	-994.226	0.000	8777.997	1568.776	-173.50	180.00
327.27	-8711.301	-1020.033	0.000	8770.817	1567.613	-173.32	180.00

*** S H A B E R T H / B R L ** TECHNOLOGY DIVISION S K F INDUSTRIES INC. ** S H A B E R T H / B R L ***

P&W FLUID FILM BEARING / ROLLING ELEMENT TESTER (WITH 2 PEBBS & 1 FLUID BRG)

R O L L I N G E L E M E N T O U T P U T FOR BEARING NUMBER 2 METRIC UNITS

AZIMUTH	NORMAL FORCES (NEWTONS)			HZ STRESS (N/MM**2)		LOAD RATIO QASP/QTOT		CONTACT ANGLES (DEG.)	
ANGLE (DEG.)	CAGE	OUTER	INNER	OUTER	INNER	OUTER	INNER	OUTER	INNER
0.00	-0.006	2726.359	1056.279	1755.472	2074.149	0.0000	0.0000	-8.1900	-21.5780
32.73	-33.447	2713.313	1041.658	1752.561	2064.535	0.0000	0.0000	-8.1262	-21.6045
65.45	-57.266	2670.015	995.044	1743.188	2033.268	0.0000	0.0000	-7.9134	-21.6922
98.18	-63.473	2613.180	933.354	1730.731	1990.349	0.0000	0.0000	-7.6178	-21.7868
130.91	-49.325	2561.628	877.077	1719.274	1949.515	0.0000	0.0000	-7.3325	-21.8852
163.64	-18.607	2530.129	842.535	1712.198	1923.578	0.0000	0.0000	-7.1493	-21.9459
196.36	18.608	2530.129	831.266	1712.198	1914.964	0.0000	0.0000	-7.1493	-21.9442
229.09	49.326	2561.628	846.516	1719.274	1926.603	0.0000	0.0000	-7.3325	-21.8804
261.82	63.474	2613.180	892.574	1730.731	1960.929	0.0000	0.0000	-7.6178	-21.7805
294.55	57.267	2670.015	956.796	1743.188	2006.875	0.0000	0.0000	-7.9134	-21.6764
327.27	33.448	2713.313	1018.532	1752.561	2049.142	0.0000	0.0000	-8.1262	-21.6010

DSW FLUID FILM BEARING / ROLLING ELEMENT TESTER (WITH 2 PEBBS & 1 FLUID BRG)

F R I C T I O N A L H E A T G E N E R A T I O N I N C O N T A C T E L L I P S E

------ BRG NO. 1 ------

I N N E R R A C E

# LAMINA	CONTACT AREA (IN**2)	SEMI-MAJOR AXIS (IN)	SEMI-MINOR AXIS (IN)
20	0.1251E-02	0.4123E-01	0.9652E-02

WIDTH OF LAMINUM (INCHES)	HEAT GEN. PER LAM. (WATTS)
0.0040520010	1.835
0.0040520010	4.755
0.0040520010	6.722
0.0040520010	7.796
0.0040520010	8.051
0.0040520010	7.567
0.0040520010	6.427
0.0040520010	4.703
0.0040520010	2.312
0.0040520010	0.272
0.0041940900	0.314
0.0041940900	2.853
0.0041940900	5.742
0.0041940900	8.089
0.0041940900	9.866
0.0041940900	10.889
0.0041940900	10.941
0.0041940900	9.791
0.0041940900	7.190
0.0041940900	2.880

O U T E R R A C E

# LAMINA	CONTACT AREA (IN**2)	SEMI-MAJOR AXIS (IN)	SEMI-MINOR AXIS (IN)
20	0.3682E-02	0.9214E-01	0.1272E-01

WIDTH OF LAMINUM (INCHES)	HEAT GEN. PER LAM. (WATTS)
0.0092141270	3.417
0.0092141270	7.698
0.0092141270	9.288
0.0092141270	8.935
0.0092141270	7.232
0.0092141270	4.475
0.0092141270	2.064
0.0092141270	0.774
0.0092141270	0.238
0.0092141270	0.081
0.0092141270	0.081
0.0092141270	0.238
0.0092141270	0.777
0.0092141270	2.072
0.0092141270	4.499
0.0092141270	7.250
0.0092141270	8.948
0.0092141270	9.298
0.0092141270	7.704
0.0092141270	3.419

*** S H A B E R T H / B R L ** TECHNOLOGY DIVISION S K F INDUSTRIES INC. ** S H A B E R T H / B R L ***

[illegible] FLUID FILM BEARING / ROLLING ELEMENT TESTER (WITH 2 PEBBS & 1 FLUID BRG)

* * * * * * * * * A V E R A G E N U M B E R S * * * * * * * * * *

F R I C T I O N A L H E A T G E N E R A T I O N I N C O N T A C T E L L I P S E

------ BRG NO. 1 ------

I N N E R R A C E

# LAMINA	CONTACT AREA (IN**2)	SEMI-MAJOR AXIS (IN)	SEMI-MINOR AXIS (IN)
20	0.1146E-02	0.3943E-01	0.9240E-02

WIDTH OF LAMINUM (INCHES)	HEAT GEN. PER LAM. (WATTS)
0.0038773220	1.635
0.0038773220	4.229
0.0038773220	5.967
0.0038773220	6.909
0.0038773220	7.124
0.0038773220	6.684
0.0038773220	5.668
0.0038773220	4.142
0.0038773220	2.035
0.0038773220	0.239
0.0040087390	0.274
0.0040087390	2.485
0.0040087390	5.002
0.0040087390	7.040
0.0040087390	8.577
0.0040087390	9.455
0.0040087390	9.490
0.0040087390	8.483
0.0040087390	6.223
0.0040087390	2.490

*** PRESSURE IS SUPERCRITICAL ***
PRESSURE = 2000.00

O U T E R R A C E

# LAMINA	CONTACT AREA (IN**2)	SEMI-MAJOR AXIS (IN)	SEMI-MINOR AXIS (IN)
20	0.3553E-02	0.9051E-01	0.1249E-01

WIDTH OF LAMINUM (INCHES)	HEAT GEN. PER LAM. (WATTS)
0.0088159000	2.980
0.0088159000	6.762
0.0088159000	8.234
0.0088159000	8.017
0.0088159000	6.605
0.0088159000	4.264
0.0088159000	2.076
0.0088159000	0.838
0.0088159000	0.279
0.0088159000	0.092
0.0088159000	0.065
0.0088159000	0.154
0.0088159000	0.494
0.0088159000	1.356
0.0088159000	3.048
0.0088159000	5.443
0.0088159000	7.337
0.0088159000	8.182
0.0088159000	7.592
0.0088159000	5.005

S R S I T E R A T I O N P R O G R A M O U T P U T

	UPSTREAM BRG	DOWNSTREAM BRG
FLUID DRAG CAGE FORCE (LB/BALL) =>	2.65338	2.65338
P.A. CAGE FORCE (LB/BALL) =>	-4.46247	-4.46247
RESULTANT FORCE ON CAGE(LB/BALL)=>	5.19173	5.19173
CAGE FRICTION HEAT (BTU/HR.BALL)=>	363.803	363.803
FLUID VISCOUS WORK (BTU/HR.BALL)=>	3565.95	3565.95

BRG 1 EXIT FLUID TEMP = 0.000000 DEG R

COOLANT QUALITY DUE TO FLASHING FROM BRG 1= 1.65701

*** S H A B E R T H / B R L ** TECHNOLOGY DIVISION S K F INDUSTRIES INC. ** S H A B E R T H / B R L ***

P&W FLUID FILM BEARING / ROLLING ELEMENT TESTER (WITH 2 PEBBS & 1 FLUID BRG)

F R I C T I O N A L H E A T G E N E R A T I O N I N C O N T A C T E L L I P S E

------ BRG NO. 2 ------

I N N E R R A C E

# LAMINA	CONTACT AREA (IN**2)	SEMI-MAJOR AXIS (IN)	SEMI-MINOR AXIS (IN)
20	0.1184E-02	0.4010E-01	0.9398E-02

WIDTH OF LAMINUM (INCHES)	HEAT GEN. PER LAM. (WATTS)
0.0039308600	1.783
0.0039308600	4.611
0.0039308600	6.506
0.0039308600	7.534
0.0039308600	7.771
0.0039308600	7.297
0.0039308600	6.198
0.0039308600	4.550
0.0039308600	2.300
0.0039308600	0.271
0.0040898660	0.316
0.0040898660	2.828
0.0040898660	5.561
0.0040898660	7.796
0.0040898660	9.484
0.0040898660	10.447
0.0040898660	10.480
0.0040898660	9.364
0.0040898660	6.868
0.0040898660	2.748
0.0000000000	0.000

O U T E R R A C E

# LAMINA	CONTACT AREA (IN**2)	SEMI-MAJOR AXIS (IN)	SEMI-MINOR AXIS (IN)
21	0.3612E-02	0.9126E-01	0.1260E-01

WIDTH OF LAMINUM (INCHES)	HEAT GEN. PER LAM. (WATTS)
0.0086911970	2.996
0.0086911970	6.859
0.0086911970	8.448
0.0086911970	8.361
0.0086911970	7.085
0.0086911970	4.913
0.0086911970	2.527
0.0086911970	1.099
0.0086911970	0.404
0.0086911970	0.143
0.0086911970	0.085
0.0086911970	0.144
0.0086911970	0.405
0.0086911970	1.102
0.0086911970	2.538
0.0086911970	4.935
0.0086911970	7.100
0.0086911970	8.372
0.0086911970	8.456
0.0086911970	6.864
0.0086911970	2.998

*** S H A B E R T H / B R L ** TECHNOLOGY DIVISION S K F INDUSTRIES INC. ** S H A B E R T H / B R L ***

P&W FLUID FILM BEARING / ROLLING ELEMENT TESTER (WITH 2 PE88S & 1 FLUID BRG)

* * * * * * * * AVERAGE NUMBERS * * * * * * * * * *

F R I C T I O N A L H E A T G E N E R A T I O N I N C O N T A C T E L L I P S E

------ BRG NO. 2 ------

I N N E R R A C E

# LAMINA	CONTACT AREA (IN**2)	SEMI-MAJOR AXIS (IN)	SEMI-MINOR AXIS (IN)
20	0.1091E-02	0.3848E-01	0.9018E-02

WIDTH OF LAMINUM (INCHES)	HEAT GEN. PER LAM. (WATTS)
0.0037759330	1.588
0.0037759330	4.101
0.0037759330	5.777
0.0037759330	6.681
0.0037759330	6.881
0.0037759330	6.452
0.0037759330	5.472
0.0037759330	4.009
0.0037759330	2.016
0.0037759330	0.237
0.0039207620	0.274
0.0039207620	2.455
0.0039207620	4.847
0.0039207620	6.793
0.0039207620	8.258
0.0039207620	9.089
0.0039207620	9.110
0.0039207620	8.133
0.0039207620	5.960
0.0039207620	2.382

*** PRESSURE IS SUPERCRITICAL ***
PRESSURE = 2000.00

O U T E R R A C E

# LAMINA	CONTACT AREA (IN**2)	SEMI-MAJOR AXIS (IN)	SEMI-MINOR AXIS (IN)
20	0.3523E-02	0.9013E-01	0.1244E-01

WIDTH OF LAMINUM (INCHES)	HEAT GEN. PER LAM. (WATTS)
0.0086607720	2.864
0.0086607720	6.537
0.0086607720	8.018
0.0086607720	7.887
0.0086607720	6.611
0.0086607720	4.455
0.0086607720	2.262
0.0086607720	0.972
0.0086607720	0.355
0.0086607720	0.128
0.0086607720	0.083
0.0086607720	0.154
0.0086607720	0.439
0.0086607720	1.169
0.0086607720	2.628
0.0086607720	4.909
0.0086607720	6.893
0.0086607720	7.953
0.0086607720	7.780
0.0086607720	5.881

SRS ITERATION PROGRAM OUTPUT

	UPSTREAM BRG	DOWNSTREAM BRG
FLUID DRAG CAGE FORCE (LB/BALL) =>	2.67921	2.67921
P.A. CAGE FORCE (LB/BALL) =>-	4.46247	-4.46247
RESULTANT FORCE ON CAGE(LB/BALL)=>	5.20498	5.20498
CAGE FRICTION HEAT (BTU/HR.BALL)=>	368.676	368.676
FLUID VISCOUS WORK (BTU/HR.BALL)=>	3616.40	3616.40

BRG 2 EXIT FLUID TEMP = 0.000000 DEG R

COOLANT QUALITY DUE TO FLASHING FROM BRG 2= 1.65701

FLAG SET TO NOSPRNG-NO SPRING PROCESSED --- STOP

ATTACHMENT B

MATHCAD SPREADSHEET FOR THREE RING FIT ANALYSIS OF BEARINGS

THREE RING FIT ANALYSIS FOR BEARING APPLICATIONS

ENTER GRAVITY CONSTANT

$G := 386.4$

ENTER RING DIAMETERS

$DIAA := .76$ Shaft Inner Diameter or Outer Race Effective Inner Diameter

$DIAB := 2$ Shaft Outer Diameter or Outer Race Outer Diameter

$DIAC := 2.8739$ Inner Race Sleeve Outer Diameter or Outer Race Sleeve Outer Diameter

$DIAD := 3.35$ Inner Race Effective Outer Diameter or Outer Race Outer Diameter

Calculate Radius'

$$a := \frac{DIAA}{2} \quad b := \frac{DIAB}{2} \quad c := \frac{DIAC}{2} \quad d := \frac{DIAD}{2}$$

ENTER RING MATERIAL PROPERTIES (E = Modulus of Elasticity; ν = Poisson's Ratio; α = Coefficient of Thermal Expansion; ρ = Weight Density)

RING 1 - Inner Ring

$E1 := 32.42\,10^{6}$ $\nu 1 := .288$ $\alpha 1 := 4.788\,10^{-6}$ $\rho 1 := .284$

RING 2 - Middle Ring

$E2 := 32.42\,10^{6}$ $\nu 2 := .288$ $\alpha 2 := 4.788\,10^{-6}$ $\rho 2 := .284$

RING 3 - Outer Ring

$E3 := 32.0\,10^{6}$ $\nu 3 := .260$ $\alpha 3 := 3.8\,10^{-6}$ $\rho 3 := .283$

ENTER RADIAL INTERFERENCE FITS BASED ON BUILD SPEC'S (NEGATIVE FOR INTERFERENCE)

$$\delta 12 := -\frac{.003}{2}$$ Ring 1 / Ring 2

$$\delta 23 := -\frac{.004}{2}$$ Ring 2 / Ring 3

ENTER RING TEMPERATURES (UNITS CONSISTENT WITHα)

$Tref := 68$ Reference Temperature

$T1 := -355$ $T2 := -355$ $T3 := -353$

ENTER ROTATIONAL SPEED OF RING SET (RPM)

$\omega := 37000$ Convertω to rad/sec $\omega := \omega \cdot 2 \cdot \frac{\pi}{60}$

CALCULATE RADIAL FIT CHANGES DUE TO THERMAL EFFECTS

$\delta 12 := \delta 12 - (\alpha 1 \cdot b \cdot (T1 - Tref) - \alpha 2 \cdot b \cdot (T2 - Tref))$

$\delta 23 := \delta 23 - (\alpha 2 \cdot c \cdot (T2 - Tref) - \alpha 3 \cdot c \cdot (T3 - Tref))$

Display Static Chilled Fits $\delta 12 = -0.0015$ Diametrical Static Chilled Fits $2 \cdot \delta 12 = -0.003$

$\delta 23 = -0.00139$

$2 \cdot \delta 23 = -0.00278$

CALCULATE RADIAL DIMENSIONAL CHANGES DUE TO SPINNING

Inner Ring Inner Radius

$\delta as1 := \frac{1}{4} \cdot \frac{\rho 1 \cdot \omega^2}{G} \cdot \frac{a}{E1} \cdot \left[(3 + \nu 1) \cdot b^2 + (1 - \nu 1) \cdot a^2\right]$ $\delta as1 = 1.096371 \cdot 10^{-4}$

Inner Ring Outer Radius

$\delta bs1 := \frac{1}{4} \cdot \frac{\rho 1 \cdot \omega^2}{G} \cdot \left(\frac{b}{E1}\right) \cdot \left[(1 - \nu 1) \cdot b^2 + (3 + \nu 1) \cdot a^2\right]$ $\delta bs1 = 1.009811 \cdot 10^{-4}$

Middle Ring Inner Radius

$\delta bs2 := \frac{1}{4} \cdot \frac{\rho 2 \cdot \omega^2}{G} \cdot \frac{b}{E2} \cdot \left[(3 + \nu 2) \cdot c^2 + (1 - \nu 2) \cdot b^2\right]$ $\delta bs2 = 6.382581 \cdot 10^{-4}$

Middle Ring Outer Radius

$\delta cs2 := \frac{1}{4} \cdot \frac{\rho 2 \cdot \omega^2}{G} \cdot \left(\frac{c}{E2}\right) \cdot \left[(1 - \nu 2) \cdot c^2 + (3 + \nu 2) \cdot b^2\right]$ $\delta cs2 = 5.817671 \cdot 10^{-4}$

Outer Ring Inner Radius

$\delta cs3 := \frac{1}{4} \cdot \frac{\rho 3 \cdot \omega^2}{G} \cdot \frac{c}{E3} \cdot \left[(3 + \nu 3) \cdot d^2 + (1 - \nu 3) \cdot c^2\right]$ $\delta cs3 = 0.00132$

Outer Ring Outer Radius

$$\delta ds3 := \frac{1}{4}\cdot\frac{\rho 3\cdot\omega^2}{G}\cdot\left(\frac{d}{E3}\right)\cdot\left[(1-\nu 3)\cdot d^2+(3+\nu 3)\cdot c^2\right] \qquad \delta ds3 = 0.00127$$

CALCULATE CHANGES IN INTERFERENCE FIT DUE TO SPINNING

$$\delta 12 := \delta 12 + \delta bs2 - \delta bs1$$

$$\delta 23 := \delta 23 + \delta cs3 - \delta cs2$$

INTERFERENCE FITS AFTER EFFECTS OF SPIN AND TEMPERATURI

$$\delta 12 = -9.627231\,0^{-4} \qquad \delta 23 = -6.527171\,0^{-4}$$

NOW USE A SOLVE BLOCK TO SOLVE FOR THE FIT PRESSURES

GUESS VALUES

$$p12 := 10000 \qquad p23 := 10000$$

SOLVE

Given

$$-p12\cdot\frac{b}{E1}\cdot\left(\frac{b^2+a^2}{b^2-a^2}-\nu 1\right)-p12\cdot\frac{b}{E2}\cdot\left(\frac{c^2+b^2}{c^2-b^2}+\nu 2\right)+\frac{p23}{E2}\cdot\frac{2\cdot c^2\cdot b}{c^2-b^2}=\delta 12$$

$$\left[-p23\cdot\frac{c}{E2}\cdot\left(\frac{c^2+b^2}{c^2-b^2}-\nu 2\right)-p23\cdot\frac{c}{E3}\cdot\left(\frac{d^2+c^2}{d^2-c^2}+\nu 3\right)+\frac{p12}{E2}\cdot\frac{2\cdot c\cdot b^2}{c^2-b^2}\right]=\delta 23$$

Return Solution Vector

$$\begin{pmatrix} p12 \\ p23 \end{pmatrix} := \text{Find}(p12, p23)$$

Ring1/Ring2 Fit Pressure

$$p12 = 1.078611\,0^4$$

Ring2/Ring3 Fit Pressure

$$p23 = 3.677041\,0^3$$

Now Calculate the Inner Ring, Inner Diametrical Change (- for Reduction)

Thermal

$\delta at := a \cdot \alpha 1 \cdot (T1 - Tref)$

Spin

$\delta as1 = 1.0963710^{-4}$

Pressure

$$\delta ap := -\frac{p12}{E1} \cdot \frac{2 \cdot a^2 \cdot b}{b^2 - a^2}$$

SUM EFFECTS TO DETERMINE CHANGE IN INNER RING, INNER DIAMETER

$\delta Dinner := 2 \cdot (\delta at + \delta as1 + \delta ap)$ $\delta Dinner = -0.00154$

Now Calculate the Outer Ring, Outer Diametrical Change (- for Reductior

Thermal

$\delta dt := d \cdot \alpha 3 \cdot (T3 - Tref)$

Spin

$\delta ds3 = 0.00127$

Pressure

$$\delta dp := \frac{p23 \cdot d}{E3} \cdot \frac{\left[c^2 \cdot (2 - \nu 3)\right]}{\left(d^2 - c^2\right)}$$

SUM EFFECTS TO DETERMINE CHANGE IN OUTER RING, OUTER DIAMETER

$\delta Douter := 2 \cdot (\delta dt + \delta ds3 + \delta dp)$ $\delta Douter = -9.5788310^{-4}$

ATTACHMENT C

MATHCAD SIMULATION OF
85MM LPOTP BEARING BALL EXCURSIONS

Evaluation of Ball Excursion Resulting From Ball Size Variations for the 85mm LPOTP with 250lb Axial Preload. The Calculations Performed Determine the Number of Shaft Revolutions Required to Cause an Offsize Ball to Lead or Lag the Average Ball Train Position by a Distance Equal To 1/2 the Cage Pocket Clearance. An Excursion of this Magnitude Would Cause Binding and an Increase In Torque

$D := .8125$ (IN) Nominal Ball Dia.

$dm := 6.625$ (IN) Pitch Dia.

$K := 175000$ (psi) Deflection Constant

$Fa := 250$ (lbs) Axial Preload

$Z := 13$ Number of Balls

$Ni := 1$ (RPM) Arbitrary Shaft Speed

$fi := .52$ Nominal Inner Race Curvature

$fo := .53$ Nominal Outer Race Curvature

$A := (fo + fi - 1) \cdot D$ $B := (fo + fi - 1)$

$ri := fi \cdot D$ Inner Race Radius Of Curvature

$ro := fo \cdot D$ Outer Race Radius Of Curvature

$Pd := .0046$ (IN) Diameterical Clearance

Calculate Nominal Free Contact Angle

$$\alpha o := \operatorname{acos}\left[1 - \frac{Pd}{2 \cdot A}\right]$$

Initial Guess for Loaded Contact Angle

$$\alpha l := \alpha o + 1 \cdot \frac{\pi}{180}$$

Use a Root Search Method To Solve For the Nominal Loaded Contact Angle (Equation 6.34 T. Harris, 'Roller Bearing Analysis',Second Edition.)

$$T1 := \left[\frac{Fa}{Z \cdot D^{2} \cdot K}\right] - \sin(\alpha l) \cdot \left[\frac{\cos(\alpha o)}{\cos(\alpha l)} - 1\right]^{1.5}$$

$$T2 := \cos(\alpha l) \cdot \left[\frac{\cos(\alpha o)}{\cos(\alpha l)} - 1\right]^{1.5} + 1.5 \cdot \tan(\alpha l)^{2} \cdot \left[\frac{\cos(\alpha o)}{\cos(\alpha l)} - 1\right]^{.5} \cdot \cos(\alpha o)$$

$$\alpha p := \alpha l + \frac{T1}{T2}$$

$\alpha l := \operatorname{root}(\alpha p - \alpha l, \alpha l)$ $\alpha l \cdot \frac{180}{\pi} = 20.372044$ (Deg) Nominal Loaded Contact Angle

$$\Gamma := D \cdot \frac{\cos(\alpha l)}{dm}$$

$$Vcage := \pi \cdot \frac{dm}{120} \cdot (Ni \cdot (1 - \Gamma))$$

Ncage := .5·(Ni·(1 - Γ))
Ncage = 0.442503 # Cage Rev/Shaft Rev

Vcage = 0.153497 (IN/S) Average Ball Train Velocity

NOW CALCULATE SPEED FOR OFF-SIZE BALL

f(apl,all,i) := root(apl - all,all) i := 0 ..9 Function to Evaluate the Contact Angle For the Offsize Ball

DEFINE RANGE OF BALL SIZE VARIATION TO EVALUATE (1 MIL TO ZERO)

$\delta D_i := -.001 + .0001 \cdot i$ (UNDERSIZE)

$DP_i := D - \delta D_i$

REPEAT ABOVE CALCULATIONS FOR OFF SIZE BALLS TO DETERMINE THE ORBITAL SPEED OF THE OFF SIZE BALLS

$$fi_i := \frac{ri}{DP_i} \qquad fo_i := \frac{ro}{DP_i}$$

$$A_i := \left[fo_i + fi_i - 1\right] \cdot DP_i \qquad B_i := \left[fo_i + fi_i - 1\right]$$

Pd := .0046

$$\alpha o_i := \operatorname{acos}\left[1 - \frac{Pd}{2 \cdot A_i}\right] \qquad \alpha l_i := \alpha o_i + 1 \cdot \frac{\pi}{180}$$

δD_i
$-1 \cdot 10^{-3}$
$-9 \cdot 10^{-4}$
$-8 \cdot 10^{-4}$
$-7 \cdot 10^{-4}$
$-6 \cdot 10^{-4}$
$-5 \cdot 10^{-4}$
$-4 \cdot 10^{-4}$
$-3 \cdot 10^{-4}$
$-2 \cdot 10^{-4}$
$-1 \cdot 10^{-4}$

$$T1_i := \left[\frac{Fa}{Z \cdot DP_i^2 \cdot K}\right] - \sin\left[\alpha l_i\right] \cdot \left[\frac{\cos\left[\alpha o_i\right]}{\cos\left[\alpha l_i\right]} - 1\right]^{1.5}$$

$$T2_i := \cos\left[\alpha l_i\right] \cdot \left[\frac{\cos\left[\alpha o_i\right]}{\cos\left[\alpha l_i\right]} - 1\right]^{1.5}$$

$$T3_i := 1.5 \cdot \tan\left[\alpha l_i\right]^2 \cdot \left[\left[\frac{\cos\left[\alpha o_i\right]}{\cos\left[\alpha l_i\right]} - 1\right]^{.5}\right] \cdot \cos\left[\alpha o_i\right]$$

$$\alpha p_i := \alpha l_i + \frac{T1_i}{T2_i + T3_i} \qquad \alpha l_i := f\left[\alpha p_i, \alpha l_i, i\right]$$

$$\Gamma_i := DP_i \cdot \frac{\cos\left[\alpha l_i\right]}{dm}$$

$$Voff_i := \pi \cdot \frac{dm}{120} \cdot \left[Ni \cdot \left[1 - \Gamma_i\right]\right]$$ (IN/S) OBRBITAL SPEED FOR OFF SIZE BALL

$$Cpl := \frac{.8395 - D}{2} \qquad Cpl = 0.0135$$ (IN) 1/2 CAGE POCKET CLEARANCE

$$time_i := \frac{Cpl}{.000000001 + Vcage - Voff_i} \qquad Noff_i := .5 \cdot \left[Ni \cdot \left[1 - \Gamma_i \right] \right]$$

$$NUMBER_i := time_i \cdot \frac{Ni}{i \; 60}$$ NUMBER OF SHAFT REVOLUTIONS REQUIRED FOR DELTA VELOCITY TO CAUSE AN EXCURSION EXCEEDING 1/2 THE CAGE POCKET CLEARANCE

i	DP i	NUMBER i
0	0.8135	-47.629219
1	0.8134	-53.845865
2	0.8133	-61.648546
3	0.8132	-71.718891
4	0.8131	-85.193258
5	0.813	-104.11771
6	0.8129	-132.585884
7	0.8128	-180.154535
8	0.8127	-275.518747
9	0.8126	-562.447579

BALL SIZE DEVIATION FROM NOMINAL (IN)

$$bsv_i := -.001 + .0001 \cdot i$$

BALL SIZE VARIATION VERSES # OF SHAFT
REVOLUTIONS FOR TORQUE INCREASE

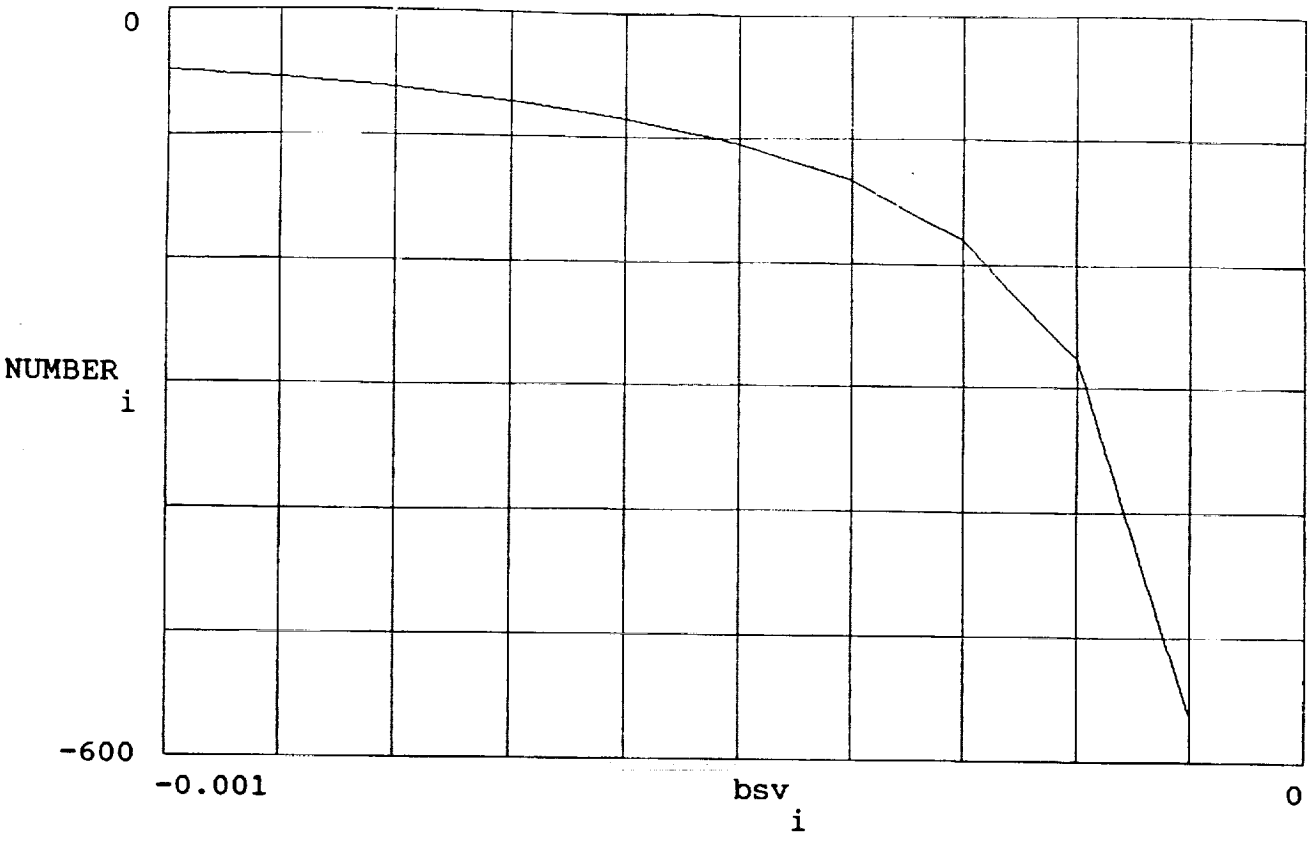

REPORT DOCUMENTATION PAGE

Form Approved
OMB No. 0704-0188

1. AGENCY USE ONLY (*Leave blank*)	2. REPORT DATE	3. REPORT TYPE AND DATES COVERED
	January 31, 2000	Final Report Jan 92 - Jan 00

4. TITLE AND SUBTITLE
SSME Bearing and Seal Tester Data Compilation Analysis, and Reporting; and Refinement of the Cryogenic Bearing Analysis Mathematical Model

5. FUNDING NUMBERS
NAS8-39379

6. AUTHOR(S)
James Moore, Dave Marty, and Joe Cody

7. PERFORMING ORGANIZATION NAME(S) AND ADDRESS(ES).
SRS Technologies
500 Discovery Drive
Huntsville, AL 35806

8. PERFORMING ORGANIZATION REPORT NUMBER
TR00-1017

9. SPONSORING/MONITORING AGENCY NAME(S) AND ADDRESS(ES)
NASA MSFC
Marshall Space Flight Center
Marshall Space Flight Center, AL 35812

10. SPONSORING/MONITORING AGENCY REPORT NUMBER

11. SUPPLEMENTARY NOTES
N/A

12a. DISTRIBUTION/AVAILABILITY STATEMENT
N/A

12b. DISTRIBUTION CODE

13. ABSTRACT (*Maximum 200 words*)

SRS and NASA/MSFC have developed software with unique capabilities to couple bearing kinematic modeling with high fidelity thermal modeling. The core thermomechanical modeling software was developed by SRS and others in the late 1980's and early 1990's under various different contractual efforts. SRS originally developed software that enabled SHABERTH (Shaft Bearing Thermal Model) and SINDA (Systems Improved Numerical Differencing Analyzer) to exchange data and autonomously allowing bearing component temperature effects to propagate into the steady state bearing mechanical model. A separate contract was issued in 1990 to create a personal computer version of the software. At that time SRS performed major improvements to the code. Both SHABERTH and SINDA were independently ported to the PC and compiled. SRS them integrated the two programs into a single program that was named SINSHA. This was a major code improvement.

14. SUBJECT TERMS	15. NUMBER OF PAGES
Rolling element bearings, cryogenic cooling, turbopump bearings, bearing analysis	310
	16. PRICE CODE

17. SECURITY CLASSIFICATION OF REPORT	18. SECURITY CLASSIFICATION OF THIS PAGE	19. SECURITY CLASSIFICATION OF ABSTRACT	20. LIMITATION OF ABSTRACT
Unclassified	**Unclassified**	**Unclassified**	**SAR**